APPENDICES

APPENDICES
ACADIANA BAYS REEF RESTORATION PROJECT

A. HYDRODYNAMIC, SALINITY AND MODELING OF REEF REPORT – TAYLOR ENGINEERING, INC.

B. GEOTECHNICAL REPORT –LOURIE CONSULTANTS

C. BOTTOM CROSS SECTIONS – ORIGINAL SECTIONS A-E, ELEVATION 0.0 AND – 3.0 AND REEF A AND B, ELEVATION – 3.0

D. REDUCED LOWER ATCHAFALAYA RIVER FLOW AND SEGMENTED REEF MODELING.

E. REEF VOLUME REQUIRED FOR SUBMERGED FILL WEIGHT OF 70 PCF-ORIGINAL CROSS SECTIONS A-E

F. PUBLIC OUTREACH PROGRAM

APPENDIX
A

APPENDIX A
ACADIANA BAYS REEF RESTORATION PROJECT

HYDRODYNAMIC, SALINITY AND MODELING OF REEF REPORT –
TAYLOR ENGINEERING, INC.

Acadiana Bays Feasibility Study

Acadiana Bays, Louisiana

February 2006

Acadiana Bays Feasibility Study
Acadiana Bays, Louisiana

Prepared for:

Louisiana Department of Natural Resources
Baton Rouge, Louisiana

by:

Taylor Engineering, Inc.
251 Florida Street
Suite 215
Baton Rouge, LA 70801
(225)387-0001

As Subconsultant to:
Waldemar S. Nelson and Co., Inc.
New Orleans, LA

February 2006
C2003-046

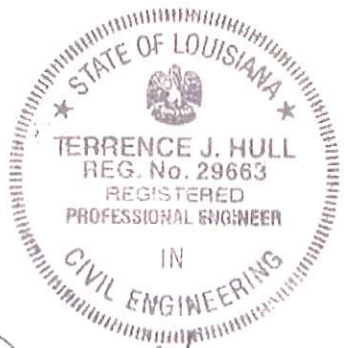

Terrence J. Hull P.E. # 29663
February 27, 2006

TABLE OF CONTENTS

LIST OF FIGURES

LIST OF TABLES

1.0 INTRODUCTION

1.1 Background

The Acadiana Bays system — located in the center of Louisiana's coast and approximately 120 mi west of the modern Mississippi River delta — constitutes Louisiana's largest estuary encompassing about 580 square mi (Walker and Hammack, 2000). The bay system consists of four major bays (from west to east): Vermilion Bay, West Cote Blanche Bay, East Cote Blanche Bay, and Atchafalaya Bay (Figure 1.1). A fifth and significantly smaller bay, Four League Bay, lies at the eastern extent of the bay system. A distance of approximately 70 mi separates eastern Four League Bay from western Vermilion Bay. The region comprises parts of Vermilion, Iberia, St Mary, and Terrebonne Parishes in Louisiana.

At one time the bay complex reportedly contained the largest concentration of oyster reefs in the United States; however, a combination of man's activities, most importantly dredging from the 1940s to 1950s (USACE, 2002), destroyed most of these beds. Shell dredging in the 1960s and 1970s almost completely removed what remained of the oyster population.

This dredging and shell mining removed natural baffles between the Gulf of Mexico and Atchafalaya Bay as well as between Atchafalaya and East Cote Blanche Bays. The area began to change from a brackish-type estuarine habitat to a fresher environment as the Atchafalaya River began to capture flow from the Mississippi River following human modifications at Old River in the 1930s and 1940s (Roberts, 1998). This change has adversely impacted the fishing, shrimping and crabbing industries. In addition, siltation due to sediment carried by the additional river flow entering the system has endangered navigation and further impacted the marine industries (Coastal Environments, Inc. 1977).

1.2 Study Purpose and Methods

The goal of this study is to examine the feasibility of influencing the salinity and turbidity regimes of the Acadiana Bays system by reestablishing reefs historically located in the area. The study applies numerical models, with existing and new data, to determine whether the presence of artificial reefs changes existing salinity and turbidity regimes.

1.3 Report Organization

The report documents the modeling effort for the Acadiana Bays restoration project. Chapter 2 describes the study area. Chapter 3 presents the project modeling needs and summarizes key features of the selected models. Chapter 4 details the hydrodynamic and transport model calibrations. Chapter 5

details the wave model calibration. Chapter 6 presents the hydrodynamic and transport model results. Chapter 7 presents the wave model results. Chapter 8 describes the effort to model the historical characteristics of the area. Finally, Chapter 9 summarizes and presents the findings of this study.

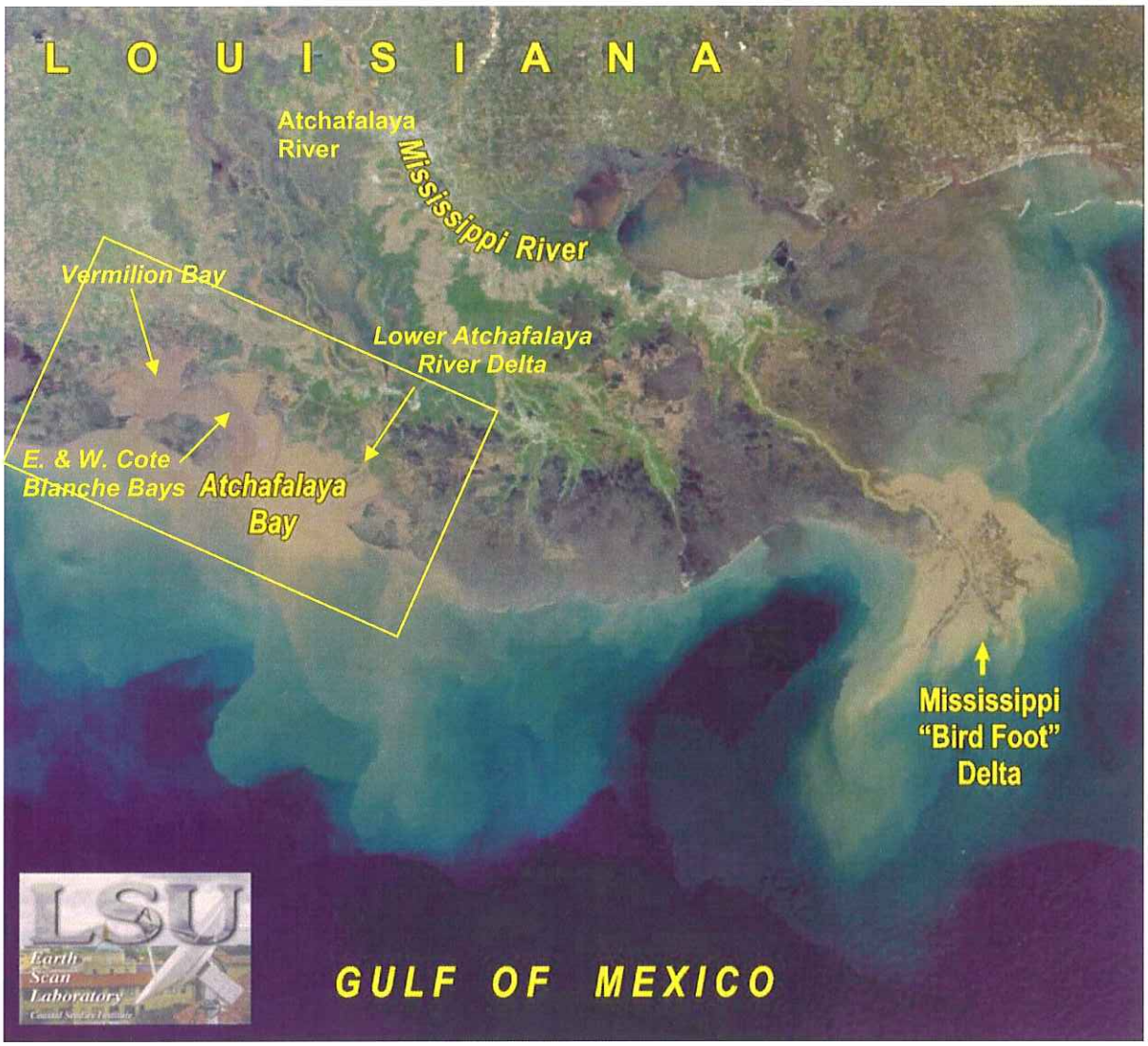

Figure 1.1 Acadiana Bays System

2.0 STUDY AREA

2.1 History of the Area

Coastal Environments, Inc. (1977) detailed the geologic history of the Acadiana Bays region (Figure 1.1). The highly dynamic Louisiana coastal zone requires significant amounts of sediment to replace material lost to erosion and to offset sea level rise and land subsidence. Historically, the Mississippi River and its tributaries delivered sufficient sediment to coastal Louisiana to maintain the deltaic and coastal processes of the natural environment.

The Acadiana Bays system formed when the Mississippi River flowed into the Gulf of Mexico through Bayou Teche, Bayou Sale and Cypremort (about 6,000 yrs ago). The natural delta building process eventually isolated the region from the river and cut off its sustaining sediment supply. With no sediment supply, the processes of subsidence and wave erosion shaped the shoreline. The open bays and narrow zones of fresh, brackish, and saline marshes of the Acadiana Bays region signify the deterioration and abandonment stage (fourth stage) of delta development.

According to Fisk (1952), as cited by Roberts (1998), explorers recognized the Atchafalaya as a distributary of the Mississippi River as early as the 1500s. These and later accounts identified the diversion as choked with debris from the Mississippi and Red Rivers (Latimer and Schweitzer, 1951 as cited in Mashriqui, 2003). In the early 1800s, local runoff provided the main freshwater input into the Acadiana Bays region with the Atchafalaya River conveying less than 10% of the flow from the Mississippi and Red Rivers (Powell, 2003). The removal of a log jam at Simmesport in 1839 (Letter, 1983) and the construction of Shreve's Cutoff on the Mississippi River positioned the Atchafalaya River to become a major distributary of the Mississippi River (Powell, 2003).

Construction of the Old River Control Structure in 1963 managed and maintained the flow distribution of the Mississippi River entering the Atchafalaya River. An auxiliary structure, constructed in 1986, augmented the original structure after damage by high floods in 1973 (Roberts, 1998). The Atchafalaya River has captured 30% of the Mississippi River's flow since construction of the original control structure (Roberts, 1998).

In 1942, the USACE dredged an artificial channel — Wax Lake Outlet — from Six-Mile Lake into Atchafalaya Bay to diminish flood levels on the Lower Atchafalaya River near Morgan City (Roberts, 1998). Designed to capture 20% of the Atchafalaya River flow, conveyance by Wax Lake

Outlet increased to 40 – 50% of the low to average Atchafalaya River flows (Powell, 2003; and Goree et al., 2002 as cited in Powell, 2003).

To halt the increasing capture of the Atchafalaya River flow, the USACE constructed a weir above the entrance of Wax Lake Outlet in 1988 (Kemp et al, 1995 as cited in Majersky et al., 1997). Hydraulic pressure through Wax Lake Outlet caused a widening of the outlet's cross section while the cross section of the Lower Atchafalaya River decreased (Shlemon, 1975 as cited in Majersky et al., 1997). The control structure reduced the Wax Lake Outlet discharge during average flows but increased discharge during high flows. This condition, along with control structure-induced changes to sediment flow and increased river stages near Morgan City, led to the removal of the structure in 1994 (Majersky et al, 1997). The removal of the control structure returned outlet channel flow to pre-weir conditions (USACE, 1995 as cited in Majersky et al., 1997).

Following the historic flood of 1973, the subaqueous portions of the Lower Atchafalaya River and Wax Lake Outlet deltas emerged as subaerial features (Roberts, 1998). At 700,000 cubic feet per second (cfs), the average peak discharge of the Atchafalaya River during the 1973 flood constituted a marked increase over the average peak discharge of 400,000 cfs from 1938 to 1972 (USACE, 1974 as cited in Roberts, 1998). Roberts (1998) classifies 1973 to 1975 as high water years. During this period the average annual suspended sediment load in the Atchafalaya River more than doubled to 88.9 million metric tons. This increase in suspended sediment introduced 30.9 million metric tons of sand to the bay through the Lower Atchafalaya River and Wax Lake Outlet — more than seven times the total of the previous four years (Roberts, 1998). Deposition of this sand led to the emergence and development of the Lower Atchafalaya River and Wax Lake Outlet deltas. These processes continue today.

2.2 Present Conditions

Classified as a micro-tidal coastal region (tides < 1.5 ft) and with water depths averaging 6 – 7 ft, diurnal tides (Walker, 2001) dominate the Acadiana Bays; however, semidiurnal tides do occur. Tidal energy, winds, muddy bottoms, and salinity and sediment fluxes influence the hydrodynamic, wave, salinity, and turbidity regimes in Acadiana Bays.

As noted, deposition continues to build two major deltas where the Atchafalaya River enters Atchafalaya Bay — the Lower Atchafalaya River and Wax Lake Outlet deltas. Both riverine (freshwater) and tidal processes (saltwater) influence the hydrodynamics of the system.

Estimates of annual water and sediment discharge from the Mississippi River average 650,000 cfs and 210 million tons/yr (Milliman and Meade 1983, as cited in Myint and Walker, 2002). The Atchafalaya River carries 30% of the Mississippi River flow and approximately 40% of the sediment load (Mossa and Roberts, 1990 as cited in Walker, 2001). Wax Lake Outlet carries 45% of the average Atchafalaya River flows, and the Lower Atchafalaya River carries the rest. The entrance of these two flows into Atchafalaya Bay provides the majority of the freshwater input into the system and a significant forcing mechanism for circulation within the region.

Wax Lake Outlet receives Atchafalaya River flow through the Gulf Intracoastal Waterway (GIWW). The GIWW distributes some Atchafalaya River flow and sediment to all the bays in the system. Vermilion, West Cote Blanche, and East Cote Blanche Bays receive significantly less direct freshwater input than Atchafalaya Bay.

Other less significant freshwater inputs into the region include the combined GIWW and Charenton Drainage Canal flow at "The Jaws" in West Cote Blanche Bay (average flow of 12,000 cfs, USGS, 2003 as cited in Powell, 2003), the Vermilion River into Vermilion Bay, and several smaller bayous.

Runoff from local precipitation constitutes an insignificant freshwater input into Acadiana Bays compared to the Atchafalaya River discharge. Analysis by Gagliano et al. (1970) as cited in Coastal Environments, Inc. (1977) shows that the Atchafalaya River provides 20 to 30 times more freshwater inflow than local rainfall.

Marsh Island separates West Cote Blanche Bay and part of Vermilion Bay from the Gulf of Mexico. Southwest Pass — with depths exceeding 100 ft and an average width of about 0.6 mi — connects eastern Vermilion Bay and West Cote Blanche Bay to the Gulf of Mexico. A 30 mi opening between eastern Marsh Island and Point Au Fer directly connects East Cote Blanche Bay and Atchafalaya Bay to the Gulf of Mexico; average depths along this reach approach 10 ft. A 10 mi opening between the northeast tip of Marsh Island and Point Chevreuil to the east provides wide access to the Gulf of Mexico. This access, along with Southwest Pass, provides flushing for Vermilion, West Cote Blanche, and East Cote Blanche Bays.

As previously noted, dredging of the oyster reefs removed the natural baffles between the Gulf of Mexico and Atchafalaya Bay as well as between Atchafalaya and East Cote Blanche Bays. Mining the reefs extending into East Cote Blanche Bay removed a natural barrier between the freshwater discharge from the Atchafalaya River and the bays to the west (USACE, 2002). In addition, removal of the barrier may have increased the flow of sediments into the bays and so contributed to shoaling in southern Vermilion Bay (USACE, 2002).

This combination of freshwater intrusion and siltation disrupted the marine habitat, killing some species and forcing others to abandon the area. The effect on the fisheries delivered a severe financial blow to fishermen, small shrimp boat operators, and the crabbing industry (Coastal Environments Inc, 1977). Siltation also impacted navigation which further affected the fishing and marine industries. Previous studies (Coastal Environments, Inc., 1977) and anecdotal evidence have indicated that restoration of the historical reefs between the East Cote Blanche and Atchafalaya Bays may reduce the siltation and freshwater intrusion due to the Atchafalaya River discharge.

2.3 Proposed Reef Alternatives

As noted, the primary goal of this study is to evaluate the potential of influencing salinity and turbidity regimes in the Acadiana Bays system by reestablishing reefs historically present in the study area. Anecdotal accounts attribute the freshening of the western bays to the removal of oyster beds lying between Marsh Island and Pt. Chevreuil (USACE 2002). Flow streamlines (pathways) derived from preliminary model simulations partially support this contention by indicating that flood tides from the Gulf of Mexico push the Wax Lake Outlet and Lower Atchafalaya River freshwater discharge plumes back into East Cote Blanche Bay via the Marsh Island-Pt. Chevreuil passage. Predominant southeast winds exacerbate this process by driving the freshwater plumes into the western bays. Presumably, suspended sediment (carried in the riverine discharge) also enters the western bays by these mechanisms.

Anecdotal evidence, an understanding of the conditions influencing salinity and turbidity in the bays, and model results formed the basis to establish artificial reef alternatives that address the concept of blocking freshwater (and suspended sediment) discharge from entering East Cote Blanche Bay (and those to the west). Table 2.1 and Figure 2.1 describe four alternatives identified. The alternatives comprised two reef orientations with two reef crest heights. All four reef alternatives extend from Pt. Chevreuil. Alternative A extends 12.5 miles with an orientation of South, 45° West (S 45°W). Alternative B extends 14 miles with an orientation of South 90° West (S 90°W) and connects to Marsh Island. Each of these

alternatives considered two different crest elevations – one at 3 feet below Mean Low Water (MLW) and one at Mean High Water (MHW).

Table 2.1 Reef Alternative Descriptions

Reef/Model Alternative	Description
A1	12.5 mi from Point Chevreuil at an angle of S 45°W Crest at -3 ft-MLW
A2	12.5 mi from Point Chevreuil at an angle of S 45°W Crest at MHW
B1	14 mi from Point Chevreuil to Marsh Island at an angle of S 90°W Crest at -3 ft-MLW
B2	14 mi from Point Chevreuil to Marsh Island at an angle of S 90°W Crest at MHW

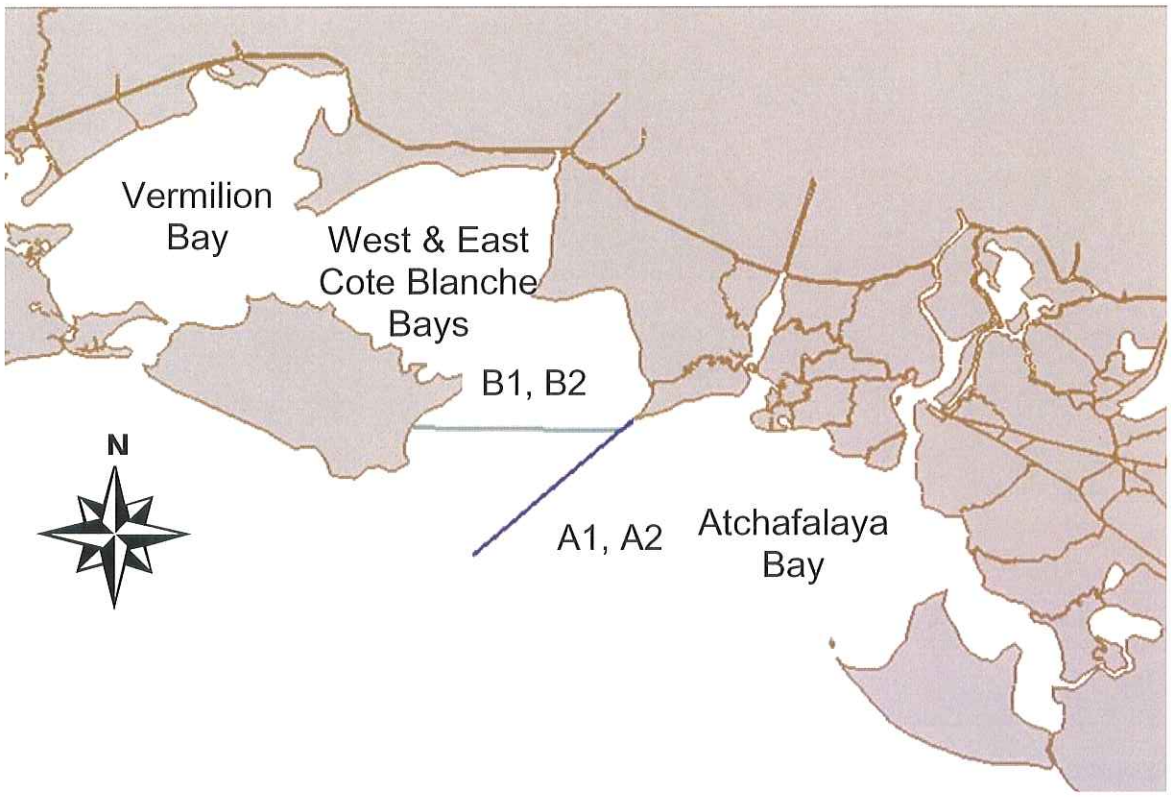

Figure 2.1 Reef Alternatives

Alternative B2 would completely block the Marsh Island-Pt. Chevreuil opening. Consequently, it would block boat traffic into the bays and, thus, make this alternative less desirable. This study addressed a complete blockage to evaluate the maximum benefit for this alternative. If benefits for this alternative prove promising, a refined alternative could consider limited openings in the reef to allow boat passage. However, boat passage would remain constrained.

A more suitable alternative (Alternative A) would allow boats easier access to East Cote Blanche Bay while still restricting the freshwater discharge from moving westward into the bay. Furthermore, since the alignment of Alternative A generally follows the natural flood and ebb flow streamlines (determined from model results), it would not significantly impede the momentum of the ebb flow carrying the freshwater (discharged by Wax Lake Outlet and the Lower Atchafalaya River) to sea. It would tend to jet the freshwater farther offshore where it could mix with more saline (and less turbid) water before returning to the bay system. The alignment also would allow the natural tidal (and saline) communication between the bay and the Gulf of Mexico on the reef's western side.

Again, this study considered two reef elevations. A reef covering the entire water column – with its crest at MHW – clearly would provide the most security against freshwater intrusion. However, a submerged reef – with its crest at -3 ft MLW – would require less material and provide a more economical solution.

For modeling purposes, the reefs with their crests at MHW constituted a complete blockage of the flow, while the reef alternatives with their crests at -3 ft MLW permitted flows above the crests. The model treated the reefs in all four cases as impermeable structures.

The four reef alternatives represent a range of possibilities. While they do not necessarily represent the most efficient, economical, or feasible solution for all considerations (including navigation), their evaluation does estimate the expected benefits that an artificial reef might realize.

3.0 DESCRIPTION OF MODELS AND PROCEDURES

3.1 Model Requirements

The circulation within the model domain and the flow, salinity, and turbidity influx and efflux across the model boundaries determine the salinity and turbidity patterns in the Acadiana system. Stream flow, tides, winds, and wind waves are the primary drivers of circulation in the bays. Not only do winds directly drive steady currents in the bays, their ability to generate waves also causes wave-related (primarily) oscillatory currents. Given this understanding, this study requires numerical models for tidal, riverine, and wind-related hydrodynamics; wave propagation; and salinity and turbidity transport over non-uniform sea and bay bottoms.

In addition to the ability to simulate these physical parameters and mechanisms, other factors control model selection. For example, the complexity of the flow through some irregular systems is inherently a three-dimensional problem, which requires a three-dimensional solution. However, in spite of significant recent technical advances, state of the art numerical models still cannot be applied in a blindfolded manner with great confidence; calibration of multiple parameters, site-specific in nature, is necessary to develop confidence in their predictive ability. In particular, three-dimensional numerical models have intense requirements for calibration data, far more than were available for the study area. Furthermore, given the relatively shallow depths within the vertically well-mixed bays, a two-dimensional depth-averaged model should appropriately simulate the processes necessary to achieve the study objectives. Consequently, only two-dimensional models were considered in the model selection process of this feasibility study. The small improvement gained from applying a three-dimensional model does not justify the considerably higher cost associated with such a model.

The model must be able to represent a large area with reasonable run times. The nature of the study area, the purpose of the modeling effort, and the simulation parameters (salinity and turbidity) dictate an expansive model domain. The large size of the model domain along with the necessity to resolve the influence of small features (such as small creeks and the proposed artificial reef) dictates the use of a model with variable grid size capability such as a finite-element model or a nested grid finite-difference model. Additional parameters of interest include model availability (public domain or reasonably priced commercial model), model acceptance, and the model's capability to address fine sediment transport, flow control structures, and wetting and drying elements.

3.2 Model Selection

Several models can simulate most or all of the physical parameters necessary to accomplish the study objectives. For hydrodynamics, salinity, and turbidity, the list includes the U.S. Army Corps of Engineers (USACE) TABS modeling suite, the Danish Hydraulics Institute (DHI) MIKE21C models, the Delft Hydraulics DELFT2D models, and a few less recognized others. Of these, the USACE TABS model suite — which includes RMA2 (hydrodynamics) and RMA4 (salinity and turbidity) — best suits this study. Its suitability is based on the model's capability to simulate the physical parameters, its public domain availability (a Louisiana Department of Natural Resources preference), and its previously successful use in large domains in coastal Louisiana (Donnell et al., 1991; USACE, 2000; USACE, 2002; Mashriqui, 2003). Other works with the TABS suite for the Acadiana Bays region have focused more narrowly on the Atchafalaya River and its delta (Donnell et al., 1991; USACE, 2002; Mashriqui, 2003).

For wave propagation, the common models include REFDIF, STWAVE, WISWAVE, FUNWAVE, and wave modules of the DHI MIKE21 and Delft Hydraulics DELFT2D packages. Among widely accepted public domain models, REFDIF and STWAVE constitute viable options. REFDIF simulates shoaling, refraction, diffraction, and surface (breaking) and bottom dissipation (bottom friction and percolation); it does not simulate wave generation or wave-wave interactions. STWAVE simulates shoaling, refraction, surface dissipation, wave generation, and wave-wave interactions; it does not simulate bottom dissipation and applies a somewhat heuristic method to address diffraction. Previous studies indicate that local wave generation is a key process for Acadiana Bays, a finding that supports the use of STWAVE over REFDIF. This study adds bottom dissipation mechanisms to the commercially available version of STWAVE to address this limitation (Chapter 5). For settings like Acadiana Bays, one expects bottom-induced diffraction to be a relatively minor process relative to wave generation, shoaling, refraction, and breaking. Structure-induced diffraction is typically important only in its immediate vicinity (the shadow zone of the structure) where a model without an ability to simulate diffraction would underpredict wave heights. Given these findings, STWAVE proves to be the best available tool for application in this study.

3.3 Description of Selected Models

3.3.1 Hydrodynamic Model

The USACE Waterways Experiment Station maintains RMA2, the one- and two-dimensional, transient, depth-averaged, finite-element, hydrodynamic model component of the TABS modeling suite. The governing equations treat conservation of mass, conservation of momentum in the x- and y-direction,

and turbulence closure. Model capabilities include wetting and drying, Coriolis acceleration, wind stress, radiation stress, dynamic friction assignment by depth, Peclet or Smagorinski definition of turbulent exchange coefficients, and two choices for boundary conditions (flow or elevation).

Typical RMA2 applications in the coastal zone simulate the effects of flow discharges and tidal forcing to estimate water surface elevations and currents in the model domain. In addition to calculating such currents, RMA2 (version 4.20 or later) accepts optional wind input cards that describe a spatially- and temporally-varying wind field that occurs simultaneously with the currents. The model calculates and superimposes wind induced-currents during the hydrodynamic computations.

The RMA2 hydrodynamic model has several optional wind shear stress formulations. These include (1) the RMA2 Original Formula, (2) Van Dorn Formula, (3) Wu Formula, (4) Safaie Formula, (5) Ekman Formula, and (6) a Generic Formula. Two additional options include prescription of the default parameter values for the Van Dorn and Wu Formulas. These eight formulas provide considerable flexibility in handling wind effects.

The application of RMA2 serves to establish the baseline circulation in the Acadiana Bays region and establish changes in circulation due to proposed alternatives. Model results then drive the companion RMA4 salinity and turbidity transport models discussed later in this section.

3.3.2 Wave Model

The Acadiana Bays region provides a challenging environment for the numerical modeling of waves. In this region, the irregularity of the coastline, soft bottom material, lack of detailed, comprehensive wave data, and the importance and frequency of the wind and storm events all contribute to modeling difficulties. The soft bottom material that dominates the bays induces significant wave energy dissipation not accounted for in most numerical wave models. Previous studies document significant wave energy dissipation over relatively small distances for waves traveling over mudbanks and regions of soft bottom material (Mathew el al., 1995; Forristall and Reece, 1985; Tubman and Suhayda, 1976).

To understand recent changes and simulate the evolution of the region requires a comprehensive understanding of the system processes and numerical models that can handle the physical properties of the region. To achieve this understanding one must employ models developed specifically for regions with a soft bottom (mud) or modify a model developed for locations with coarse bottom material (sand).

The wave modeling component applies the steady-state spectral wave model STWAVE 3.0 (Smith et al., 2001) to model the wave environment in the Acadiana Bays region. STWAVE, a finite-difference model based on the wave-action balance equation, estimates nearshore wind-wave growth and propagation by simulating wave generation, bottom- and current-induced wave refraction and shoaling, and steepness-induced wave breaking. STWAVE provides a flexible and robust wave model that works within the software package employed for the Acadiana Bays hydrodynamic and salinity transport models.

The public domain version of the STWAVE model does not incorporate wave dissipation by bottom processes; this limits its use to relatively small propagation distances — tens of miles (Smith et al., 2001) — and regions where dissipation caused by bottom effects is negligible (deep water and sandy seabeds). Thus, the public domain version of the model does not provide an ideal representation of the project area with bottom sediments comprised primarily of a mixture of silts and clays; such sediments in shallow water depths cause substantial wave attenuation not simulated in the public domain version. Modifying the public domain model to include the effects of bottom dissipation on wave transformation overcomes this model deficiency. Chapter 5 describes calibration of the wave modeling and modifications required by the cohesive sediment within the Acadiana Bays.

3.3.3 Salinity and Turbidity Transport Model

The USACE Waterways Experiment Station developed RMA4 – a companion to RMA2 – as the finite-element, water quality transport model component of the TABS modeling suite. RMA4 applies the RMA2-supplied hydrodynamic field to simulate depth averaged advection-diffusion processes for up to six conservative or non-conservative constituents within a one- or two-dimensional mesh domain. RMA4 simulates the processes of depth-averaged advection, dispersion, decay, local mass sources, and rainfall/evaporation effects. Common applications of RMA4 simulate salinity or pollutant transport, calculate water temperature distribution, calculate residence time in harbors or basins, evaluate turbidity plume extents, define mixing zones, describe BOD-DO interaction, and analyze flushing.

Application of RMA4 establishes baseline salinity and turbidity distributions in Acadiana Bays and evaluates changes in salinity and turbidity distributions attributable to the proposed alternatives.

3.3.4 A Note on the Applied Sediment Transport Methodology

The USACE TABS modeling suite does include the morphodynamic model SED2D-WES, which was initially considered for application in this study. A finite element model, it calculates bed elevation

changes through deposition and erosion by employing a hydrodynamic solution of water elevations and velocities from the RMA2 model with appropriate sediment transport equations. Unfortunately, the amount of information required to correctly apply this model was unavailable. Consequently, this study applied RMA4 to model turbidity. The following discussion highlights SED2D-WES and the rationale for not applying it in this study.

Though SED2D-WES simulates transport of both cohesive (clay) and non-cohesive (sand and silt) sediments, in any given simulation the model can only simulate the transport of a single sediment type represented by a single grain size. The Acadiana Bays region features sediment beds comprised of sands, silts, and clays (Mehta et al., 1989). The sand portion resides close to the delta while silt and clay occur more frequently in the bays and on the shelf. In domains with more than one type of sediment, SED2D-WES individually calculates and linearly superimposes bed changes for each material type.

In its implementation, SED2D-WES incorporates four computations — the basic convection-diffusion equation with the suspended sediment concentration and a bed source term, bed shear stress, bed source quantity, and bed model (Donnell, 2001). Applying the RMA2-supplied hydrodynamic field and suspended sediment concentrations at the beginning of a time step, SED2D-WES calculates the suspended sediment concentrations and bed elevations across the entire model domain. Effective diffusion coefficients for the longitudinal and transverse directions describe the effects of diffusion, dispersion, and time averaging on the suspended sediment (Donnell, 2001). Initial suspended sediment concentrations are either directly specified as a parameter or by employing the results of a previous solution (in a hot start mode). Furthermore, SED2D-WES requires specifications of bottom shear stress and the amount and type of bed material. For non-cohesive beds, it requires grain size, specific gravity, grain shape factor, characteristic length factors for erosion and deposition, fall velocity, and thickness of the sediment bed. Cohesive beds, modeled as a series of layers, require specification for each layer a characteristic thickness, critical shear stress for erosion of a particle and for the layer, erosion rate constant for particle erosion, initial dry density, consolidation coefficient, and age; the critical shear stress for deposition and settling velocity are the same for all layers.

The above discussion indicates that application of SED2D-WES requires specification of a multitude of parameters — critical shear stress for bed particles and layers, bed age, consolidation coefficient, bed geotechnical properties, etc. — unavailable in this study. Calibrating the model to represent prototype conditions is again difficult given the lack of adequate appropriate data including comprehensive, multi-year bathymetric comparison data that includes no effects of mining or subsidence. In light of these limitations, this study used the RMA4 model to simulate the transport of turbidity in

Acadiana Bays. This approach models the advection-diffusion of neutrally buoyant sediment particles introduced into the bays by riverine sources; it does not model sediment exchange between the water column and the bed. Nevertheless, RMA4 provides an excellent tool for evaluating turbidity response to reef alternatives in the Acadiana Bay system.

3.4 Data Sources for Modeling

3.4.1 Bathymetric Data

In 2004, as part of this study, Fugro Chance, Inc. collected bathymetry data in and offshore Acadiana Bays. In addition, Dr. Joe Letter (USACE Coastal Hydraulics Laboratory, Vicksburg, MS) provided the bathymetric data used in the USACE (2002) study. Bathymetric data collected as part of this study supplemented data from USACE (2002) to develop a composite bathymetric data file for the model domain. When merging the two data sets, the new data superseded the USACE data in areas where both new and old (USACE, 2002) data were available. A check of the revised bathymetric file ensured smooth transitions in bathymetry from the new to old data sets.

3.4.2 Wave, Current, Salinity, and Turbidity Data

The Coastal Studies Institute at Louisiana State University (LSU) maintains the Wave-Current-Surge Information System for Coastal Louisiana (WAVCIS). Deployed under this program, two gages lie in the study area. The WAVCIS gage located offshore Point Chevreuil, designated CSI-14, was deployed on February 8, 2004 as part of this study. WAVCIS gage CSI-3 located offshore Marsh Island has been operational since October 20, 2000. These stations record a variety of data including water level, ocean current speed and direction, wind speed and direction, conductivity (to provide salinity), turbidity, and water temperature. Figure 3.1 locates these stations as well as salinity monitoring stations 622 and 623 maintained by the Louisiana Department of Wildlife and Fisheries (LDWF). Data from all these gages helped calibrate the numerical models of this study.

Wave gages WG-66 and WG-68, whose locations are shown in Figure 3.1, recorded wave height and period data in 1981. Data from these gages and those from CSI-6, CSI-5, and CSI-11 (outside the study area) were used in the wave modeling portion of this study.

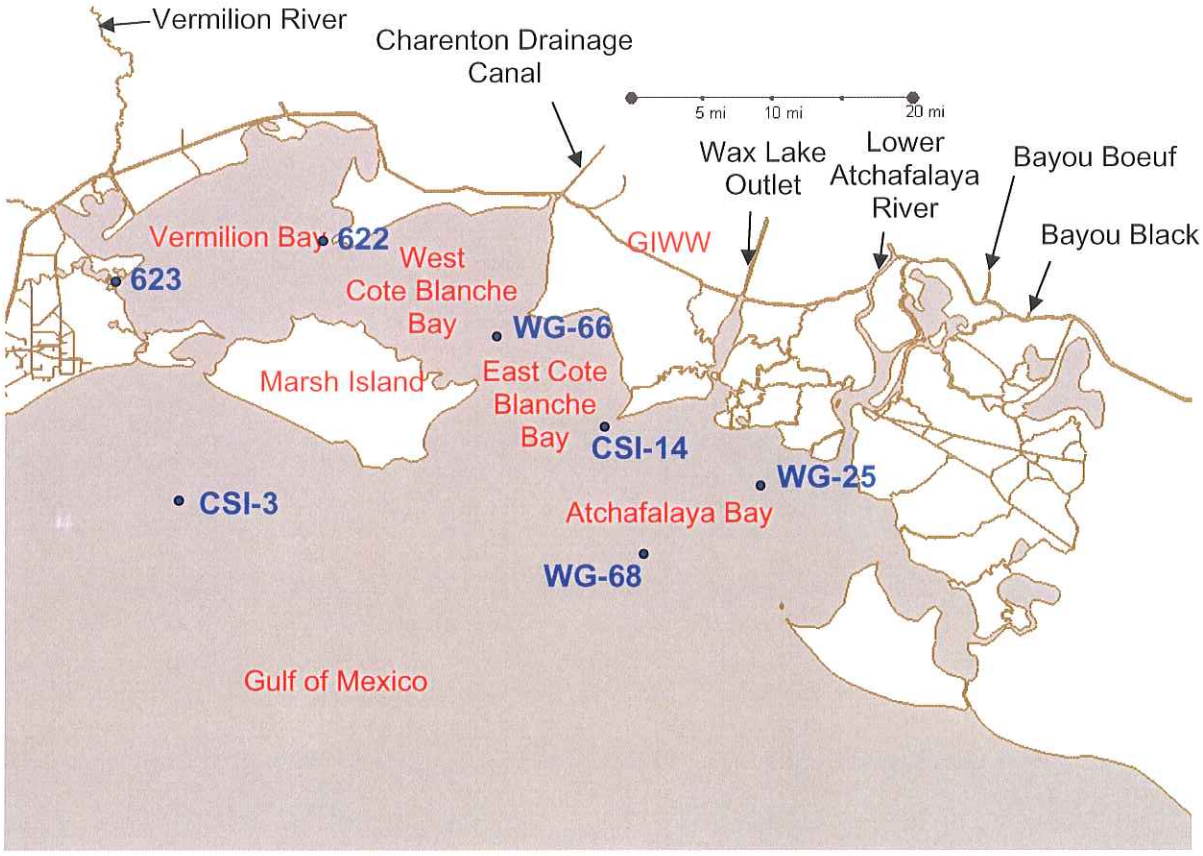

Figure 3.1 Data Sensor Locations

3.4.3 Flow Data

United States Geological Survey (USGS) gages provided daily stream flow data for Wax Lake Outlet at Calumet, Lower Atchafalaya River at Morgan City, Vermilion River at Perry, Charenton Drainage Canal at Baldwin, Bayou Boeuf at Amelia, and Bayou Black near Bay Wallace east of Morgan City.

3.4.4 Wind Data

The WAVCIS stations (CSI-3 and CSI-14) and a USACE station at Cypremort Point in Vermilion Bay (near station 622 in Figure 3.1) provided the local wind data for this study. The CSI-3 and CSI-14 stations provided hourly wind speed and direction boundary data from 2000 through 2004, and the USACE station provided data from 1999 through 2002.

3.5 General Features of Models

3.5.1 Hydrodynamic and Transport Model Mesh

Figure 3.2 shows the RMA2/RMA4 model extent (including the bays of interest) and Figure 3.3 shows the RMA2/RMA4 model mesh for present conditions. The finite-element mesh consists of 10,334 two-dimensional triangular and quadratic elements and 34,370 nodes. The mesh covers a total area of about 10,700 mi^2, with the largest element covering 180 mi^2 and the smallest 1,500 ft^2. Note the high mesh resolution along several alignments extending from Point Chevreuil. This resolution allows for inserting alternative artificial reef structures into the model without changing the mesh resolution. This eliminates the introduction of possible effects due solely to mesh resolution changes required to accommodate the structures.

Manning's roughness (Manning's n) for the model ranged from 0.015 to 0.035, with reef locations assigned a value of 0.05. Modifications to the mesh accounted for land areas for storm inundation and historical tributaries.

3.5.2 Hydrodynamic Model General Boundary Conditions

The USACE maintains a tidal stage database (EC2001) of the Gulf of Mexico determined with the Advanced Circulation (ADCIRC) model for shelves, coasts, and estuaries. This database provides a time series of water surface elevations based on astronomical tide for any location in the ADCIRC domain. The hydrodynamic model applies the tidal stage conditions developed from the database along the boundary indicated in Figure 3.4. Because of the large extent of the mesh (nearly 200 mi, Figure 3.2), the model applies unique tidal stages at the 57 individual mesh boundary points to reproduce tidal phase variations over the mesh and simulate the corresponding offshore circulation.

Figure 3 .4 also indicates the stream flow boundaries for Wax Lake Outlet at Calumet, the Lower Atchafalaya River at Morgan City, the Vermilion River at Perry, the Charenton Drainage Canal at Baldwin, Bayou Boeuf at Amelia, and Bayou Black near Bay Wallace east of Morgan City.

3.5.3 Wave Model Mesh

To examine the required wave characteristics, the wave model applies multiple meshes with several orientations. The basic wave model mesh consists of about 2,000 cross-shore and 1,500 longshore elements with the mesh covering about 1,300 mi^2. Chapter 5 contains the details for each wave model mesh.

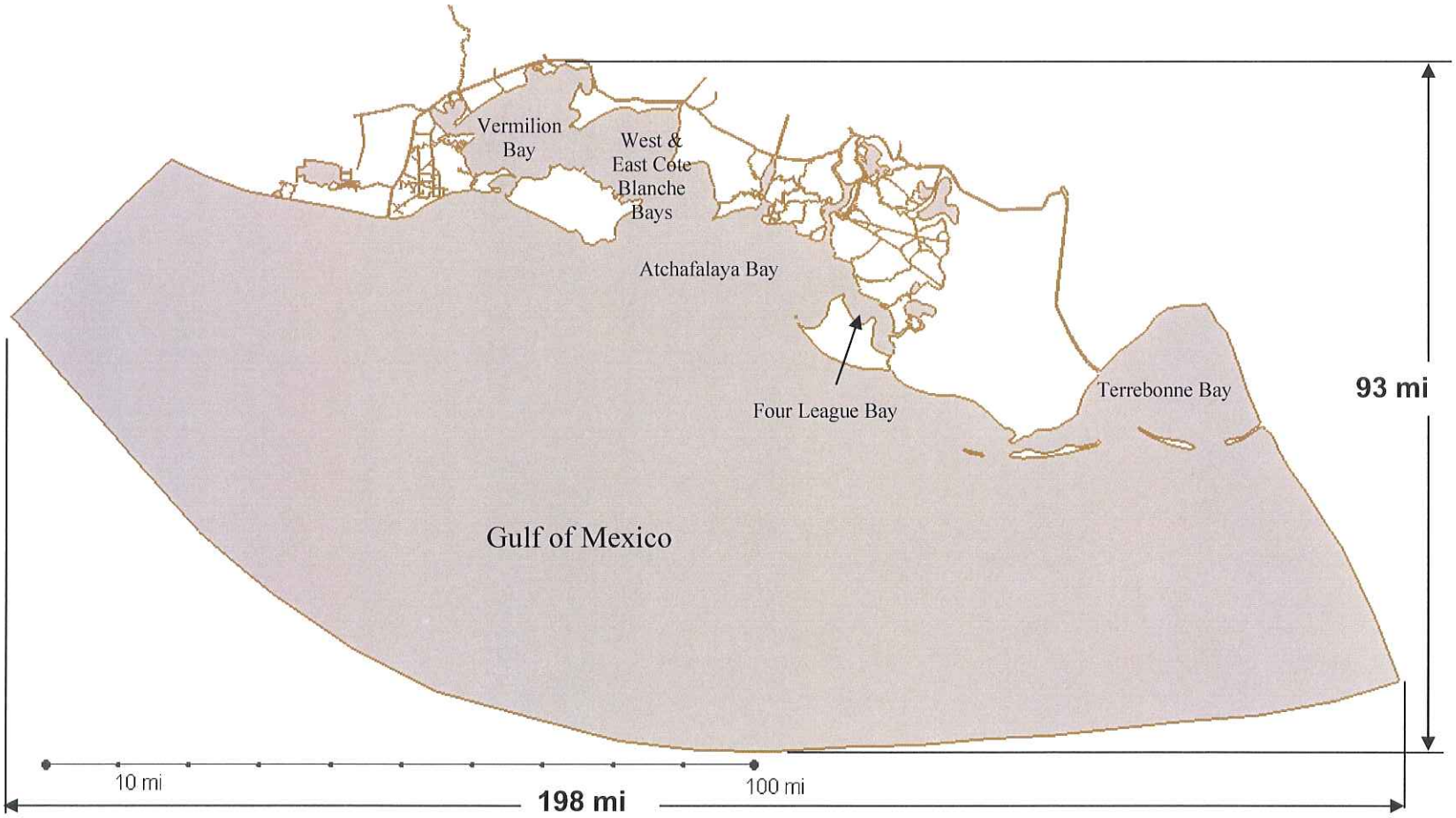

Figure 3.2 Model Extents

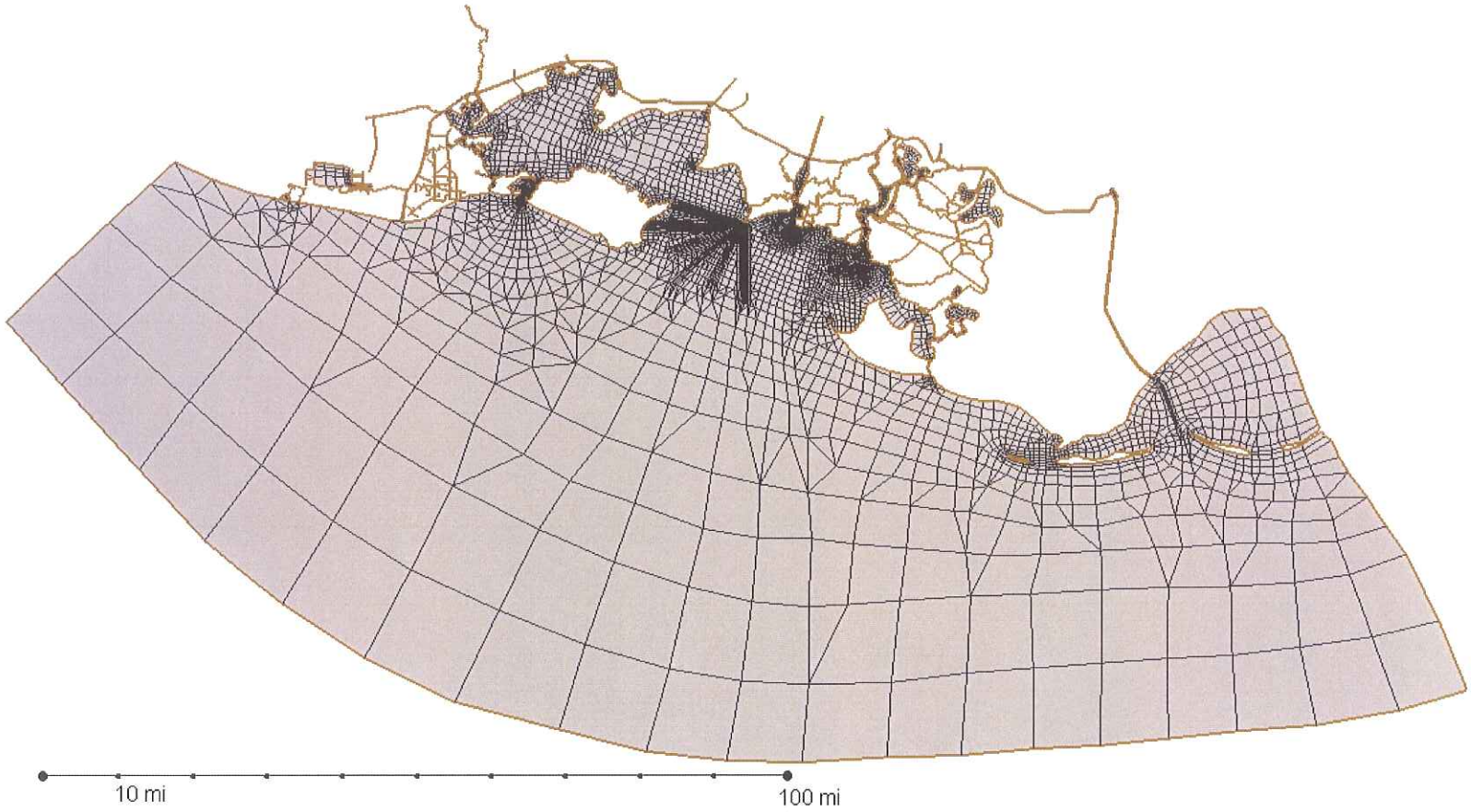

Figure 3.3 Model Mesh

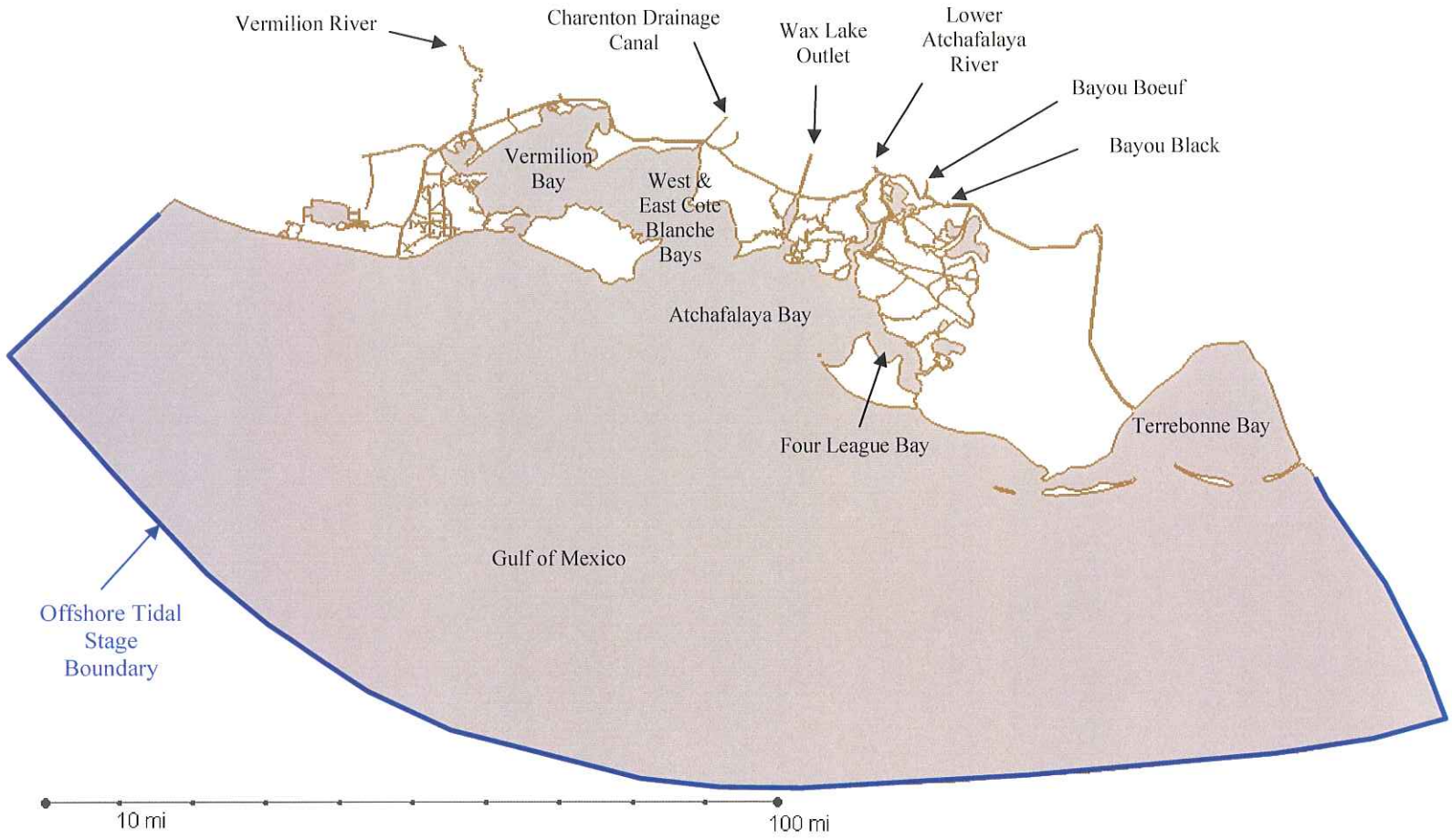

Figure 3.4 Locations of Imposed Boundary Conditions

4.0 HYDRODYNAMIC AND TRANSPORT MODEL CALIBRATIONS

This chapter describes the calibration procedures, boundary conditions, and results for the hydrodynamic model and the salinity and turbidity transport models. In each case, the calibration shows the ability of the model to reproduce measured data.

4.1 Boundary Conditions

4.1.1 Hydrodynamic Model Boundary Conditions

Model calibration covered the 30-day period from 24 May 2004 to 23 June 2004. Model boundary conditions consisted of tidal stage applied on the offshore boundary, stream flow (both constant and time varying) applied along the northern inflow points indicated in Figure 3.4, and variable wind speed and direction applied over the entire mesh. Figure 4.1 shows a representative plot of the tidal stage boundary condition developed from the ADCIRC database covering the calibration period.

The USGS station daily stream flow record provided time varying boundary conditions at Wax Lake Outlet at Calumet and Lower Atchafalaya River. Figure 4.2 presents this variable stream flow data for the calibration period.

The USGS daily stream flow database for the Vermilion River, Charenton Drainage Canal, Bayou Boeuf, and Bayou Black contained either incomplete data or no data for these stations in 2004. An analysis of the available data at these stations yielded the long-term average stream flow in Table 4.1. Combined, the stream flows at these locations contribute less than 3% of the Wax Lake Outlet and Lower Atchafalaya River stream flows. Therefore, the model applied a constant, long-term average stream flow input at the Vermilion River, Charenton Drainage Canal, Bayou Boeuf, and Bayou Black boundaries (Table 4.1).

Table 4.1 Constant Stream Flow Boundary Conditions

Stream Flow Location	Stream Flow (m^3/s)	Stream Flow (cfs)
Vermilion River	38	1,342
Charenton Drainage Canal	50	1,766
Bayou Boeuf	60	2,119
Bayou Black	28	989

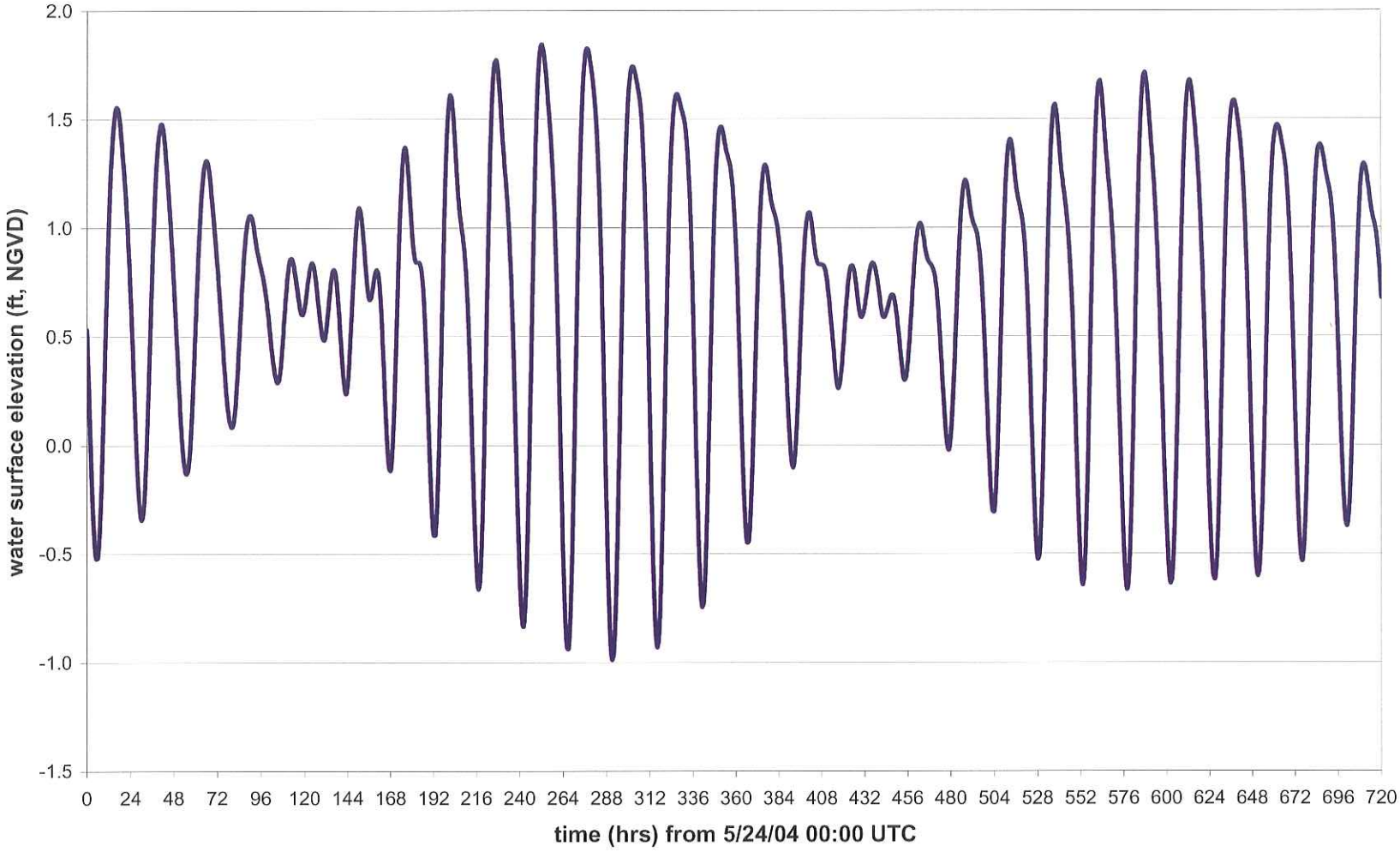

Figure 4.1 Representative Tidal Stage Boundary Condition for the Calibration Period

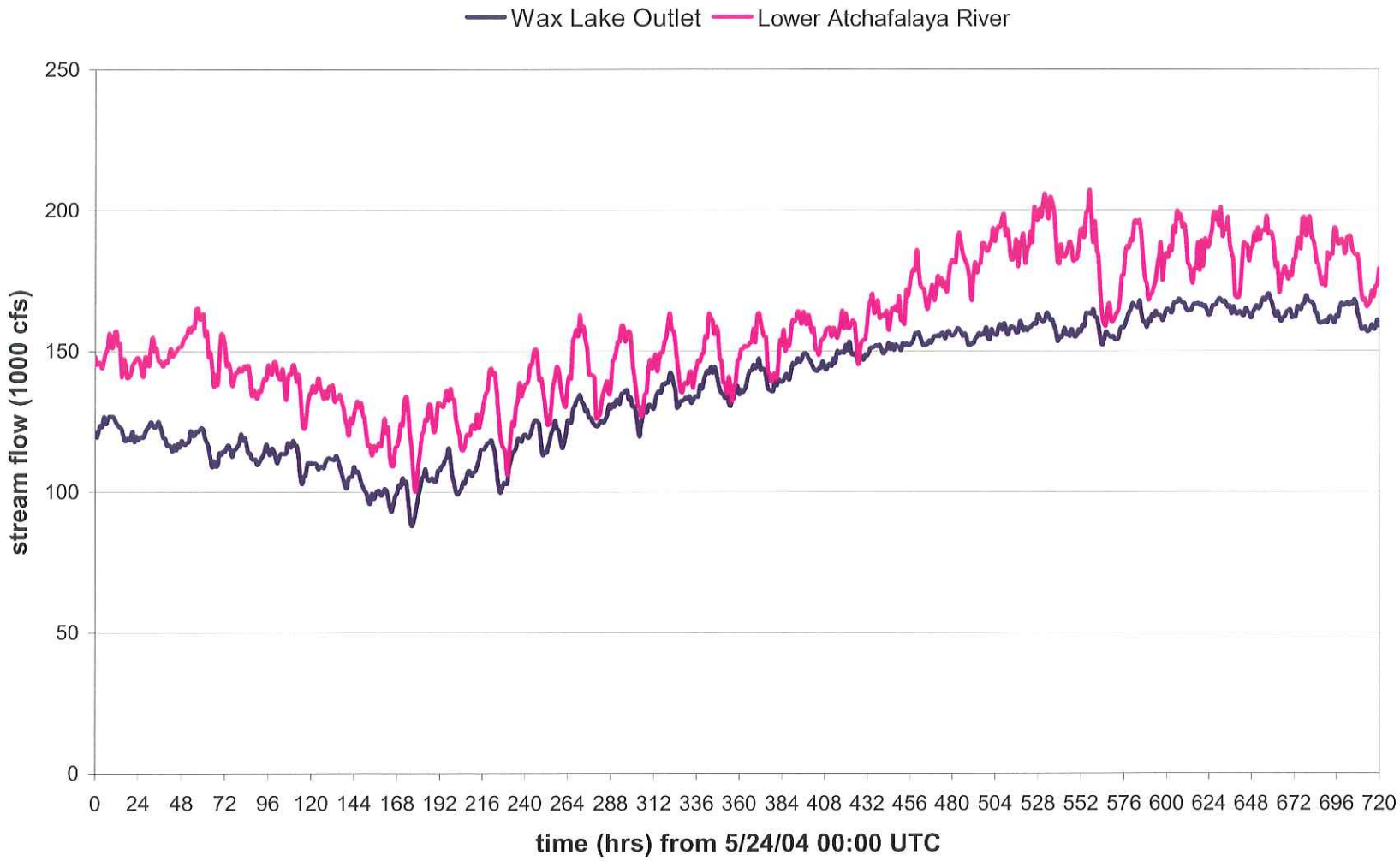

Figure 4.2 Stream Flow at Wax Lake Outlet and Lower Atchafalaya River for the Calibration Period

WAVCIS gages CSI-3 and CSI-14 (Figure 4.3) provided surface boundary condition wind data. While CSI-3 and CSI-14 recorded similar wind speeds, large fluctuations in wind direction recorded at CSI-14 but not at CSI-3 rendered the CSI-14 directional data suspect. Therefore, the model boundary conditions consisted of the CSI-3 wind direction applied over the entire mesh, the CSI-3 wind speed applied over the nearshore and offshore mesh, and the CSI-14 wind speed applied to the mesh near CSI-14. Figure 4.4 shows the wind speed boundary conditions, and Figure 4.5 shows the wind direction boundary condition (with wind direction indicating the origin of the wind).

WAVCIS stations CSI-3 and CSI-14 also provided the measured stage and current data for comparison with hydrodynamic model predictions.

4.1.2 Transport Model Initial and Boundary Condition

The WAVCIS stations provided both salinity and turbidity information, while the LDWF stations provided only salinity information for the model. Examination of the salinity data showed salinity values of about 8 ppt just offshore of Marsh Island (CSI-3), 0.3 ppt between Atchafalaya and East Cote Blanche Bays (CSI-14), 0.8 ppt on the eastern side of Vermilion Bay, and 1.8 ppt on the western side of Vermilion Bay at the beginning of the calibration period. This data agreed with Day et al. (1998) which reported salinities of about 1 – 2 ppt in Vermilion and East and West Cote Blanche Bays and 5 ppt nearshore off Point Au Fer during spring 1997.

Day et al. (1998) and TAMU (1996) indicated a Gulf of Mexico salinity of 30 ppt for the spring – summer period (the calibration period). To expedite the solution, the initial model conditions transitioned the Gulf of Mexico salinity from 30 ppt at the boundary to 8 ppt at CSI-3. Salinity at all stream flow input points remained 0 ppt throughout the simulation.

In addition to providing data for the model initial conditions, the WAVCIS and LDWF stations provided the measured salinity data for comparison with the modeled results in the salinity transport model calibration. Special point S1 served as a special monitoring point for the salinity model. Comparison of models salinity predictions at S1 to measurements at CSI-3 provided insights into the effects of flow stratification.

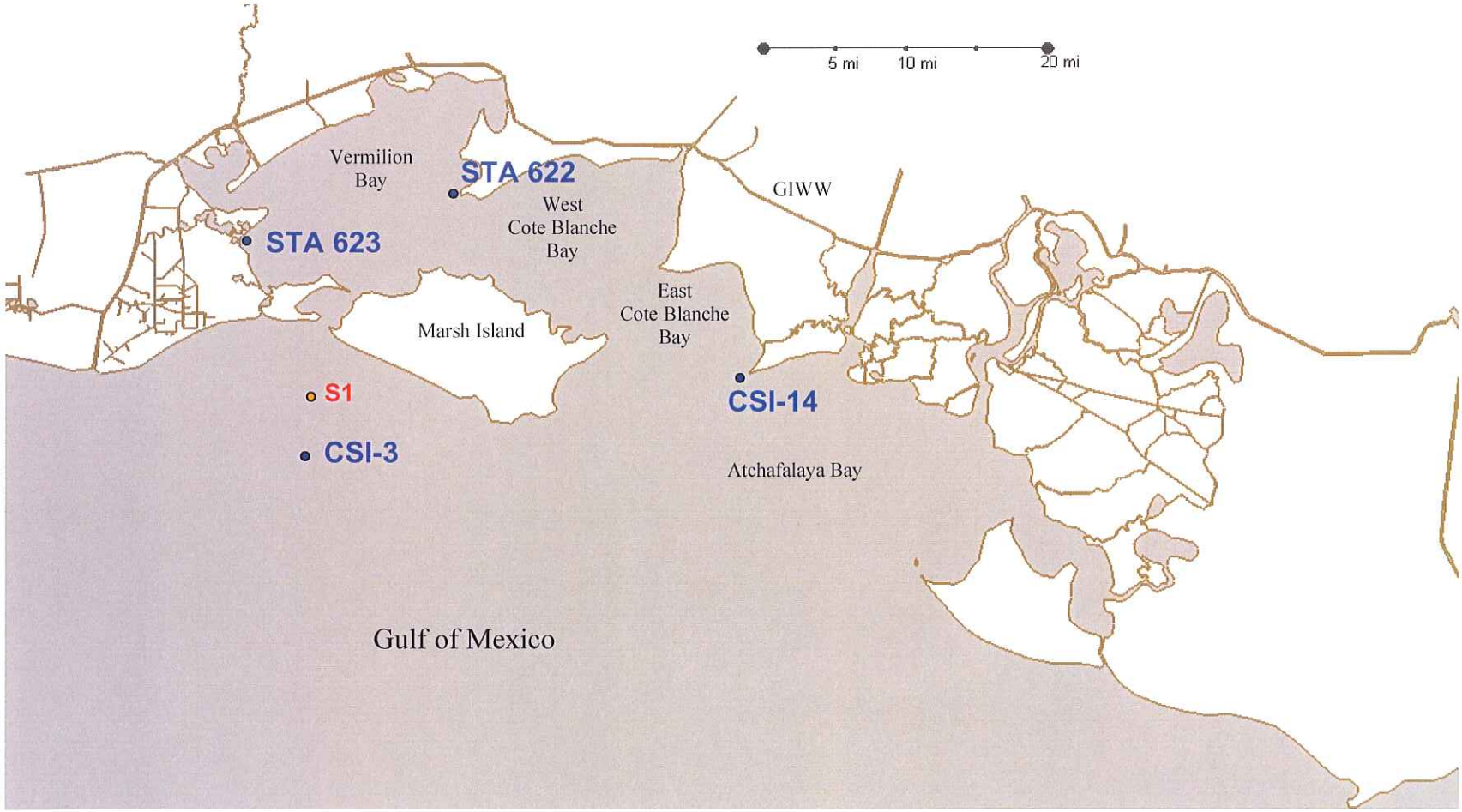

Figure 4.3 Data Collection and Model Calibration Points

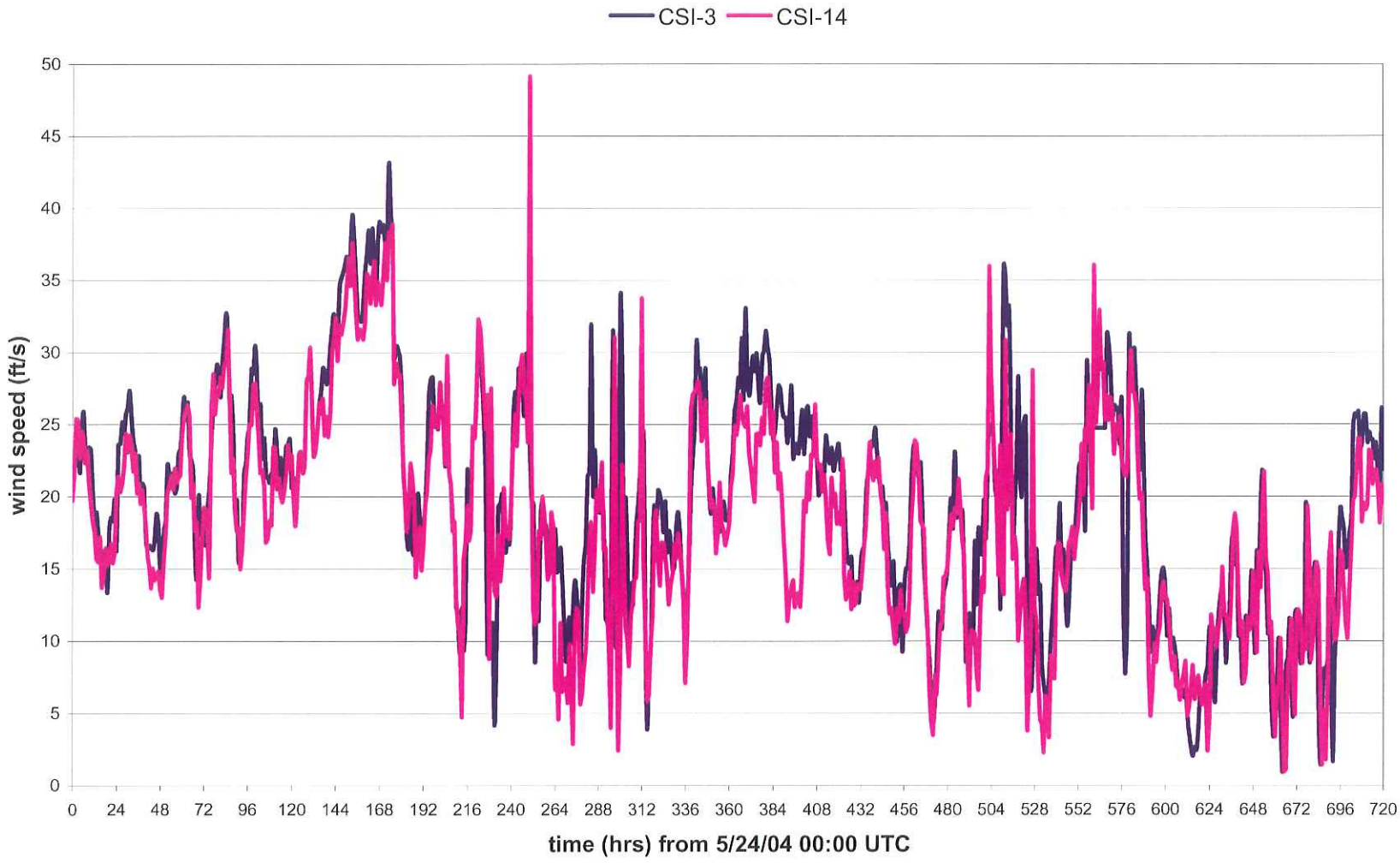

Figure 4.4 Wind Speed Boundary Conditions for the Calibration Period

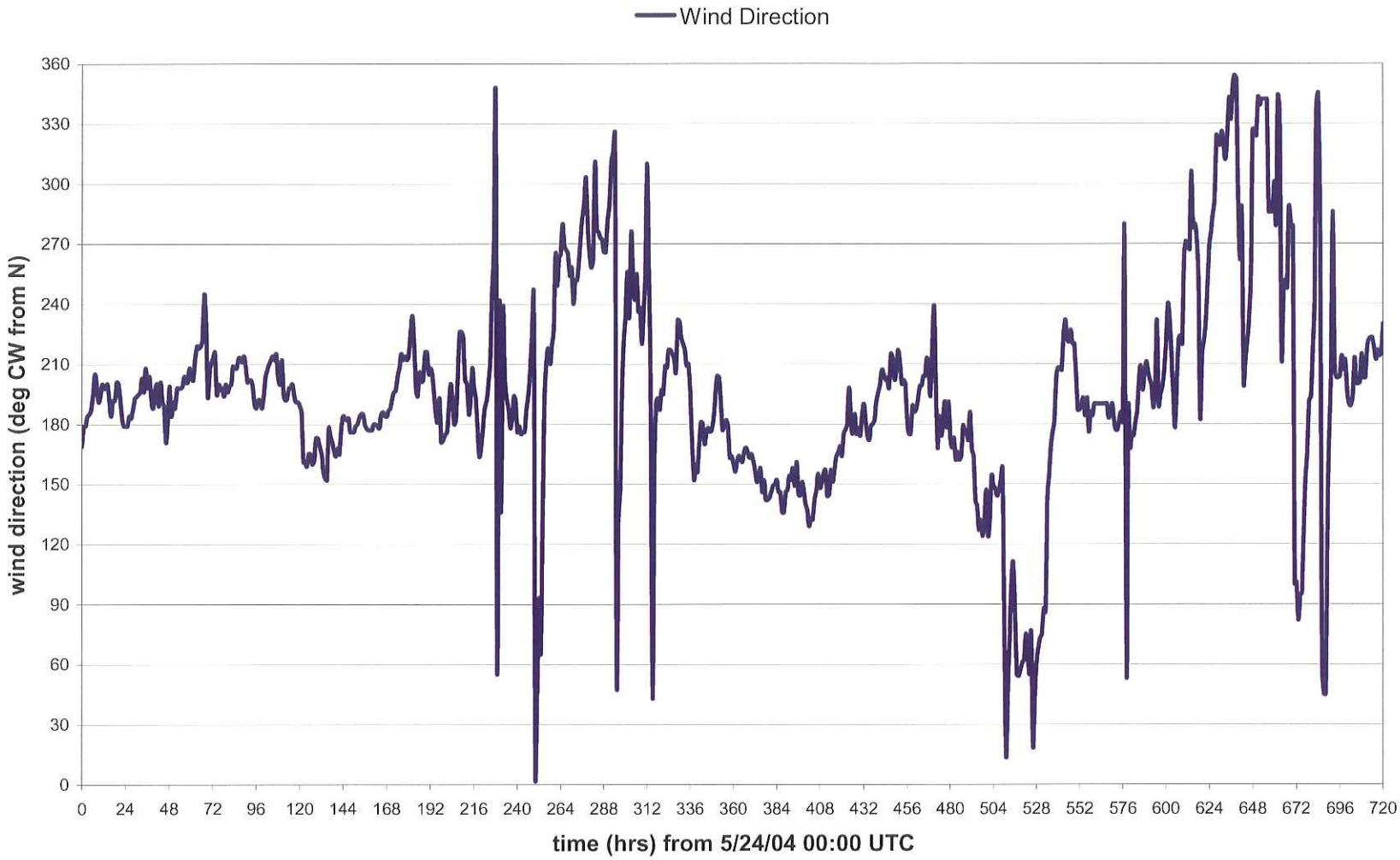

Figure 4.5 Wind Direction (Wind Origin) Boundary Condition for the Calibration Period

Myint and Walker (2002) and Walker et al. (2002a) indicated that suspended sediment concentrations during March – April 1996 ranged from 25 – 150 mg/l in Atchafalaya Bay, 50 – 150 mg/l near the Wax Lake Outlet and Lower Atchafalaya deltas, 70 – 150 mg/l in East and West Cote Blanche Bays, and 10 – 150 mg/l in Vermilion Bay. Walker et al. (2002a) and USACE (2002) reported suspended sediment levels of 40 – 640 mg/l at Morgan City (Lower Atchafalaya) and 60 –500 mg/l at Calumet (Wax Lake Outlet). USACE (2002) modeled sediment loads of 10 mg/l at the other stream flow boundaries.

Measured turbidity levels at the beginning of the calibration period reached roughly 100 mg/l just offshore Marsh Island (CSI-3) and 125 mg/l between Atchafalaya and East Cote Blanche Bays (CSI-14). Because these levels correspond to the middle to upper end of the ranges (Myint and Walker, 2002; Walker et al., 2002a; and USACE, 2002), the turbidity transport model applied initial turbidity concentrations at the middle to upper end of the range. These concentrations included 100 mg/l in the nearshore (near CSI-3), 125 mg/l in Atchafalaya and the southern portion of East Cote Blanche Bay (CSI-14), and 100 mg/l in Vermilion and West Cote Blanche Bays. Satellite imagery in Walker and Hammack (2000), Huh et al. (2001), Walker (2001), Myint and Walker (2002), Walker et al. (2002a), and Walker et al. (2002) indicated turbidities below 10 mg/l seaward of CSI-3; therefore, the turbidity was set to zero seaward of CSI-3.

In addition, analysis of biweekly USGS sediment load data at Lower Atchafalaya at Morgan City and Wax Lake Outlet at Calumet (1998 – 2002) showed that stream flows carried a sediment load roughly equal to 0.2% of their volume flow rate. The model applied this relationship at the Lower Atchafalaya and Wax Lake stream flow input points to obtain a time-varying turbidity input boundary condition dependent on the stream flow. Concentrations found in Myint and Walker (2002) and Walker et al. (2002) do not support the USACE (2002) level of 10 mg/l at the other stream flow boundaries — applying this low level to the model would dilute turbidities in the bays. The model applied a more representative sediment concentration of 80 mg/l to all other stream flow input points. At this level, the influence of the stream flow boundaries should remain neutral (neither diluting nor excessively increasing the turbidities in the bays).

CSI-3 and CSI-14 provided the measured turbidity data for comparison with the modeled results in the turbidity transport model.

4.2 Calibration Procedure

The hydrodynamic model calibration followed an iterative procedure. After adjusting the mesh to obtain a stable model with a manageable run time, iterative adjustments to the bed roughness at various

points within the mesh and wind stress parameters developed a reasonable match between the modeled tidal stage and currents and the measured data at stations CSI-3 and CSI-14. Similarly, adjusting the transport model diffusion coefficients developed a reasonable agreement between the modeled salinities and measured values at CSI-3, CSI-14, as well as the LDWF stations (stations 622 and 623). Finally, the turbidity model calibration considered turbidity levels at CSI-3 and CSI-14 and used the diffusion coefficients determined in the salinity calibration.

4.3 Hydrodynamic Model Calibration Results

4.3.1 Tidal Stage Calibration

Figures 4.6 and 4.7 and Tables 4.2 and 4.3 give the tidal stage calibration results at CSI-3 and CSI-14. Equation 4.1 defines the Root Mean Square (RMS) value for each time series.

$$RMS = \sqrt{\frac{\sum_{i=1}^{N} x_i^2}{N}} \tag{4.1}$$

where x_i = the data value at time increment i and N = the total number of values or time increments.

Equation 4.2 defines the RMS error (RMSΔ).

$$RMS\Delta = \sqrt{\frac{\sum_{i=1}^{N} \left(modeled_i - measured_i\right)^2}{N}} \tag{4.2}$$

where $modeled_i$ = the modeled value and $measured_i$ = the measured value. As RMSΔ approaches zero, the differences between the measured data and model predictions diminish.

With the RMSΔ within 30% of the RMS values and the modeled tide range within 20% of the measured value at both CSI-3 and CSI-14, the model predictions of tidal stage demonstrated reasonable agreement with measurements.

Table 4.2 CSI-3 Tidal Stage Calibration Results

	Measured	**Model**
Mean High Water (MHW, ft NGVD)	1.7	1.6
Mean Low Water (MLW, ft NGVD)	-0.7	-0.3
Range (MHW – MLW, ft)	2.4	1.9
Mean Tide Level (MTL, ft NGVD)	0.6	0.8
Root Mean Square (RMS, ft NGVD)	1.1	1.1
RMSΔ (ft NGVD)		0.3

Table 4.3 CSI-14 Tidal Stage Calibration Results

	Measured	**Model**
Mean High Water (MHW, ft NGVD)	1.9	1.7
Mean Low Water (MLW, ft NGVD)	-0.2	-0.1
Range (MHW – MLW, ft)	2.1	1.8
Mean Tide Level (MTL, ft NGVD)	1.0	0.9
Root Mean Square (RMS, ft NGVD)	1.3	1.2
RMSΔ (ft NGVD)		0.4

4.3.2 Current Calibration

CSI-14 provided the only current data in the study area. Figure 4.8 and Table 4.4 give the current speed calibration results, and Figure 4.9 gives the current direction calibration results at CSI-14. Again, Equation 4.2 defines RMSΔ.

The model smoothed some of the measured data peaks (Figure 4.8). However, the modeled maximum, minimum, and average current speeds remained within 10 – 20% of the measured data. The inherent difficulties in measuring currents for comparison to model simulations makes exact agreement nearly impossible. In fact, the measured data give the current at a specific point within the water column (about half the depth) while the model produces a depth-averaged current. For logarithmic vertical current profiles, any current measurement in the upper two-thirds of the water column generally exceeds the depth-averaged current. Therefore, the modeled current shows reasonable agreement with the measured data.

Table 4.4 CSI-14 Current Speed Calibration Results

	Measured (fps)	**Model (fps)**
Maximum Flood Current	1.3	1.3
Minimum Ebb Current	0.0	0.1
Average Current	0.7	0.6
RMSΔ		0.2

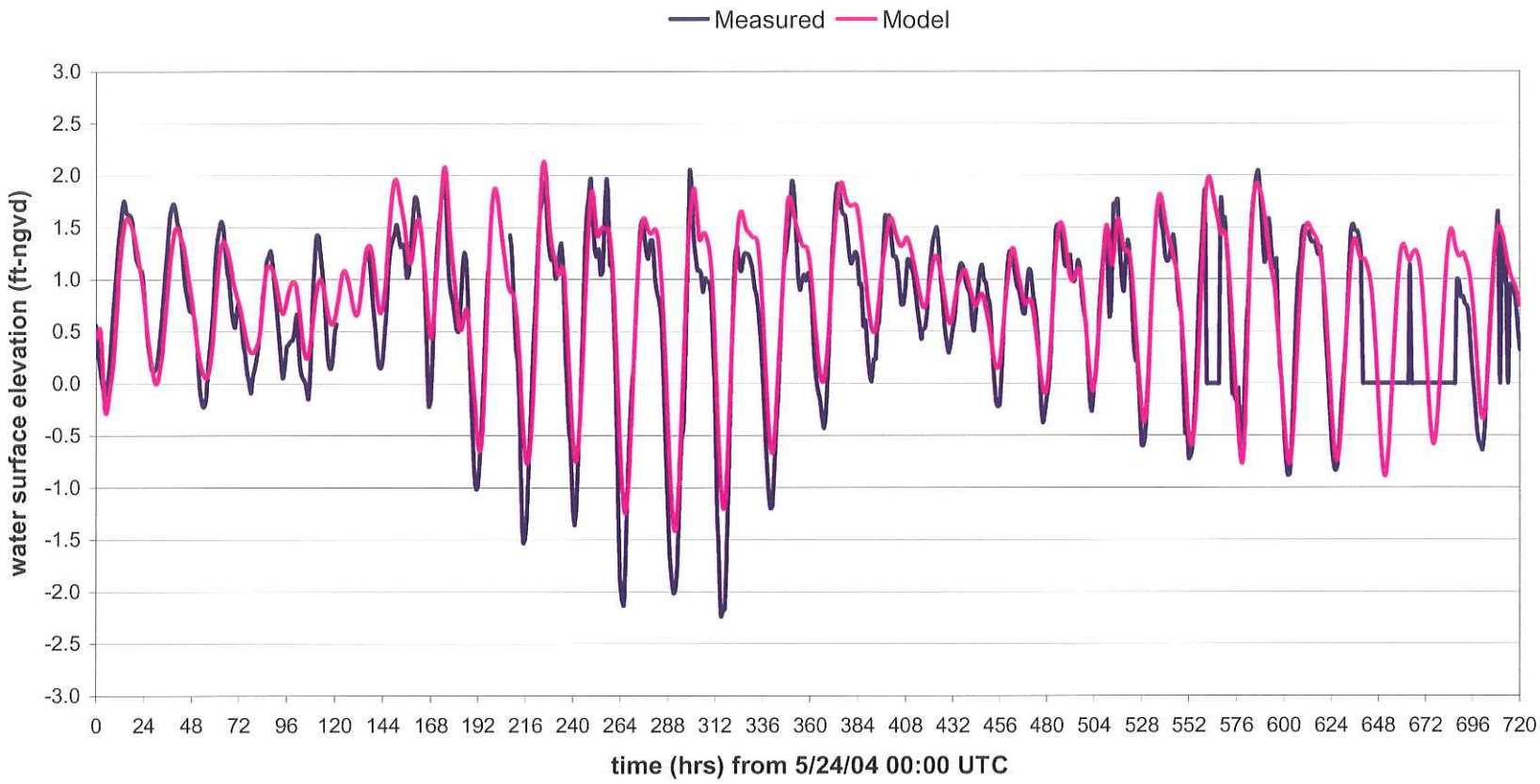

Figure 4.6 CSI-3 Tidal Stage Calibration Results

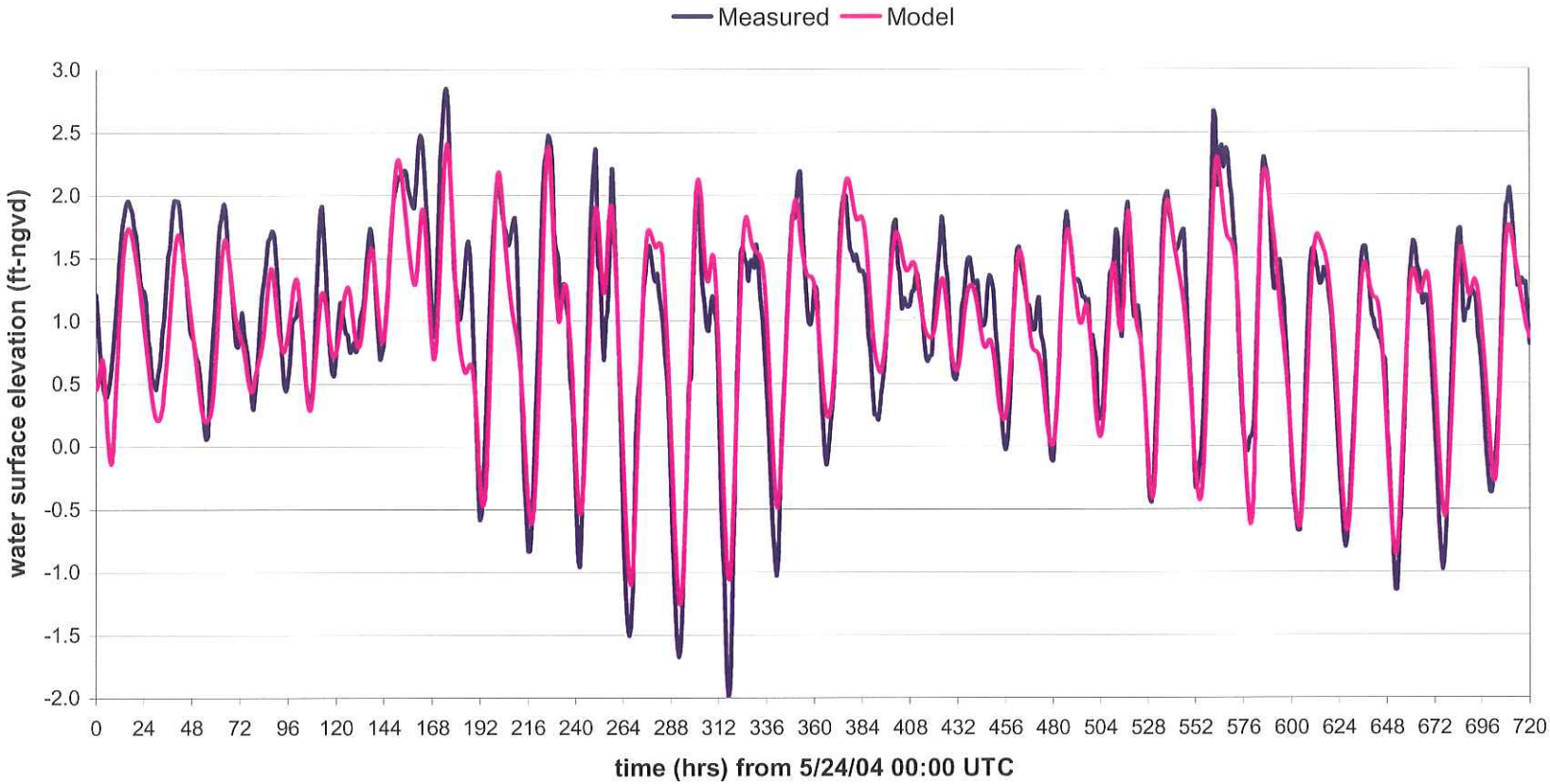

Figure 4.7 CSI-14 Tidal Stage Calibration Results

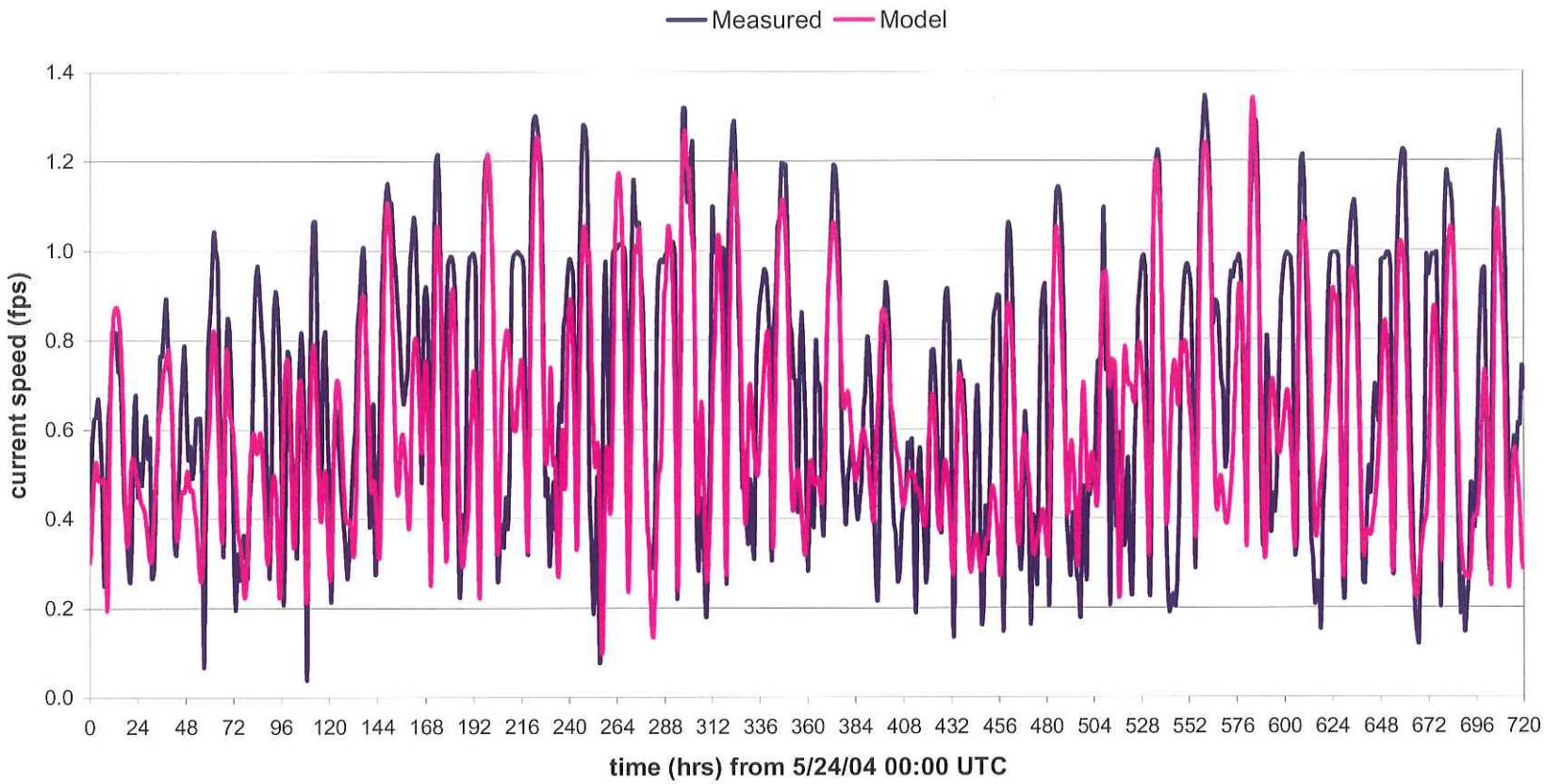

Figure 4.8 CSI-14 Current Speed Calibration Results

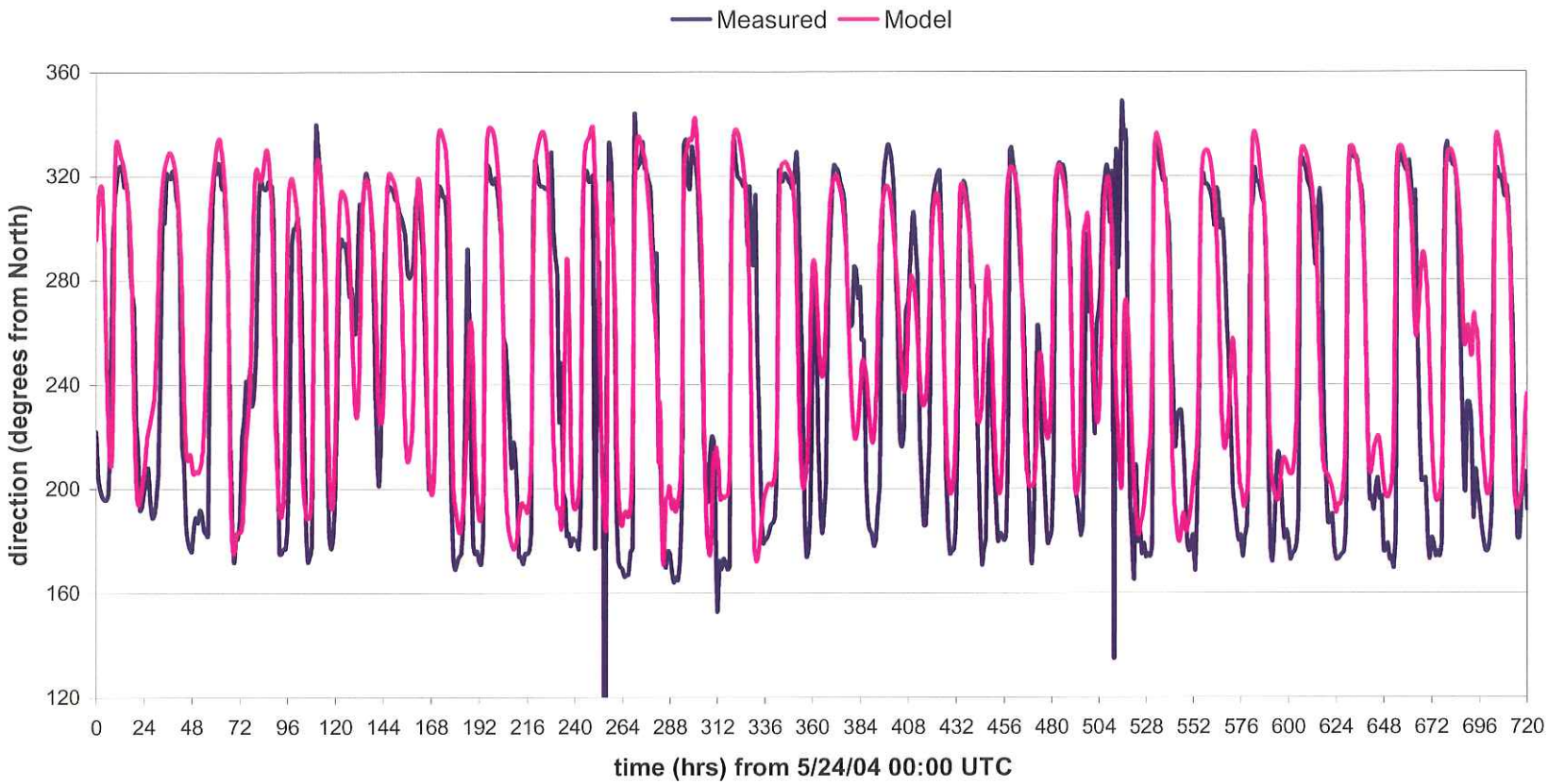

Figure 4.9 CSI-14 Current Direction Calibration Results

4.3.3 *Terrebonne Bay Stream Flow*

Other than data (described previously) used to drive upstream inflow boundaries, minimal information was available to provide estimates of flows within the waterways for comparison to model results. However, one source provided a localized comparison. The U.S. Environmental Protection Agency (EPA) in the 2002 Bayou Lafourche Restoration Feasibility Study (EPA, 2002) estimated that Terrebonne Bay, on the eastern extreme of the model (Figure 3.3), typically experiences about 1,700 cfs total inflow from the GIWW, Bayou Lafourche, and Company Canal. The calibrated model simulates a mean stream flow into Terrebonne Bay of 2,000 cfs. Therefore, the model agrees reasonably well with the EPA estimate particularly given the approximation of both estimates.

4.3.4 *Possible Reasons for Inconsistencies between Model Predictions and Gage Measurements*

Although the model simulates stage and current reasonably well, model results and corresponding measurements do not match perfectly. The paragraphs below discuss possible reasons for discrepancies between model results and measurements.

Lack of Measured Tidal Forcing at the Offshore Boundary — Ideally, when calibrating a hydrodynamics model, one applies *measured* tidal stage values at the model's offshore boundary and compares model predictions of stage and current with measured values in the model's interior. Unfortunately, the scope of this study precluded the collection of measured offshore stage data. Elaborating, the model required a relatively large model domain to separate the offshore boundaries from the zone of influence of the Wax Lake Outlet and Lower Atchafalaya River discharge plumes, key determinants of the salinity and turbidity regimes in the Acadiana Bays.

Given this requirement and the large east-west dimension of the Acadiana Bays system, the offshore boundary must extend, at a minimum, in excess of 150 mi. This length of the model's offshore edge would require several deepwater offshore gages to collect tidal stage measurements capturing the tidal stage phase difference across the long boundary. The limited resources available for this project precluded the deployment of these gages. Also, given the lack of offshore gage data for salinity, moving the offshore boundary farther offshore (away from the influence of freshwater discharges) allowed the specification of ambient salinities of the Gulf of Mexico at the offshore boundary.

In lieu of measured tidal stages at the offshore boundary, a global ADCIRC model (EC2001) established the offshore tidal boundary conditions. As a result, the offshore boundary condition used in

the present application contained only the effects of astronomical forcing; it contained no effects of short-term meteorological forcing. One expects this limitation to cause most of the deviations between measured and predicted tidal stages and currents at the calibration locations. However, this limitation does not negatively affect the purpose of this study. Note that the model captured the influences of local meteorological forcing — that is, those within the model domain — since the model applied the measured wind as a surface boundary condition.

Lack of High-Density Bathymetric Data — USACE (2002) supplied bathymetric data for significant portions of the model domain; the dates and quality of that data remain somewhat uncertain. A sensitivity analysis investigated the effects of potential errors in bathymetry over large portions of the model domain (see Section 4.6). The analysis demonstrated that varying the model depth 2 – 3 ft can increase tidal range and current speeds as much as 10%. Thus, more accurate bathymetry could have improved the calibration comparisons with measured data. Furthermore, patching together data from different dates and differing quality may cause some of the observed differences in tidal currents and tidal stages. Fortunately, the model depth sensitivity analysis showed that salinity was somewhat insensitive to errors in model depth; therefore, study objectives were not compromised by small depth errors.

Lack of High-Density Wind Data — Ideally, for the surface boundary condition of the model, given the size of the domain one prefers several gages providing measured wind speed and direction data at multiple locations scattered throughout the model domain. In contrast, resource constraints and data quality limited the wind speed data to two locations and wind direction data to one location. One expects this limitation to have some effect on the accuracy of comparisons to measurements.

High costs prohibited the installation of tide, current, salinity, turbidity, and meteorological gages to thoroughly cover such a large study area. Notwithstanding the above limitations, the available data did demonstrate the suitability of the model to represent the study area conditions and to accomplish the goals of the study. The hydrodynamic model predictions represented measurements well enough to deem the hydrodynamic model adequately calibrated.

4.4 Salinity Model Calibration Results

4.4.1 Salinity Model Results

Figures 4.10 – 4.13 and Tables 4.5 – 4.8 give the salinity model calibration results at CSI-3, CSI-14, STA-622, and STA-623 (see Figure 4.3 for the locations). In the tables, mean high salinity refers to the average of all salinity peaks in the time series (Figures 4.10 – 4.13) and mean low salinity refers to the

average of all salinity troughs. The model predictions at CSI-14, STA-622, and STA-623 (Figures 4.11 – 4.13) show reasonable agreement with measured data at Point Chevreuil and in Vermilion Bay. In contrast, the model predictions do not appear to agree well with measurements at CSI-3. Nearshore flow stratification (discussed in the next section), a process not represented in the vertically-averaged two-dimensional model, may have caused this discrepancy.

Table 4.5 CSI-3 Salinity Calibration Results

	Measured	**Modeled**
Mean High Salinity (ppt)	9.8	13.6
Mean Low Salinity (ppt)	7.6	11.2
Salinity Range (ppt)	2.2	2.4
Mean Salinity (ppt)	7.9	12.7
RMS (ppt)	10.7	13.1
RMSΔ (ppt)		6.9

Table 4.6 CSI-14 Salinity Calibration Results

	Measured	**Modeled**
Mean High Salinity (ppt)	0.2	0.1
Mean Low Salinity (ppt)	0.2	0.1
Salinity Range (ppt)	0.0	0.0
Mean Salinity (ppt)	0.1	0.1
RMS (ppt)	0.1	0.2
RMSΔ (ppt)		0.1

Table 4.7 STA-622 Salinity Calibration Results

	Measured	**Model**
Mean High Salinity (ppt)	0.8	0.6
Mean Low Salinity (ppt)	0.7	0.5
Salinity Range (ppt)	0.1	0.2
Mean Salinity (ppt)	0.8	0.6
RMS (ppt)	0.8	0.6
RMSΔ (ppt)		0.3

Table 4.8 STA-623 Salinity Calibration Results

	Measured	**Model**
Mean High Salinity (ppt)	1.8	1.7
Mean Low Salinity (ppt)	1.6	1.7
Salinity Range (ppt)	0.2	0.0
Mean Salinity (ppt)	1.7	1.7
RMS (ppt)	1.7	1.7
RMSΔ (ppt)		0.2

4.4.2 Discussion of Salinity Model Results at CSI-3

The measured data from CSI-3 shows a marked period of low salinity followed by a period of high salinity. Given the CSI-3 conductivity/salinity sensor's location at mid-depth, a saline layer (or salt wedge with the heavier saline layer lying below the freshwater) with a saltwater/freshwater interface oscillating around the sensor — alternately covering and uncovering it — could account for the low and high salinity pattern.

The depth-averaged transport model, representing a vertically well-mixed system, cannot accurately describe point measurements made by a sensor in stratified flows. In general, for stratified two-layer (freshwater-saltwater) flows where a sharp halocline separates individually well-mixed layers, the depth-averaged salinity concentration exceeds the point measurement recorded by a sensor in the freshwater layer. In contrast, the depth-averaged salinity concentration falls below the point measurement recorded by a sensor in the saltwater layer. Consequently, the depth-averaged model is expected to predict higher salinity than that recorded by a sensor in the freshwater layer and lower salinity than that recorded

by a sensor in the saltwater layer. Along these lines of reasoning, when the tidal range decreases toward neap tide (less tidal energy), one expects freshwater exiting Southwest Pass to force the saline layer deeper in the water column; consequently, the mid-depth sensor (now located in the freshwater layer) registers low salinity. Conversely, when the tidal range increases toward spring tide, the saline layer should rise toward the surface, and the sensor will register high salinity. Figures 4.14 suggests that such a condition exists during the calibration period.

A model correctly calibrated for depth-averaged values should agree better with the salinity of the water closer to Southwest Pass where high velocities tend to mix the water vertically. To illustrate this improved agreement, Figure 4.15 shows the model response at point S1 (Figure 4.3) compared to the measured data at CSI-3. The good agreement between the modeled and measured salinity up to 288 hrs and after about 400 hours supports the above hypothesis. Given these findings, the salinity model appears to represent depth-averaged concentrations reasonably well. Notably, stratification calibration problems did not occur within the bay system, the area of interest.

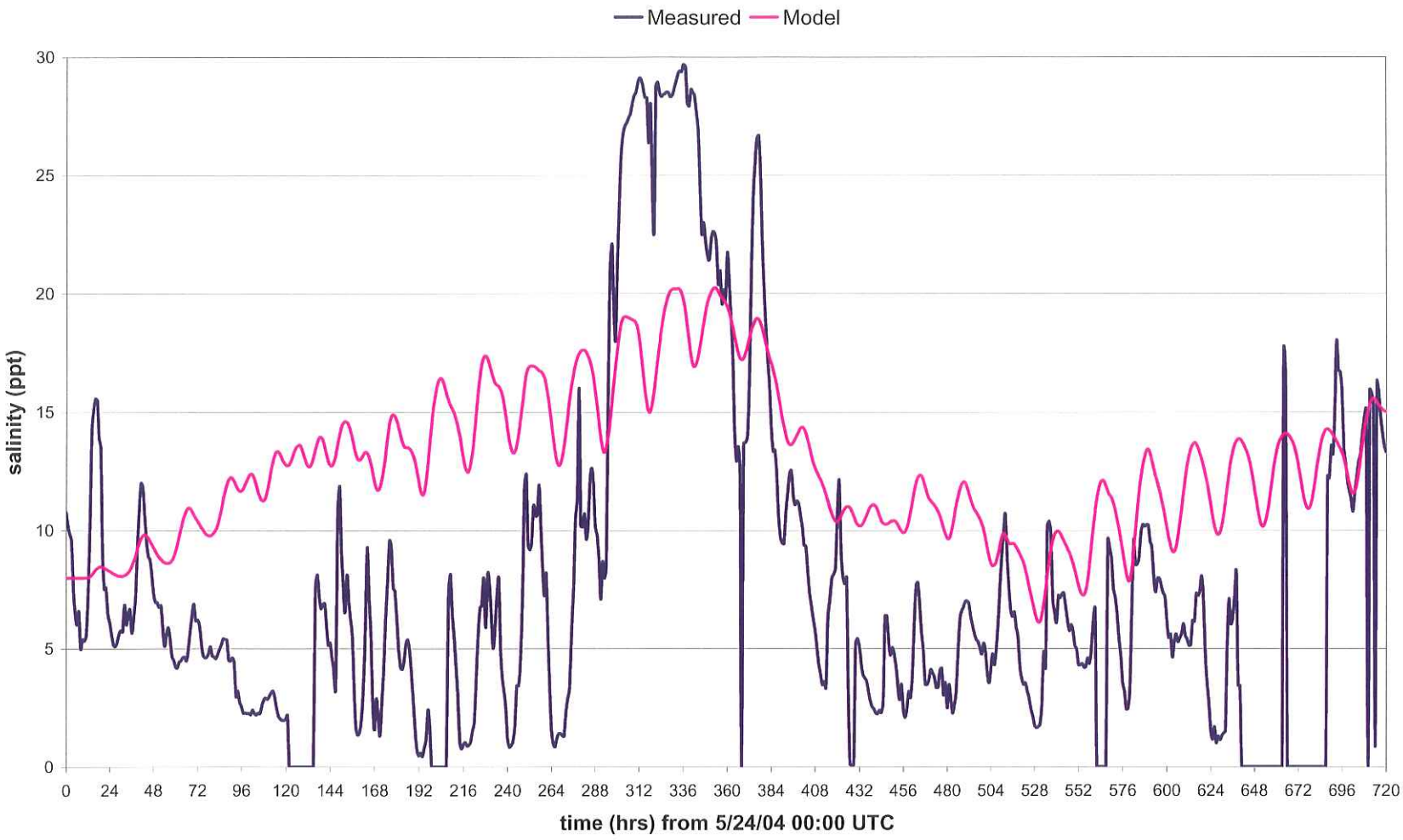

Figure 4.10 CSI-3 Salinity Calibration Results

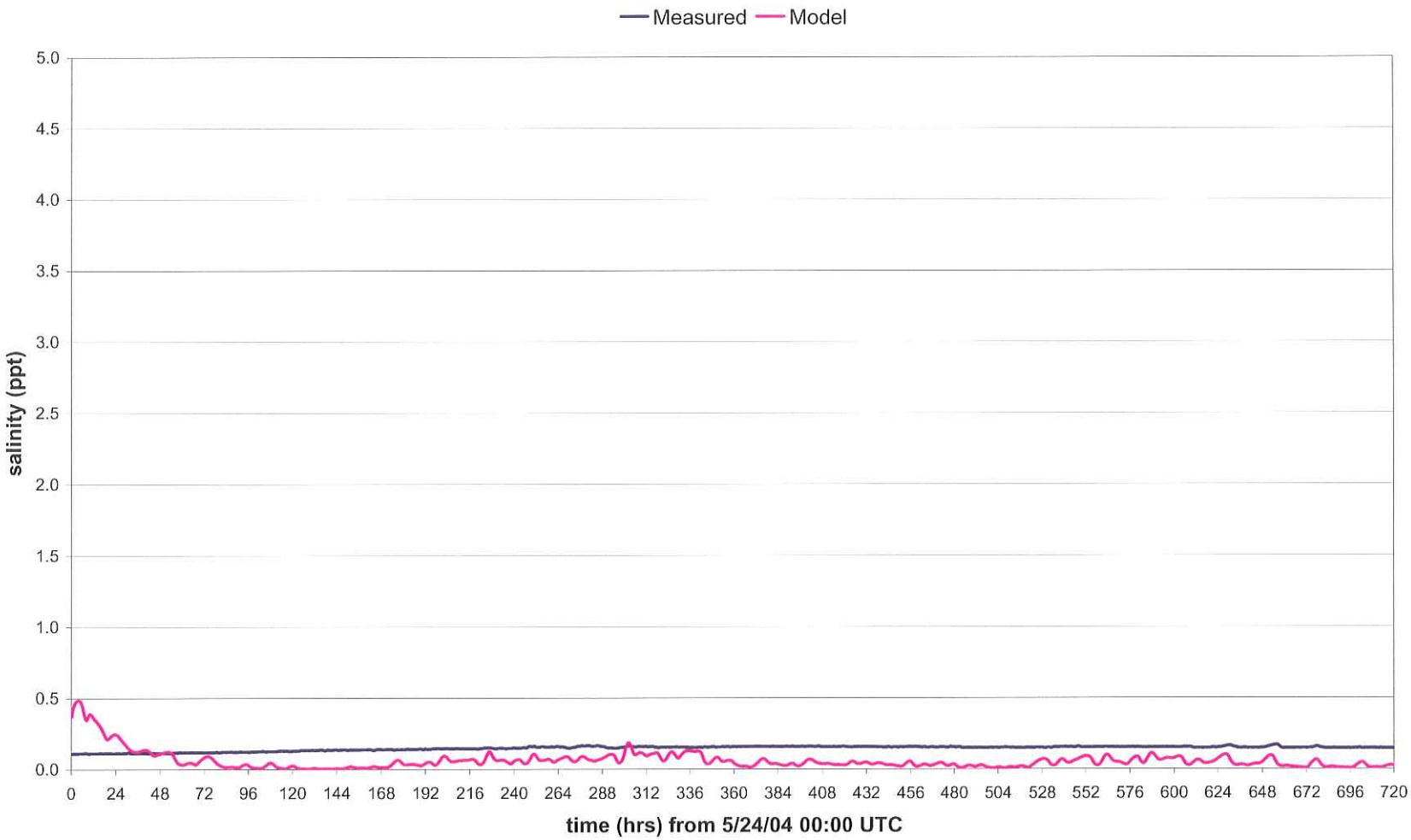

Figure 4.11 CSI-14 Salinity Calibration Results

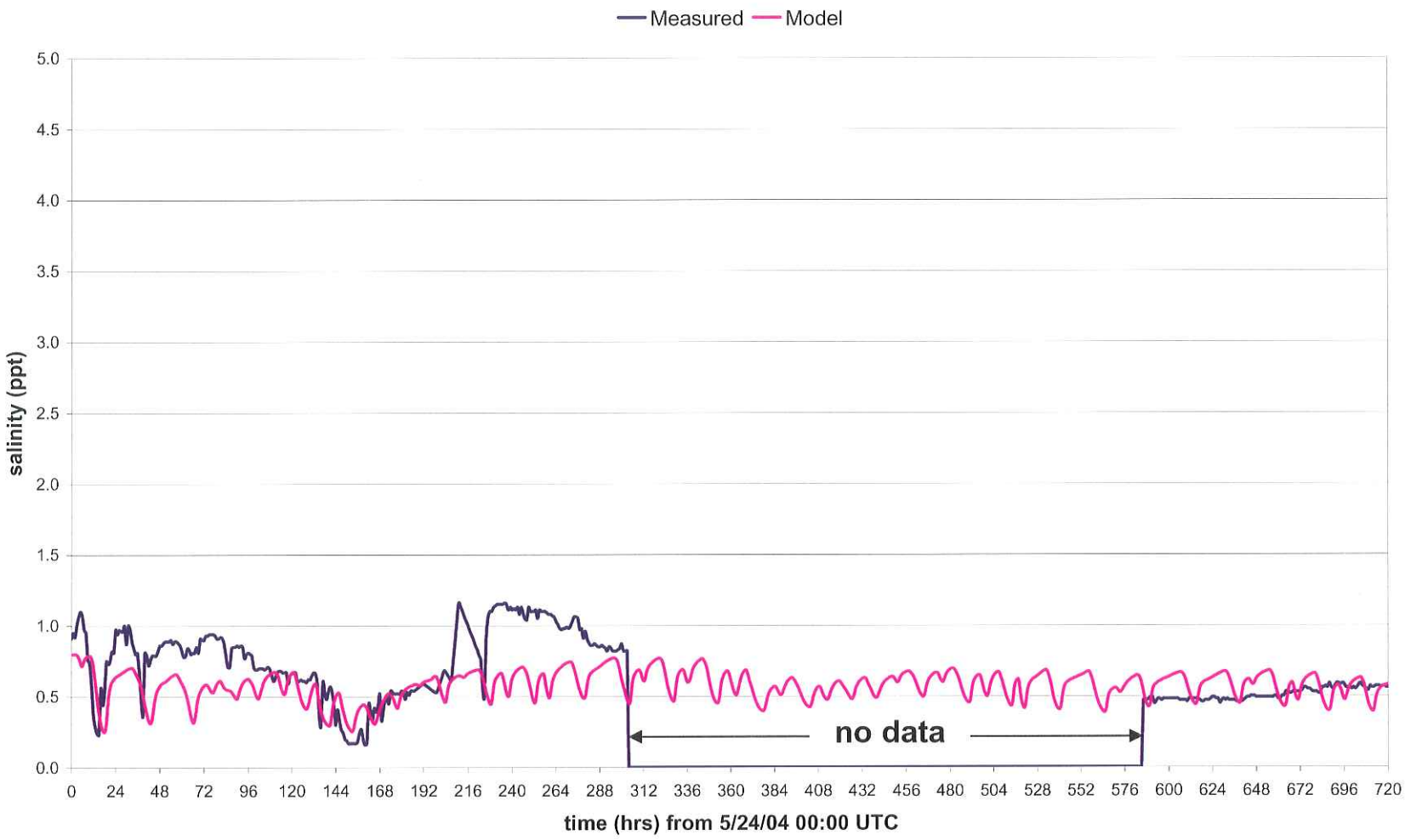

Figure 4.12 STA 622 Salinity Calibration Results

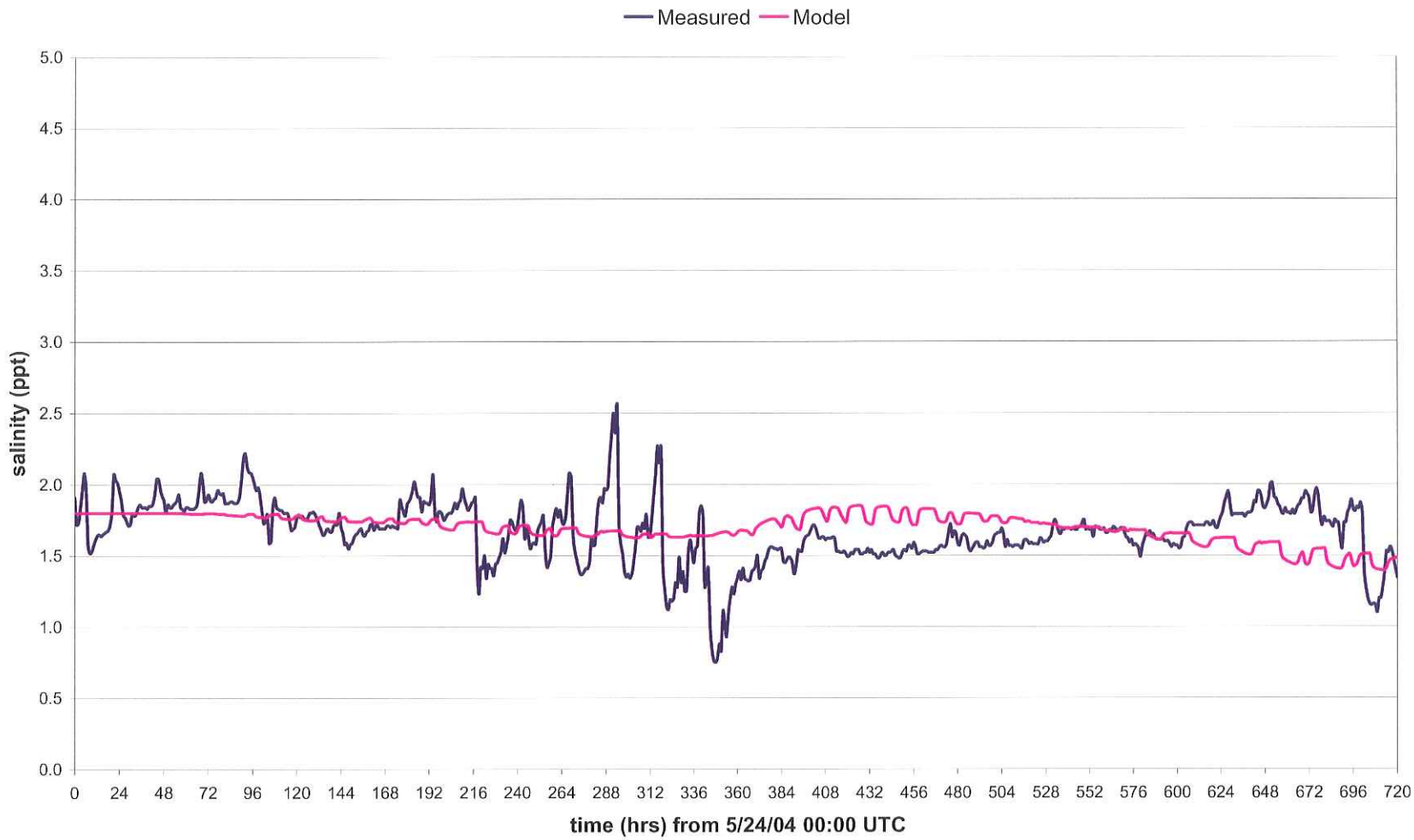

Figure 4.13 STA 623 Salinity Calibration Results

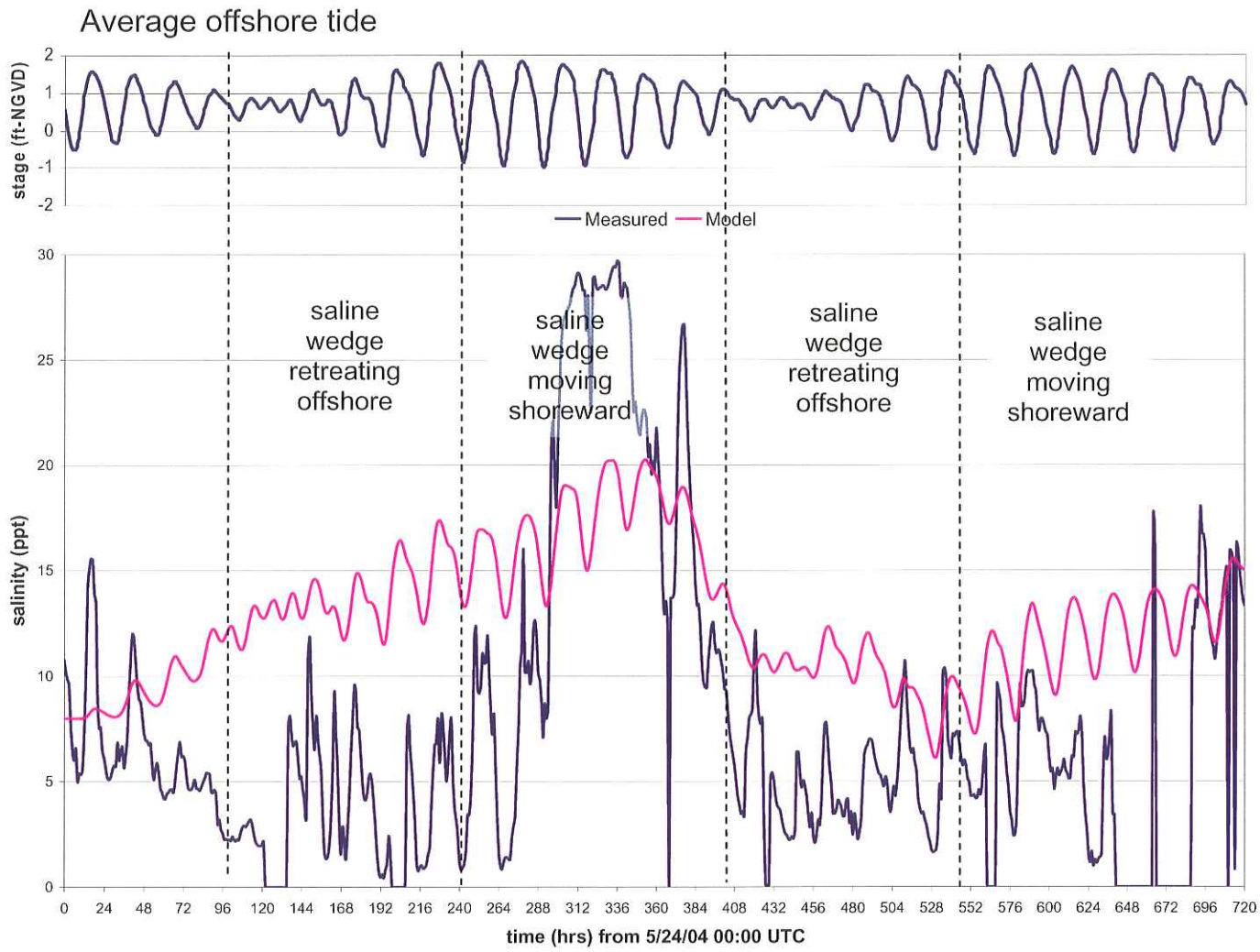

Figure 4.14 CSI-3 Salinity vs. Tidal Stage

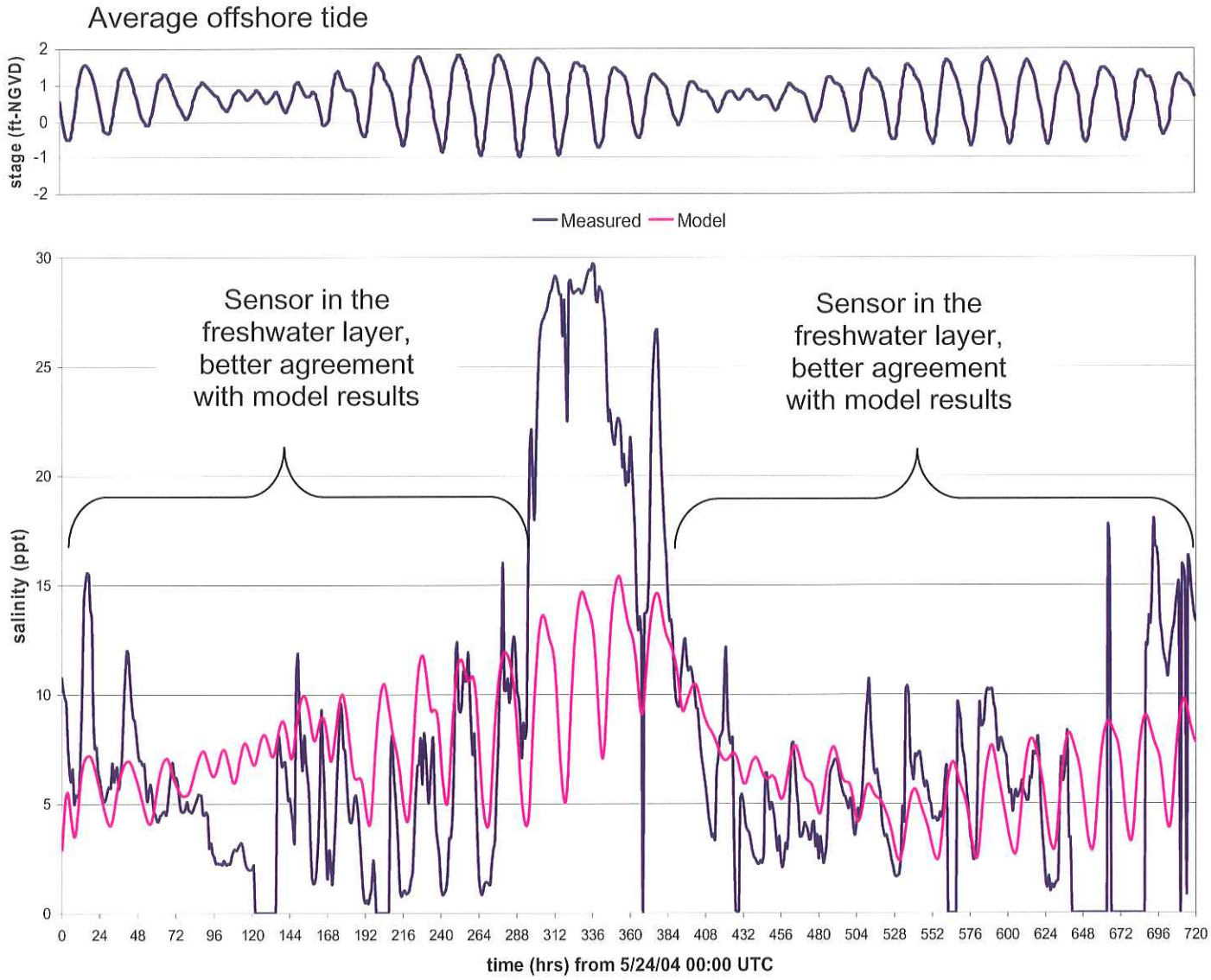

Figure 4.15 S1 Model Salinity vs. CSI-3 Measured Salinity

4.4.3 Model Mass Balance Results

A mass balance analysis verifies that the model correctly accounts for the material added and removed from the system (does not artificially gain or loose material). For the salinity transport model, saline water (salt) entered and left the system through the offshore boundary. The stream flow boundaries continually added freshwater and, thus, only affected the system volume. The model treated all other mesh boundaries as impenetrable walls.

Table 4.9 shows an example mass balance analysis over a tidal cycle in terms of metric gigatons of salt in the system. As the table shows, the transport model balanced the total system mass and mass transport into and out of the system.

Table 4.9 Salinity Transport Model Mass Balance Results

System Mass		Model Time		
		635 hrs	658 hrs	System Mass Difference
System Mass (G-tons)		11.008	10.901	-0.107
Mass Transport	Seaward Boundary	East Boundary	West Boundary	Total Mass Transport
Mass Added/Removed at the Boundaries (G-tons)	-0.194	-0.009	+0.096	-0.107
Remaining System Mass (G-tons)				0.000

4.5 Turbidity Model Calibration Results

Figures 4.16 and 4.17 compare the turbidity model predictions with measured data at CSI-3 and CSI-14. Figure 4.16 indicates that the model predicted the ambient turbidity level at CSI-3 quite well but failed to predict the episodic spikes. The ambient turbidity at CSI-3 appears to result from the river discharges feeding Acadiana Bays. The model should simulate this process well given the success of the hydrodynamics model (which drives the turbidity model) in simulating measured currents.

The measured time series of turbidity shows that the sediment concentration increased episodically and then fell back to the ambient level. These episodic concentration spikes may have resulted from local entrainment of sediments from a soft bed during periods of high bottom shear stress

caused by high currents or waves. Figure 4.4 reveals that wind speeds consistently exceeded 25 ft/s for hours 132 to 180 while Figure 4.16 reveals that the period with sustained, elevated levels of turbidity extended from hour 140 to 208. This comparison suggests that a short duration of high waves (a result of high winds) may have developed a bed shear stress greater than the critical bed shear stress; with the critical bed shear stress exceeded, the soft bed eroded and sediment suspension increased the concentration of sediment in the water column (see, for example, Parchure and Mehta, 1985). The low settling velocity of the fine particles caused the concentration of the water column to remain above ambient levels for a short period after the winds slowed. The applied turbidity model cannot simulate such effects. However, this inability is relatively minor for this study as its main objective is to model the net advection-diffusion mechanism of turbidity from the river discharges. The model appears to model this mechanism reasonably well given its ability to replicate the longer-term ambient/background turbidity levels.

Consistent with the above discussion, Figure 4.17 shows reasonable agreement with the measured ambient turbidity levels at CSI-14 during the first half of the calibration period. The model reasonably reproduced the average turbidity at Point Chevreuil but missed the short-term variations.

In the second half of the calibration period, the modeled turbidity exceeded the measured ambient turbidity levels. A closer examination of the methods used to quantify turbidity input into the Bays offers a plausible explanation for this discrepancy. Figure 4.3 shows that CSI-14 lies just off Point Chevreuil, relatively close to the major rivers discharging sediments into Atchafalaya Bay. As mentioned earlier, due to the lack of appropriate data, this study assumed turbidity discharge volume from the rivers to be a function of flow discharge rate. This approach resulted in increased volumes of turbidity discharged from the Lower Atchafalaya River and Wax Lake Outlet after approximately hour 200 (see Figure 4.2). With a small phase lag, Figure 4.17 shows a similar trend — the predicted turbidity increased after approximately hour 240. Accurate estimates of sediment discharge from the rivers should improve the agreement between measured and predicted turbidities.

Based on the above discussions, the turbidity model was deemed calibrated and capable of reproducing ambient turbidity concentrations for Acadiana Bays.

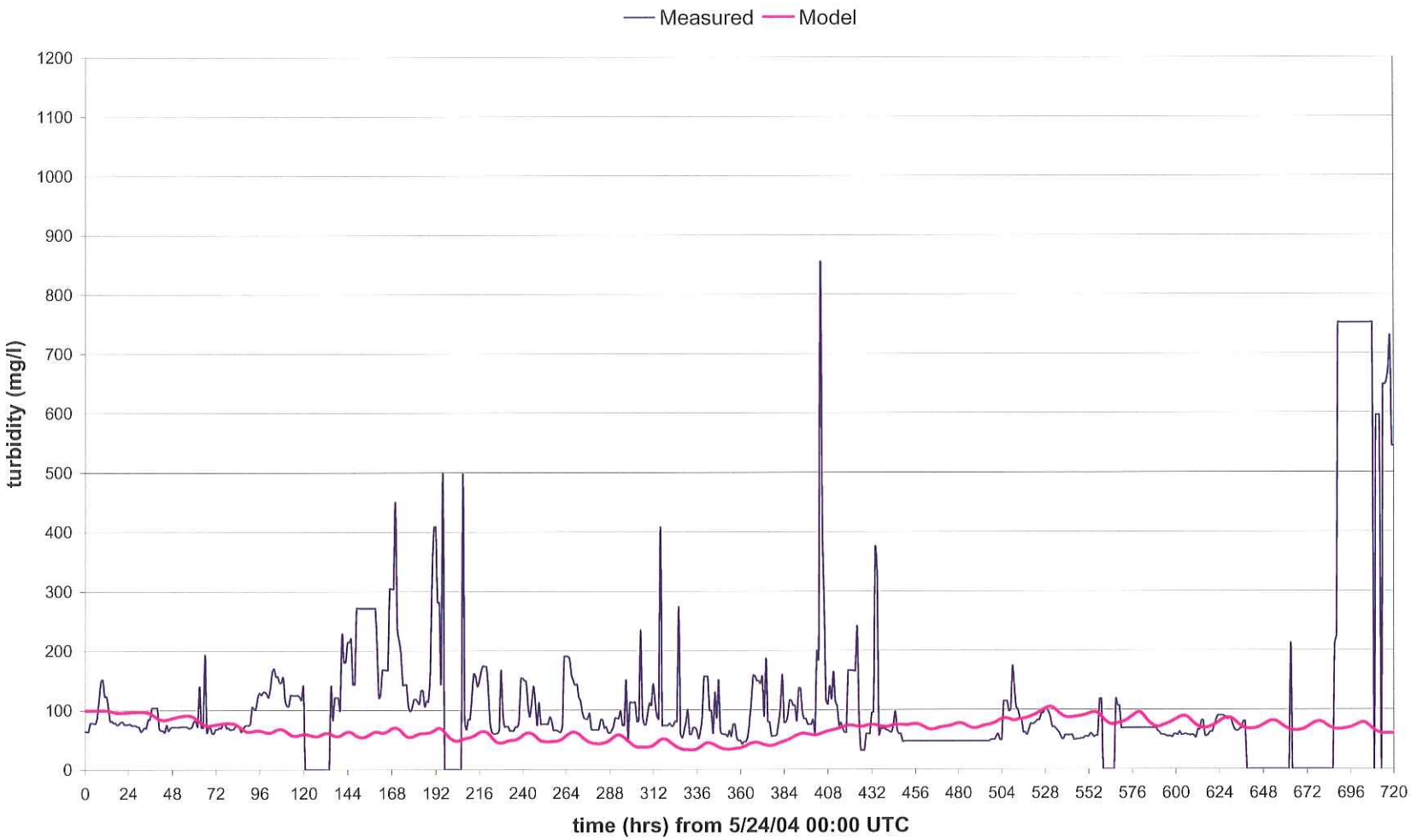

Figure 4.16 CSI-3 Turbidity Model Calibration

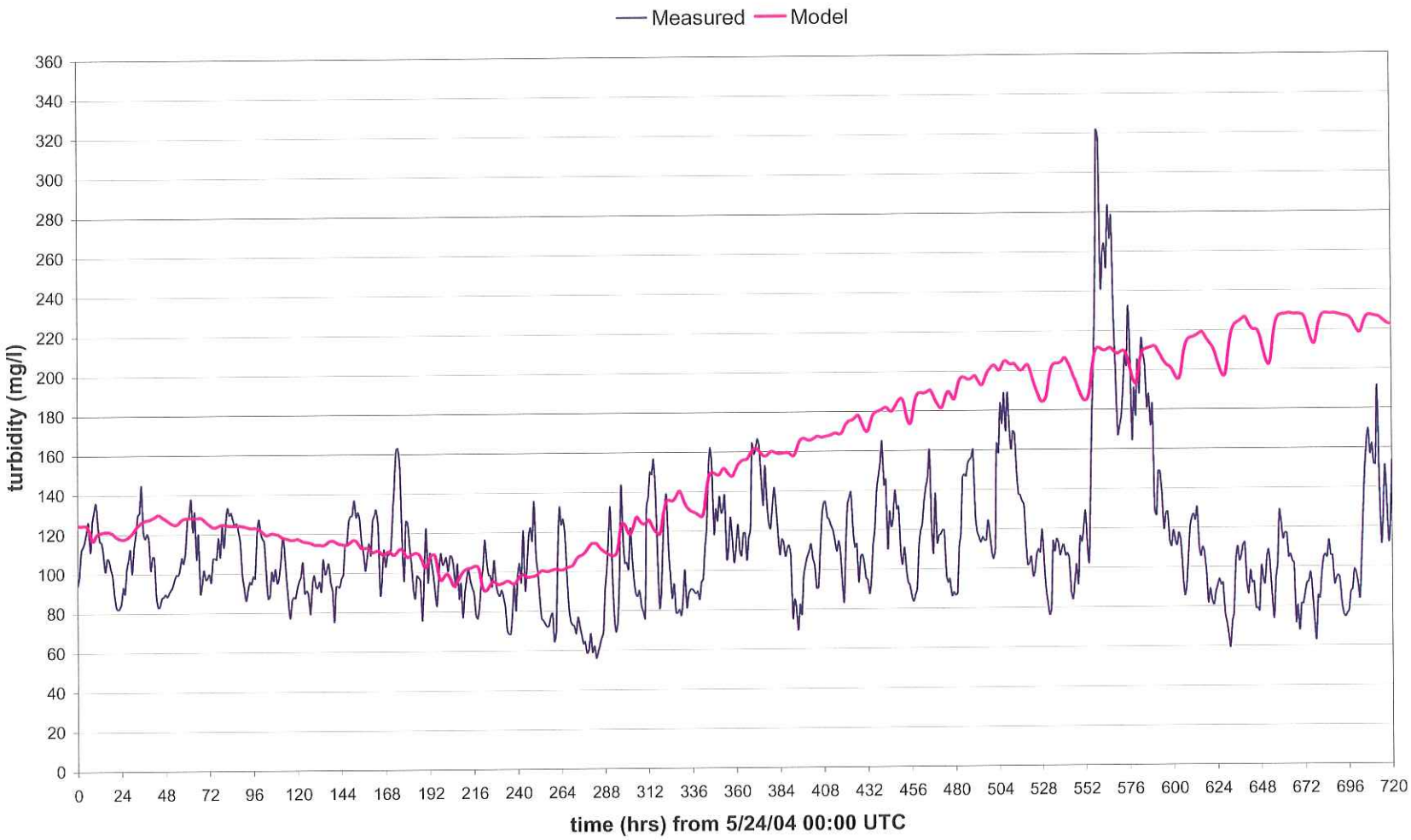

Figure 4.17 CSI-14 Turbidity Model Calibration

4.6 Model Depth Sensitivity Tests

The lack of a comprehensive, updated bathymetric survey for this study (precluded by the high cost associated with such an effort), warranted a sensitivity analysis to determine the effects of water depth inaccuracies on model results. This study examined the sensitivity of the model predictions to depth inaccuracies by running the hydrodynamics model with the following depth variation alternatives:

- The depth as surveyed and interpolated to the model mesh (surveyed depths)
- The surveyed depths deepened by 1.6 ft (0.5 m) throughout the model mesh (depths -1.6 ft)
- The surveyed depths deepened by 3.3 ft (1 m) throughout the model mesh (depths -3.3 ft)
- The surveyed depths deepened by 3.3 ft only in the Acadiana Bays portion of the model mesh (depth in bays -3.3 ft) (i.e., the offshore depths remained at the surveyed levels)

Tables 4.10 and 4.11 and Figures 4.18 and 4.19 show the modeled tidal stage results at CSI-3 and CSI-14. The depth variations increased the modeled tide ranges at CSI-3 and CSI-14 – up to +0.2 ft.

Tables 4.12 and 4.13 and Figures 4.20 and 4.21 show the modeled current speed results at CSI-3 and CSI-14. Deepening the mesh increased the current speeds by 0.1 – 0.3 ft/s.

Finally, Figure 4.22 and 4.23 show the modeled current direction at CSI-3 and CSI-14. Although depth changes did affect the current direction, their effects were insignificant.

Based on the above results, the current direction predictions appear relatively insensitive to minor depth inaccuracies, but the model tide range and current speed predictions increased about 10% with increased depths of 1 – 3 ft.

Table 4.10 CSI-3 Tidal Stage Depth Sensitivity Results

	Surveyed depths	**Depths -1.6 ft**	**Depths -3.3 ft**	**Depths -3.3 ft (bays only)**
MHW (ft NGVD)	1.3	1.3	1.2	1.3
MLW (ft NGVD)	0.4	0.4	0.3	0.2
Range (ft)	0.9	0.9	0.9	1.1
MTL (ft NGVD)	0.8	0.8	0.8	0.8
RMS (ft NGVD)	0.9	0.9	0.9	0.9
RMSΔ (ft NGVD)		0.0	0.1	0.0

Table 4.11 CSI-14 Tidal Stage Depth Sensitivity Results

	Surveyed depths	**Depths -1.6 ft**	**Depths -3.3 ft**	**Depths -3.3 ft (bays only)**
MHW (ft NGVD)	1.5	1.5	1.5	1.5
MLW (ft NGVD)	0.5	0.4	0.4	0.4
Range (ft)	1.0	1.1	1.1	0.8
MTL (ft NGVD)	1.0	0.9	0.9	1.0
RMS (ft NGVD)	1.1	1.1	1.1	1.1
RMSΔ (ft NGVD)		0.0	0.0	0.0

Table 4.12 CSI-3 Current Speed Depth Sensitivity Results

	Surveyed depths	**Depths -1.6 ft**	**Depths -3.3 ft**	**Depths -3.3 ft (bays only)**
Mean Flood (ft/s)	0.5	0.5	0.5	0.6
Mean Ebb (ft/s)	0.5	0.5	0.5	0.5
Peak Flood (ft/s)	0.7	0.7	0.6	0.7
Peak Ebb (ft/s)	0.6	0.6	0.6	0.6
RMS (ft/s)	0.4	0.4	0.4	0.4
RMSΔ (ft/s)		0.0	0.0	0.0

Table 4.13 CSI-14 Current Speed Depth Sensitivity Results

	Surveyed depths	**Depths -1.6 ft**	**Depths -3.3 ft**	**Depths -3.3 ft (bays only)**
Mean Flood (ft/s)	0.7	0.8	0.8	0.8
Mean Ebb (ft/s)	0.5	0.6	0.6	0.6
Peak Flood (ft/s)	0.9	1.2	1.2	1.2
Peak Ebb (ft/s)	0.8	0.9	0.9	0.9
RMS (ft/s)	0.6	0.6	0.6	0.6
RMSΔ (ft/s)		0	0.1	0.1

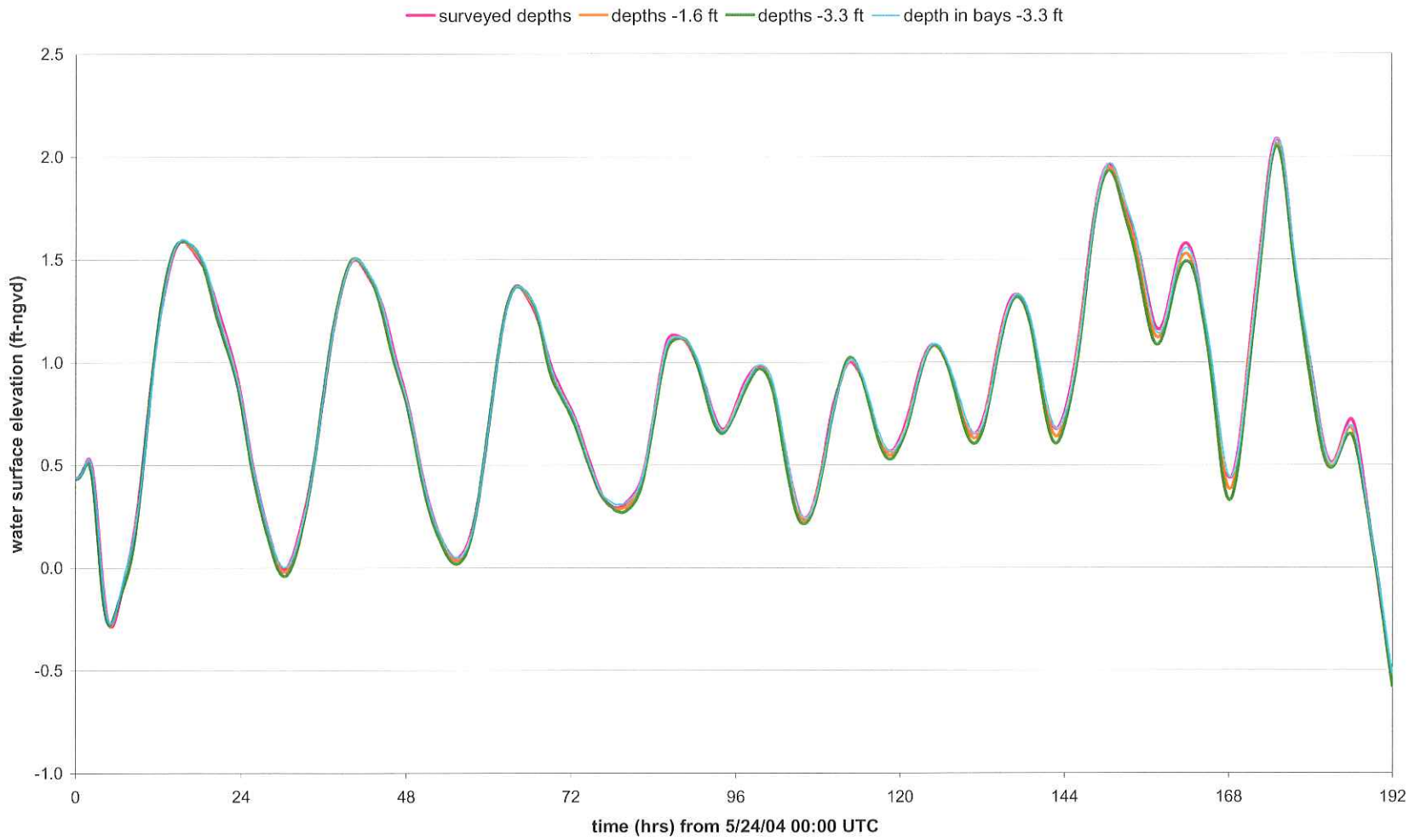

Figure 4.18 CSI-3 Tidal Stage/Model Depth Sensitivity

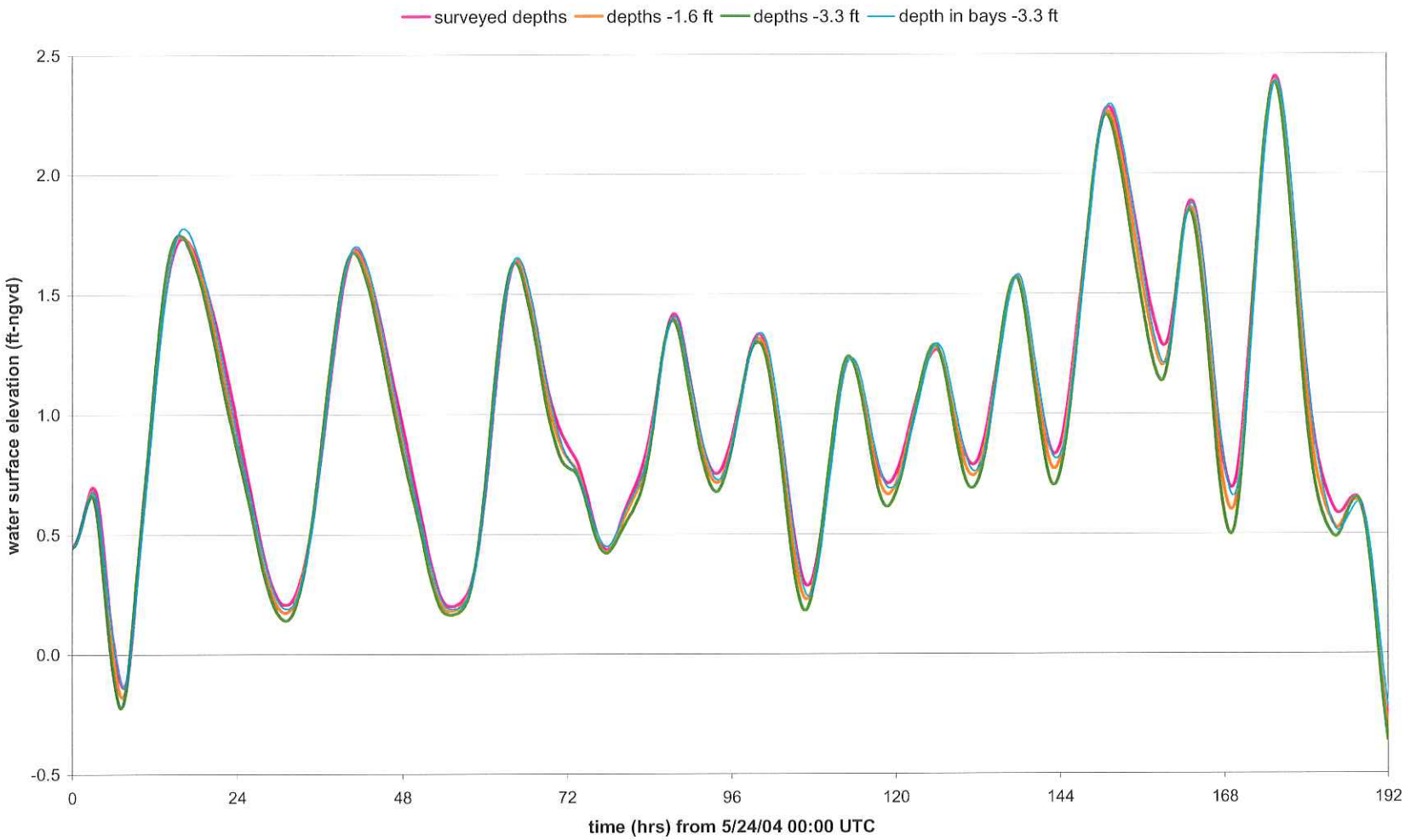

Figure 4.19 CSI-14 Tidal Stage/Model Depth Sensitivity

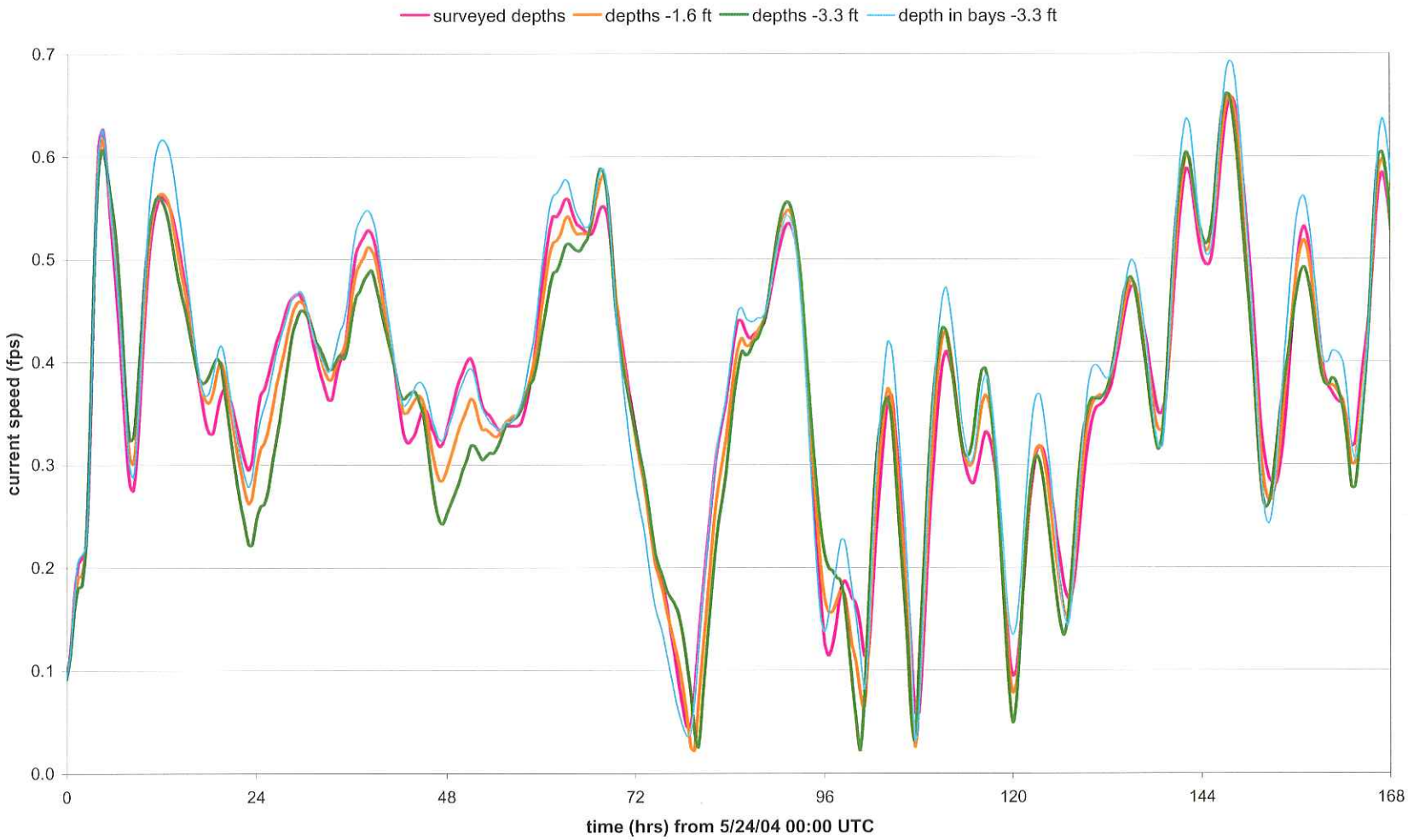

Figure 4.20 CSI-3 Current Speed/Model Depth Sensitivity

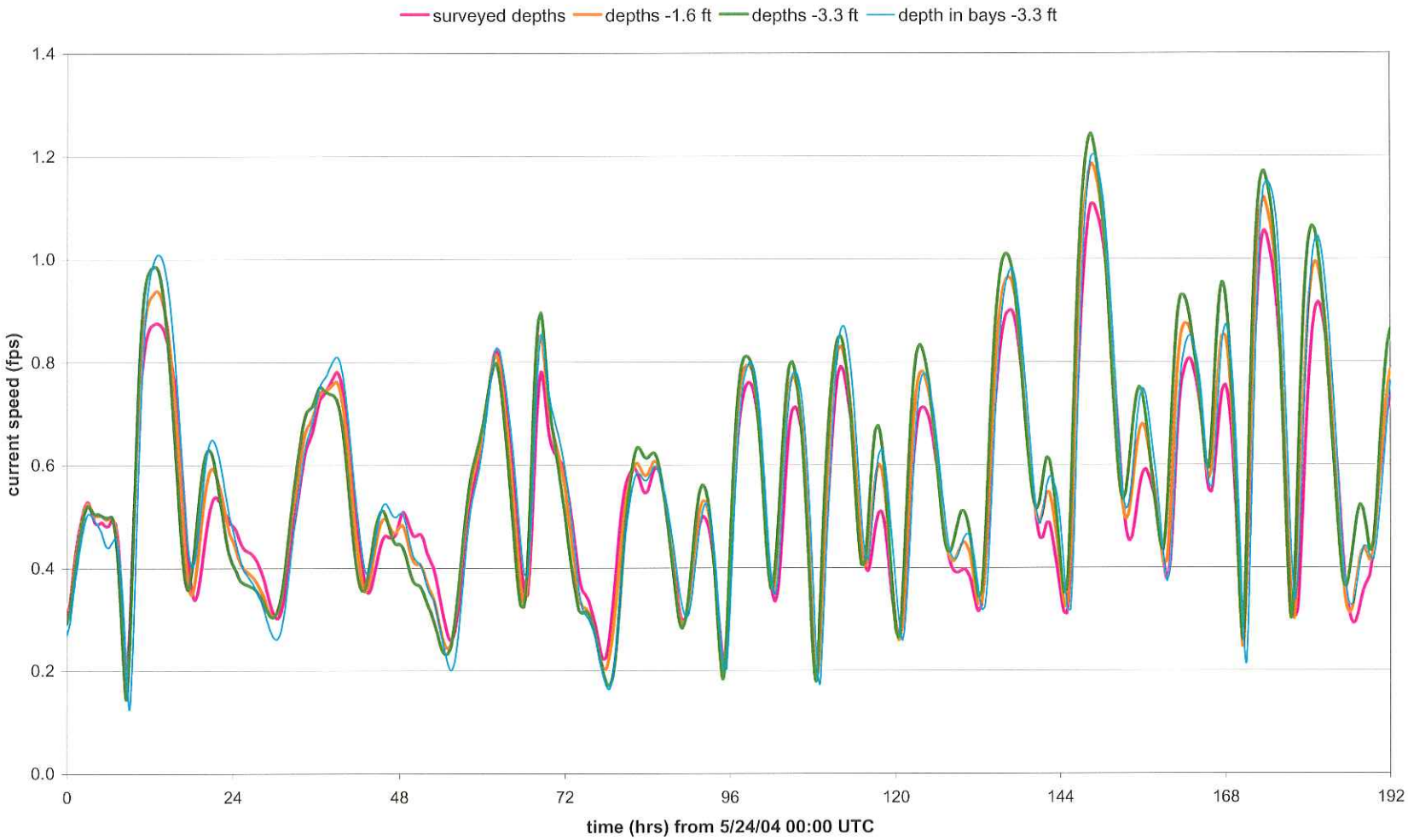

Figure 4.21 CSI-14 Current Speed/Model Depth Sensitivity

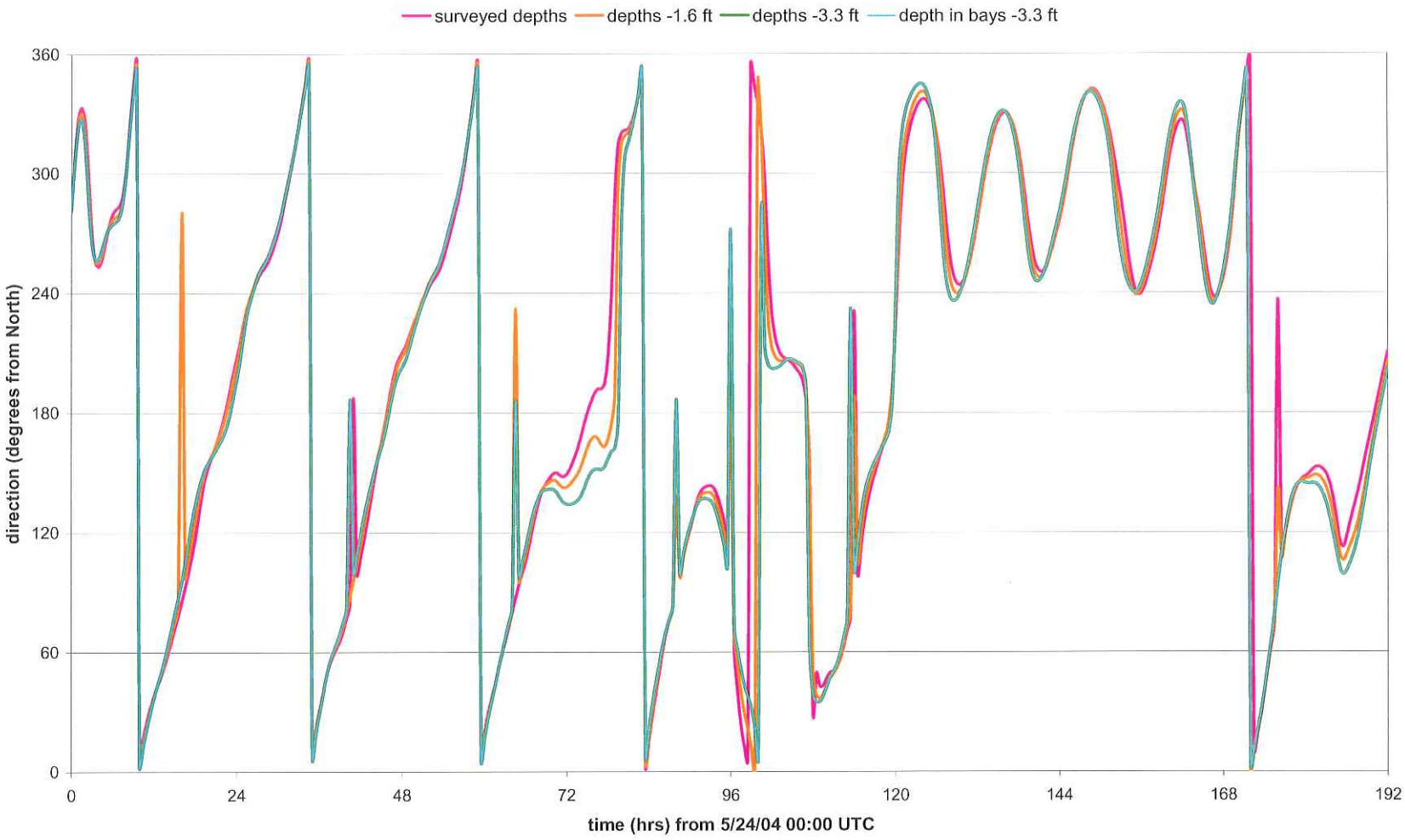

Figure 4.22 CSI-3 Current Direction/Model Depth Sensitivity

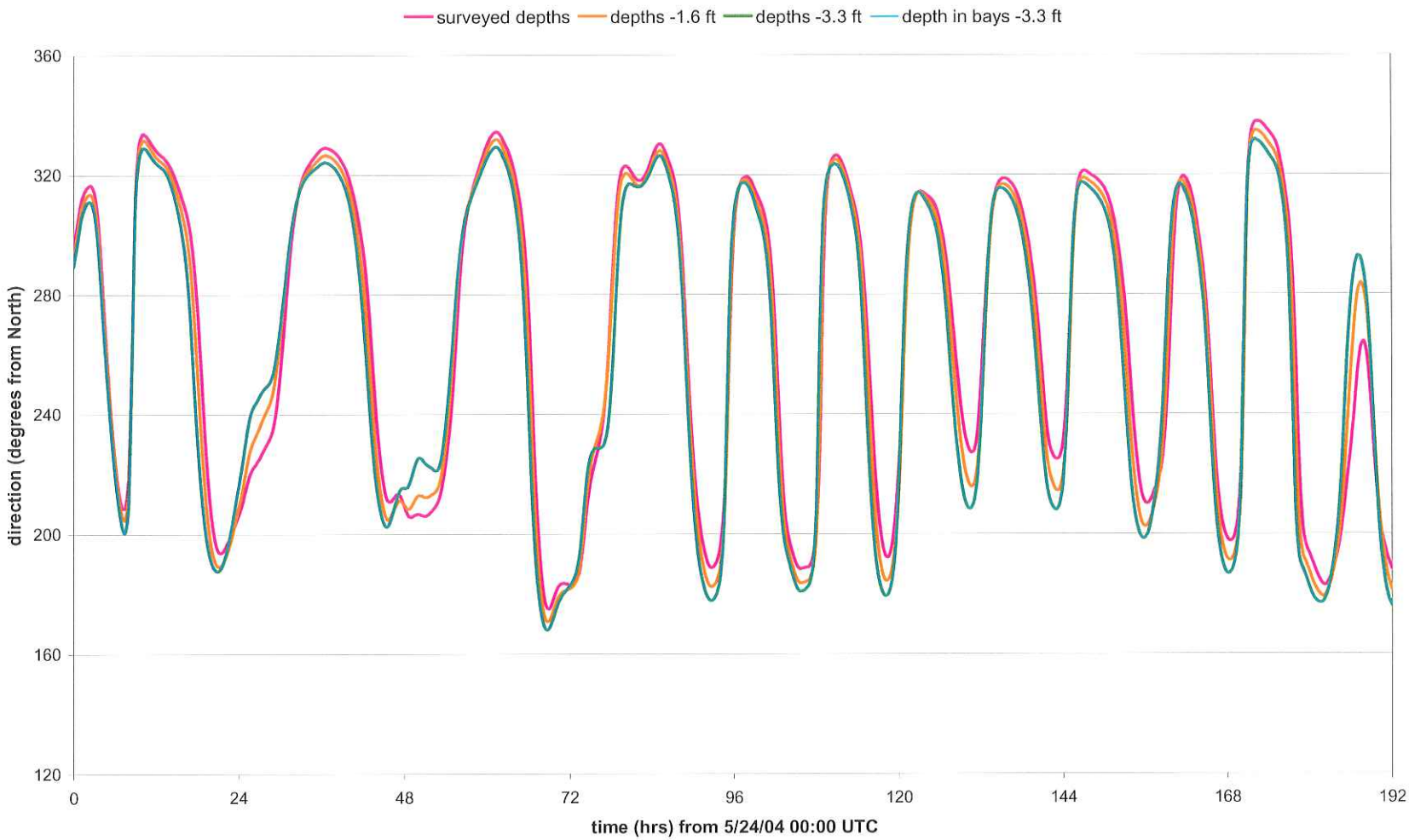

Figure 4.23 CSI-14 Current Direction/Model Depth Sensitivity

Tables 4.14 – 4.17 and Figures 4.24 – 4.27 show the effects of varying the model depths on salinity. In the tables, mean high salinity refers to the average of all salinity peaks in the time series (Figures 4.24 – 4.25) and mean low salinity refers to the average of all salinity troughs. Table 4.14 shows that the depth variations resulted in less than a 2% change in predicted mean salinity at CSI-3. Though the depth variations changed the mean salinities at CSI-14 and STA-622 by 10 – 20%, the absolute value of mean salinity at these locations approaches zero; thus, these changes are insignificant. Depth variations had negligible effects on salinity estimates at STA-623.

Overall, the salinity variations were well under 1 ppt at all locations, showing that the calibrated transport model was relatively insensitive to depth variations up to 3 ft.

Table 4.14 CSI-3 Salinity Depth Sensitivity Results

	Surveyed depths	**Depths -1.6 ft**	**Depths -3.3 ft**	**Depths -3.3 ft (bays only)**
Mean High Salinity (ppt)	12.16	11.92	12.02	12.02
Mean Low Salinity (ppt)	11.41	11.65	11.68	11.68
Salinity Range (ppt)	0.75	0.27	0.34	0.34
Mean Salinity (ppt)	10.70	10.49	10.58	10.58
RMS (ppt)	10.90	10.68	10.77	10.77
RMSΔ (ppt)		0.17	0.31	0.16

Table 4.15 CSI-14 Salinity Depth Sensitivity Results

	Surveyed depths	**Depths -1.6 ft**	**Depths -3.3 ft**	**Depths -3.3 ft (bays only)**
Mean High Salinity (ppt)	0.24	0.23	0.14	0.23
Mean Low Salinity (ppt)	0.18	0.14	0.13	0.17
Salinity Range (ppt)	0.06	0.09	0.01	0.06
Mean Salinity (ppt)	0.10	0.12	0.11	0.12
RMS (ppt)	0.16	0.16	0.16	0.16
RMSΔ (ppt)		0.01	0.02	0.02

Table 4.16 STA-622 Salinity Depth Sensitivity Results

	Surveyed depths	Depths -1.6 ft	Depths -3.3 ft	Depths -3.3 ft (bays only)
Mean High Salinity (ppt)	0.64	0.69	0.64	0.66
Mean Low Salinity (ppt)	0.38	0.47	0.46	0.49
Salinity Range (ppt)	0.26	0.23	0.18	0.17
Mean Salinity (ppt)	0.55	0.61	0.58	0.60
RMS (ppt)	0.56	0.62	0.59	0.61
RMSΔ (ppt)		0.05	0.10	0.08

Table 4.17 STA-623 Salinity Depth Sensitivity Results

	Surveyed depths	Depths -1.6 ft	Depths -3.3 ft	Depths -3.3 ft (bays only)
Mean High Salinity (ppt)	1.78	1.78	1.79	1.79
Mean Low Salinity (ppt)	1.77	1.77	1.77	1.77
Salinity Range (ppt)	0.01	0.01	0.01	0.01
Mean Salinity (ppt)	1.78	1.78	1.78	1.78
RMS (ppt)	1.78	1.78	1.78	1.78
RMSΔ (ppt)		0.00	0.01	0.01

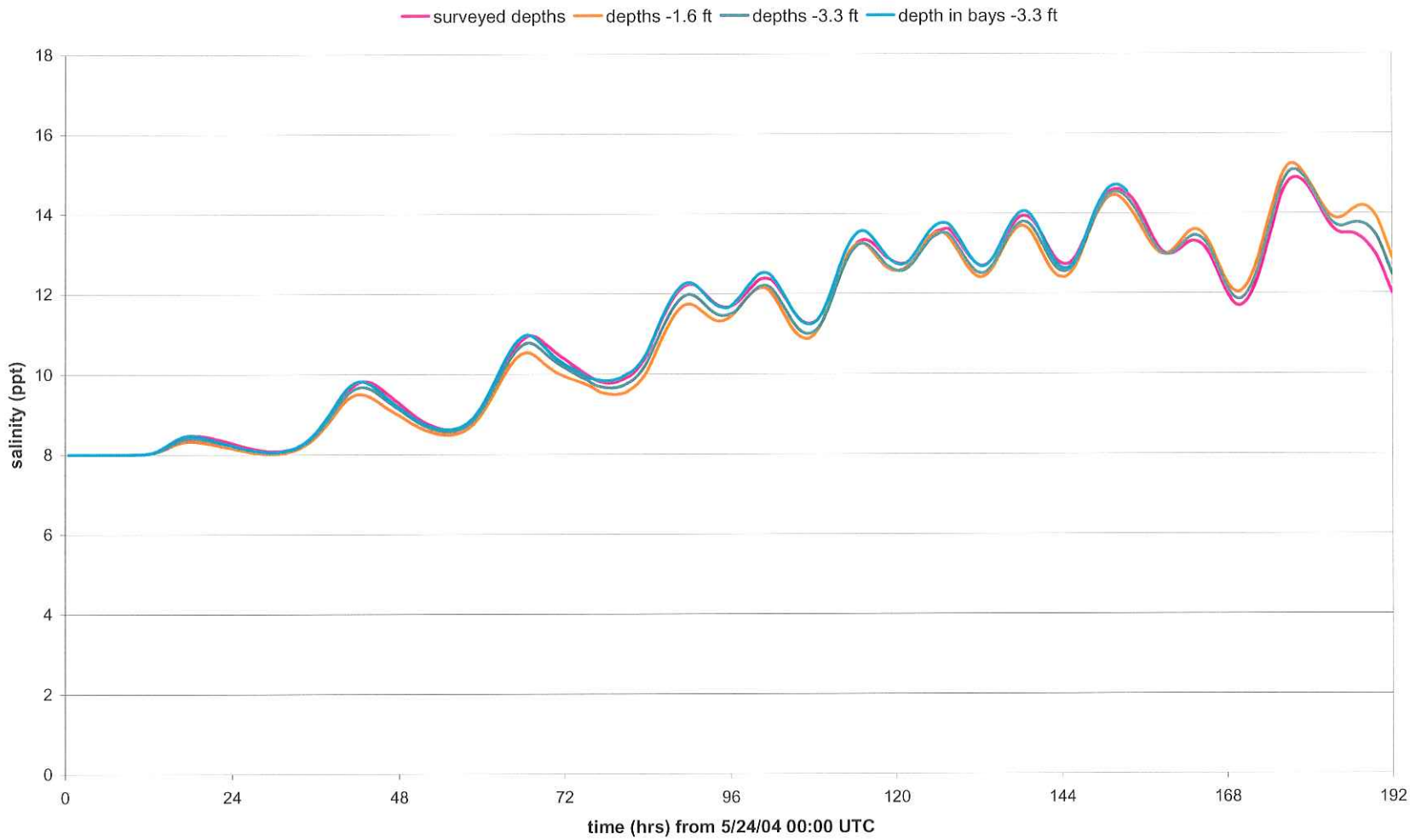

Figure 4.24 CSI-3 Salinity/Model Depth Sensitivity

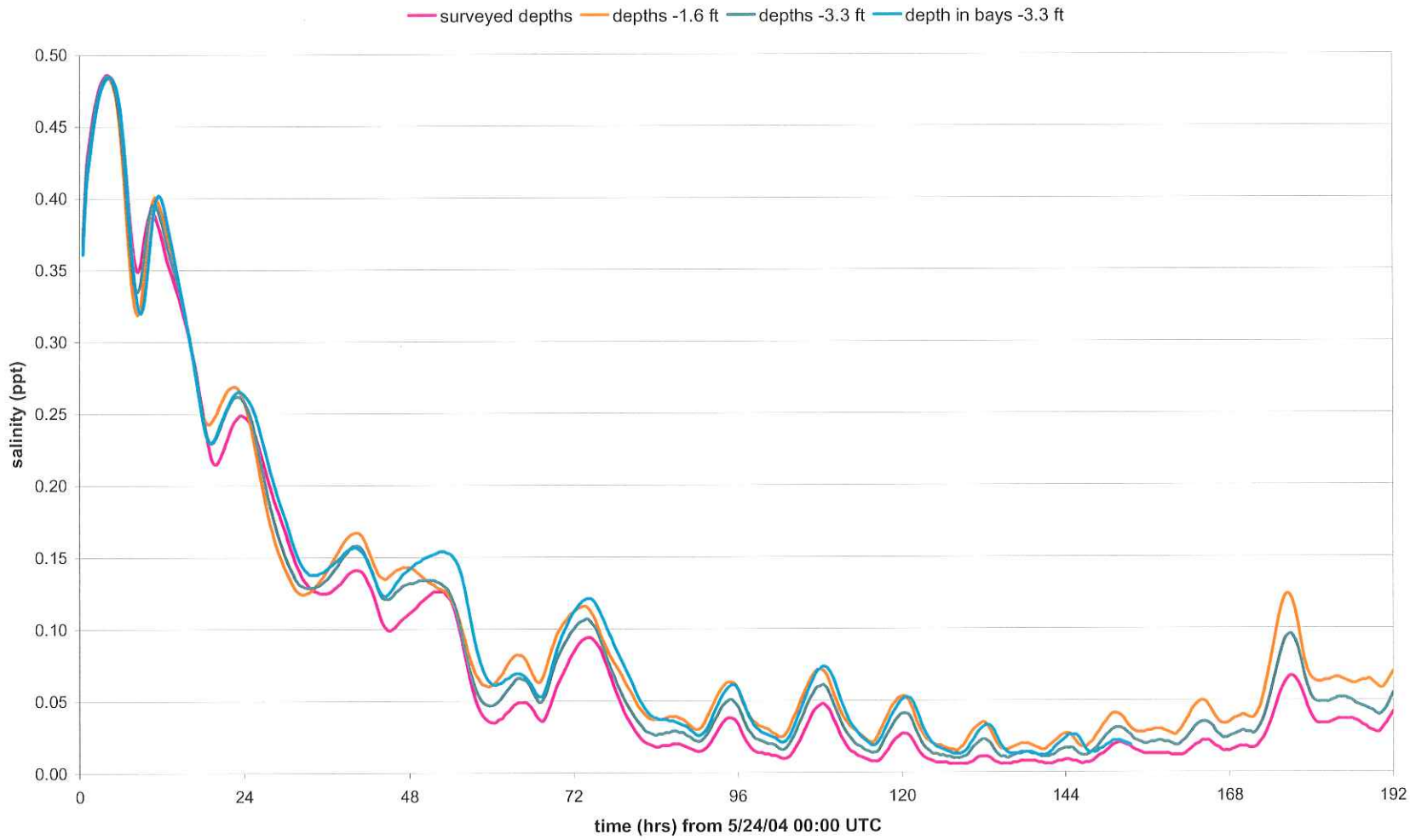

Figure 4.25 CSI-14 Salinity/Model Depth Sensitivity

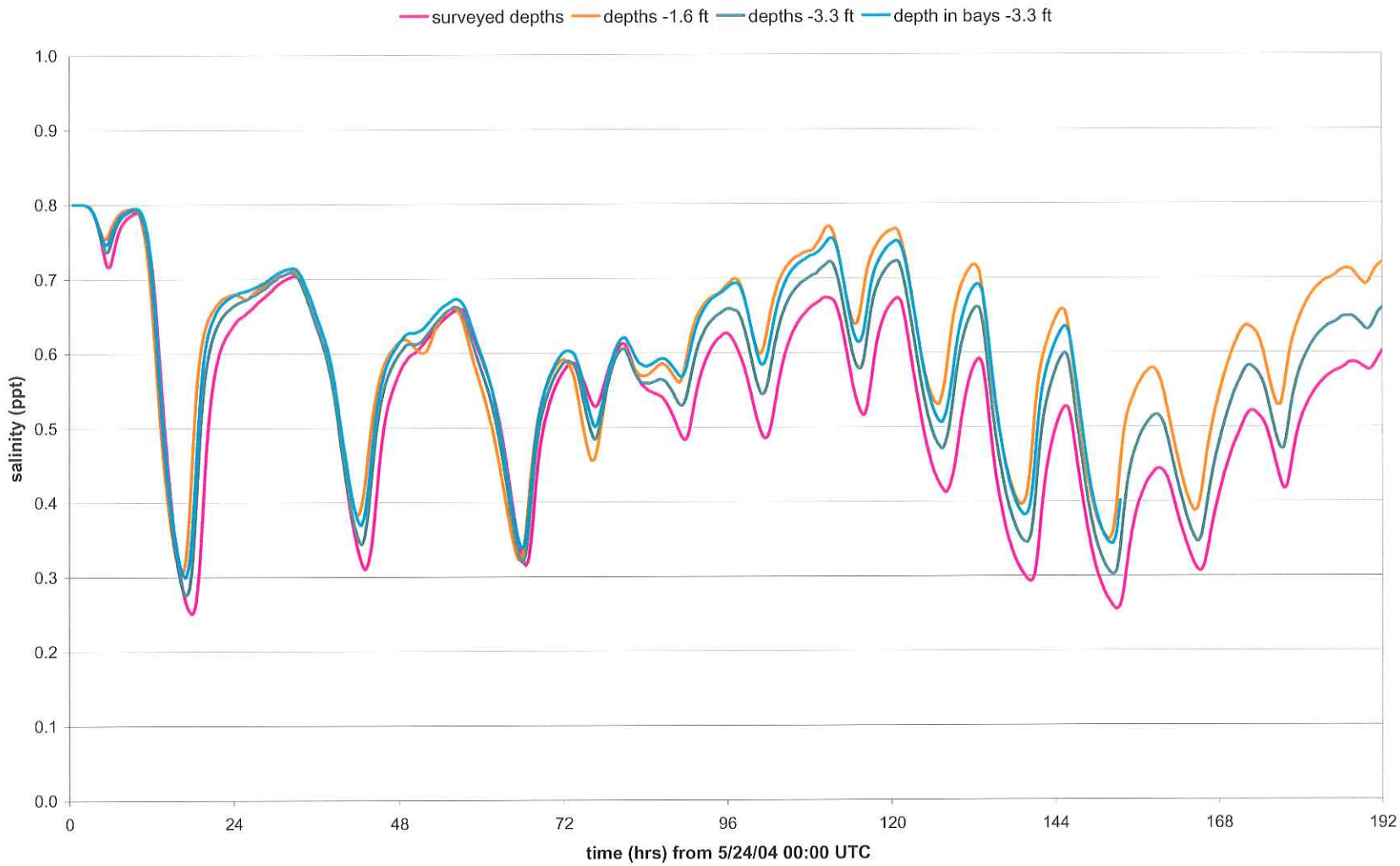

Figure 4.26 STA-622 Salinity/Model Depth Sensitivity

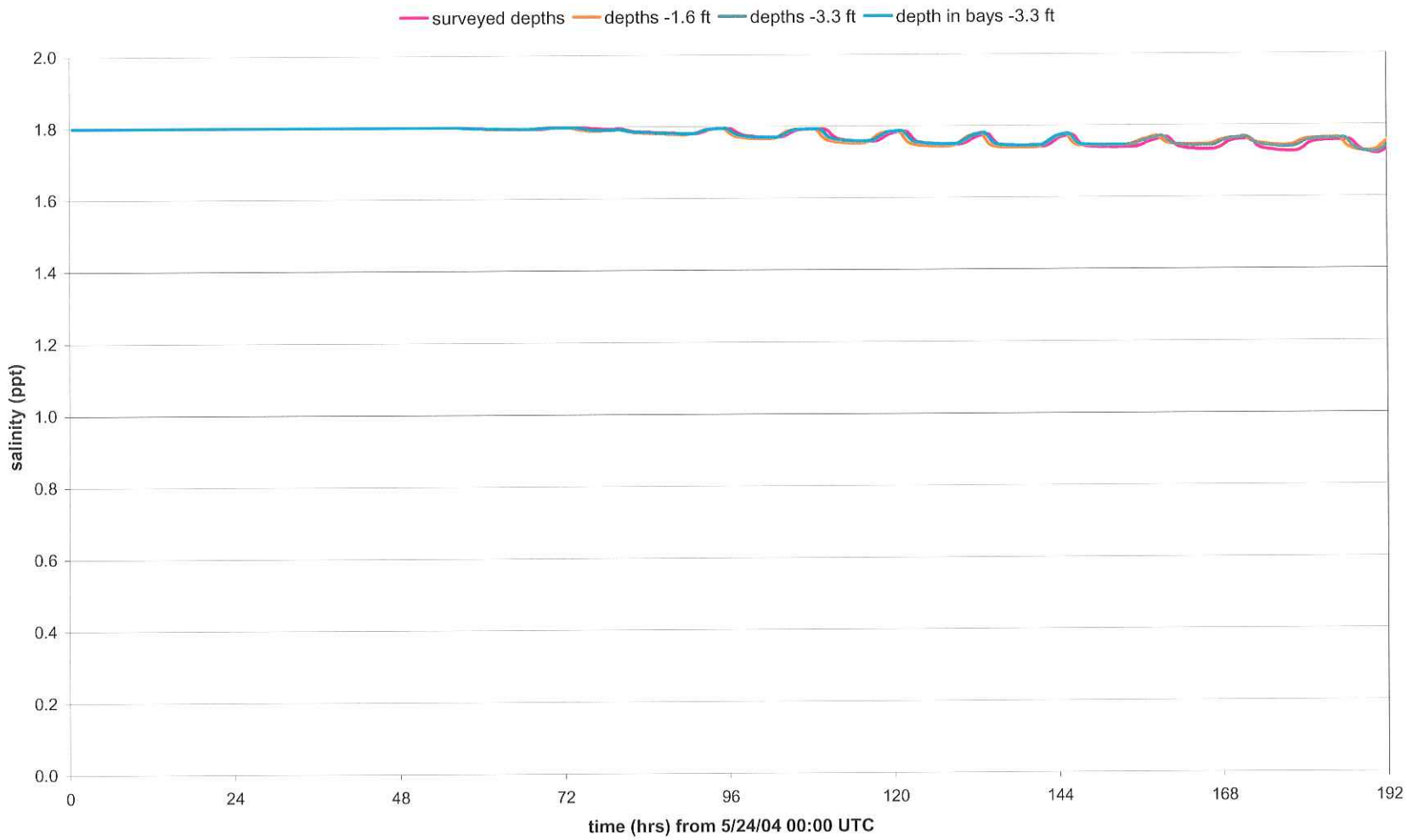

Figure 4.27 STA-623 Salinity/Model Depth Sensitivity

4.7 Model Wind Sensitivity Tests

Simulations with identical flow and tidal stage boundary conditions but different wind boundary conditions examined the effect of wind on the model. For each flow condition examined, one simulation applied a variable wind as the wind boundary condition over the entire mesh and a second simulation applied no wind. Following completion of the hydrodynamic simulations, transport simulations examined the development of the freshwater plume by tracking salinity and a freshwater tracer. The tracer model applied a constant conservative tracer concentration at the freshwater stream flow input points. The model results directly tracked the spread of freshwater through the system.

Figures 4.28 – 4.31 present the model results. Figures 4.28 and 4.29 show salinity contours and Figures 4.30 and 4.31 show freshwater tracer contours at model simulation hour 468.5. The presence of a southeast wind restricted the offshore penetration of freshwater discharged from Lower Atchafalaya River and Wax Lake Outlet (Figures 4.28 and 4.30). Without the wind (Figures 4.29 and 4.31), tides carried the bulk of the freshwater into the Gulf of Mexico. Figure 4.30 shows that the wind drove the freshwater plume toward the northwest into the Acadiana Bays.

In summary, wind plays a significant role in the evolution of the freshwater plume emanating from the mouths of Wax Lake Outlet and the Lower Atchafalaya River.

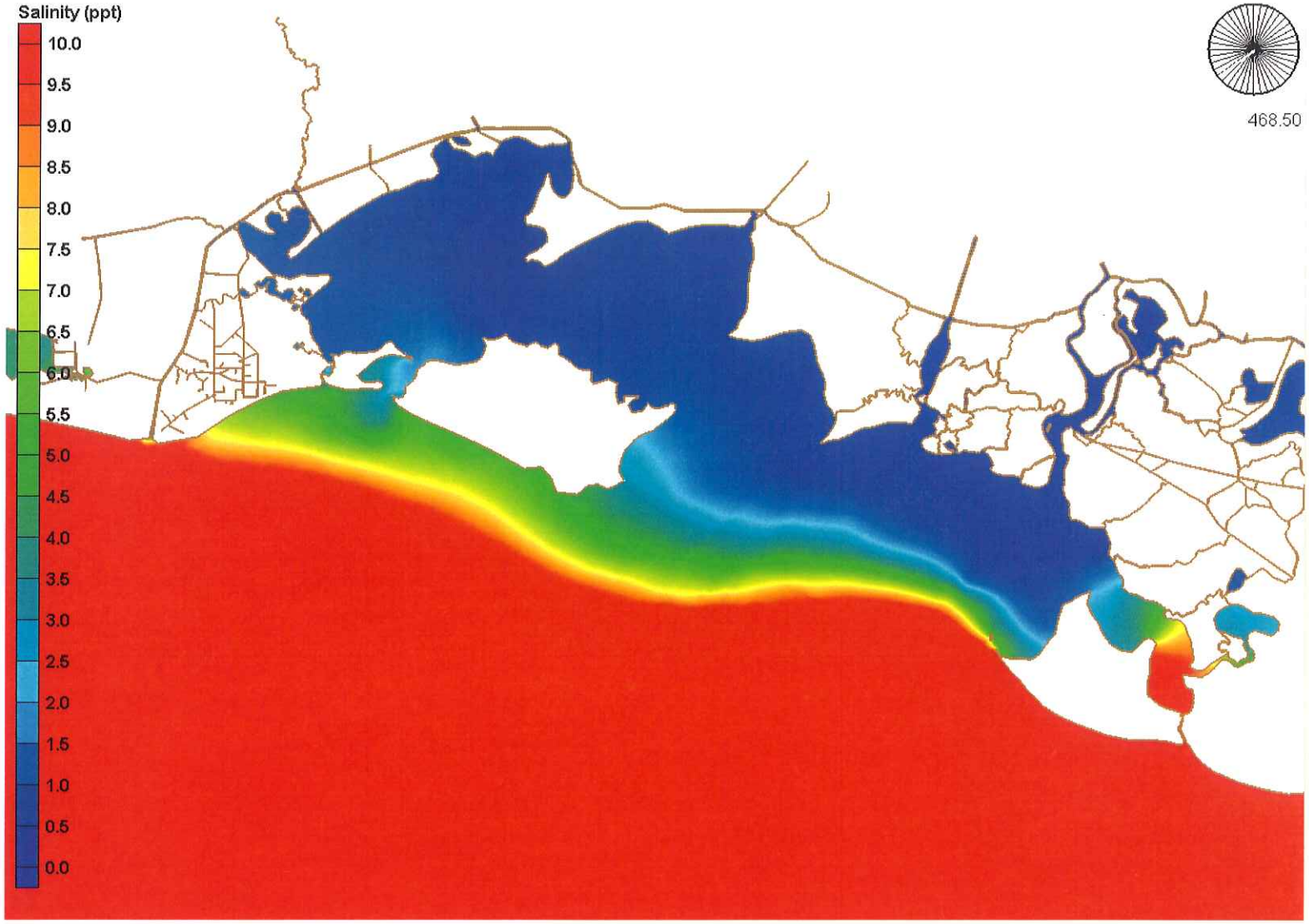

Figure 4.28 Salinity Model with Southeast Wind

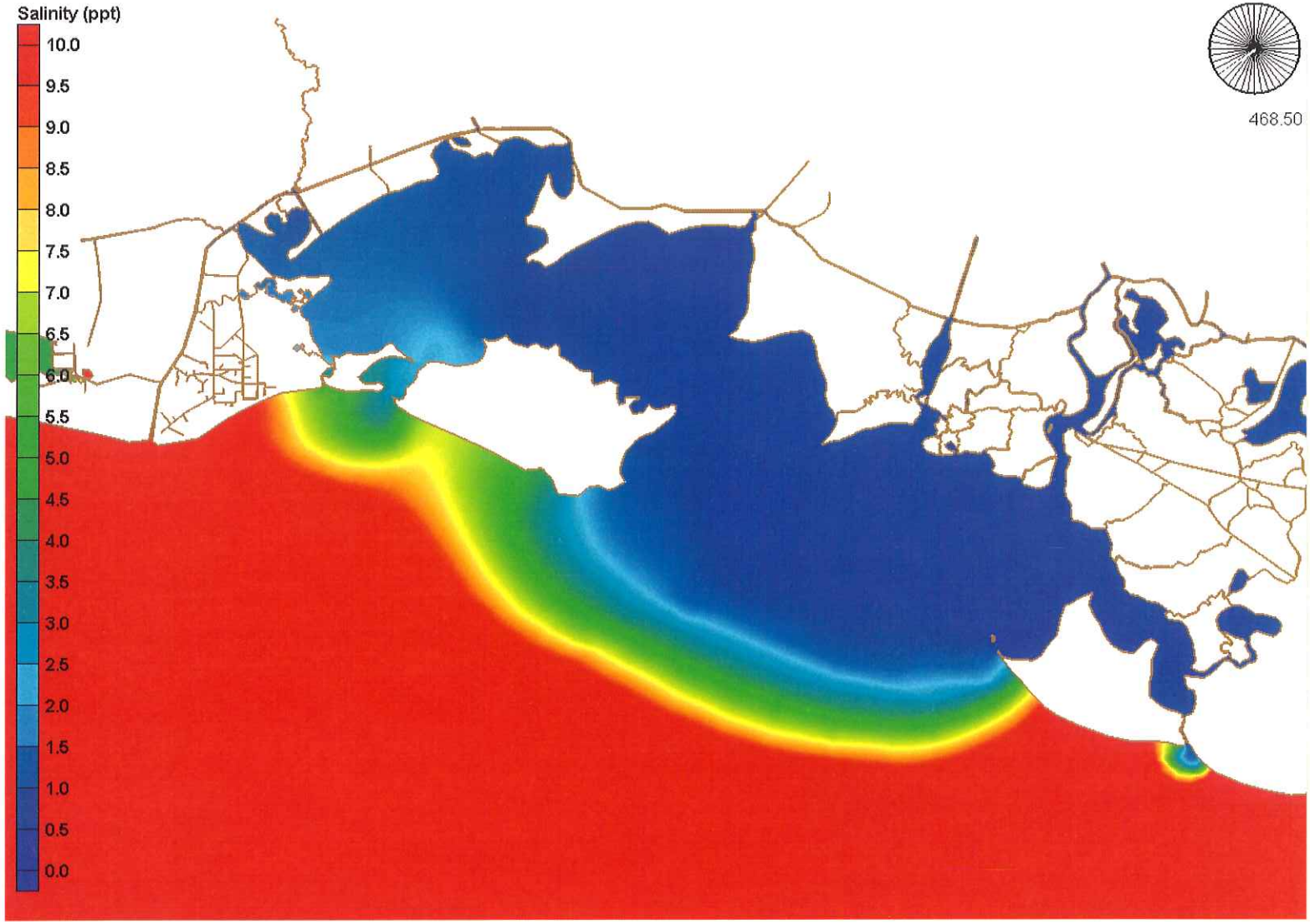

Figure 4.29 Salinity Model with No Wind

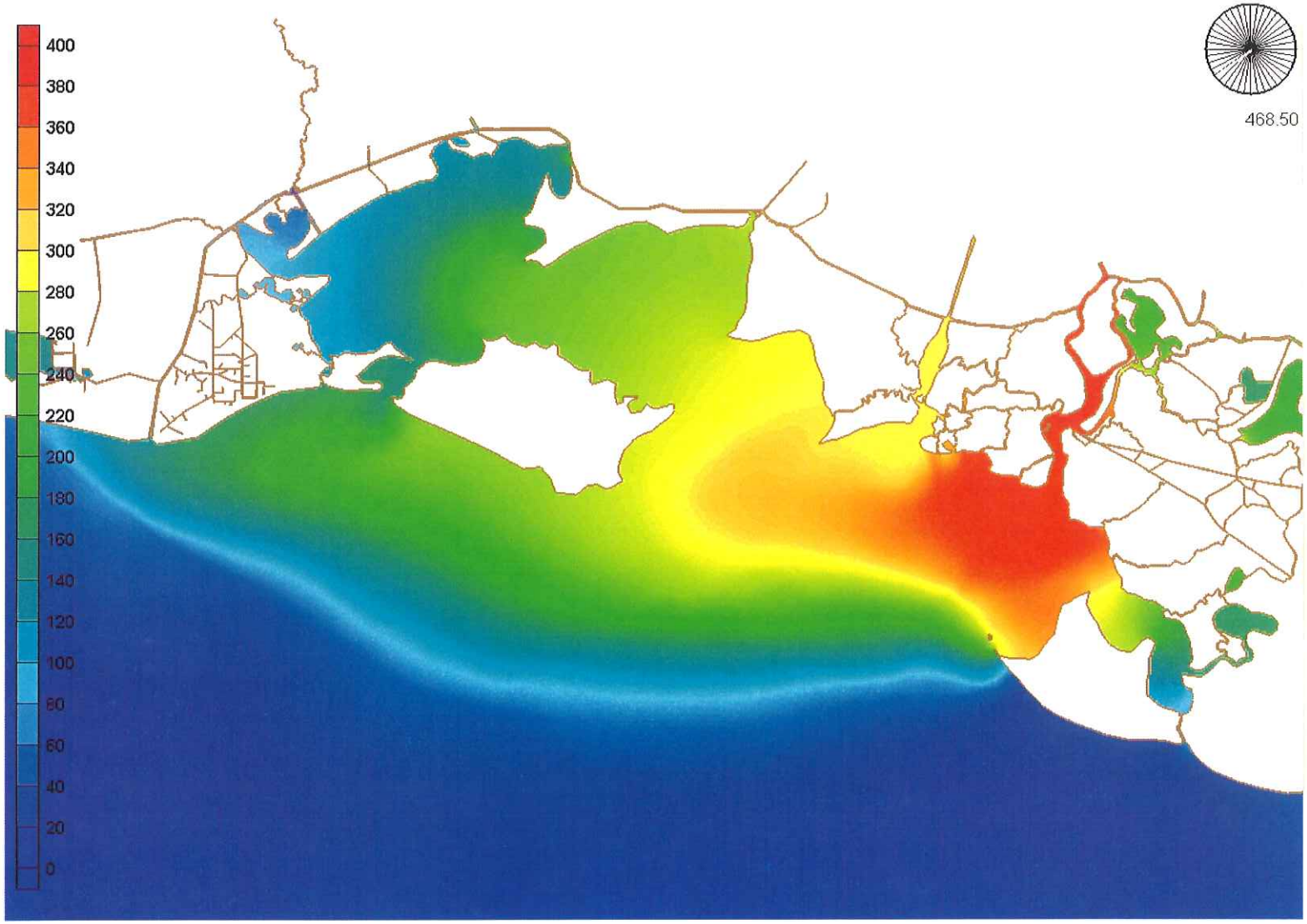

Figure 4.30 Freshwater Tracer Model with Southeast Wind

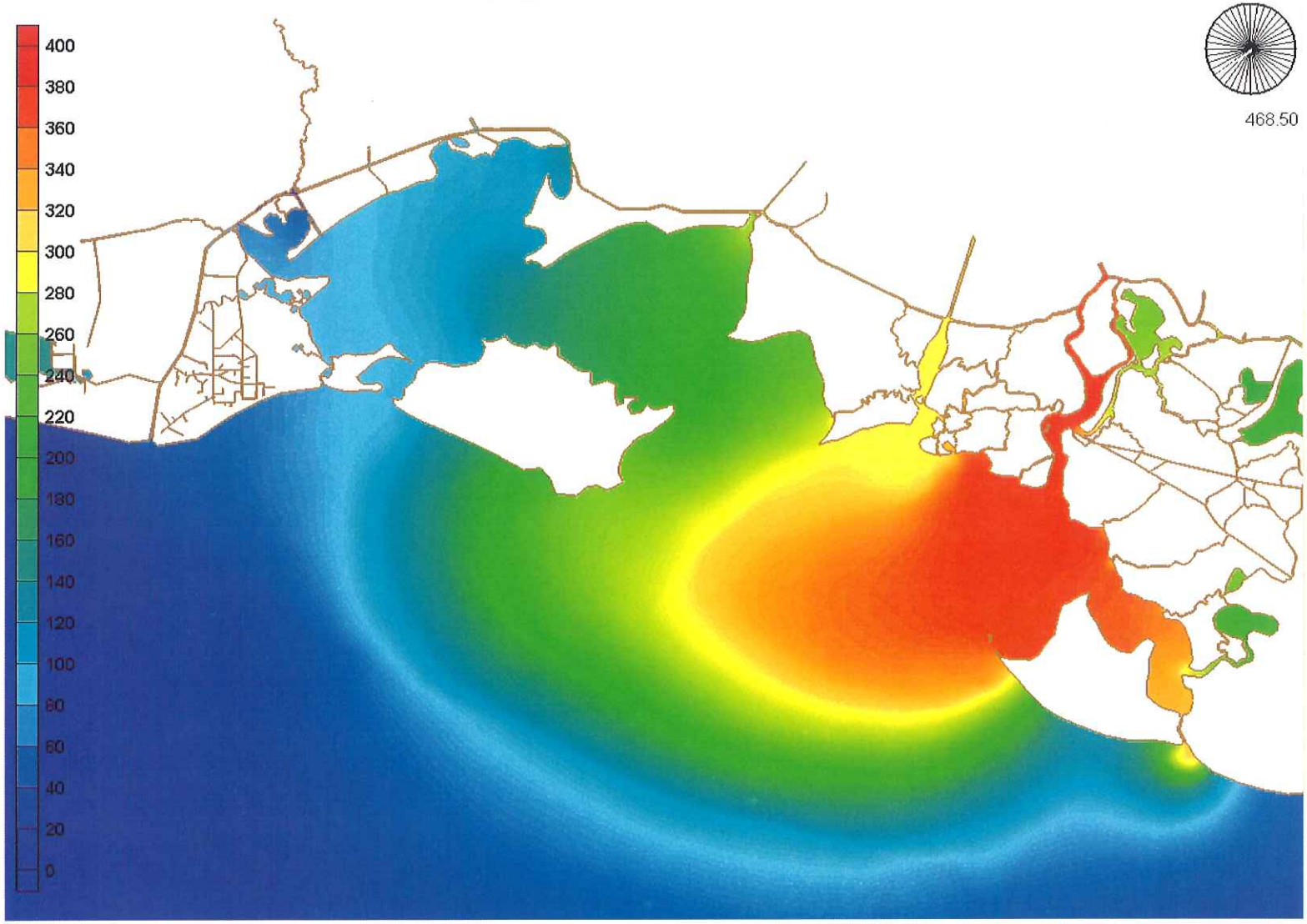

Figure 4.31 Freshwater Tracer Model with No Wind

5.0 CALIBRATION OF WAVE MODEL

5.1 A Review of Previous Wave Studies

Early studies on the Acadiana Bays and surrounding areas pertaining to coastal engineering focused on the geologic aspects of the region and the influence of the Mississippi and Atchafalaya Rivers and their modifications. Recent research focuses on the influence of wind and storm events on hydrodynamics, salinity and sediment fluxes, suspended-sediment plume extent and translation, and wave attenuation due to the soft bottom prevalent in the area. Changes to water quality within the bays and rapid loss of subaerial marsh have increased research initiatives in these areas.

Jensen (1985) describes a 1981 U.S. Army Corps of Engineers (USACE) wave study specific to Atchafalaya Bay. The report includes the only known concurrent wave measurements within Atchafalaya Bay, East Cote Blanche Bay, and West Cote Blanche Bay before 2004. Jensen (1985) states "the most puzzling feature of all the measured results, regardless of the wind and presumed direction of propagation, was the lack of high wave conditions." The maximum wave heights recorded for the three gages — labeled WG-XX in Figure 5.1 — reached 2.04 ft, 1.54 ft, and 1.82 ft [0.62 m, 0.47 m, 0.55 m] with typical wave heights (H_{mo}) from 0.5 – 0.8 ft [0.15 – 0.24 m] and periods (T_p) of 2.0 – 2.5 sec. From previous studies, regions with comparable fetch lengths and water depths show wave heights of 2 – 4 ft [0.61 – 1.22 m] with periods of 3 – 5 sec. The 1985 report concludes that part of the energy loss occurs due to wave–soft bottom interaction.

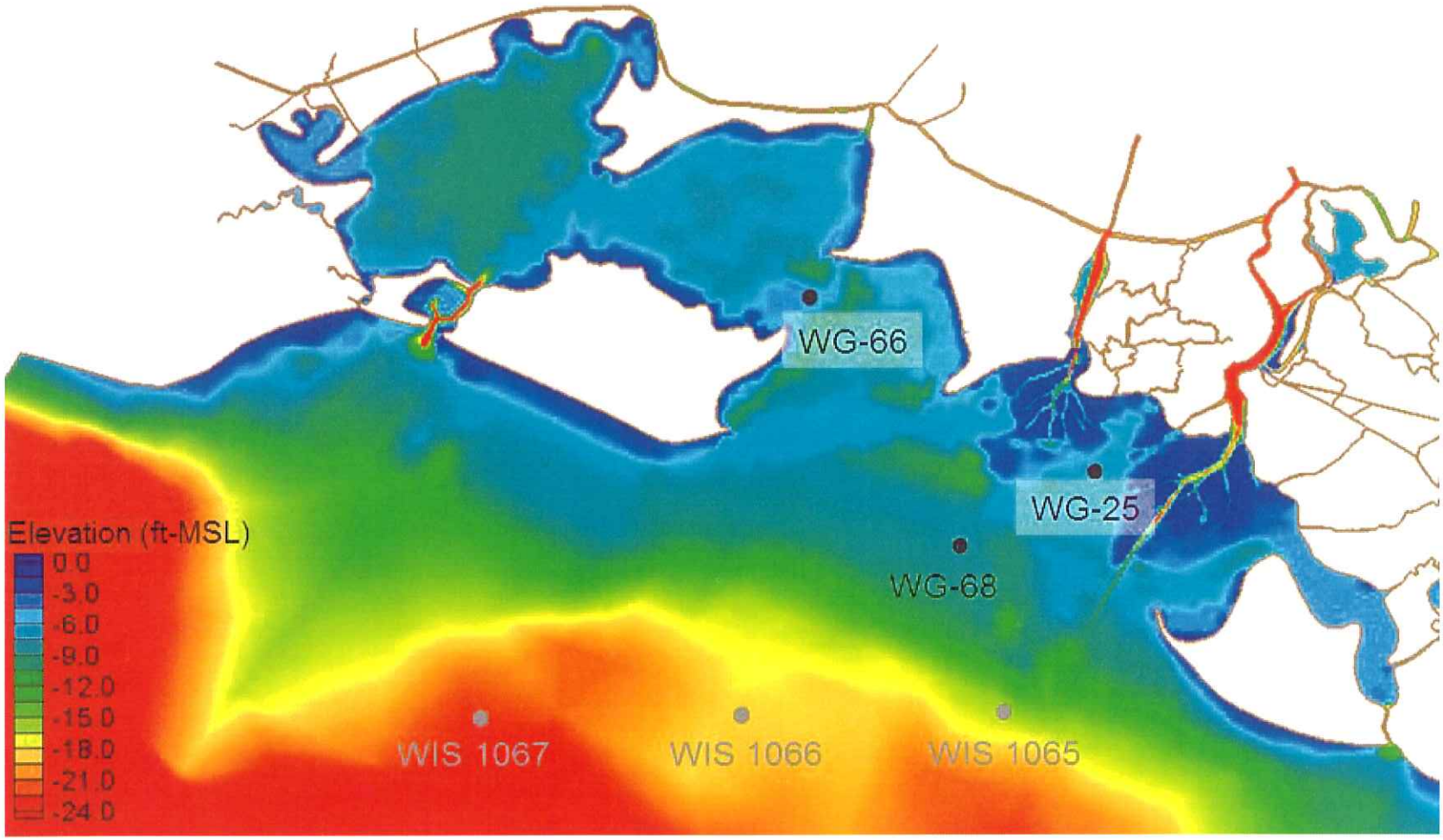

Figure 5.1 Acadiana Bays Vicinity Showing Jensen's (1985) Wave Gages and WIS Station Locations

Analysis of storm events with southerly winds indicates "very little long-period wave energy derived from Gulf-generated waves is capable of retaining a significant energy level within Atchafalaya Bay" (Jensen, 1985). Specific comparison between wave records for gages WG-68, located at the offshore edge of Atchafalaya Bay, and WG-66, located between Point Chevreuil and Marsh Island, indicates substantial energy loss between the gages. The USACE report concludes "an energy sink must exist between the two gage locations that reduces long-period wave energy while permitting short-period waves to remain unchanged in a near uniform fashion."

Though the two inshore gages show greatly reduced energy (80% reduction at WG-25 and 90% reduction at WG-66) relative to that at the offshore gage, the three gages record generally similar spectral shapes. Notably, one would expect energy losses from a linear process to cause a uniform change to the spectral shape. Energy loss due to most bottom dissipation mechanisms occur nonlinearly (Collins, 1972 as cited in Jensen, 1985). Consequently, one expects such dissipation mechanisms to change the spectral shape; this change may result in spectral energy redistribution and the formation of a new spectral peak period. As mentioned, Jensen (1985) noted preservation of spectral shapes across gages. The constant spectral shape in the gage data indicates that an exponential decay for the energy dissipation is appropriate for Acadiana Bays (Hsiao, 1978).

Other studies not specific to the Acadiana Bays region provide valuable information for coastal environments with soft bottom-wave interaction. Tubman and Suhayda (1976) provide a study of wave action over fine sediments near East Bay, Louisiana (east of the Acadiana Bays region). The study contains wave properties and bottom movement records at two locations in water depths of 63 and 17.3 ft (19.2 and 5.3 m). The results of Tubman and Suhayda indicate that energy loss due to the muddy bottom reached at least an order of magnitude greater than that resulting from either bottom percolation or bottom frictional effects. The data of Tubman and Suhayda (1976) indicate a 48% reduction in wave energy near East Bay, LA. Exponential decay with distance provides one method to describe wave energy losses in a muddy environment; Section 5.2 provides a detailed description of wave attenuation theory. Lee and Mehta (1997) applied the data of Tubman and Suhayda (1976) to calculate an exponential decay attenuation coefficient, k_i, of 0.0002 m^{-1} [0.00066 ft^{-1}]. This value provides the only known data for the wave attenuation for a location near the Acadiana Bays.

The study by Forristall and Reece (1985) contains results from an experiment measuring the attenuation of waves as they travel from deep water in the Gulf of Mexico to a relatively shallow water region near East Bay, LA. The results indicate that theoretically calculated refraction and shoaling can explain the changes in the spectra given a low wave height. "As the wave height increases, a non-linear

attenuation mechanism becomes increasingly strong" (Forristall and Reece, 1985). The attenuation was a strong function of deep-water wave height and a weak function of wave frequency.

Wells and Kemp (1986) provide a study on the interaction of surface waves and cohesive sediments. Wave data from an experiment in a muddy region off the coast of Surinam indicate an 88% loss in wave energy between two stations located 6.8 miles (11 km) apart. The study found 96% energy loss after the waves traveled an additional 4.3 miles (7 km). The final water depth equaled 4.9 ft (1.5 m). While the authors give no wave attenuation results for locations near Louisiana, they state that in southwestern Louisiana, shrimpers often take refuge during storms in waters over localized accumulations of fluid mud; they do so, presumably, to take advantage of wave attenuation caused by the fluid mud.

Sheremet and Stone (2003a) present a study on the wave dissipation caused by regions with different bottom sediment on the inner Louisiana Shelf along the West Louisiana coast. The study contains data from WAVCIS, a coastal observing system of the Coastal Studies Institute at Louisiana State University. Wave propagation during a cold front passage was monitored at two WAVCIS stations with one station (CSI-5) in a sandy sedimentary environment and the other (CSI-3) in a muddy environment; both stations were located at the 16.4 ft (5 m) depth contour. The attenuation of the swell at CSI-3 (the muddy site) exceeded in variance by an order of magnitude the attenuation at CSI-5 (the sandy environment). At sea frequencies ($f > 0.2$ hz) the wave energy at CSI-3 decreases significantly as the wind forcing drops; this drop does not occur at CSI-5. This indicates a dissipation mechanism for low period wave energy — possibly increased viscosity due to sediment resuspension — in the muddy environment that is not present in the sandy environment.

In conclusion, the above discussion indicates that wave modeling of the Acadiana Bays vicinity should consider the dissipation effects of the muddy bottom in attenuating wave heights in the study area. The following section briefly reviews existing theory on wave attenuation due to soft beds.

5.2 Wave Attenuation Theory

Dalrymple and Liu (1978) present a theory for the propagation of small amplitude linear waves in a two-layered viscous system with laminar flow in both layers. The model results compare well with the experimental results of Gade (1958). The results of Dalrymple and Liu indicate significant wave attenuation rates when the thickness of the lower (mud) layer approaches the same order as the internal boundary layer thickness, and for a thick lower layer.

Jiang and Mehta (1996) develop a relationship between progressive water waves and a dissipative bottom mud represented as a standard solid viscoelastic continuum. The model requires the dynamic viscosity, elastic moduli (two values), density, and depth of the mud. The authors cite the works of Mathew (1992) and Mathew et al. (1995) that demonstrate an 85% reduction in the wave energy over a fluid mud bank (thickness of 3.28 ft [1 m]) off the coast of India for two stations approximately 0.5 miles (0.8 km) apart (depths of 32.8 and 16.4 ft [10 and 5 m]). The same two stations recorded minimal wave energy dissipation in the absence of a mud bank. Jiang (1993) contains the formulation for a wave attenuation model valid over a mud bottom represented as a standard linear solid. The wave attenuation model compares well with the data of Mathew (1992).

The USACE Coastal Engineering Manual (CEM) provides some guidance on wave propagation in areas with soft bottoms, specifically fluid mud. In such areas, "the predominant mechanism of wave attenuation is the thick, viscous boundary layer of fluid mud" (Lee, 1995). The CEM cites the formulation of Lee (1995) and Lee and Mehta (1994) to describe an exponential decay model for wave heights across a muddy profile

$$H = H_0 e^{-k_i x} \tag{5.1}$$

where x equals the distance along the wave ray towards shore, H_o equals the incident wave height, H equals the wave height at distance x, and k_i equals the wave height attenuation coefficient (m^{-1}). The wave height attenuation coefficient relates to the bed rheology and wave characteristics and usually acts as a tuning parameter. Lee (1995) gives values of k_i in the range of $0.0001 \leq k_i \leq 0.05\ m^{-1}$. Dalrymple and Liu (1978) also present the wave damping equation (Eq. 5.1); however their two-layer fluid model determines their value of k_i. Mehta and Jiang (1996) refer to this type of exponential decay with distance and cite the experimental verification by Maa and Mehta (1987).

The presence of fluid mud at the bottom also results in a change in the wavelength — the effective water depth increases when a layer of fluid mud exists below the elevation of the prescribed bottom. The increased water depth leads to longer wavelengths through the dispersion relationship for the two-layer system. However, the change in wavelength due to the wave-fluid mud interaction is relatively small compared to the effect of the increased depth attributed to the fluid mud. Referencing Wehausen and Laitone (1960), Rodriquez (2000) states that "the fluid mud layer has only a minor effect on the wave number, and that the main influence of the mud layer is on wave damping." In an example where the water depth equals the fluid mud depth (3 ft), Rodriquez (2000) demonstrates that including the extra depth of the fluid mud increases the wavelength by approximately 20 to 30% for wave periods from 4 to

16 seconds (s). However, the process of fluid-mud interaction only changes the wavelength approximately 4 – 7% for the same wave periods.

The concept of a fixed water depth proves much less applicable in muddy environments than in sandy environments. In areas with soft bottoms, wave forcing induces the development of a fluid mud layer. Assuming that area sediments remain temporally and spatially uniform, the depth of the fluid mud layer at any time depends on the wave height, wave period, and water depth. Therefore, the water depth and fluid mud depth constantly change under changing wave conditions. Measured water depths depend on the surveying technique as well as the wave conditions during the measurement. The low viscosity of the fluid mud layer may lead to different surveying techniques giving different depth values as the surveying method, i.e. rod versus acoustic methods, may or may not "feel" the fluid mud layer. That the reported depth values indicate a value between the water depth from the free surface to the top or the bottom of the fluid mud layer is a reasonable assumption. Thus, even traditional wave analysis methods that disregard soft bottom effects but use water depths derived from a surveying technique recording a portion of the fluid mud layer in its reported depth should capture some of the fluid mud's effect on wavelength. This study considers the effect of the change in wavelength secondary to the change in wave height caused by the mud.

5.3 Modifications to STWAVE

Bottom friction, bottom percolation, and viscous bottom effects represent some of the physical processes at the seafloor capable of wave energy dissipation and attenuation. One may apply standard linear wave theory to modify STWAVE and describe the effects of bottom friction and percolation (Dr. W.R. Dally, Surfbreak Engineering and Sciences — personal communication). However, in this study, the effects of these two mechanisms are assumed secondary compared to the effects of a muddy bottom that comprises the majority of the Acadiana Bays region.

To model wave-mud interaction, the exponential wave decay function, with a wave attenuation coefficient k_i (cited in the CEM), was judged suitable for incorporation into STWAVE. The scarcity of detailed geotechnical data for the cohesive sediments in the region and the requirement of these sediment parameters in Dalrymple and Liu (1978) and Jiang and Mehta (1996) models (described in the previous section) preclude the effective use of solutions dependent on multiple sediment characteristics. General sediment characteristics such as sediment type (Coastal Environments, 1977), fall velocity (Teeter and Pankow, 1989), and grain size distribution (Pankow et al., 1990) exist for some or all of the study area. However, specific cohesive sediment geotechnical characteristics determined through extensive testing

such as critical shear stress for erosion and deposition, erosion rate constant, elastic modulus, and consolidation characteristics are not known to exist.

Therefore, wave attenuation with a single attenuation coefficient, such as in Equation 5.1, proves preferable to more complex models with many sediment characteristics unknown for the Acadiana Bays sediments. The model depth values do not add the depth of the mud layer, as the mud layer depth remains unknown; therefore, with this method the wave number does not change due to the mud.

The development of the wave attenuation by mud dissipation concept for STWAVE occurred in the following manner based on the theory presented in Section 5.2. The method employs the wave height definition of Equation 5.1 with the notion that spatially uniform rate of wave energy dissipation (per unit bed area) is attributable to viscous dissipation due to wave-induced motion of the soft bottom material (Lee, 1995). For steady state conditions, dissipation balances the gradient of the energy flux in the direction of wave propagation (x):

$$\frac{d\left(EC_g\right)}{dx} = \overline{\varepsilon}_d \tag{5.2}$$

where E equals the wave energy, C_g represents the surface wave's group velocity and $\overline{\varepsilon}_d$ represents the rate of wave-averaged energy dissipation (per unit bed area). One may develop an expression for the energy dissipation across a single STWAVE grid with the wave height described by Equation 5.1 and with the assumption of locally uniform depth conditions. Using the parameter definitions of STWAVE, the energy loss due to mud dissipation

$$\overline{\varepsilon}_d = \frac{C_g}{dx} E\left[1 - \left(e^{-k_i dx}\right)^2\right] \tag{5.3}$$

where dx equals the grid element width and t represents a characteristic time dependent on the wave travel speed across the grid cell (Resio, 1988).

To simulate the effects of dissipation by muddy bottoms, the Equation 5.3 formulation was included in the public domain version of STWAVE. The new version of STWAVE with wave attenuation by mud dissipation, termed STWAVE Taylor, must undergo rigorous calibration and verification with wave data within the region to ensure the validity of the model. The following sections describe this process.

5.4 Calibration Data Sources

Historical wave data within the five bays that comprise Acadiana Bays prove limited. LSU collected additional, although limited, data as part of this study to supplement existing data. The paragraphs below describe both historical and recent data.

Jensen (1985) contains the only known wave measurements in the five bays before 2004. The study contains wave data records at three locations beginning in the fall of 1981 and continuing for approximately one year with spectral wave properties (H_{mo} and T_p) recorded every three hours. The report contains tables of wave height, wave period, wind speed, and wind direction for over 10 storms including both northerly and southerly storms.

Jensen's (1985) report only considered locally generated waves in its analysis. This study applied hindcast wave information from the USACE Wave Information Study (WIS) to account for wave energy propagating into the Acadiana Bays region from the Gulf of Mexico. WIS stations 1065, 1066, and 1067 lie offshore the Acadiana Bays region at a water depth near 20 ft and provide data from 1976 to 1995.

The WAVCIS (wavcis.csi.lsu.edu) program encompasses a wave information system developed and maintained by the Coastal Studies Institute (CSI) at Louisiana State University. As of November 2005, the system comprised five stations with the first installed in the spring of 2000. CSI installed gage CSI-14 within the East Cote Blanche Bay for this study. CSI plans to install eight more stations, which will cover the entire coast of Louisiana. The stations generally record the wave height and spectral characteristics, period, direction of propagation, water level, surge, current velocity profile meteorological conditions on a real time basis; however, each station does not record all the above listed parameters. The WAVCIS system provides nearshore wave data for the coast of Louisiana. This data was unavailable before 2000 when the closest gage locations were over 100 miles away from the Acadiana Bays region. (National Data Buoy Center stations — NDBC 42040, NDBC 42001, and NDBC 42041).

The WAVCIS stations closest to the Acadiana Bays region are stations CSI-3 and CSI-14; however, CSI-14 came on-line following much of this study's wave modeling work. CSI-3 lies in 15 ft of water and south of Vermilion Bay approximately 15 miles from Marsh Island. Sheremet and Stone (2003b) report the bottom sediment near CSI-3 contains mostly cohesive mud. CSI-14 lies in 10 ft of water in East Cote Blanche Bay.

Three WAVCIS stations (CSI-6, CSI-5, and CSI-11) lie in the Terrebonne Bay region approximately 31 miles east of Four League Bay. Bottom sediments in the region near CSI-6 and CSI-5 consist mainly of non-cohesive, sandy material (Sheremet and Stone, 2003b). The locations of stations CSI-6 and CSI-5 — along a shore-perpendicular transect surrounded by generally straight and parallel bottom contours — provide an opportunity for local wave transformation analysis with STWAVE. Station CSI-11 lies within Terrebonne Bay, shoreward of two barrier islands near the Houma Navigation Channel outlet and in an area of muddy bed sediment characteristics. Appendix A contains wave modeling results at these locations from additional testing of the STWAVE Taylor model developed in this study.

5.5 Calibration Procedures and Results

To calibrate the STWAVE model in the Acadiana Bays region, model predictions were compared to the data of Jensen (1985). Selected southerly and northerly storms from the USACE study provided the input wind speed and directions. For southerly events the wave model also applied WIS data — from Station 1065 — for wave height, period, and direction of the Gulf-generated waves entering the model domain.

To approximate the bathymetric conditions of the Jensen (1985) study, this study used bathymetric data digitized from 1982 NOAA Nautical Charts (11349, Vermilion Bay and Approaches; 11351, Point au Fer to Marsh Island; 11352, Intracoastal Waterway New Orleans to Calcasieu River East Section). Data collected as part of this study and those provided by Dr. Joe Letter (see Chapter 4) supplemented the NOAA data.

The historic oyster shell reefs located in the Acadiana Bays region remain on the 1982 NOAA charts (and the 2003 charts) for the region despite evidence of dredging over 30 years ago. When encountering the shell reef in the nautical chart, the digitizing procedure selected a value similar to the depth on each side of the reef, in effect removing the reef. The paucity of historic bathymetry data for the entire region and rapid bathymetric changes due to the high sediment influx into the region require such measures to best recreate the bathymetry at the time of the 1981 USACE study (Jensen, 1985). Differences between the published water depths of the wave gages and tide stations listed in Jensen (1985) and the depths at those locations on the Letter mesh indicated changes in the bathymetry (Table 5.1). Generally, the depths digitized from the 1982 NOAA charts lie closer to the Jensen (1985) data than do the values of the Letter mesh. All comparisons of the STWAVE simulations with the Jensen (1985)

wave height data apply bathymetry almost entirely from the NOAA charts; the Letter mesh only provides data to fill gaps in the NOAA chart data.

Table 5.1 Water Depth Comparison for Different Locations and Sources

	Jensen (1985) USACE Data			Letter Mesh	1982 NOAA Chart	Comparisons	
	Latitude	Longitude	Depth	Depth	Digitized Depth	Letter Mesh - USACE Data	NOAA Chart - USACE Data
Wave Gage	(deg)	(deg)	(ft)	(ft)	(ft)	(ft)	(ft)
WG 25	29.45	91.41	9.5	5.8	6.7	-3.7	-2.8
WG 68	29.39	91.54	10.0	7.4	7.6	-2.6	-2.4
WG 66	29.60	91.68	11.0	4.0	11.2	-7.0	0.2
Tide Station							
1	29.35	91.41	5.5	6.5	5.3	1.0	-0.2
4	29.45	91.69	6.0	7.2	6.1	1.2	0.1
5	29.51	91.60	3.0	8.4	2.6	5.4	-0.4
7	29.69	91.74	7.0	6.6	7.8	-0.4	0.8
8	29.67	91.87	6.0	6.0	7.3	0.0	1.3
9	29.68	92.03	8.0	9.0	9.0	1.0	1.0
10	29.77	91.93	8.0	9.0	9.0	1.0	1.0

In addition to calibrating to Jensen's (1985) data, this study also evaluated model predictions for the conditions of Hurricane Rita, a severe storm which affected the study area in 2005. For this evaluation, the model applies the existing conditions bathymetry described in Chapter 4 along with water level, wind, and wave data from gages CSI-3 and CSI-14.

5.5.1 Southerly Storms

Applying the appropriate input conditions and bathymetry to the STWAVE models allows comparison to the wave data of the 1981 USACE Study. The following plots present STWAVE results from three versions of STWAVE: (1) the original code that excludes bottom friction (STWAVE Original); (2) an STWAVE model that accounts for turbulent bottom boundary layer effects developed by Dr. Bill Dally of Surfbreak Engineering Sciences (STWAVE Surfbreak); and (3) an STWAVE model developed in this study that accounts for viscous dissipation with an exponential decay function (STWAVE Taylor).

Figure 5.2 presents the STWAVE grid applied for the modeling with storms from the south. The grid contains 1,300 elements in the cross-shore and longshore directions with equal grid spacing of 114.8 ft (35 m) in both directions. The offshore boundary lies at the approximate location of the WIS stations closest to the Acadiana Bays. Figure 5.3 presents the wave height and wave period measured at WIS

Station 1065 for "Southerly Storm 3"; the data show wave heights exceeding 6 ft and periods representative of swell waves. Figure 5.4 presents the wind conditions from WIS Station 1065 for the period of record for "Southerly Storm 3" of the 1981 USACE study.

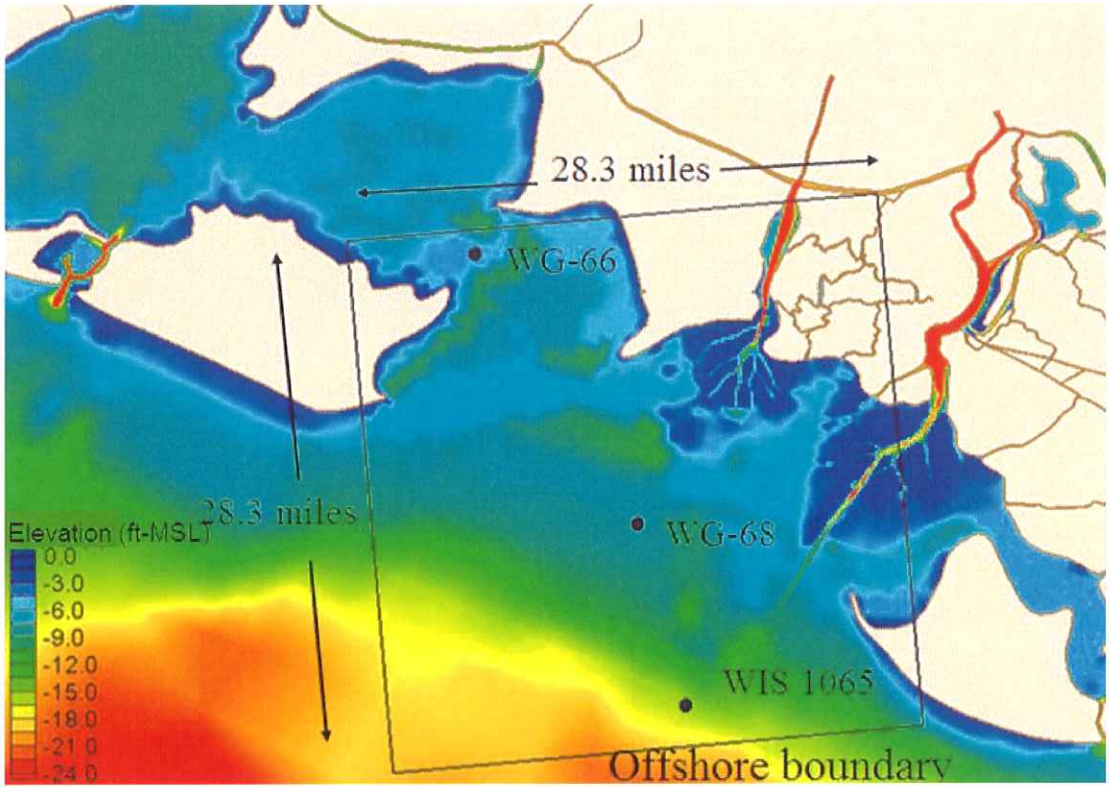

Figure 5.2 STWAVE Grid for Southerly Storm 1 with Jensen (1985) Gage Locations

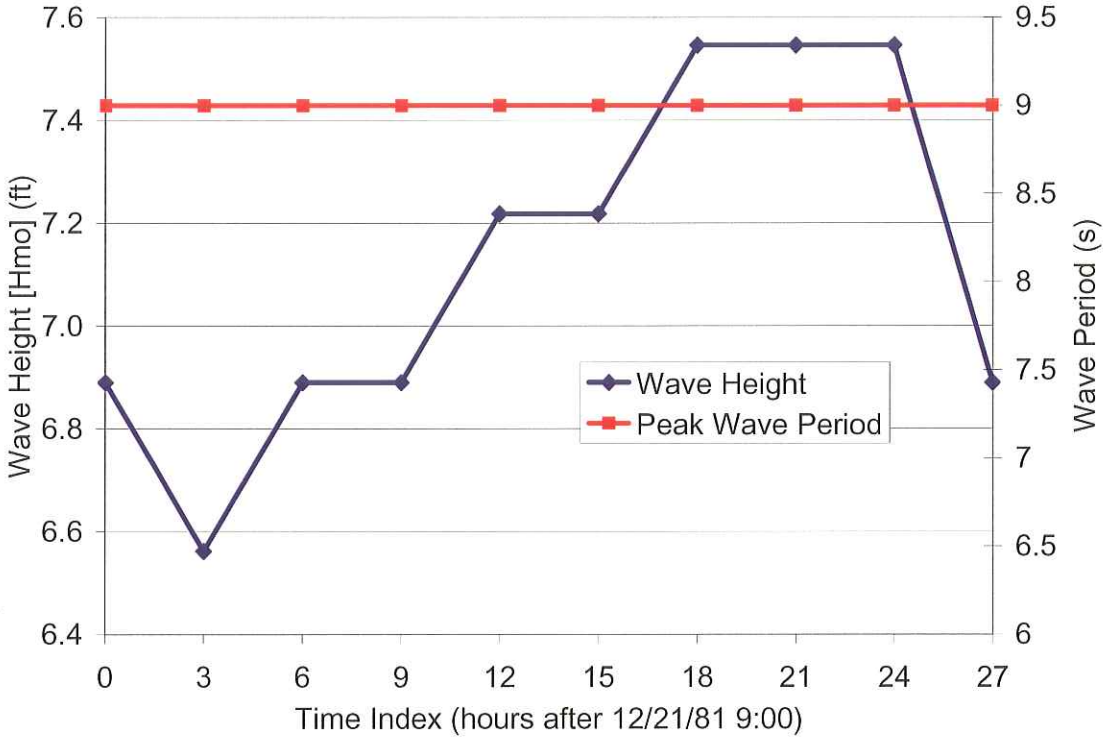

Figure 5.3 WIS Station 1065 Wave Record for Southerly Storm 3

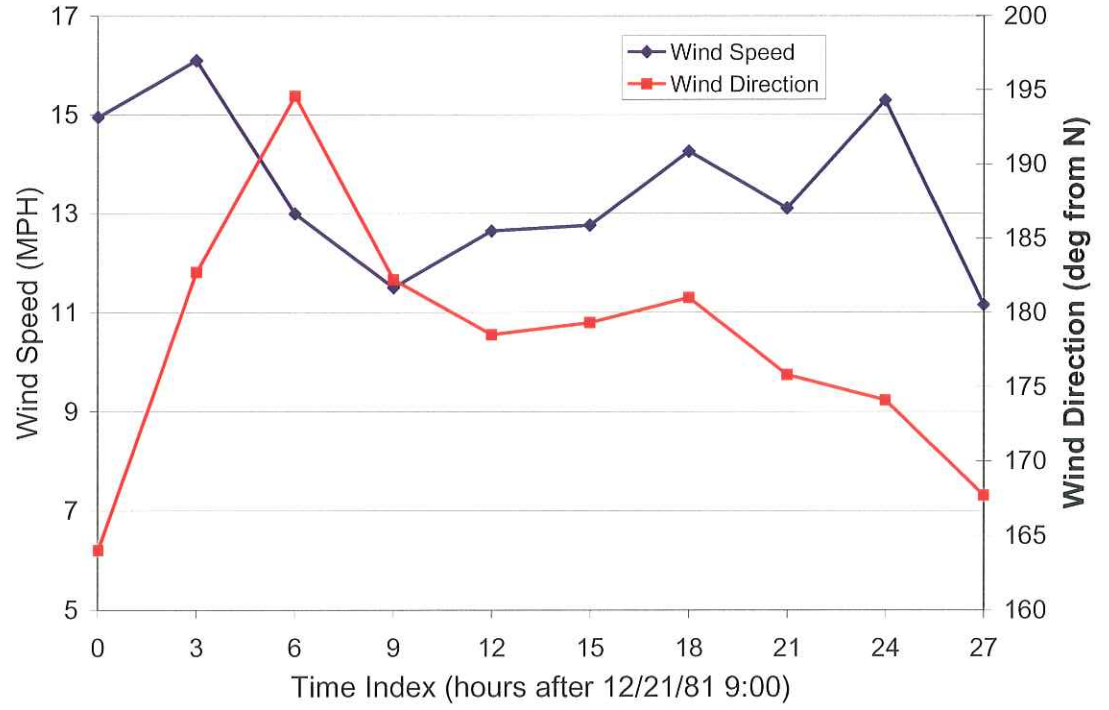

Figure 5.4 WIS Station 1065 Wind Record for Southerly Storm 3

Figures 5.5 through 5.8 present comparisons of the STWAVE models for Southerly Storm 3 at wave gage WG-68 — the most offshore gage — for input conditions including the Gulf of Mexico generated swell and wind conditions. Each figure shows two STWAVE Taylor models ($k_i = 0.0001\ m^{-1}$ and $k_i = 0.0005\ m^{-1}$) to investigate the sensitivity of the mud dissipation to the attenuation coefficient, and to locate a value applicable to the conditions in the Acadiana Bays. Figures 5.9 through 5.12 present comparisons of STWAVE models for Southerly Storm 3 at wave gage WG-66 — stationed at the entrance to West Cote Blanche Bay. This report presents no analysis of the modeling results at WG-25 due to the proximity of wave gage WG-25 to the Lower Atchafalaya River and Wax Lake Outlet deltas and the lack of accurate bathymetric data for this area characterized by rapid shoaling.

Figures 5.5 and 5.9 present the measured and modeled wave heights as a time series showing the value every three hours for a 27-hour record, while Figures 5.6 and 5.10 present an average height value at those locations — with the standard deviation shown with error bars. STWAVE models steady-state conditions; therefore, the wind duration does not limit the waves, and for a set of input parameters the wave heights develop with no reference to time. This presents some issues when results compare a steady state wave model to wave height data recorded every three hours. In an ideal case, one would track a single wave from one gage to another, and track the wave transformation. In the field, this proves difficult as many individual waves comprise the wave field. Thus, for a generally steady wave field, one may apply a method of averaging the wave values over the period of record to compare the recorded results to the modeled results.

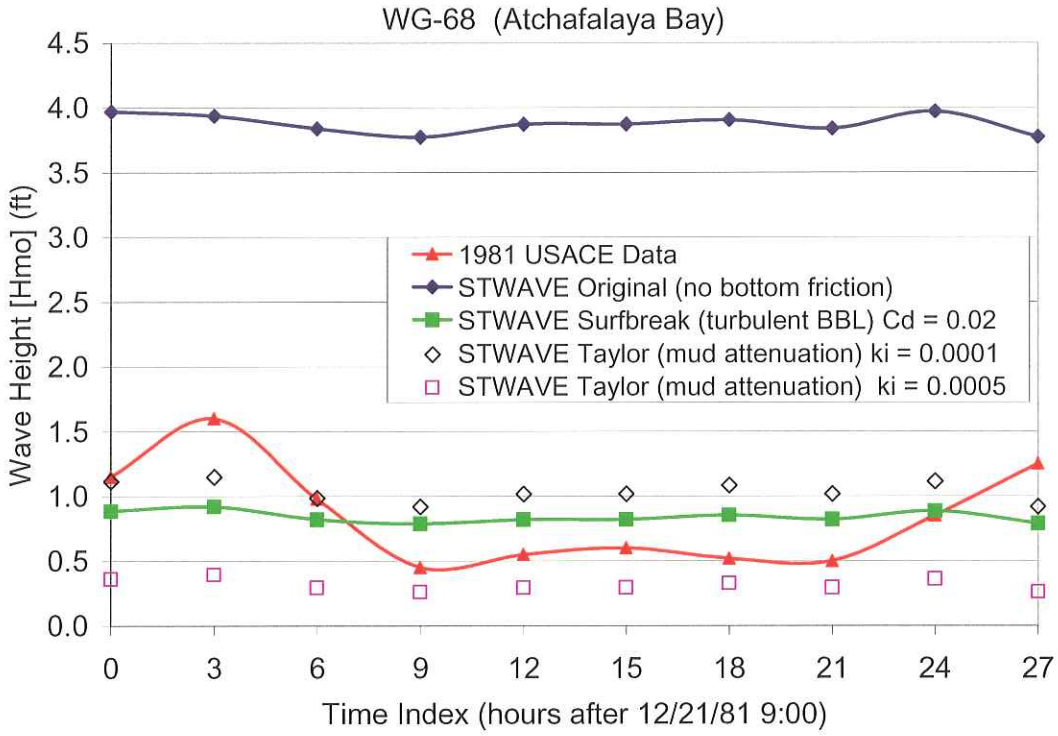

Figure 5.5 Wave Height Record Comparison at WG-68 for Southerly Storm 3

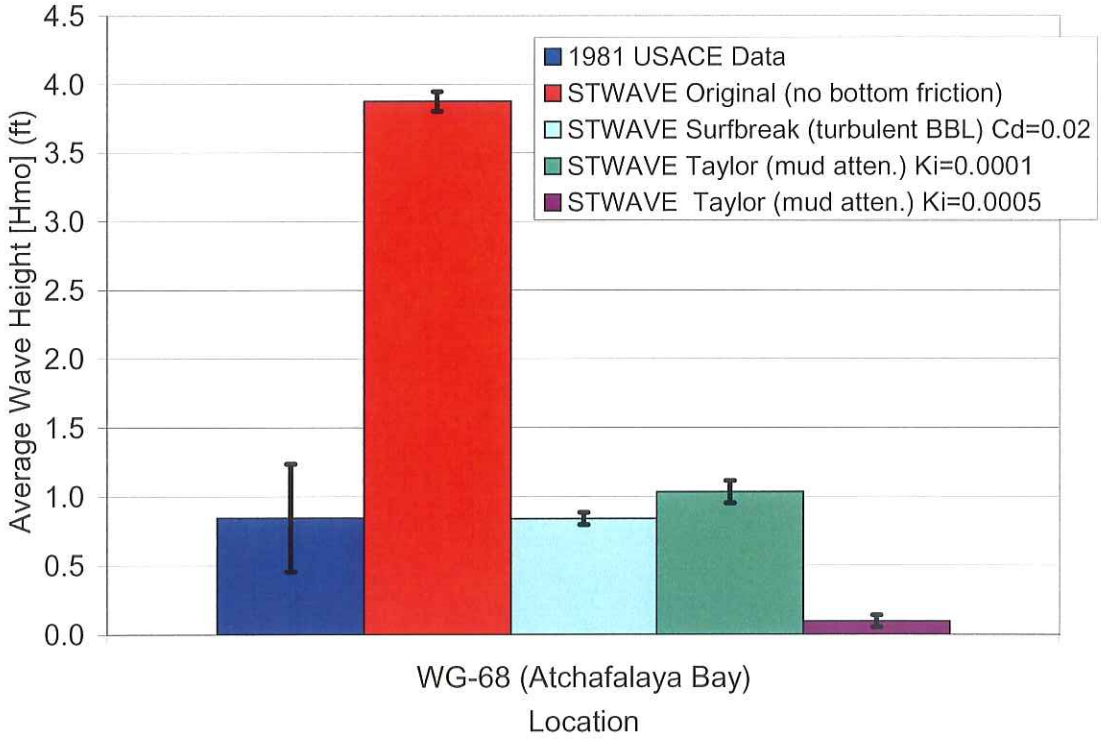

Figure 5.6 Wave Height Averages Comparison at WG-68 for Southerly Storm 3

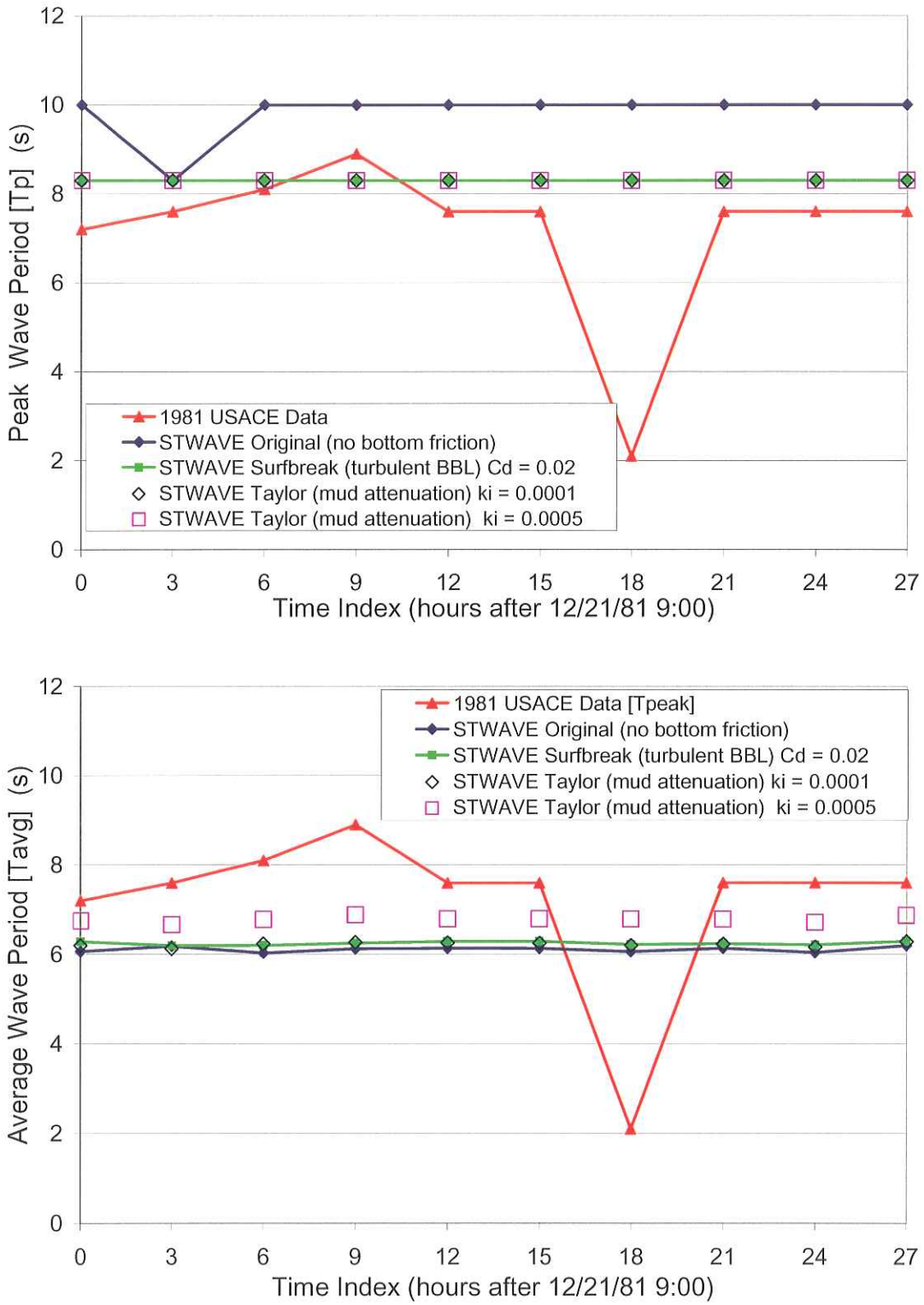

Figure 5.7 Wave Period Record Comparisons at WG-68 for Southerly Storm 3: Peak Period (top) and Average Period (bottom)

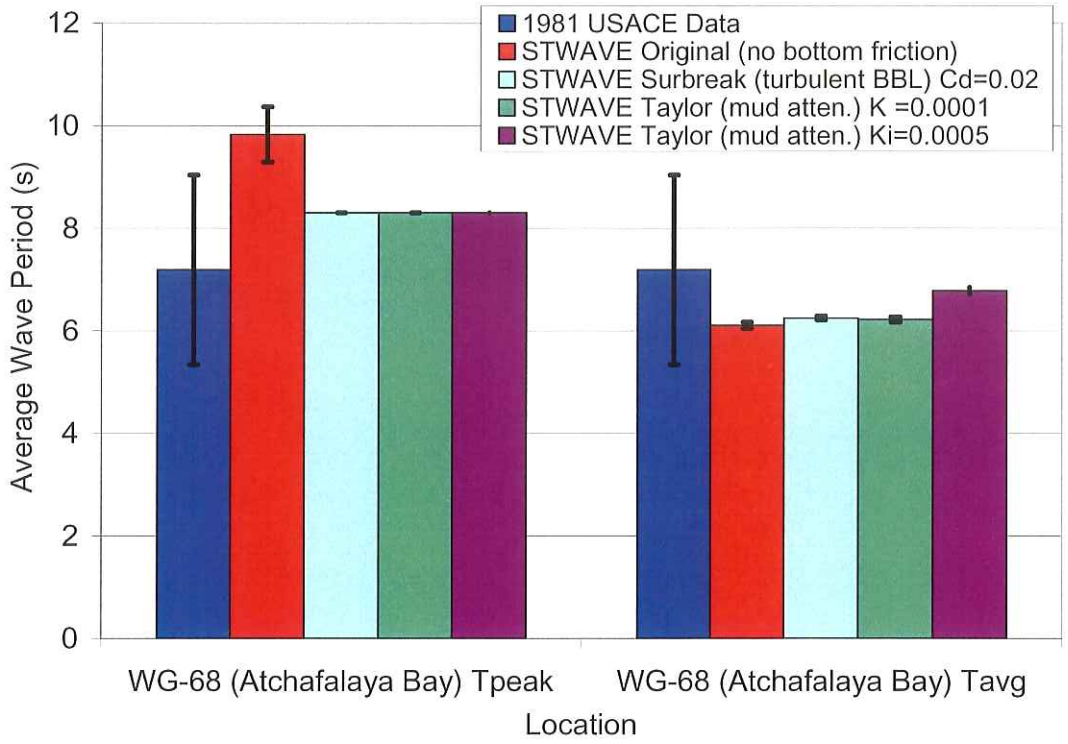

Figure 5.8 Wave Period Averages Comparison at WG-68 for Southerly Storm 3

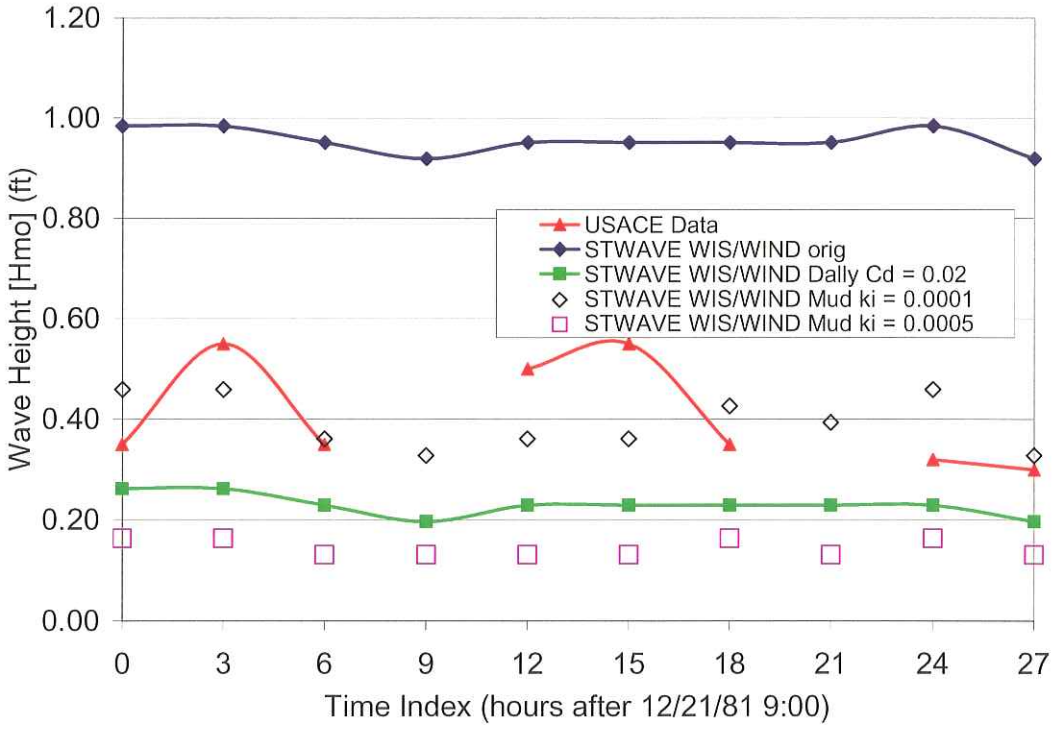

Figure 5.9 Wave Height Record Comparison at WG-66 for Southerly Storm 3

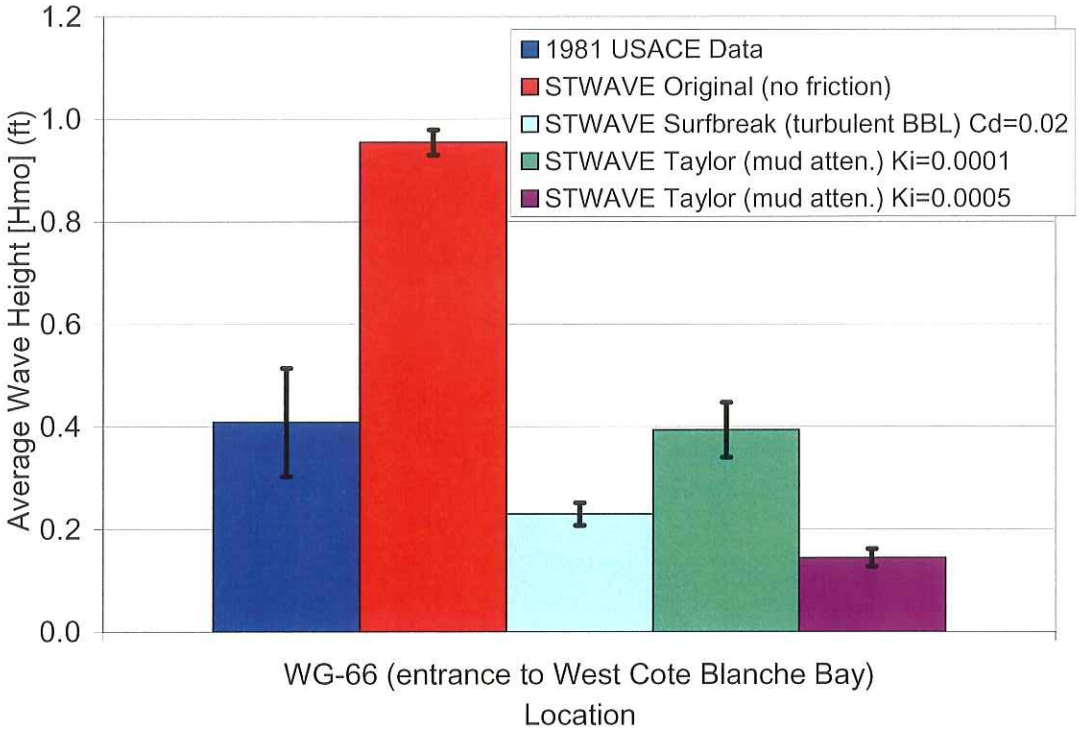

Figure 5.10 Wave Height Averages Comparison at WG-66 for Southerly Storm 3

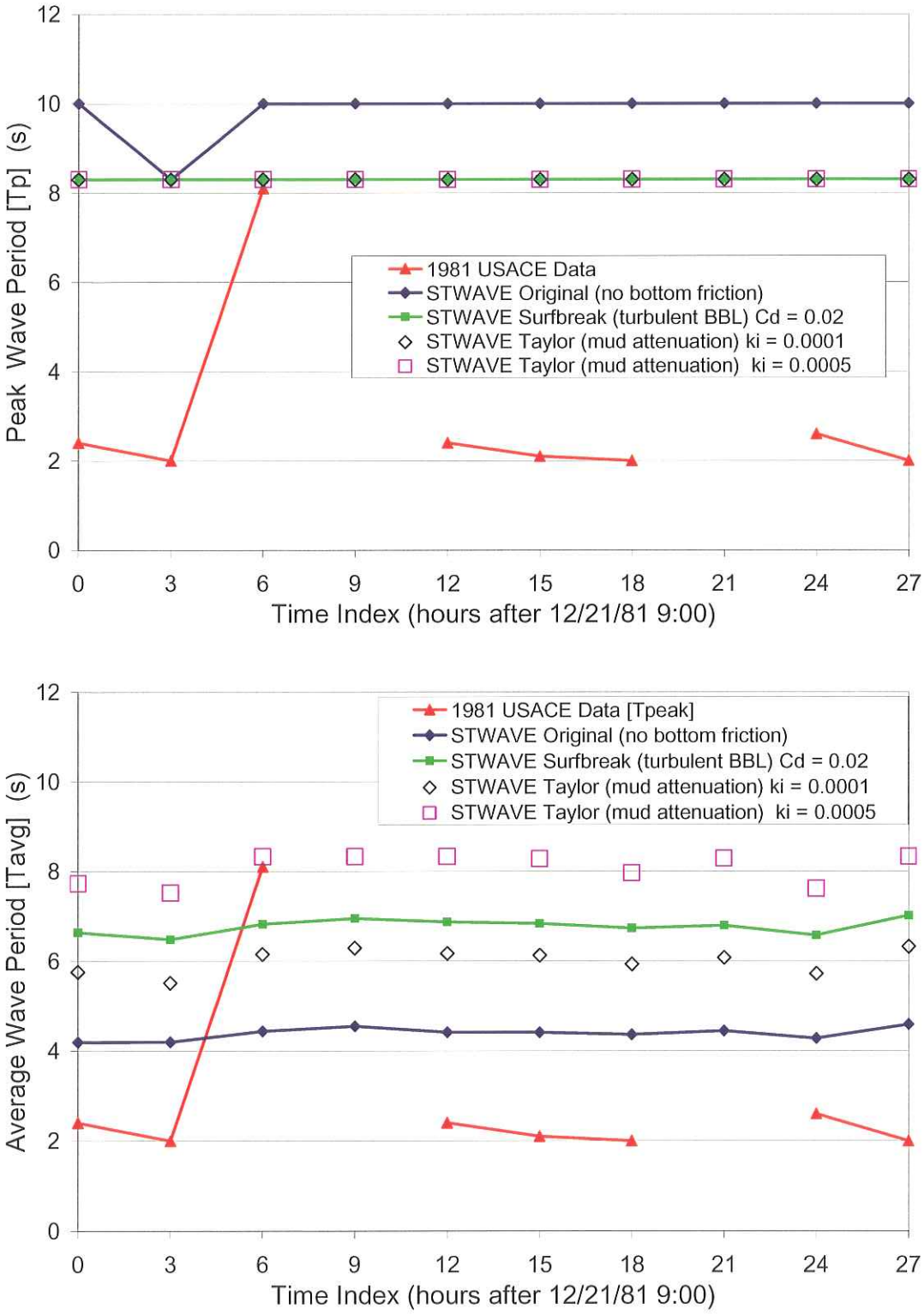

Figure 5.11 Wave Period Record Comparison at WG-66 for Southerly Storm 3: Peak Period (top) and Average Period (bottom)

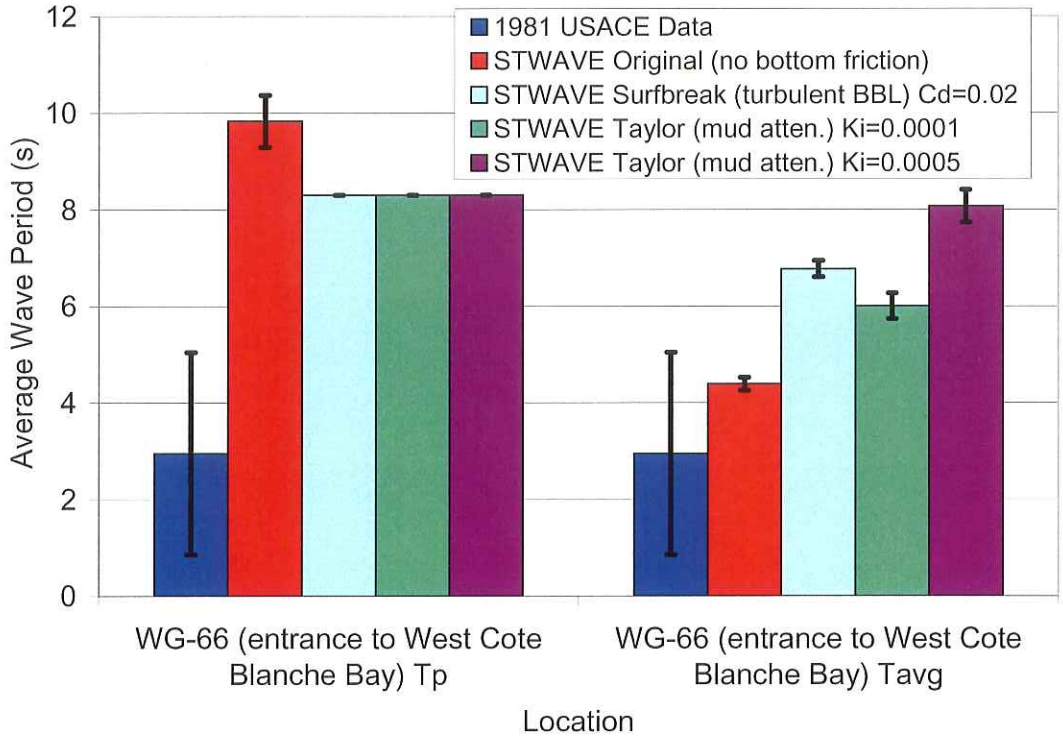

Figure 5.12 Wave Period Averages Comparison at WG-66 for Southerly Storm 3

The results demonstrate the need to include some form of bottom dissipation when the input wave conditions include the Gulf-generated waves present in a southerly storm. At both WG-68 and WG-66 the wave height simulated by STWAVE Original severely overestimates the measured wave heights. At WG-68, both STWAVE Surfbreak and STWAVE Taylor (k_i = 0.0001 m^{-1}) have average wave heights that almost match the measured values, while at WG-66 the STWAVE Surfbreak model underestimates the measured wave height. The STWAVE Taylor (k_i = 0.0001 m^{-1}) nearly matches the measured wave height. For this and all other cases, the STWAVE Taylor model with larger k_i values (i.e., 0.0005 m^{-1}) induced excessive wave dissipation.

Figures 5.7 and 5.11 present the time series for the measured wave period reported by Jensen (1985) for Southerly Storm 3. These figures also show the peak, T_p, and average, T_{avg}, periods simulated by STWAVE. Figures 5.8 and 5.12 show the integrated wave period results for the peak and average wave periods. Wave attenuation by bottom dissipation within the bays can result in wave spectra with two significant peaks (Jensen, 1985). Wave spectra with two significant peaks (i.e., a bichromatic spectra) can contain dramatic switching of the peak period. The period parameter reported by Jensen (1985) indicates

switching of the peak period from a swell condition ($T_p \sim 7$ s) that suggests Gulf-generated waves, to a sea condition ($T_p \sim 3$ s) indicative of locally generated wind waves. The switching of the peak period occurs when the energies in the sea and swell bands of the spectra are similar, and slight changes to either result in one band becoming larger than the other band. This situation can lead to difficulty when a model requires a single wave value to define a spectrum for further analysis. Calculation of an average wave period provides another view of the wave period conditions with the average wave period defined as:

$$T_{avg} = \frac{m_{0f}}{m_{1f}} \tag{5.4}$$

$$m_j = \int_0^\infty f^j S(f) df \tag{5.5}$$

where S equals the energy spectra in terms of frequency integrated over direction.

The wave period records for Southerly Storm 3 demonstrate the fluctuations between sea-dominated and swell-dominated environments. The large error bars for 1981 USACE data in Figures 5.8 and 5.12 illustrate this condition. The plots of the average wave period values indicate that at WG-68, the simulated peak period overestimates the measurements by over 2 s, while the average wave period underestimates the period by less than 1 s. At WG-66 the simulated peak period overestimates the measurements by over 5 s, while the average wave period overestimates the period by approximately 3 s.

The results suggest good agreement between measured data and wave height simulations when the STWAVE model incorporates bottom dissipation into the simulations. Wave period simulations, although not as good, are reasonable. The STWAVE Taylor model with $k_i = 0.0001$ appears best suited to model waves in Acadiana Bays.

5.5.2 Northerly Storm 1

Jensen (1985) also presents measured values for storms from the north or northwest. Figure 5.13 contains the STWAVE grid applied for this modeling. The grid consists of 1,900 elements in the cross-shore and 1,300 elements in longshore directions with equal spacing of 114.8 ft (35 m) in both directions. Figure 5.14 presents the measured wind speed and direction for "Northerly Storm 1." When modeling this storm, this study assumes only wind-generated waves exist in the model domain. The half-plane limitation of STWAVE requires the assumption that no swell enters the region from the Gulf.

Figures 5.15 and 5.16 present three-hourly, 27-hour time series of measured and modeled wave heights at WG-68 (the most offshore gage) and WG-66 (stationed at the entrance to West Cote Blanche Bay). Figure 5.17 presents comparisons of wave height for STWAVE Original, STWAVE Surfbreak, and STWAVE Taylor for Northerly Storm 1 at wave gages WG-68 and WG-66. Figures 5.18 and 5.19 present wave period comparisons for the three STWAVE models for Northerly Storm 1 at wave gage WG-68 and WG-66.

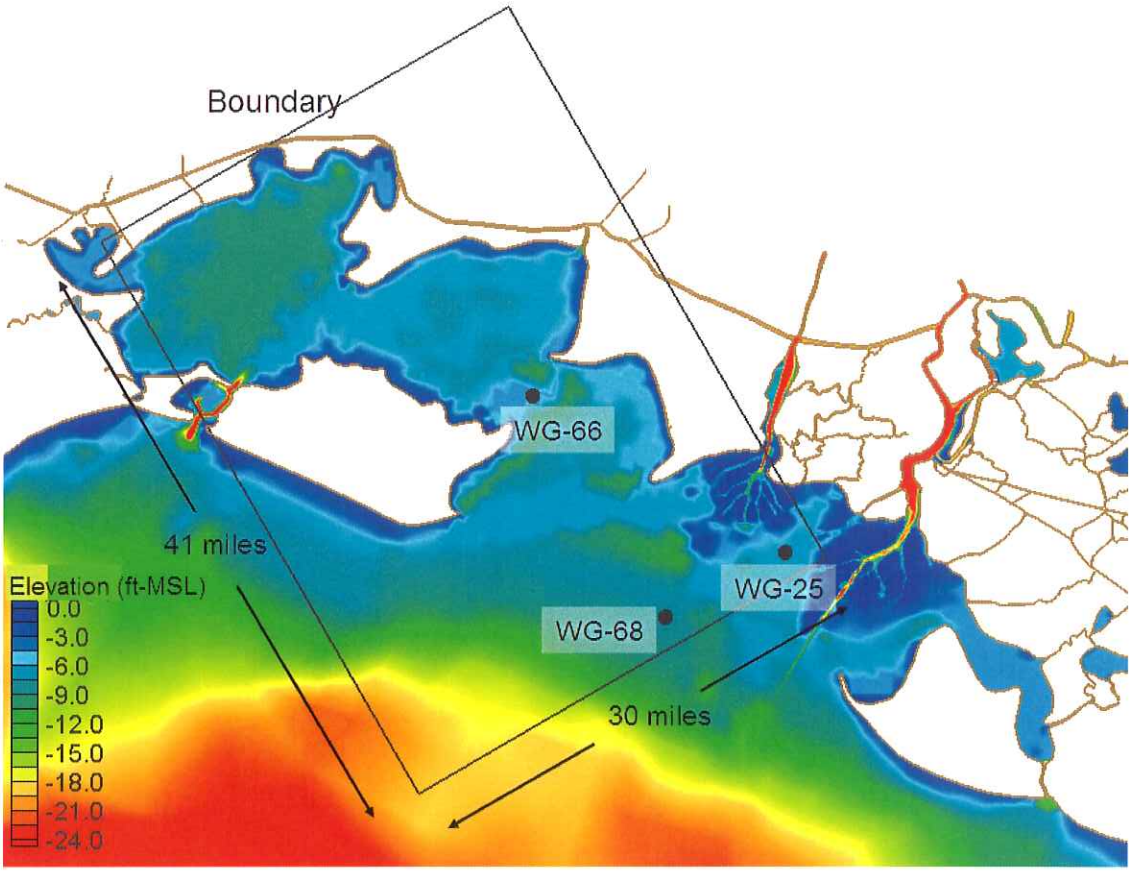

Figure 5.13 STWAVE Grid for Northerly Storm 1 with Jensen (1985) Gage Locations

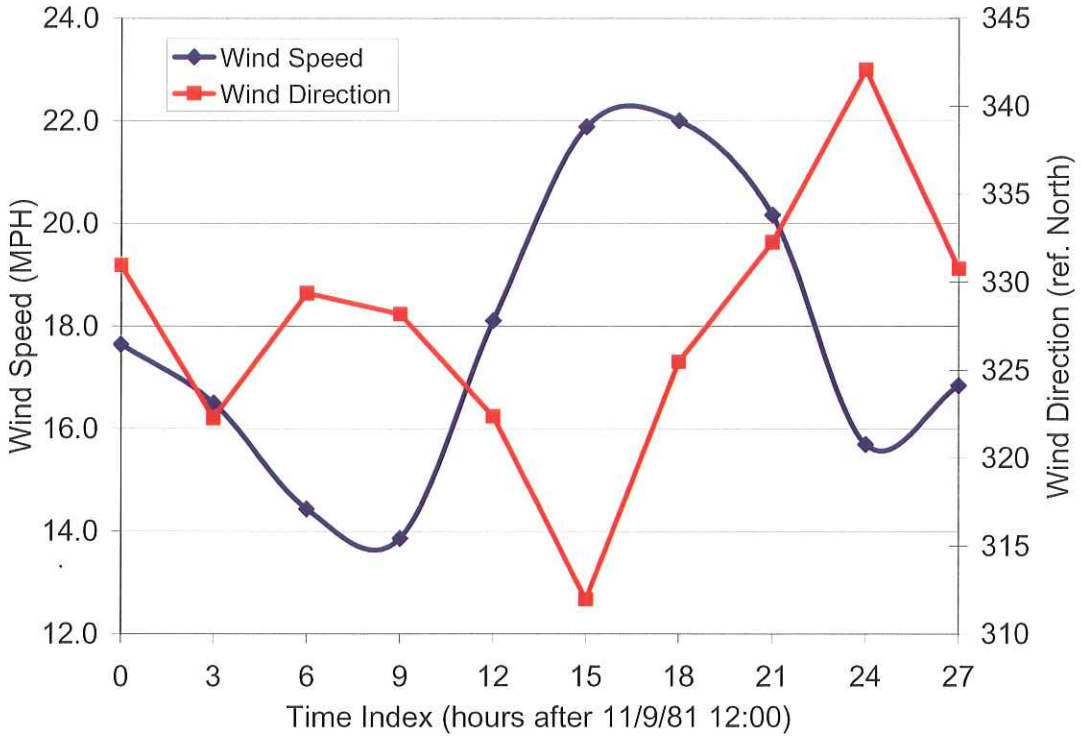

Figure 5.14 Jensen (1985) Wind Speed and Direction Record for Northerly Storm 1

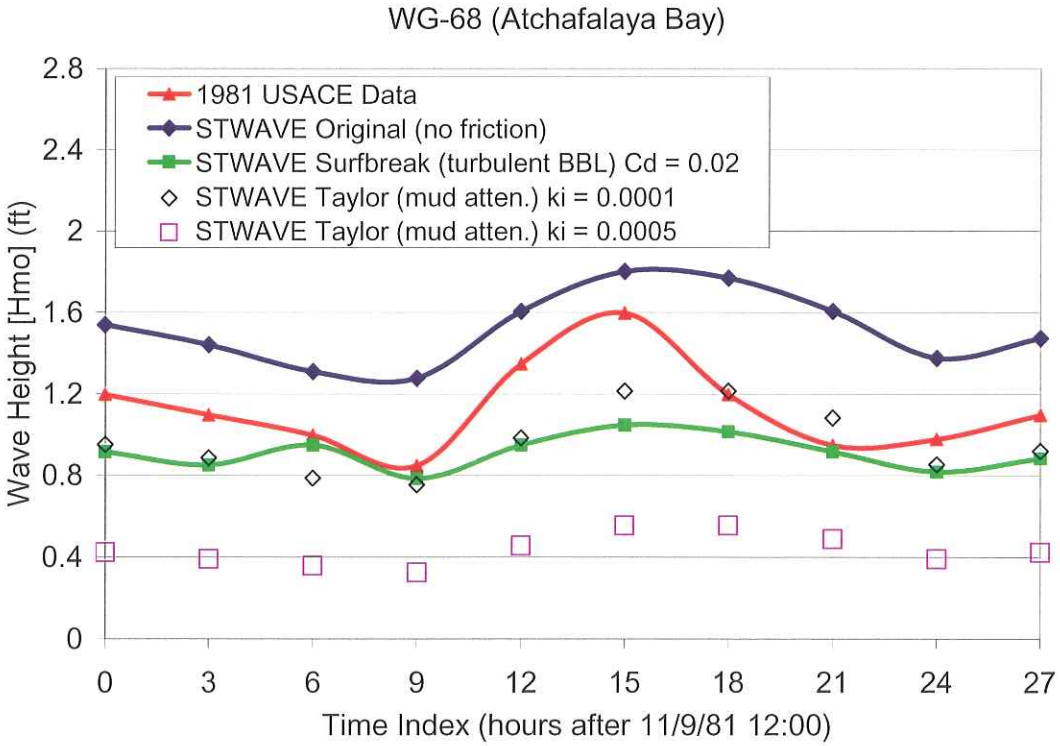

Figure 5.15 Wave Height Record Comparisons at WG-68 for Northerly Storm 1

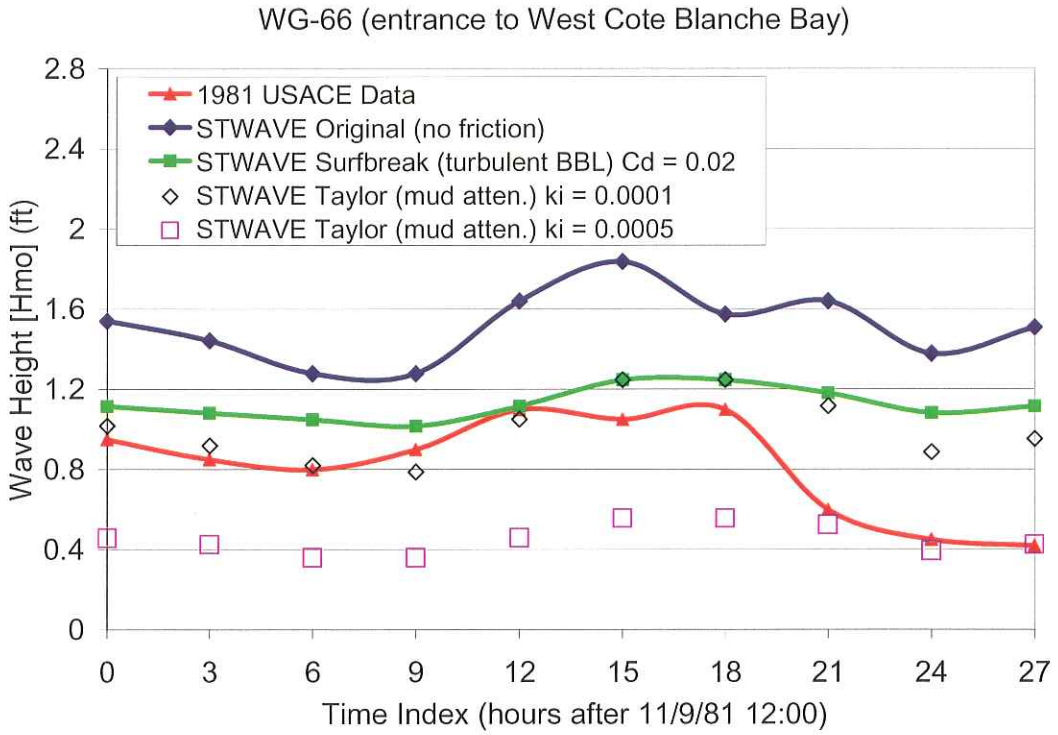

Figure 5.16 Wave Height Record Comparison at WG-66 for Northerly Storm 1

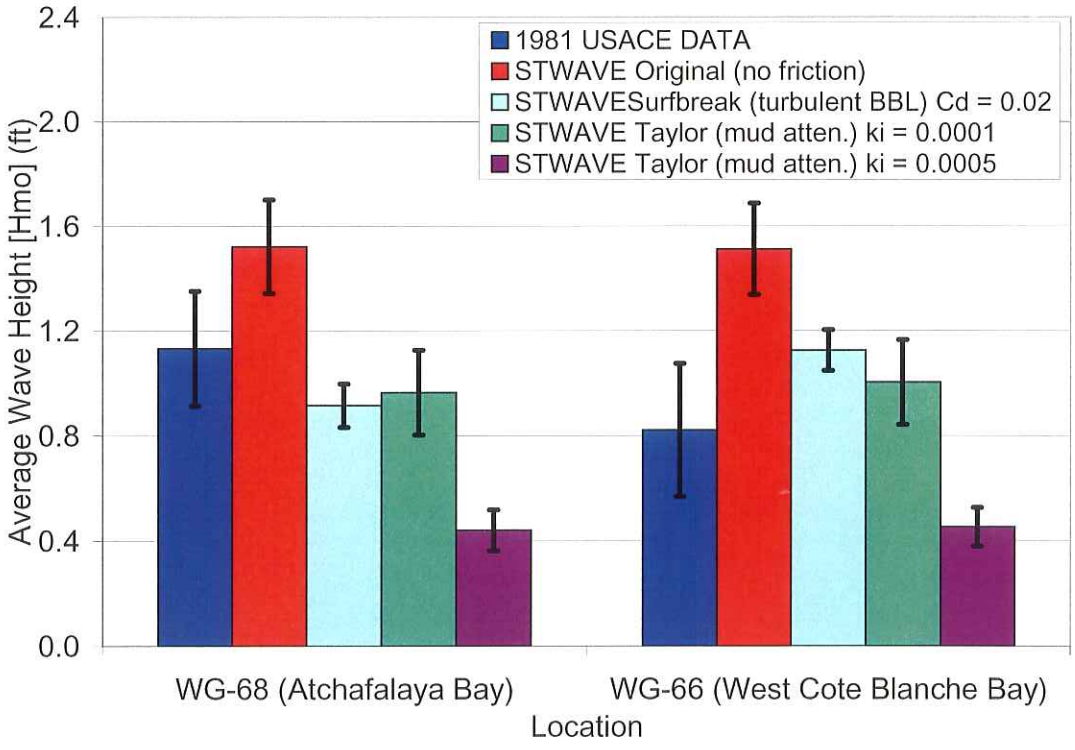

Figure 5.17 Wave Height Averages Comparison at WG-68 and WG-66 for Northerly Storm 1

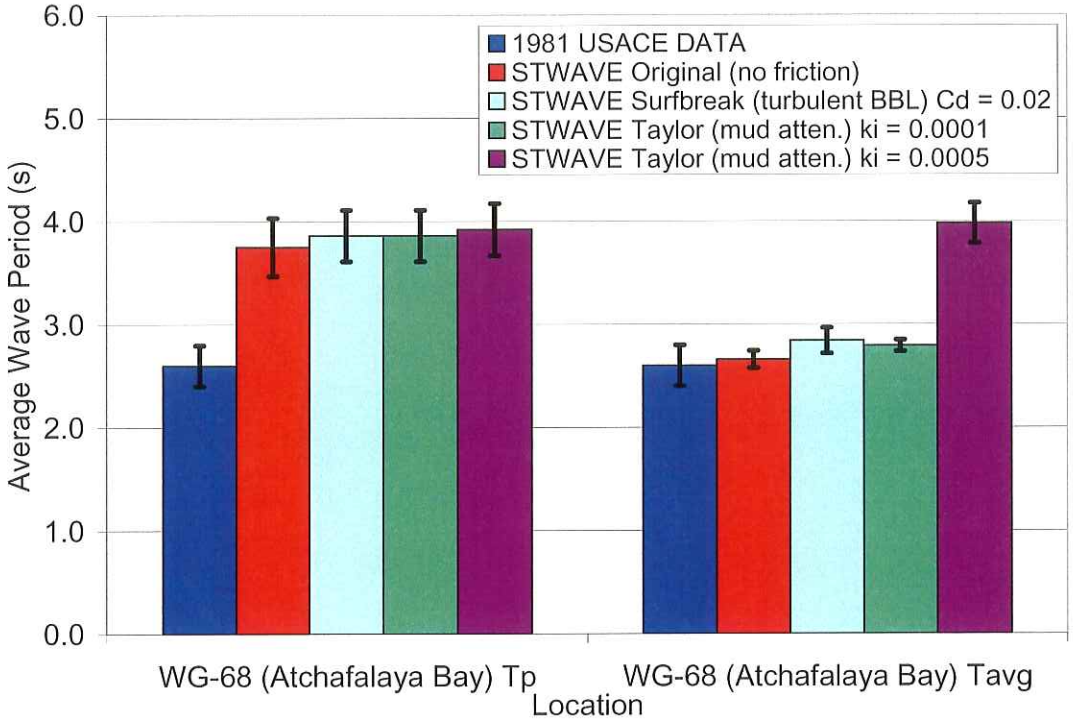

Figure 5.18 Wave Period Averages Comparison at WG-68 for Northerly Storm 1

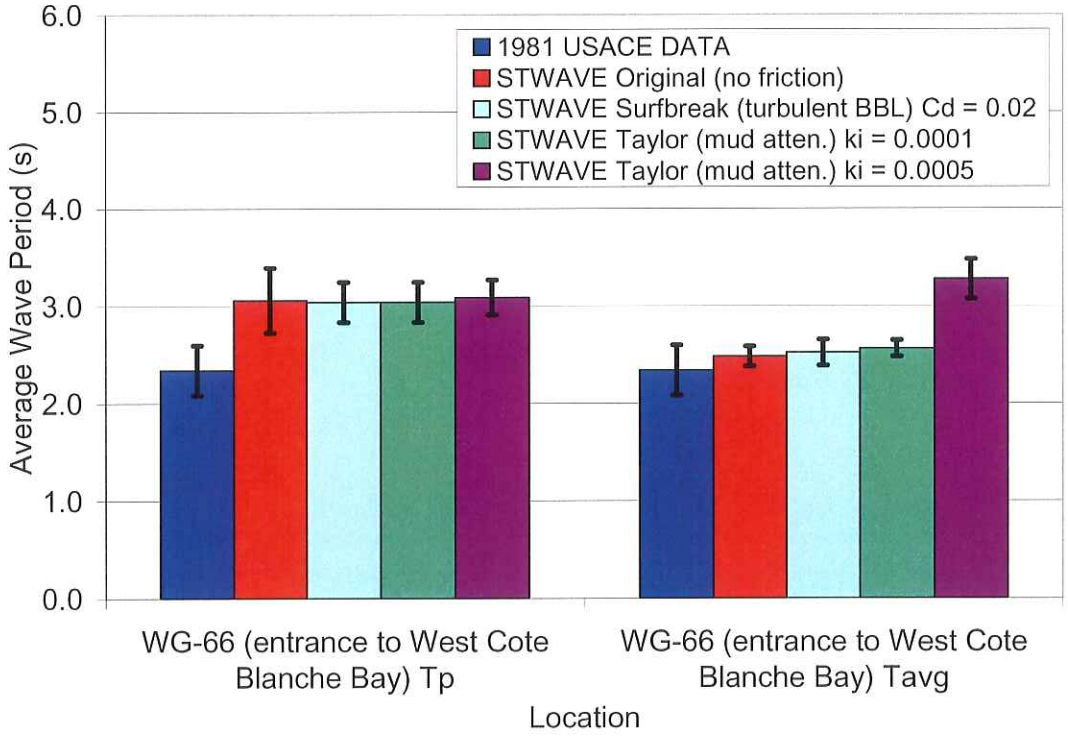

Figure 5.19 Wave Period Averages Comparison at WG-66 for Northerly Storm 1

The results for Northerly Storm 1 verify the need for some form of bottom dissipation within the wave model for high frequency storms, even for this case of only wind-generated waves. At both WG-68 and WG-66, STWAVE Original over estimates the average wave heights, while STWAVE Surfbreak and STWAVE Taylor provide average values much closer to those measured. The wave period results indicate that at both WG-68 and WG-66, the modeled peak period values overestimate those measured, while the average periods match those measured reasonably well.

5.5.3 Locally Generated Conditions

The Northerly Storm 1 comparison between the STWAVE models and the 1981 USACE study includes only locally-generated wind waves as long period swell cannot enter the bays from the north. For storms that approach from the south, long period (swell) waves generated in the Gulf of Mexico can theoretically enter Atchafalaya Bay and propagate to other bays in the region. The Jensen (1985) study did not include these Gulf-generated waves in its analysis based on its hypothesis that while swell waves generated in the Gulf exist at the entrance to Atchafalaya Bay, they are "limited in number of occurrences and also in the amount of energy they contain." To test whether swell energy from the Gulf penetrates Acadiana Bays, this study next modeled Southerly Storm 3 to compare simulations for two conditions: (a) both local winds and the wave energy recorded by WIS Station 1065 as boundary conditions (termed *WIS plus wind*) and (b) only local winds as the boundary condition (termed *wind only*).

Figure 5.20 shows the average wave height at Station WG-68 for the case of *WIS plus wind* input and for the case of *wind only* input. Figure 5.20 demonstrates that, even with *wind only* input, excluding bottom dissipation leads the STWAVE Original model to overestimate wave height at WG-68. A mud attenuation coefficient of k_i =0.0001 m^{-1} provides a good fit with the 1981 USACE measurements reported by Jensen (1985). Figure 5.21 presents the average wave period at Station WG-68 for the case of *WIS plus wind* input and for the case of *wind only* input. Applying a *wind only* condition results in simulated average wave periods much smaller than those measured. The larger measured wave periods suggest the measurements include some influence from Gulf-generated long period swell waves. Figures 5.22 and 5.23 contain information for WG-66 similar to those in the two previous figures. Figure 5.22 demonstrates that, even with *wind only* input, excluding bottom dissipation leads the STWAVE Original model to overestimate wave height at WG-66. Surprisingly, the *WIS plus wind* simulated wave heights smaller than the *wind only* wave heights; some form of destructive interference caused by non-coincident wind and wave propagation angles may explain this result. The inconclusive results at WG-66 do not resolve the issue whether modeling wave climate inside Acadiana Bays requires offshore swell data. For the STWAVE Taylor model with k_i =0.0001 m^{-1}, the *WIS plus wind* simulations of wave height are

superior to the *wind only* simulations; however, the *WIS plus wind* simulations of wave period are inferior to the *wind only* simulations.

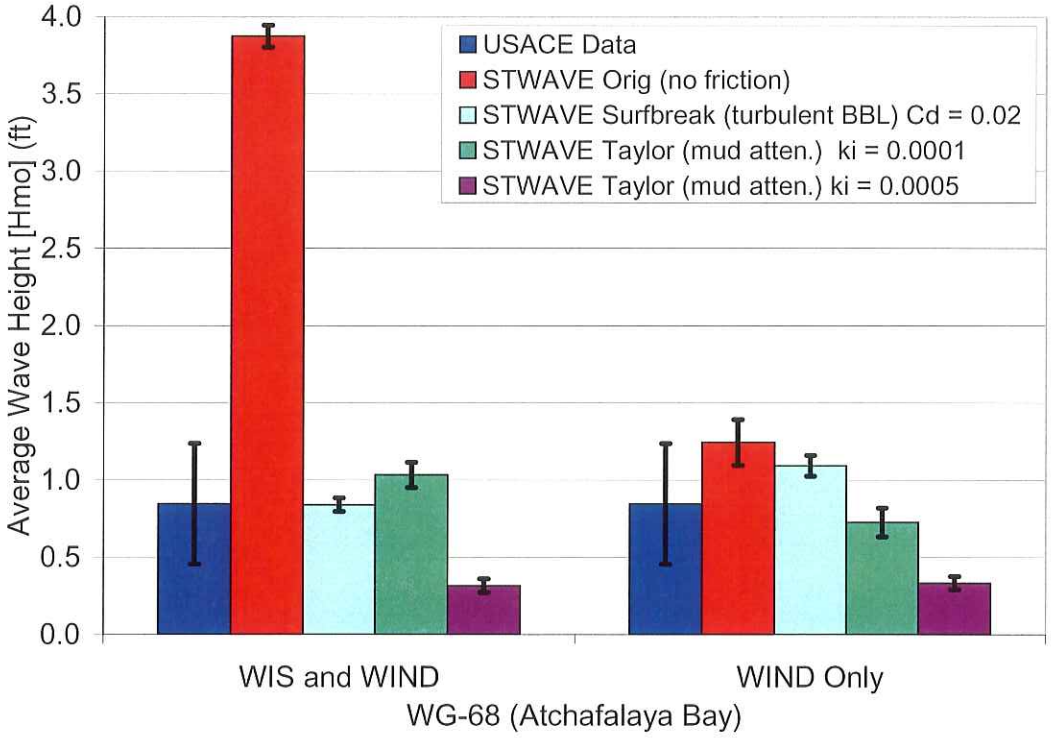

Figure 5.20 Wave Height Averages at WG-68 for Southerly Storm 3 for Two Input Conditions

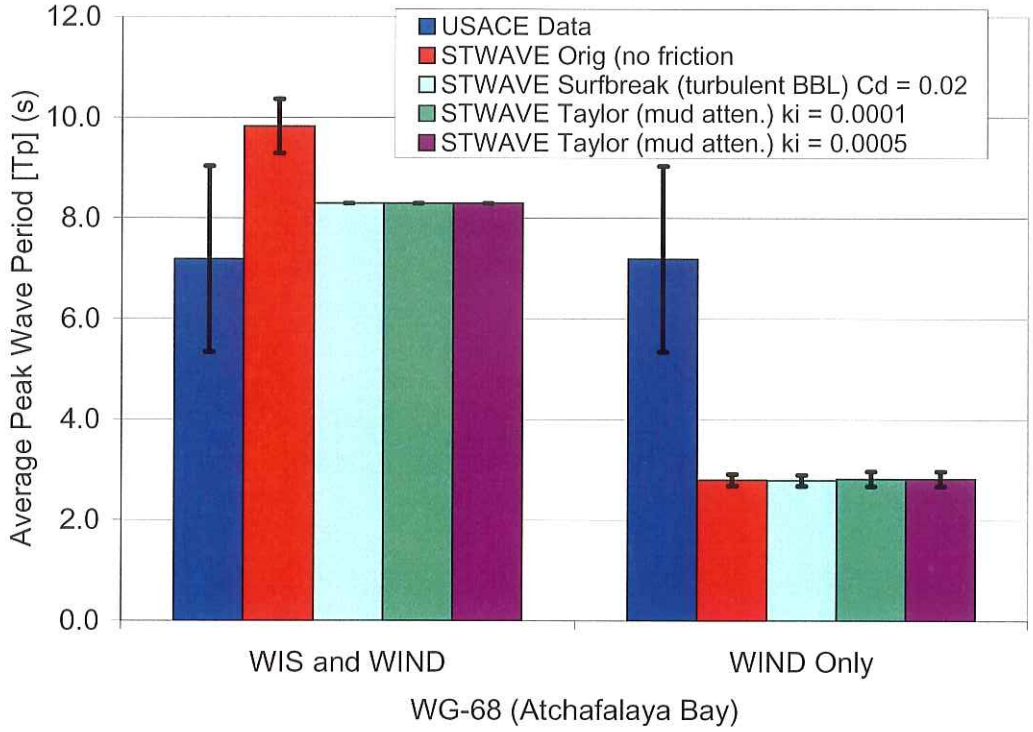

Figure 5.21 Wave Period Averages at WG-68 for Southerly Storm 3 for Two Input Conditions

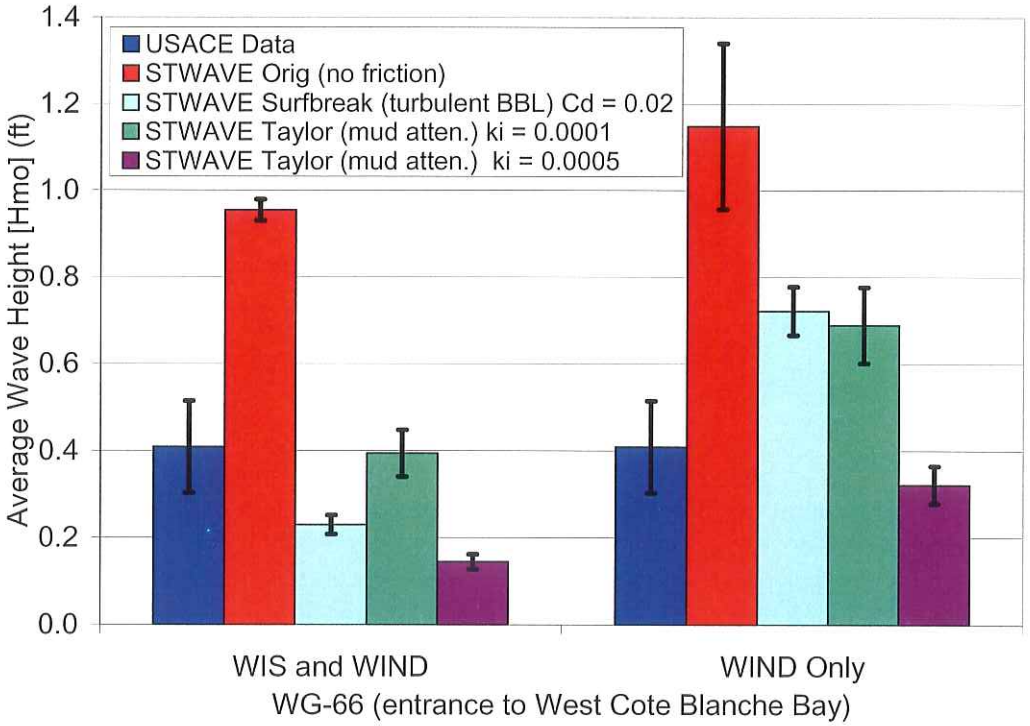

Figure 5.22 Wave Height Averages at WG-66 for Southerly Storm 1 for Two Input Conditions

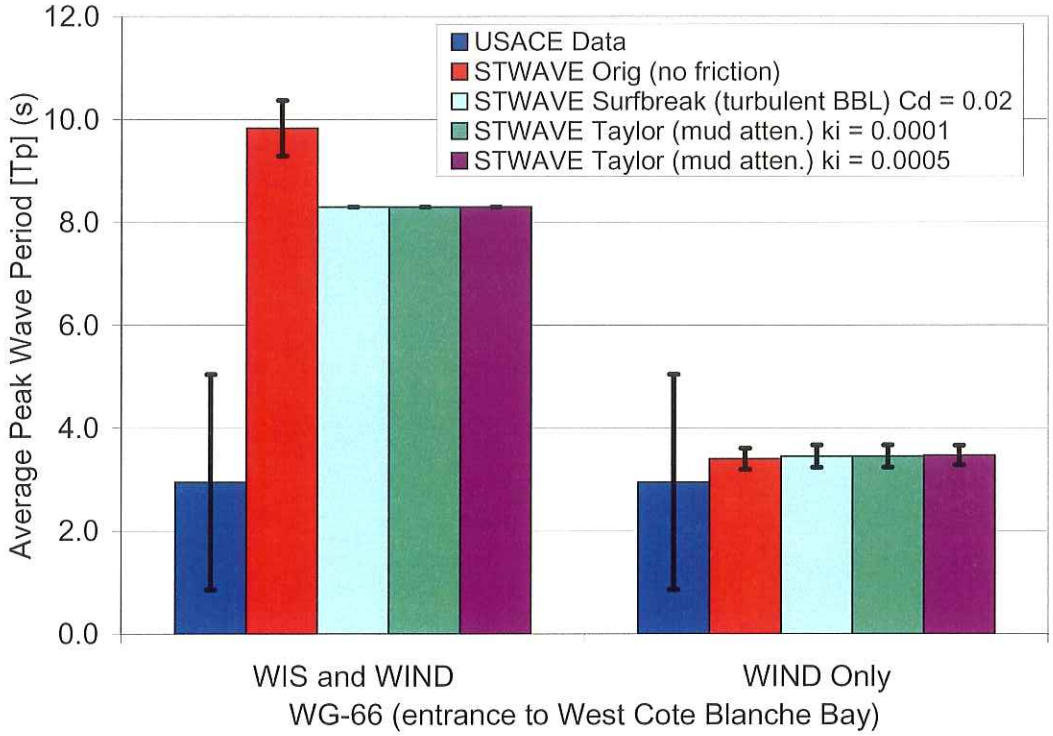

Figure 5.23 Wave Period Averages at WG-66 for Southerly Storm 3 for Two Input Conditions

5.5.4 Average of Three Southerly Storms

Figures 5.24 and 5.25 compare simulations of three versions of STWAVE for the average wave height during three southerly storms. Figure 5.24 presents the average wave heights at WG-68 and WG-66 for *WIS plus wind* data input. Figure 5.25 presents the average wave heights at WG-68 and WG-66 for *wind only* data input. This analysis suggests that model predictions of wave heights in Acadiana Bays are relatively insensitive to the inclusion of Gulf-generated waves in the model boundary condition. Given the STWAVE Original model consistently overestimates wave height, both figures reinforce the need for some form of a bottom dissipation mechanism to attenuate wave energy, during high frequency events, estimated by STWAVE Original. In comparison, the STWAVE Surfbreak (turbulent bottom boundary layer dissipation) and STWAVE Taylor (viscous mud dissipation) results indicate improved agreement. While both forms of bottom dissipation (turbulent BBL and viscous) attenuate wave energy and improve the model results, the known soft bottom material within the Acadiana Bays points to a viscous dissipation mechanism for wave attenuation. Therefore, this study selects the STWAVE Taylor model as the preferred model to simulate waves during typical conditions in the Acadiana Bays. Testing of various attenuation coefficients (k_i) indicates a value of 0.0001 m^{-1} provides reasonable general agreement with

the measured data. Note, the limited availability of wave data and sparse bathymetric data within the study area makes general agreement with the measured data a realistic goal.

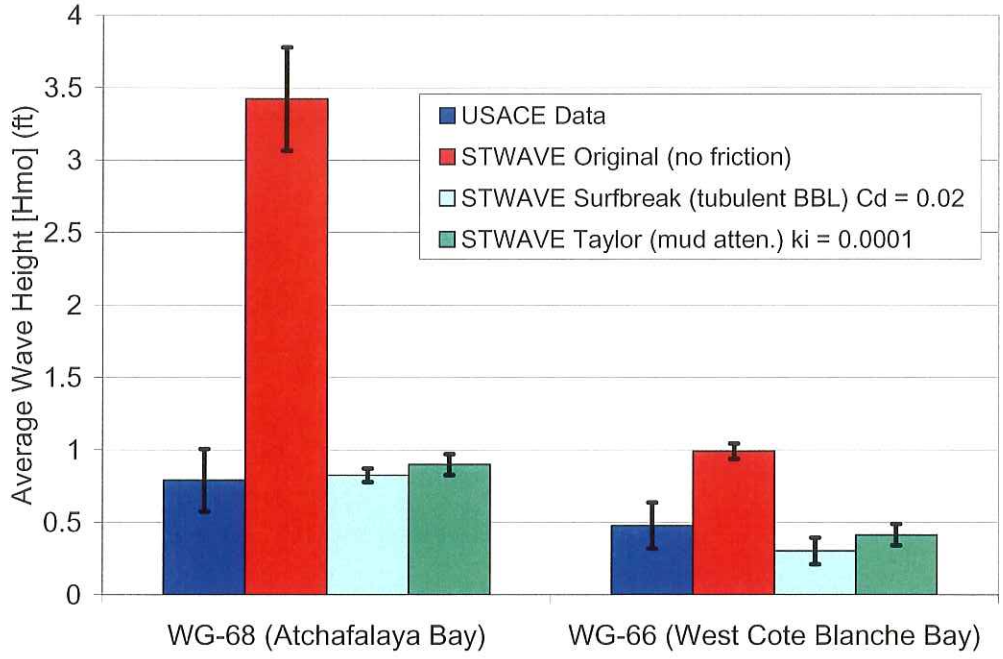

Figure 5.24 Average Wave Heights from Southerly Storms 1, 2, and 3 at WG-66 and WG-68 with WIS Hindcast Wave Data and Wind Only Input.

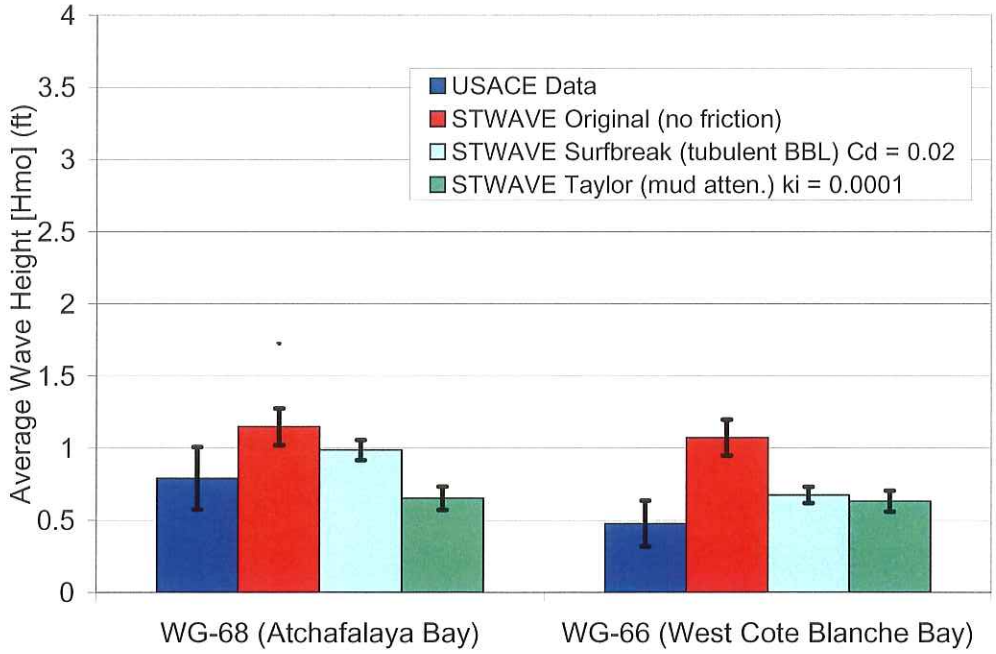

Figure 5.25 Average Wave Heights from Southerly Storms 1, 2, and 3 at WG-66 and WG-68 with Wind Only Input

5.5.5 Hurricane Rita

Hurricane Rita made landfall west of the study area, along the Louisiana-Texas border on September 24, 2005. WAVCIS gage CSI-14 recorded peak wind speeds of 80 ft/s, a total surge of about 8 ft NGVD, and wave heights of 6 ft during the storm. Assuming that the winds approached the study area from S15°E, this study modeled the effects of the recorded wind speed and storm surge to assess the effectiveness of STWAVE for extreme events. The STWAVE model domain contains 1,520 by 2,012 cells with a 115-ft grid spacing and an offshore orientation perpendicular to S15°E

Figures 5.26 and 5.27 present the wave heights in the Acadiana Bays simulated by STWAVE Original and STWAVE Taylor (k_i = 0.0001 m^{-1}). STWAVE Original estimates wave heights of about 5.75 ft, while STWAVE Taylor estimates wave heights of about 3.75 ft at CSI-14. The results demonstrate that the STWAVE Original model provides good simulation of wave heights during extreme events; in contrast, the STWAVE Taylor model underestimates wave heights.

The most probable reason for this discrepancy is the form of the dissipation function used in STWAVE Taylor. This model represents energy dissipation due to soft beds by assuming an exponential

decay of wave height with distance. The STWAVE Taylor model considers the attenuation coefficient a constant, in practice a tuning parameter, in this formulation. From a physical standpoint, one expects this coefficient to depend on the water depth. In other words, the effects of soft bed-induced viscous damping should decrease in larger relative water depth (with relative water depth normally defined as a ratio of water depth to wave length). Noting that the calibration process essentially considered relatively high frequency storm conditions to set the attenuation parameter, understandably the model does not accurately simulate the effects of surge associated with extremely low frequency events.

This comparison shows that for modeling extreme storm events where storm surge reduces (if not mostly eliminates) bottom dissipation effects, application of the STWAVE Original model may prove preferable to the STWAVE Taylor model.

5.6 Conclusions

The analysis presented in this chapter demonstrates that wave propagation models for Acadiana Bays must account for bottom dissipation. The analysis revealed that, for normal and high-frequency storm conditions, formulations of dissipation in terms of either bottom friction (rough beds) or viscous damping (soft beds) are equally effective in helping the STWAVE model replicate measured wave heights reasonably well. Though the inclusion of bottom dissipation generally improves model simulations of period, especially when the simulated average wave period is compared to measured peak period values, in general the model does not consistently estimate wave periods very well. Because wave period plays a secondary role relative to wave height in determining most parameters of interest (e.g., sediment transport, transport-diffusion, wave forces on structures, etc.) in the nearshore zone, this finding does not represent a significant limitation of this study.

Given the soft bed nature of the Acadiana Bays system, this study selects, with one caveat, the STWAVE Taylor model — describing energy loss by viscous dissipation over soft beds — with an attenuation factor (k_i) of 0.0001 m^{-1} for general application. For extreme, low frequency storm events, note that the STWAVE Original model provides simulations of wave height better than those of STWAVE Taylor.

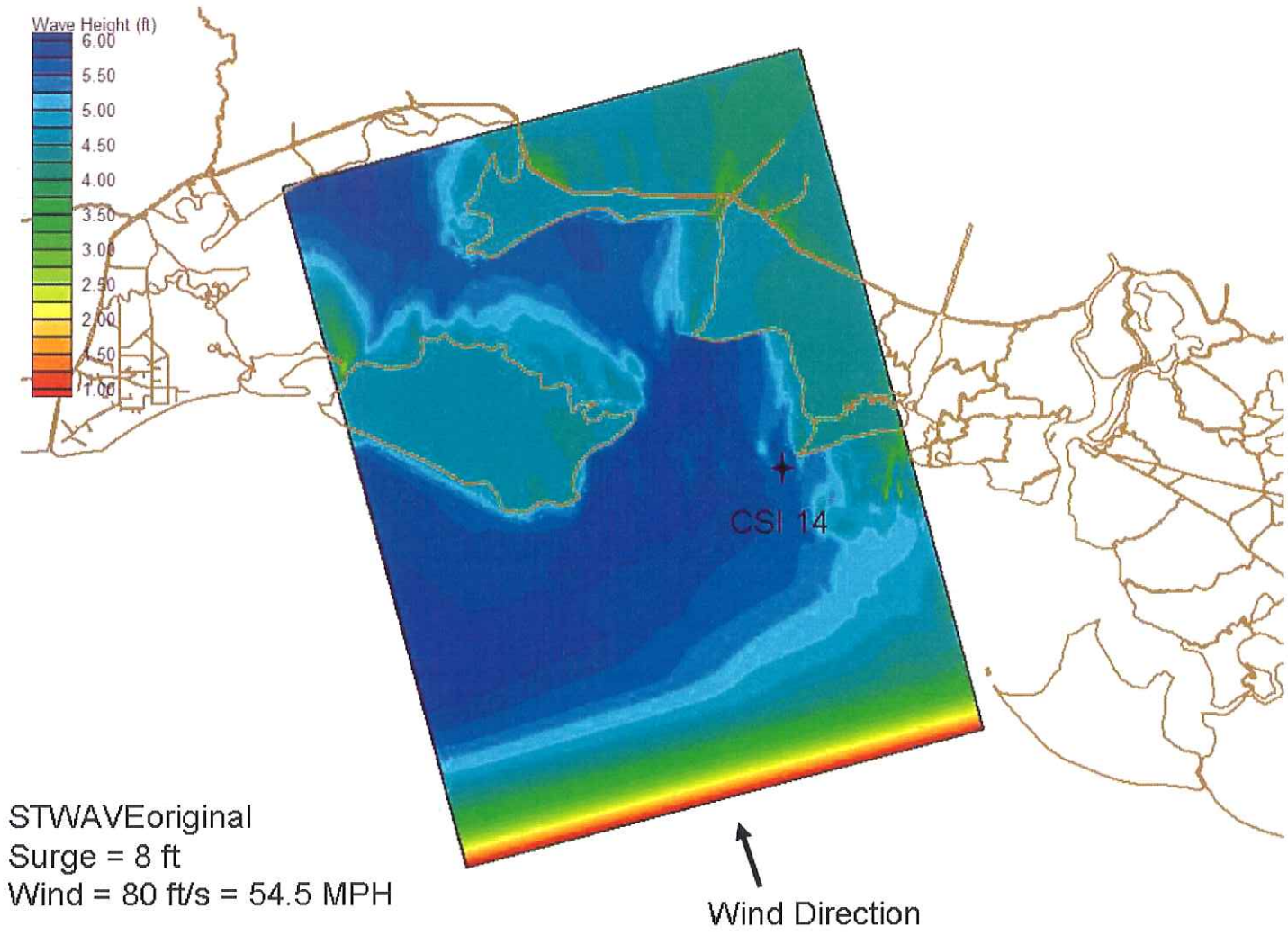

Figure 5.26 STWAVE Original Predictions of Wave Height for Approximate Conditions of Hurricane Rita

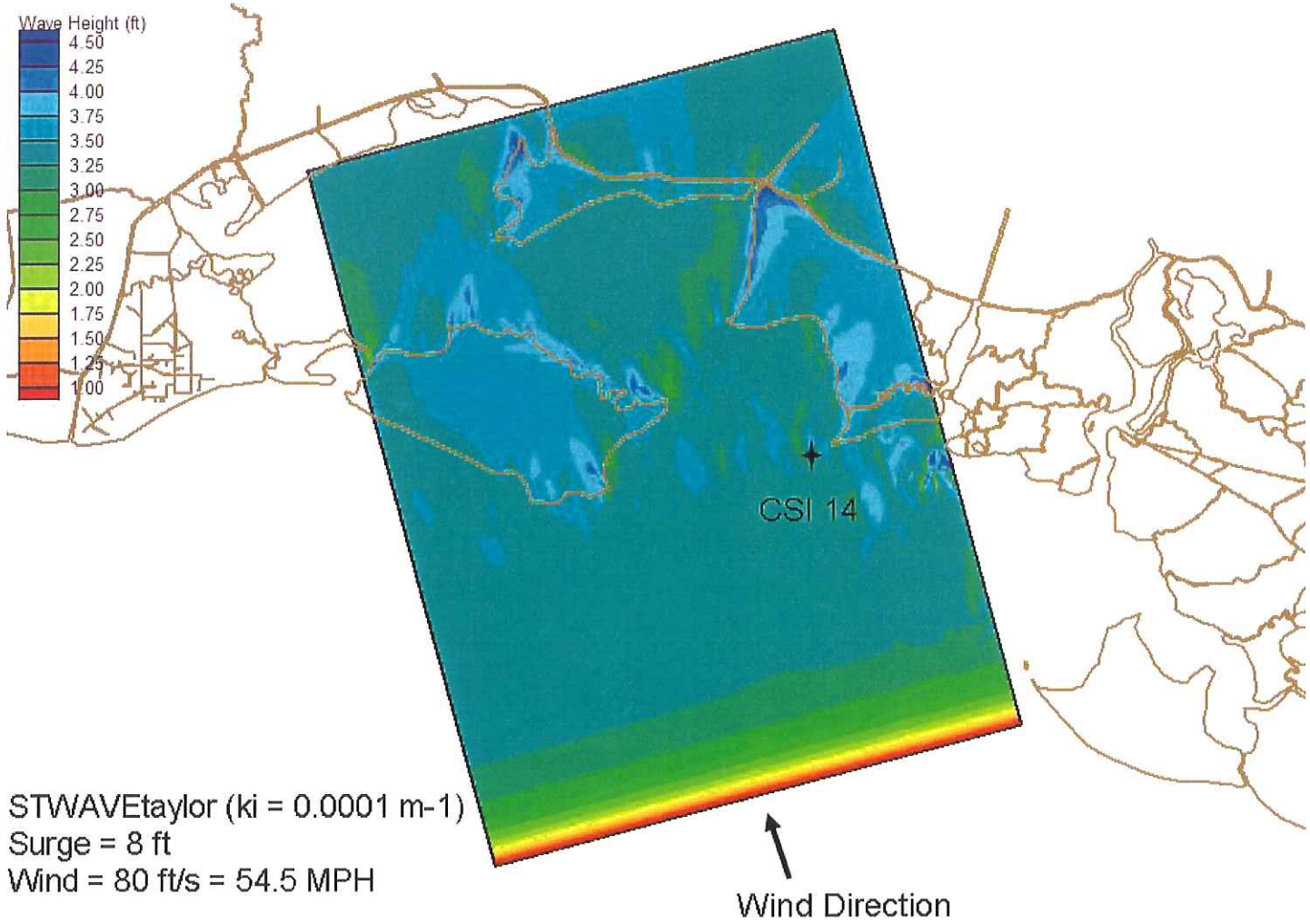

Figure 5.27 STWAVE Taylor Predictions of Wave Height for Approximate Conditions of Hurricane Rita

6.0 HYDRODYNAMIC, SALINITY, AND TURBIDITY MODELING OF REEF ALTERNATIVES

6.1 Model Simulation Periods and Methods

This study analyzed the effects, relative to existing conditions, of four reef alternatives on the salinity and turbidity regimes in Acadiana Bays. Long model run times and large solution file sizes made running continuous simulations of several years for all alternatives impractical. Furthermore, continuously changing inflow conditions, generally varying significantly on a monthly basis, suggested long-term simulations were unnecessary. The fact that the salinity and turbidity regimes in Acadiana Bays depend greatly on freshwater stream flows from the Atchafalaya River and Wax Lake Outlet suggested a more efficient approach to achieve reasonable run times and solution file sizes. An analysis of the multi-year historic daily stream flow records for the Lower Atchafalaya River and Wax Lake Outlet determined characteristic values representative of high, mean, low, summer, and winter stream flow regimes. The coincidence and similarity of the summer and low stream flow conditions reduced the total number of required simulation periods to four.

Further examination of the flow hydrographs determined the months when these representative flows occurred. Analysis of historic nearshore tidal and wind records (recorded at gage CSI-3) determined their representative time-varying values for these months. After running the hydrodynamic and transport models for these months, analysis of the model predictions ascertained which reef alternative caused the largest changes in salinity and turbidity regimes, relative to existing conditions, in Acadiana Bays.

6.1.1 Stream Flow Boundary Conditions

Figure 6.1 shows the annual average daily stream flows for the Lower Atchafalaya River at Morgan City and Wax Lake Outlet at Calumet representative of 7- and 17-year periods, respectively. To limit the number of variables considered in the study, the model applied a constant stream flow to each stream flow boundary (Figure 3.4). Table 6.1 lists the stream flow boundary data. The table also lists the representative month for each stream flow period.

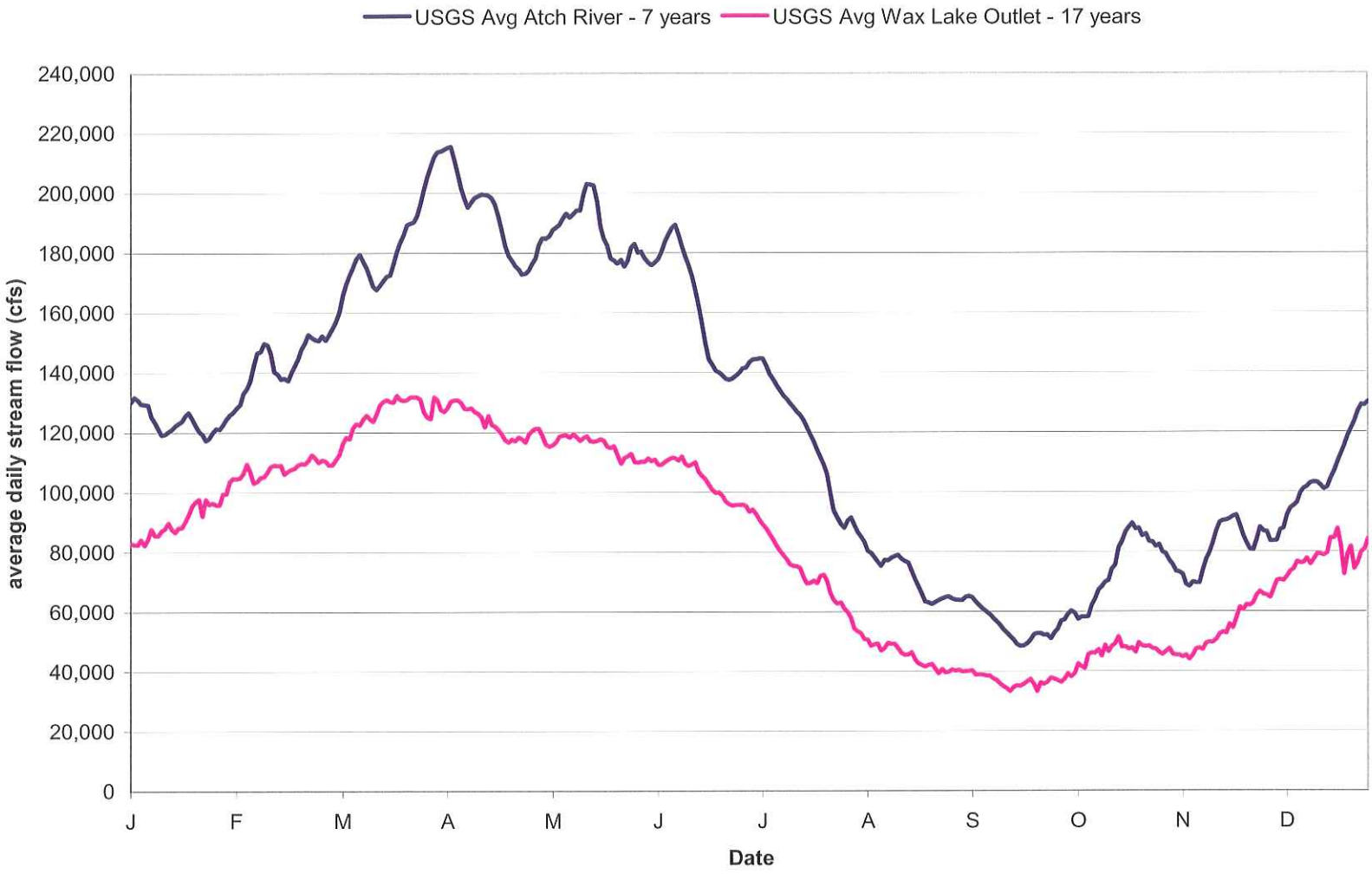

Figure 6.1 Annual Average Daily Stream Flows

Table 6.1 Production Run Stream Flow Boundary Conditions

	Stream Flow Period and Boundary Condition (cfs)				
Stream Flow Location	**High (Apr)**	**Mean (Jan)**	**Low (Aug)**	**Summer (Aug)**	**Winter (Feb)**
Vermilion River at Perry	1340	1340	1340	1340	1340
Charenton Drainage Canal	1770	1770	1770	1770	1770
Wax Lake Outlet at Calumet	124,000	83,000	40,000	40,000	108,000
Lower Atchafalaya River	192,000	125,000	62,000	62,000	150,000
Bayou Boeuf	2120	2120	2120	2120	2120
Bayou Black	990	990	990	990	990

For the months listed in Table 6.1, an analysis of the available data determined the typical hydrological year and winds by analyzing the stream flow record at the Lower Atchafalaya River at Morgan City and the CSI-3 wind record.

The seven-year flow records at the Lower Atchafalaya River station provided the means to select the calendar year that best represents an average hydrologic year. A comparison of the measured flow at this station with the average flow from the seven-year record (referred to as the average hydrologic year) showed that the time series of recorded daily flows in the year 2001 are closest to the flows for the average hydrologic year. Thus, 2001 provided the representative hydrologic year and provided the stream flow boundary conditions for the simulations. Consistent with this finding, the 2001 tides provided the offshore tidal stage boundary conditions.

A comparison of the four-year wind record (speed and direction) for CSI-3 yielded the statistical wind information in Tables 6.2 and 6.3. Table 6.2 clearly shows that the wind speed experienced in 2001 most closely follows the four-year record. The four-year wind direction record (Table 6.3) provides a less clear "typical year"; however, given that wind direction variations less than ±10 degrees generally have little affect on the model, the absolute values do not show an excessive variability within the record period. Therefore, the model applied the appropriate portions of the 2001 wind record as wind boundary conditions.

Table 6.2 Four Year (2001 – 2004) Wind Speed Statistics

	2001 – 2004	2001	2002	2003	2004
Median Wind Speed (ft/s)	12.4	12.8	13.2	11.8	11.9
Mean Wind Speed (ft/s)	12.8	13.2	13.6	12.4	12.1
Wind Speed Standard Deviation (ft/s)	6.7	6.4	7.7	6.1	6.4
Upper Half Median Wind Speed (ft/s)	17.0	17.3	18.2	16.0	16.6
Lower Half Median Wind Speed (ft/s)	8.0	8.5	8.5	7.9	7.2
IQR* (ft/s)	9.0	8.8	9.7	8.1	9.3

* Interquartile Range (IQR): the difference in the medians of the upper and lower halves of the data set

Table 6.3 Four Year (2001 – 2004) Wind Direction Statistics

	2001 – 2004	2001	2002	2003	2004
Median Wind Direction (degrees from N)	142	133	133	156	150
Mean Wind Direction (degrees from N)	96	93	97	97	95
Wind Speed Standard Deviation (degrees from N)	207	198	195	230	206
Upper Half Median Wind Direction (degrees from N)	73	72	65	82	80
Lower Half Median Wind Direction (degrees from N)	134	126	130	148	126
IQR* (degrees from N)	142	133	133	156	150

* Interquartile Range (IQR): the difference in the medians of the upper and lower halves of the data set

Table 6.4 lists the general characteristics of the tidal stage and wind boundary conditions for each model simulation period. Figures 6.2 – 6.5 show typical offshore tide boundary conditions. Figure 6.6 shows the wind rose for each simulation period.

In addition to the boundary conditions, the transport model requires initial conditions, specifically initial salinity and turbidity concentrations throughout the system. Subject to large local variations depending on local disturbances (e.g., storms), salinity and turbidity vary within the bays throughout the year. These disturbances can raise the salinity in the bays as high as 20 ppt (Walker, 2001).

Because the goal of this study is to examine the feasibility of influencing the salinity and turbidity regimes of the Acadiana Bays system, the relatively low levels of salinity consistent with the calibration period served as the initial conditions for all model simulation scenarios (production runs). Setting the

initial conditions at this level removes the influence of highly variable local disturbances, establishes the influence of the reefs following the worst initial conditions (low salinity), and allows meaningful comparison of results for different flow conditions. Measured salinity records indicate low salinity conditions do occur throughout the year, even during periods of low stream flow. Thus, the use of low initial salinity conditions establishes the benefits of the reefs during these periods (when low salinity stresses the ecology). The use of low initial salinity also serves to maximize the influence of the reefs on salinity (if salinity is already high, the reefs will have less effect on increasing salinity further).

Table 6.4 General Features of Production Runs' Tidal Stage and Wind Boundary Conditions

Simulation (Month)	Tidal Stage Time Series Boundary	Wind Time Series Boundary
Mean (Jan)	January 2001 2 spring tides of 2 – 2.3 ft range 2 neap tides of 0.2 ft range	January 2001 CSI-3 wind average speed of 16 mph maximum speed of 33 mph variable direction, primarily from the NE
High (Apr)	April 2001 2 spring tides of 2 – 2.3 ft range 2 neap tides of 0.5 ft range	CSI-3 Data for April 2001 average speed of 13 mph maximum speed of 34 mph variable direction, , primarily from the SE
Low/Summer (Aug)	August 2001 2 spring tides of 2 – 2.2 ft range 2 neap tides of 0.3 ft range	CSI-3 Data for August 2001 average speed of 11 mph maximum speed of 28 mph variable direction, primarily from the SW
Winter (Feb)	February 2001 2 spring tides of 2 – 2.3 ft range 2 neap tides of 0.2 ft range	CSI-3 Data for February 2001 average speed of 14 mph maximum speed of 38 mph variable direction, primarily from the SE

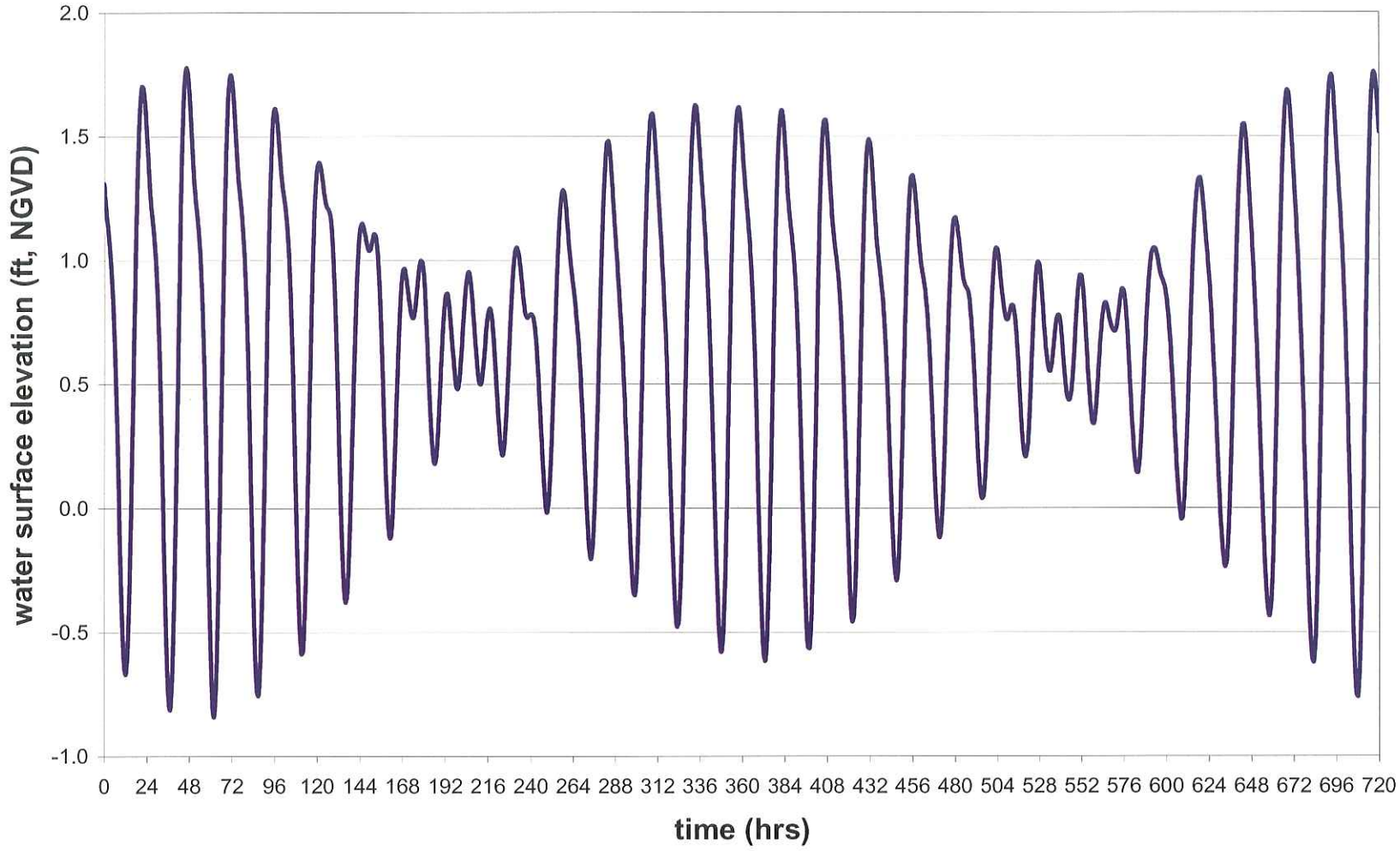

Figure 6.2 Typical January 2001 Offshore Tide (Mean Stream Flow Simulation)

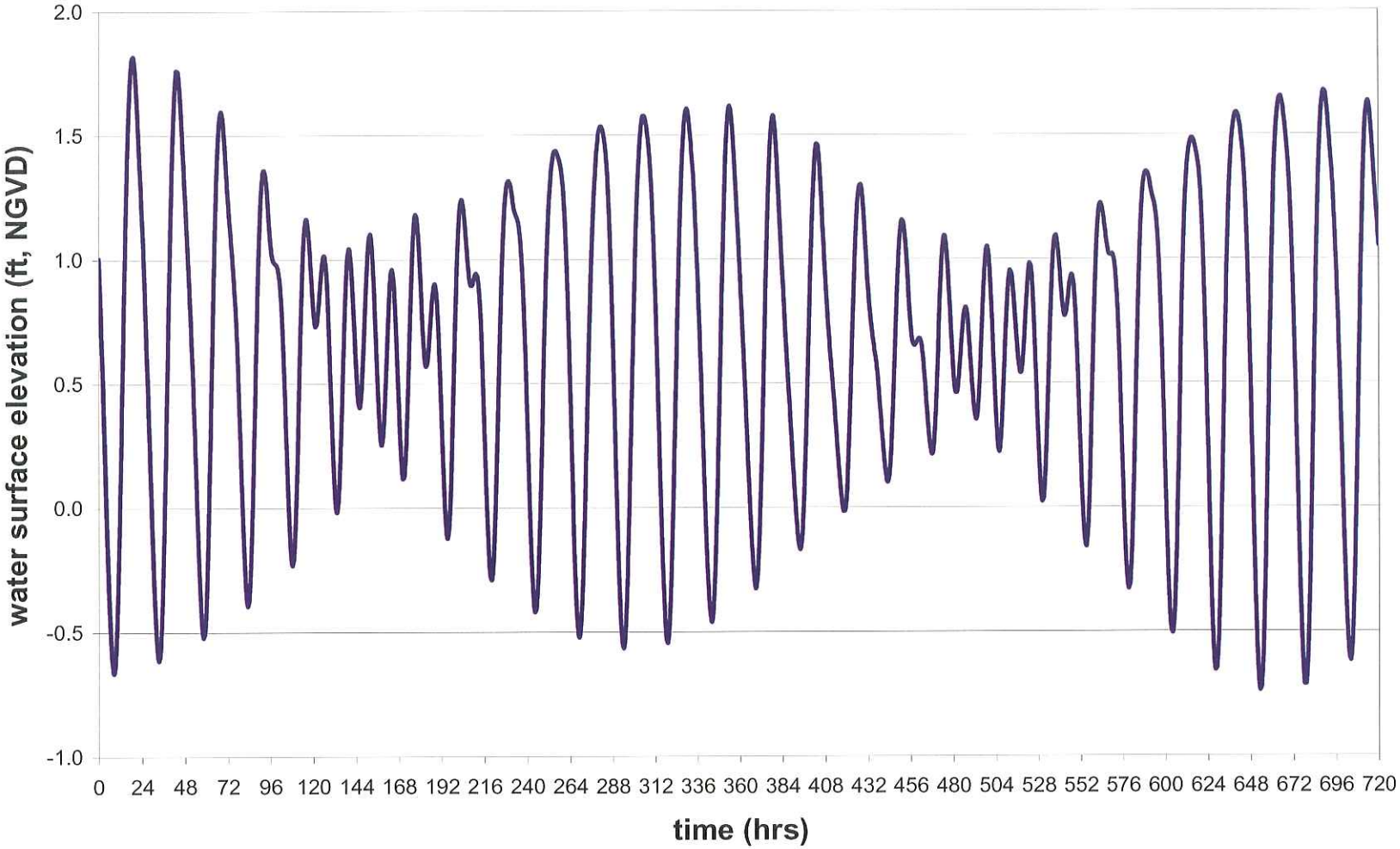

Figure 6.3 Typical April 2001 Offshore Tide (High Stream Flow Simulation)

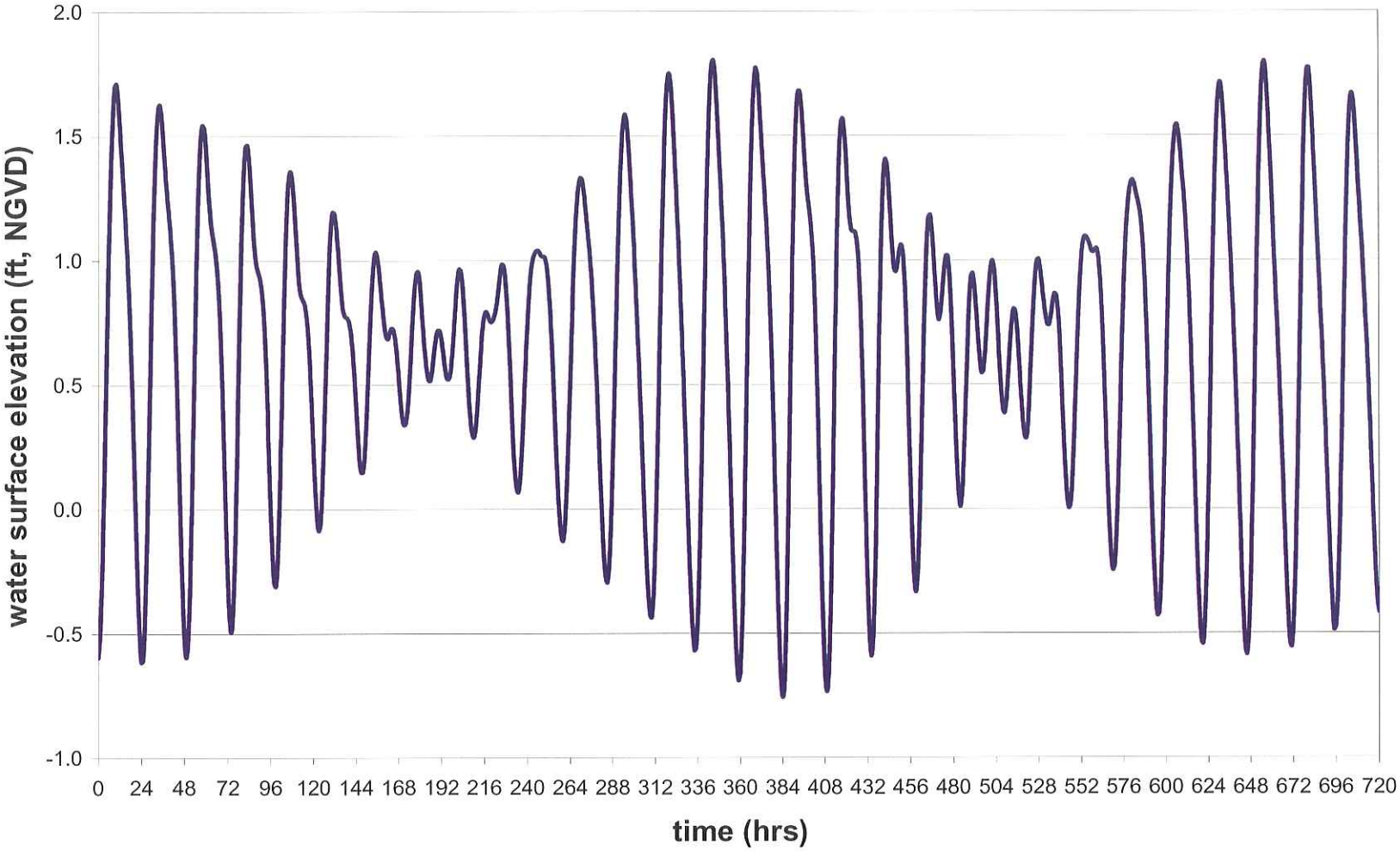

Figure 6.4 Typical August 2001 Offshore Tide (Low/Summer Stream Flow Simulation)

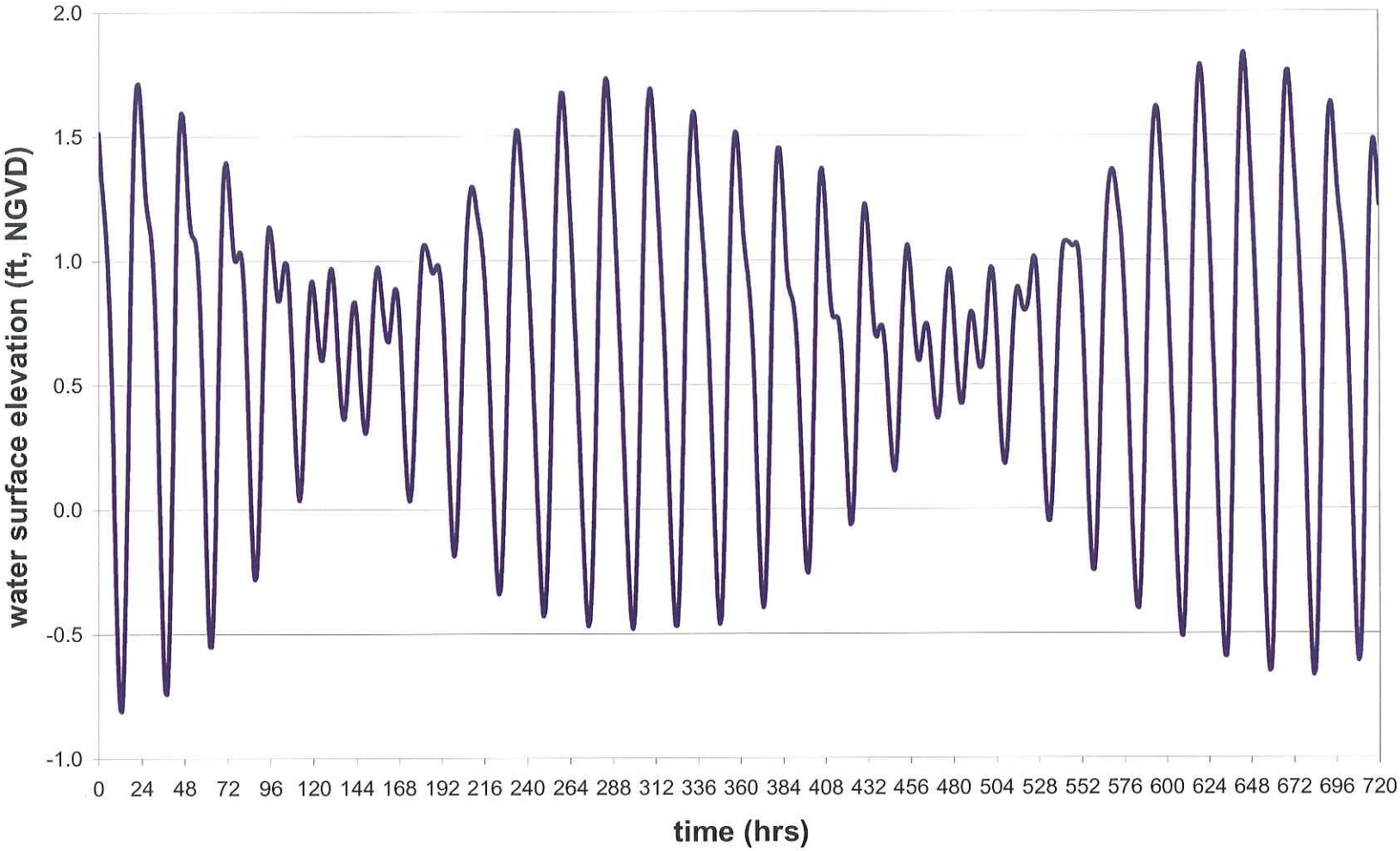

Figure 6.5 Typical February 2001 Offshore Tide (Winter/Intermediate Stream Flow Simulation)

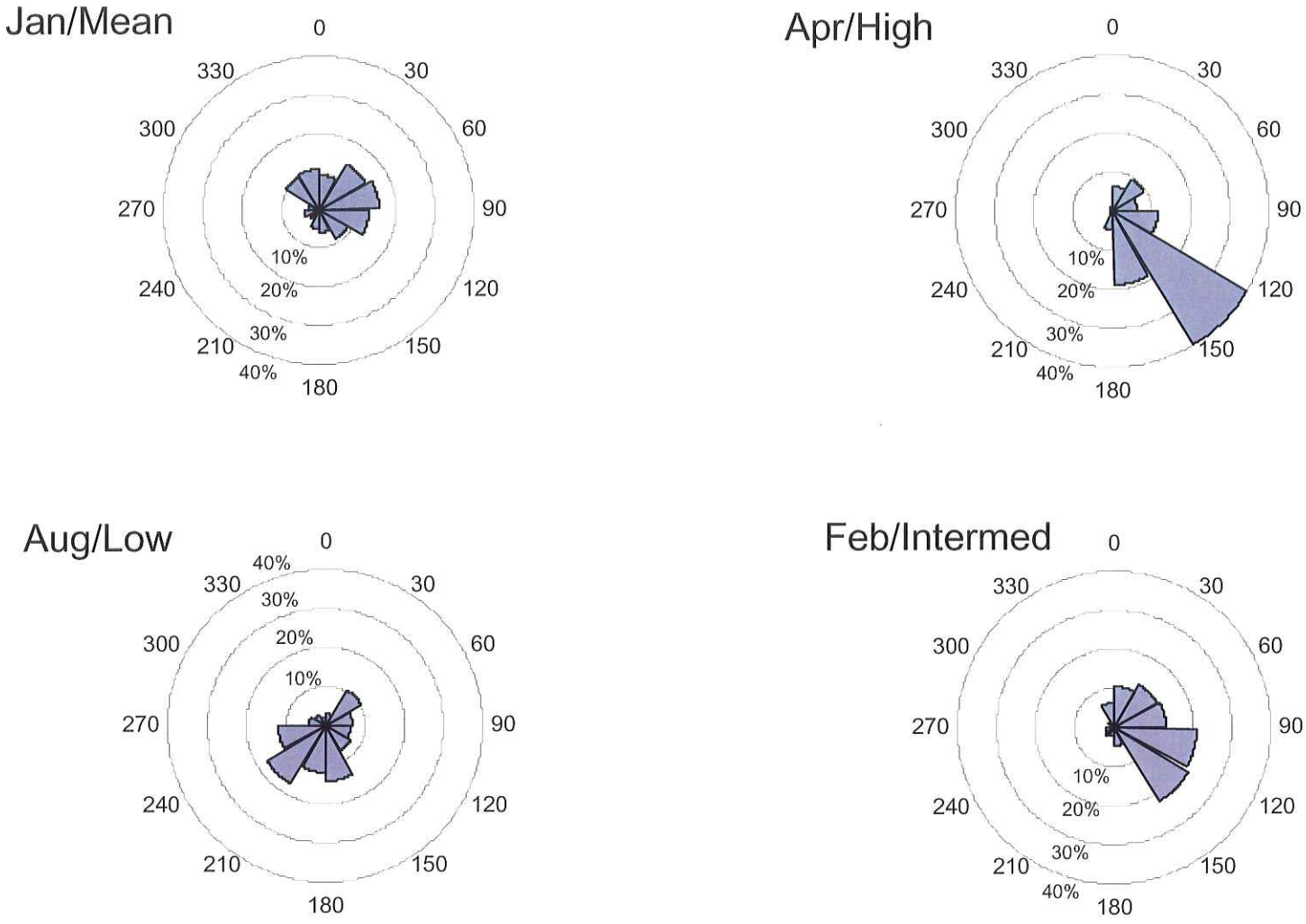

Figure 6.6 Wind Roses for the Wind Boundary Conditions

6.1.2 Model Results Sample Locations and Model Output Presentation

Figure 6.7 shows the location of the transport-diffusion model sample stations selected for the presentation of model results. For each model scenario (conditions listed in Tables 6.1 and 6.4) a 28-day simulation was conducted for each reef alternative (Table 2.1) and existing bathymetric conditions. For each flow condition/scenario, the model results provided representative quasi-equilibrium salinity and turbidity concentrations (at the end of the simulation) at the stations shown in Figure 6.7 for all reef alternatives and for existing conditions. The results were grouped according to the simulation period (mean, high, low/summer, and intermediate/winter) and plotted in bar plots for comparison purposes to evaluate the relative effectiveness of each reef alternative. For each case, the first figure illustrates the simulated values (either salinity or turbidity) for each alternative and existing conditions. The second figure illustrates the same data but presents the results relative to existing conditions (i.e., illustrates the *changes* in values caused by the reef compared to existing conditions).

6.2 Mean Stream Flow Model Results

6.2.1 Reef Effect on Salinity

Figures 6.8 and 6.9 show the effects the reefs have on salinity during mean flow conditions. Figure 6.9 shows that the A2 and B2 reefs with their crests at MHW cause the greatest changes. The B2 reef (totally blocking the flow at the entrance to East Cote Blanche Bay) causes the greatest increases in Vermilion Bay (up to 1.5 ppt); however, B2 decreases salinity in West Cote and East Cote Blanche Bays (0.5 – 1 ppt). B2 also decreases salinity in the Gulf of Mexico at the western entrance to Atchafalaya Bay (W Ent Atcha Bay), near Marsh Island (Marsh Island GoM), and offshore of Southwest Pass (SW Pass). These decreases indicate some build up of freshwater from inflows that enter West and East Cote Blanche Bays but cannot exit to the Gulf due to the B2 reef blockage of tidal communication. Also, freshwater discharged by the Lower Atchafalaya River and Wax Lake Outlet into Atchafalaya Bay migrates directly to the west and along Marsh Island without any diversion into the western Bays .

The A2 reef causes the greatest increase in salinity in West Cote and East Cote Blanche Bays (2 – 3 ppt) and nearly a 1 ppt increase in salinity in Vermilion Bay. This reef alignment forces the freshwater from Atchafalaya Bay toward the south into deeper water before migrating to the west (after mixing with saline water). A2 allows tidal communication with East Cote Blanche Bay and the resulting mixing and exchange of the freshwater entering the bay from the Jaws and other sources. A2 decreases salinity at the Atchafalaya Bay, East Entrance of Atchafalaya Bay, and Four League Bay stations. This condition probably results from the reef confining the freshwater and allowing more mixing to the east.

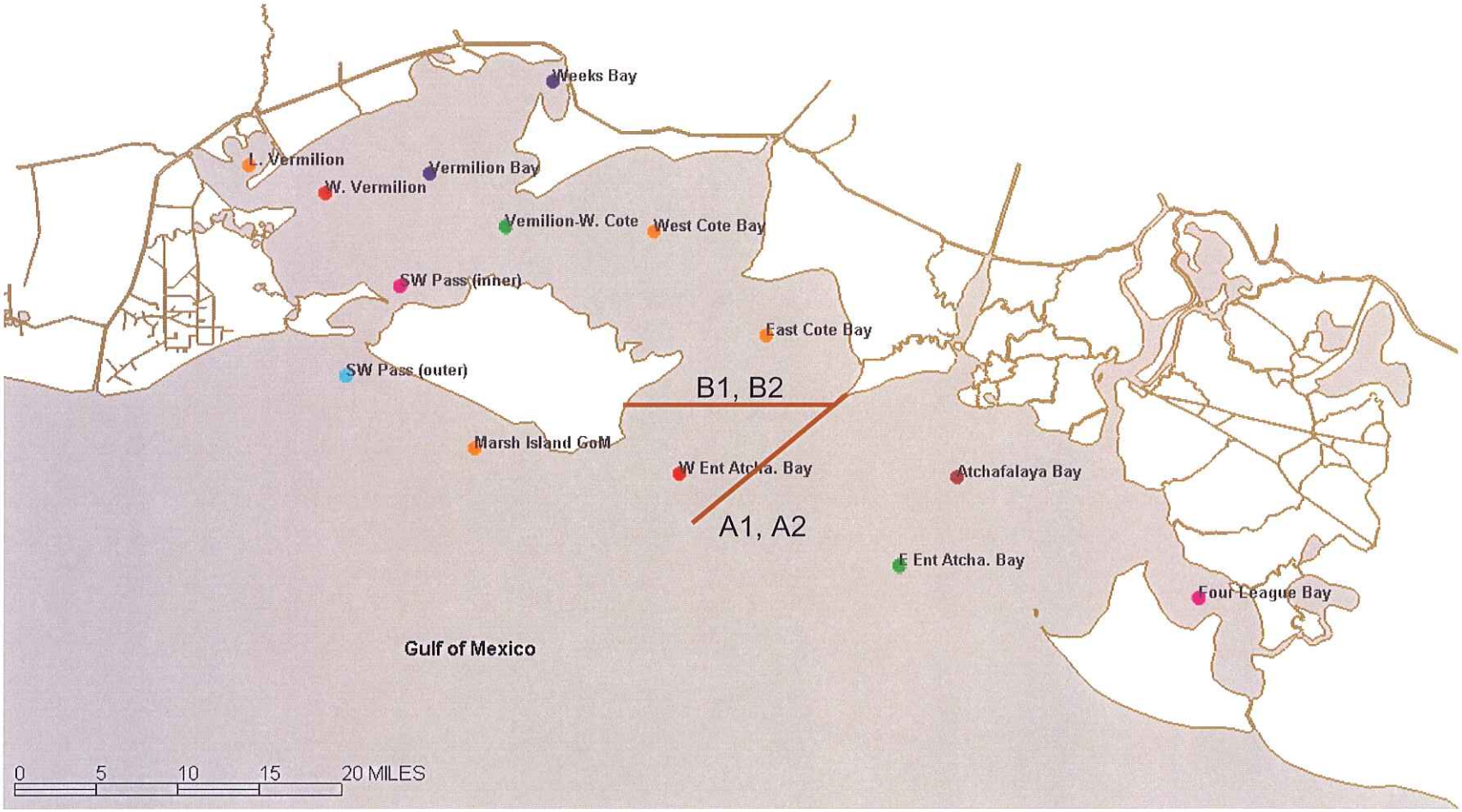

Figure 6.7 Model Results Sample Stations and Reef Alternatives

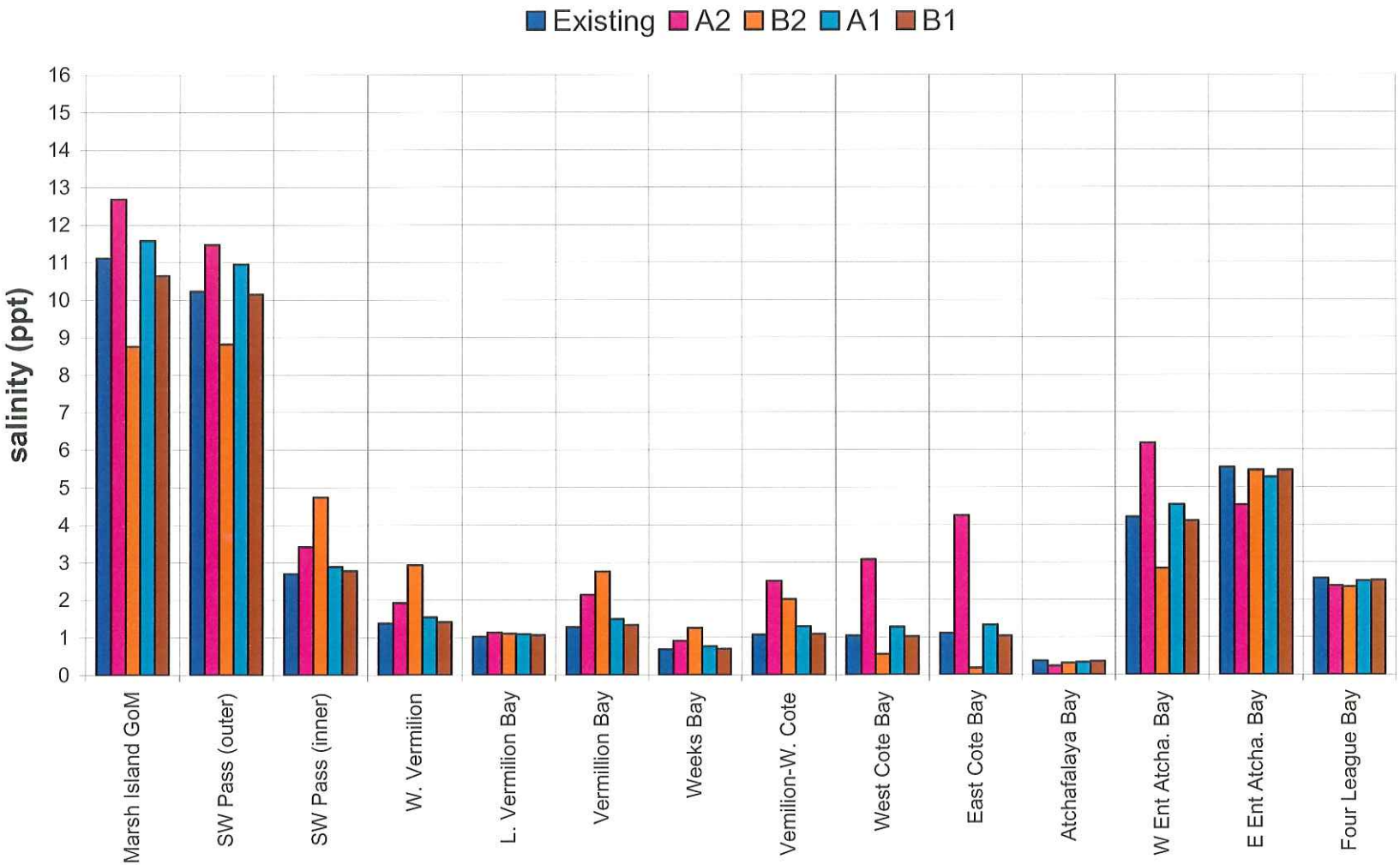

Figure 6.8 Modeled Salinity for Mean Stream Flow Conditions

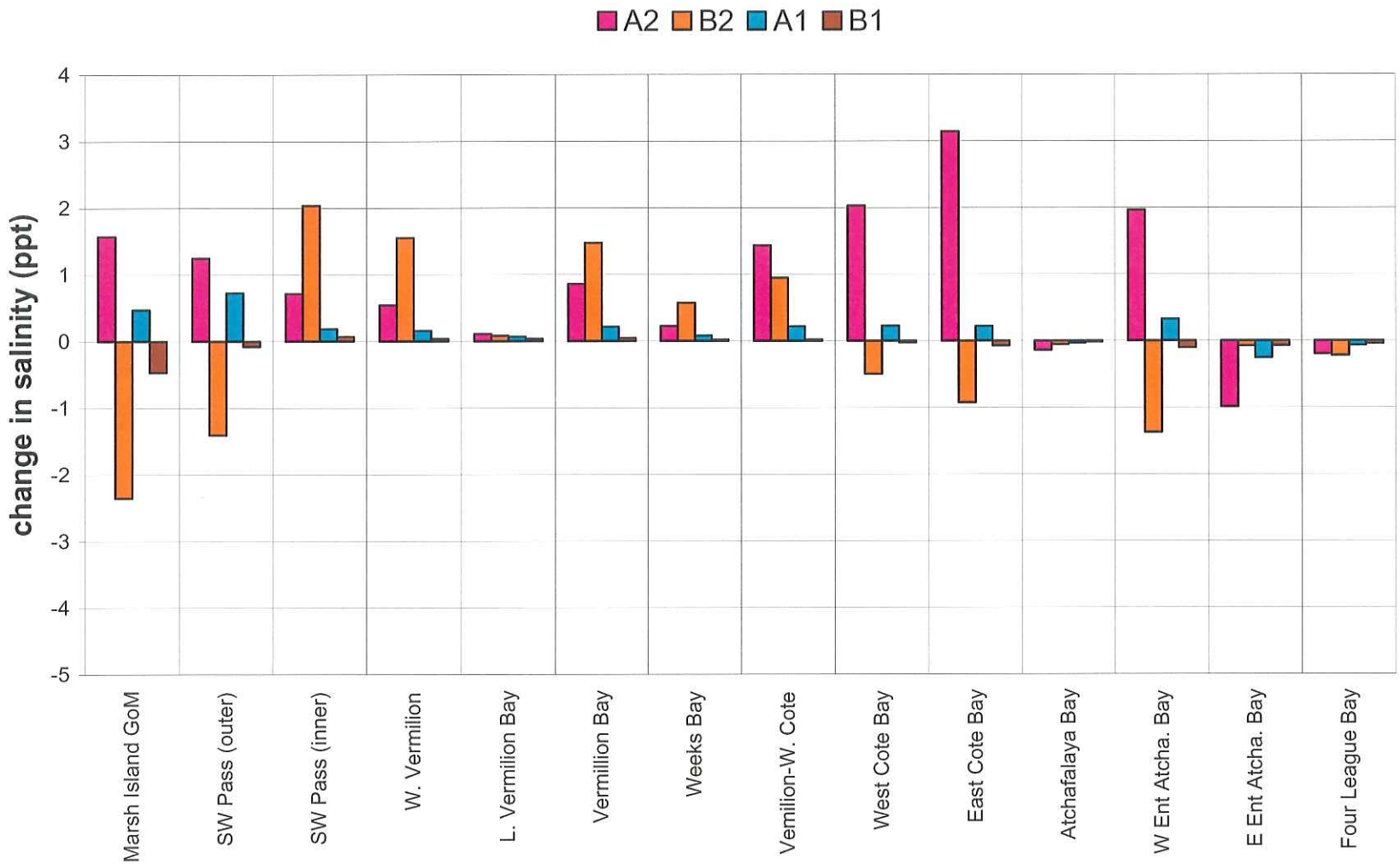

Figure 6.9 Modeled Salinity Change for Mean Stream Flow Conditions

Under the mean stream flow conditions, the A1 reef with a crest at -3 ft MLW slightly increases the salinity in the bays west of Atchafalaya Bay, at the western entrance to Atchafalaya Bay, and in the Gulf of Mexico near Marsh Island and Southwest Pass. The increases within the bays generally remain below 0.2 ppt. The increases in salinity in the Gulf of Mexico indicate that the reef redirected the freshwater plume seaward of the coastline but to a lesser degree than the A2 reef.

The B1 reef causes the least changes in salinities in the system. The greatest B1 change occurs in the Gulf of Mexico near Marsh Island where salinity decreases about 0.5 ppt. This indicates the reef redirects some freshwater along the coast rather than into the bays. However, within the bays salinities increase marginally (less than 0.1 ppt).

In summary, reef alternative A2 causes the most consistent and significant salinity increases (as much as 3 ppt) in western Acadiana Bays (west of the reef). B2 increases salinity as much as 1.5 ppt but decreases salinity in West and East Cote Blanche Bays. In the bays west of the reefs, salinities do not reach 5 ppt for any alternative.

6.2.2 Reef Effect on Turbidity

Figures 6.10 and 6.11 show the effects the reefs have on the turbidity distribution due to discharges from freshwater sources. Both of the MHW crested reefs, A2 and B2, cause significant decreases in turbidity in Vermilion, West Cote Blanche, and East Cote Blanche Bays. By completely eliminating the direct connection between East Cote Blanche Bay and Atchafalaya Bay, reef alternative B2 causes an appreciable reduction in turbidity in Vermilion, West Cote Blanche, and East Cote Blanche Bays. Alternative A2 causes similar, albeit more muted, effects in these bays. Apparently, the communication provided by the A2 opening between its terminus and Marsh Island allows some turbid water to enter the western bays. Neither of the -3 ft MLW crested reefs causes appreciable changes in turbidity anywhere in the model.

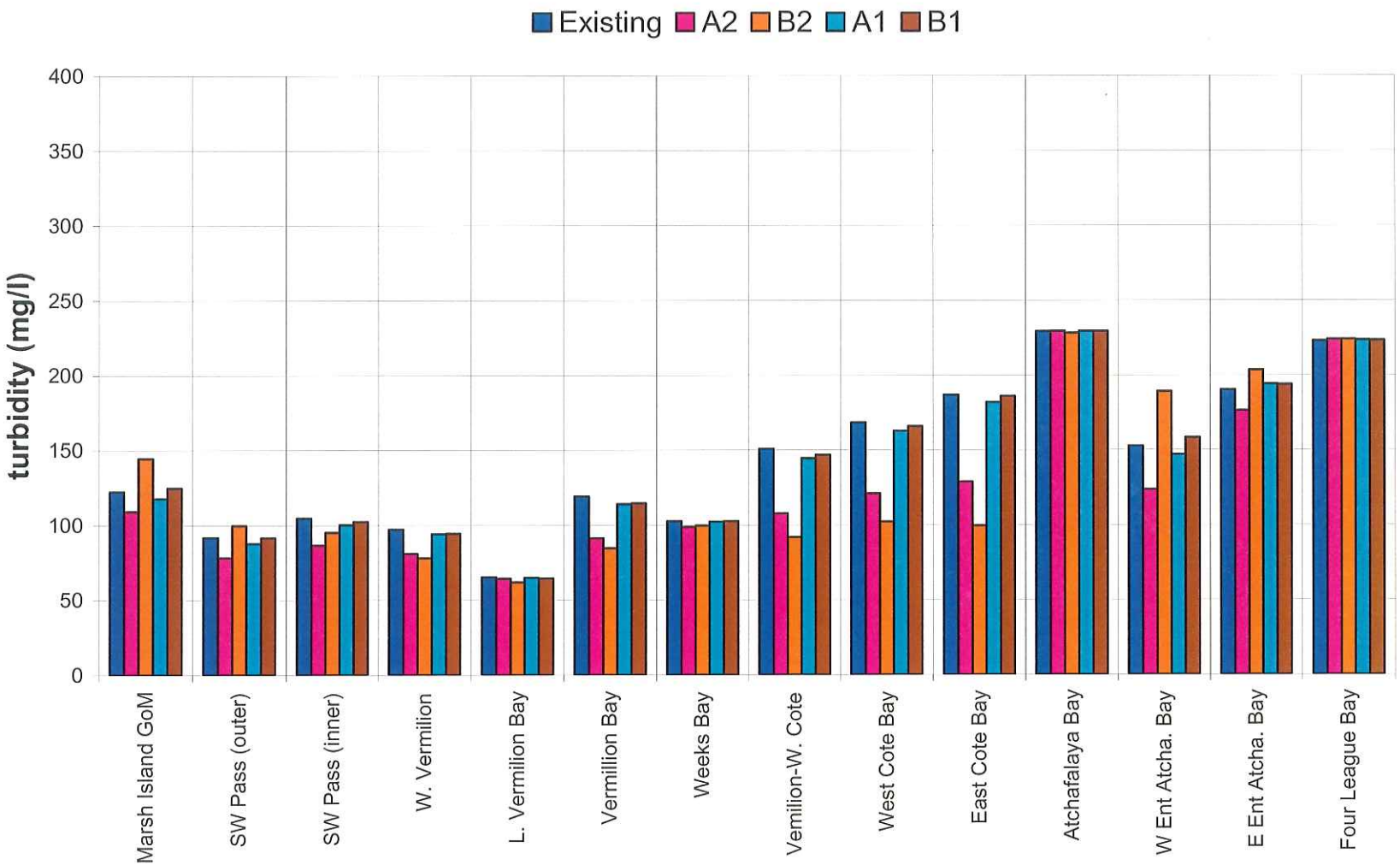

Figure 6.10 Modeled Turbidity for Mean Stream Flow Conditions

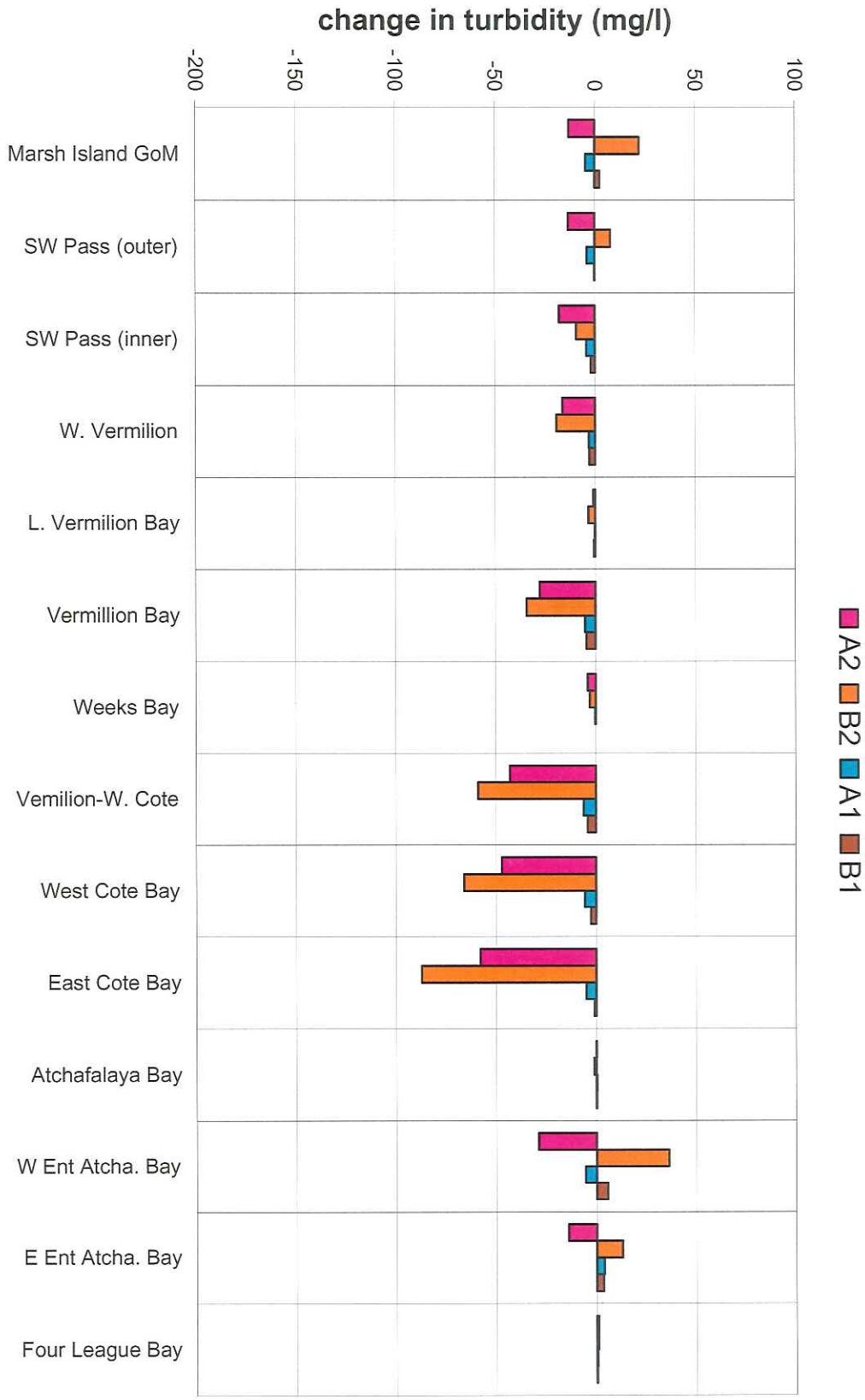

Figure 6.11 Modeled Turbidity Change for Mean Stream Flow Conditions

6.3 High Stream Flow Model Results

6.3.1 Reef Effect on Salinity

Figures 6.12 and 6.13 show the effects the reefs have on salinity during high flow conditions. Figure 6.13 shows that the A2 and B2 reefs with their crests at MHW again cause the greatest changes. The A2 reef causes the greatest increases in West Cote and East Cote Blanche Bays (1.8 – 3.3 ppt) and a smaller increase in Vermilion Bay. The A2 reef also increases the salinity at the western entrance to Atchafalaya Bay (about 2 ppt). Salinity increases west of Atchafalaya Bay (W Ent Atcha Bay, Marsh Island GoM, and SW Pass) indicate that the A2 reef reduces the volume of freshwater reaching these locations by displacing the Lower Atchafalaya River and Wax Lake Outlet freshwater plumes farther seaward where they mix with higher salinity water before migrating west.

The B2 reef causes a small salinity increase in Vermilion Bay (less than 1 ppt) and small decreases in salinity in West Cote and East Cote Blanche Bays (about 0.3 ppt). Salinity decreases (3 – 4 ppt) in the Gulf of Mexico near Marsh Island and Southwest Pass suggest that the B2 reef alignment allows more freshwater to reach these areas because no freshwater flow enters the western bays – all is diverted along the seaward side of Marsh Island. Unlike the A2 alignment, the plume is not directed offshore.

Under high stream flow conditions, the A1 and B1 reefs with their crests at -3 ft MLW caused little change in salinity in the bays west of Atchafalaya Bay.

In general, reef alternative A2 causes the most significant salinity increases (as much as 3 ppt) in the bays west of the reef. B2 has a similar effect in most of these areas, but decreases salinity in West and East Cote Blanche Bays. In the bays west of the reefs, salinities do not reach 5 ppt for any alternative.

6.3.2 Reef Effect on Turbidity

Figures 6.14 and 6.15 show the effects the reefs have on the turbidity distribution in the system during high flow conditions. Both of the MHW crested reefs cause significant decreases in turbidity in West Vermilion through East Cote Blanche Bays. Reef alternative B2, which eliminates the direct connection between East Cote Blanche Bay and Atchafalaya Bay, causes greater decreases in turbidity than does A2. Neither of the -3 ft MLW crested reefs causes appreciable changes in turbidity anywhere in the model.

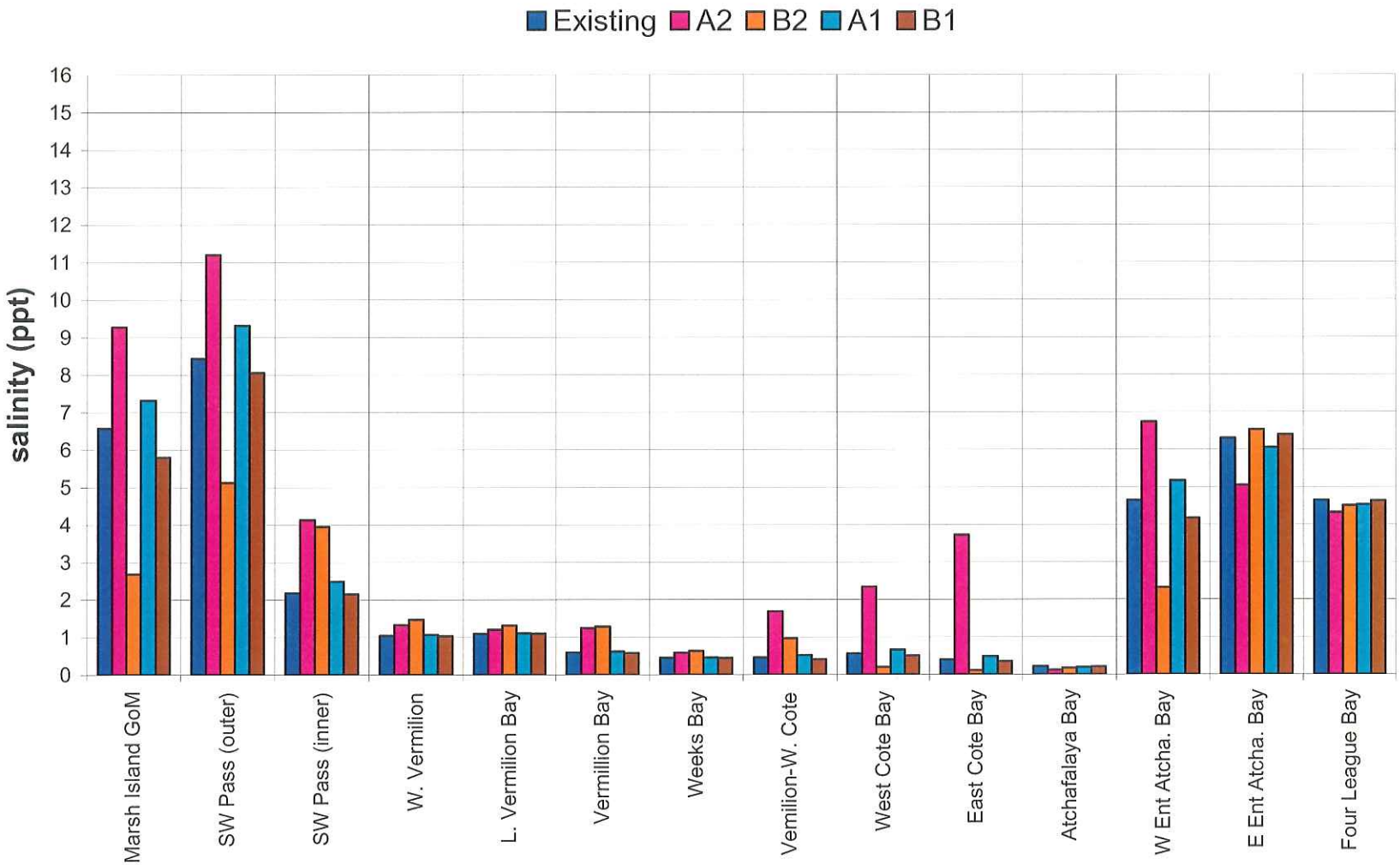

Figure 6.12 Modeled Salinity for High Stream Flow Conditions

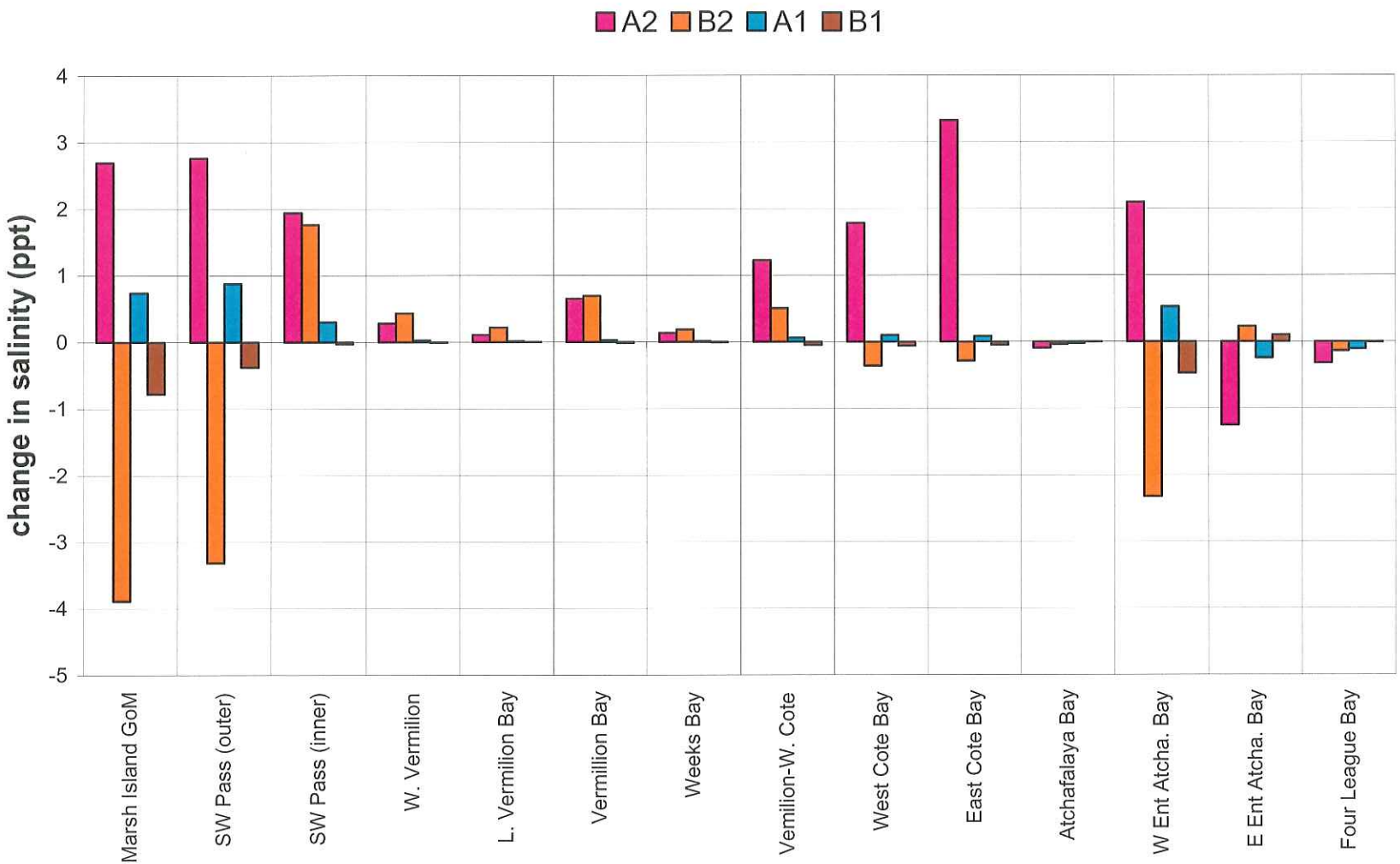

Figure 6.13 Modeled Salinity Change for High Stream Flow Conditions

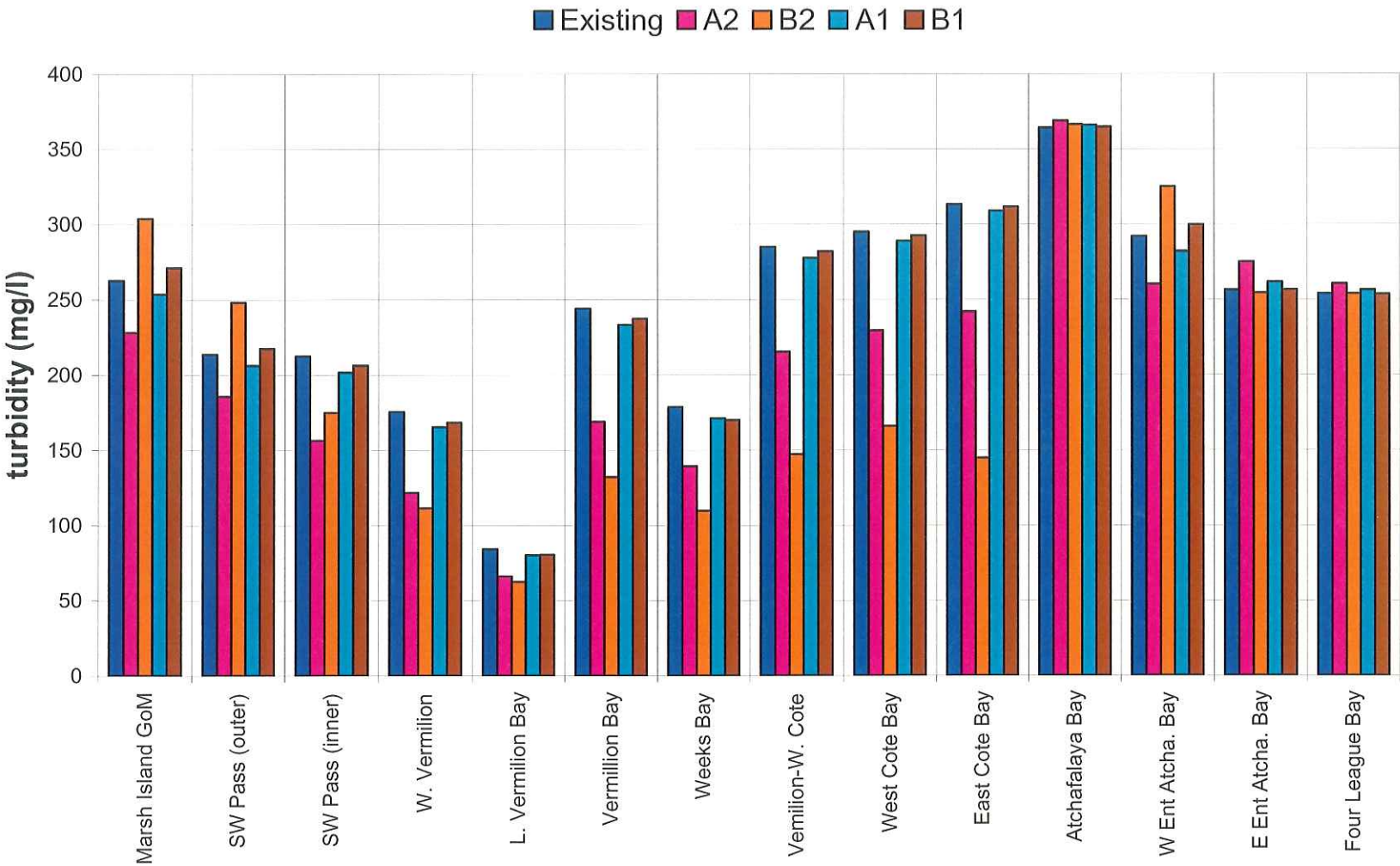

Figure 6.14 Modeled Turbidity for High Stream Flow Conditions

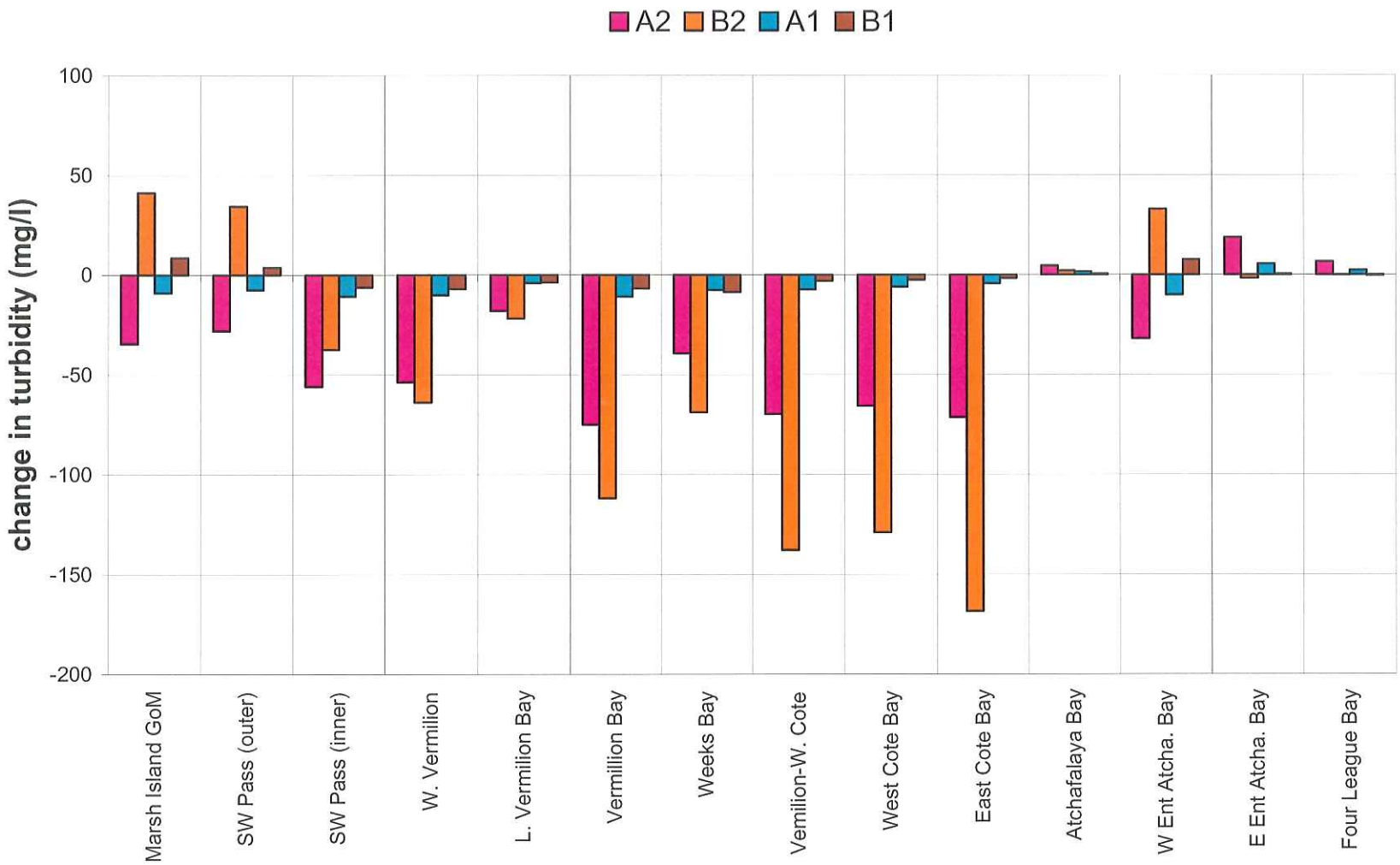

Figure 6.15 Modeled Turbidity Change for High Stream Flow Conditions

6.4 Low Stream Flow Model Results

6.4.1 Reef Effect on Salinity

Figures 6.16 and 6.17 show the effects the reefs have on salinity during low, summer flow conditions. Figure 6.17 shows that the A2 and B2 reefs (crests at MHW) cause the greatest changes. The A2 reef generally causes the greatest salinity increases (up to 3.3 ppt in East Cote Blanche Bay and near 2 ppt in West Cote Blanche Bay and at the western entrance to Atchafalaya Bay). To the east, the A2 reef decreases salinity by up to 0.5 ppt. Higher salinity in the Gulf of Mexico near Marsh Island and Southwest Pass indicate that the A2 reef directs the freshwater plume farther seaward where it mixes with salt water before migrating westward along Marsh Island.

The B2 reef increases salinity by about 1 ppt in Vermilion Bay and the area where Vermilion Bay becomes West Cote Blanche Bay (Vermilion-W. Cote). However, cutting off the East Cote Blanche Bay tidal exchange connection to the Gulf of Mexico (and so the bulk of the saline water supply), the reef decreases salinity by about 2 to 3 ppt in West Cote and East Cote Blanche Bays. Lower salinity in the Gulf of Mexico (at the western and eastern entrances to Atchafalaya Bay and near Marsh Island) indicate a tendency of the B2 reef to freshen the water close to the coast by blocking the Atchafalaya Bay freshwater from entering East Cote Blanche Bay and redirecting the freshwater westward along the seaward side of Marsh Island.

Both low crested reef alternatives, A1 and B1, cause only marginal changes in salinity (0.3 ppt or less) throughout the area of interest.

In summary, reef alternative A2 causes the greatest salinity increase (3.3 ppt) in the system and generally increases salinity west of the reef. B2 increases salinity as much as 1.4 ppt in Vermilion Bay but decreases salinity in West and East Cote Blanche Bays and other locations. In the bays west of the reefs, alternative A2 causes salinities to reach 5 ppt at one location (East Cote Blanche Bay). For the other alternatives salinities do not reach 5 ppt in the bays west of the reefs.

6.4.2 Reef Effect on Turbidity

Figures 6.18 and 6.19 show the effect the reefs have on the turbidity distribution during low, summer flow conditions. None of the reef alternatives appreciably affect the turbidity in the system under these conditions.

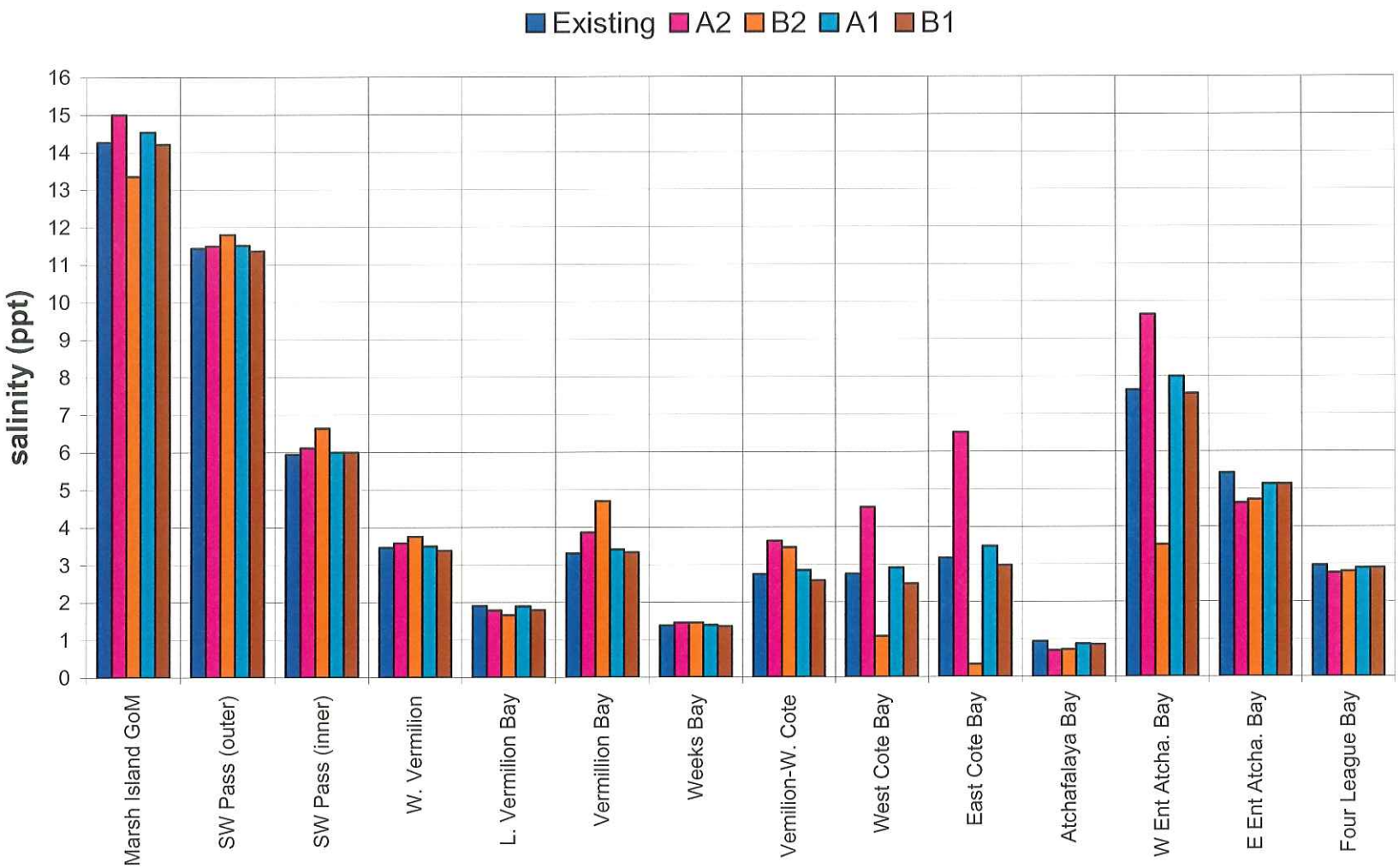

Figure 6.16 Modeled Salinity for Low/Summer Stream Flow Conditions

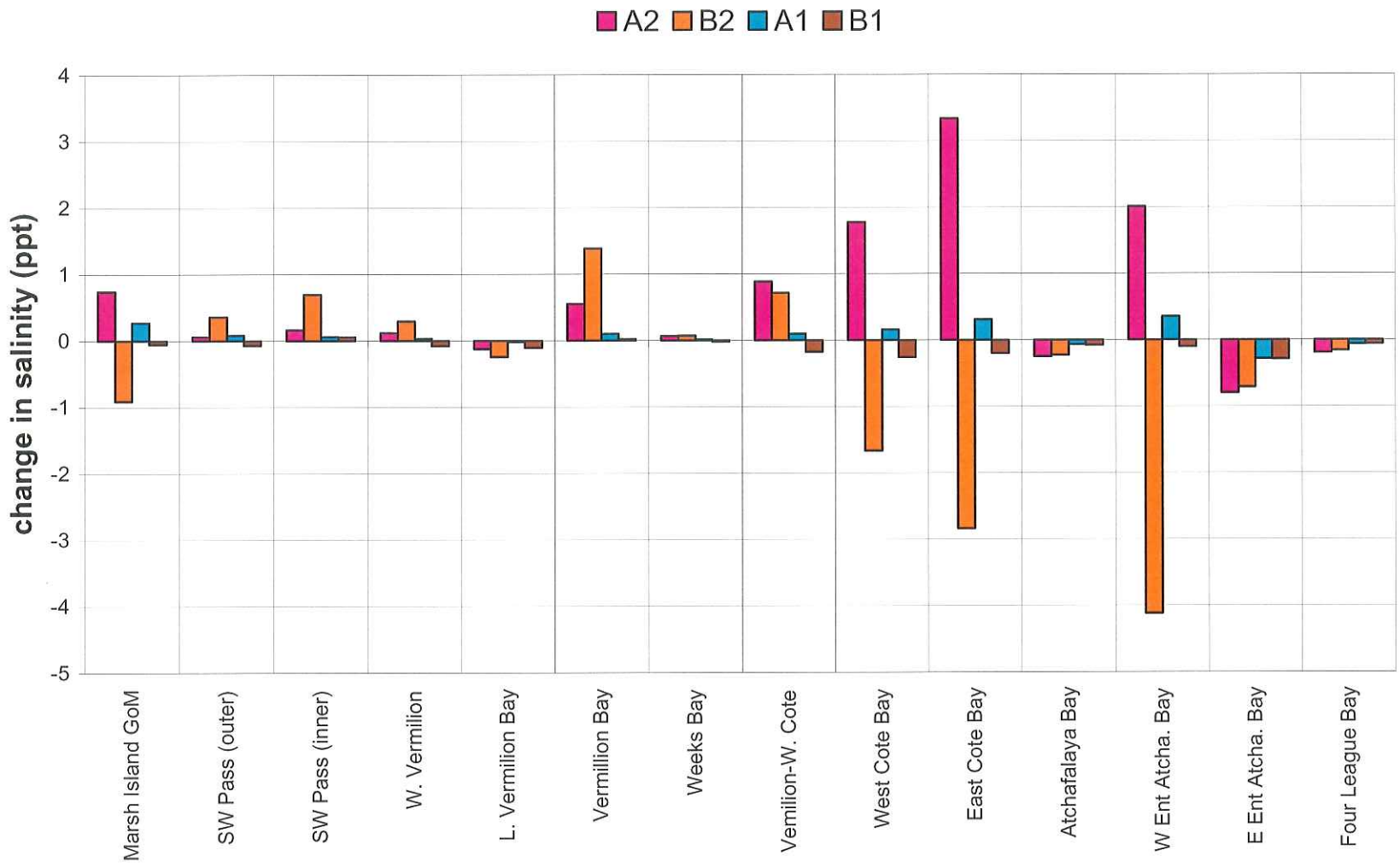

Figure 6.17 Modeled Salinity Change for Low/Summer Stream Flow Conditions

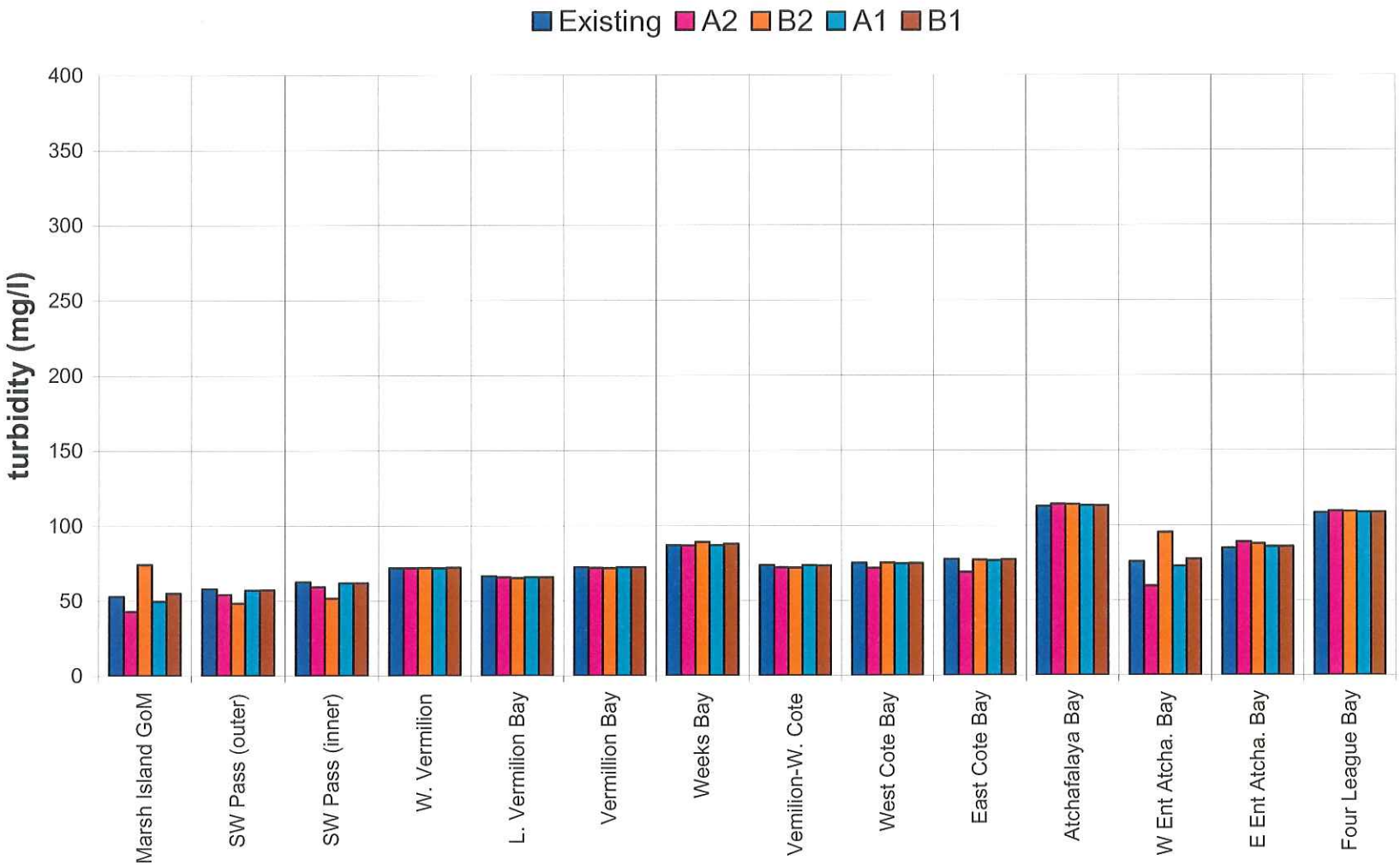

Figure 6.18 Modeled Turbidity for Low/Summer Stream Flow Conditions

Figure 6.19 Modeled Turbidity Change for Low/Summer Stream Flow Conditions

6.5 Intermediate Stream Flow Model Results

6.5.1 Reef Effect on Salinity

Figures 6.20 and 6.21 show the effects the reefs have on salinity during intermediate flow/winter conditions. Figure 6.21 shows that the A2 and B2 reefs (crests at MHW) cause the largest changes. The A2 reef causes the greatest increase of 1.7 – 2.3 ppt (West Cote and East Cote Blanche Bays); it causes small increases (less than 1 ppt) in the bays west of West Cote Blanche Bay. Also, higher salinity in nearshore areas west of Atchafalaya Bay (W Ent Atcha Bay, Marsh Island GoM, and SW Pass) indicate that the A2 reef displaces the Lower Atchafalaya River and Wax Lake Outlet freshwater plumes farther seaward than existing conditions. In deeper, higher saline water, the freshwater plumes become more saline before migrating to the west.

The B2 reef causes a small salinity increase, about 0.5 ppt, in Vermilion Bay and small decreases in salinity (about 0.5 – 1 ppt) in West Cote and East Cote Blanche Bays under intermediate stream flow conditions. Lower salinity (by 1 – 2 ppt) at the western entrance to Atchafalaya Bay and in the Gulf of Mexico near Marsh Island suggest that the reef, while preventing Atchafalaya Bay freshwater from entering East Cote Blanche Bay, redirected all of the Atchafalaya Bay freshwater to these locations.

Under the intermediate/winter stream flow conditions, the A1 reef with a crest at -3 ft MLW generally increases the salinity (as much as 0.5 ppt in West Vermilion Bay) west of the reef. The B1 reef generally causes smaller changes in salinity.

In summary, reef alternative A2 causes the greatest salinity increase (2.3 ppt) in the system and generally increases salinity west of the reef. B2 increases salinity as much as 0.4 ppt in the bays west of the reef but decreases salinity in West and East Cote Blanche Bays and other locations. In the bays west of the reefs, salinities do not reach 5 ppt for any alternative, although A2 increases salinity to 5.1 ppt in the Western Entrance to Atchafalaya Bay.

6.5.2 Reef Effect on Turbidity

Figures 6.22 and 6.23 show the effects the reefs have on the turbidity distribution during intermediate/winter flow. Both of the MHW crested reefs considerably decrease (40 mg/l or more) turbidity in Vermilion, West Cote, and East Cote Blanche Bays. This change represents about a 25 percent decrease. Reef alternative B2, which eliminates the direct connection between East Cote Blanche Bay and Atchafalaya Bay, causes larger decreases in turbidity than does A2. Neither of the -3 ft MLW crested reef alternatives appreciably change turbidity anywhere in the area of interest.

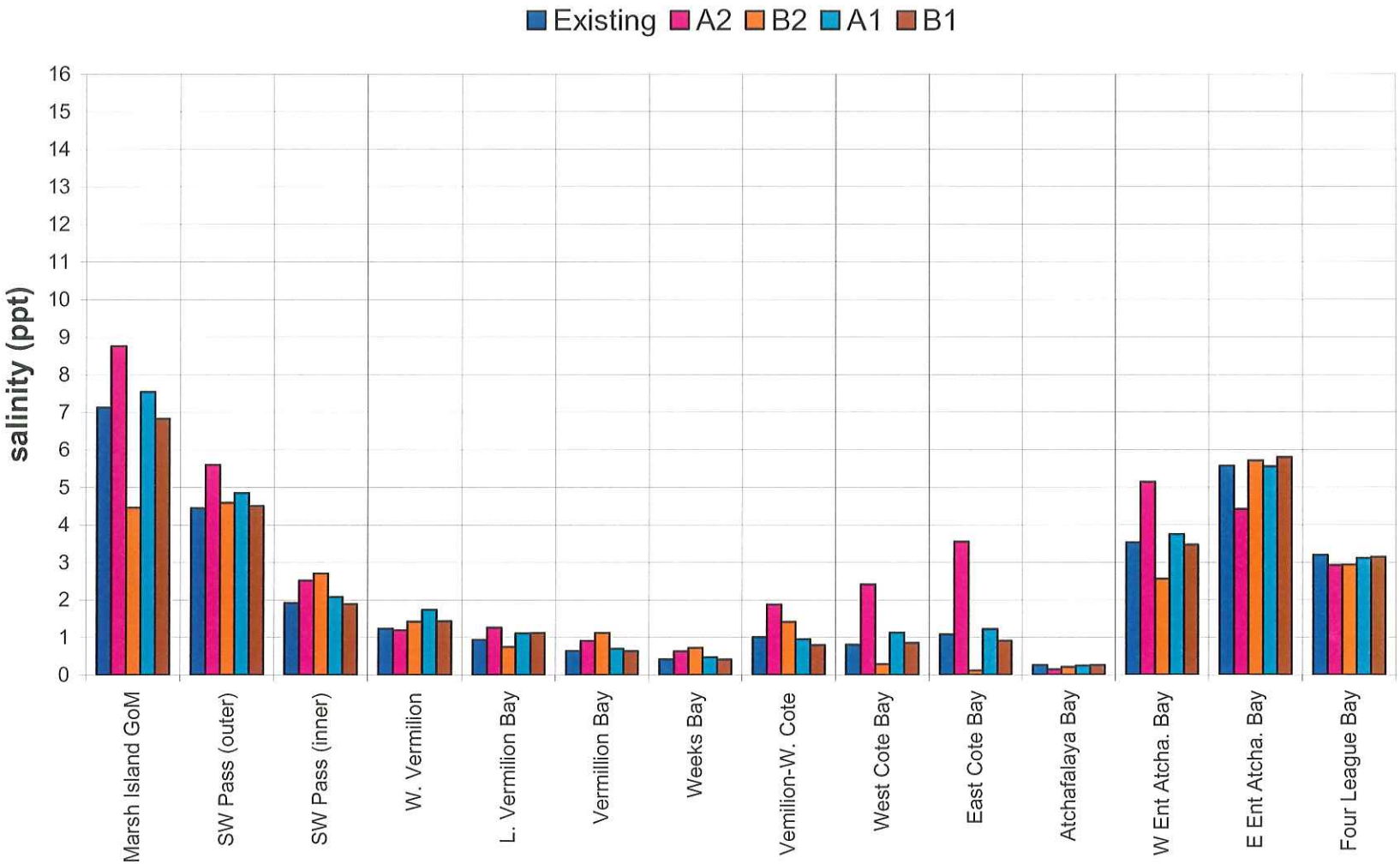

Figure 6.20 Modeled Salinity for Intermediate/Winter Stream Flow Conditions

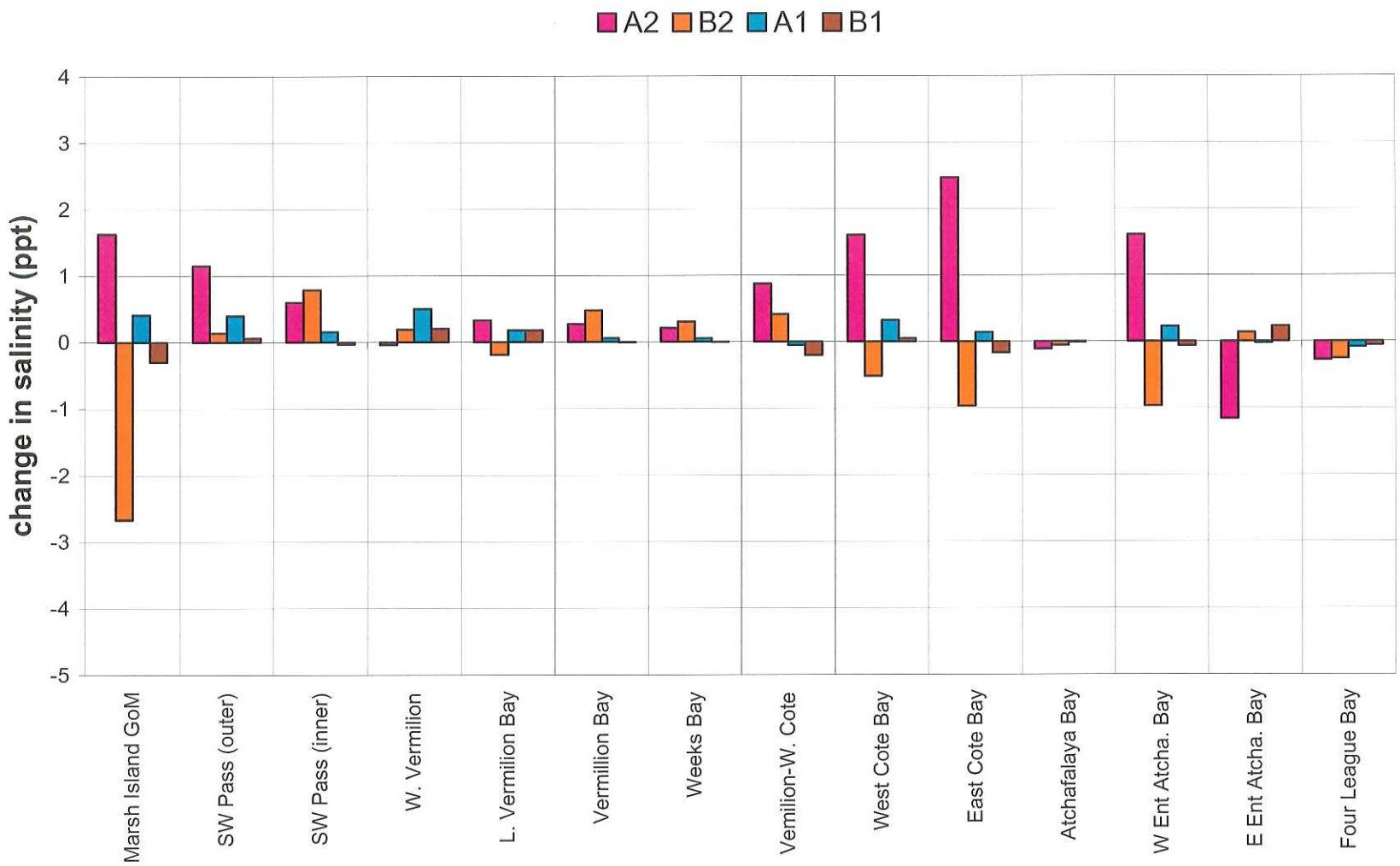

Figure 6.21 Modeled Salinity Change for Intermediate/Winter Stream Flow Conditions

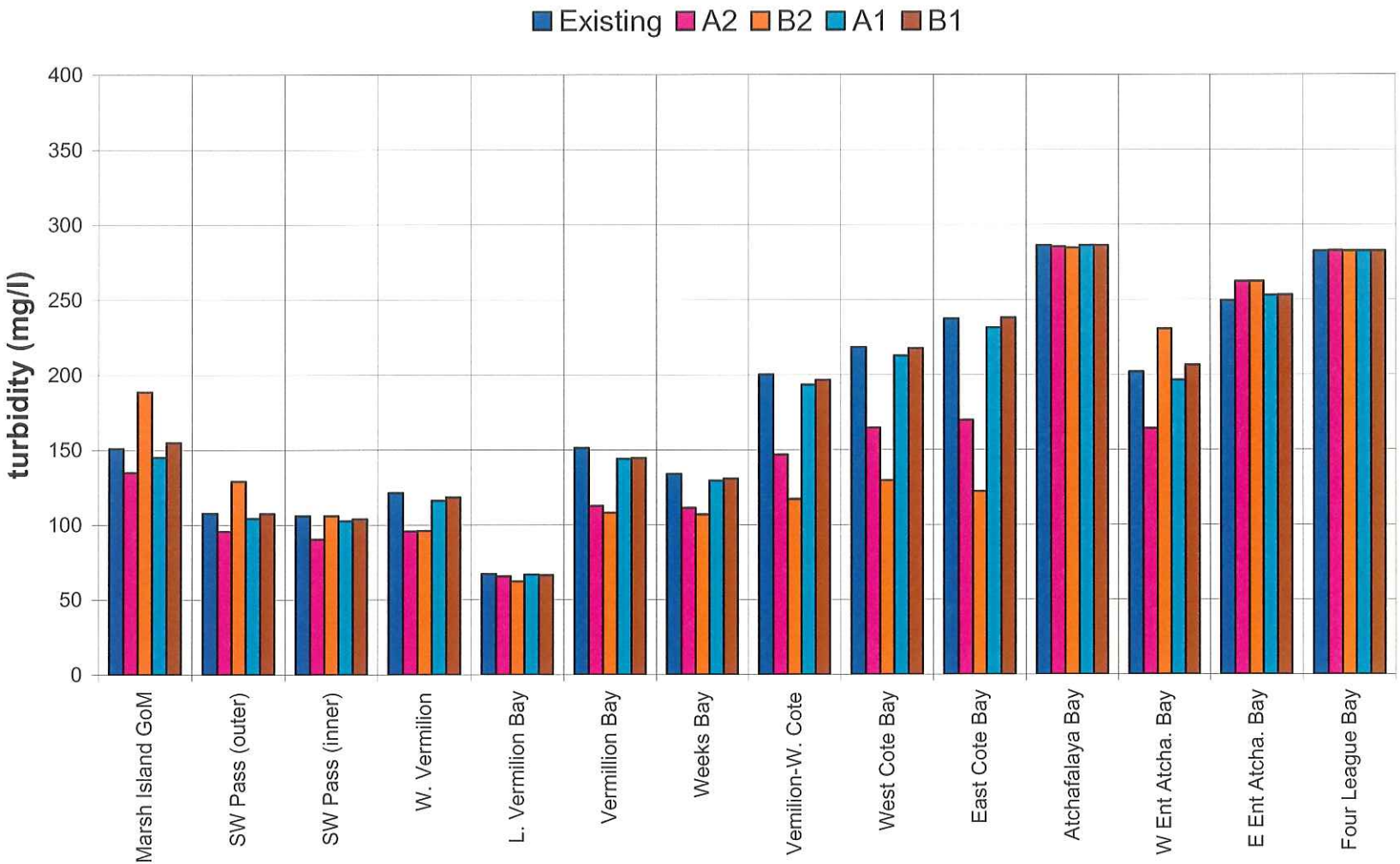

Figure 6.22 Modeled Turbidity for Intermediate/Winter Stream Flow Conditions

Figure 6.23 Modeled Turbidity Change for Intermediate/Winter Stream Flow Conditions

6.6 Summary of Findings on Reef Effects on Salinity and Turbidity

6.6.1 Effects on Salinity

In general terms, the horizontal momentum of the freshwater plumes exiting the Lower Atchafalaya River and Wax Lake Outlet into Atchafalaya Bay carries them longitudinally in a southerly direction. In addition, mixing processes between the plume and ambient bay waters, and the effect of wind action, cause the plumes to move and grow laterally (approximately east-west). The salinity concentration of the plumes increases with this mixing.

Reef B2 blocks the freshwater plume from directly entering East Cote Blanche Bay. Relative to existing conditions, this blocking effect causes a larger volume of freshwater to move farther seaward; in turn, the westerly growth/penetration of the freshwater plume occurs farther seaward. These processes cause the observed decreases in salinity at the western entrance to Atchafalaya Bay and offshore Marsh Island. In addition to blocking freshwater, the B2 reef also blocks saline Gulf water from entering East Cote Blanche and West Cote Blanche Bays. Generally, model results suggest that the effect of blocking saline water has greater impact than that of blocking freshwater; thus, salinity decreases at these locations as freshwater from the Jaws and other inputs builds behind the reef. Increase in saline water entering through Southwest Pass causes small increases in salinity in Vermilion Bay.

The effects of reef B1 are similar to those of reef B2; however, B1 causes much smaller magnitude changes than B2.

The effects of reef A2 are somewhat different. The reef restricts the westerly growth of the freshwater plume (exiting the Lower Atchafalaya River and Wax Lake Outlet into Atchafalaya Bay) until it passes the seaward tip of the reef. Consequently, given the relative orientations of reefs A2 and B2, the westerly growth of the freshwater plume for A2 occurs well seaward of that for B2 (and even more seaward relative to that for existing conditions). The A2 alignment maintains the southerly momentum of the plume and directs it farther seaward where it mixes with higher salinity concentrations before migrating (typically westward). The reduction of freshwater reaching the western entrance to Atchafalaya Bay, offshore Marsh Island, and offshore Southwest Pass increases salinity at these locations.

Reef A2 is effective in blocking the freshwater plume from entering West Cote Blanche and East Cote Blanche Bays. By blocking the freshwater and allowing Gulf saline water to enter the bays, reef A2 causes salinity concentrations to increase at these locations.

The effects of reef A1 are similar to those of reef A2; however, A1 causes much smaller magnitude changes than A2.

6.6.2 Effects on Turbidity

As modeled, the primary sources of turbidity are the Lower Atchafalaya River and Wax Lake Outlet. Both A2 and B2 reefs block, in varying degrees, freshwater (turbidity) from these rivers from entering the Acadiana Bays system west of Atchafalaya Bay. Consequently, East Cote Blanche, West Cote Blanche, and Vermilion Bays see reductions in turbidity. The magnitudes of the reductions are functions of the stream flow phase — reductions are significantly high during high and intermediate flows, substantial during the mean flow, and negligible during low flow. Since reef B2 completely prevents the turbid waters of the two major rivers from entering the western bays (whereas A2 only partially blocks these waters), reef B2 causes larger turbidity reductions than does A2. Reefs A1 and B1 have negligible effects.

6.7 Reef Effect on Storm Surge

This study also examined the potential effects of the reefs on storm surge elevations in the bays. This section discusses the assumptions, model modifications, and results.

6.7.1 Storm Surge Assumptions

The simulation applied a +10.8 ft NGVD peak storm surge elevation (8 ft above MHW) offshore, approximately corresponding to that experienced during Hurricane Lili (which made landfall in coastal Louisiana on October 3, 2002). The hydrograph shape (Figure 6.24) used in this model came from the Escambia County, Florida hydrographs recommended by the Florida Department of Transportation (Sheppard and Miller, 2003). The model assumed mean stream flow boundary conditions. The model applied no wind boundary condition; a wave model application (Chapter 7) describes the reefs' effects on storm surge waves.

6.7.2 Modifications to the Model

Figure 6.25 shows the model mesh with added floodable land areas (shown in green) that the storm surge overtops. Adequate consideration of flooded land (upland storage) comprises an important aspect of surge modeling. The typical floodable land elevation rose to about +2 ft NGVD. The model applied Manning's roughness values of 0.05 to the reefs.

6.7.3 Effects on Storm Surge at the Shoreline

To investigate the effects of the reef on storm surge, the model estimated — for existing and reef alternative conditions— the peak storm surge elevation at locations along the interior bay shorelines (Figure 6.26). Figure 6.27 shows the change in peak storm surge elevation at these shoreline points. As seen in this figure, the B2 reef alternative yields the greatest effect — the reef decreases the maximum storm surge by about a half foot. Reefs A2 and B1 produced less effect – generally a 0.1 – 0.2 ft decrease. Reef A1 showed the least effect.

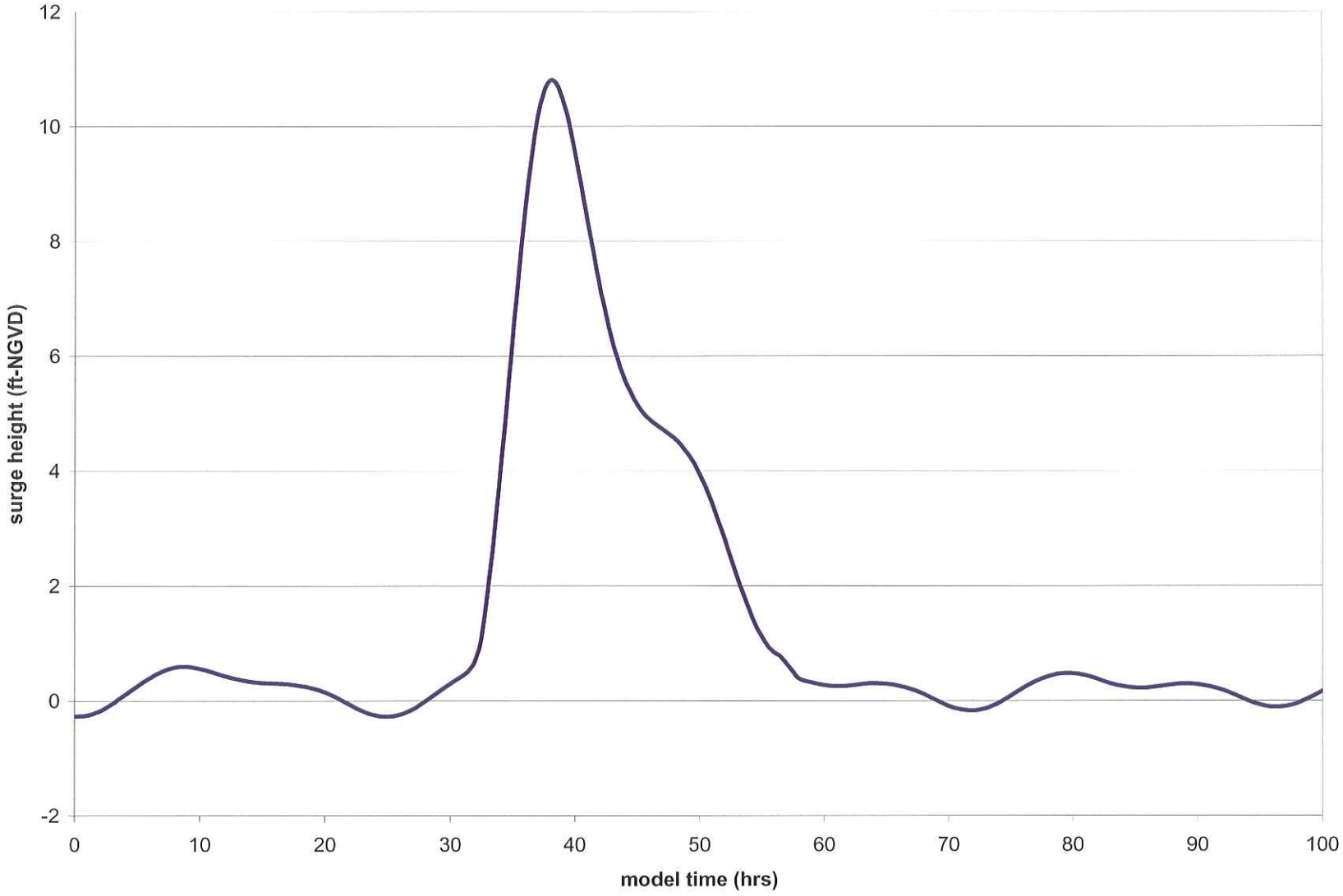

Figure 6.24 Water Level Hydrograph for the Storm Surge Simulations

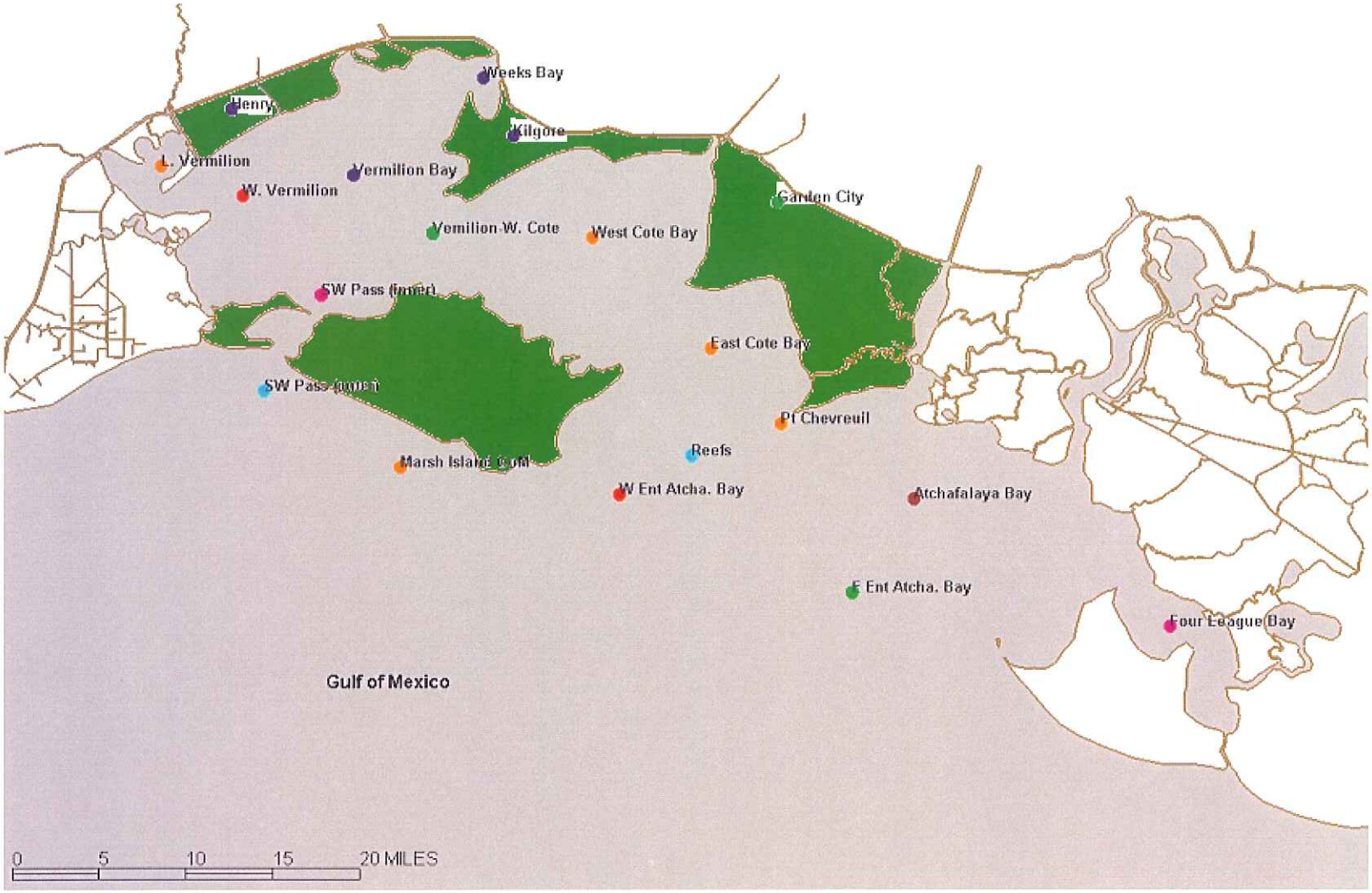

Figure 6.25 Land Area Added to Model Mesh for Storm Surge Simulations

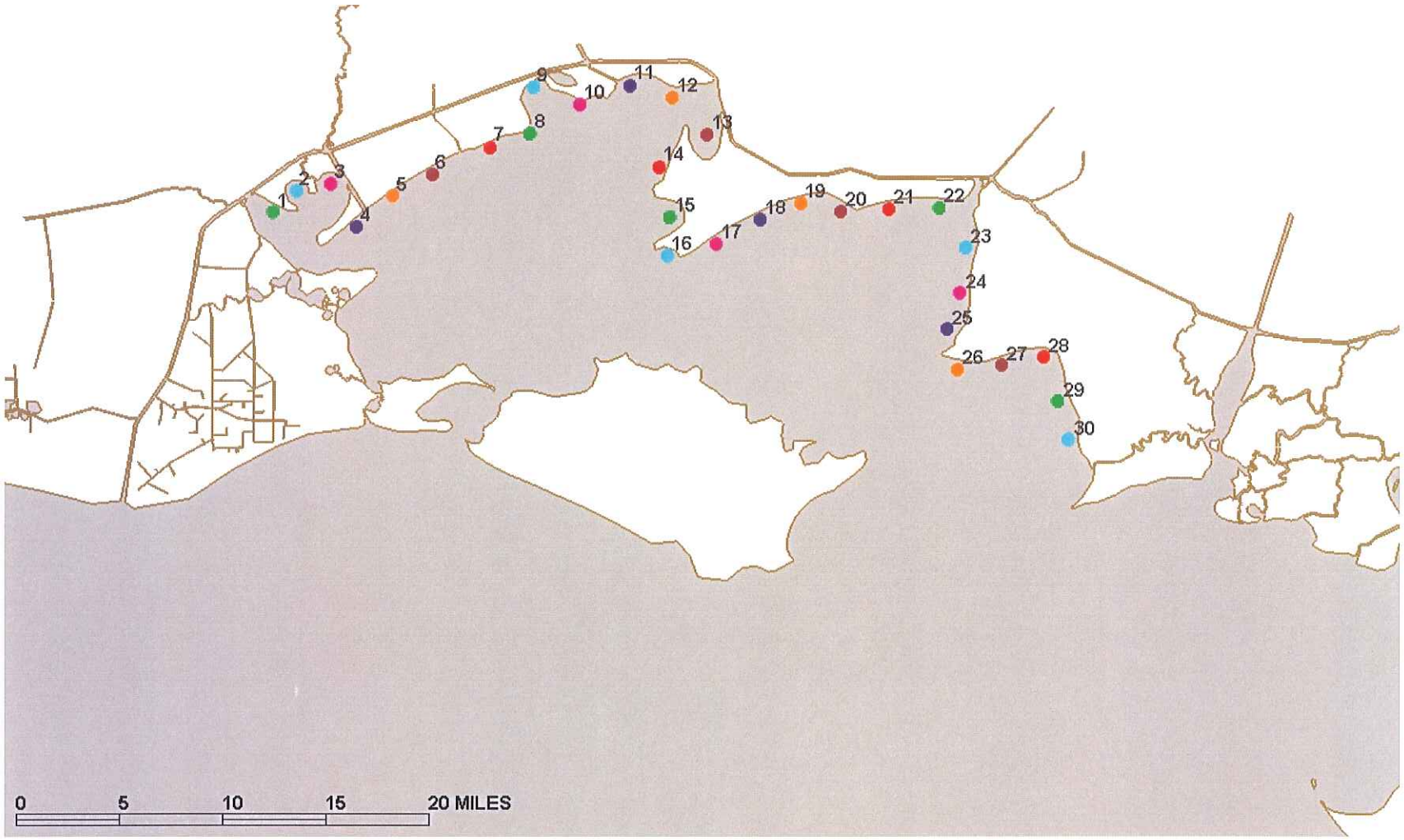

Figure 6.26 Bay Shore Simulation Observation Points

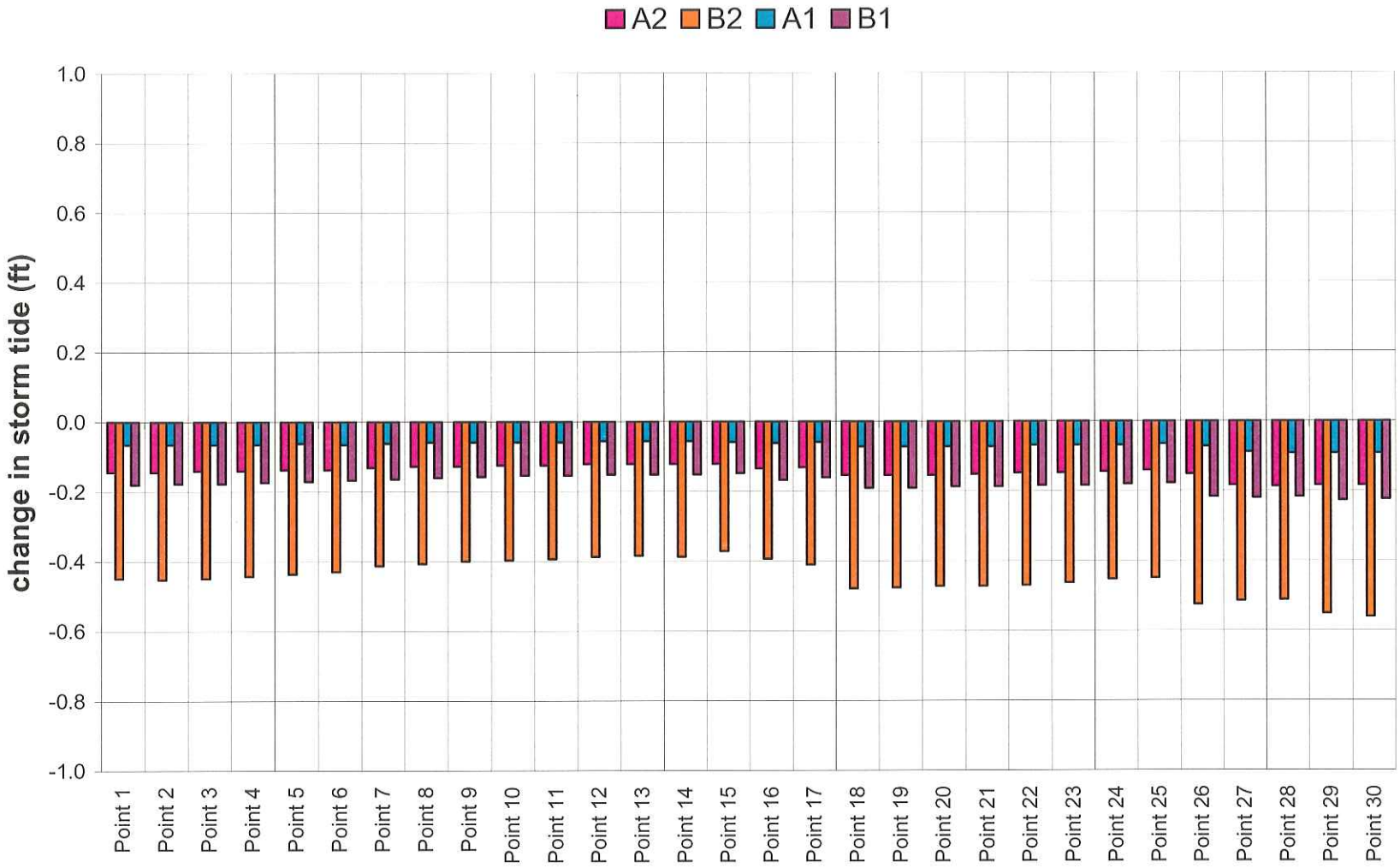

Figure 6.27 Effects on Peak Storm Surge along the Bay Shoreline

7.0 WAVE MODELING OF REEF ALTERNATIVES

The previous chapter demonstrated that, among the alternatives considered, reef alternatives A2 and B2 created the greatest changes in salinity and turbidity in Acadiana Bays. This chapter documents the application of the STWAVE Taylor model to analyze the effects of these alternatives on waves.

7.1 Model Boundary Conditions

The wind climate records of a USACE station at Cypremort Point from December 1999 to October 2002 were analyzed to select model surface boundary conditions. Table 7.1 presents the occurrence frequency of wind speeds. Given the generally small wave heights in the study area, a low-frequency wind speed return period was chosen to model the effect of the reef alternatives on reasonably large waves. In particular, modeling simulated the effects of the reef alternatives on waves generated by 22 miles per hour (mph) (10 m/s) winds, a condition with a 3% exceedance frequency.

Table 7.1 USACE Cypremort Point Station Wind Speed Exceedance Frequency

Wind Speed			Exceedance Frequency
(mph)	(ft/s)	(m/s)	
13	19.7	6	18.65
18	26.2	8	7.09
22	32.8	10	2.95
33	49.2	15	0.13
49	72.2	22	0.0082

To obtain estimates of the largest waves that may develop with the chosen wind speed, two wind directions, S15°E and N50°W, which provide the longest open fetch conditions, were chosen for modeling.

In accord with the findings of Jensen (1985) and Chapter 5 regarding wave heights, no Gulf-generated swell waves were included at the offshore boundary. At worst, this choice may slightly underestimate wave heights in the model domain.

7.2 Results

Figure 7.1 presents the domain of the STWAVE Taylor model applied to evaluate reef alternatives A2 and B2 for winds out of the south-southeast. The domain contains 1,520 by 2,012 cells with a 115-ft grid spacing and an offshore orientation perpendicular to S15°E. Figure 7.2 presents the domain of the STWAVE Taylor model applied to evaluate reef alternatives A2 and B2 for winds out of the northwest. The domain contains 1,208 by 2,427 cells with a 115-ft grid spacing and an offshore orientation perpendicular to N50°W.

Applying a uniform wind speed of 22 mph over the entire domain allows an evaluation of the wave field within the domain for wind events with a historical exceedance of approximately 3%. Figures 7.1 and 7.2 indicate the orientation of the wind field within the STWAVE domains.

Figure 7.3 presents a contour plot of the simulated wave field for existing conditions when 22 mph winds are blowing from S15°E. The wave field rapidly grows proceeding inshore from the offshore boundary. Wave heights reach about 1.2 ft in the majority of the study area; they reach about 1.5 ft in a few locations.

Figure 7.4 presents a contour plot of the simulated wave field for reef alternative A2 conditions with 22 mph winds blowing from S15°E. Again, the wave field rapidly grows proceeding inshore from the offshore boundary until it encounters the reef and dissipates. Waves regenerate on the landward side of the reef and grow as they propagate into the Cote Blanche Bays. Waves generally do not exceed 1.3 ft within the western Acadiana Bays.

Figure 7.5 presents a contour plot of the wave height difference between the reef alternative A2 and existing conditions when 22 mph winds blow from S15°E. The reef mainly reduces wave heights in its immediate vicinity in western Atchafalaya Bay; smaller changes occur in limited portions of East Cote Blanche Bay.

Applying a uniform wind field out of the northwest allows another evaluation of the reef's effect on the wave field. Figure 7.6 presents a contour plot of the simulated wave height field for existing conditions when 22 mph winds blow from N50°W.

For 22 mph winds blowing from N50°W, Figure 7.7 indicates that the significant wave height field changes caused by reef alternative A2 generally occur immediately downwind of the reef in western Atchafalaya Bay. Smaller wave height changes, generally less than 0.3 ft, persist farther east in eastern Atchafalaya Bay towards Point Au Fer.

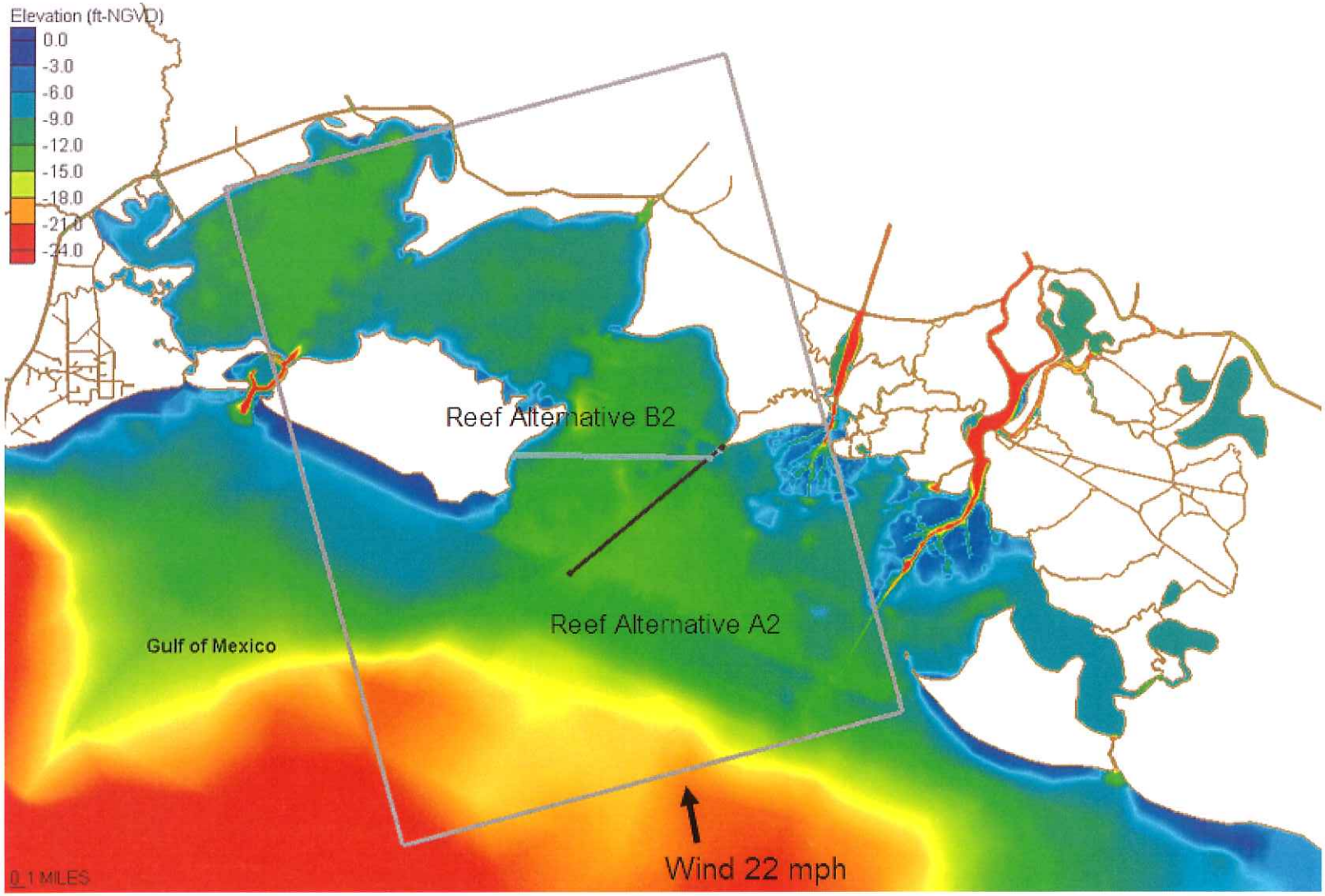

Figure 7.1 Modeling Domain and Location of Reef Alternatives A2 and B2; Winds from S15°E

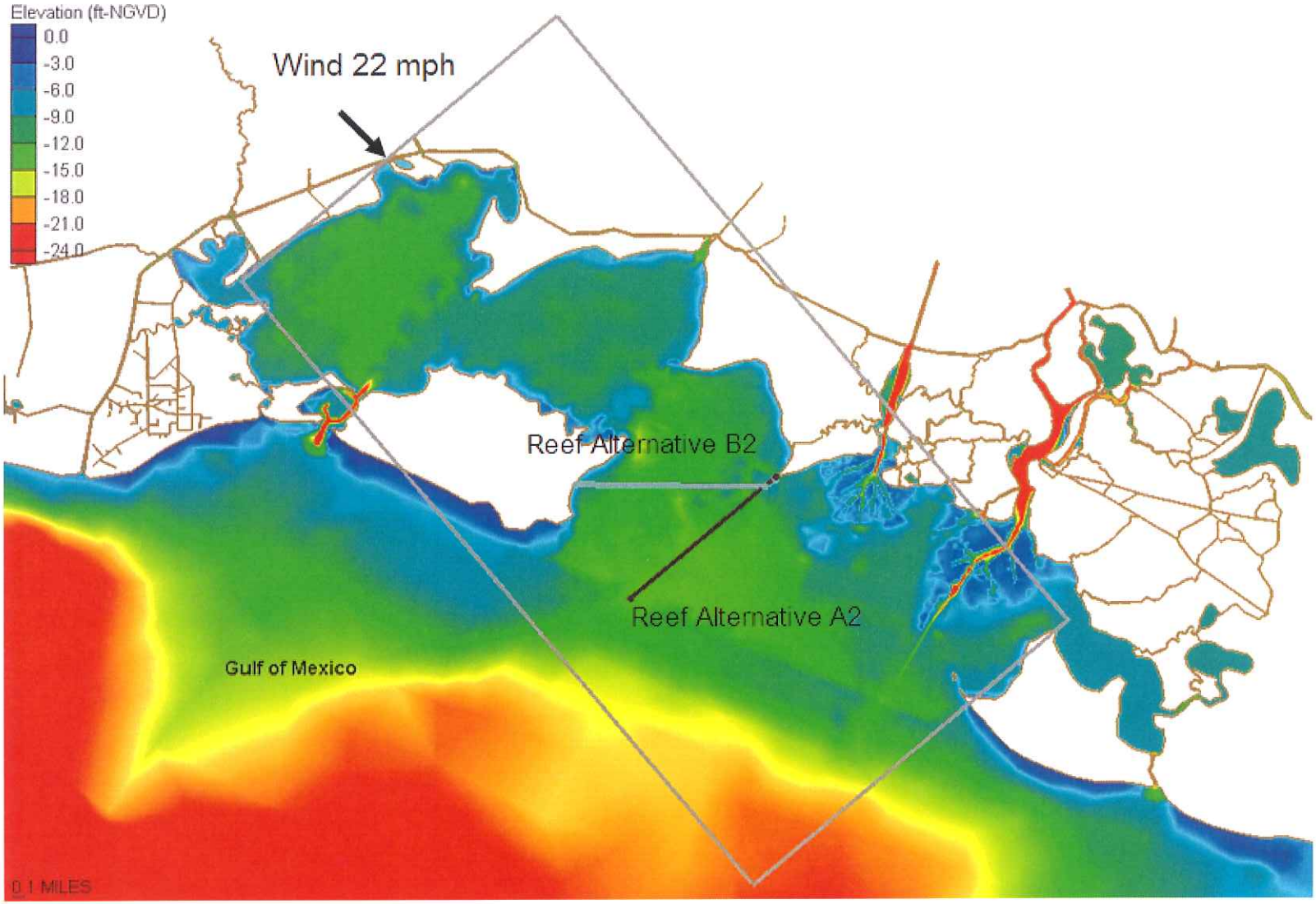

Figure 7.2 Modeling Domain and Location of Reef Alternatives A2 and B2; Winds from N50°W

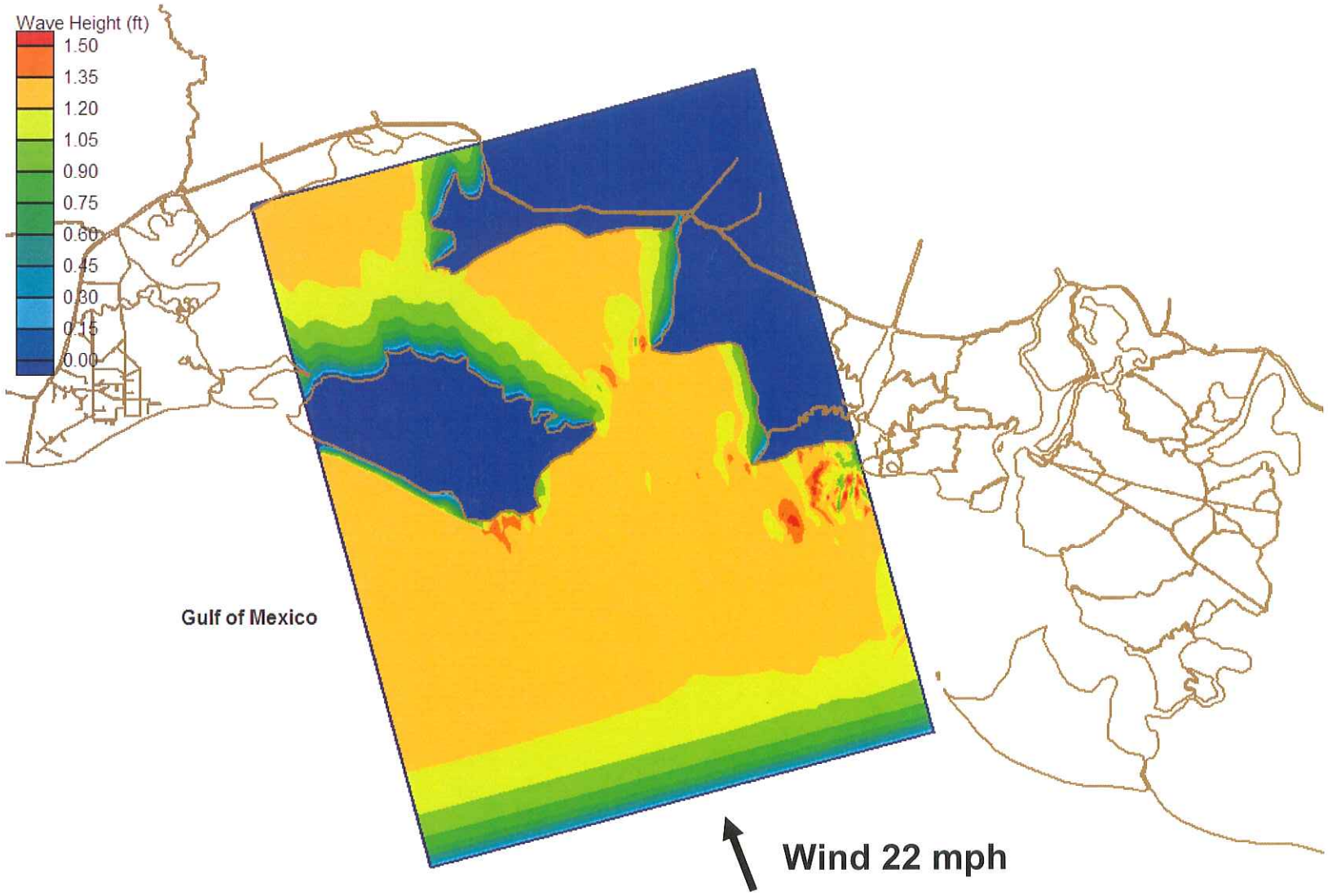

Figure 7.3 Contour Plot of Significant Wave Height for Existing Conditions; 22 mph Winds from S15°E

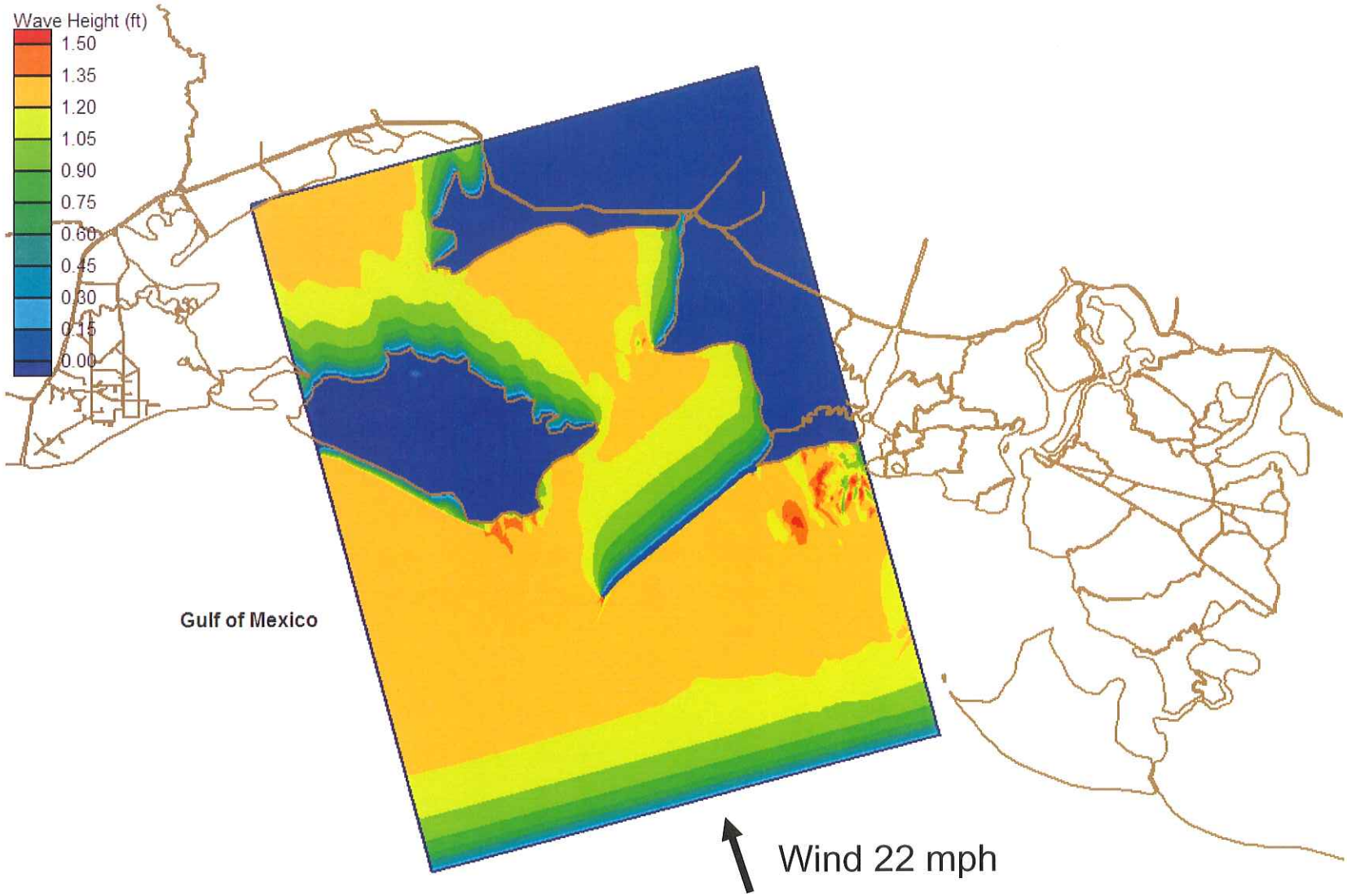

Figure 7.4 Contour Plot of Significant Wave Height for Reef Alternative A2; 22 mph Winds from S15°E

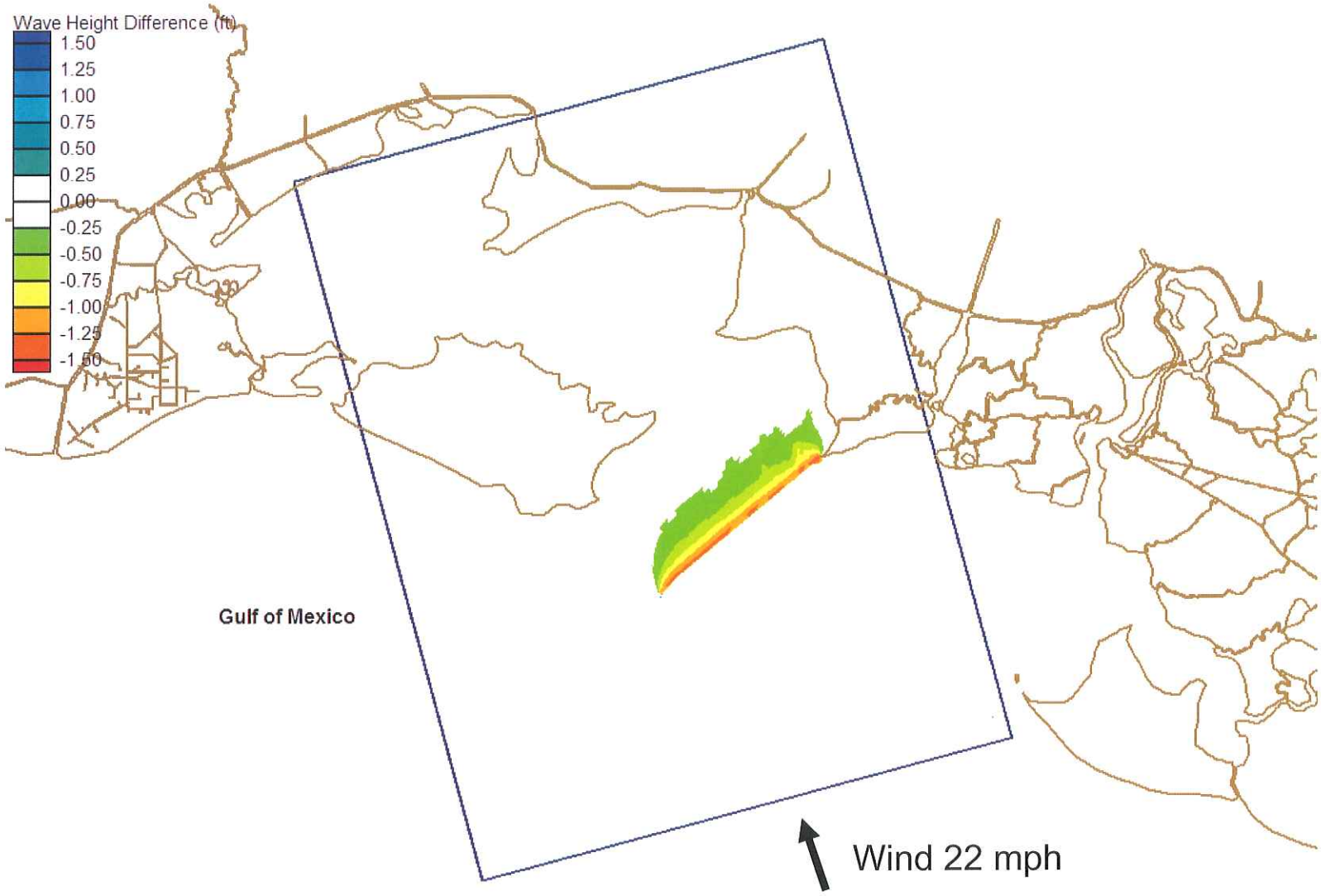

Figure 7.5 Contour Plot of Difference in Significant Wave Heights (Reef Alternative A2 versus Existing Conditions); 22 mph Winds from S15°E

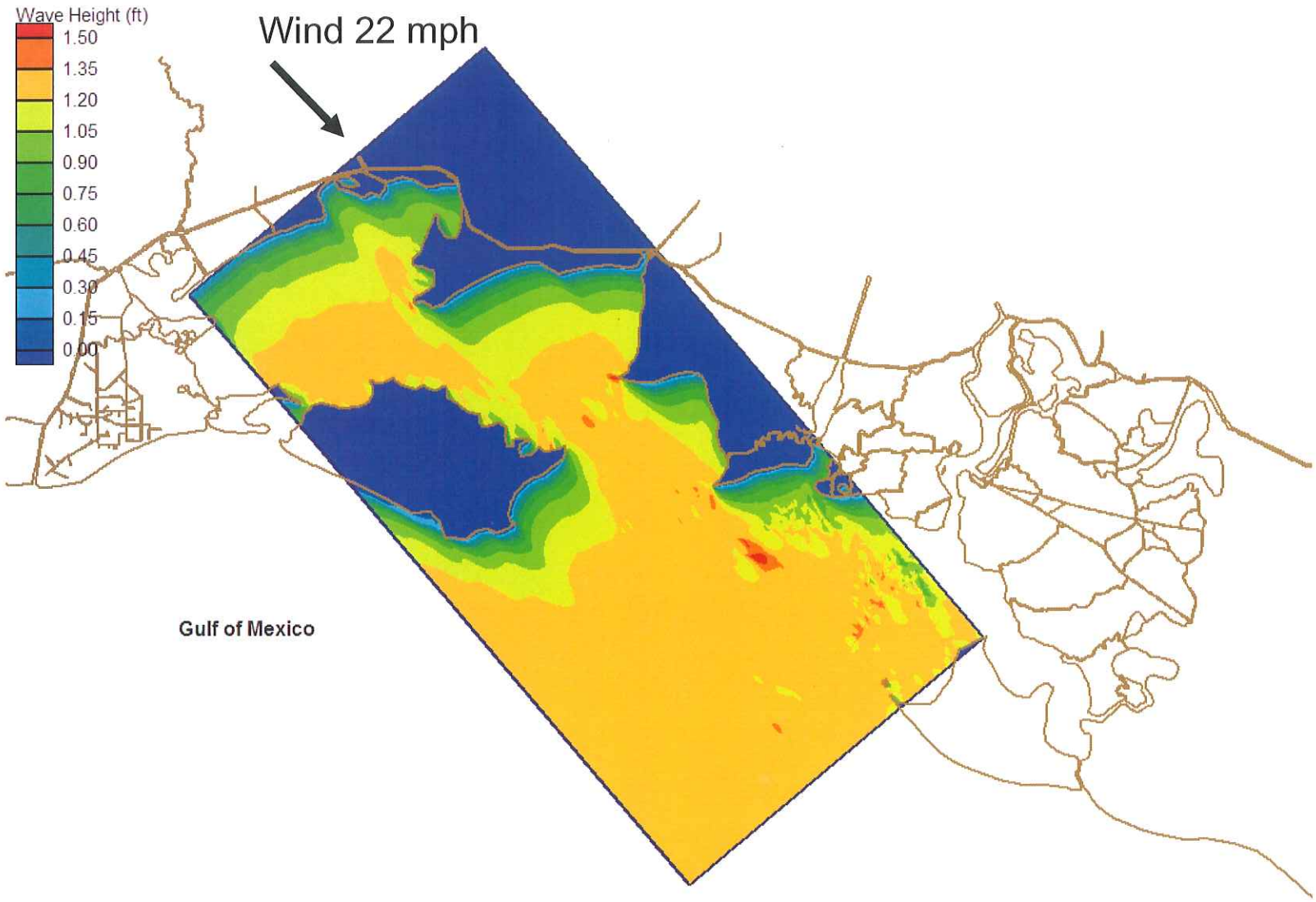

Figure 7.6 Contour Plot of Significant Wave Height for Existing Conditions; 22 mph Winds from N50°W

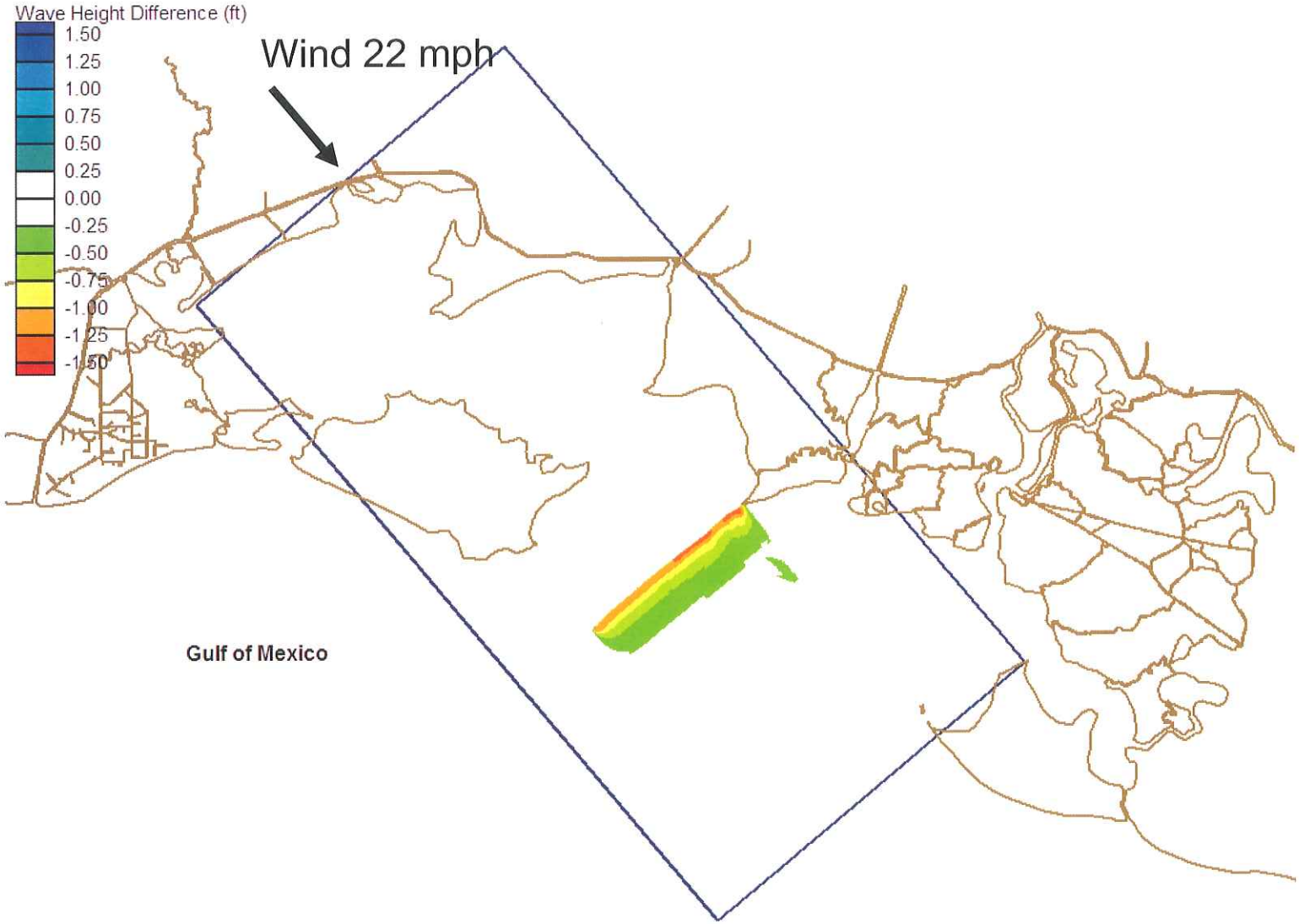

Figure 7.7 Contour Plot of Difference in Significant Wave Heights (Reef Alternative A2 versus Existing Conditions); 22 mph Winds from N50°W

Alternative B2 (Figure 7.1 and 7.2) orients in a more east-west direction than reef alternative A2. Figure 7.8 presents a contour plot of the simulated wave field for reef alternative B2 when 22 mph winds blow from S15°E. The wave field rapidly grows proceeding inshore from the offshore boundary until waves encounter the reef and dissipate. Waves regenerate on the landward side of the reef and grow as they propagate into the Cote Blanche Bays. Waves generally do not exceed 1.3 ft within the western Acadiana Bays. Figure 7.9 presents a contour plot of the wave height difference between Alternative B2 and existing conditions when 22 mph winds blow from S15°E. The reef mainly reduces wave heights in its immediate vicinity in western Atchafalaya Bay and East Cote Blanche Bay.

Figure 7.10 presents a contour plot of the simulated wave field for Alternative B2 when 22 mph winds blow from N50°W. Waves grow from the inshore boundary until they intersect with the reef, which causes dissipation of the wave energy. Waves regenerate on the southern side of reef. Figure 7.11 presents a contour plot of the wave height difference between Alternative B2 and existing conditions when 22 mph winds blow from N50°W. Results indicate Alternative B2 causes significant wave field changes, similar to reef alternative A2, in the vicinity of the structure. Changes to the wave field generally occur immediately downwind of the reef in western Atchafalaya Bay. Smaller wave height changes, generally less than 0.3 ft, persist farther east in eastern Atchafalaya Bay towards Point Au Fer.

7.3 Conclusions

The western regions of Acadiana Bays mostly experience locally generated wind waves because evidence suggests that bottom dissipation processes significantly attenuate long period swell from the Gulf of Mexico before they reach the interior Acadiana Bays. As expected, reef alternatives A2 and B2 act as complete physical barriers to wave propagation. However, absent the penetration of long period swell into Acadiana Bays, the zone of influence of reef alternatives A2 and B2 — the region over which they retard wave heights — is essentially restricted to their immediate downwind vicinity (about 10 miles or less). Even with the reefs, local wave generation processes raise, over a relatively short distance, the downwind wave heights to the levels experienced without the reefs. Thus, the wave modeling indicates the reef alternatives cause significant changes to the wave field only in the immediate downwind vicinity of the structures.

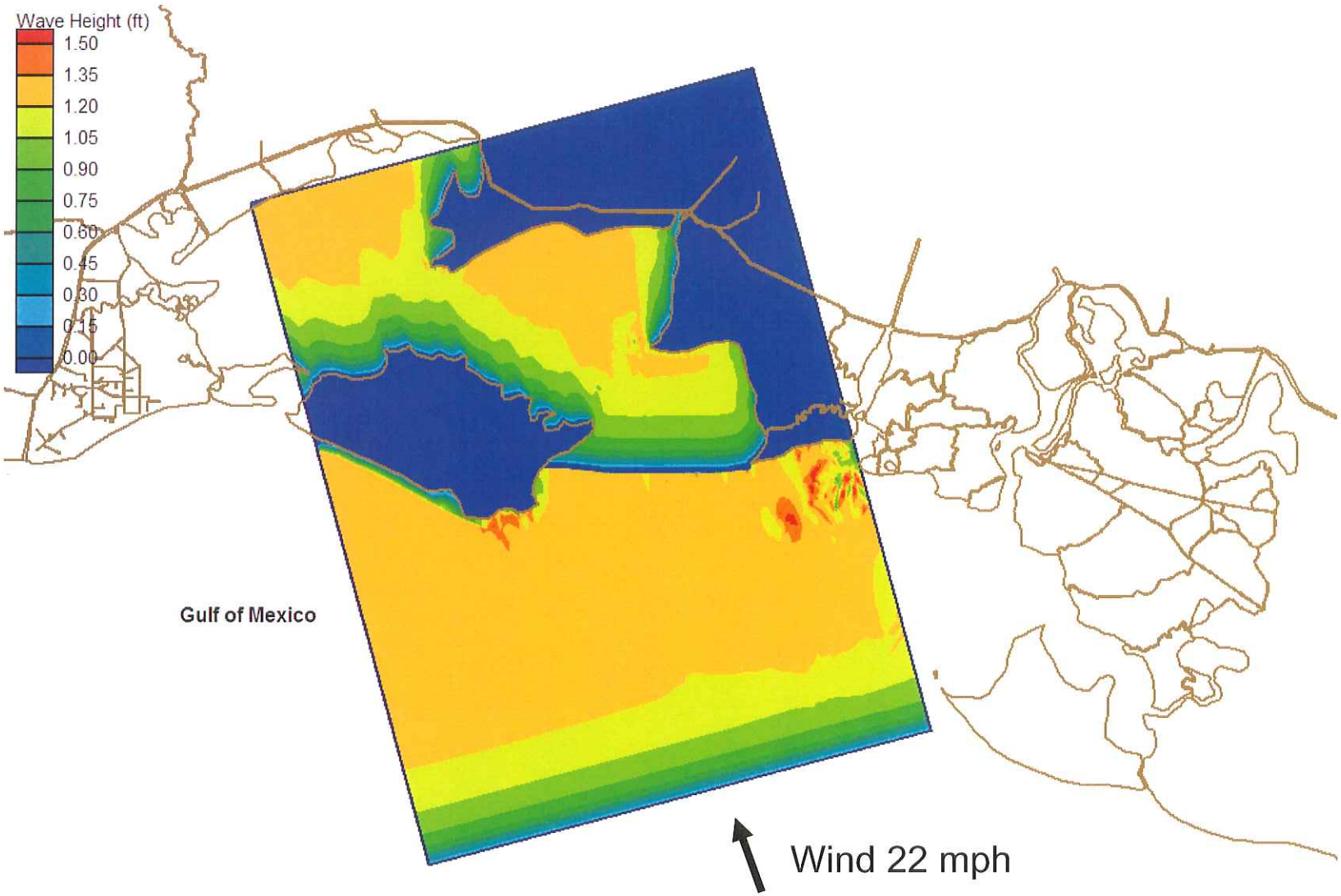

Figure 7.8 Contour Plot of Significant Wave Height for Reef Alternative B2; 22 mph Winds from S15°E

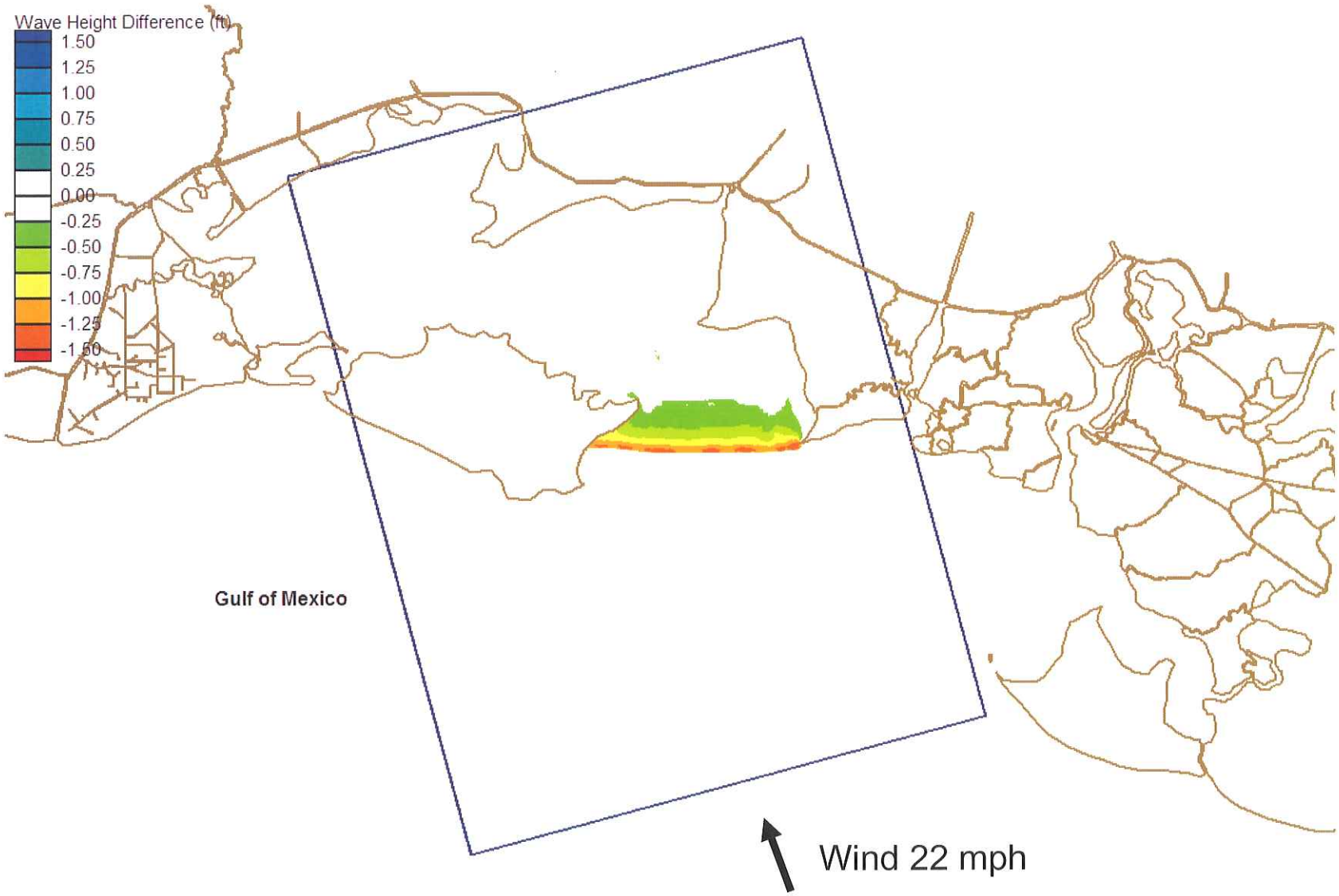

Figure 7.9 Contour Plot of Difference in Significant Wave Heights (Reef Alternative B2 versus Existing Conditions); 22 mph Winds from S15°E

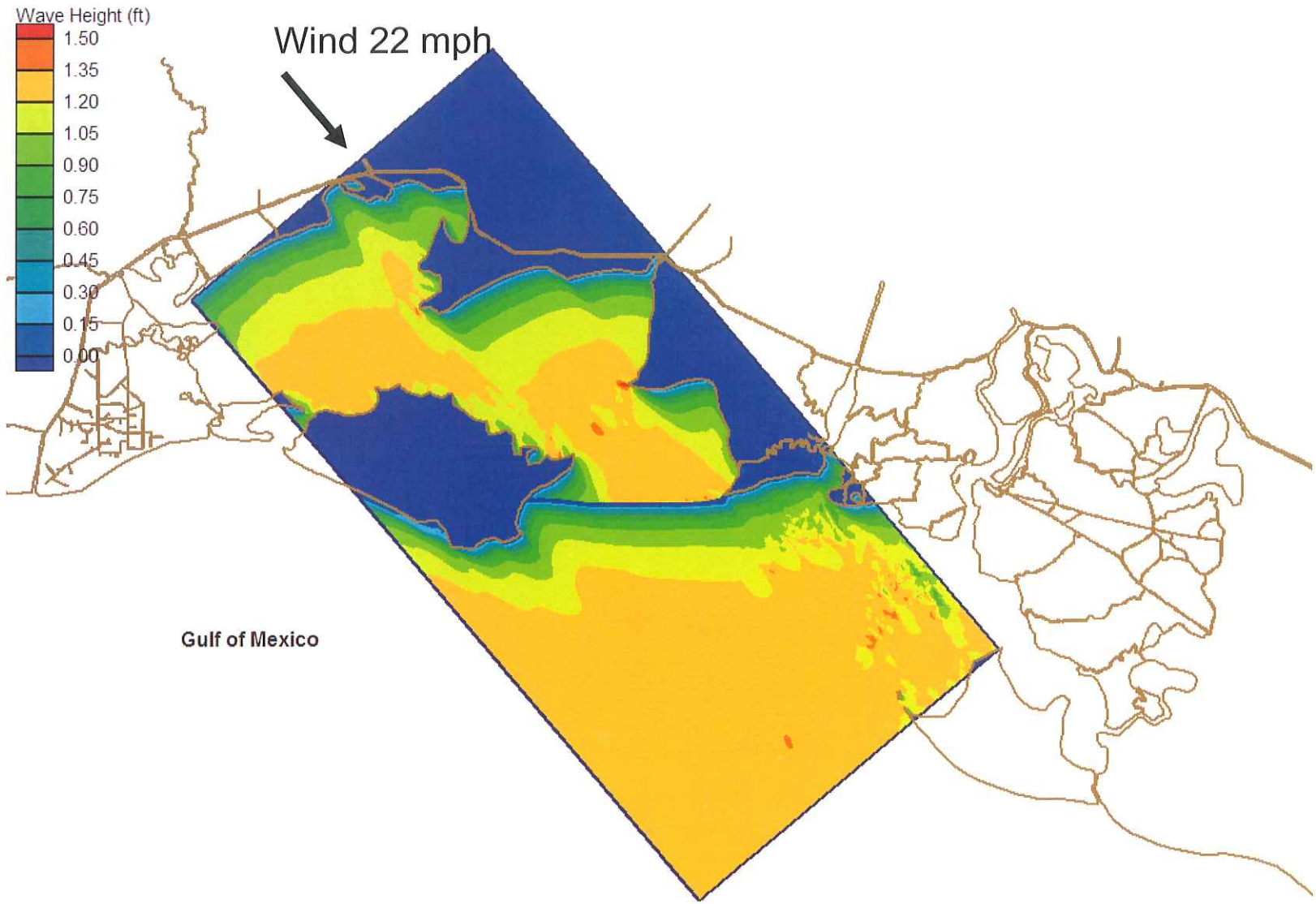

Figure 7.10 Contour Plot of Significant Wave Height for Reef Alternative B2; 22 mph Winds from N50°W

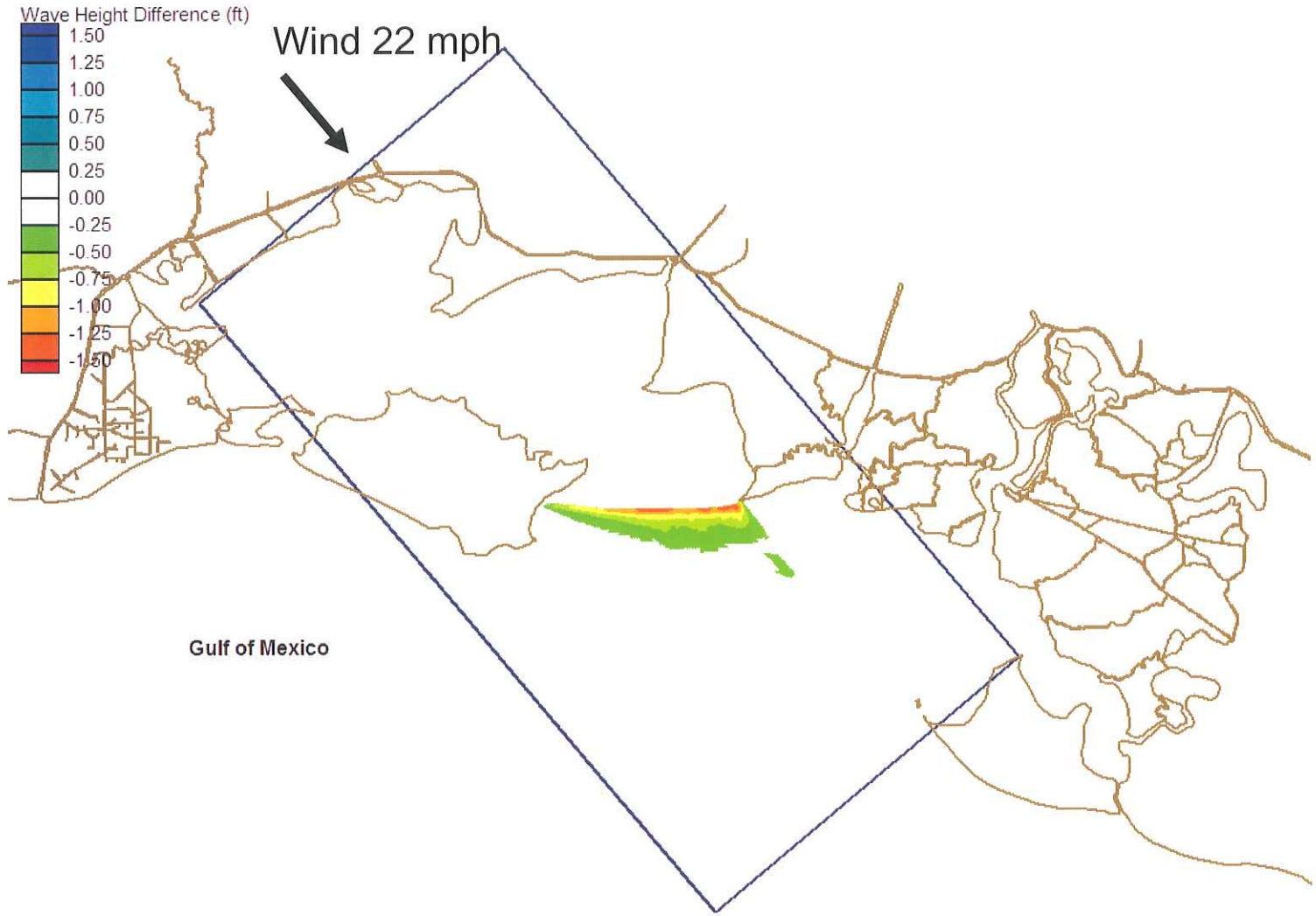

Figure 7.11 Contour Plot of Difference in Significant Wave Heights (Reef Alternative B2 versus Existing Conditions); 22 mph Winds from N50°W

8.0 APPROXIMATE HISTORICAL CONDITIONS

As discussed in Chapter 2, some anecdotal evidence suggest that the freshening of the Acadiana Bays system resulted from the removal of the oyster reefs which had prevented the Lower Atchafalaya River and Wax Lake Outlet freshwater plumes from entering the western bays. The model results described in Chapter 6 fail to support this contention in that the modeled bay salinity levels (modeled with the reefs included) did not approach the anecdotal historic levels (about 10 ppt). This begs the question: What other factors may have led to the freshening of the bays since the 1930s and 1940s?

To answer this question, Taylor Engineering considered the documented increases in freshwater discharge and the construction of the GIWW and its interconnecting freshwater channels over the past 50 – 60 years. Using historic maps and stream flow data, Taylor Engineering developed a model reflecting the general historic (pre-1940) bay system. Rather than representing a specific date and time, this model provided a means to evaluate the possible effects of historic system changes.

8.1 Description of the Historical Model Mesh and Bathymetry

An examination of historical maps of the bays before 1940 (USCSO, 1863; Holtz, c1864; Rand McNally, 1896; USACE 1915, 1928, 1929; USDOI, 1930) provided the basis for a model to simulate historical conditions. Figure 8.1 shows the model extent and configuration for the pre-1940 model. This model includes Wax Lake but not Wax Lake Outlet or the GIWW (connecting Wax Lake to the GIWW and Lower Atchafalaya River), both built after 1942.

Lacking adequate historic data, the modeled bathymetry remained unchanged from the present conditions (i.e., the 2002 – 2004 bathymetry) and did not include the historic oyster reefs. By not including the historic oyster reefs (completely removed by the 1970s) the model examines the effect of freshwater inflow changes independent of the effect of the oyster reefs (which some believe blocked freshwater and turbidity from entering the system). Thus, the historic model may also illuminate the significance of the historic reefs.

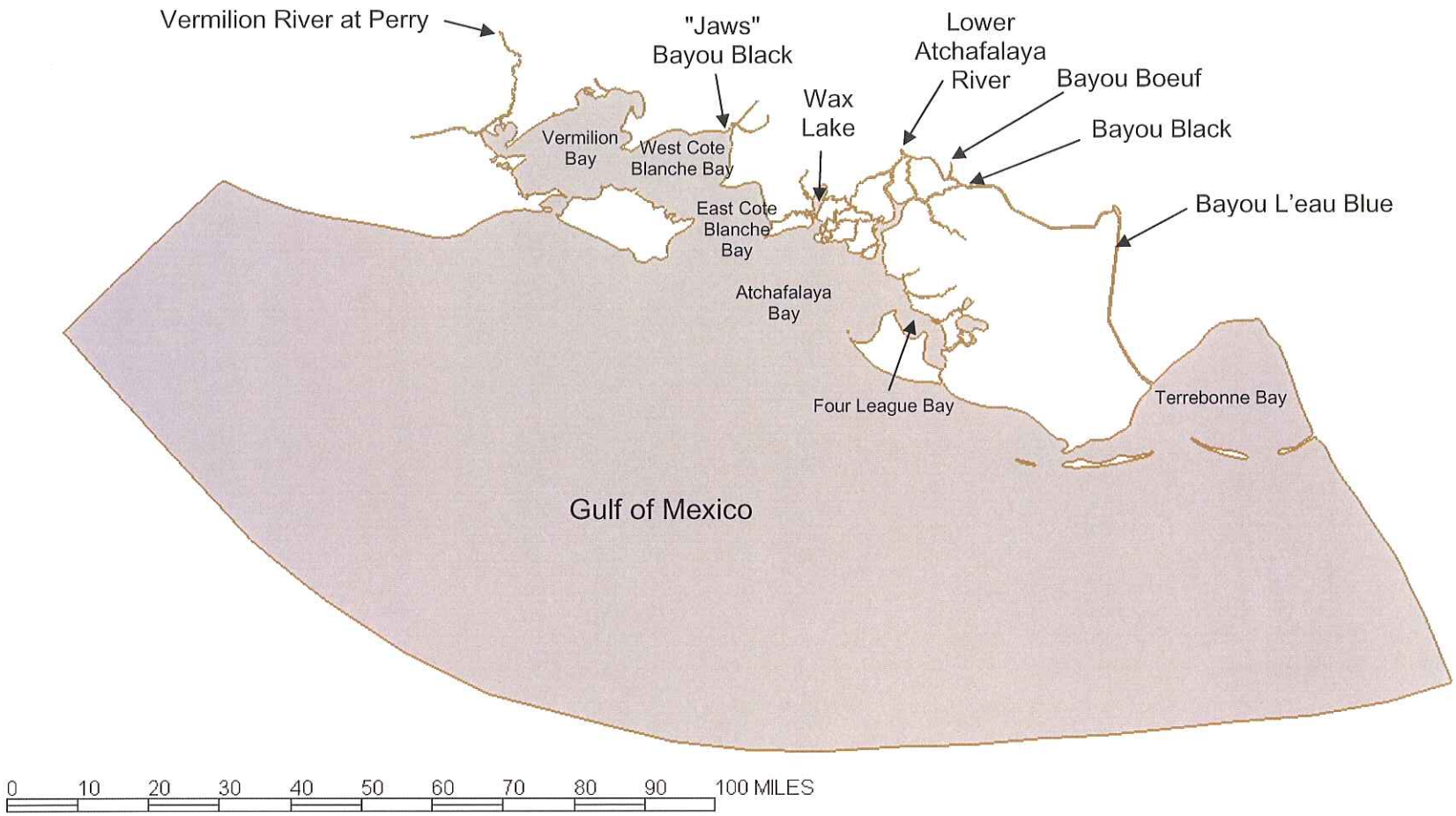

Figure 8.1 Historical, Pre-1940 Model

8.2 Historical Stream Flow

The USGS has maintained a stream flow gage on the Atchafalaya River at Simmesport, Louisiana since 1935. Figure 8.2 shows a plot of the 1-yr and 10-yr average stream flow recorded at this gage. USGS stream flow records from 1995 to 2002 provided the only concurrent data for Wax Lake Outlet at Calumet, the Lower Atchafalaya River at Morgan City, and the Atchafalaya River at Simmesport. Figure 8.3 compares the combined stream flows for Wax Lake Outlet at Calumet and the Lower Atchafalaya River at Morgan City with that of the Atchafalaya River at Simmesport for this period

Figure 8.3 demonstrates that almost all flow recorded at the Simmesport gage reaches the gages at Calumet and Morgan City and, by inference, the Atchafalaya Bay. Therefore, the stream flow plotted in Figure 8.2 should correspond to the volume entering Atchafalaya Bay in the historic model.

Notably, Figure 8.2 shows an increase in the stream flow in the early 1970s. At this time, the 10-year averaged stream flow abruptly increased from about 175,000 cfs to nearly 250,000 cfs. This increase corresponds to the 1973 flood that created changes to the conveyance of the channels discussed in Chapter 2.

Wind and tide boundary conditions from the mean stream flow simulation (roughly corresponding to the winter-spring season) provided the wind and tide boundary conditions for the historical simulation. The stream flows for the Vermilion River at Perry, the Charenton Drainage Canal, Bayou Boeuf, and Bayou Black boundaries remained constant at the mean stream flow levels listed in Table 6.1.

Figure 8.4 presents the pre-1940 stream flow, averaged by month, for the 1935 to 1939 period and the present stream flow from 1976 to 2004. The figure shows the similarity of the temporal variation of flows over the course of a year for both periods; an offset — varying between 50,000 and 100,000 cfs — separates historic flows from present flows.

Given the approximations inherent in this representation of the historical Acadiana Bays system, the modeling effort only considered one flow condition — the historic low flow condition — to examine whether historic salinity levels might exceed present conditions. In particular, the model applied a constant 50,000 cfs stream flow to the Lower Atchafalaya River boundary. The model simulation covered a period of three months. Within the limitations of this analysis, this 3-month simulation provided a very rough estimate of the maximum salinity levels historically attainable in the Acadiana Bays.

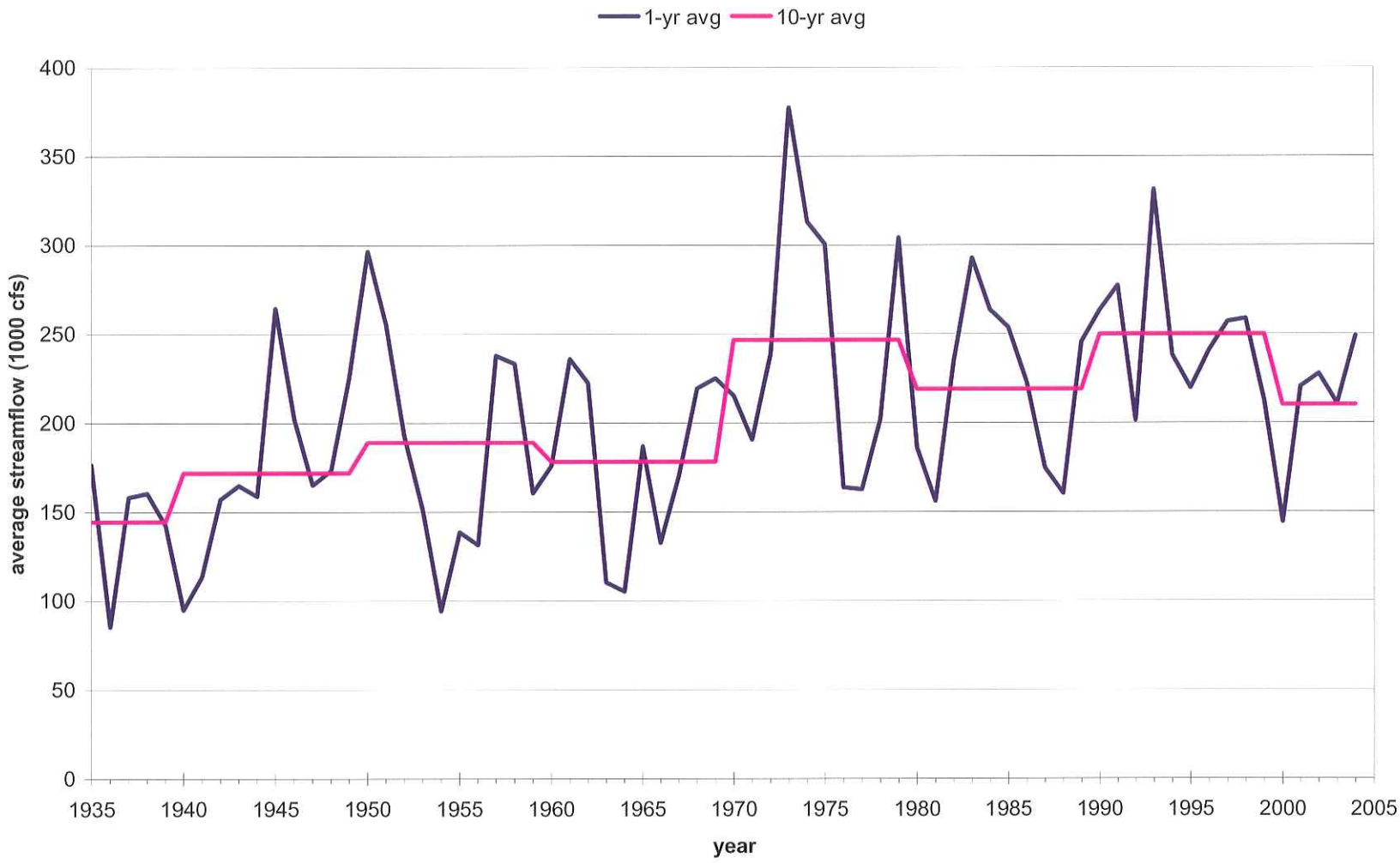

Figure 8.2 1-yr and 10-yr Average Stream Flow on the Atchafalaya River at Simmesport, LA

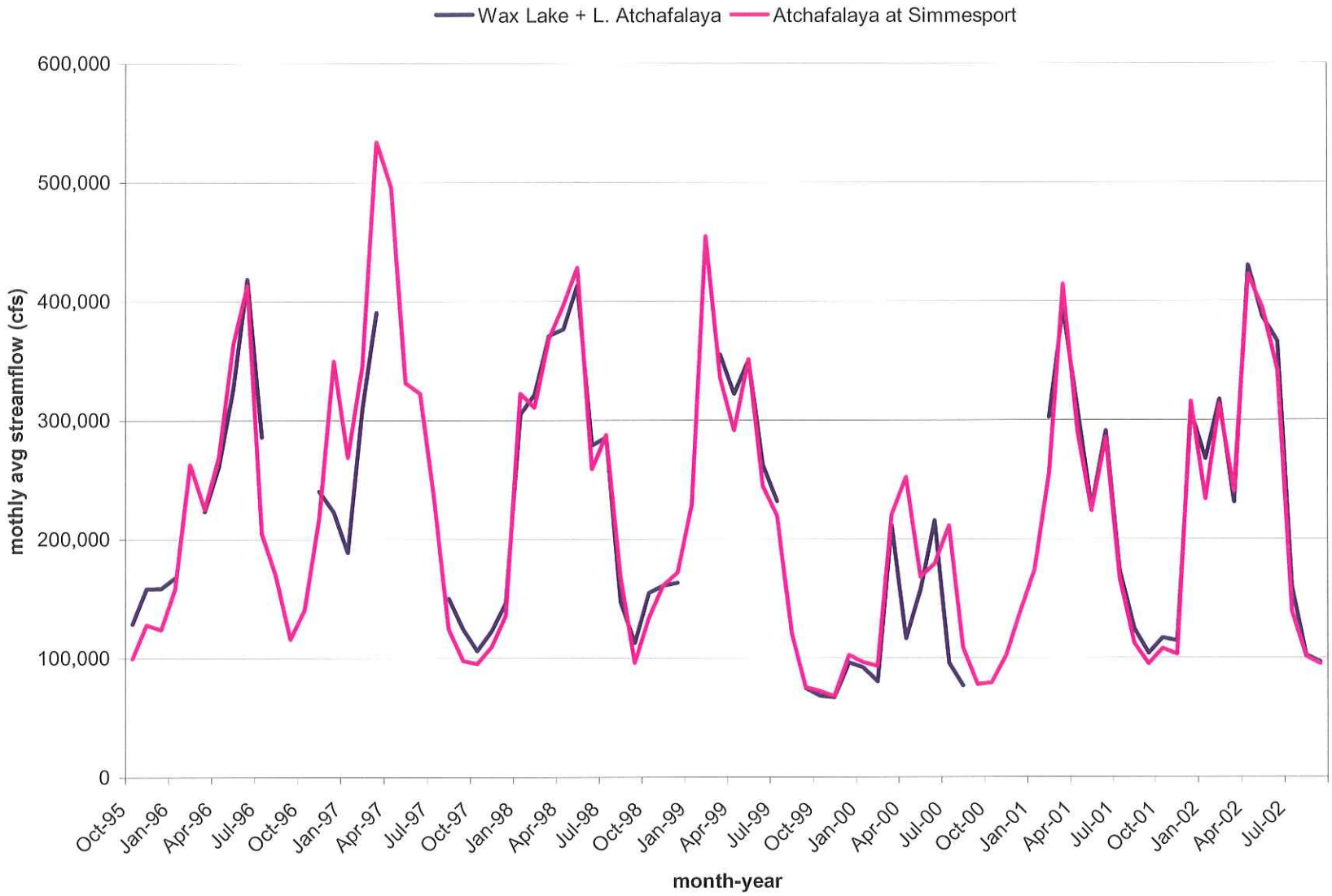

Figure 8.3 Monthly Average Stream Flow for Wax Lake Outlet, the Lower Atchafalaya River and the Atchafalaya River at Simmesport, LA

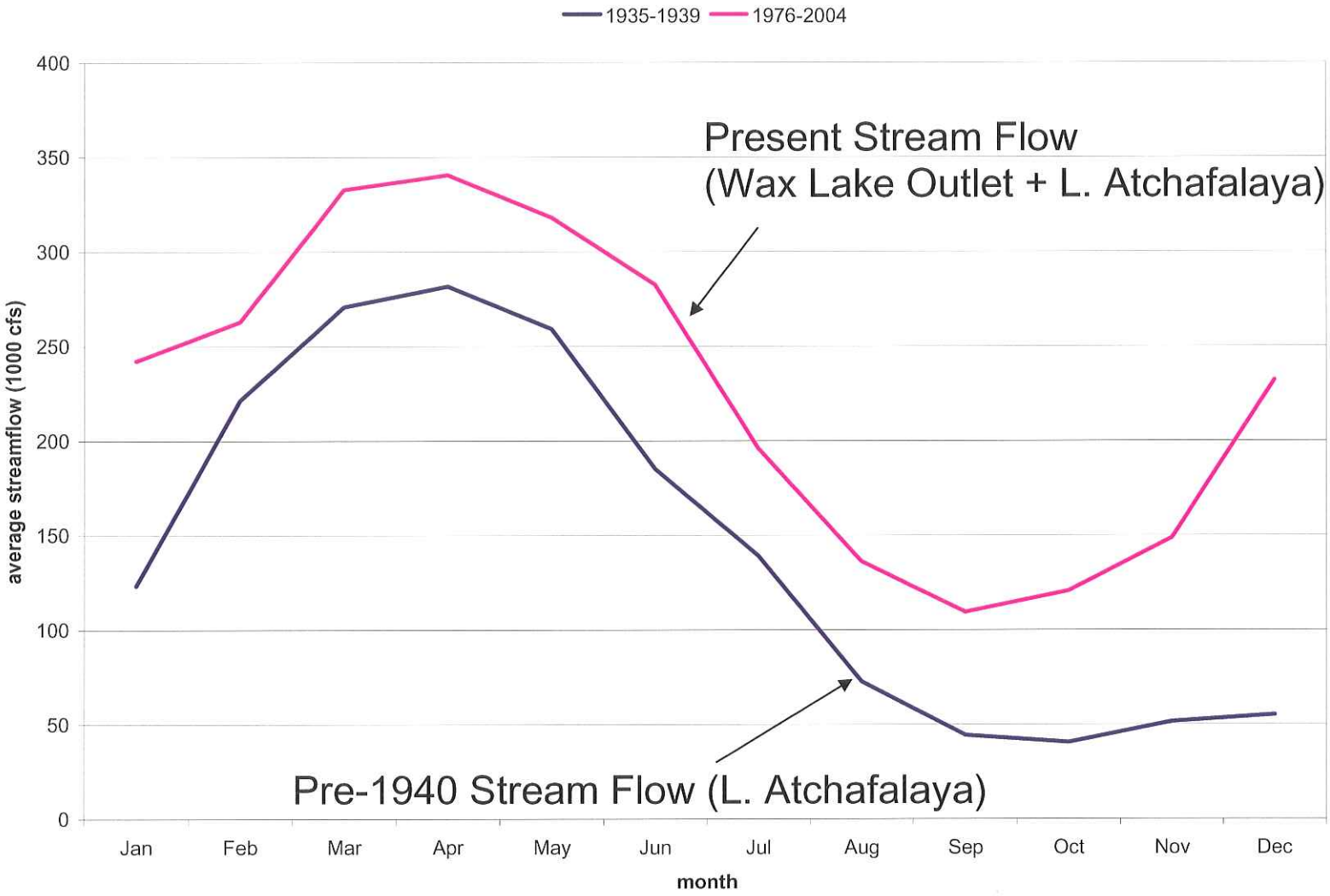

Figure 8.4 Comparison of Historical Monthly Stream Flows of Present-Day and Historical Models

8.3 Comparison of Historical Model to Existing Conditions

Figures 8.5 and 8.6 present the salinity model results after 1 and 3 months. For the 1-month simulation, salinity levels in Vermilion, East Cote Blanche and West Cote Blanche Bays ranged from 2 – 6 ppt and averaged about 3 – 4 ppt. The 3-month simulation salinity in these bays climbed as high as 13 ppt and averaged over 10 ppt. For similar wind and tide conditions, the historical salinity exceeded the existing low flow regime salinity by a factor of two to three, particularly if the low flow conditions persist for an abnormally extended period.

8.4 Conclusions Based on Historical Model

The historical model (Figures 8.5 and 8.6) shows that the combination of a lower average stream flow entering Atchafalaya Bay and the absence of the GIWW and Wax Lake Outlet allowed the salinity within the bay system to exceed 10 ppt for extended periods. This level agrees with anecdotal historical levels.

Additionally, because the historical model did not include historical reefs at the entrance to East Cote Blanche Bay, the modeling suggests that such reefs did not play a decisive role in maintaining high salinity levels in the bays. The lower stream flow and pre-1940 tributary configuration provided sufficient conditions to maintain bay salinity levels at or above 10 ppt.

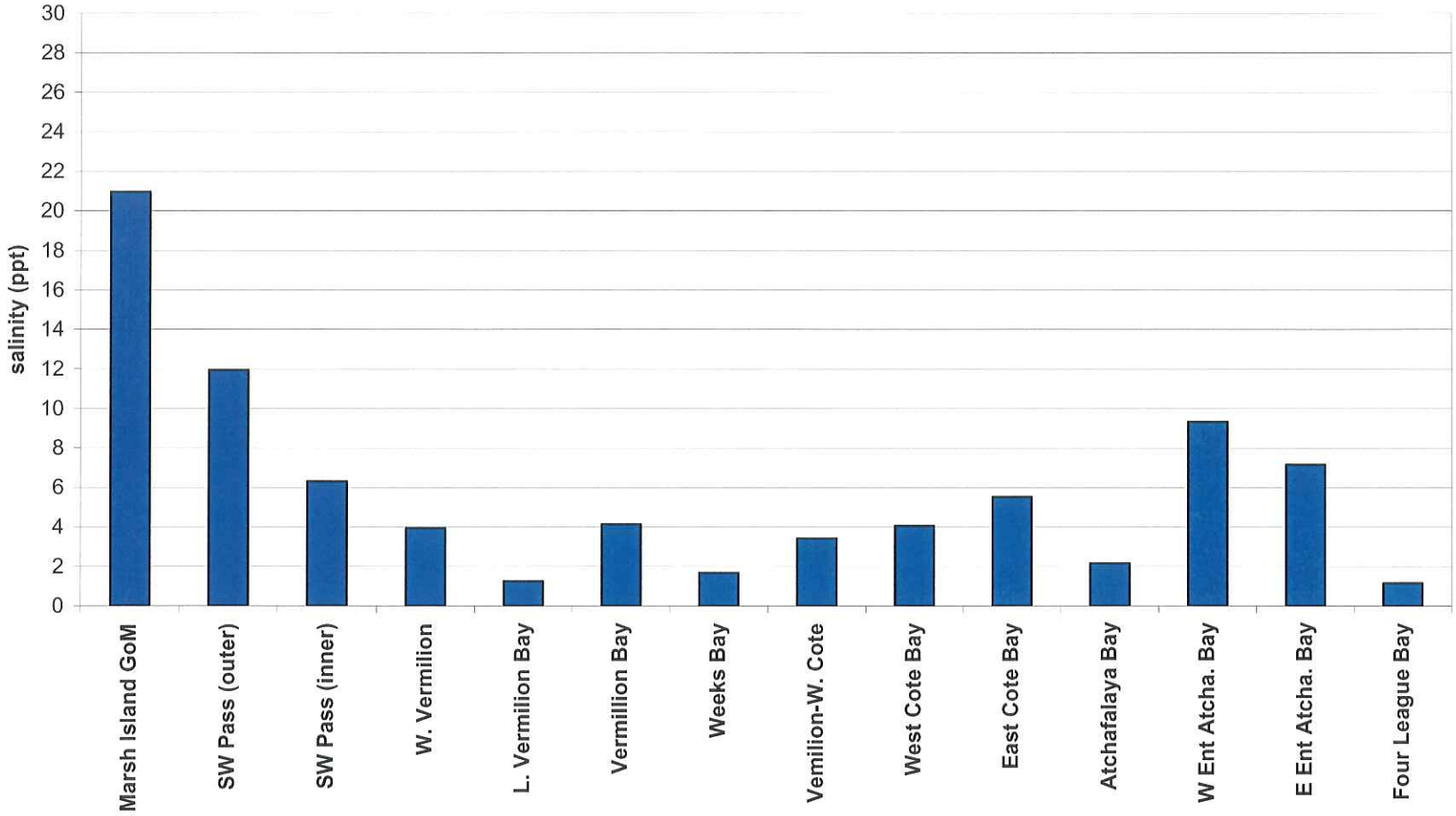

Figure 8.5 Salinity Values for the Historic 1-Month Simulation

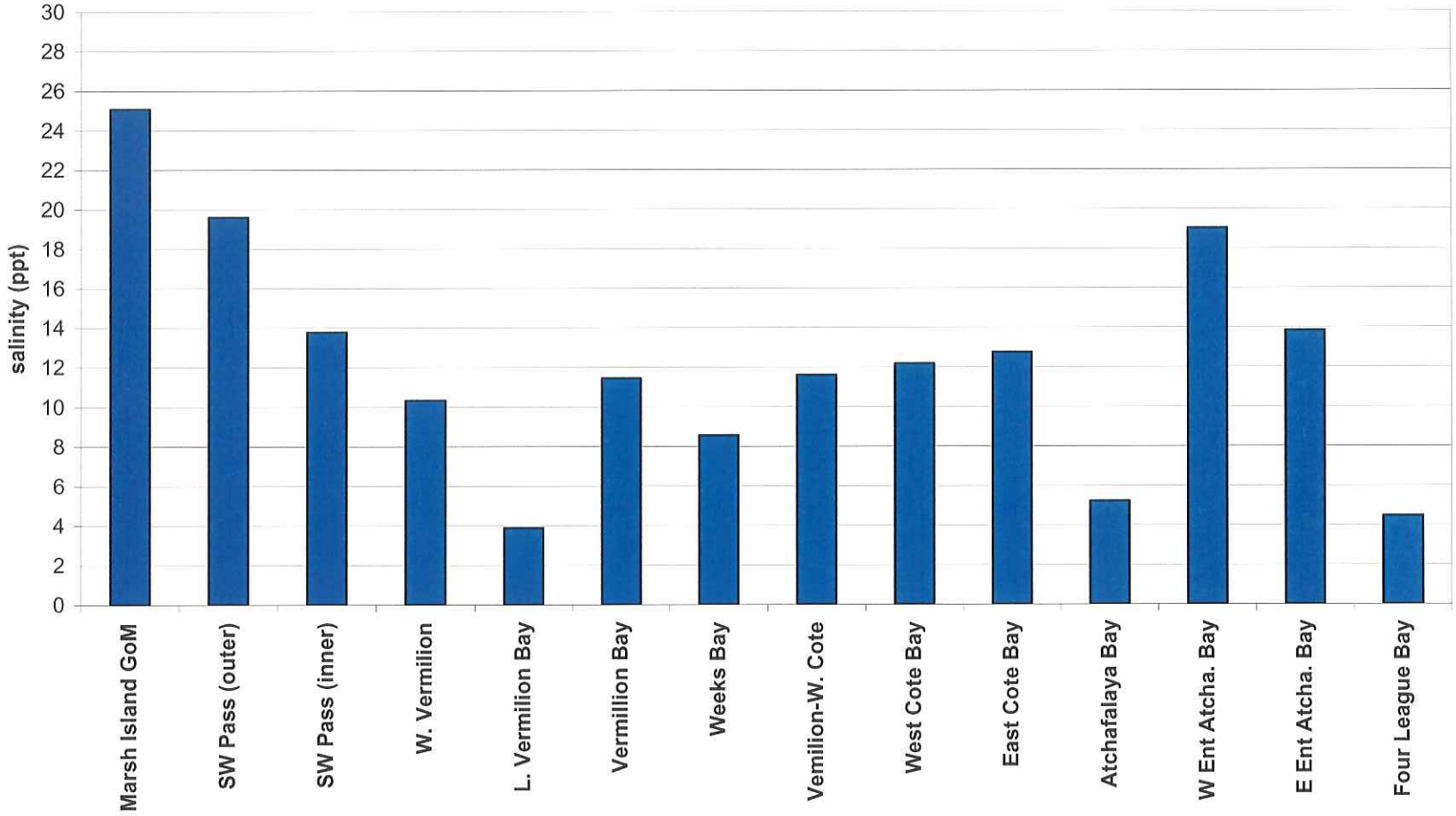

Figure 8.6 Salinity Values for the Historic 3-Month Simulation

9.0 SUMMARY AND CONCLUSIONS

9.1 Summary

This study examined the feasibility of influencing the salinity and turbidity regimes of the Acadiana Bays system — consisting of Vermilion, West Cote Blanche, East Cote Blanche, Atchafalaya, and Four League Bays — by reestablishing reefs historically located in the area. To this end, the study applied numerical models, with existing and new data, to determine whether the presence of artificial reefs changes existing salinity and turbidity regimes.

Given that stream flows, tides, winds, and wind waves are the primary drivers of circulation in the bays, this study applied numerical models for tidal, riverine, and wind-related hydrodynamics; wave propagation; and salinity and turbidity transport. Some key selection criteria — ability to simulate most, if not all, physical processes; public domain availability; and previously successful use in large domains in coastal Louisiana — guided the choice of RMA2 to model hydrodynamics, RMA4 to model salinity and turbidity, and STWAVE to model wave propagation. Model calibration and application results are summarized briefly below.

9.1.1 Model Calibration

The hydrodynamics model was calibrated to 2004 stage data measured by WAVCIS stations CSI-3 (offshore Marsh Island) and CSI-14 (offshore Point Chevreuil) and to 2004 current velocity data measured by CSI-14. By adjusting its dispersion coefficients, the salinity model was calibrated to 2004 data measured at CSI-3 and CSI-14; it was also calibrated to two additional Louisiana Department of Wildlife and Fisheries stations, 622 and 623, located in Vermilion Bay. Retaining the values of the dispersion coefficients of the salinity model, the turbidity model's predictions were compared to 2004 data measured at CSI-3 and CSI-14; the comparison indicated that predictions matched measurements reasonably well.

A review of literature and measured data from 1981 indicated that the muddy bottoms in and offshore Acadiana Bays cause significant damping of wind waves during normal conditions and high frequency (short return period) storm events. An exponential wave decay term was incorporated in STWAVE to simulate damping by soft beds. The modified wave propagation model was termed STWAVE-Taylor to distinguish it from the regular STWAVE model, termed STWAVE-Original. A calibration process determined the value for the wave attenuation coefficient appropriate for normal conditions and high frequency storms. Data for a low frequency storm, Hurricane Rita —which impacted

the project area in 2005 — indicated only a small wave damping effect of bottom dissipation during high storm surge conditions. Thus, STWAVE-Original appears appropriate for storm surge events where water depths greatly exceed normal conditions.

9.1.2 Reef Effects

Salinity and turbidity regimes in Acadiana Bays depend greatly on freshwater discharges from the Lower Atchafalaya River and Wax Lake Outlet. An analysis of the multiyear historic daily stream flow records for these freshwater sources determined characteristic values representative of high, mean, low, summer, and winter stream flow regimes. Modeling complete lunar tidal cycles based on these characteristic stream flows proved an efficient modeling approach which reduced both model run times and solution file sizes while maintaining the annual stream flow cycle effects. The coincidence and similarity of the summer and low stream flow conditions reduced the total number of required simulation periods to four.

This study analyzed the effects of four reef alternatives on the salinity and turbidity regimes in Acadiana Bays. Information on the orientation of historic reefs and the analysis of model-predicted flow streamlines (pathways) near Point Chevreuil suggested two reef orientations. The first orientation (A) at S 45°W directed the freshwater discharge from Wax Lake Outlet and the Lower Atchafalaya farther offshore, relative to existing conditions, into the Gulf of Mexico. This orientation also facilitates blocking the flood tide from carrying much of the freshwater discharged by Wax Lake Outlet and the Lower Atchafalaya River into East Cote Blanche Bay. Furthermore, this orientation provides a wide gap for boats to pass into the bays between the reef and Marsh Island. The second orientation (B) at S 90°W directly blocked communication between Atchafalaya and East Cote Blanche Bays to reduce the direct exchange of freshwater between the bays.

The modeling effort considered both submerged (crests at -3 ft MLW) and emergent (crests at MHW). The submerged reefs (designated A1 and B1) allowed some flow over the reefs during all tidal conditions. The emergent reefs (A2 and B2) allowed no flow over the reefs. For the B2 reef, this condition eliminated all communication between Atchafalaya and East Cote Blanche Bays.

The A2 reef (S 45°W, MHW crest) restricts the westerly growth of the freshwater plume until it passes the seaward tip of the reef. Consequently, the westerly growth of the freshwater plume for the A2 reef occurs well seaward of that for the existing conditions. As the freshwater plume travels to the south along the A2 reef and beyond, it mixes with increasingly saline Gulf of Mexico waters before it migrates

westward. The reduction of freshwater reaching the western entrance to Atchafalaya Bay, offshore Marsh Island, and offshore Southwest Pass increases salinity at these locations.

Additionally, the A2 reef effectively blocks much of the freshwater plume from entering West Cote Blanche and East Cote Blanche Bays. It also allows tidal communication with these bays through the opening extending from the reef tip to Marsh Island. This communication allows saline water exchange and flushes the freshwater from the Jaws and other sources. The A1 reef shows similar, though much smaller, effects on salinity compared to those of the A2 reef.

The simulations showed that the B2 reef (S 90°W, MHW crest) blocks the freshwater plume, emanating from the Lower Atchafalaya River and Wax Lake Outlet, from directly entering East Cote Blanche Bay. This blocking effect causes a larger volume of freshwater to migrate around the seaward side of Marsh Island. These processes decrease in salinity at the western entrance to Atchafalaya Bay and offshore Marsh Island. In addition to blocking freshwater, the B2 reef also blocks saline Gulf water from entering East Cote Blanche and West Cote Blanche Bays. With this saline water supply cut off, salinity falls in East Cote Blanche Bay as freshwater inflow from the Charenton Drainage Canal ("Jaws") tends to build up in the bay. West Cote Blanche Bay also experiences salinity decreases, albeit reduced in magnitude because of direct communication with Vermilion Bay and its closer proximity to saline water from Southwest Pass. With the Atchafalaya and Wax Lake freshwater source cut off, saline water entering through Southwest Pass causes small increases in salinity at Vermilion Bay. The B1 reef shows similar, though much smaller, effects on salinity compared to those of the B2 reef.

A review of the literature shows that suspended sediment carried by the Lower Atchafalaya River and Wax Lake Outlet provide the primary sources of turbidity for the bays. By blocking the freshwater plume, both A2 and B2 reefs inhibit these river's turbidity from entering the portions of Acadiana Bays west of Atchafalaya Bay. Consequently, the models show reductions in turbidity in East Cote Blanche, West Cote Blanche, and Vermilion Bays. The models considered the suspended sediment load as a function of the stream flow; therefore, the magnitudes of the reductions varied with the stream flow phase — reductions were significant during high and intermediate flows, substantial during mean flow, and negligible during low flow. The A2 reef, which only partially blocks the turbid waters of the Lower Atchafalaya River and Wax Lake Outlet from entering the western bays, causes smaller reductions of turbidity than the B2 reef, which completely blocks these waters from entering the western bays. A1 and B1 reefs produce negligible effects.

Wave modeling suggests that the western regions of Acadiana Bays mostly experience locally generated wind waves because bottom dissipation processes significantly attenuate long period swells from the Gulf of Mexico before they reach the interior Acadiana Bays. A2 and B2 reefs act as complete physical barriers to wave propagation. However, absent the penetration of long period swells into Acadiana Bays, the zone of influence of these reefs — the region over which they retard wave heights — is essentially restricted to their immediate downwind vicinity (about 10 miles or less). Even with the reefs, local wave generation processes raise, over a relatively short distance, the downwind wave heights to the levels experienced without the reefs.

The study examined the effects of the reefs on the surge height of a low frequency (100-yr) storm. Approximating Hurricane Lili (2002) surge heights, the B2 reef caused the greatest decrease in peak storm surge elevation — almost 0.5 ft — along the Acadiana Bays shoreline. The other reef alternatives caused smaller changes.

9.1.3 Modeling Historic Conditions

An approximate model of historic, pre-1940 conditions examined the effects of construction of man-made waterways and flood control systems on the salinity of the bays. The stream flow records showed that the total average freshwater discharge to Atchafalaya Bays increased by about 100,000 cfs since the 1930s. Also, the construction of the GIWW and Wax Lake Outlet redistributed the freshwater flows within the system. With lower, pre-1940 stream flow levels and without the GIWW or Wax Lake Outlet, modeling indicated that bay salinities could increase as much as 2 – 3 times present levels during certain periods and maintain levels above 10 ppt for longer periods. These results suggest that stream flow changes, not historic reef dredging, supplied the dominant driving force in decreasing salinity concentrations in the Acadiana Bays system.

9.2 Conclusions

The modeling efforts of this study concentrated on the effect of reef restoration on the salinity and turbidity levels within the bays west of Atchafalaya Bay in the Acadiana Bay system. Specifically, the study examined the relative influence of four reef alternatives on salinity and turbidity within the bays. In addition, the study examined the effect of the reefs on waves and storm surge.

Overall, the submerged reef alternatives (with crests at -3 ft MLW) only negligibly affected salinity and turbidity in the bays. Of the emergent reef alternatives, the A2 reef raised average salinities in the bays by 1 – 2 ppt while the B2 reef raised average salinities by less than 1 ppt. The A2 and B2 reefs reduced turbidity levels in the bays by about 30% at best and about 15 – 20% on average.

Storm surge modeling indicated that the reefs would have some effects on storm surge height within the bays. The B2 reef, which blocked the entrance to East Cote Blanche Bay (up to MHW), showed a 5% reduction (0.5 ft) in the storm surge heights within the bays, the maximum reduction for all the reef alternatives.

Wave model results indicated that the reefs only affected wave heights in their immediate vicinity. This result suggests that waves in the bays are largely locally wind-generated and highly dependent on bottom attenuation.

Finally, models simulating the approximate pre-1940 condition of the system (low stream flow, no GIWW, and no Wax Lake Outlet) suggested that increases in stream flow since 1940 – not reef removal – has driven the observed decreases in Acadiana Bay salinity.

REFERENCES

Coastal Environments, Inc. 1977. A Jetty from Point Chevreuil: An Evaluation of a Proposal to Reduce Sedimentation in the Cote Blanche Bays and Vermilion Bay. Atchafalaya Basin Division, Louisiana Department of Culture, Recreation, and Tourism and Louisiana State Planning Office, Baton Rouge, LA.

Day, J.W., Lane, R.R., Kemp, G.P., Marx, B. 1998. The Effects of the Atchafalaya River on the Vermilion-Terrebonne Estuarine Complex. U.S. Army Corps of Engineers, New Orleans District, New Orleans, LA.

Ebersole, B.A. 1985. The Atchafalaya River Delta: Report 9: Wind Climatology. Technical Report HL-82-15. Waterways Experiment Station, U.S. Army Corps of Engineers, Vicksburg, MS.

Forristall, G.Z. and Reece, A.M. 1985. Measurements of Wave Attenuation Due to a Soft Bottom: The SWAMP Experiment." *Journal of Geophysical Research*. 90(C2): 3367- 3380.

Holtz, H. c1864. Map of Louisiana and Arkansas. U.S. Infantry, Department of Louisiana. Library of Congress Geography and Map Division, G4010 1864 .H6 CW 230, Washington, D.C.

Hsaio, S-C.V. 1978. On the Transformation Mechanisms and the Prediction of Finite- Depth Water Waves. Ph.D. Dissertation. University of Florida, Department of Coastal and Oceanographic Engineering, Gainesville, FL.

Huh, O.K., Walker, N.D., and Moeller, C. 2001. Sedimentation along the Eastern Chenier Plain Coast: Down Drift Impact of a Delta Complex Shift. *Journal of Coastal Research*. 17(1): 72-81.

Jensen, R. 1985. The Atchafalaya River Delta, Report 10: Wave Hindcasts Main Text and Appendices A and B. Waterways Experiment Station, U.S. Army Corps of Engineers, Vicksburg, MS.

Lee, S.-C., and Mehta, A.J. 1997. Problems in Characterizing Dynamics of Mud Shore Profiles. *Journal of Hydraulic Engineering*, 123(4): 351-361.

Letter, J.V. 1982. The Atchafalaya River Delta, Report 3: Extrapolation of Delta Growth. Waterways Experiment Station, U.S. Army Corps of Engineers, Vicksburg, MS.

Majersky, S., Roberts, H.H., Cunningham, R., Kemp, G.P., and John, C.J. 1997. Facies Development in the Wax Lake Outlet Delta: Present and Future Trends. *Basin Research Institute Bulletin*, Louisiana State University, Baton Rouge, LA.

Mashriqui, H.S. 2003. Hydrodynamic and Sediment Transport Modeling of Deltaic Sediment Processes. Ph.D. Dissertation. Louisiana State University, Department of Civil and Environmental Engineering, Baton Rouge, LA.

Myint S.W. and Walker, N.D. 2002. Quantification of Surface Suspended Sediments Along a River Dominated Coast with NOAA AVHRR and SeaWIFS Measurements: Louisiana, USA. *International Journal of Remote Sensing*. 23(16): 3229-3249.

Pankow, W., Teeter, A.M., and Donnell, B.P. 1990. The Atchafalaya River Delta, Report 2: Field Data: Section 3: Grain Size Analysis of Selected Bay Sediments. Waterways Experiment Station, U.S. Army Corps of Engineers, Vicksburg, MS.

Parchure, T.M. and Mehta, A.J. 1985 Erosion of Soft Cohesive Beds. *Journal of Hydraulic Engineering*, 111 (10), 1308-1326.

Powell, N.J. 2004 Estuarine Characteristics of the Vermilion-Atchafalaya Complex. Hydrologic Engineering Section, U.S. Army Corps of Engineers, New Orleans District.

Rand McNally and Co. 1896. Map of Louisiana c1895. Chicago, 1896. Library of Congress Geography and Map Division, G4011.P3 1895 .R3 RR 228, Washington, D.C.

Roberts, H.H. 1998. Delta Switching: Early Responses to the Atchafalaya River Diversion. *Journal of Coastal Research*. 14(3): 882-899.

Roberts, H.H., Walker, N.D., Cunningham, G.P., and Majersky, S. 1997. Evolution of Sedimentary Architecture and Surface Morphology: Atchafalaya and Wax Lake Deltas, Louisiana (1973-1994). Gulf Coast Association of Geological Societies Transactions, XLVII.

Rouse, L.J., Roberts, H.H., Cunningham, R.H. 1978. Satellite Observations of Subaerial Growth of the Atchafalaya Delta. *Geology*. 6: 405-408.

Sheppard, D. M. and Miller, W. 2003. *Design* Storm Surge Hydrographs for the Florida Coast. Florida Department of Transportation Technical Report, Tallahassee, FL.

Sheremet, A. and Stone, G.W. 2003a. Observations of Nearshore Wave Dissipation over Muddy Sea Beds. *Journal of Geophysical Research*. 108(C11): 3357.

Sheremet, A. and Stone, G.W. 2003b. Wave Dissipation Due to Heterogeneous Sediments on the Inner Louisiana Shelf. *Proceedings of the International Conference on Coastal Sediments 2003, May 2003, Clearwater Beach, Florida.*

Stone, G.W., Grymes J.M., Dingler, J.R., and Pepper, D.A. 1997. Overview and Significance of Hurricanes on the Louisiana Coast, USA. *Journal of Coastal Research*. 13(3): 656-669.

Stone, G.W., Grymes J.M., Robbins, K.D., Underwood, S.G., Styer, G.D., and Muller, R.A. 1993. A Chronologic Overview of Climatological and Hydrological Aspects Associated with Hurricane Andrew and its Morphological Effects Along the Louisiana Coast, U.S.A. *Shore and Beach*. 61(2): 2-12.

Suhayda, J.N. 1984. Attenuation of Storm Waves over Muddy Bottom Sediments. Federal Emergency Management Agency, Washington, D.C.

TAMU. 1996. Studying circulation over the Texas-Louisiana shelf. *Texas A & M University, Quarterdeck*, Taxas A & M University, Collage Park, TX. Volume 4, Number 2, Summer 1996.

Teeter, A.M., and Pankow, W. 1990. The Atchafalaya River Delta, Report 2: Field Data: Section 2: Settling Characteristics of Bay Sediments. Waterways Experiment Station, U.S. Army Corps of Engineers, Vicksburg, MS.

Tubman, M.W., and Suhayda, J.N. 1976. Wave Action and Bottom Movements of Fine Sediments. *Proceeding of the 15th Coastal Engineering Conference*, Vol. 2, ASCE, New York, N.Y., 1168-1183.

USACE, 1915. Map of Southern Louisiana. U.S. Army Corps of Engineers, New Orleans District, March 1915.

USACE, 1928. Southern Louisiana. U.S. Army Corps of Engineers, New Orleans District, New Orleans, LA.

USACE, 1929. Louisiana and Texas Intracoastal Waterway, Vermilion River to Mermentau River, LA. U.S. Army Corps of Engineers, New Orleans District, New Orleans, LA.

USACE, 2002. "Mississippi River and Tributaries, Atchafalaya Basin, Louisiana, Lower Atchafalaya Basin Reevaluation Study." U.S. Army Corps of Engineers, Mississippi River Commission, New Orleans District, New Orleans, LA

USCSO, 1863. Military map of part of Louisiana. U.S. Coast Survey Office, A. D. Bache, Sept. 1863. Library of Congress Geography and Map Division, G4010 1863 .L5 CW 232.5, Washington, D.C.

USDOI, 1930. "State of Louisiana." U.S. Department of the Interior Map, General land Office, Washington, D.C .

Walker, N.D., 2001. Tropical Storm and Hurricane Effects on Water Level, Salinity, and Sediment Transport in the River-Influenced Atchafalaya-Vermilion Bay System, Louisiana, USA. *Estuaries*. 24(4): 498-508.

Walker, N.D., and Hammack, A.B. 1999. Impact of River Discharge and Wind Forcing on Circulation, Sediment Distribution, Sediment Flux, and Salinity Changes: Vermilion/Cote Blanche Bay System, Louisiana. Coastal Studies Institute, Louisiana State University, Baton Rouge, LA.

Walker, N.D., and Hammack, A.B. 2000. Impacts of Winter Storms on Circulation and Sediment Transport: Atchafalaya-Vermilion Bay Region, Louisiana, USA. *Journal of Coastal Research*. 16(4): 996-1010.

Wells, J.T. 1983. Dynamics of Fluid Muds in Low-, Moderate-, and High-Tide-Range Environments. *Canadian Journal of Fisheries and Aquatic Sciences*. 40(1): 130- 142.

Appendix A

Wave Plots

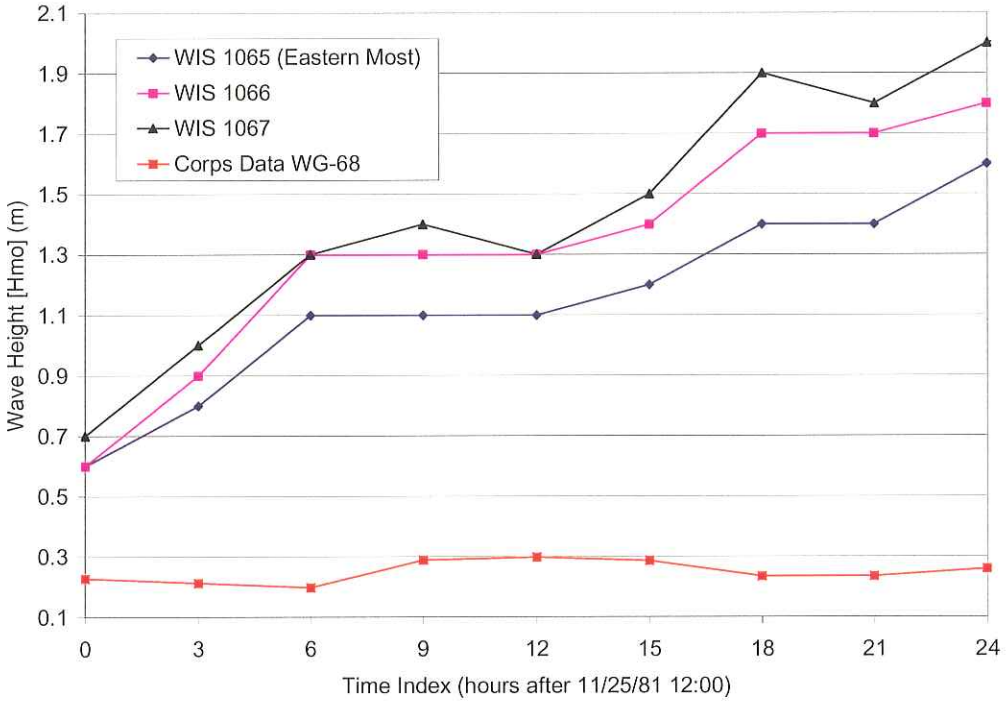

Wave height record: WIS Stations 1065, 1066, and 1067; Southerly Storm 1

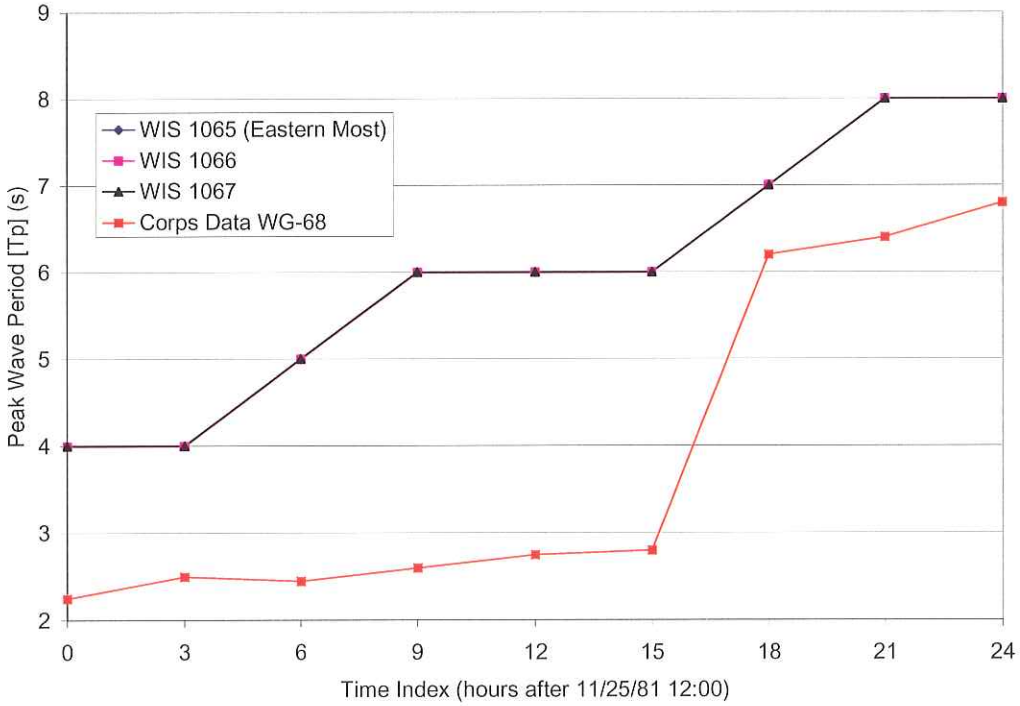

Wave period record: WIS Stations 1065, 1066, and 1067; Southerly Storm 1

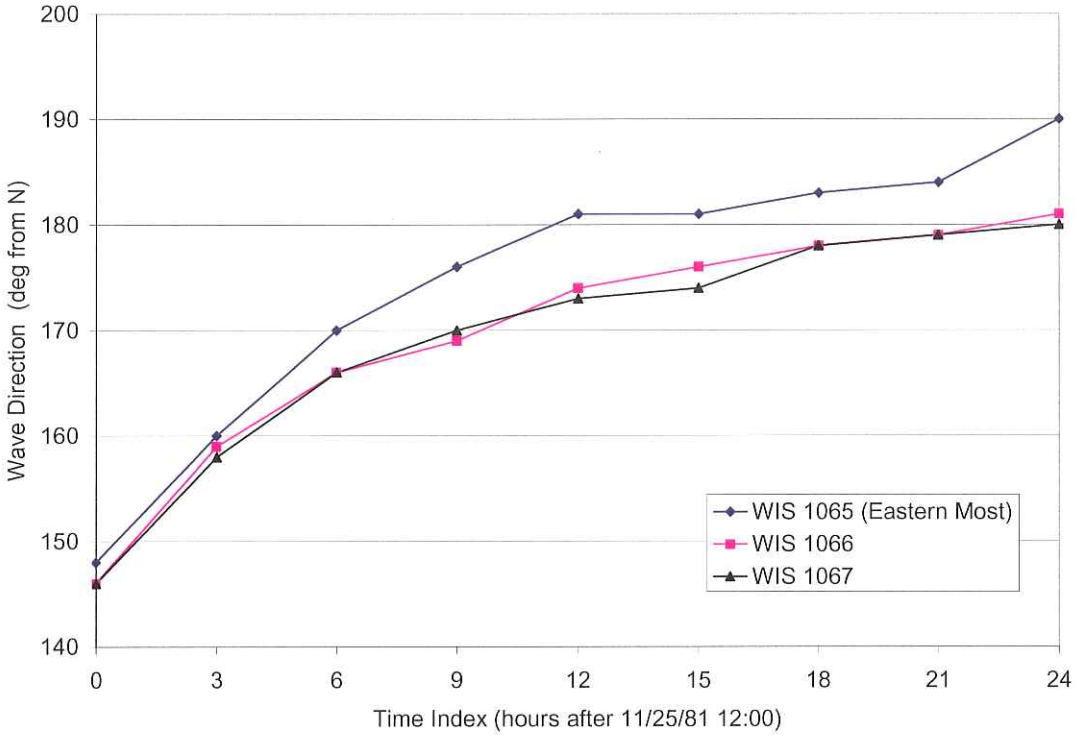

Wave Direction record: WIS Stations 1065, 1066, and 1067; Southerly Storm 1

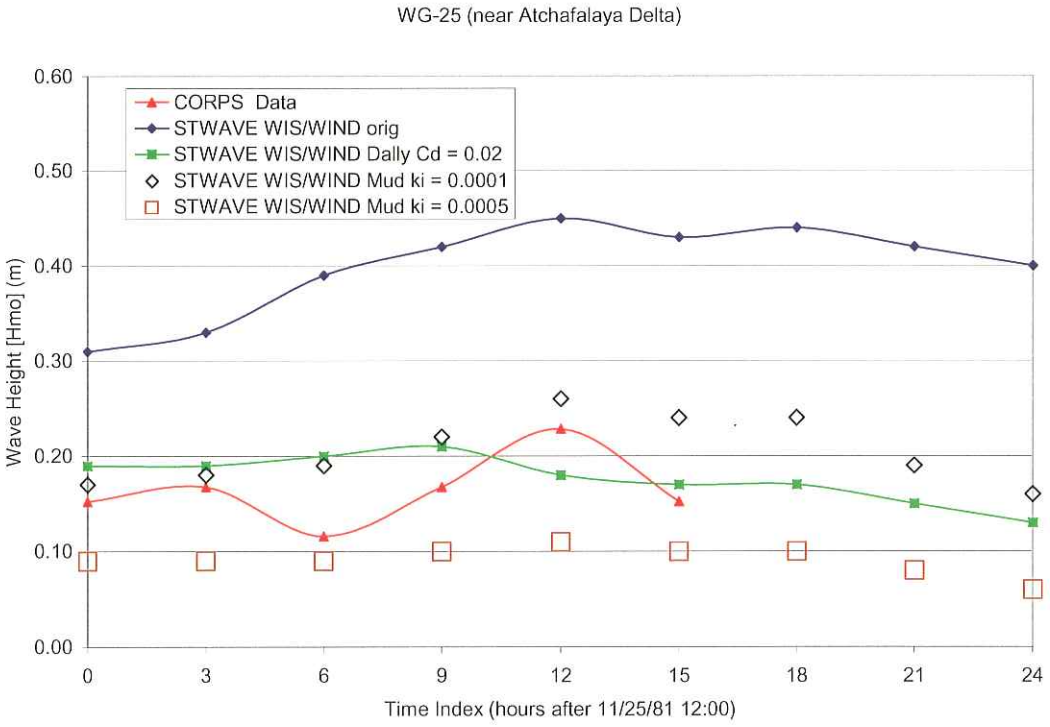

Wave height record comparison at WG-25 for Southerly Storm 1

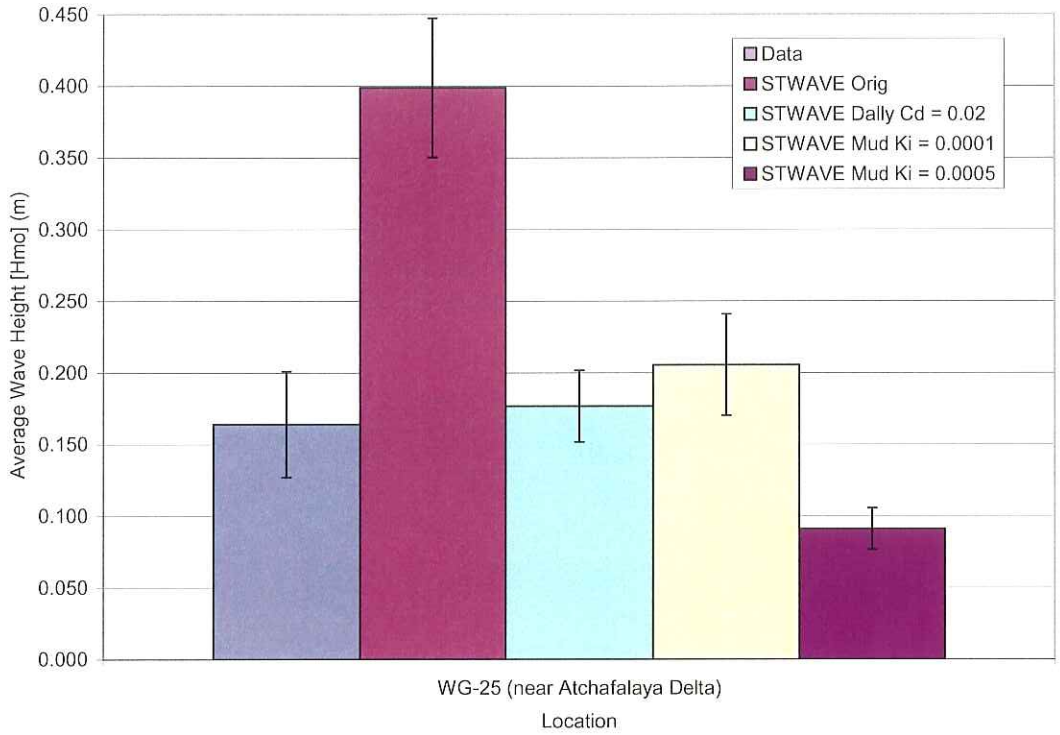

Wave height averages comparison at WG-25 for Southerly Storm 1

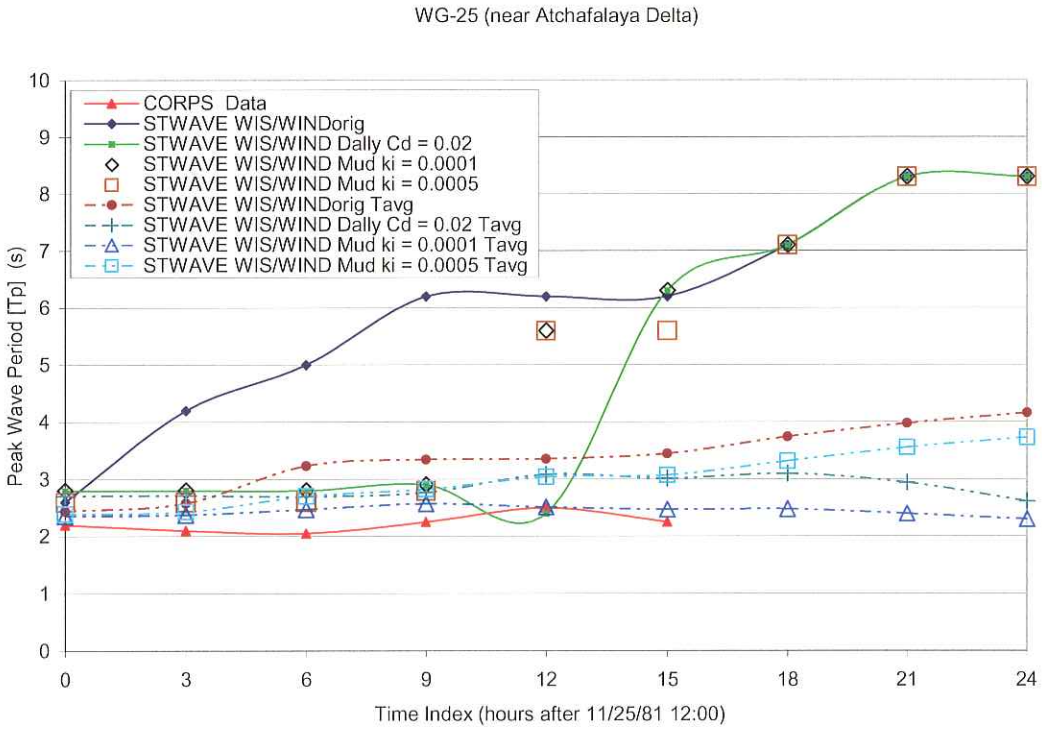

Wave period record comparison at WG-25 for Southerly Storm 1

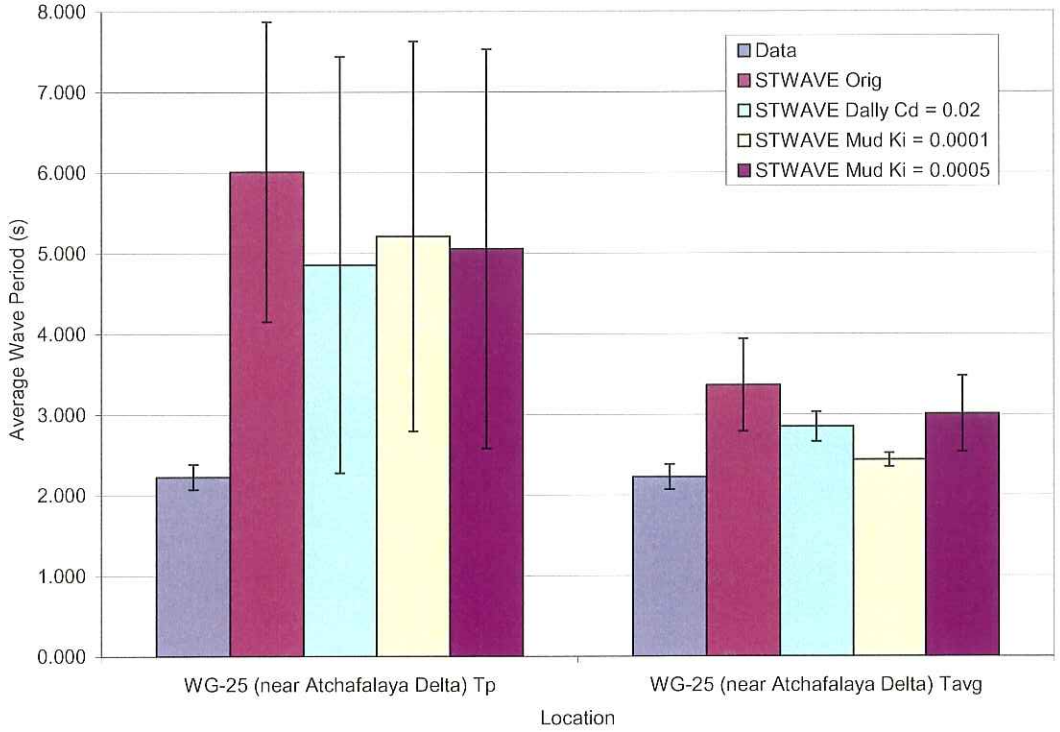

Wave period averages comparison at WG-25 for Southerly Storm 1

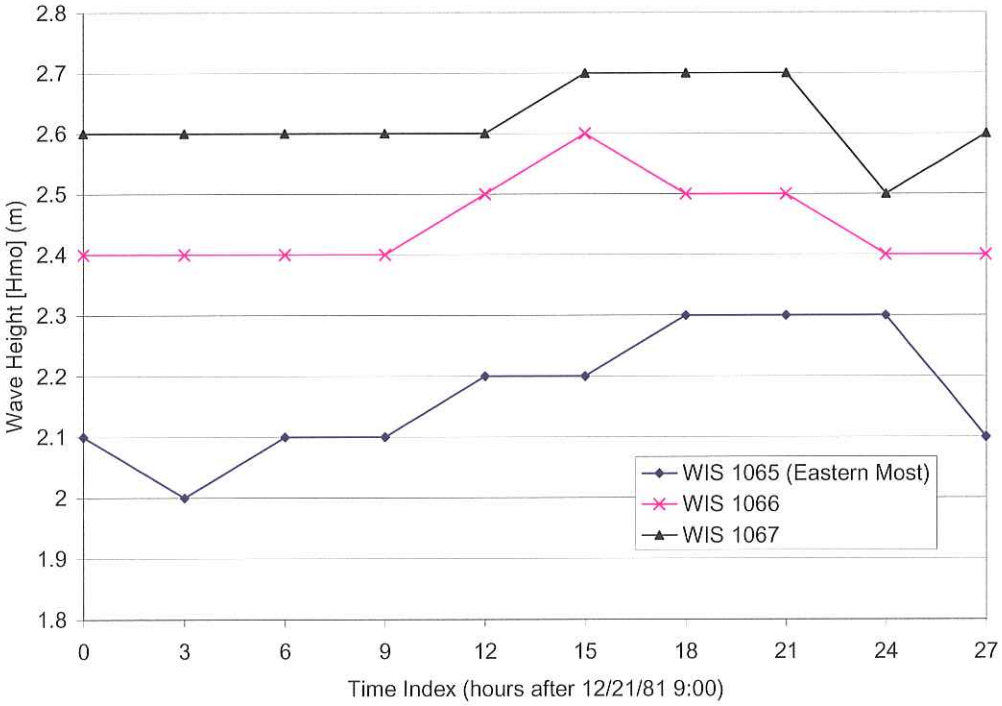

Wave height record: WIS Stations 1065, 1066, and 1067; Southerly Storm 3

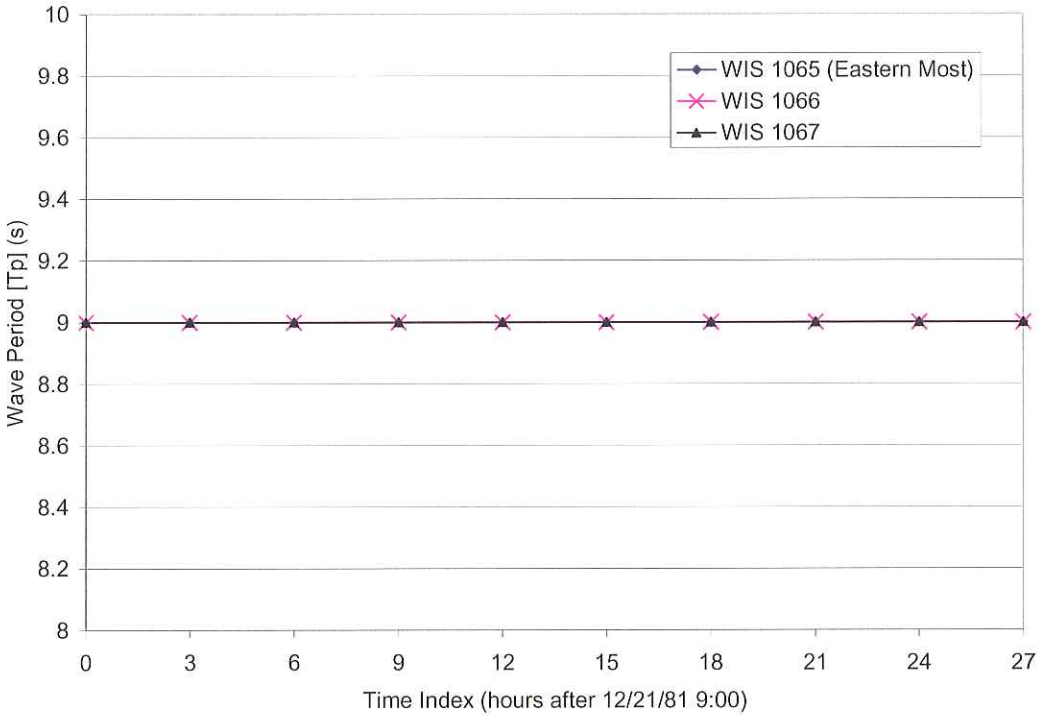

Wave period record: WIS Stations 1065, 1066, and 1067; Southerly Storm 3

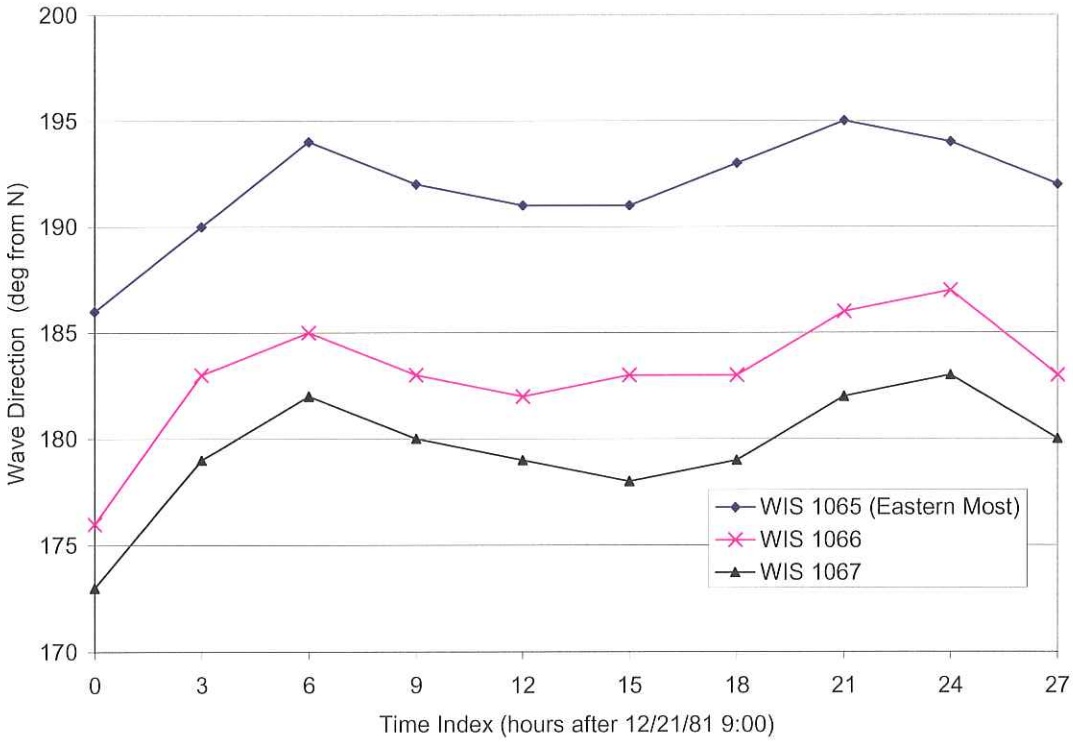

Wave direction record: WIS Stations 1065, 1066, and 1067; Southerly Storm 3

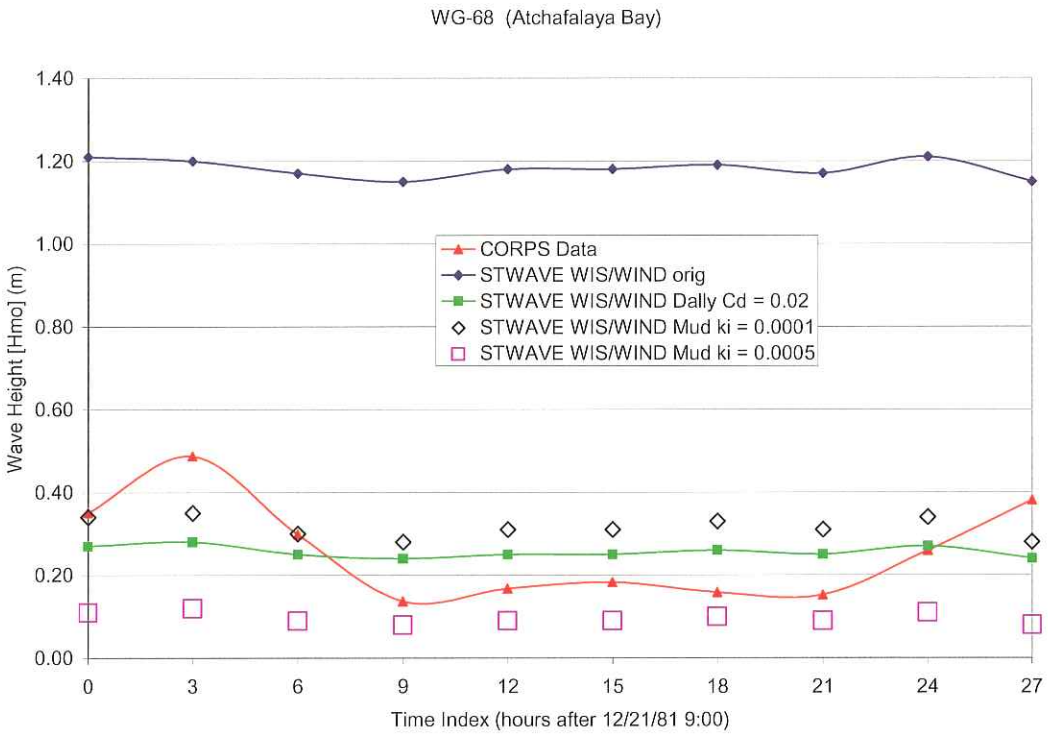

Wave height record comparison at WG-68 for Southerly Storm 3

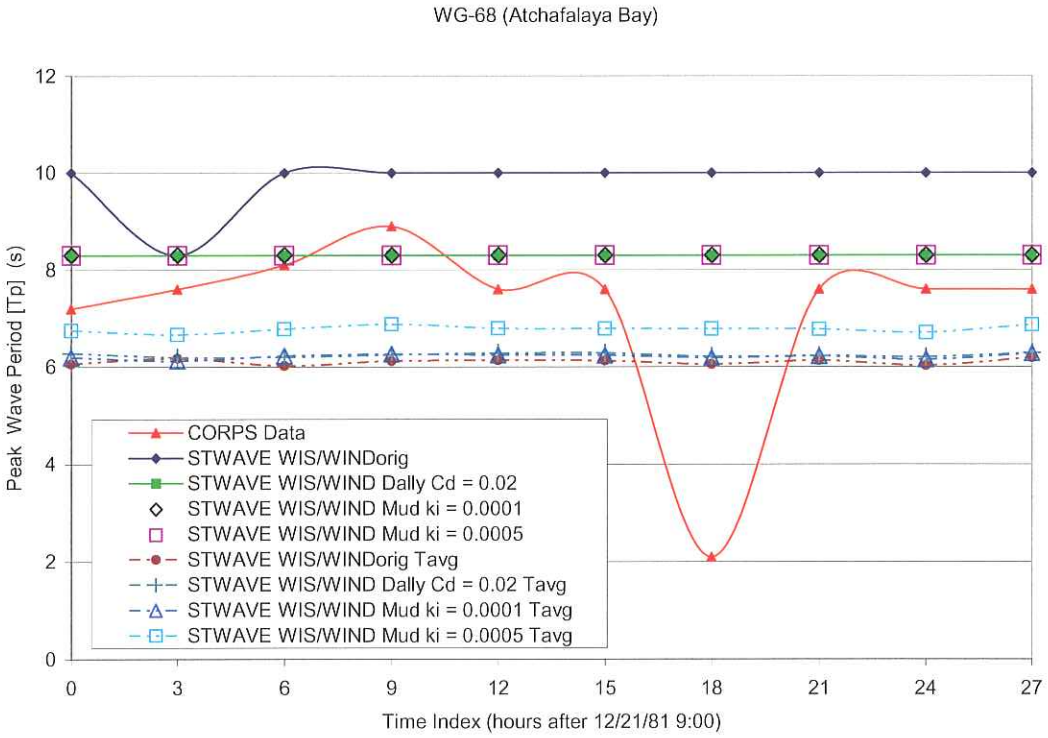

Wave period record comparison at WG-68 for Southerly Storm 3

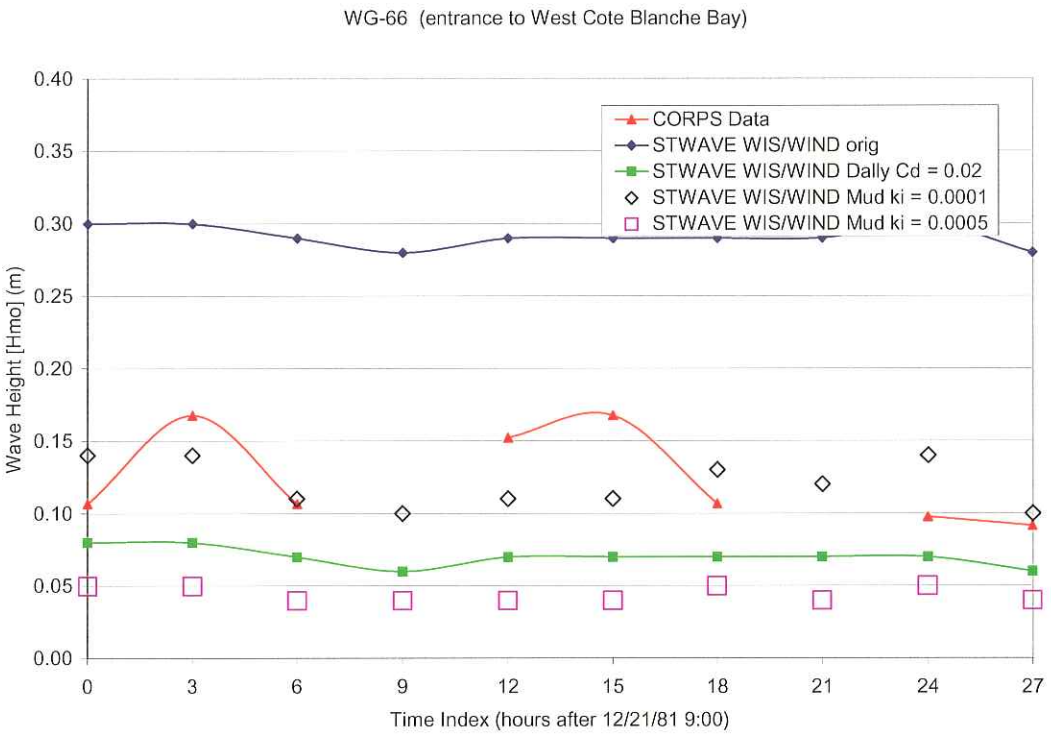

Wave height record comparison at WG-66 for Southerly Storm 3

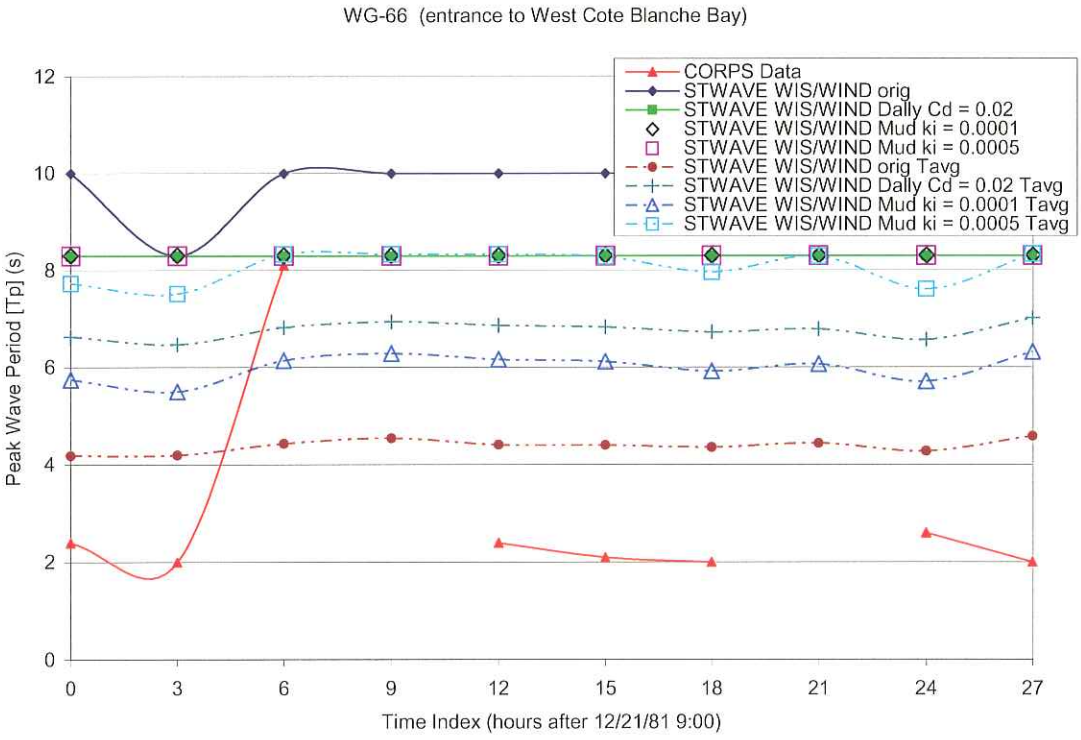

Wave period record comparison at WG-66 for Southerly Storm 3

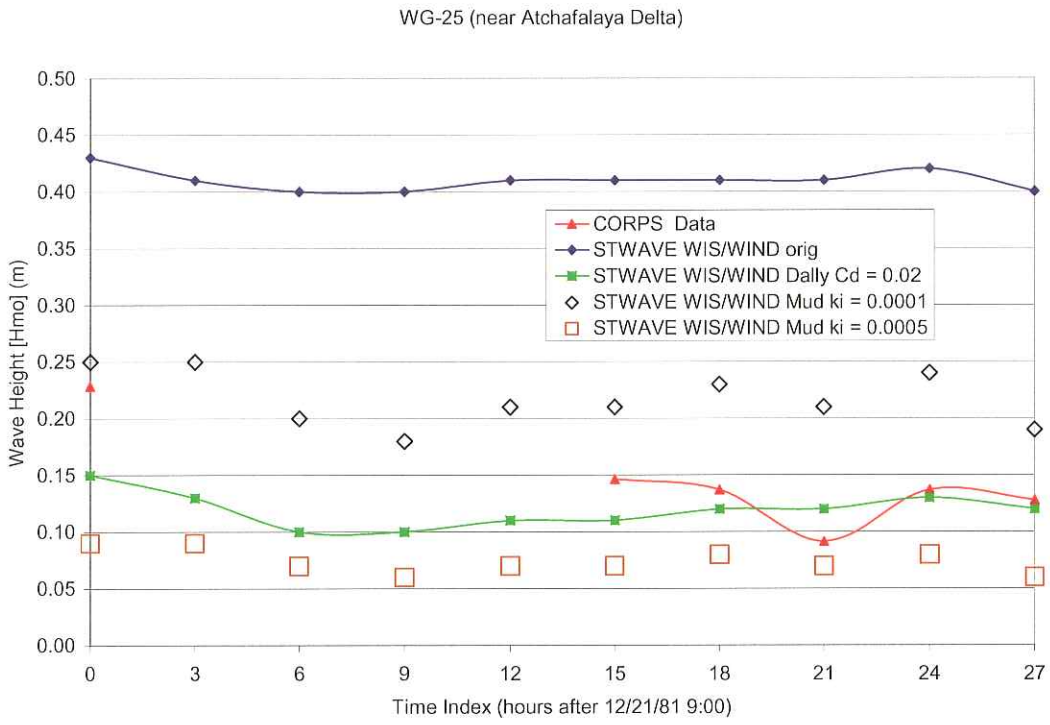

Wave height record comparison at WG-25 for Southerly Storm 3

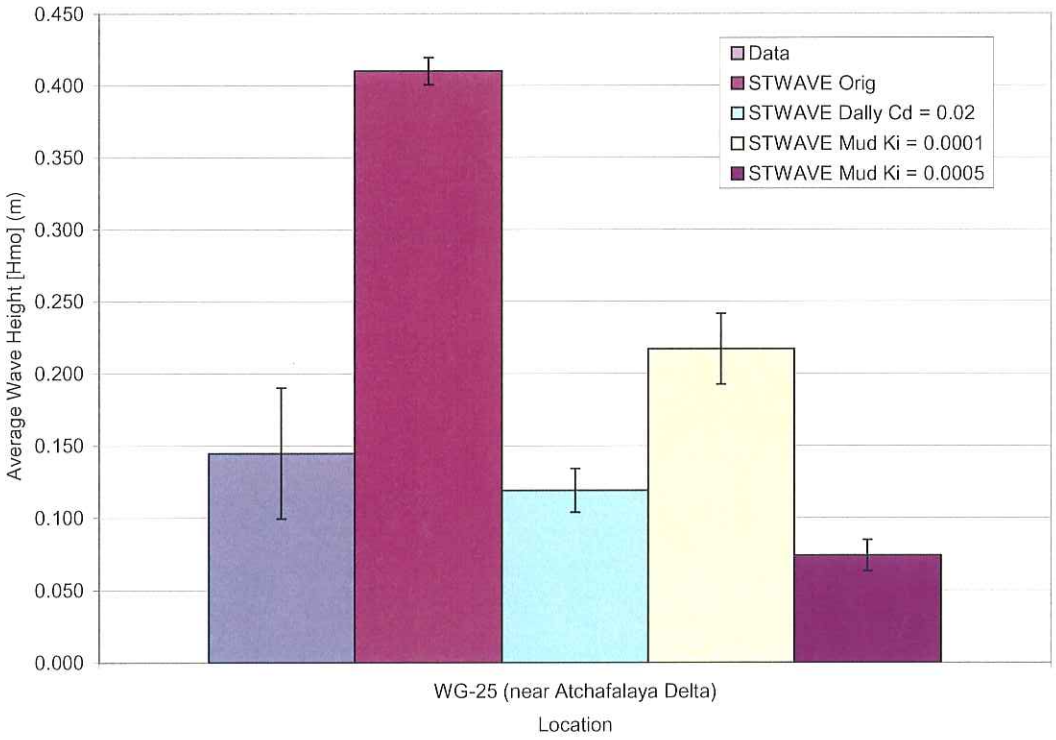

Wave height averages comparison at WG-25 for Southerly Storm 3

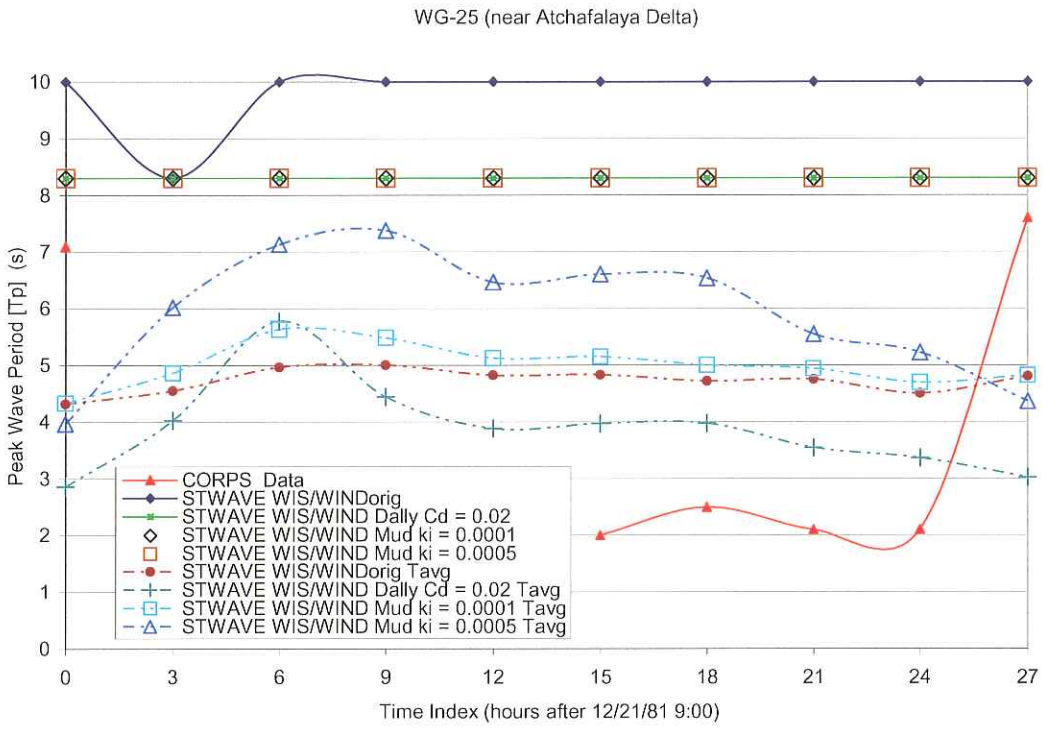

Wave period record comparison at WG-25 for Southerly Storm 3

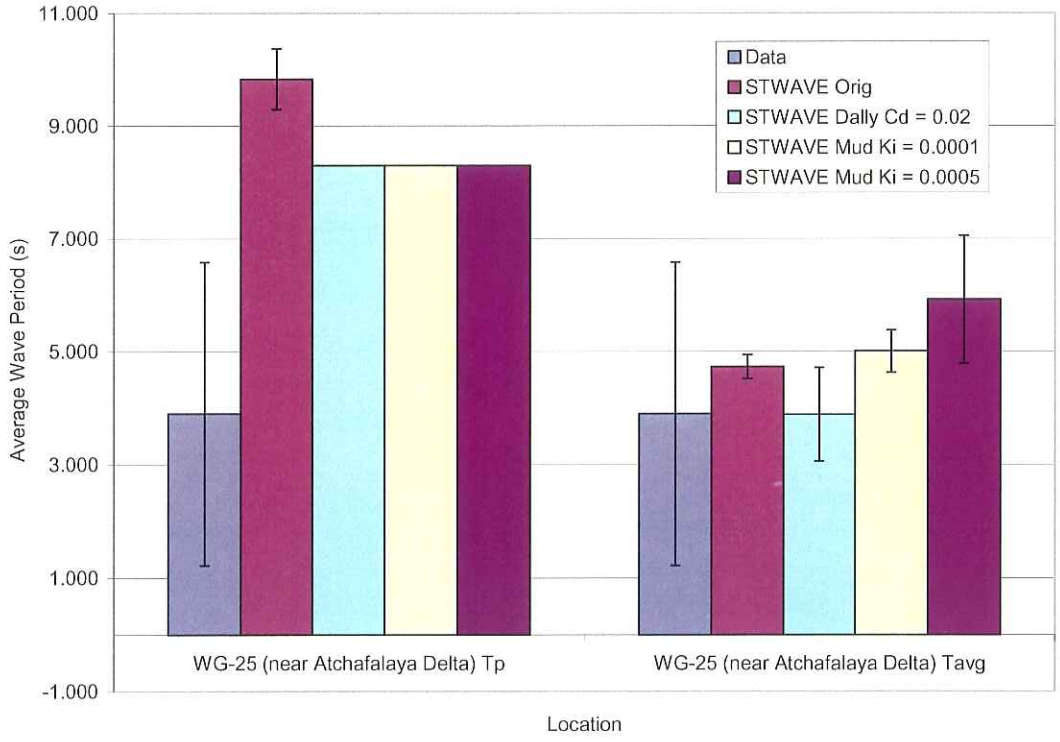

Wave period averages comparison at WG-25 for Southerly Storm 3

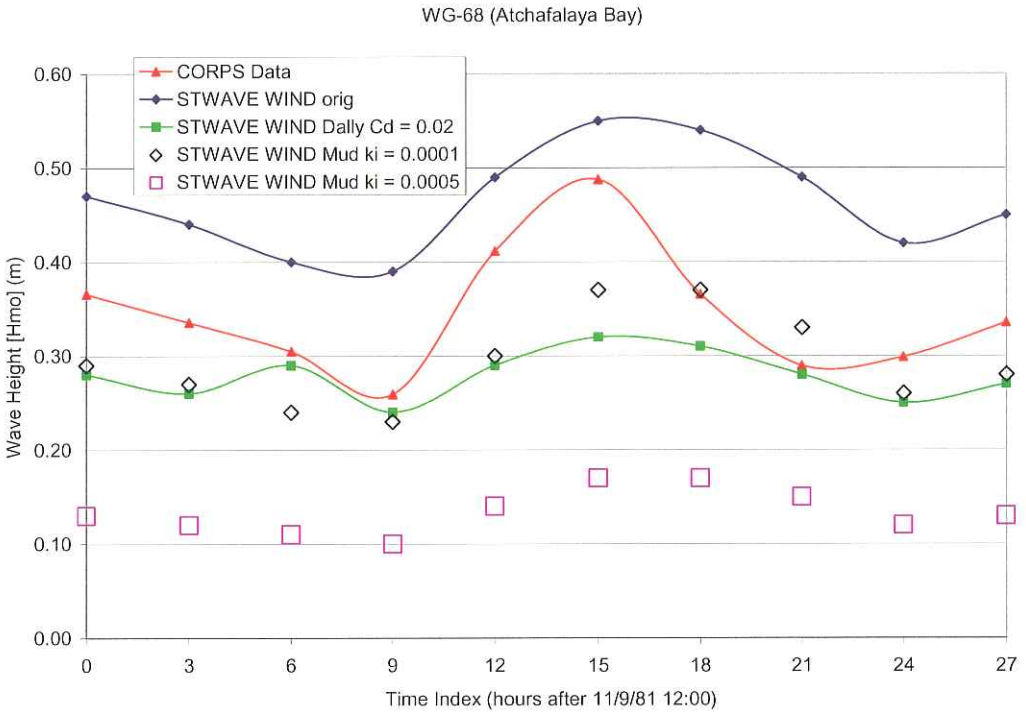

Wave height record comparison at WG-68 for Northerly Storm 1

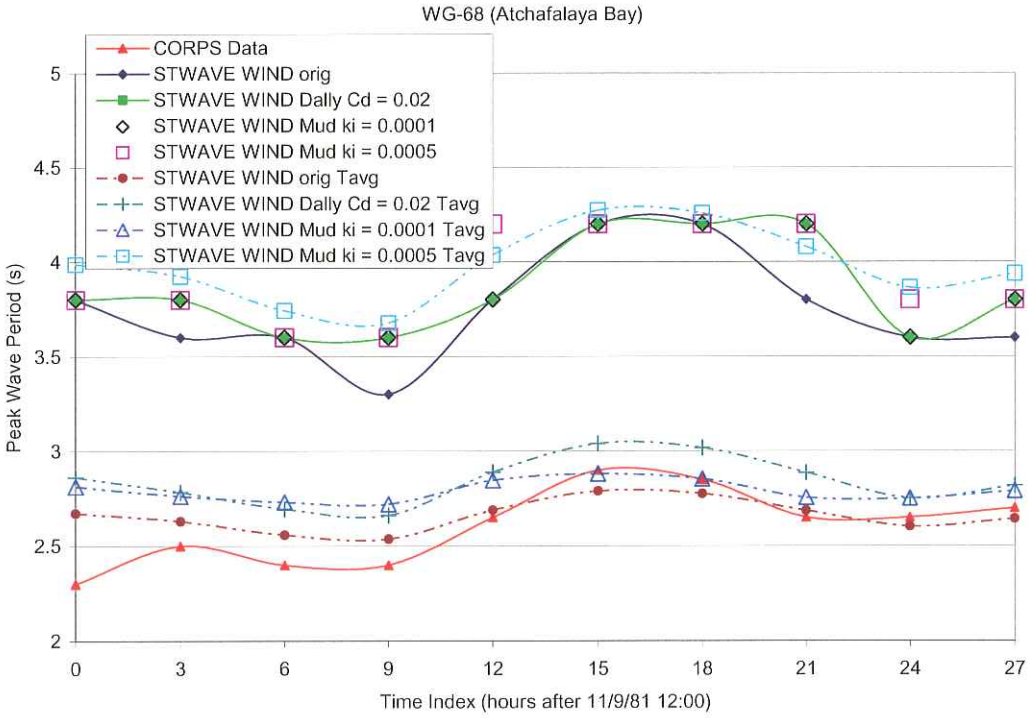

Wave period record comparison at WG-68 for Northerly Storm 1

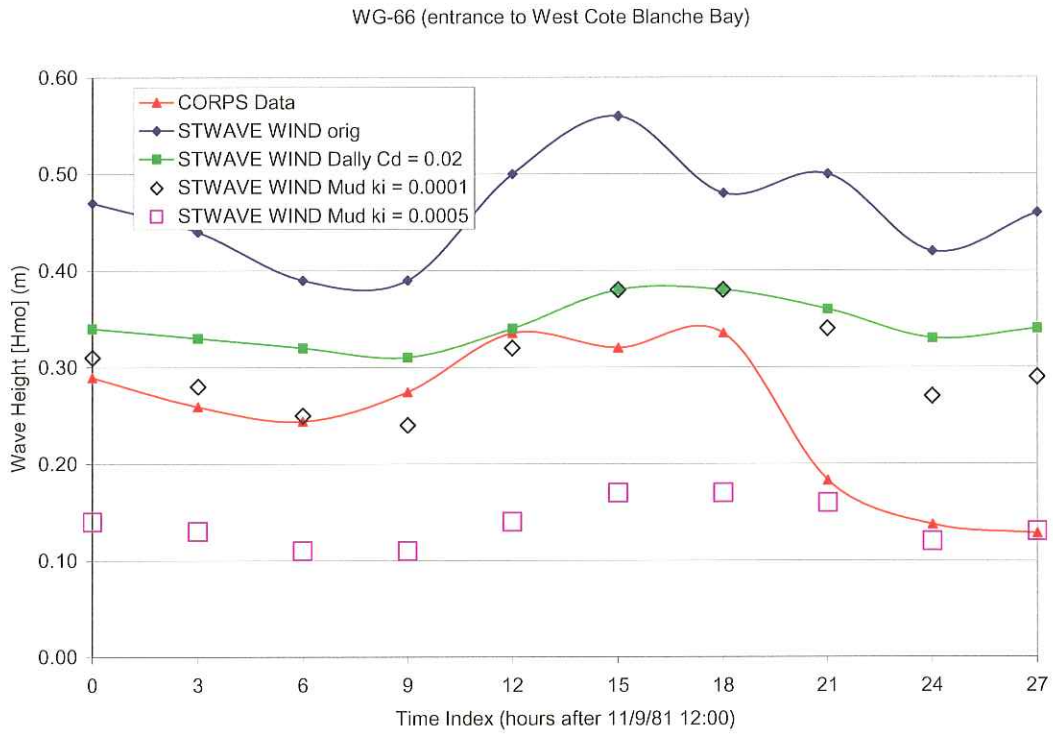

Wave height record comparison at WG-66 for Northerly Storm 1

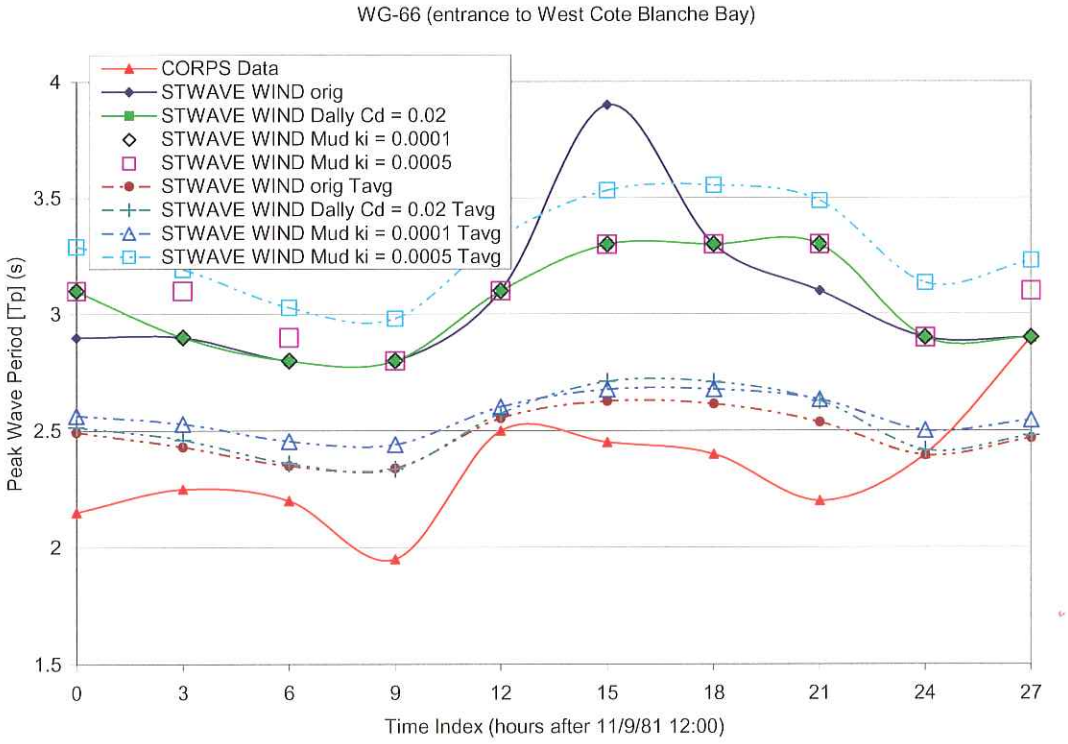

Wave period record comparison at WG-66 for Northerly Storm 1

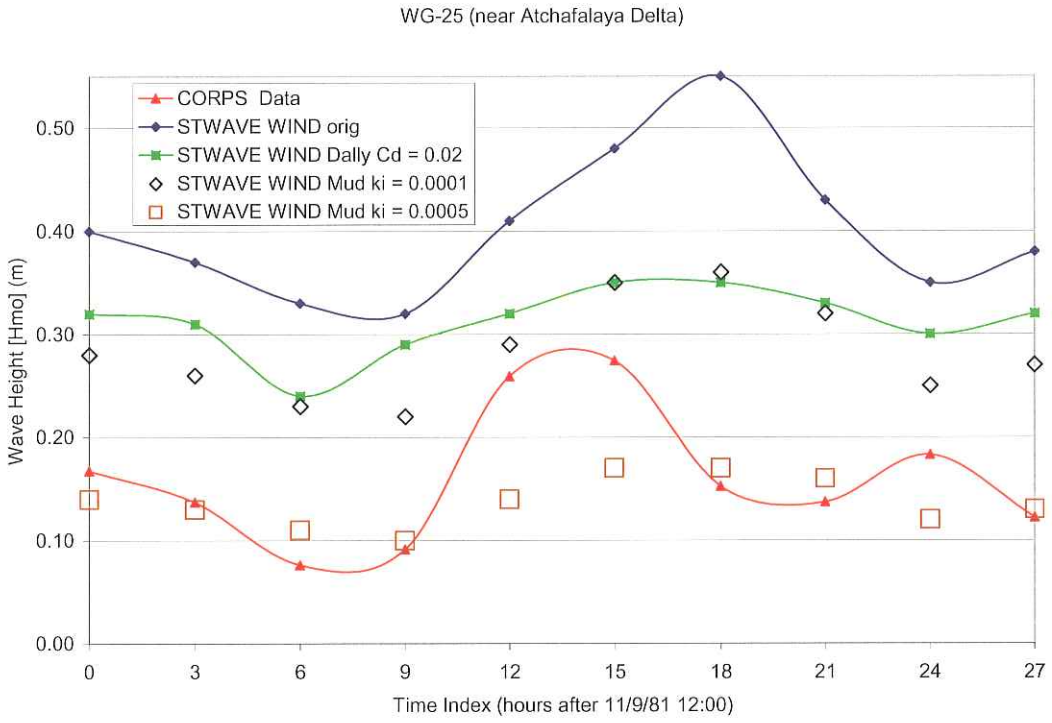

Wave height record comparison at WG-25 for Northerly Storm 1

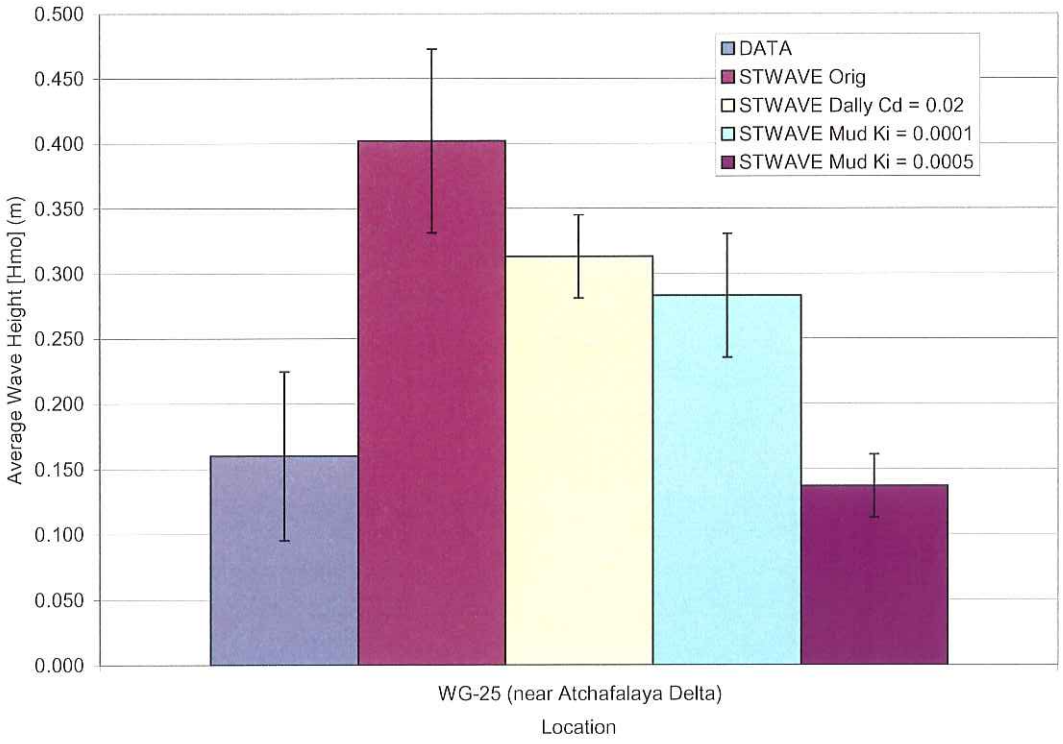

Wave height averages comparison at WG-25 for Northerly Storm 1

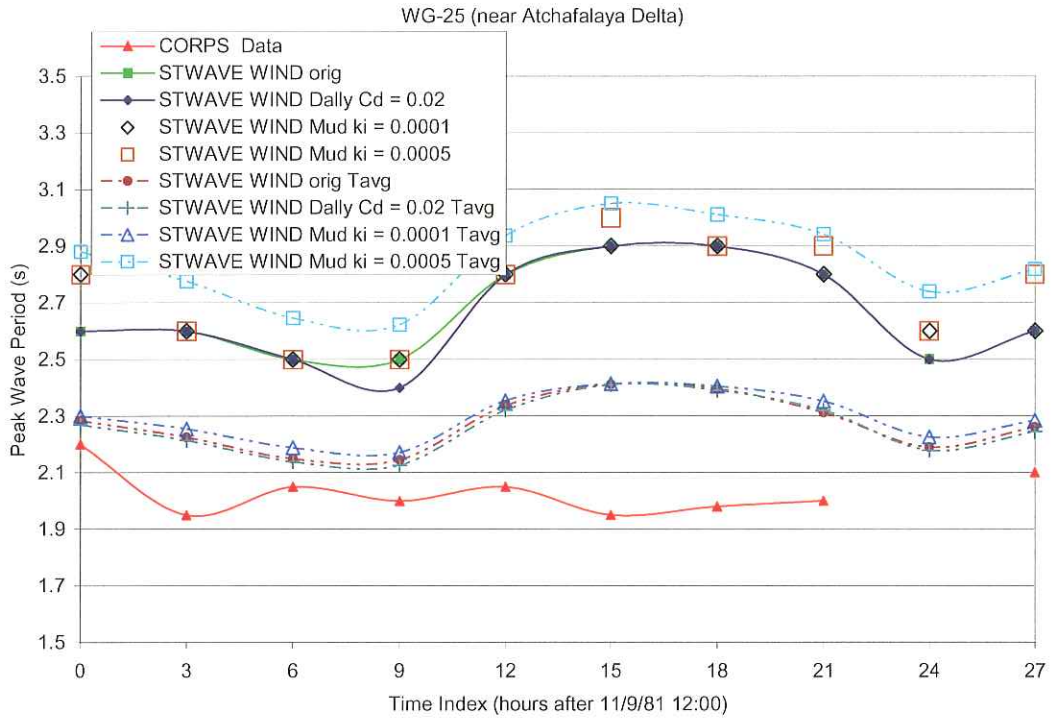

Wave period record comparison at WG-25 for Northerly Storm 1

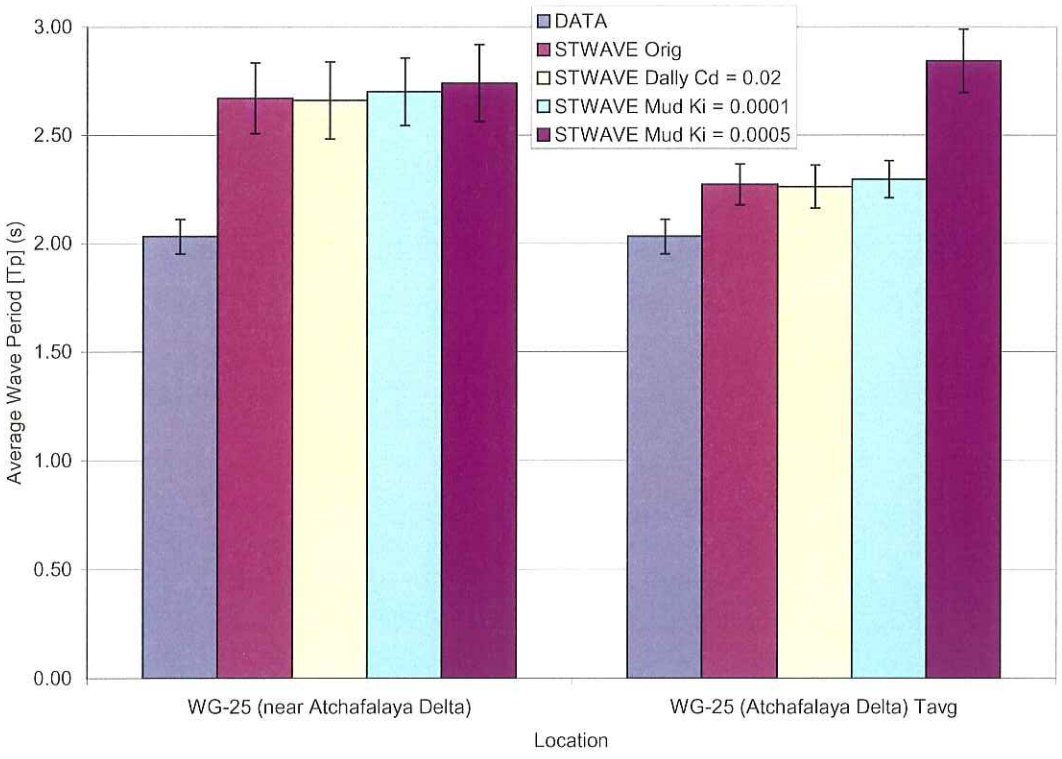

Wave period averages comparison at WG-25 for Northerly Storm 1

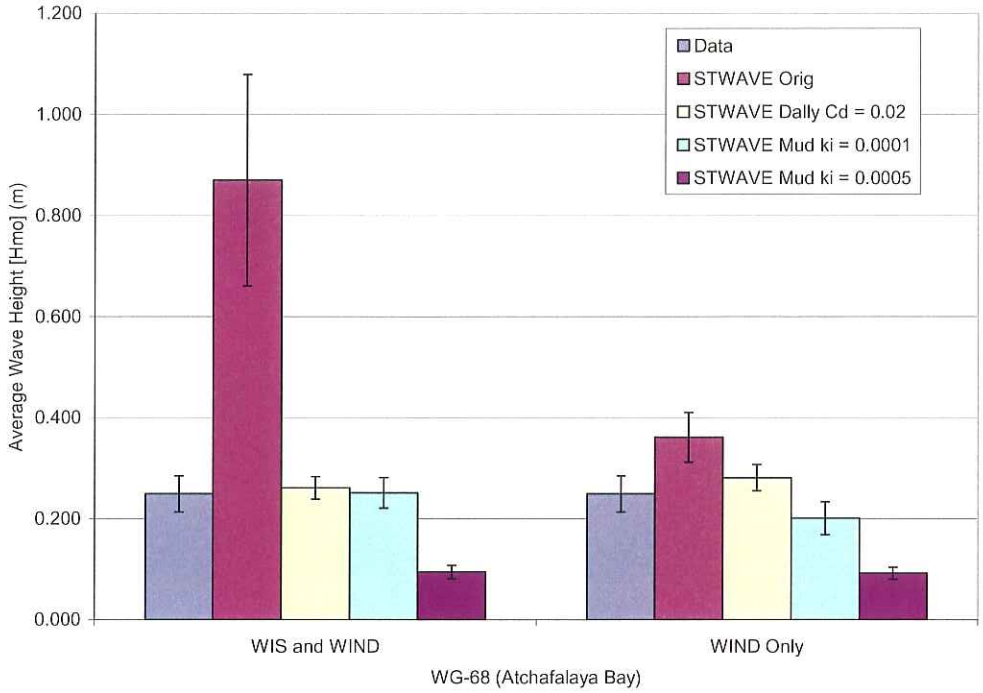

Wave height averages comparison (WIS+wind versus only locally generated wind waves) at WG-68 for Southerly Storm 1

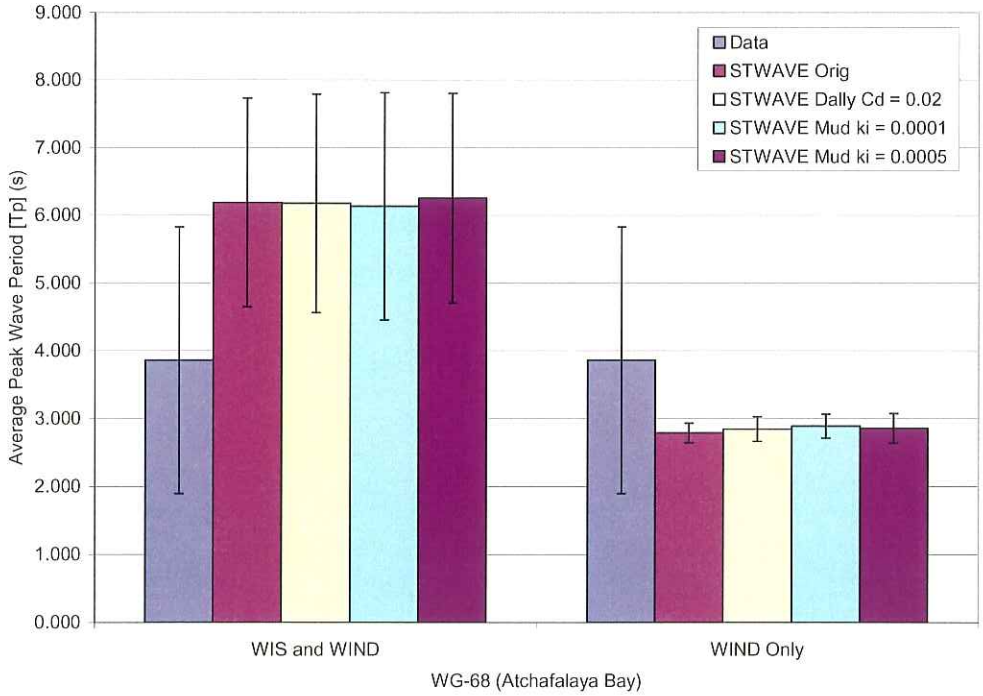

Peak wave period averages comparison (WIS+wind versus only locally generated wind waves) at WG-68 for Southerly Storm 1

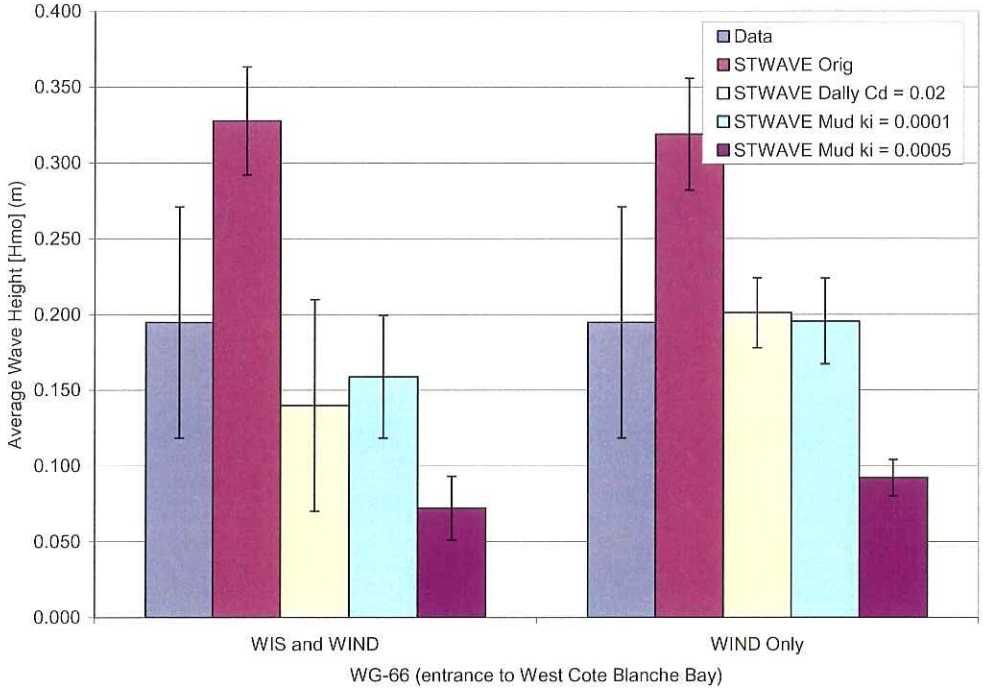

Wave height averages comparison (WIS+wind versus only locally generated wind waves) at WG-66 for Southerly Storm 1

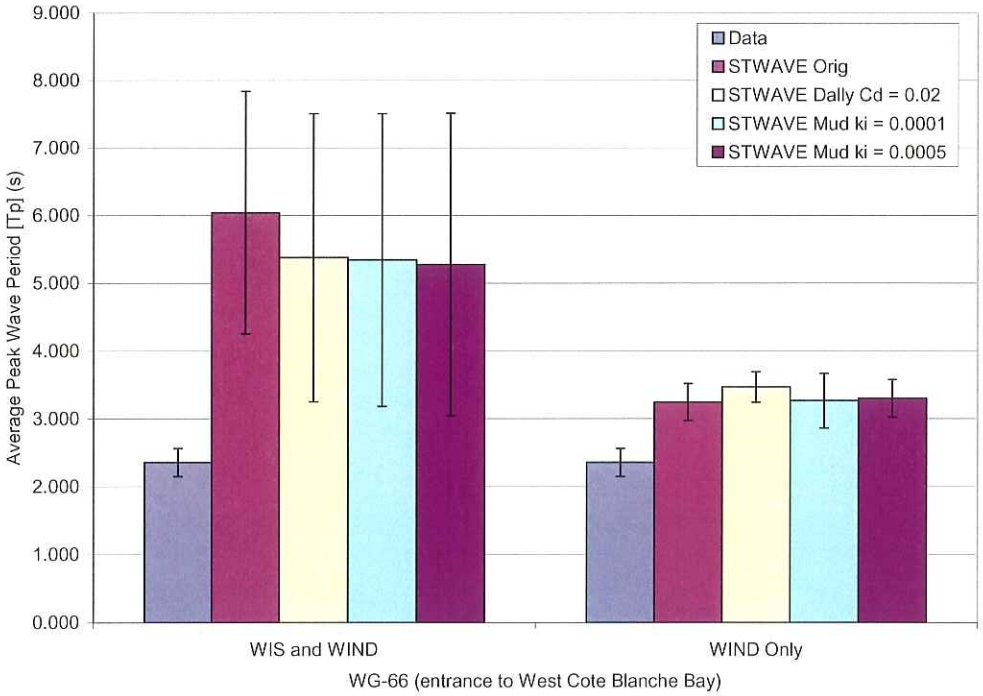

Peak wave period averages comparison (WIS+wind versus only locally generated wind waves) at WG-66 for Southerly Storm 1

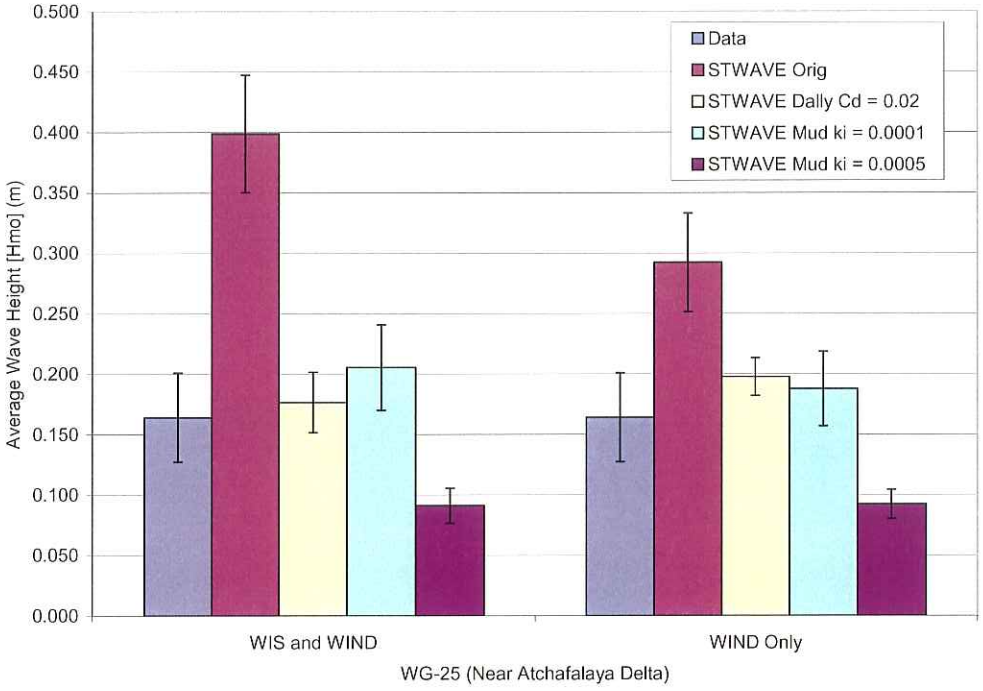

Wave height averages comparison (WIS+wind versus only locally generated wind waves) at WG-25 for Southerly Storm 1

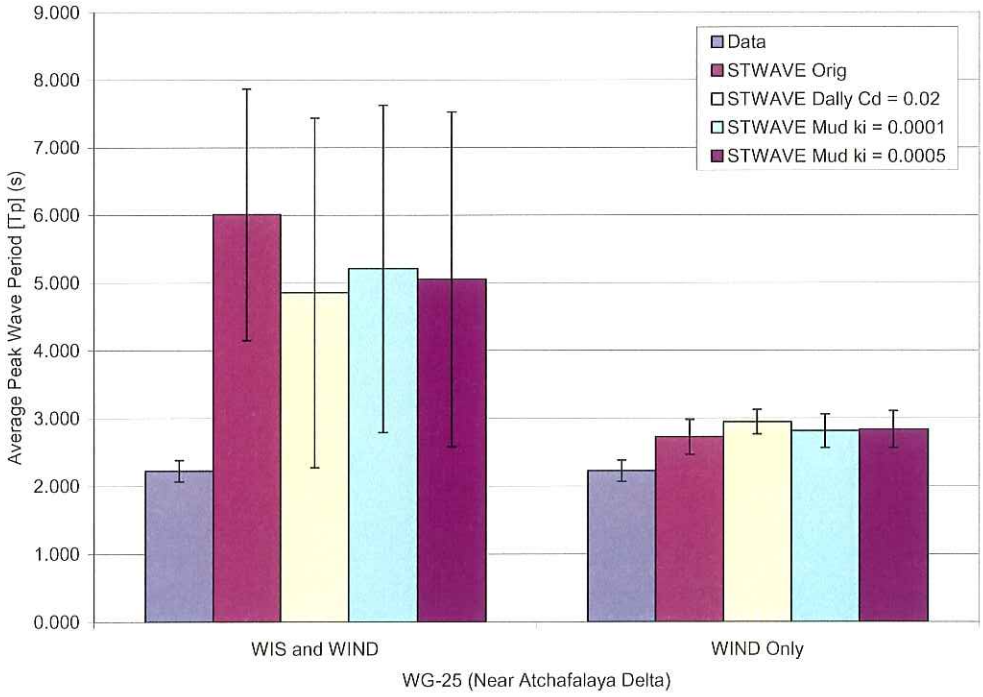

Peak wave period averages comparison (WIS+wind versus only locally generated wind waves) at WG-25 for Southerly Storm 1

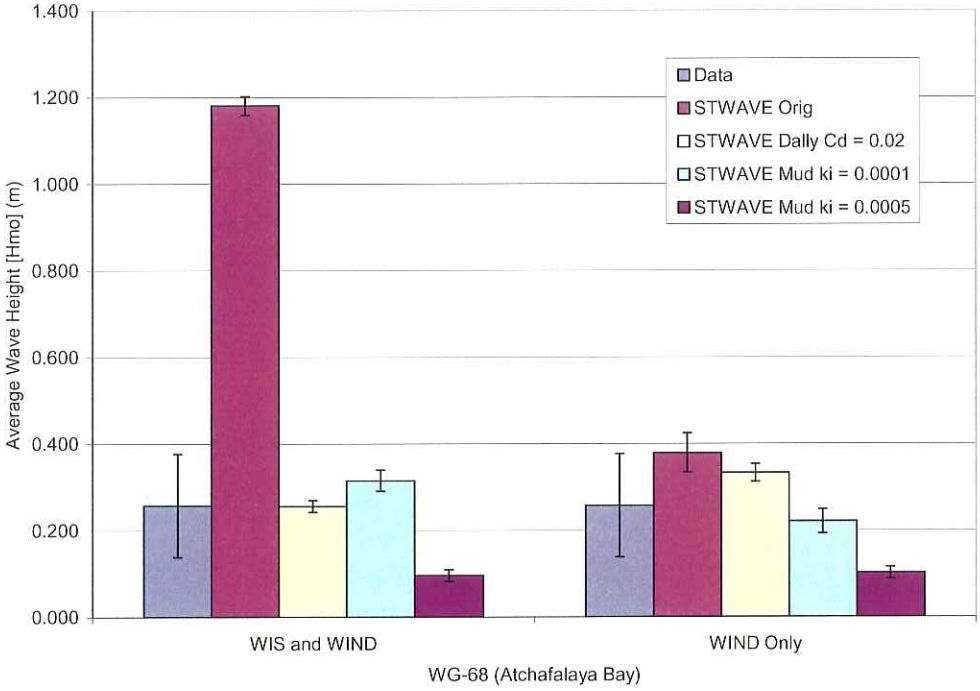

Wave height averages comparison (WIS+wind versus only locally generated wind waves) at WG-68 for Southerly Storm 3

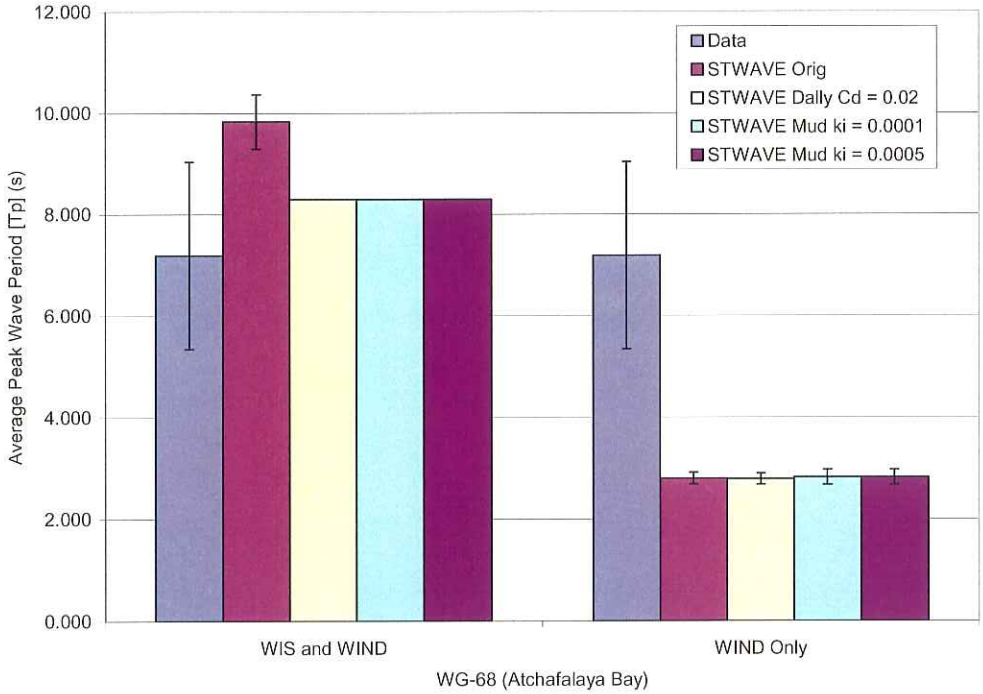

Peak wave period averages comparison (WIS+wind versus only locally generated wind waves) at WG-68 for Southerly Storm 3

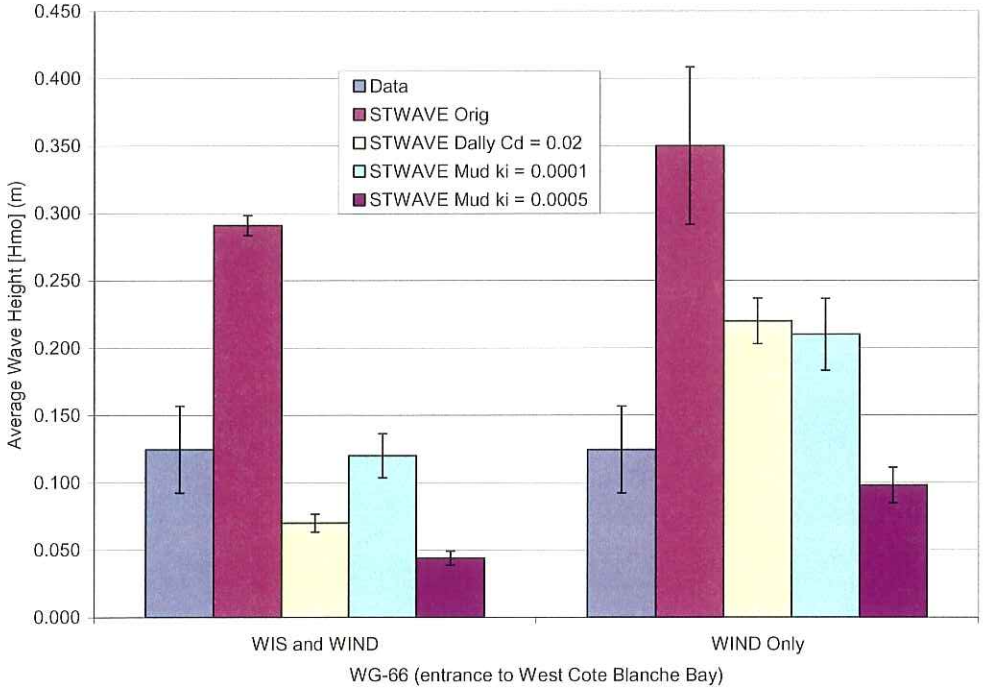

Wave height averages comparison (WIS+wind versus only locally generated wind waves) at WG-66 for Southerly Storm 3

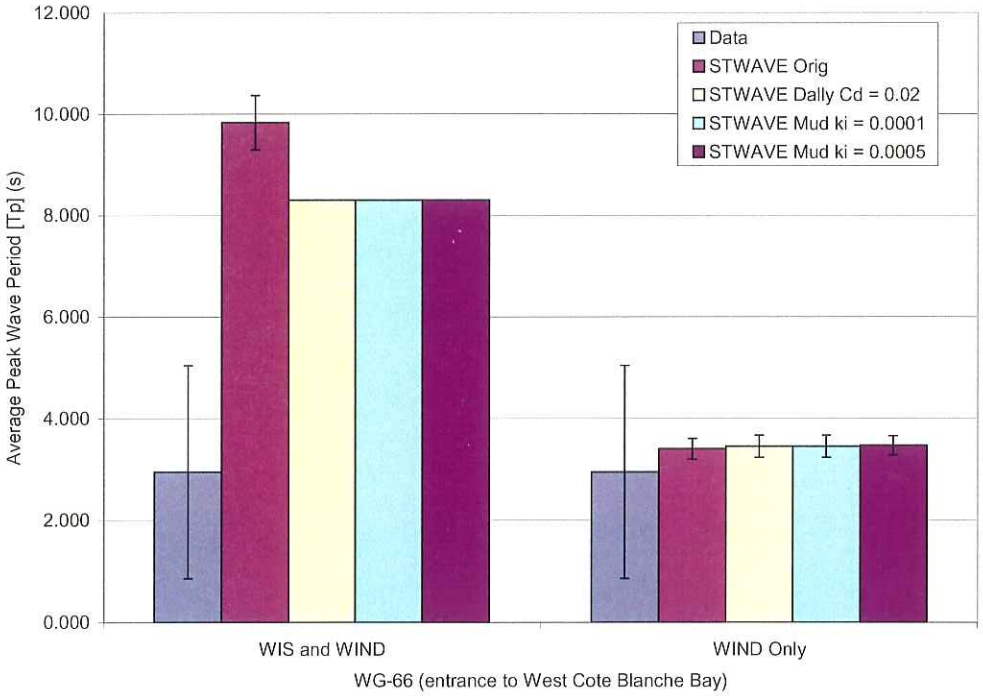

Peak wave period averages comparison (WIS+wind versus only locally generated wind waves) at WG-66 for Southerly Storm 3

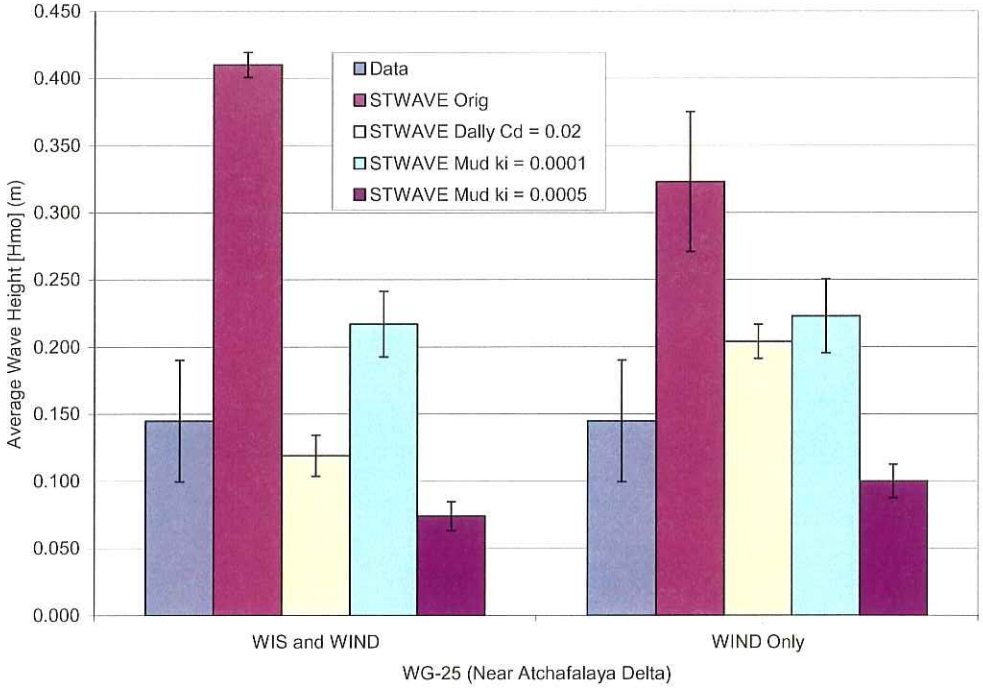

Wave height averages comparison (WIS+wind versus only locally generated wind waves) at WG-25 for Southerly Storm 3

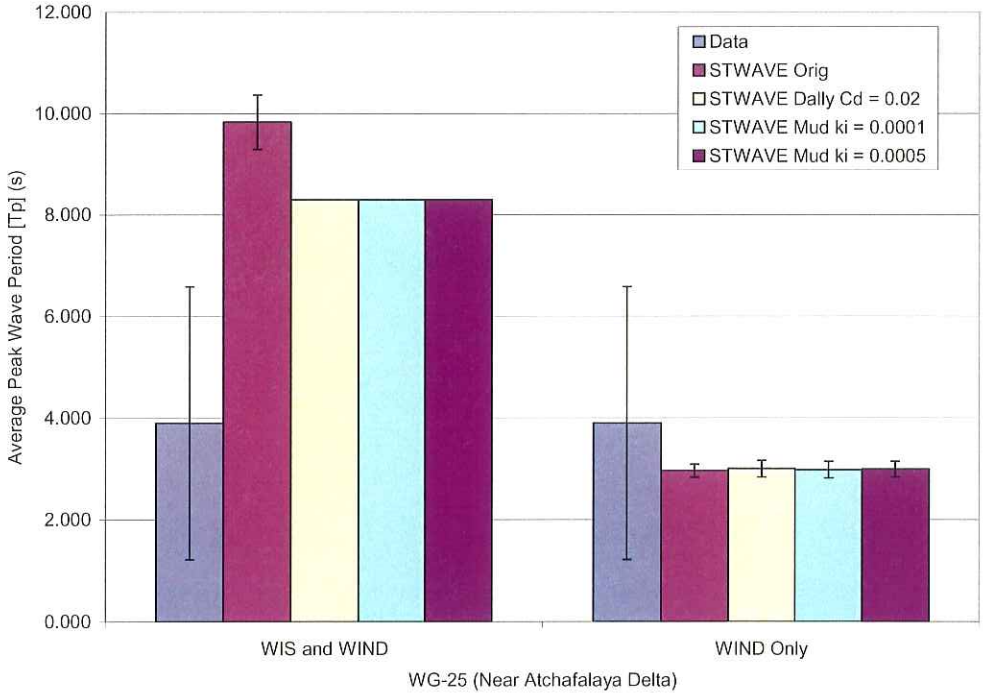

Peak wave period averages comparison (WIS+wind versus only locally generated wind waves) at WG-25 for Southerly Storm 3

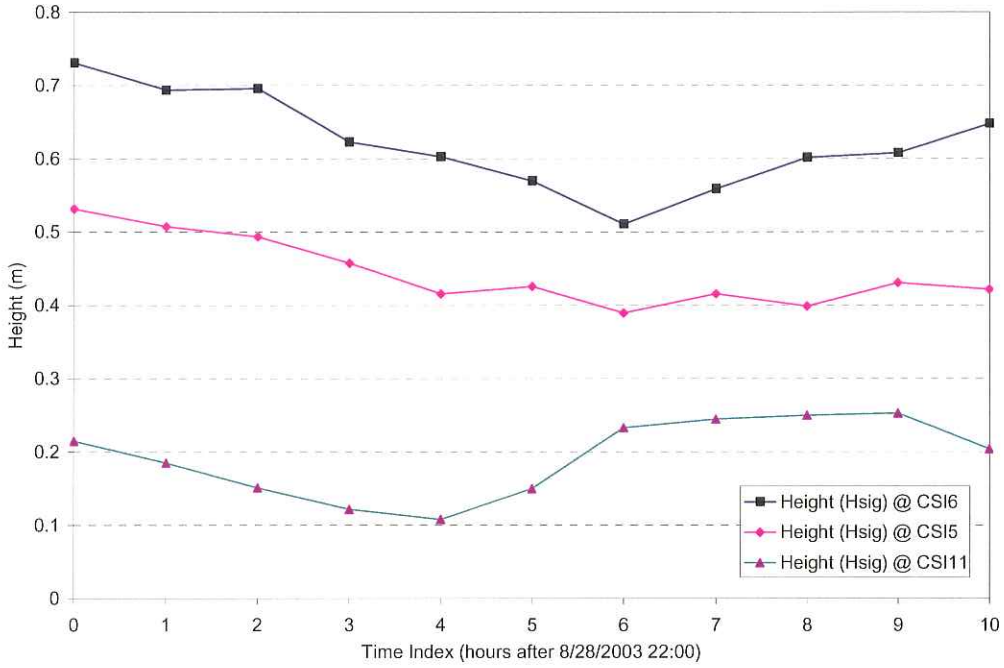

Wave height at WAVCIS stations during typical summer conditions

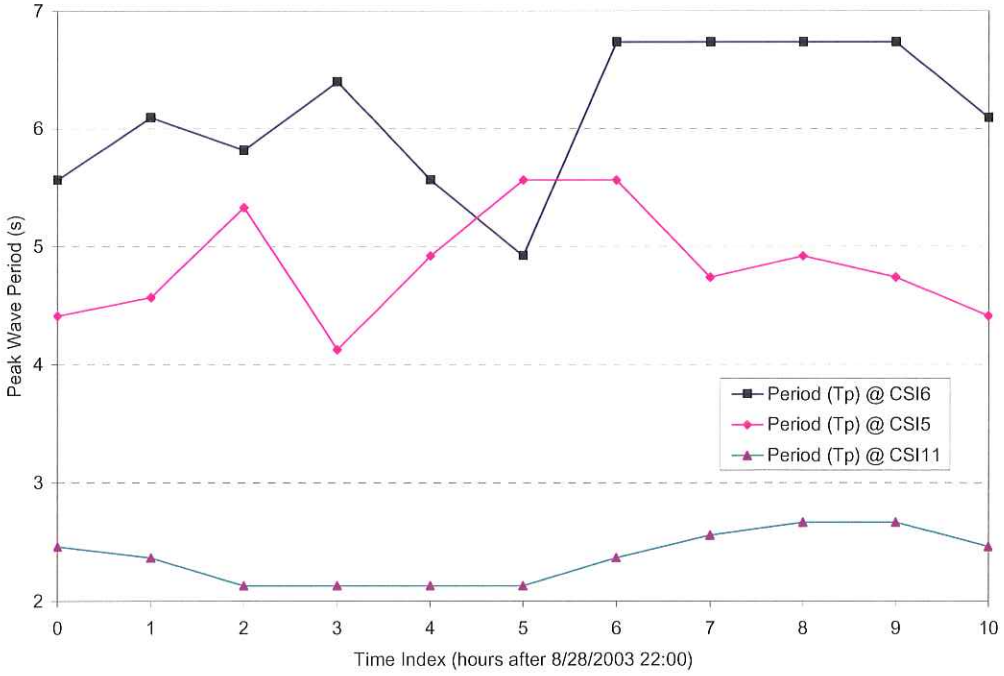

Wave period at WAVCIS stations during typical summer conditions

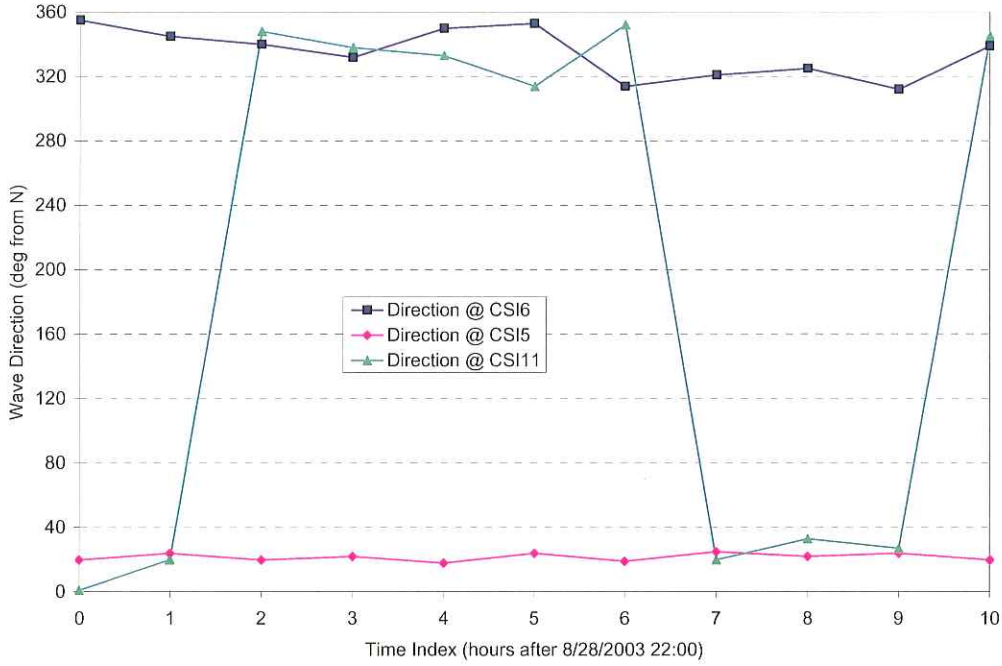

Wave direction at WAVCIS stations during typical summer conditions

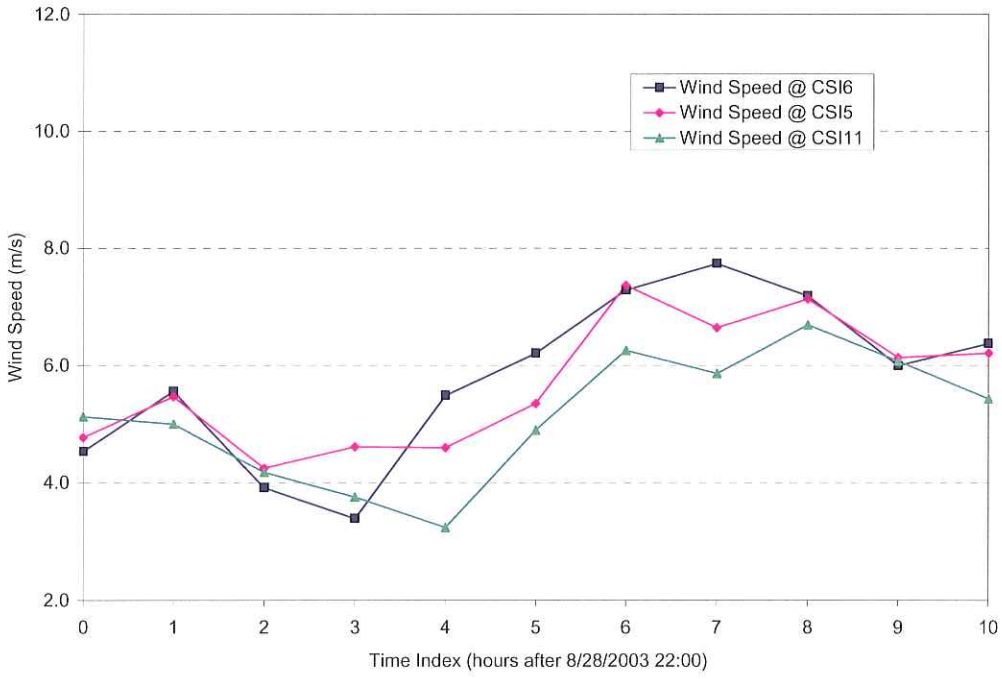

Wind speed at WAVCIS stations during typical summer conditions

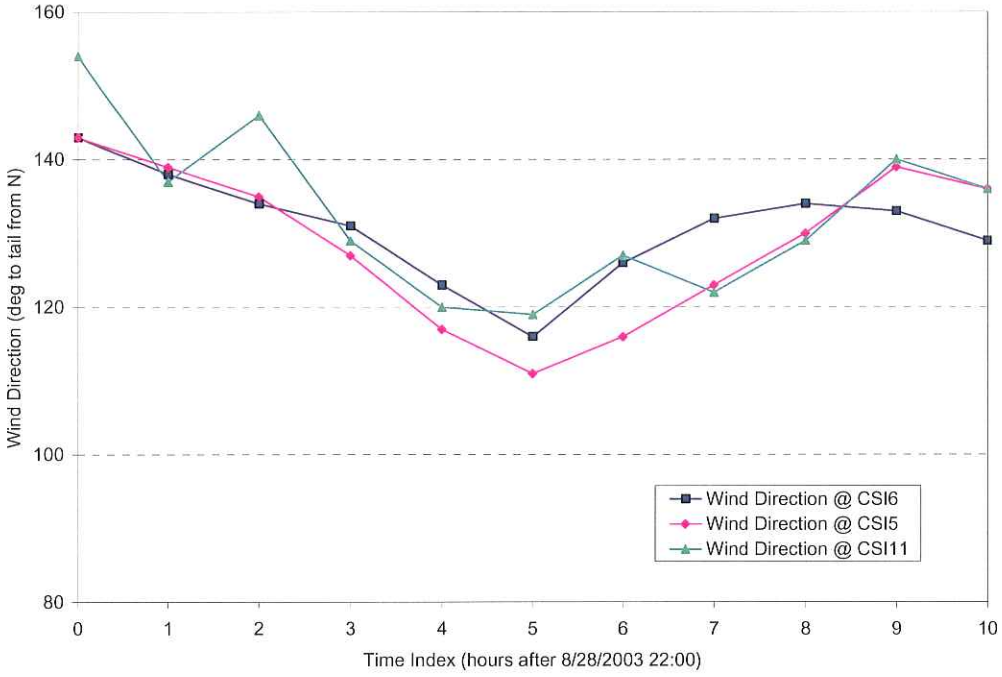

Wind direction at WAVCIS stations during typical summer conditions

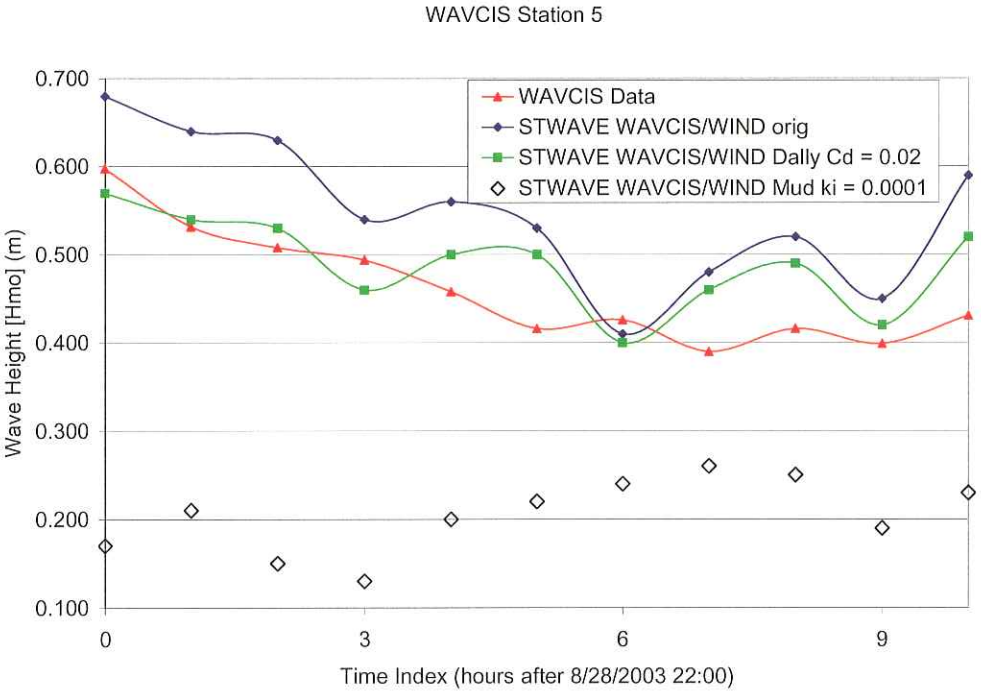

Wave height record comparison at CSI-5 for typical summer conditions

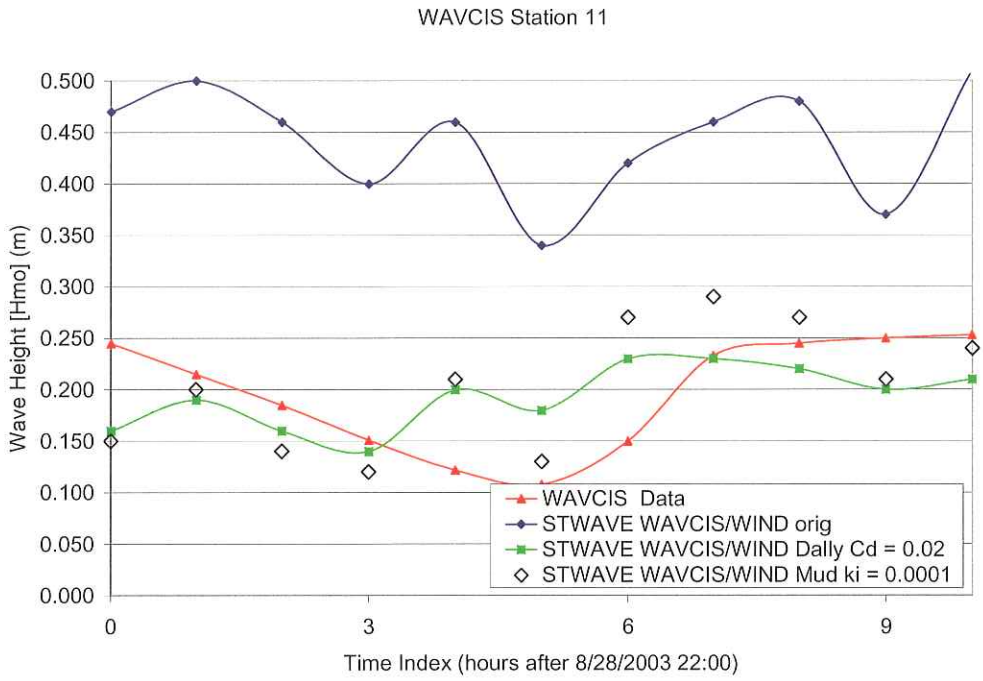

Wave height record comparison at CSI-11 for typical summer conditions

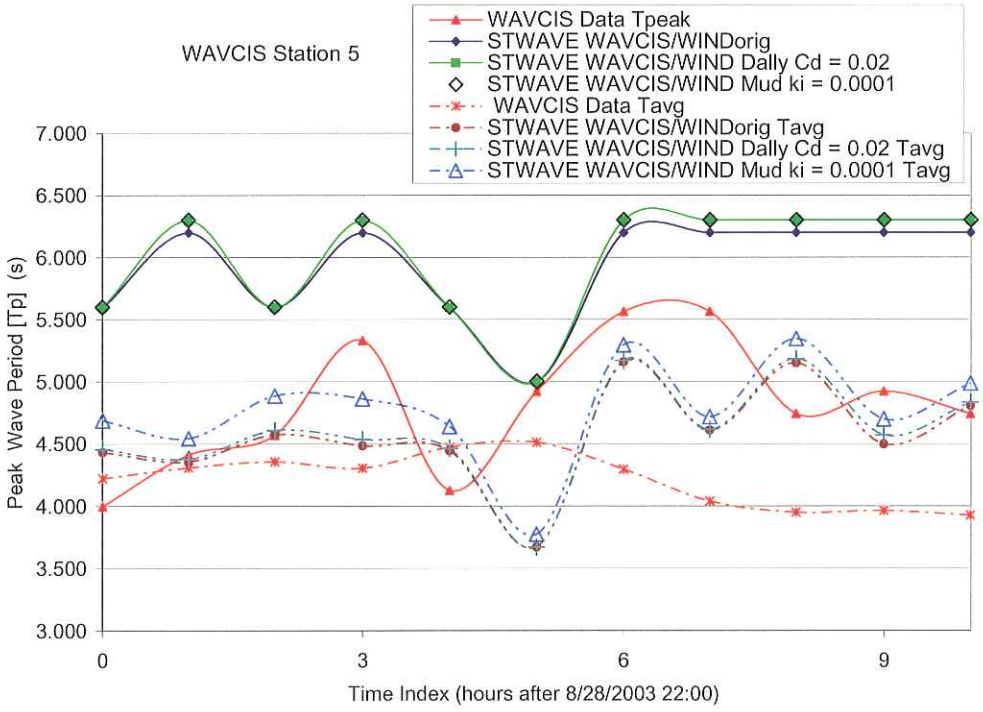

Wave period record comparison at CSI-5 for typical summer conditions

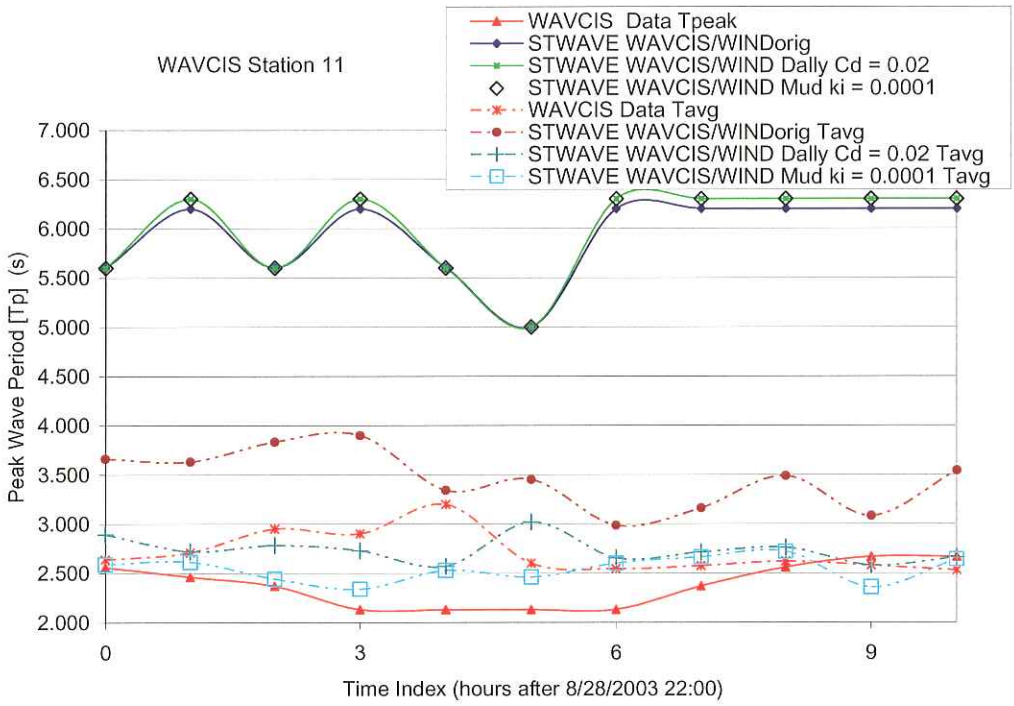

Wave period record comparison at CSI-11 for typical summer conditions

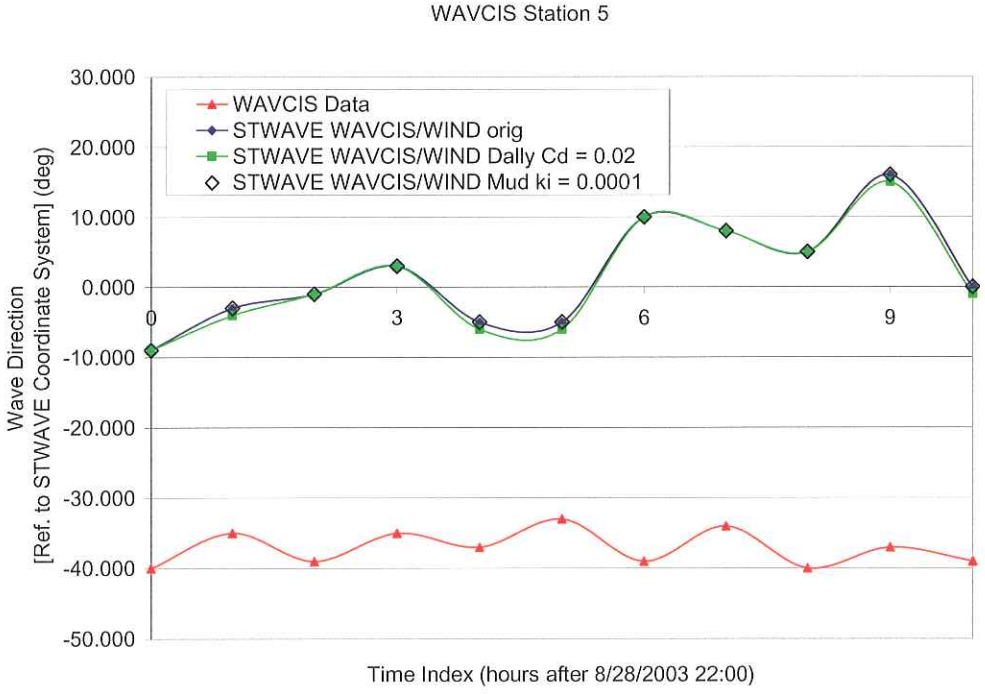

Wave direction record comparison at CSI-5 for typical summer conditions

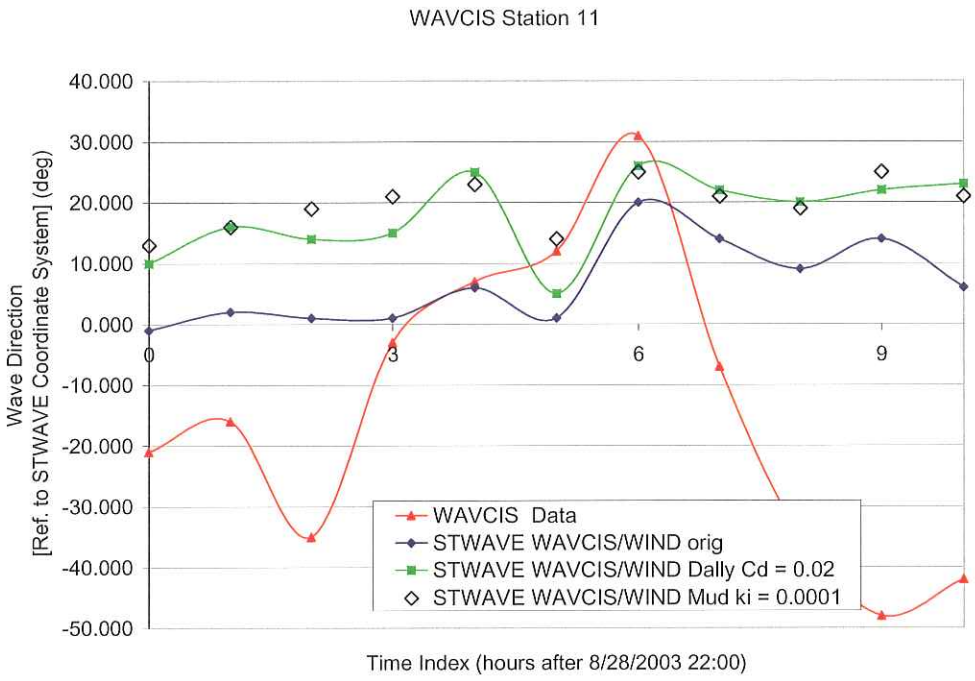

Wave direction record comparison at CSI-11 for typical summer conditions

Appendix B

Salinity Time Series Plots

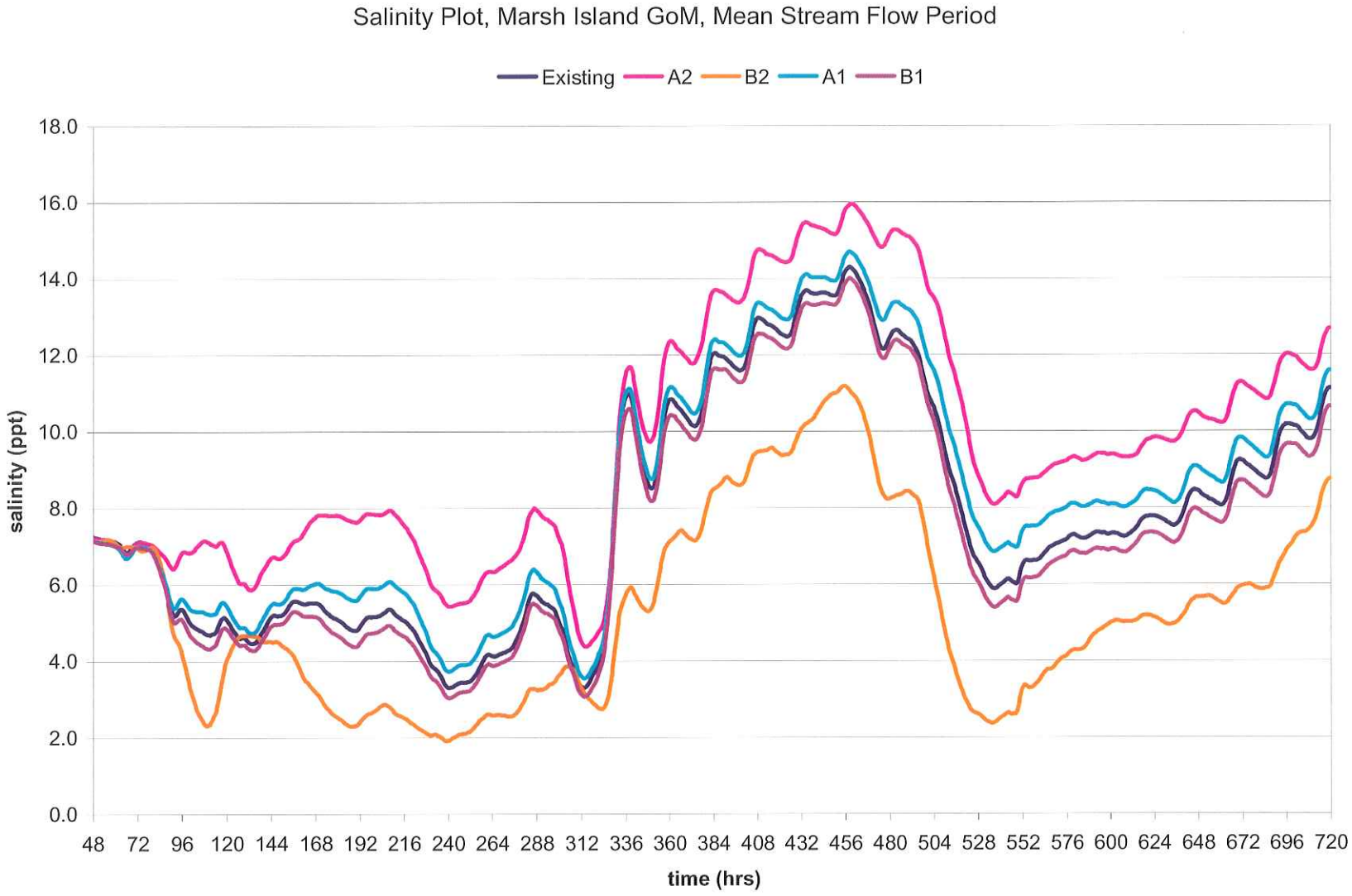
Salinity Plot, Marsh Island GoM, Mean Stream Flow Period
Existing
A2
B2
A1
B1
18.0
16.0
14.0
12.0
10.0
8.0
6.0
4.0
2.0
0.0
salinity (ppt)
48 72 96 120 144 168 192 216 240 264 288 312 336 360 384 408 432 456 480 504 528 552 576 600 624 648 672 696 720
time (hrs)

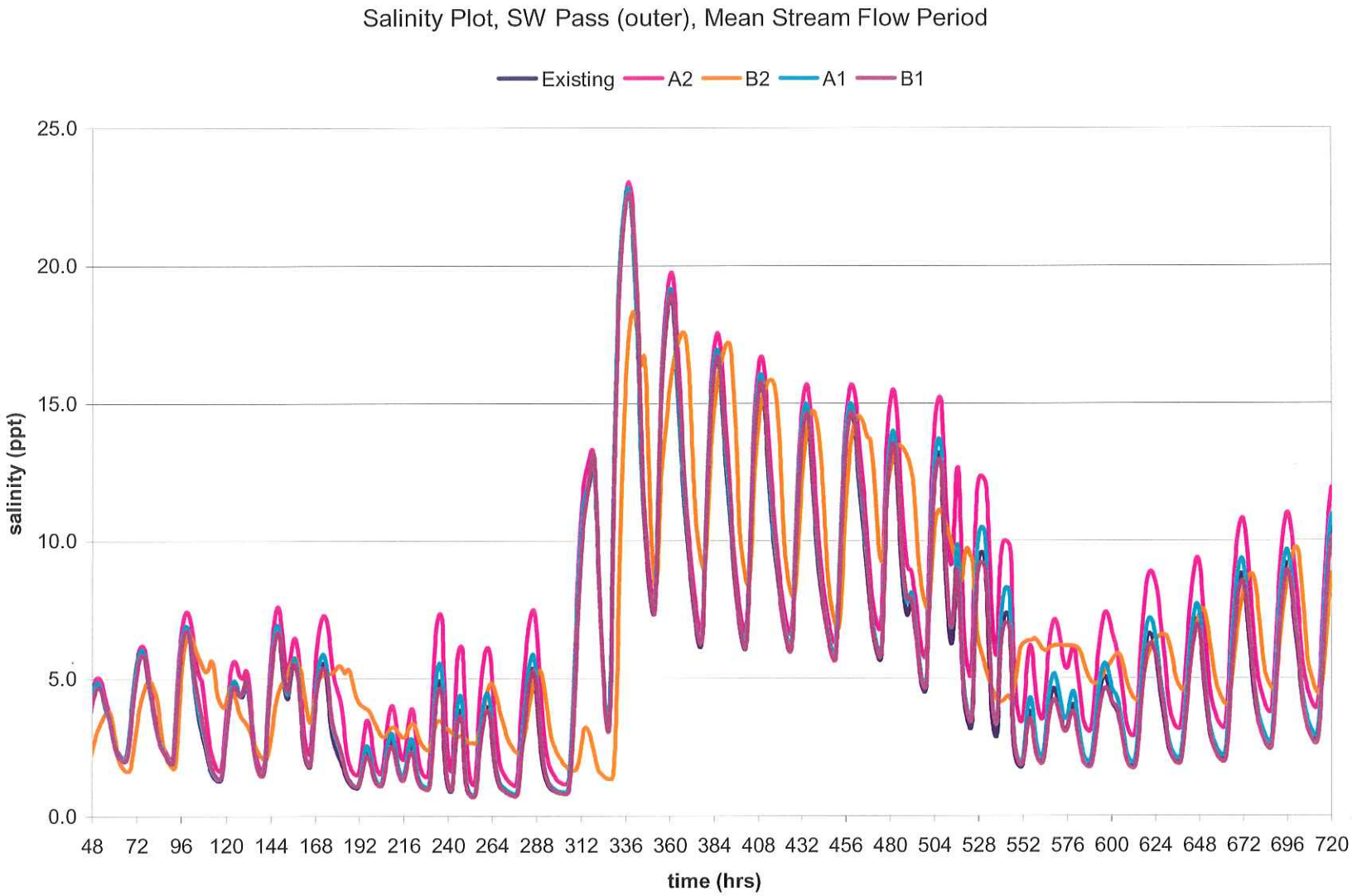
Salinity Plot, SW Pass (outer), Mean Stream Flow Period
Existing
A2
B2
A1
B1
25.0
20.0
15.0
10.0
5.0
0.0
salinity (ppt)
48 72 96 120 144 168 192 216 240 264 288 312 336 360 384 408 432 456 480 504 528 552 576 600 624 648 672 696 720
time (hrs)

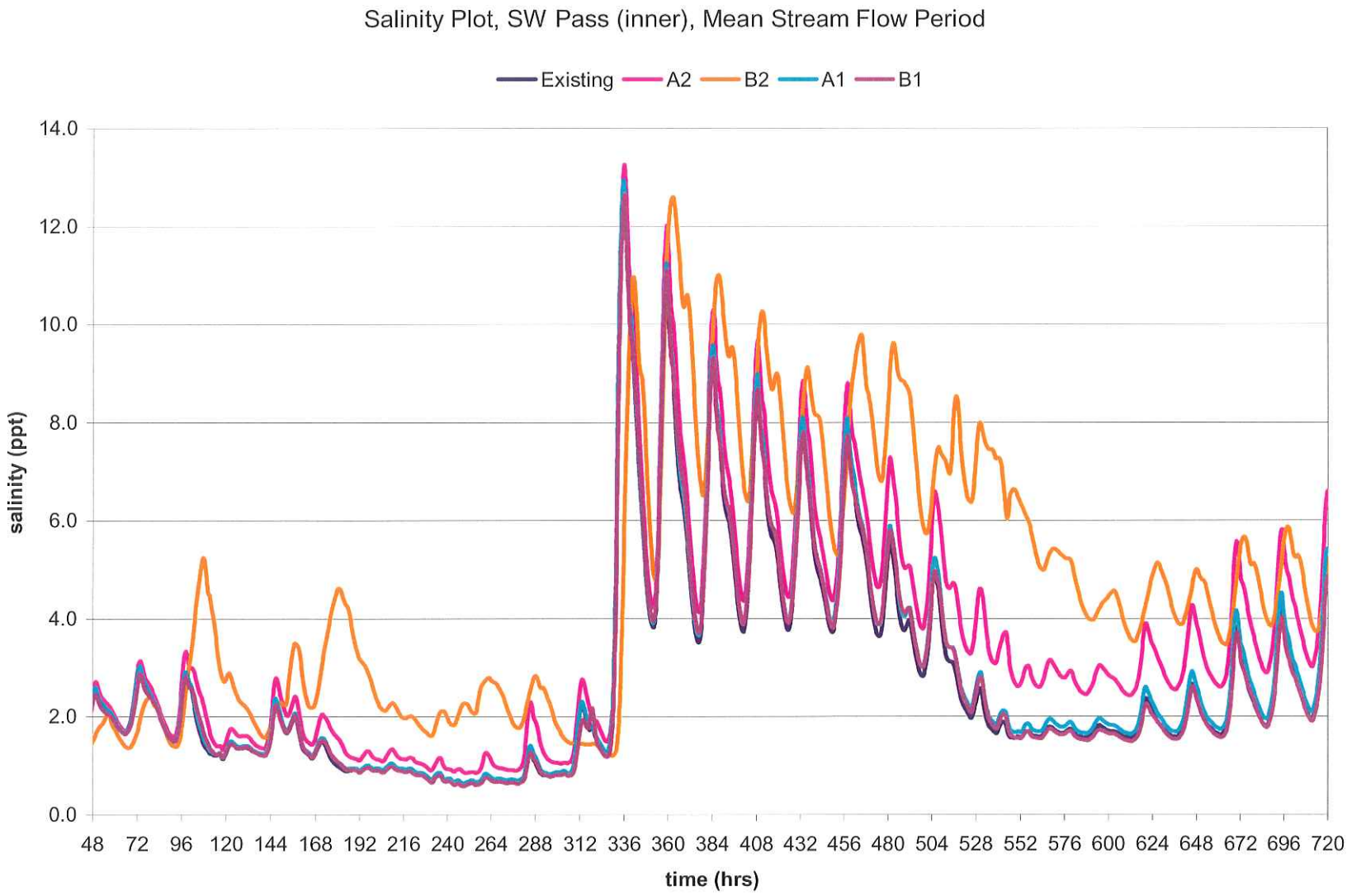
Salinity Plot, SW Pass (inner), Mean Stream Flow Period
Existing
A2
B2
A1
B1
salinity (ppt)
14.0
12.0
10.0
8.0
6.0
4.0
2.0
0.0
48 72 96 120 144 168 192 216 240 264 288 312 336 360 384 408 432 456 480 504 528 552 576 600 624 648 672 696 720
time (hrs)

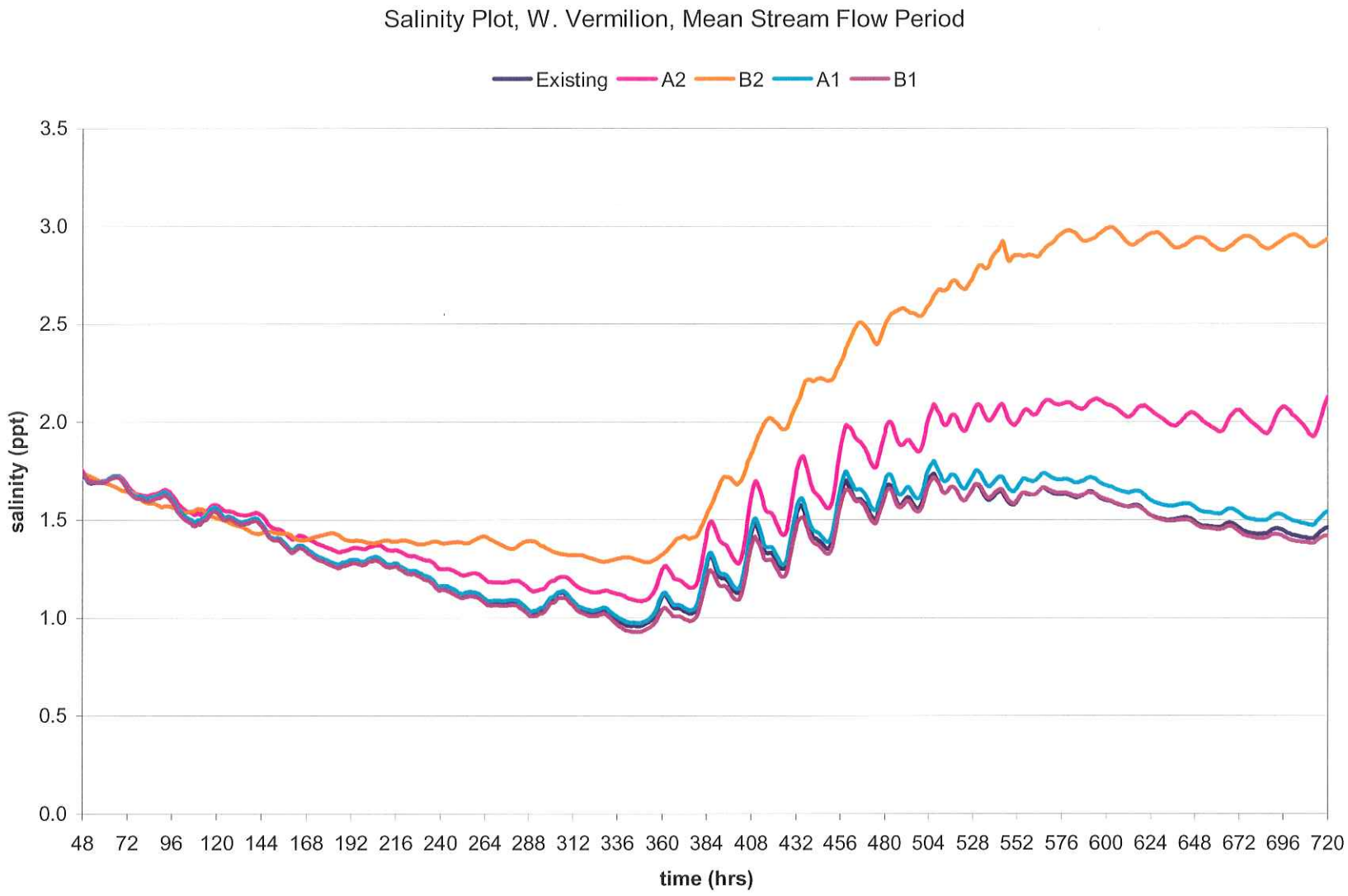
Salinity Plot, W. Vermilion, Mean Stream Flow Period
Existing
A2
B2
A1
B1
salinity (ppt)
3.5
3.0
2.5
2.0
1.5
1.0
0.5
0.0
48 72 96 120 144 168 192 216 240 264 288 312 336 360 384 408 432 456 480 504 528 552 576 600 624 648 672 696 720
time (hrs)

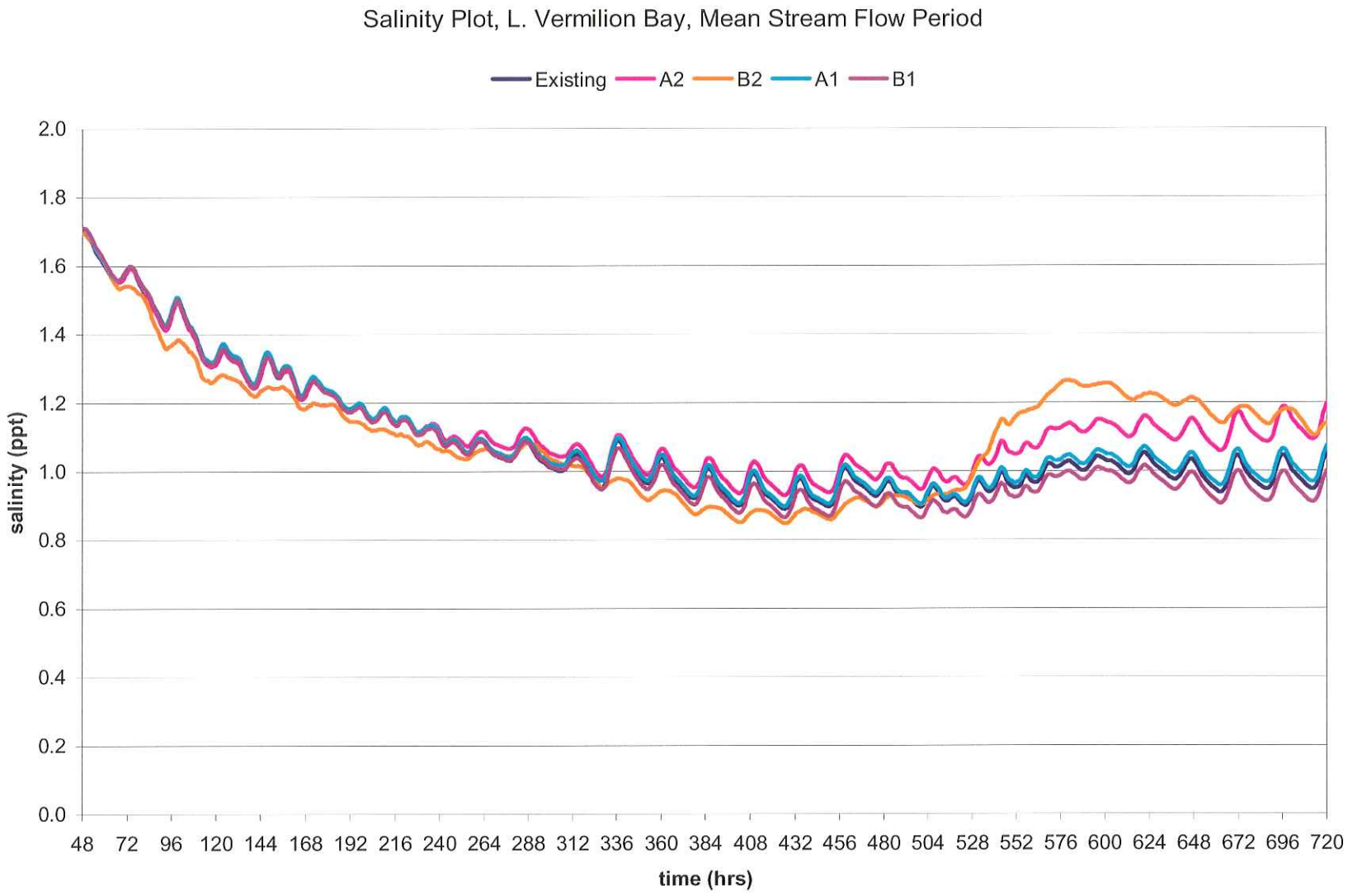
Salinity Plot, L. Vermilion Bay, Mean Stream Flow Period
Existing
A2
B2
A1
B1
salinity (ppt)
2.0
1.8
1.6
1.4
1.2
1.0
0.8
0.6
0.4
0.2
0.0
48 72 96 120 144 168 192 216 240 264 288 312 336 360 384 408 432 456 480 504 528 552 576 600 624 648 672 696 720
time (hrs)

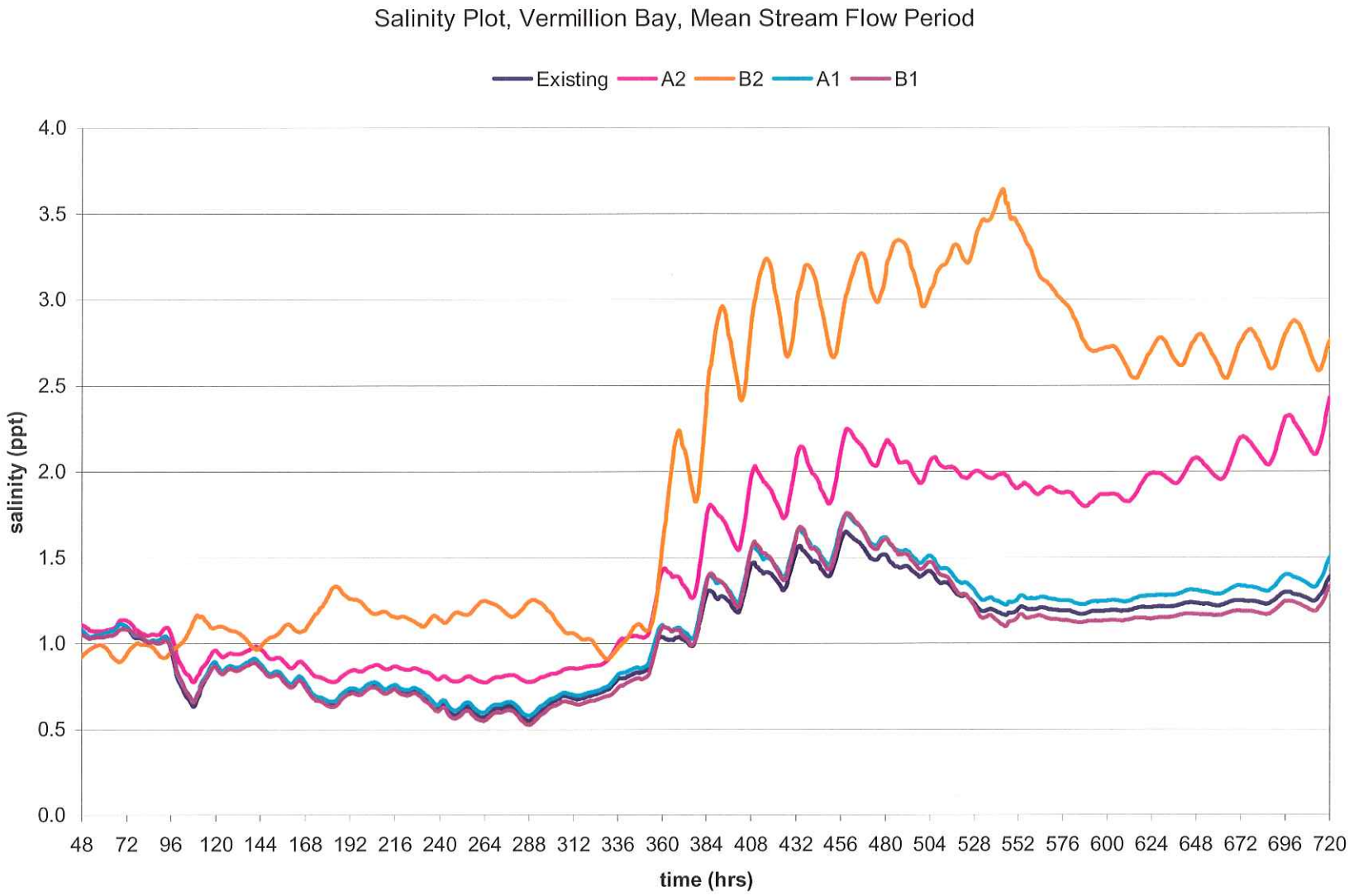
Salinity Plot, Vermillion Bay, Mean Stream Flow Period
Existing
A2
B2
A1
B1
salinity (ppt)
4.0
3.5
3.0
2.5
2.0
1.5
1.0
0.5
0.0
48 72 96 120 144 168 192 216 240 264 288 312 336 360 384 408 432 456 480 504 528 552 576 600 624 648 672 696 720
time (hrs)

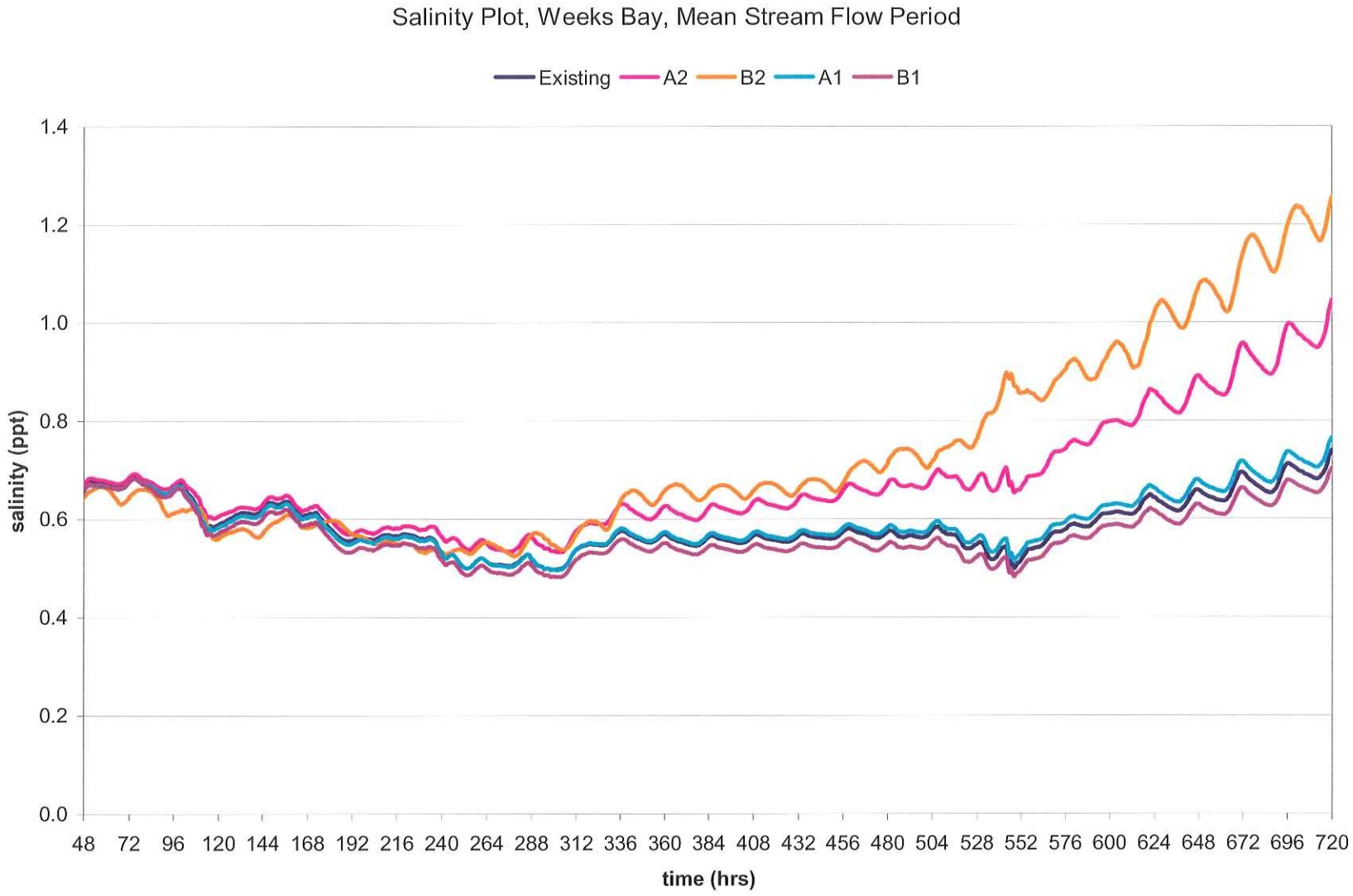
Salinity Plot, Weeks Bay, Mean Stream Flow Period
Existing
A2
B2
A1
B1
salinity (ppt)
1.4
1.2
1.0
0.8
0.6
0.4
0.2
0.0
48 72 96 120 144 168 192 216 240 264 288 312 336 360 384 408 432 456 480 504 528 552 576 600 624 648 672 696 720
time (hrs)

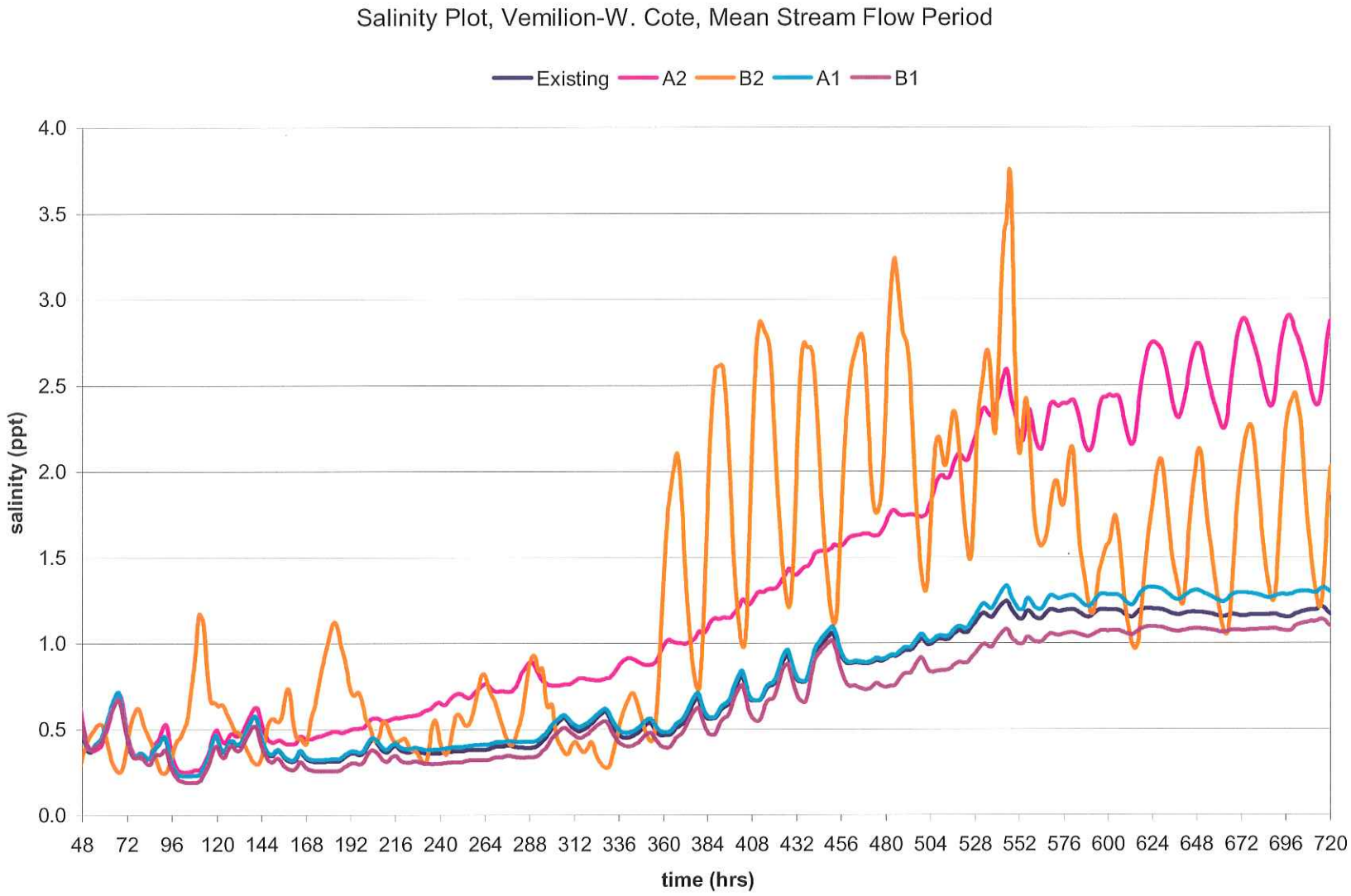
Salinity Plot, Vemilion-W. Cote, Mean Stream Flow Period
Existing
A2
B2
A1
B1
salinity (ppt)
4.0
3.5
3.0
2.5
2.0
1.5
1.0
0.5
0.0
48 72 96 120 144 168 192 216 240 264 288 312 336 360 384 408 432 456 480 504 528 552 576 600 624 648 672 696 720
time (hrs)

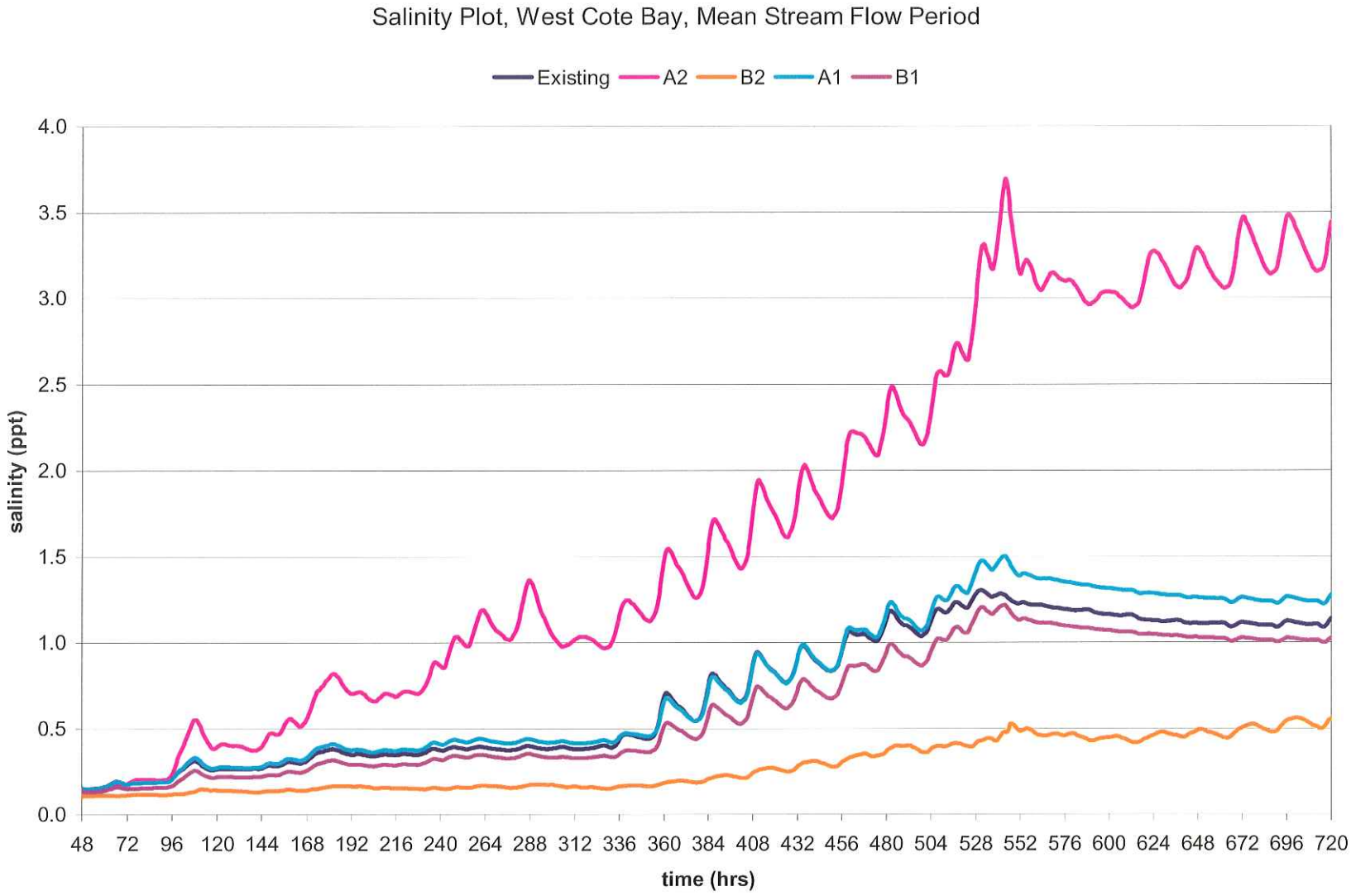
Salinity Plot, West Cote Bay, Mean Stream Flow Period
Existing
A2
B2
A1
B1
salinity (ppt)
4.0
3.5
3.0
2.5
2.0
1.5
1.0
0.5
0.0
48 72 96 120 144 168 192 216 240 264 288 312 336 360 384 408 432 456 480 504 528 552 576 600 624 648 672 696 720
time (hrs)

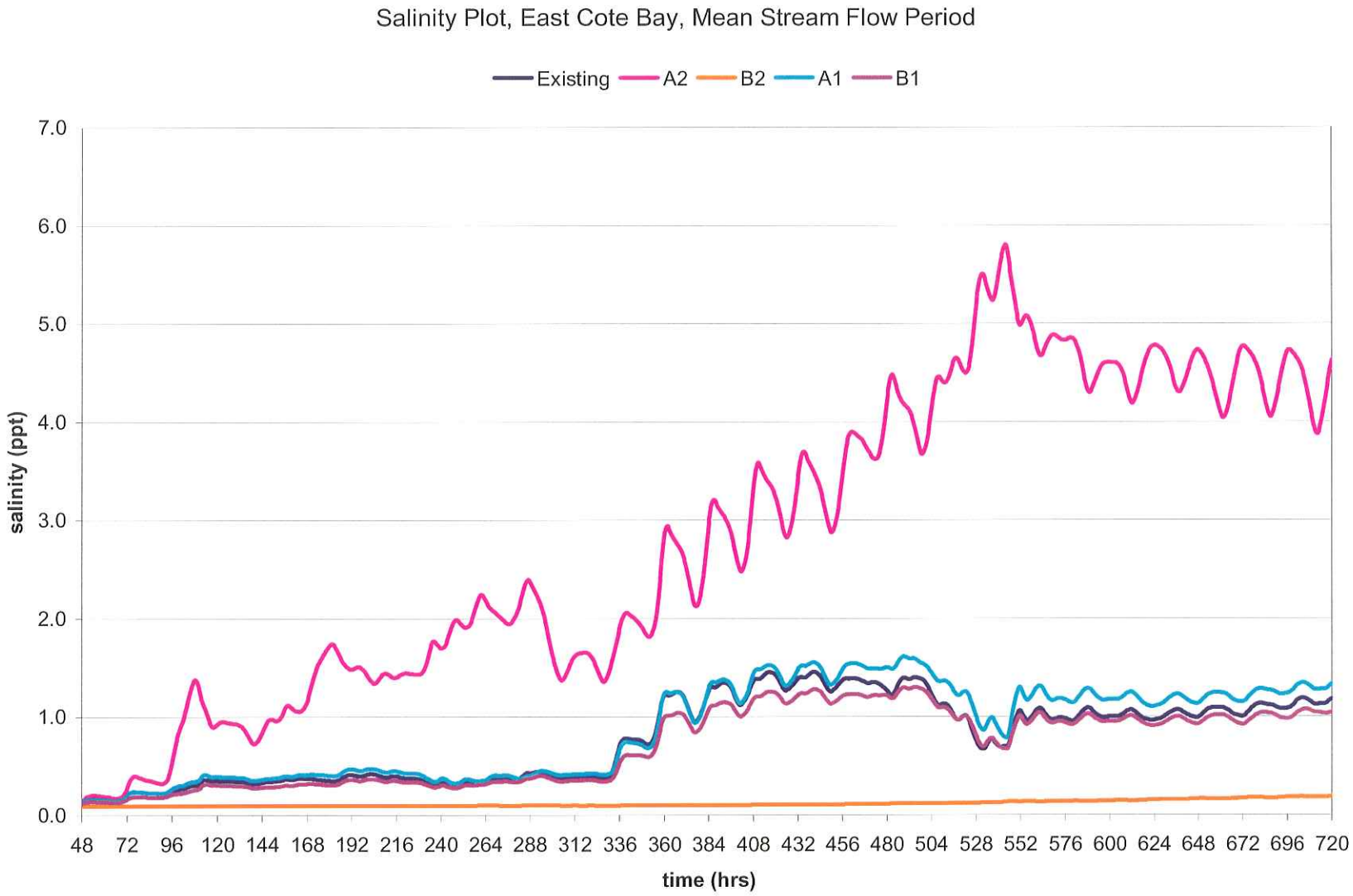
Salinity Plot, East Cote Bay, Mean Stream Flow Period
Existing
A2
B2
A1
B1
7.0
6.0
5.0
4.0
3.0
2.0
1.0
0.0
salinity (ppt)
48 72 96 120 144 168 192 216 240 264 288 312 336 360 384 408 432 456 480 504 528 552 576 600 624 648 672 696 720
time (hrs)

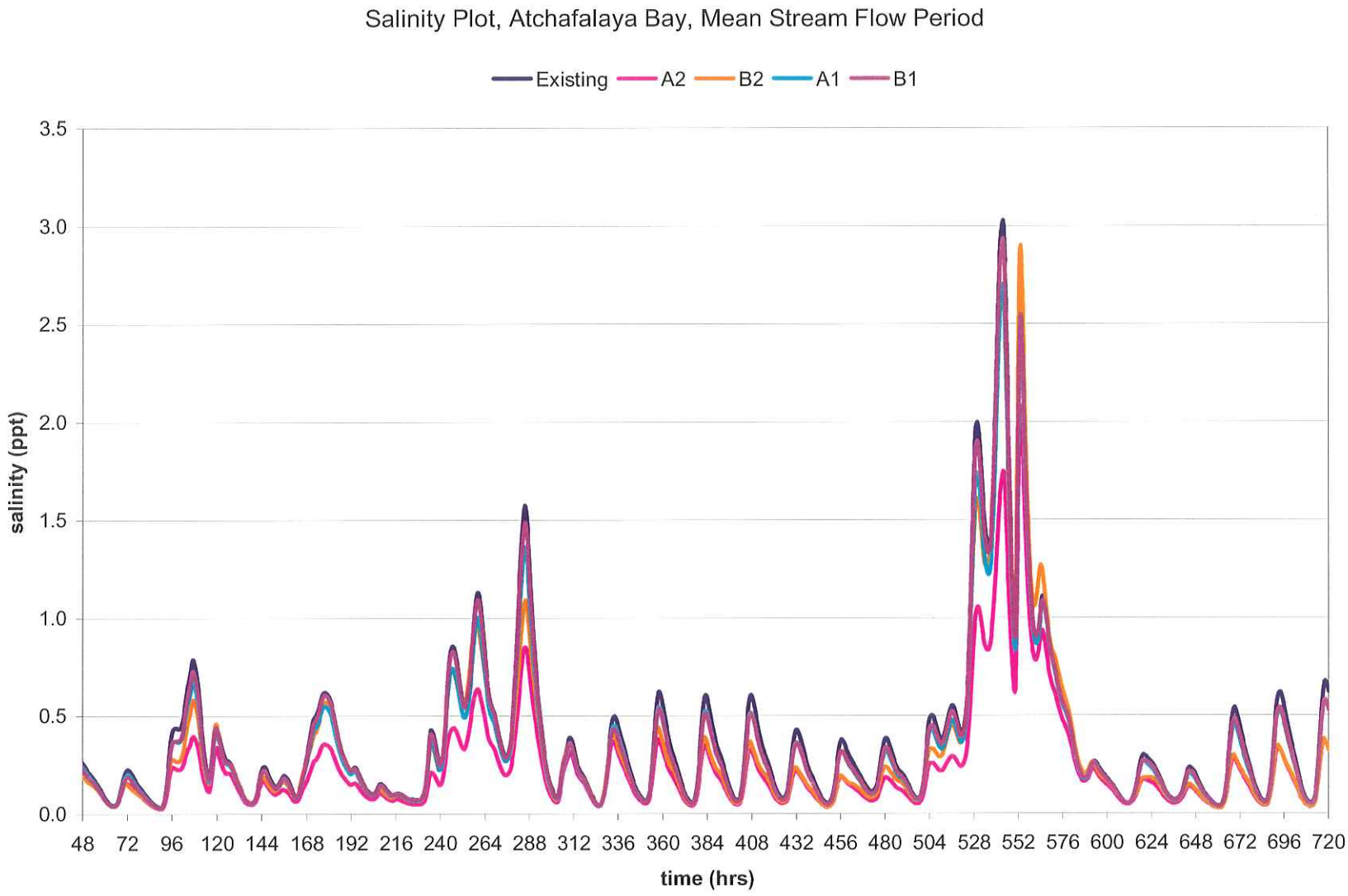
Salinity Plot, Atchafalaya Bay, Mean Stream Flow Period
Existing
A2
B2
A1
B1
salinity (ppt)
3.5
3.0
2.5
2.0
1.5
1.0
0.5
0.0
48 72 96 120 144 168 192 216 240 264 288 312 336 360 384 408 432 456 480 504 528 552 576 600 624 648 672 696 720
time (hrs)

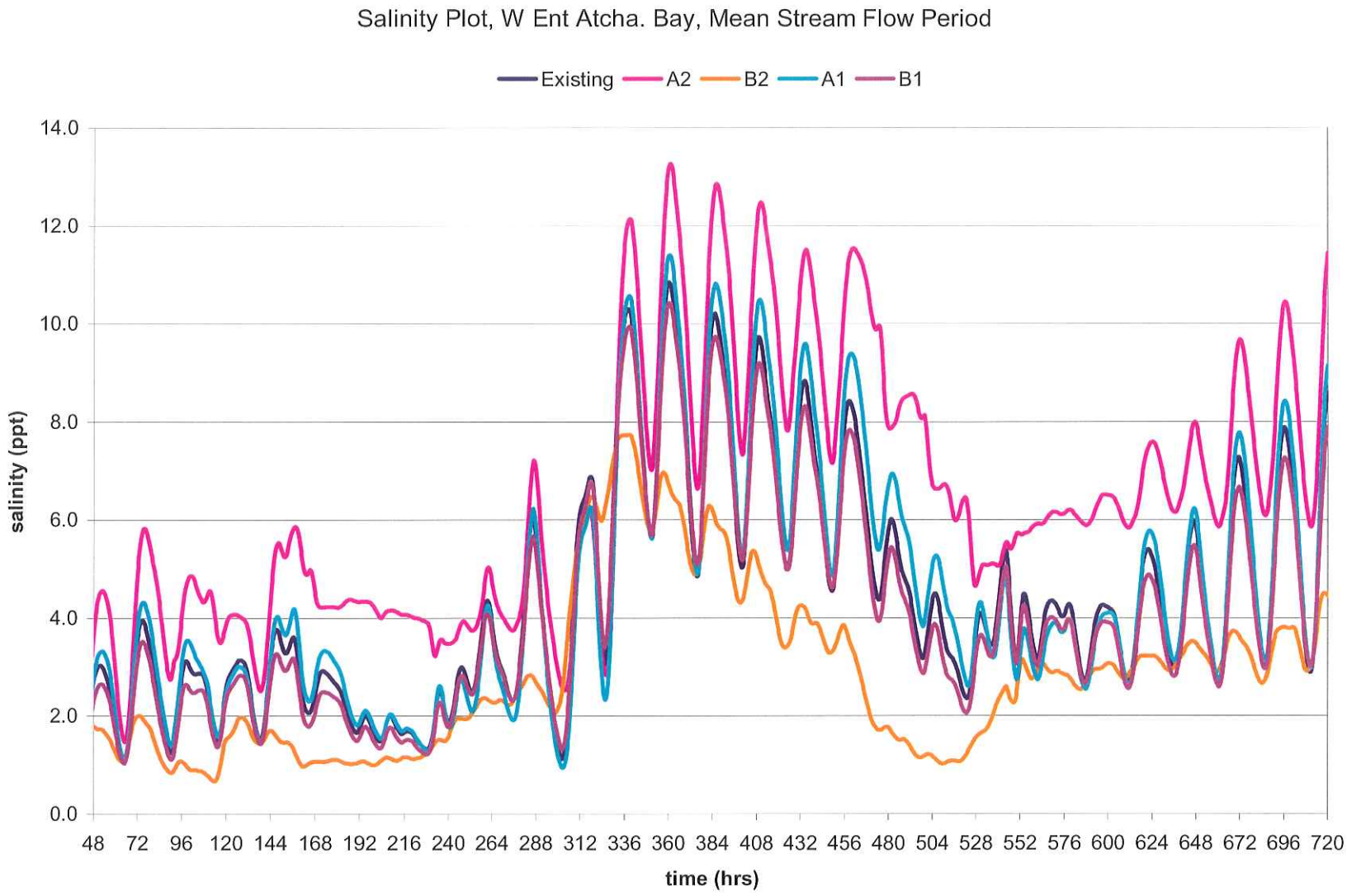
Salinity Plot, W Ent Atcha. Bay, Mean Stream Flow Period
Existing
A2
B2
A1
B1
14.0
12.0
10.0
8.0
6.0
4.0
2.0
0.0
salinity (ppt)
48 72 96 120 144 168 192 216 240 264 288 312 336 360 384 408 432 456 480 504 528 552 576 600 624 648 672 696 720
time (hrs)

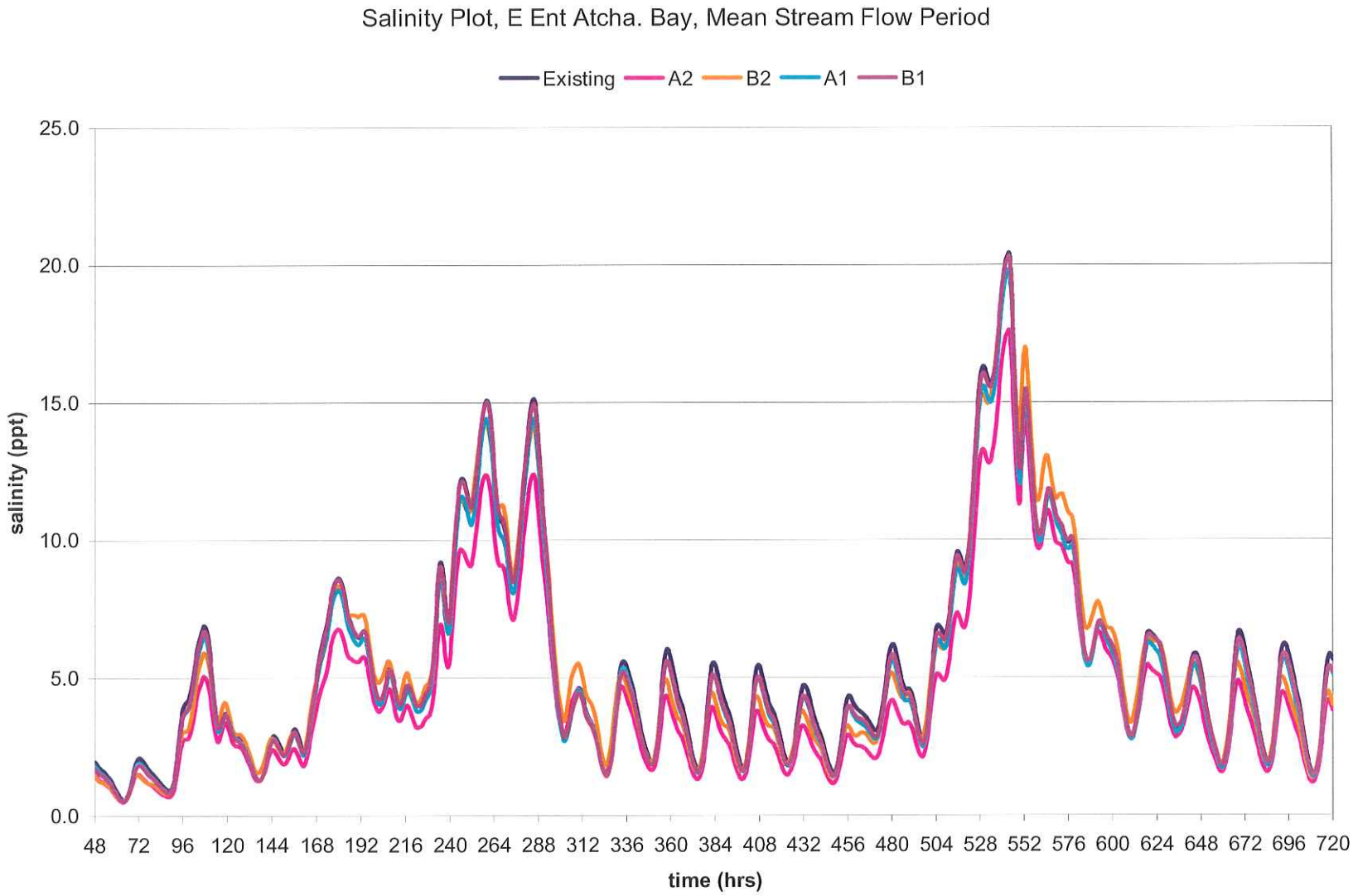
Salinity Plot, E Ent Atcha. Bay, Mean Stream Flow Period
Existing
A2
B2
A1
B1
25.0
20.0
15.0
10.0
5.0
0.0
salinity (ppt)
48 72 96 120 144 168 192 216 240 264 288 312 336 360 384 408 432 456 480 504 528 552 576 600 624 648 672 696 720
time (hrs)

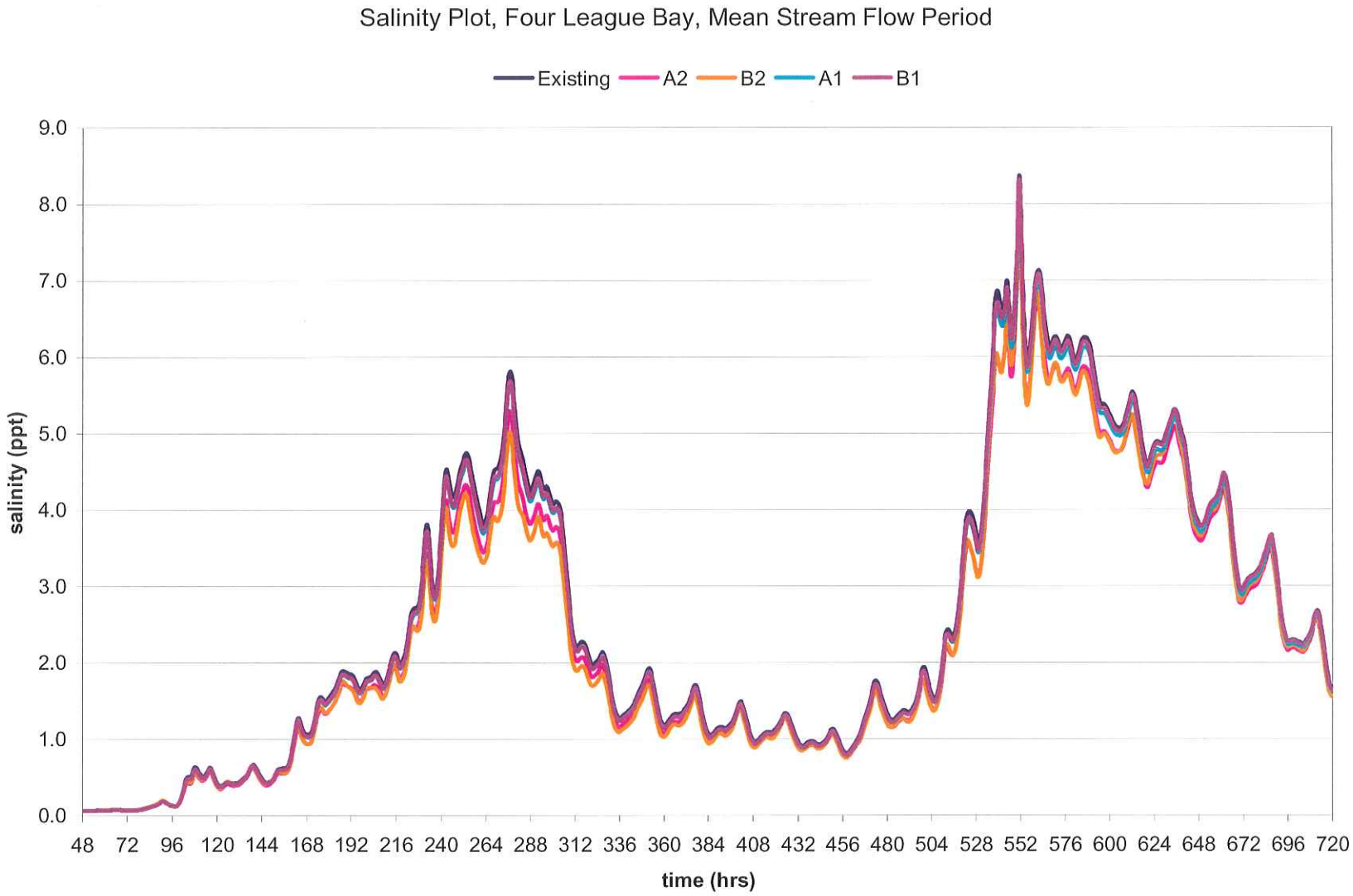
Salinity Plot, Four League Bay, Mean Stream Flow Period
Existing
A2
B2
A1
B1
9.0
8.0
7.0
6.0
5.0
4.0
3.0
2.0
1.0
0.0
salinity (ppt)
48 72 96 120 144 168 192 216 240 264 288 312 336 360 384 408 432 456 480 504 528 552 576 600 624 648 672 696 720
time (hrs)

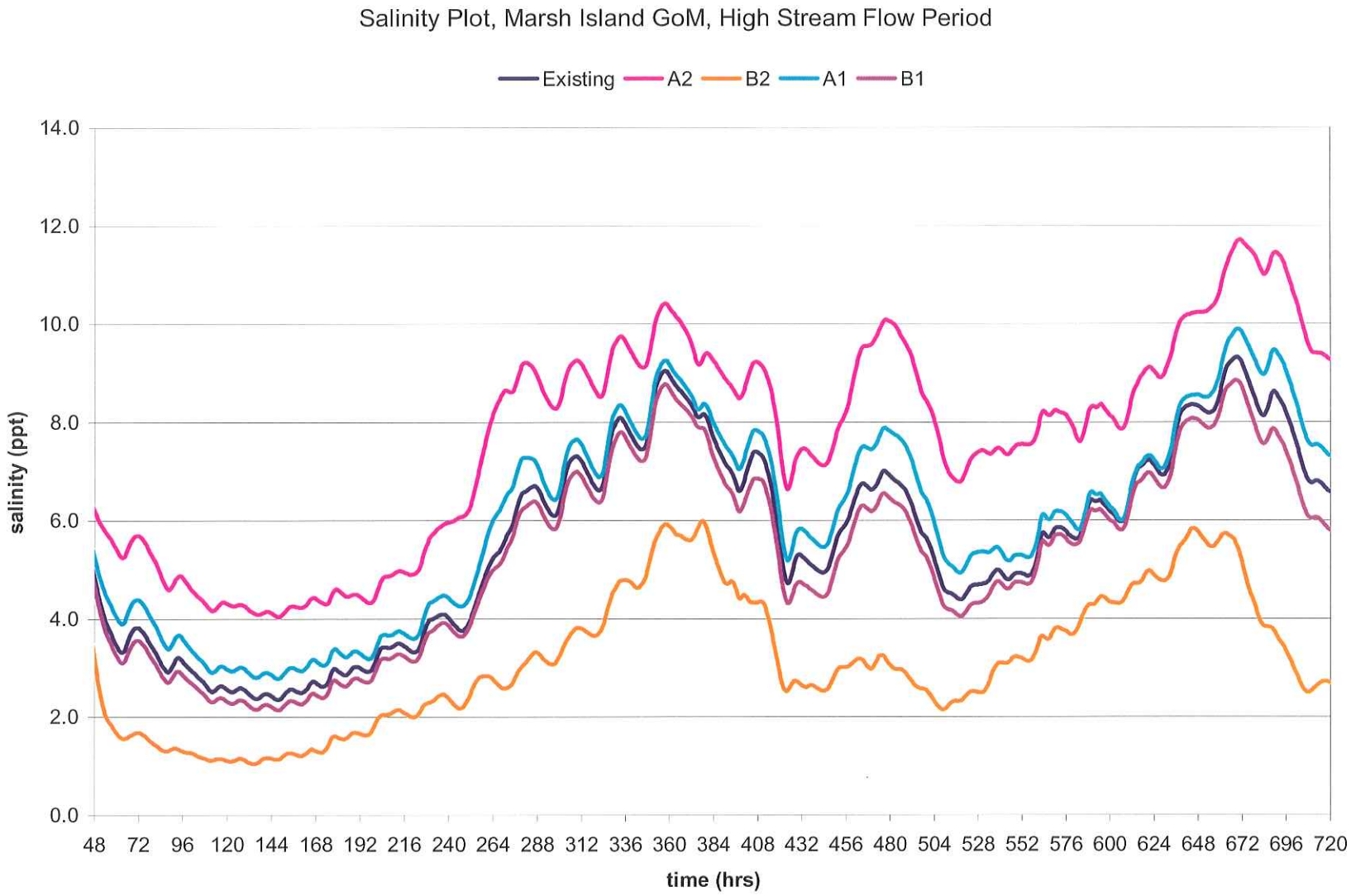
Salinity Plot, Marsh Island GoM, High Stream Flow Period
Existing
A2
B2
A1
B1
14.0
12.0
10.0
8.0
6.0
4.0
2.0
0.0
salinity (ppt)
48 72 96 120 144 168 192 216 240 264 288 312 336 360 384 408 432 456 480 504 528 552 576 600 624 648 672 696 720
time (hrs)

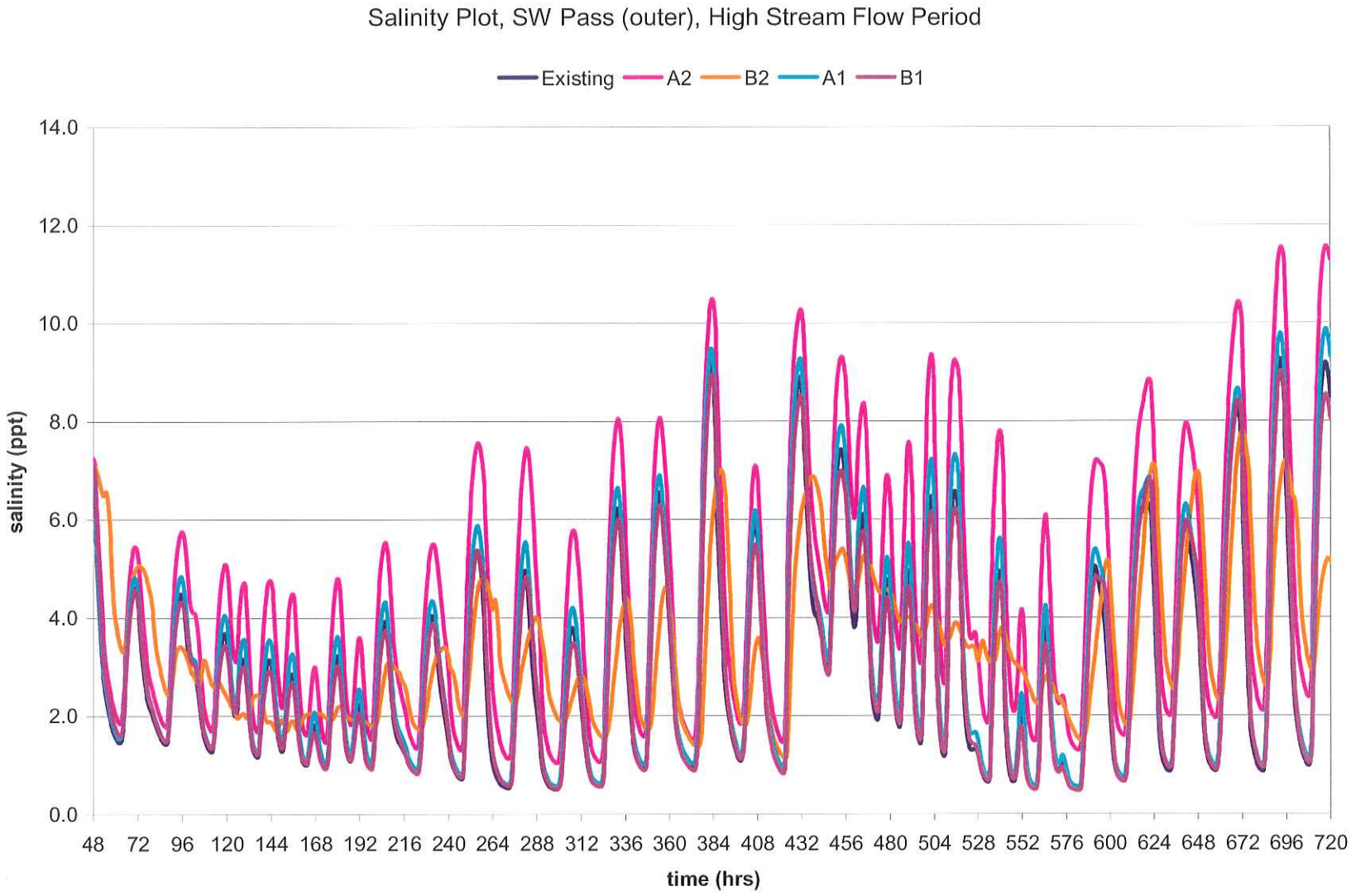
Salinity Plot, SW Pass (outer), High Stream Flow Period
Existing
A2
B2
A1
B1
14.0
12.0
10.0
8.0
6.0
4.0
2.0
0.0
salinity (ppt)
48 72 96 120 144 168 192 216 240 264 288 312 336 360 384 408 432 456 480 504 528 552 576 600 624 648 672 696 720
time (hrs)

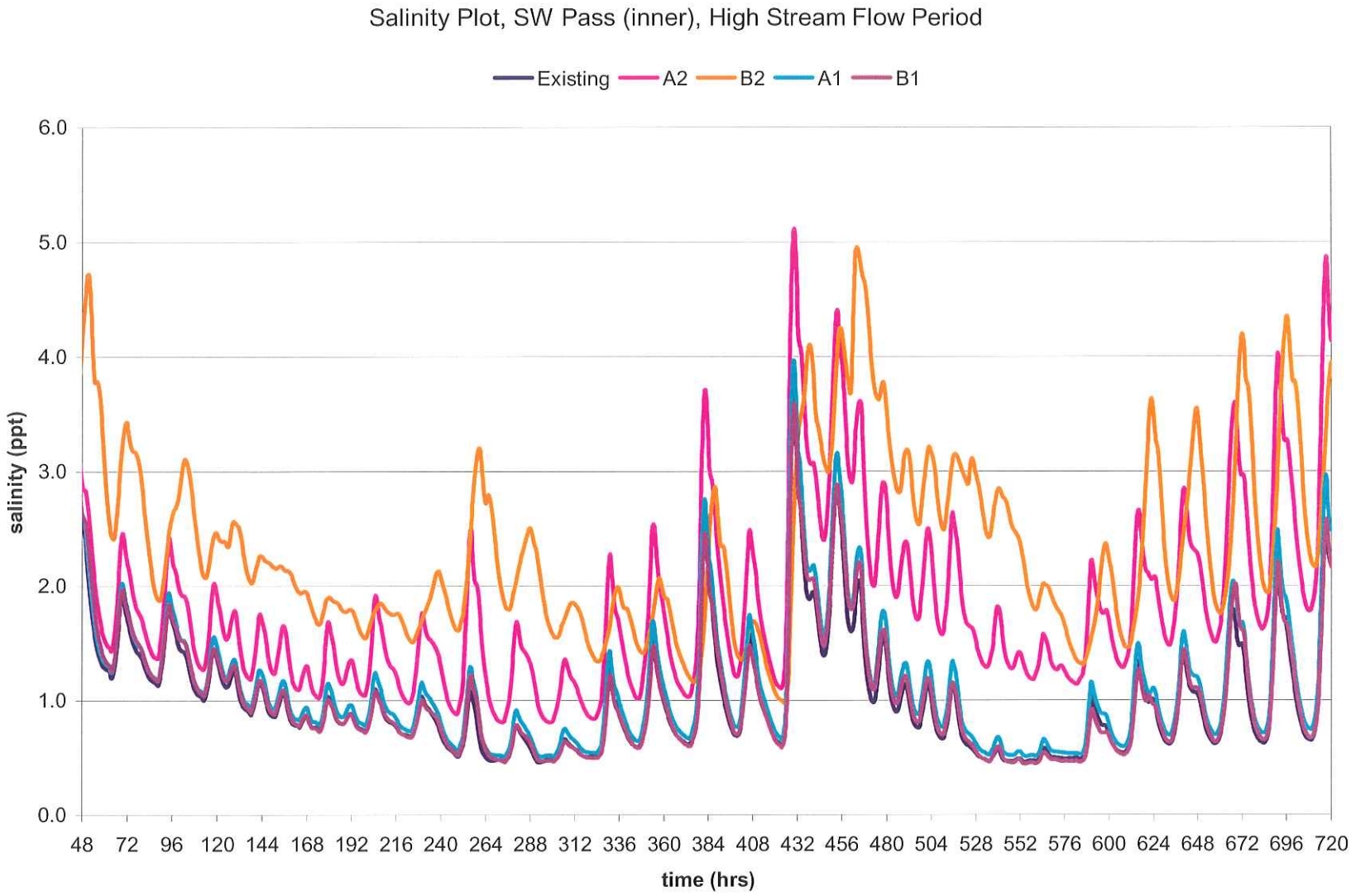
Salinity Plot, SW Pass (inner), High Stream Flow Period
Existing
A2
B2
A1
B1
6.0
5.0
4.0
3.0
2.0
1.0
0.0
salinity (ppt)
48 72 96 120 144 168 192 216 240 264 288 312 336 360 384 408 432 456 480 504 528 552 576 600 624 648 672 696 720
time (hrs)

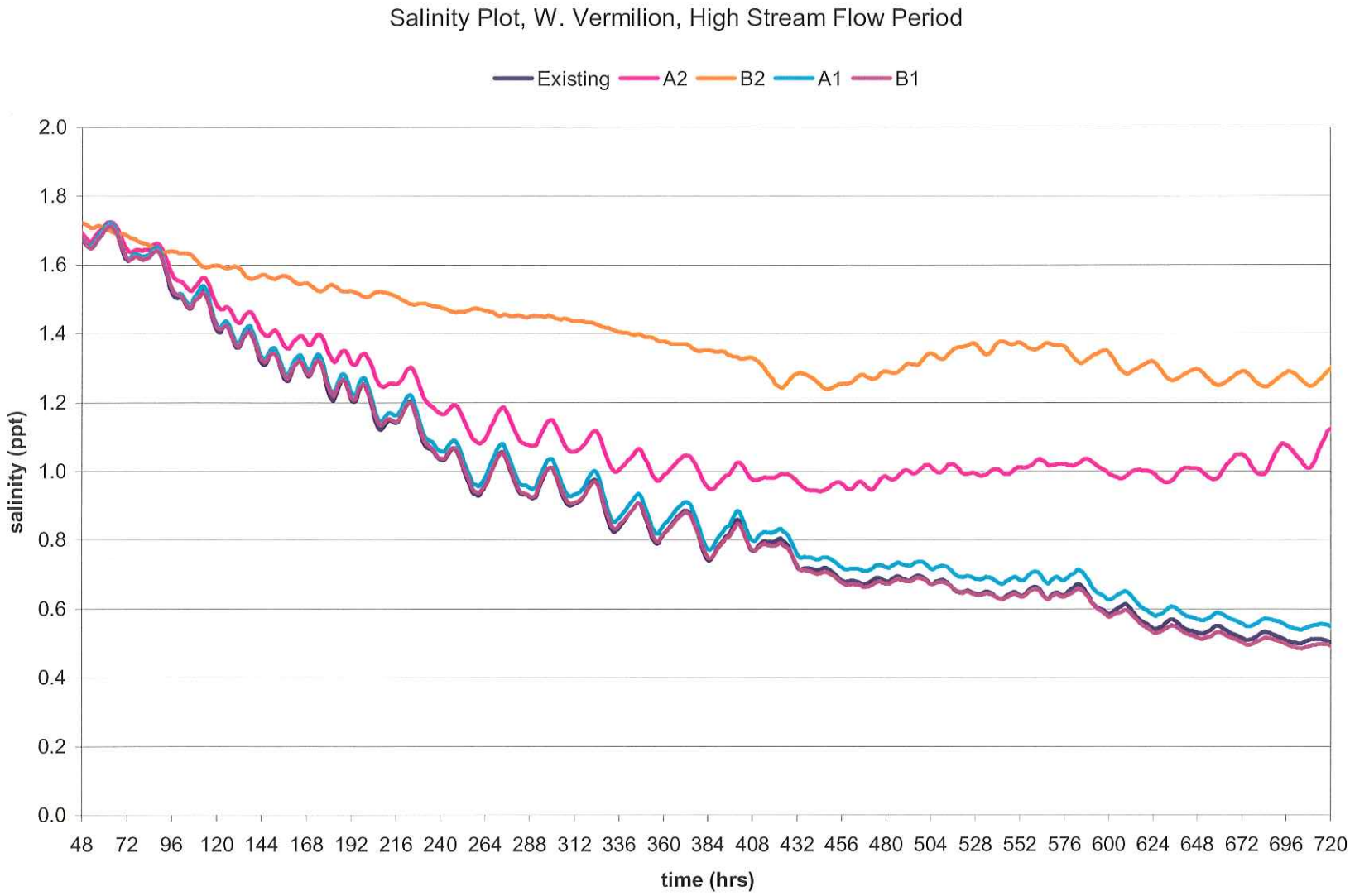
Salinity Plot, W. Vermilion, High Stream Flow Period
Existing
A2
B2
A1
B1
salinity (ppt)
2.0
1.8
1.6
1.4
1.2
1.0
0.8
0.6
0.4
0.2
0.0
48 72 96 120 144 168 192 216 240 264 288 312 336 360 384 408 432 456 480 504 528 552 576 600 624 648 672 696 720
time (hrs)

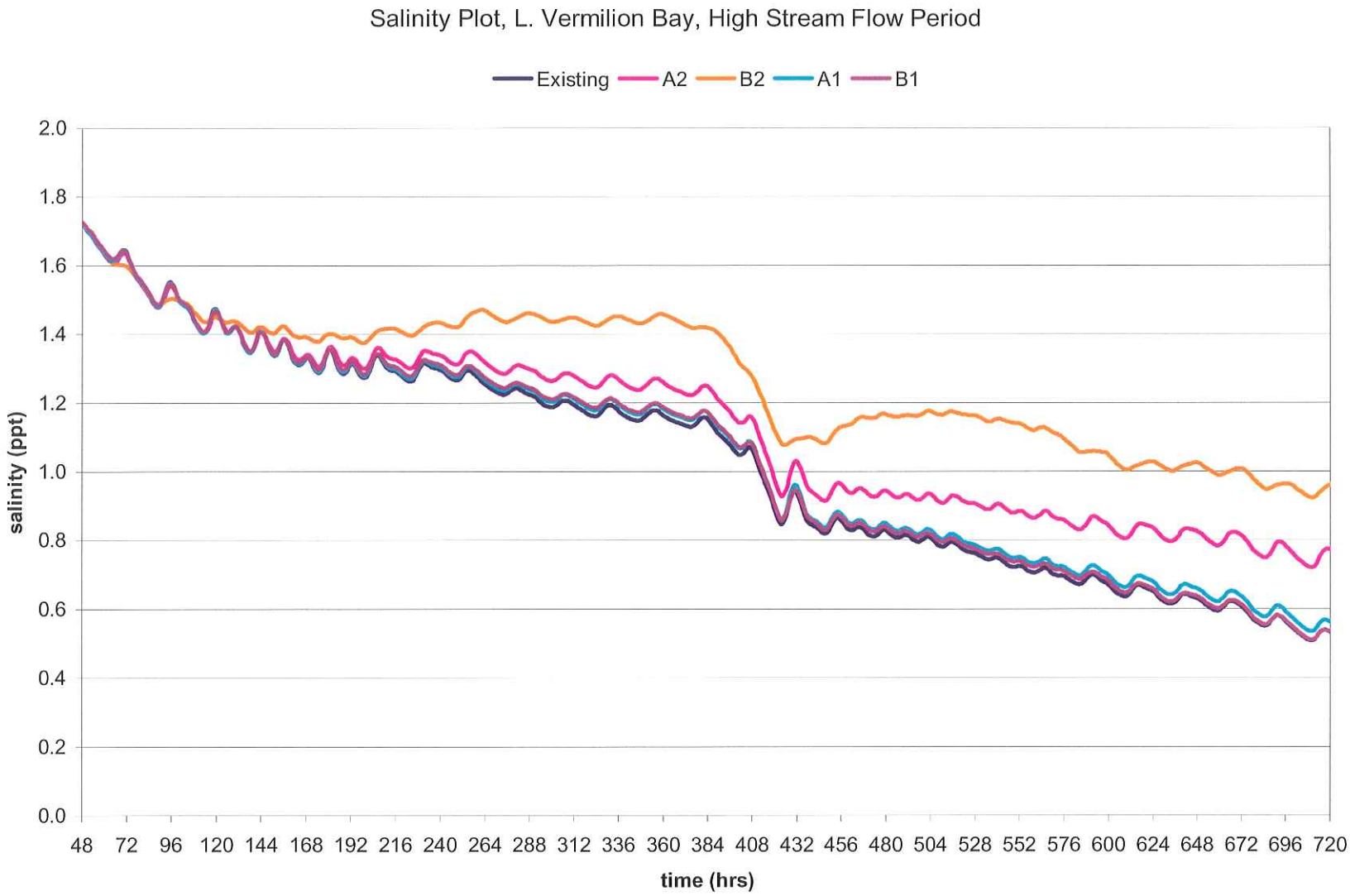
Salinity Plot, L. Vermilion Bay, High Stream Flow Period
Existing
A2
B2
A1
B1
salinity (ppt)
2.0
1.8
1.6
1.4
1.2
1.0
0.8
0.6
0.4
0.2
0.0
48 72 96 120 144 168 192 216 240 264 288 312 336 360 384 408 432 456 480 504 528 552 576 600 624 648 672 696 720
time (hrs)

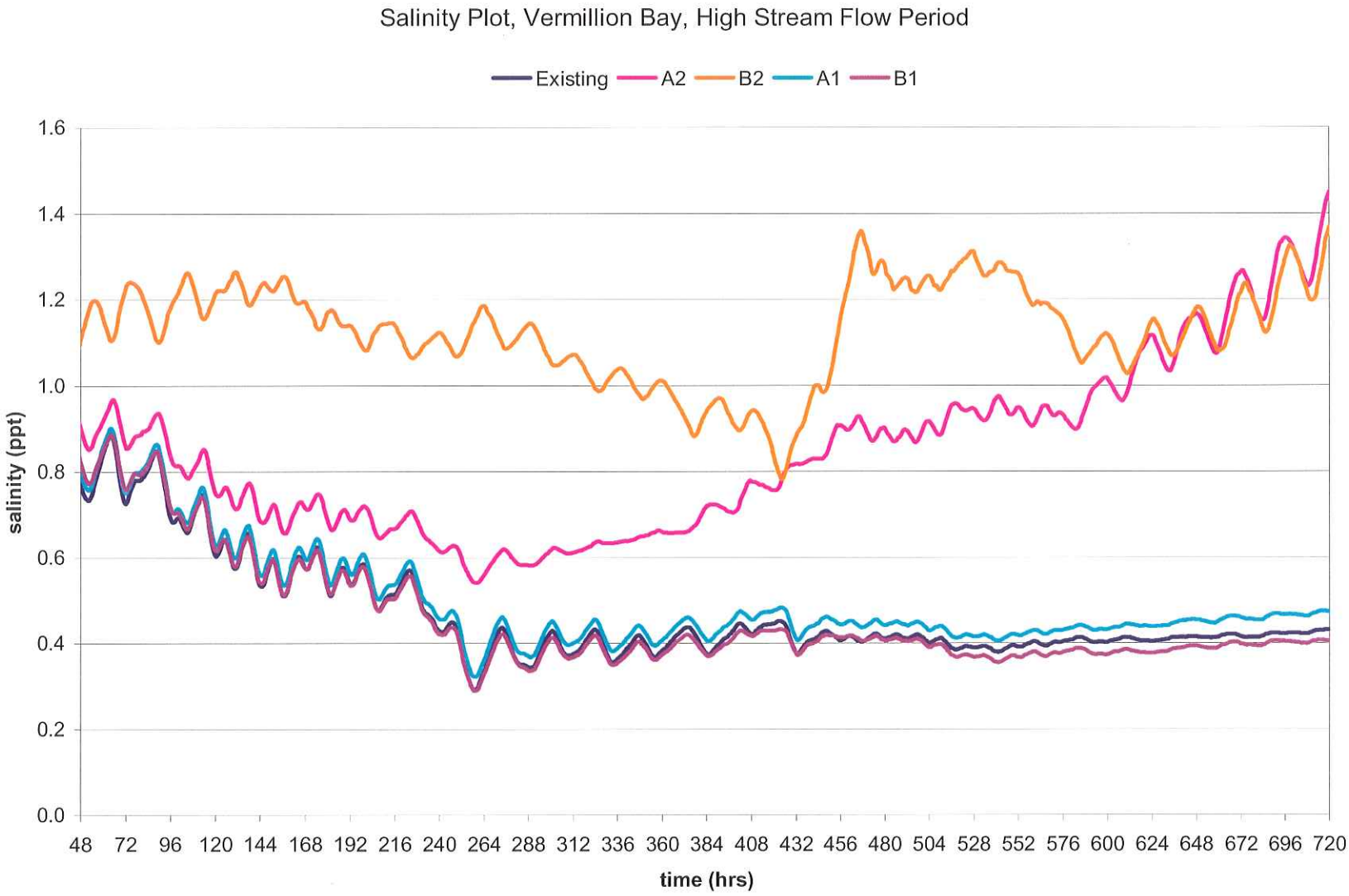
Salinity Plot, Vermillion Bay, High Stream Flow Period
Existing
A2
B2
A1
B1
salinity (ppt)
1.6
1.4
1.2
1.0
0.8
0.6
0.4
0.2
0.0
48 72 96 120 144 168 192 216 240 264 288 312 336 360 384 408 432 456 480 504 528 552 576 600 624 648 672 696 720
time (hrs)

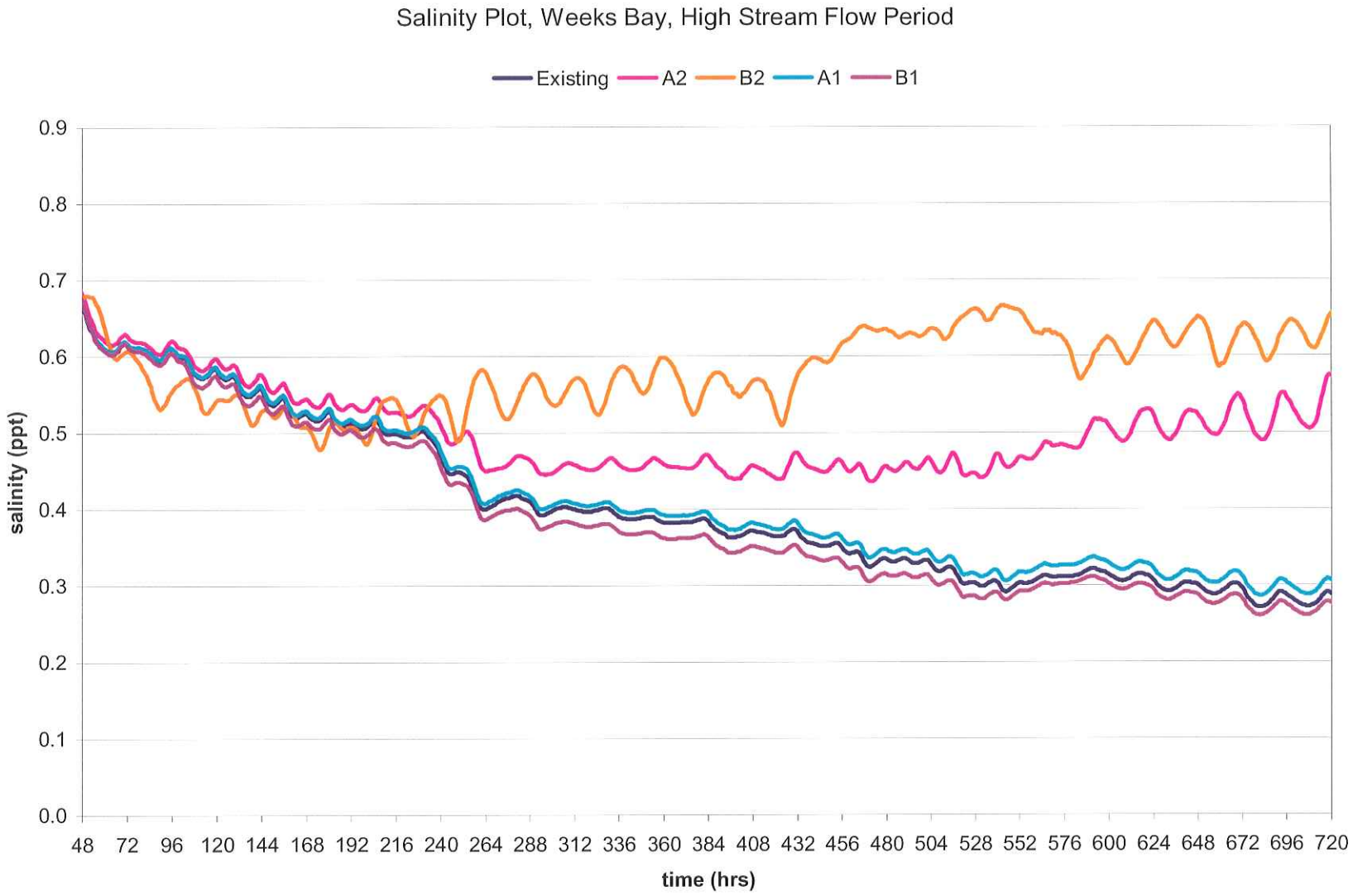
Salinity Plot, Weeks Bay, High Stream Flow Period
Existing
A2
B2
A1
B1
salinity (ppt)
0.0
0.1
0.2
0.3
0.4
0.5
0.6
0.7
0.8
0.9
48 72 96 120 144 168 192 216 240 264 288 312 336 360 384 408 432 456 480 504 528 552 576 600 624 648 672 696 720
time (hrs)

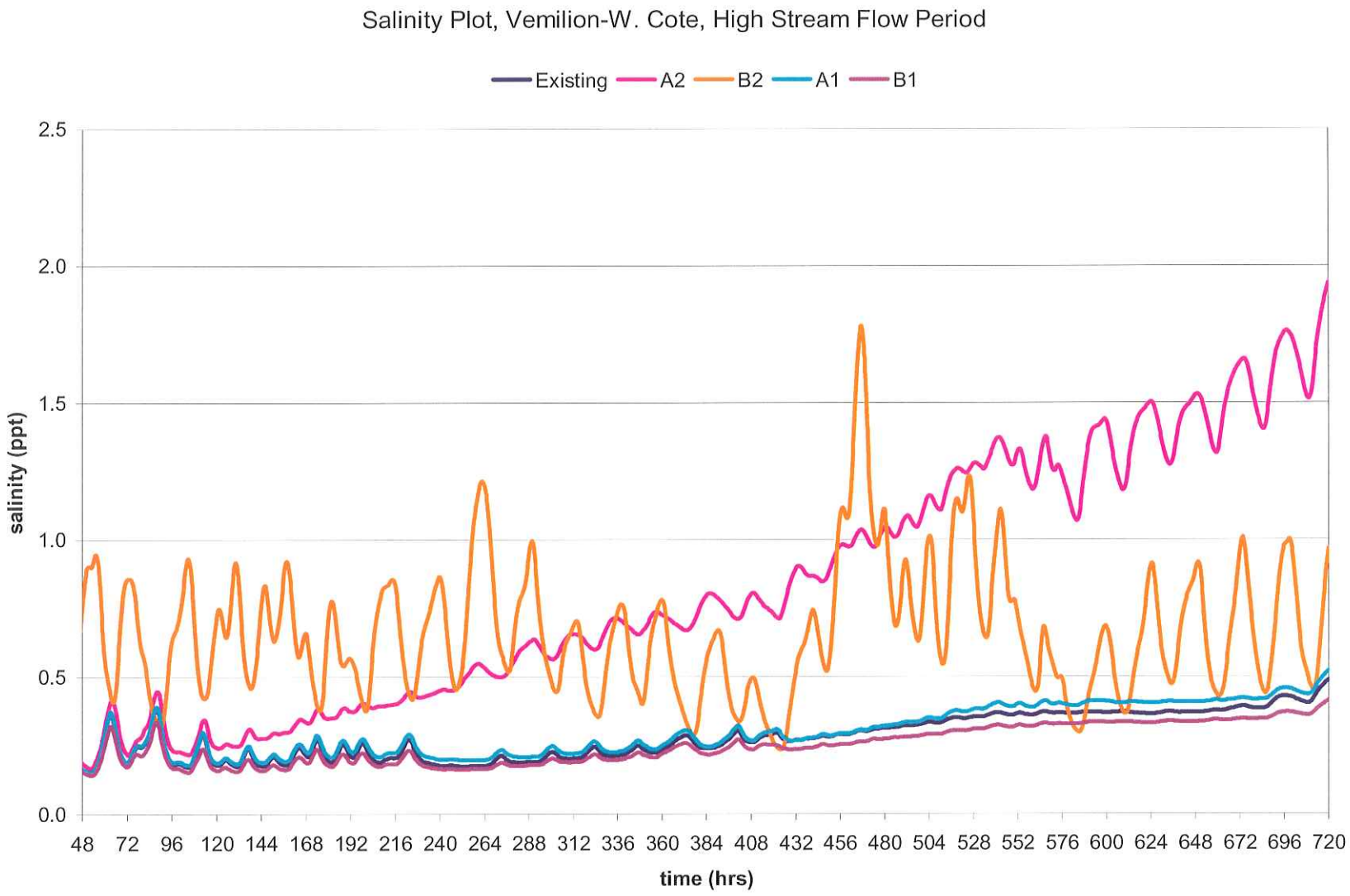
Salinity Plot, Vemilion-W. Cote, High Stream Flow Period
Existing
A2
B2
A1
B1
salinity (ppt)
2.5
2.0
1.5
1.0
0.5
0.0
48 72 96 120 144 168 192 216 240 264 288 312 336 360 384 408 432 456 480 504 528 552 576 600 624 648 672 696 720
time (hrs)

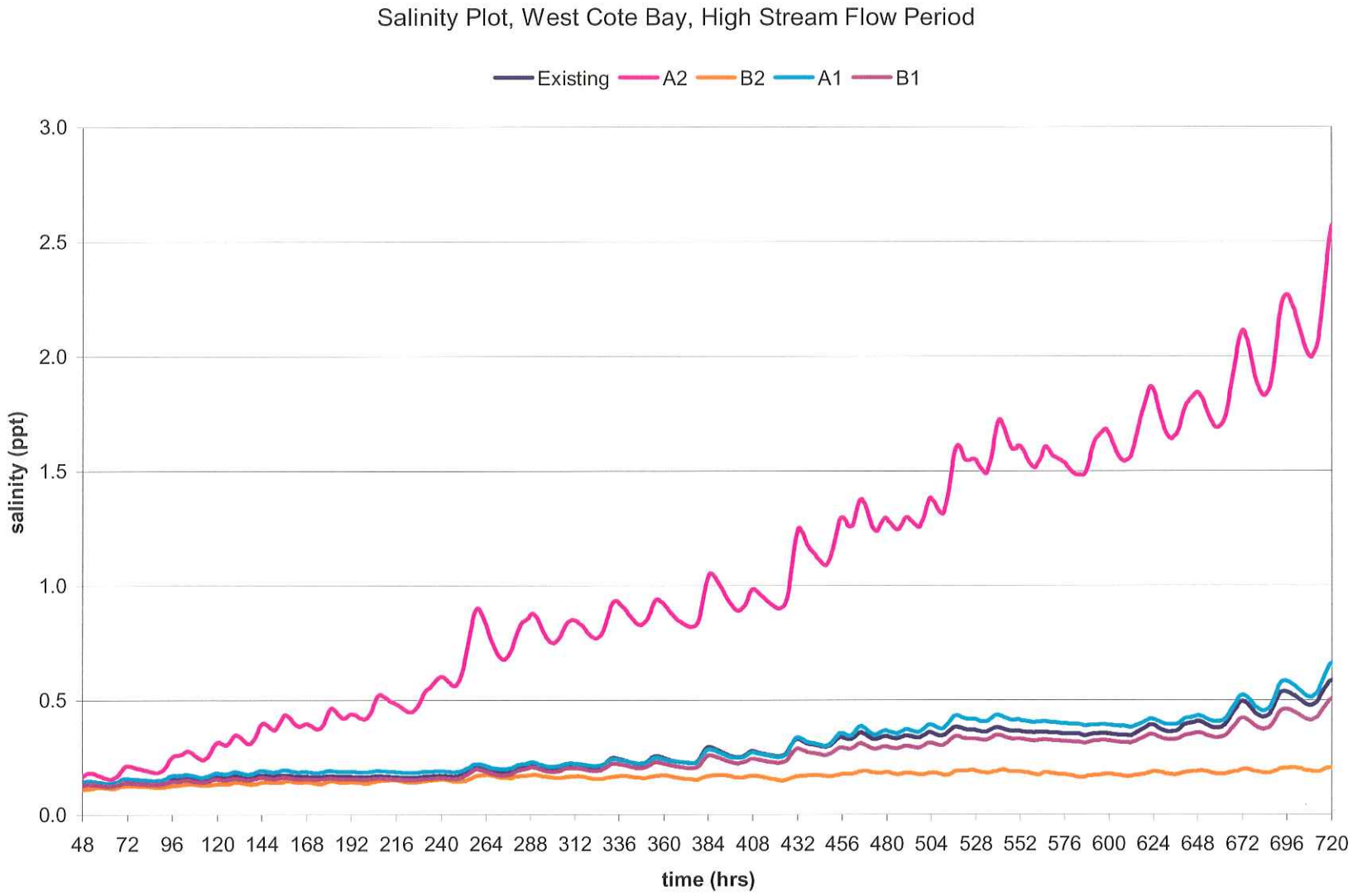
Salinity Plot, West Cote Bay, High Stream Flow Period
Existing
A2
B2
A1
B1
3.0
2.5
2.0
1.5
1.0
0.5
0.0
salinity (ppt)
48 72 96 120 144 168 192 216 240 264 288 312 336 360 384 408 432 456 480 504 528 552 576 600 624 648 672 696 720
time (hrs)

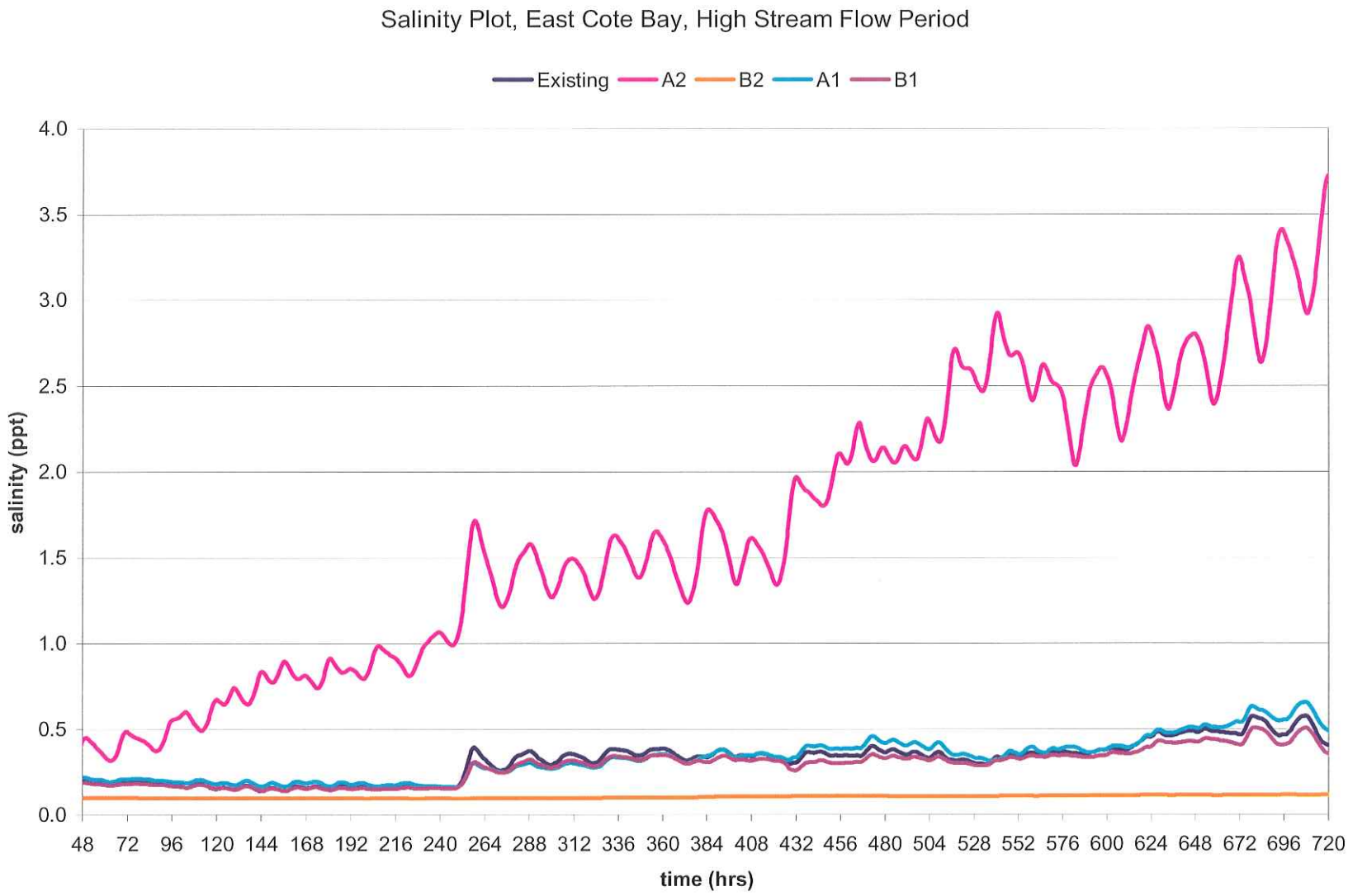
Salinity Plot, East Cote Bay, High Stream Flow Period
Existing
A2
B2
A1
B1
4.0
3.5
3.0
2.5
2.0
1.5
1.0
0.5
0.0
salinity (ppt)
48 72 96 120 144 168 192 216 240 264 288 312 336 360 384 408 432 456 480 504 528 552 576 600 624 648 672 696 720
time (hrs)

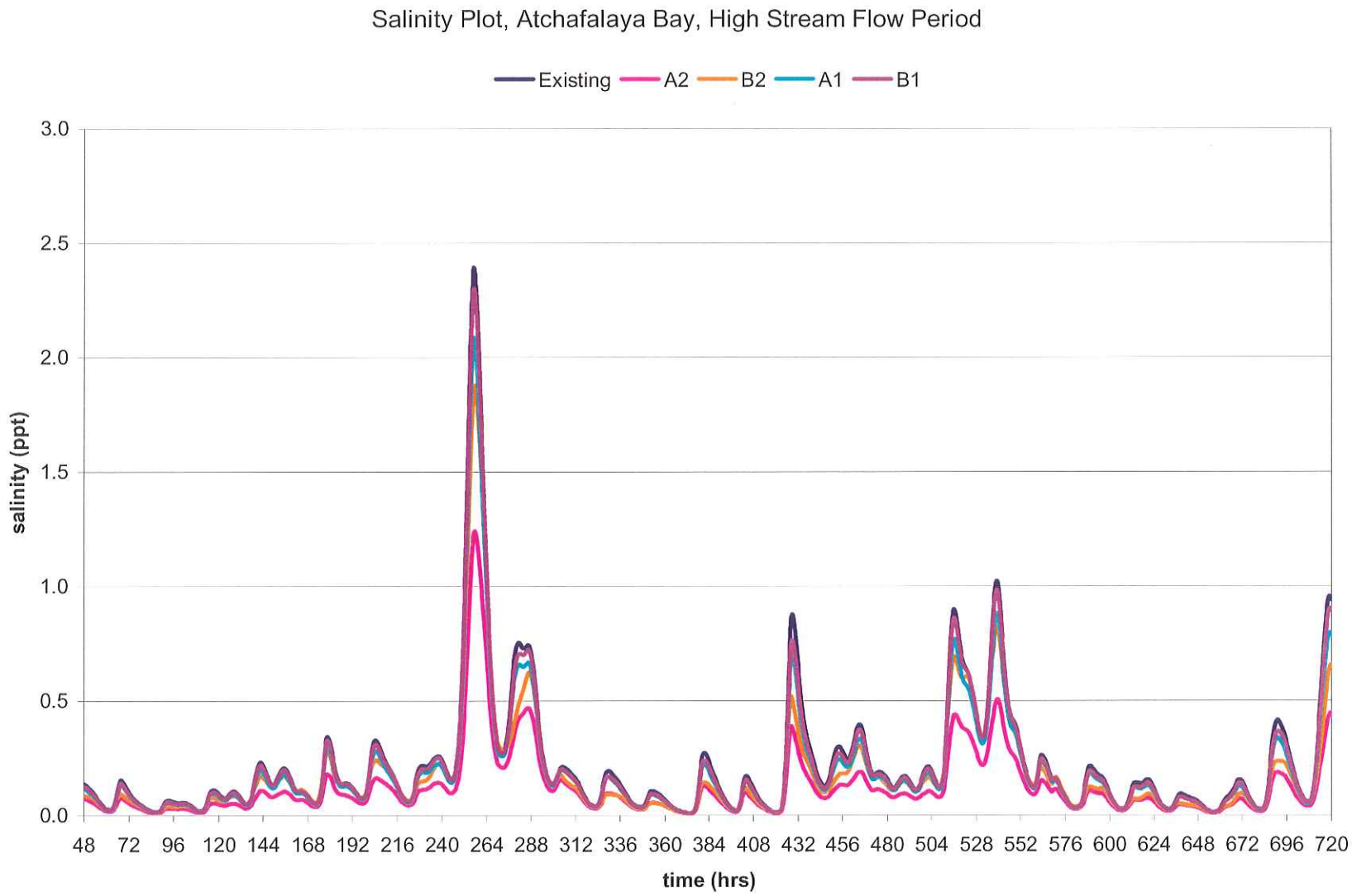
Salinity Plot, Atchafalaya Bay, High Stream Flow Period
Existing
A2
B2
A1
B1
3.0
2.5
2.0
1.5
1.0
0.5
0.0
salinity (ppt)
48 72 96 120 144 168 192 216 240 264 288 312 336 360 384 408 432 456 480 504 528 552 576 600 624 648 672 696 720
time (hrs)

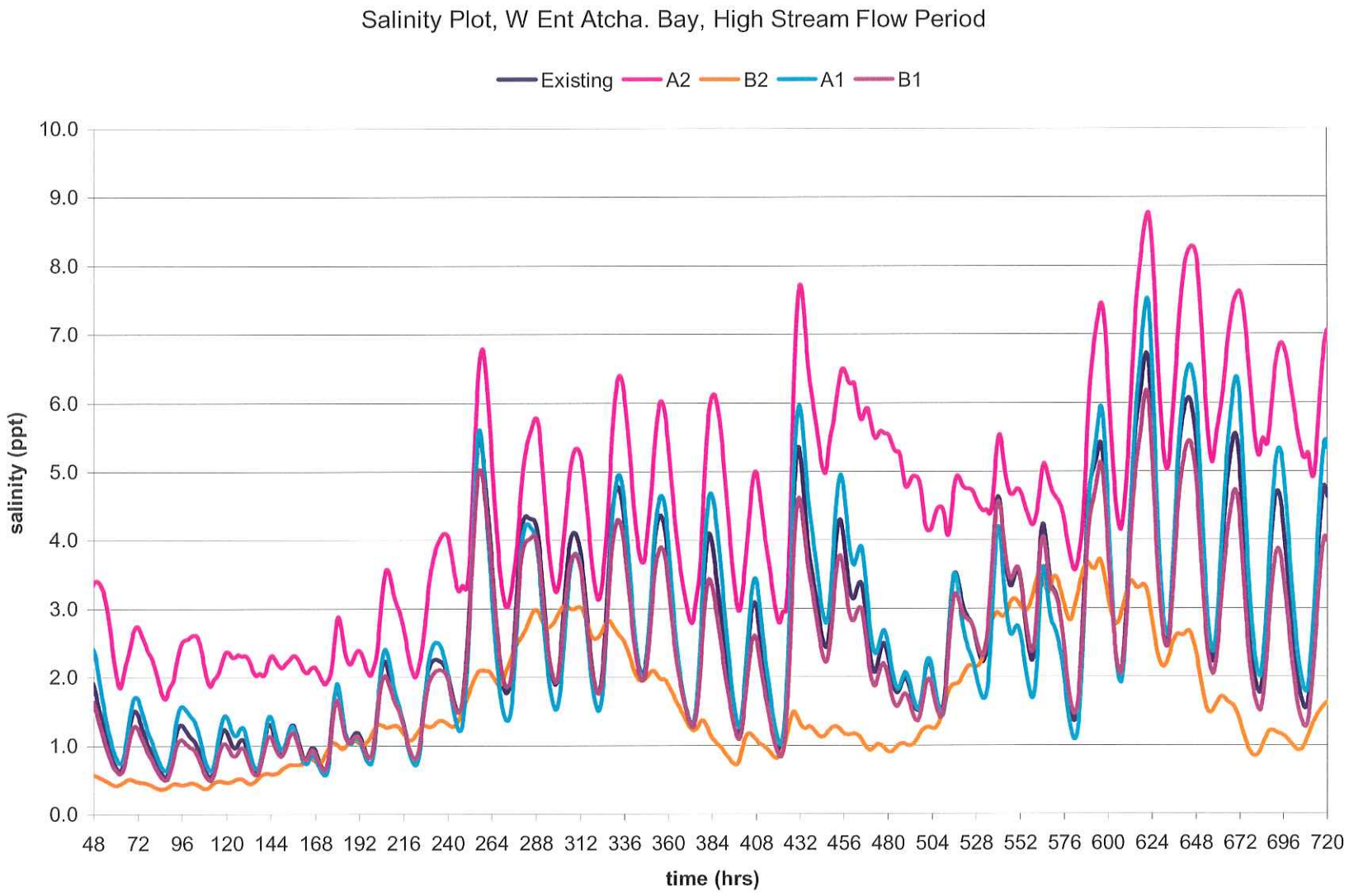
Salinity Plot, W Ent Atcha. Bay, High Stream Flow Period
Existing
A2
B2
A1
B1
10.0
9.0
8.0
7.0
6.0
5.0
4.0
3.0
2.0
1.0
0.0
salinity (ppt)
48 72 96 120 144 168 192 216 240 264 288 312 336 360 384 408 432 456 480 504 528 552 576 600 624 648 672 696 720
time (hrs)

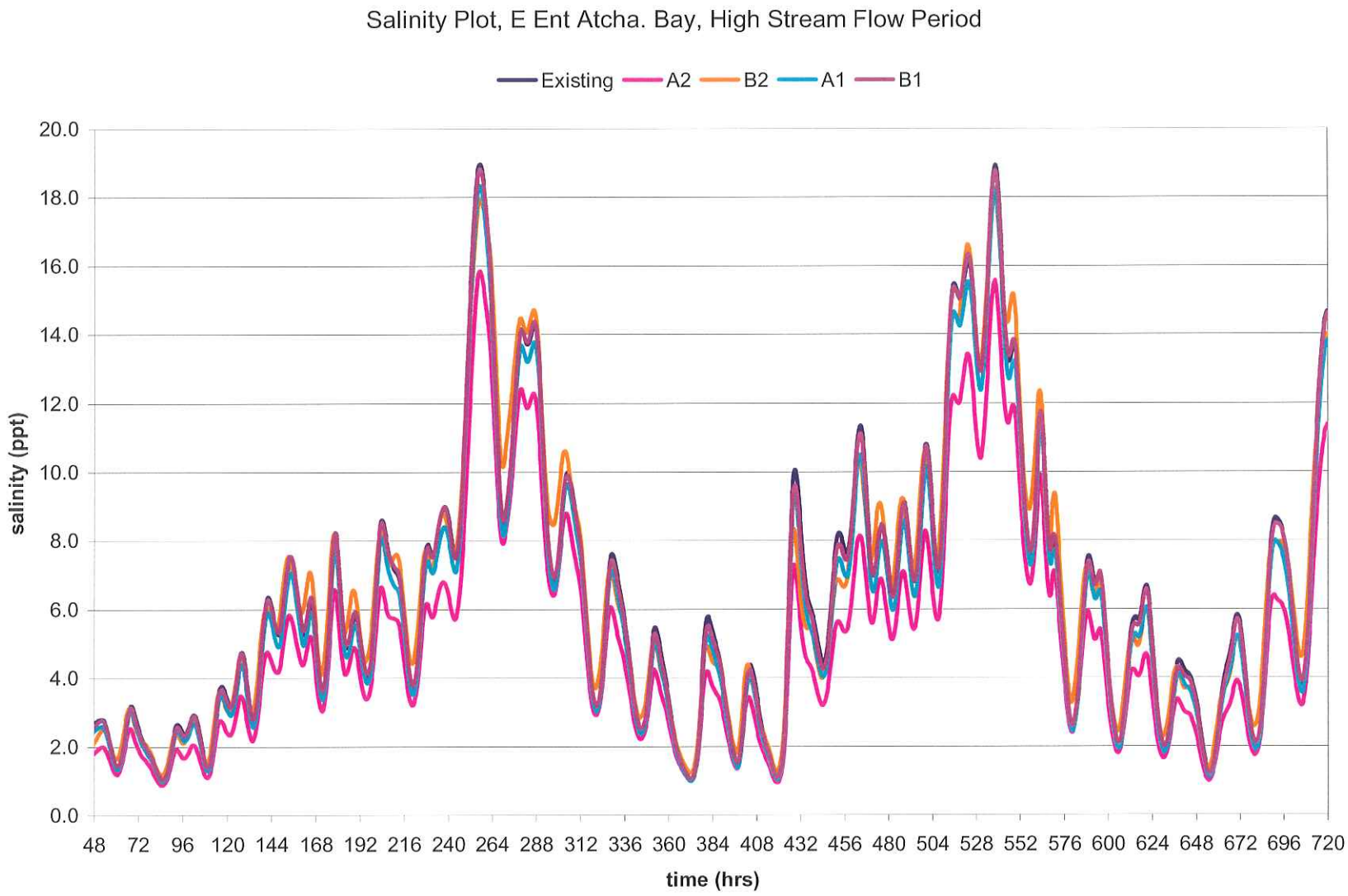
Salinity Plot, E Ent Atcha. Bay, High Stream Flow Period
Existing
A2
B2
A1
B1
salinity (ppt)
20.0
18.0
16.0
14.0
12.0
10.0
8.0
6.0
4.0
2.0
0.0
48 72 96 120 144 168 192 216 240 264 288 312 336 360 384 408 432 456 480 504 528 552 576 600 624 648 672 696 720
time (hrs)

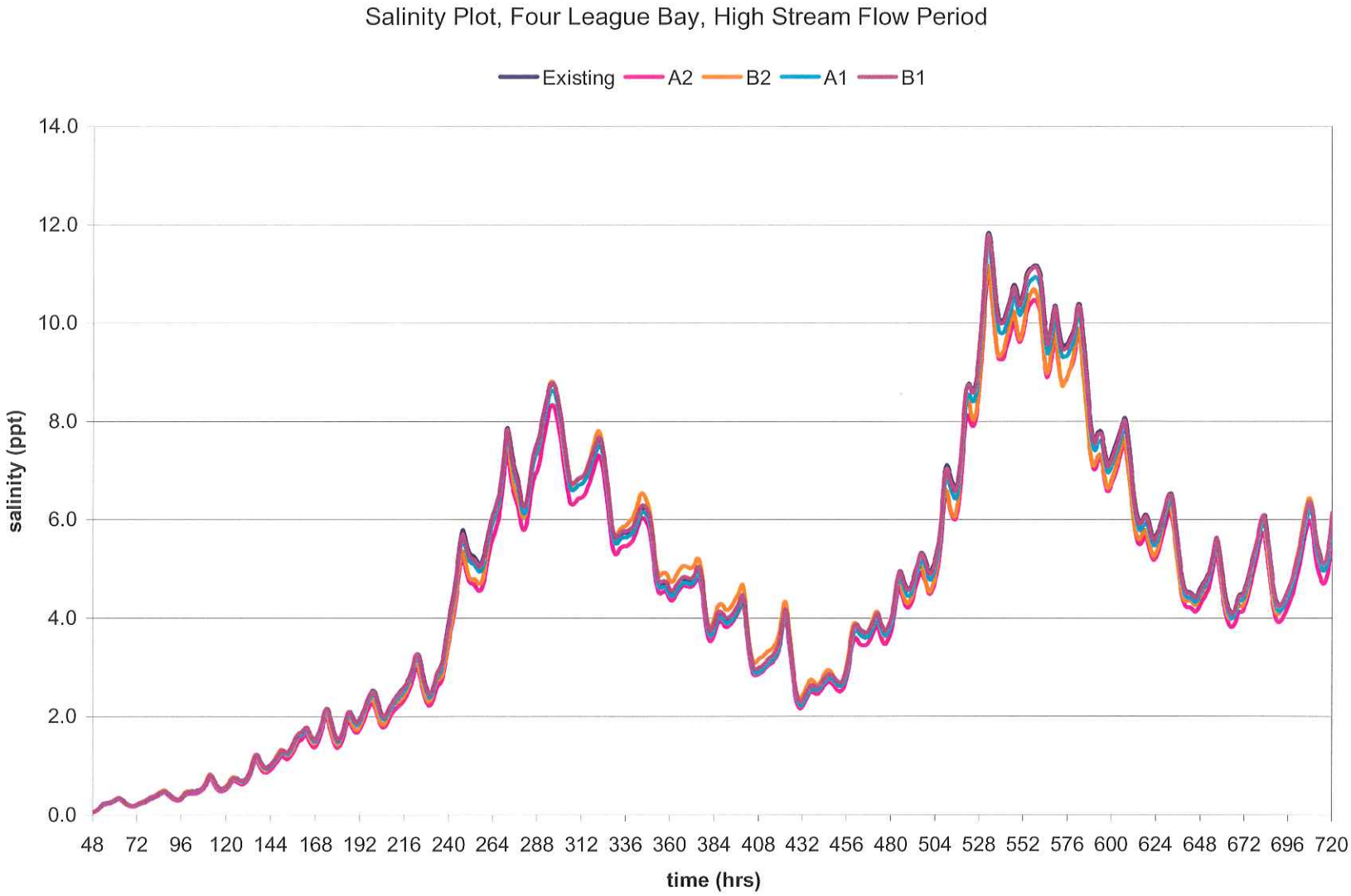
Salinity Plot, Four League Bay, High Stream Flow Period
Existing
A2
B2
A1
B1
14.0
12.0
10.0
8.0
6.0
4.0
2.0
0.0
salinity (ppt)
48 72 96 120 144 168 192 216 240 264 288 312 336 360 384 408 432 456 480 504 528 552 576 600 624 648 672 696 720
time (hrs)

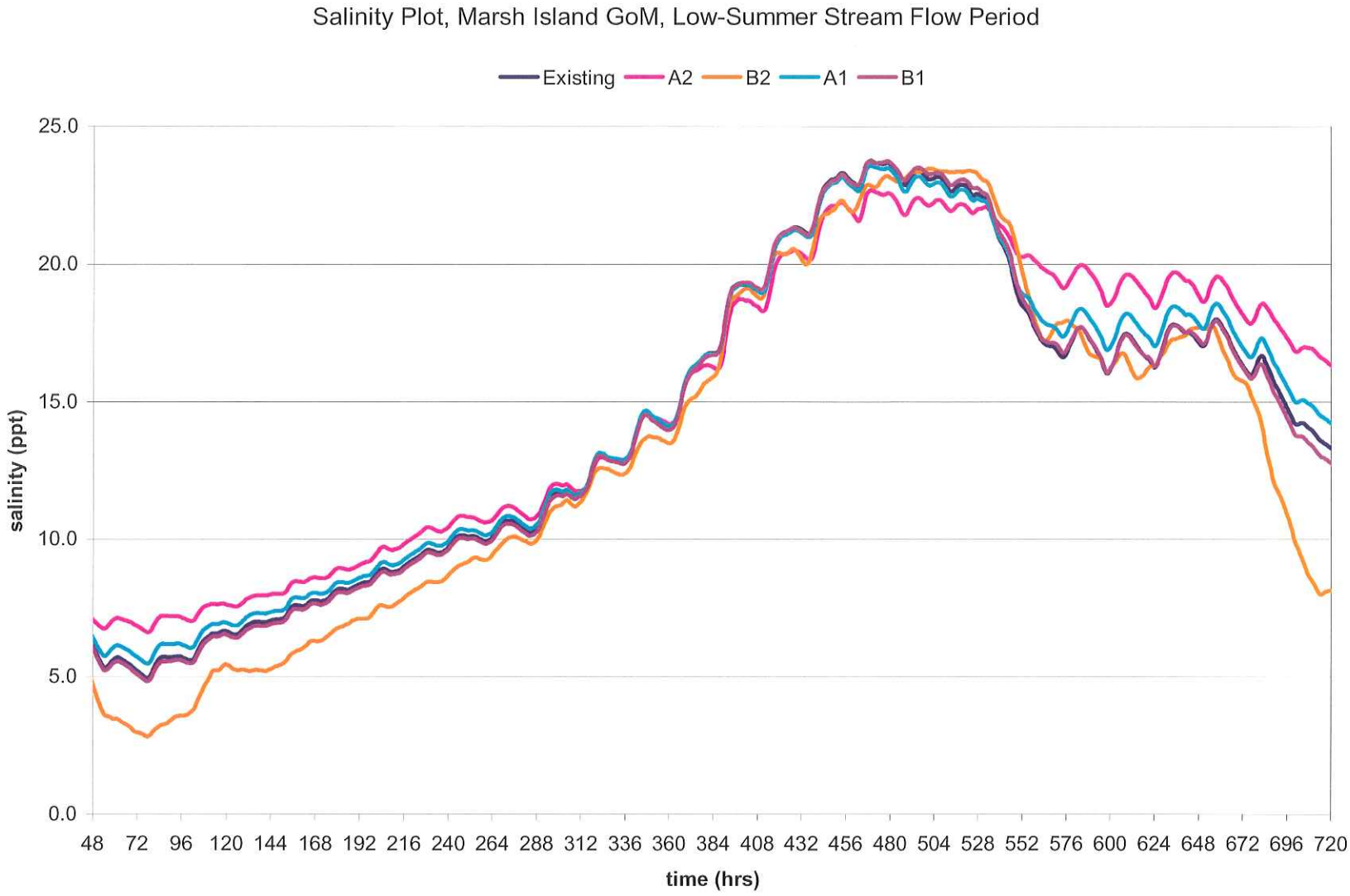
Salinity Plot, Marsh Island GoM, Low-Summer Stream Flow Period
Existing
A2
B2
A1
B1
25.0
20.0
15.0
10.0
5.0
0.0
salinity (ppt)
48 72 96 120 144 168 192 216 240 264 288 312 336 360 384 408 432 456 480 504 528 552 576 600 624 648 672 696 720
time (hrs)

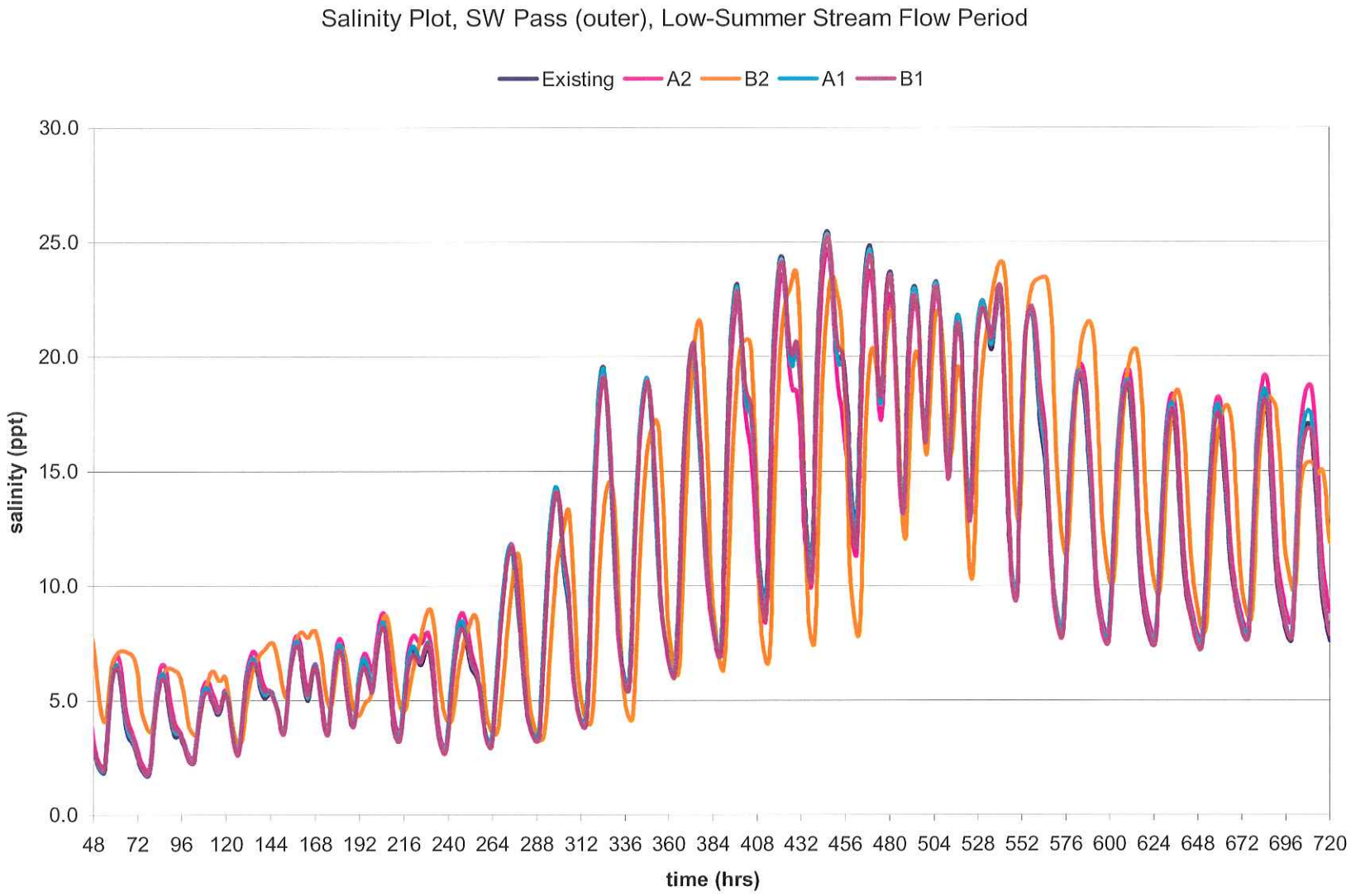
Salinity Plot, SW Pass (outer), Low-Summer Stream Flow Period
Existing
A2
B2
A1
B1
30.0
25.0
20.0
15.0
10.0
5.0
0.0
salinity (ppt)
48 72 96 120 144 168 192 216 240 264 288 312 336 360 384 408 432 456 480 504 528 552 576 600 624 648 672 696 720
time (hrs)

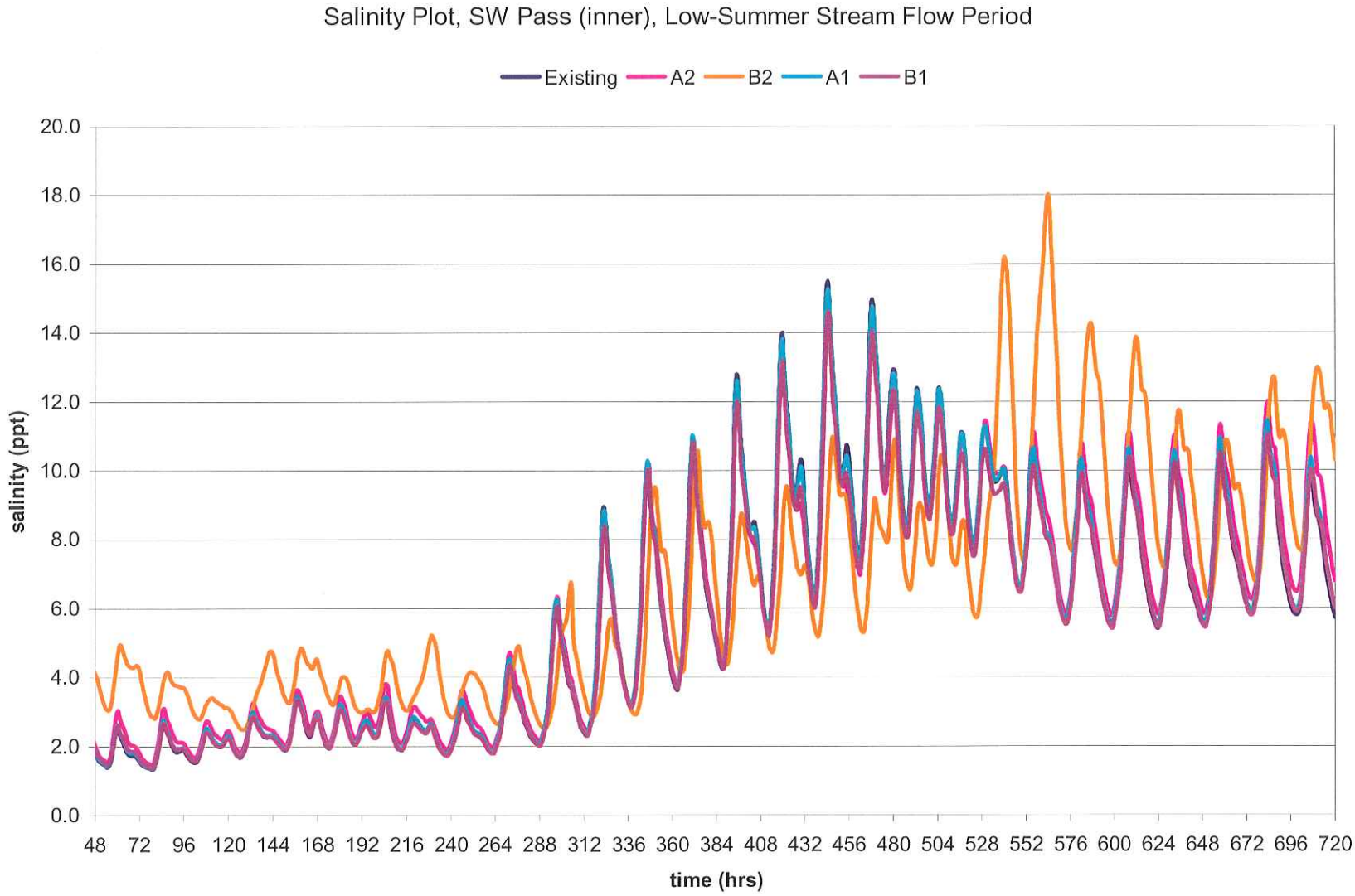
Salinity Plot, SW Pass (inner), Low-Summer Stream Flow Period
Existing
A2
B2
A1
B1
salinity (ppt)
20.0
18.0
16.0
14.0
12.0
10.0
8.0
6.0
4.0
2.0
0.0
48 72 96 120 144 168 192 216 240 264 288 312 336 360 384 408 432 456 480 504 528 552 576 600 624 648 672 696 720
time (hrs)

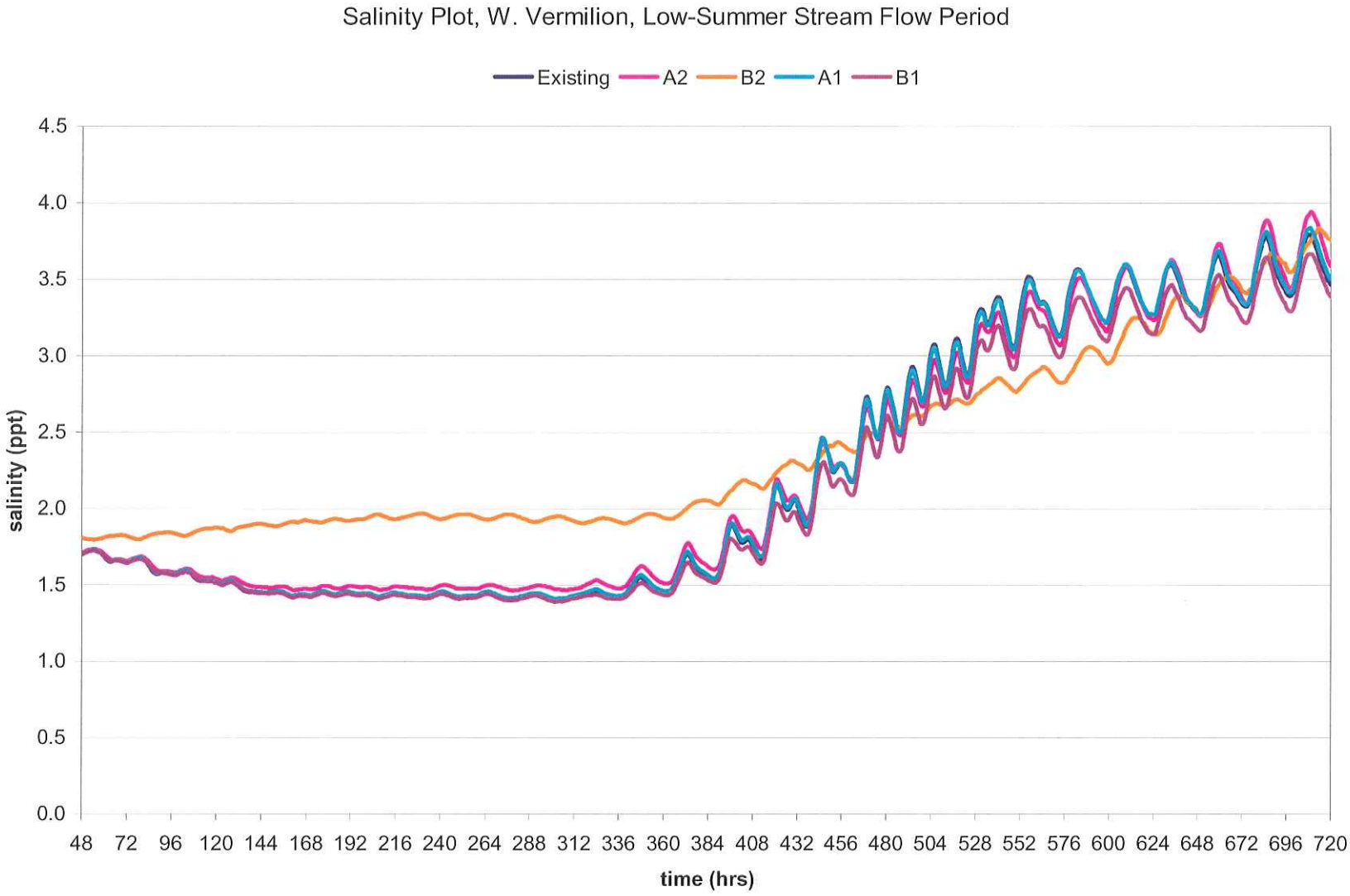
Salinity Plot, W. Vermilion, Low-Summer Stream Flow Period
Existing
A2
B2
A1
B1
salinity (ppt)
4.5
4.0
3.5
3.0
2.5
2.0
1.5
1.0
0.5
0.0
48 72 96 120 144 168 192 216 240 264 288 312 336 360 384 408 432 456 480 504 528 552 576 600 624 648 672 696 720
time (hrs)

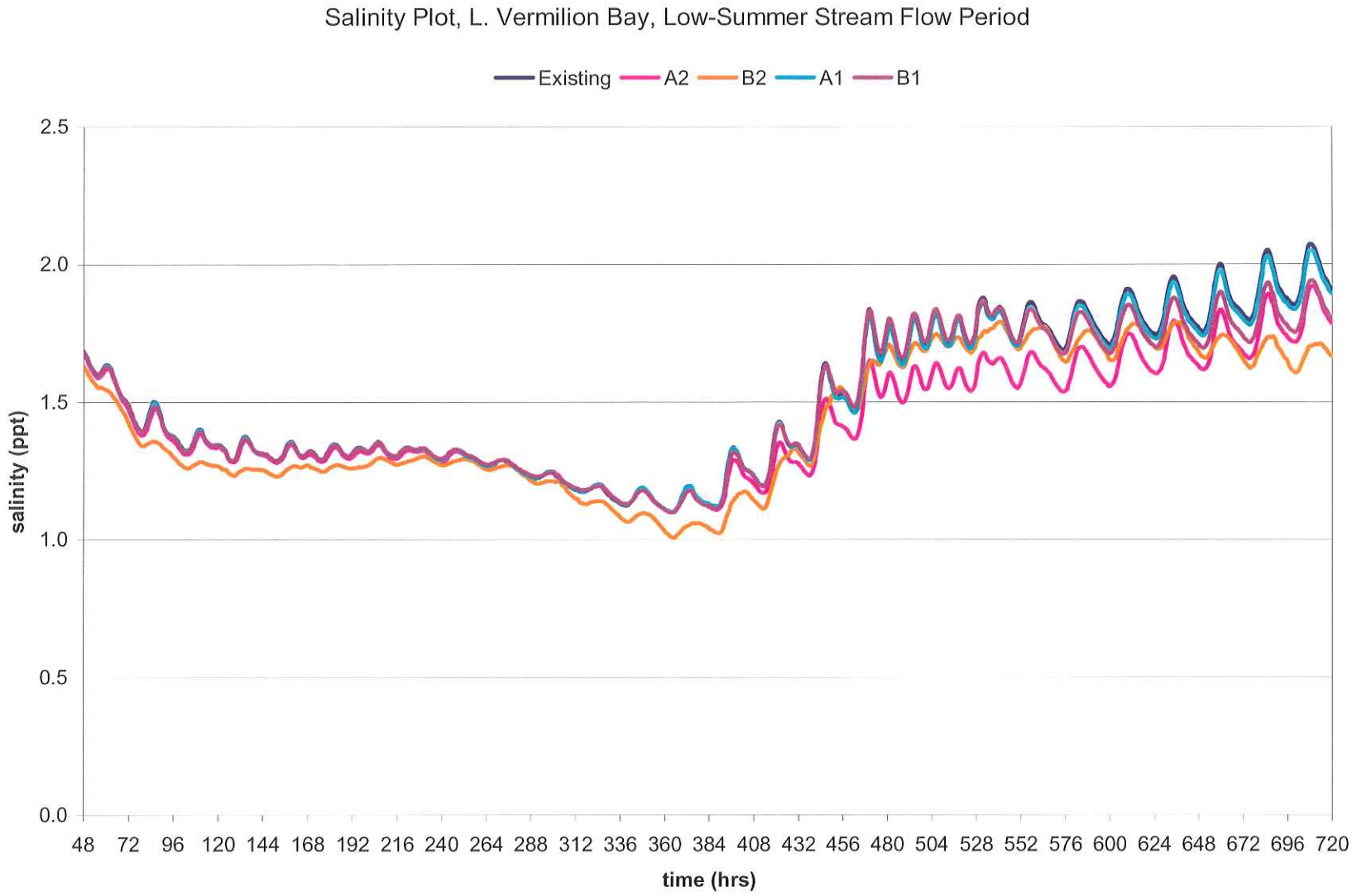
Salinity Plot, L. Vermilion Bay, Low-Summer Stream Flow Period
Existing
A2
B2
A1
B1
2.5
2.0
1.5
1.0
0.5
0.0
salinity (ppt)
48 72 96 120 144 168 192 216 240 264 288 312 336 360 384 408 432 456 480 504 528 552 576 600 624 648 672 696 720
time (hrs)

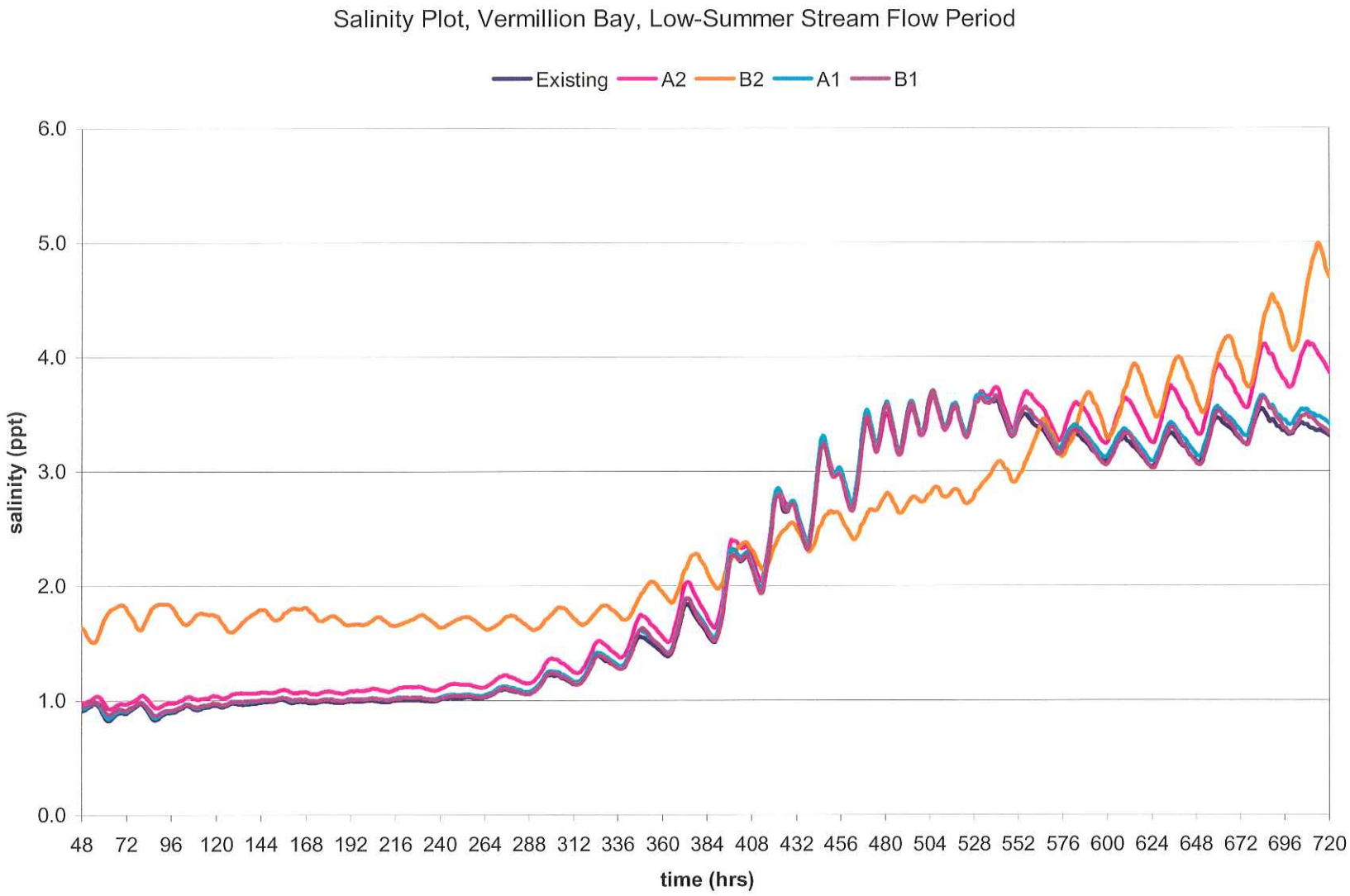
Salinity Plot, Vermillion Bay, Low-Summer Stream Flow Period
Existing
A2
B2
A1
B1
6.0
5.0
4.0
3.0
2.0
1.0
0.0
salinity (ppt)
48 72 96 120 144 168 192 216 240 264 288 312 336 360 384 408 432 456 480 504 528 552 576 600 624 648 672 696 720
time (hrs)

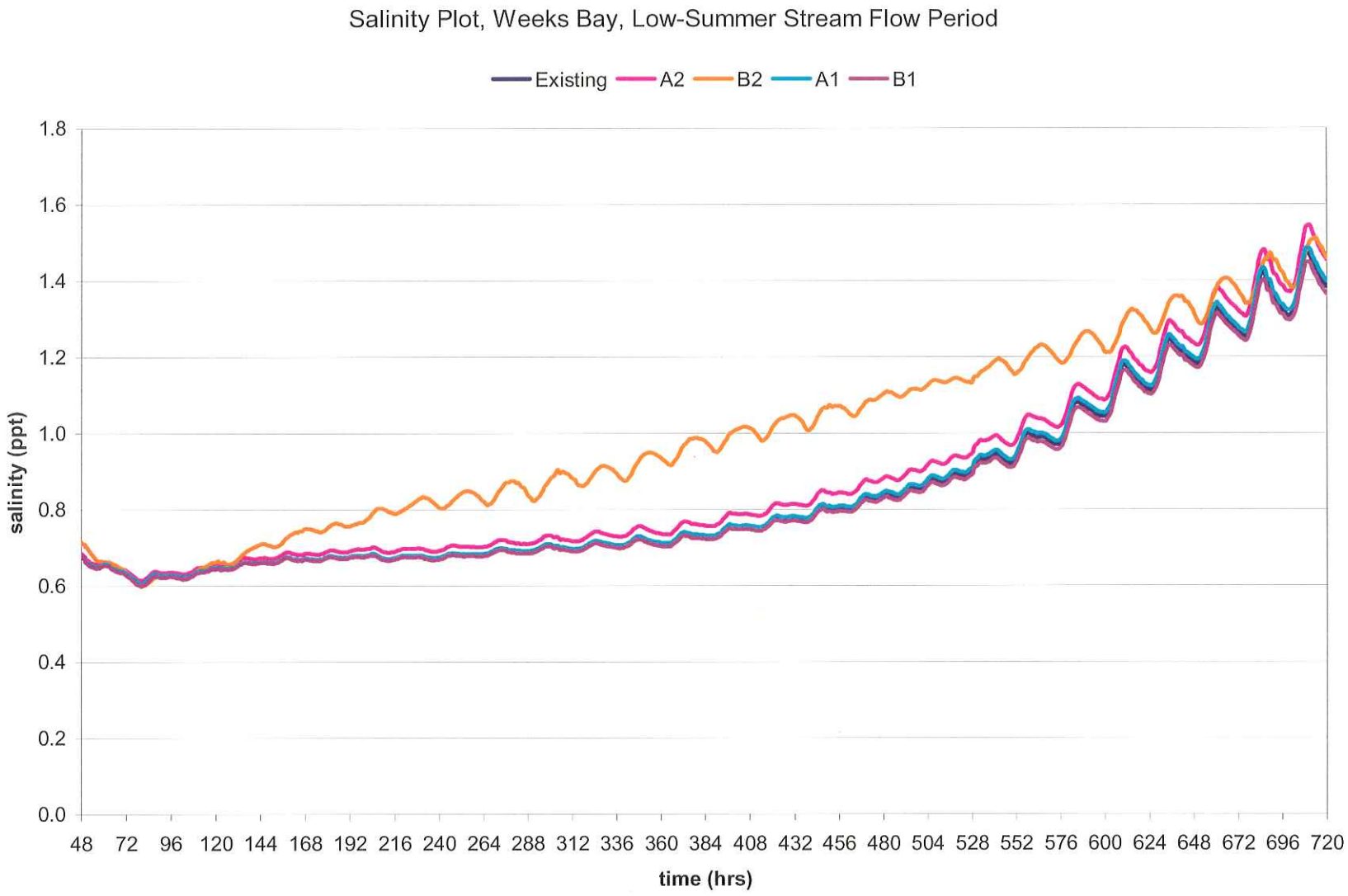
Salinity Plot, Weeks Bay, Low-Summer Stream Flow Period
Existing
A2
B2
A1
B1
salinity (ppt)
1.8
1.6
1.4
1.2
1.0
0.8
0.6
0.4
0.2
0.0
48 72 96 120 144 168 192 216 240 264 288 312 336 360 384 408 432 456 480 504 528 552 576 600 624 648 672 696 720
time (hrs)

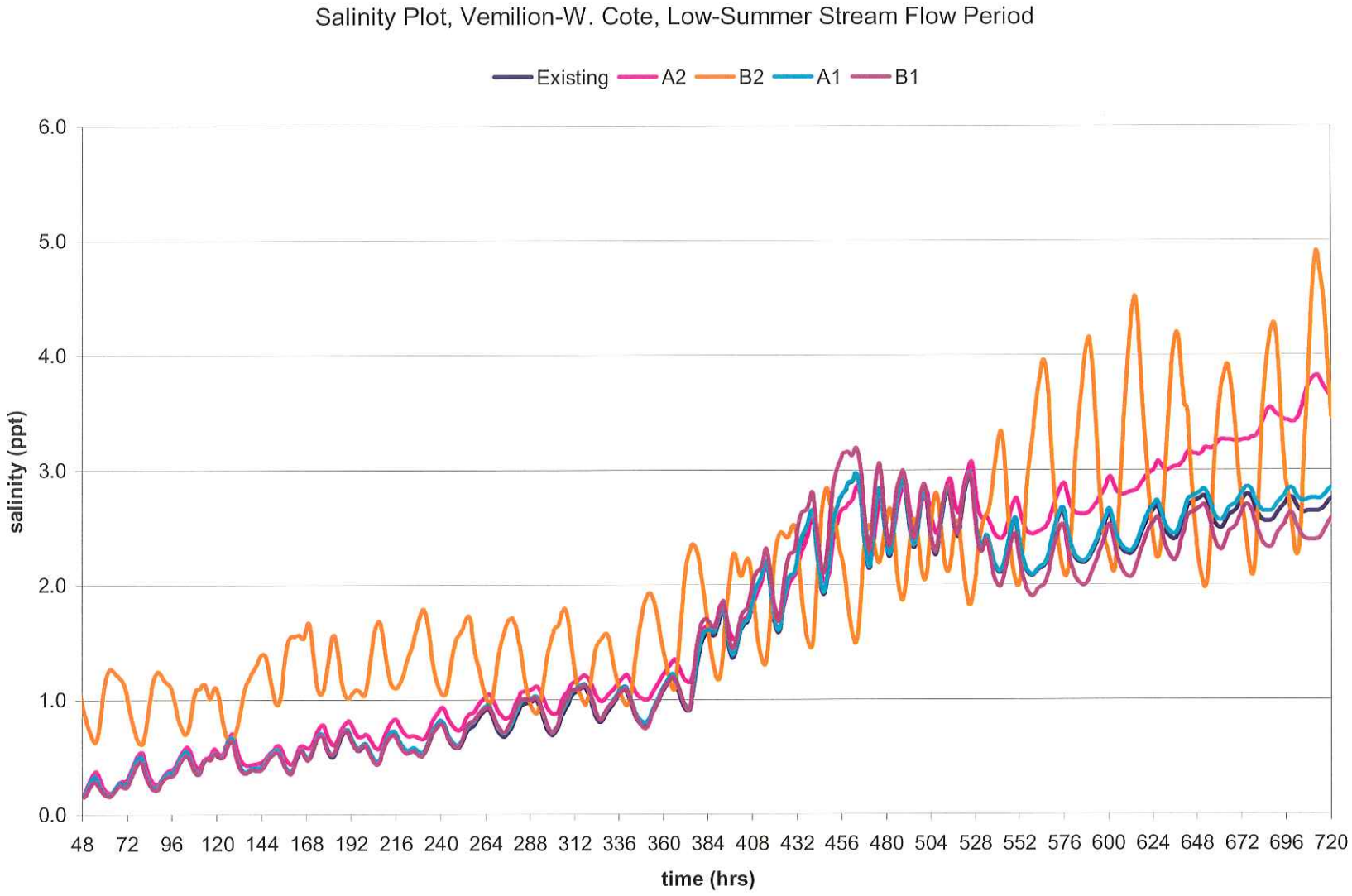
Salinity Plot, Vemilion-W. Cote, Low-Summer Stream Flow Period
Existing
A2
B2
A1
B1
salinity (ppt)
6.0
5.0
4.0
3.0
2.0
1.0
0.0
48 72 96 120 144 168 192 216 240 264 288 312 336 360 384 408 432 456 480 504 528 552 576 600 624 648 672 696 720
time (hrs)

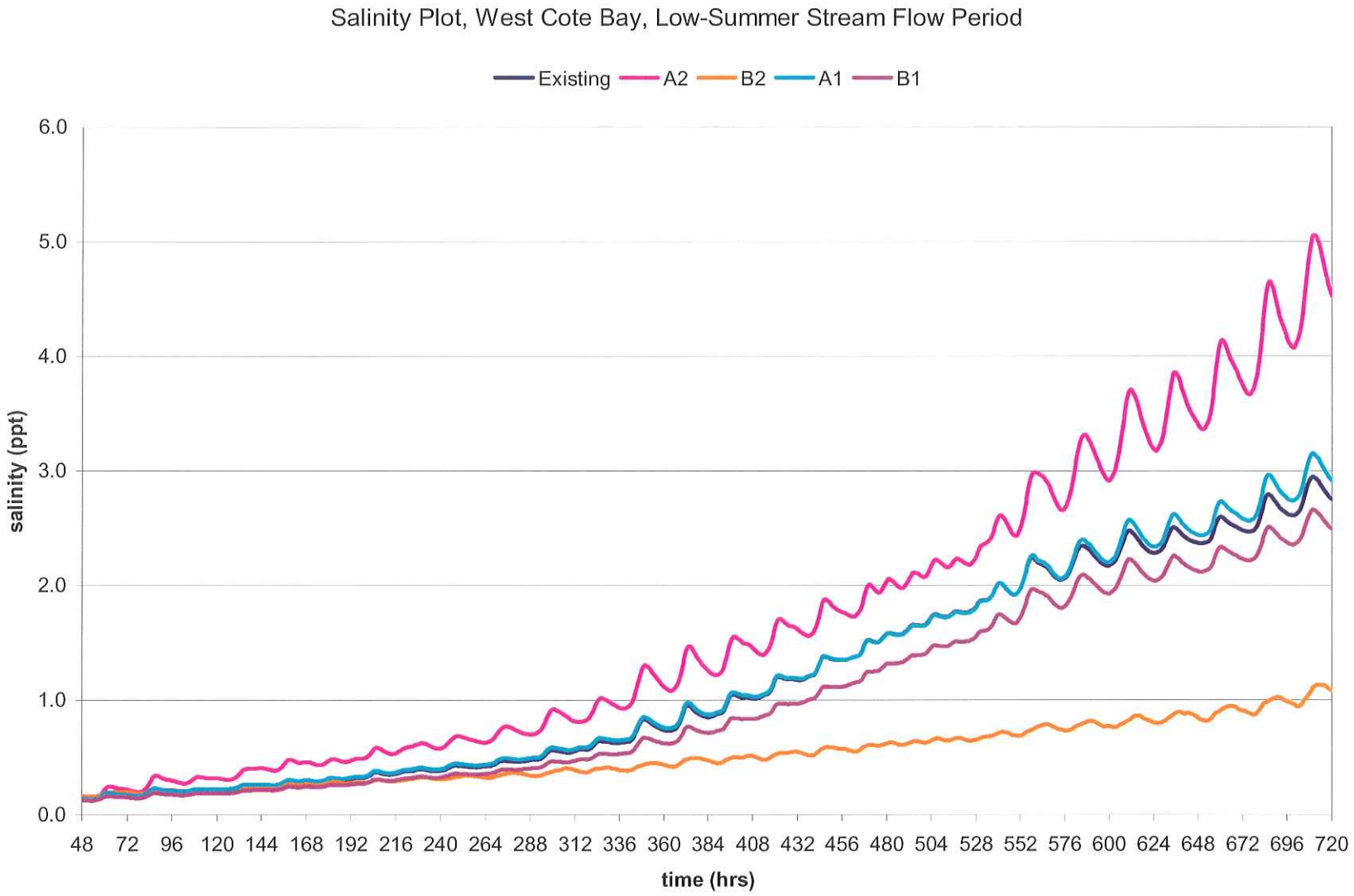
Salinity Plot, West Cote Bay, Low-Summer Stream Flow Period
Existing
A2
B2
A1
B1
6.0
5.0
4.0
3.0
2.0
1.0
0.0
salinity (ppt)
48 72 96 120 144 168 192 216 240 264 288 312 336 360 384 408 432 456 480 504 528 552 576 600 624 648 672 696 720
time (hrs)

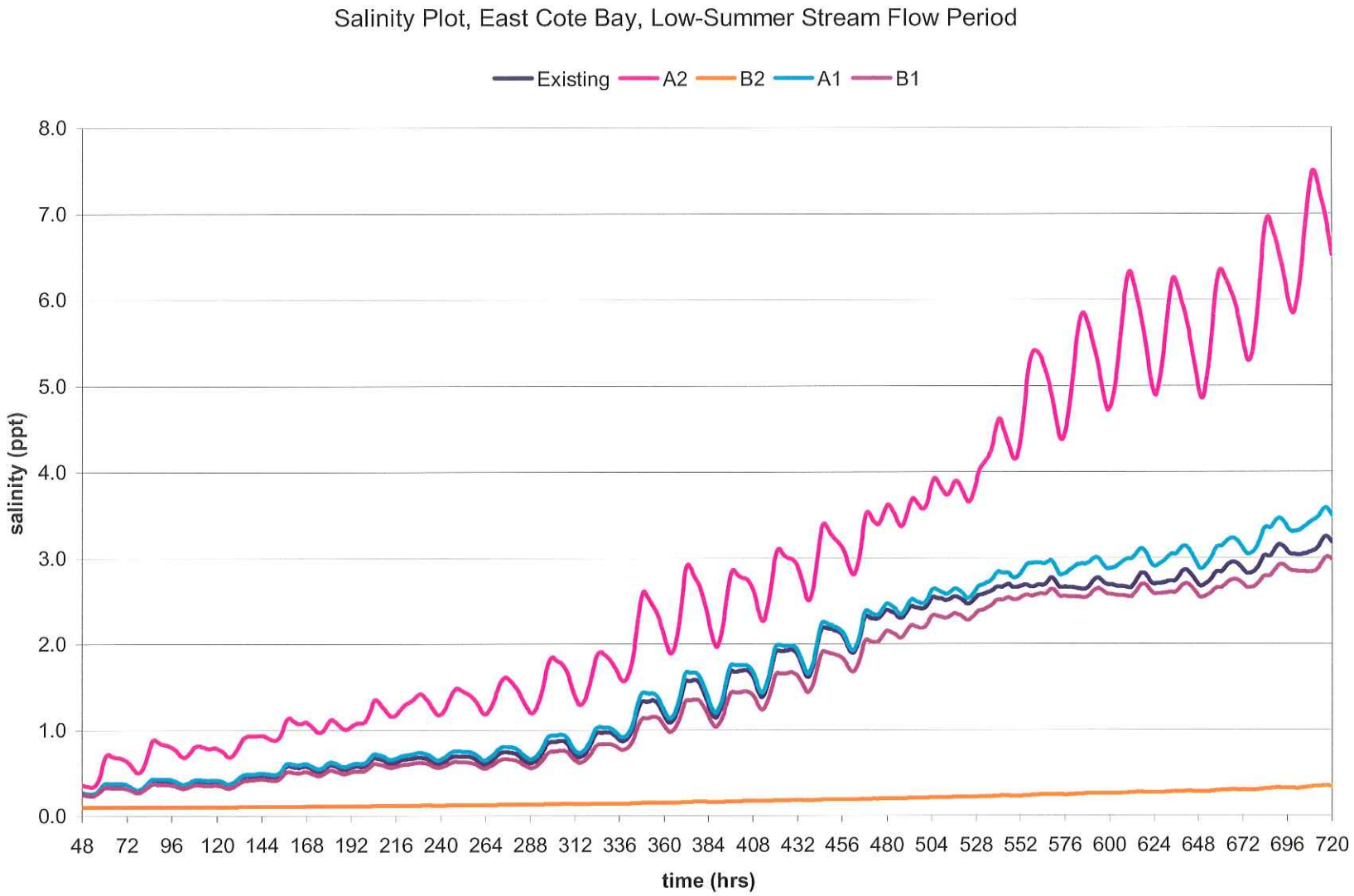
Salinity Plot, East Cote Bay, Low-Summer Stream Flow Period
Existing
A2
B2
A1
B1
salinity (ppt)
8.0
7.0
6.0
5.0
4.0
3.0
2.0
1.0
0.0
48 72 96 120 144 168 192 216 240 264 288 312 336 360 384 408 432 456 480 504 528 552 576 600 624 648 672 696 720
time (hrs)

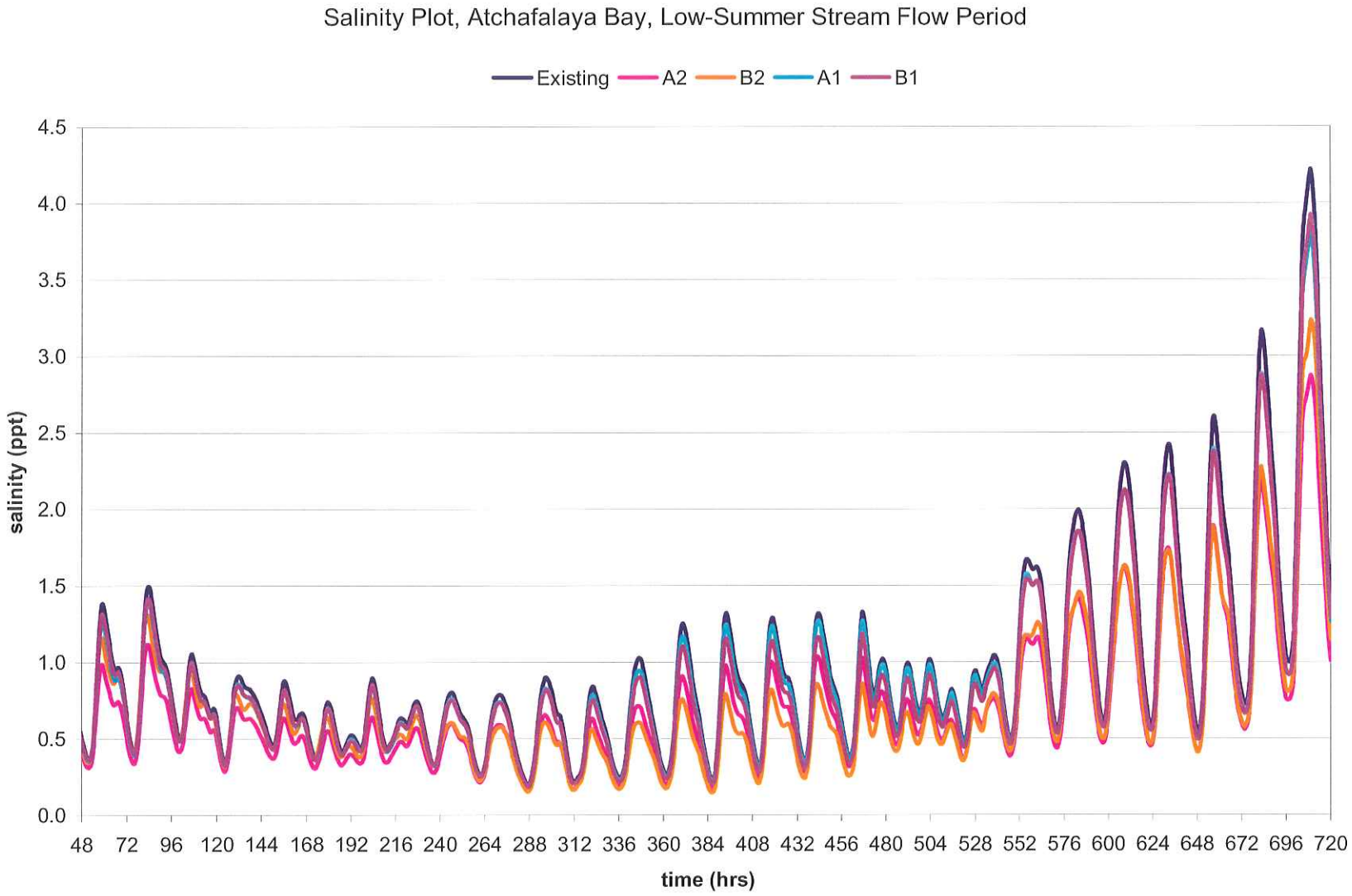
Salinity Plot, Atchafalaya Bay, Low-Summer Stream Flow Period
Existing
A2
B2
A1
B1
salinity (ppt)
4.5
4.0
3.5
3.0
2.5
2.0
1.5
1.0
0.5
0.0
48 72 96 120 144 168 192 216 240 264 288 312 336 360 384 408 432 456 480 504 528 552 576 600 624 648 672 696 720
time (hrs)

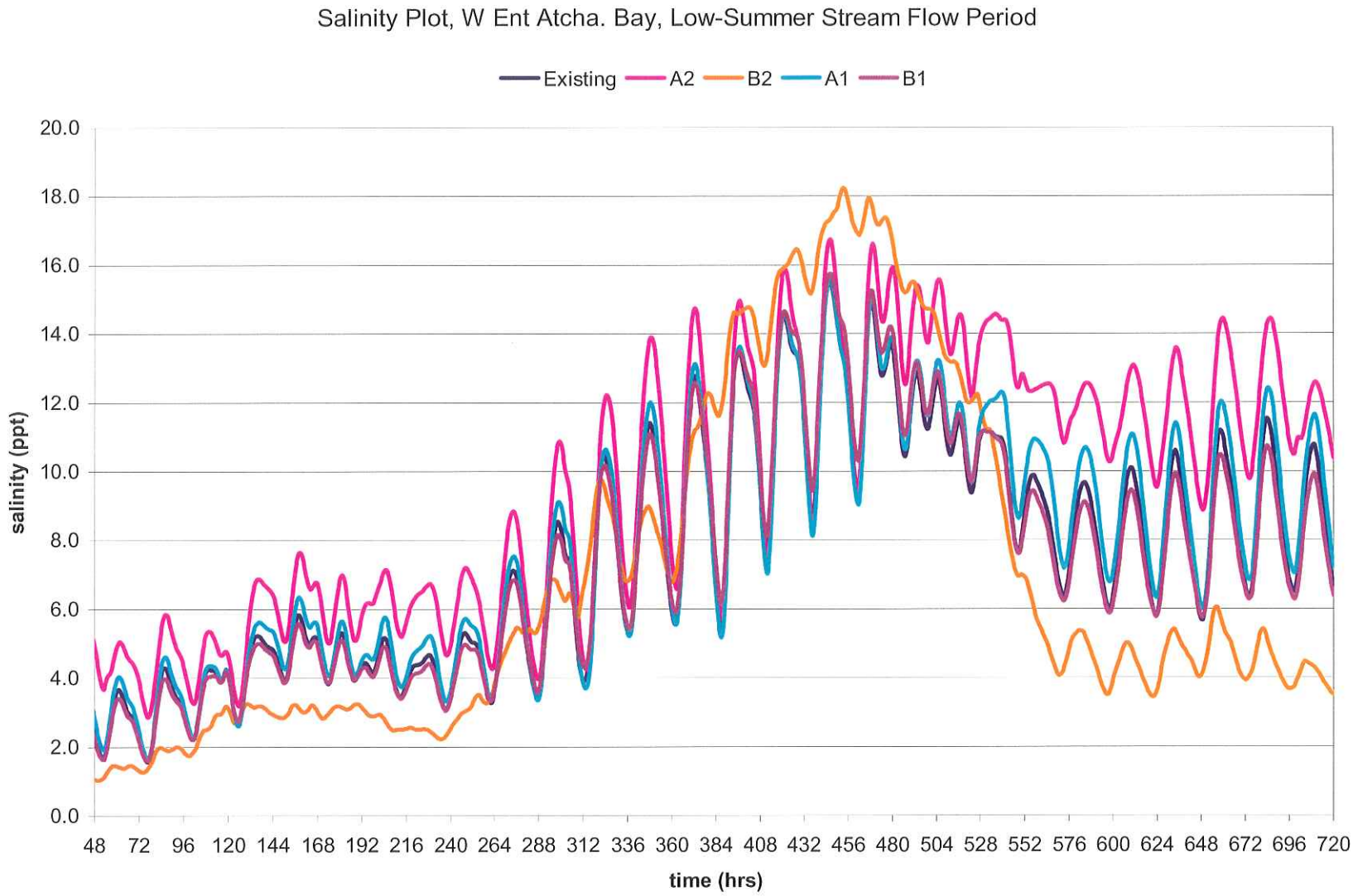
Salinity Plot, W Ent Atcha. Bay, Low-Summer Stream Flow Period
Existing
A2
B2
A1
B1
20.0
18.0
16.0
14.0
12.0
10.0
8.0
6.0
4.0
2.0
0.0
salinity (ppt)
48 72 96 120 144 168 192 216 240 264 288 312 336 360 384 408 432 456 480 504 528 552 576 600 624 648 672 696 720
time (hrs)

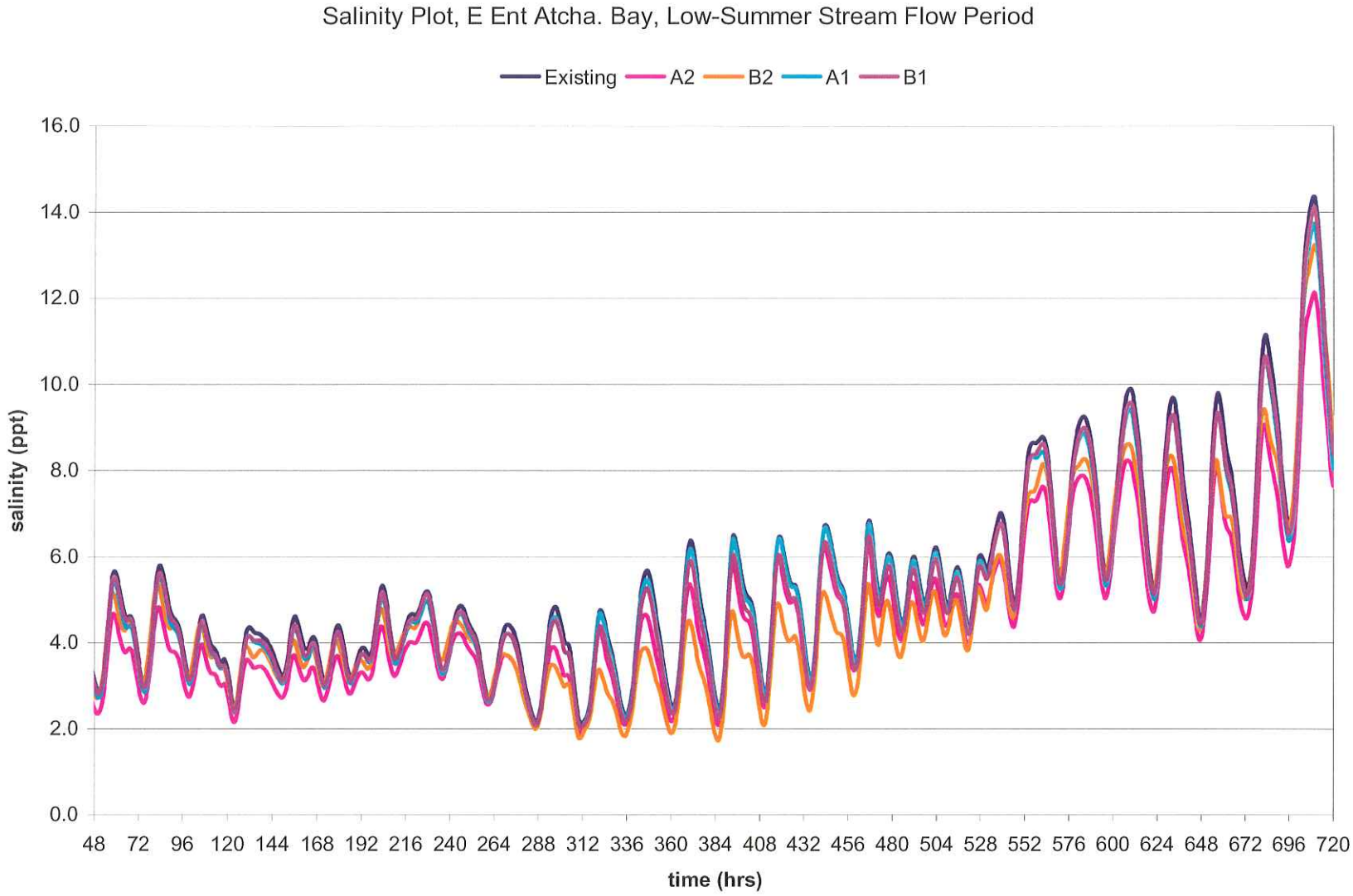
Salinity Plot, E Ent Atcha. Bay, Low-Summer Stream Flow Period
Existing
A2
B2
A1
B1
16.0
14.0
12.0
10.0
8.0
6.0
4.0
2.0
0.0
salinity (ppt)
48 72 96 120 144 168 192 216 240 264 288 312 336 360 384 408 432 456 480 504 528 552 576 600 624 648 672 696 720
time (hrs)

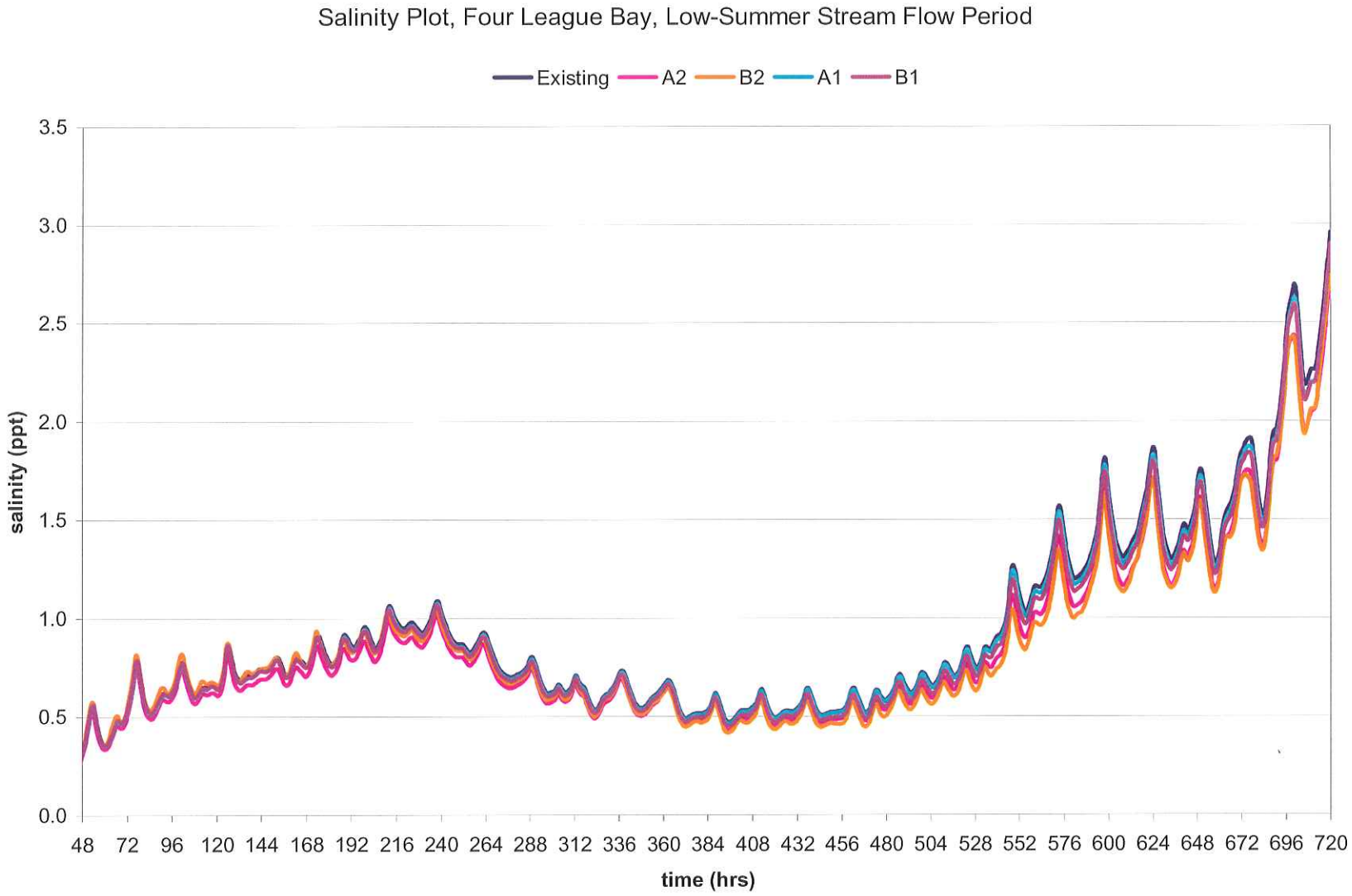
Salinity Plot, Four League Bay, Low-Summer Stream Flow Period
Existing
A2
B2
A1
B1
salinity (ppt)
3.5
3.0
2.5
2.0
1.5
1.0
0.5
0.0
48 72 96 120 144 168 192 216 240 264 288 312 336 360 384 408 432 456 480 504 528 552 576 600 624 648 672 696 720
time (hrs)

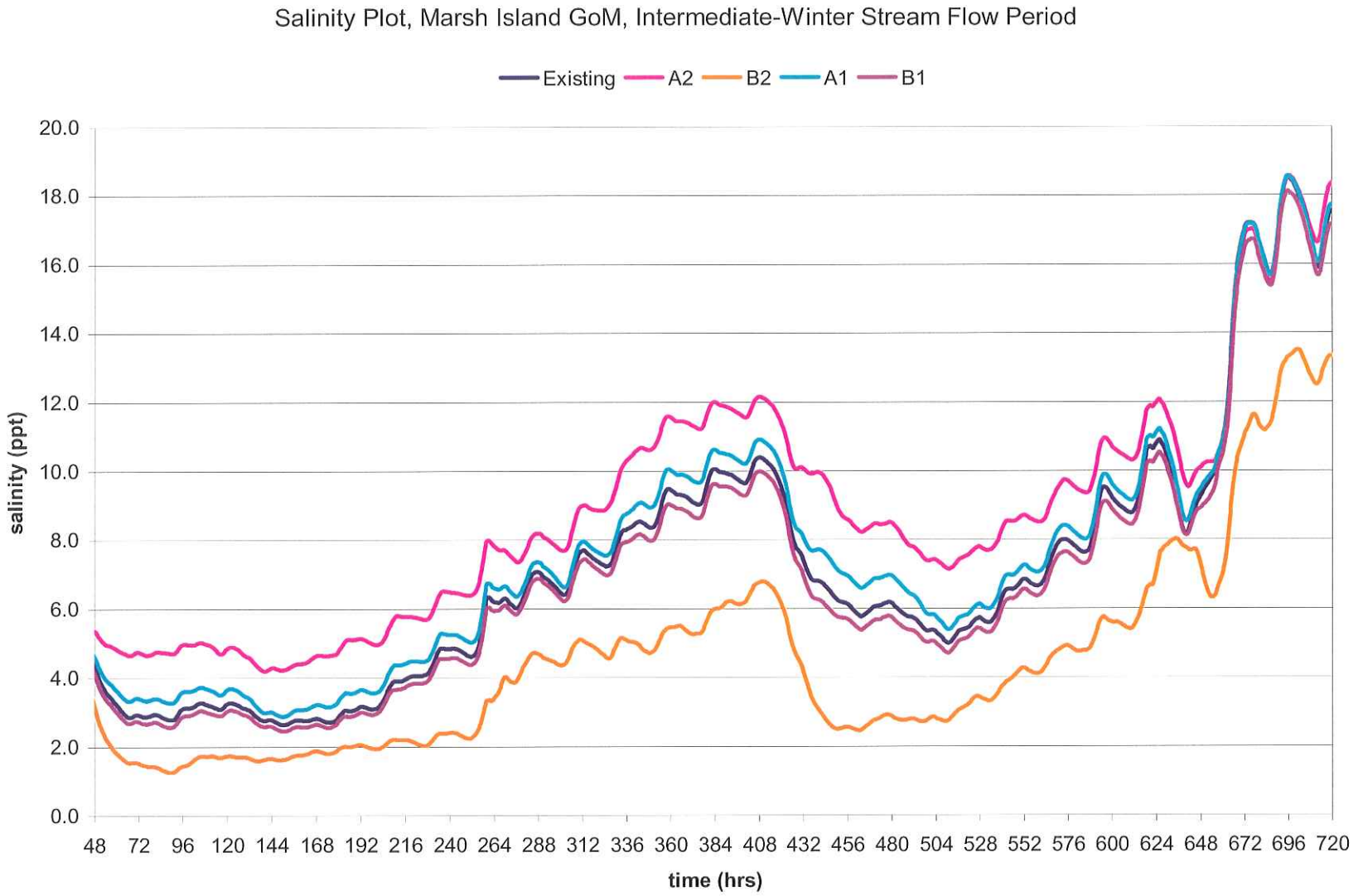
Salinity Plot, Marsh Island GoM, Intermediate-Winter Stream Flow Period
Existing
A2
B2
A1
B1
20.0
18.0
16.0
14.0
12.0
10.0
8.0
6.0
4.0
2.0
0.0
salinity (ppt)
48 72 96 120 144 168 192 216 240 264 288 312 336 360 384 408 432 456 480 504 528 552 576 600 624 648 672 696 720
time (hrs)

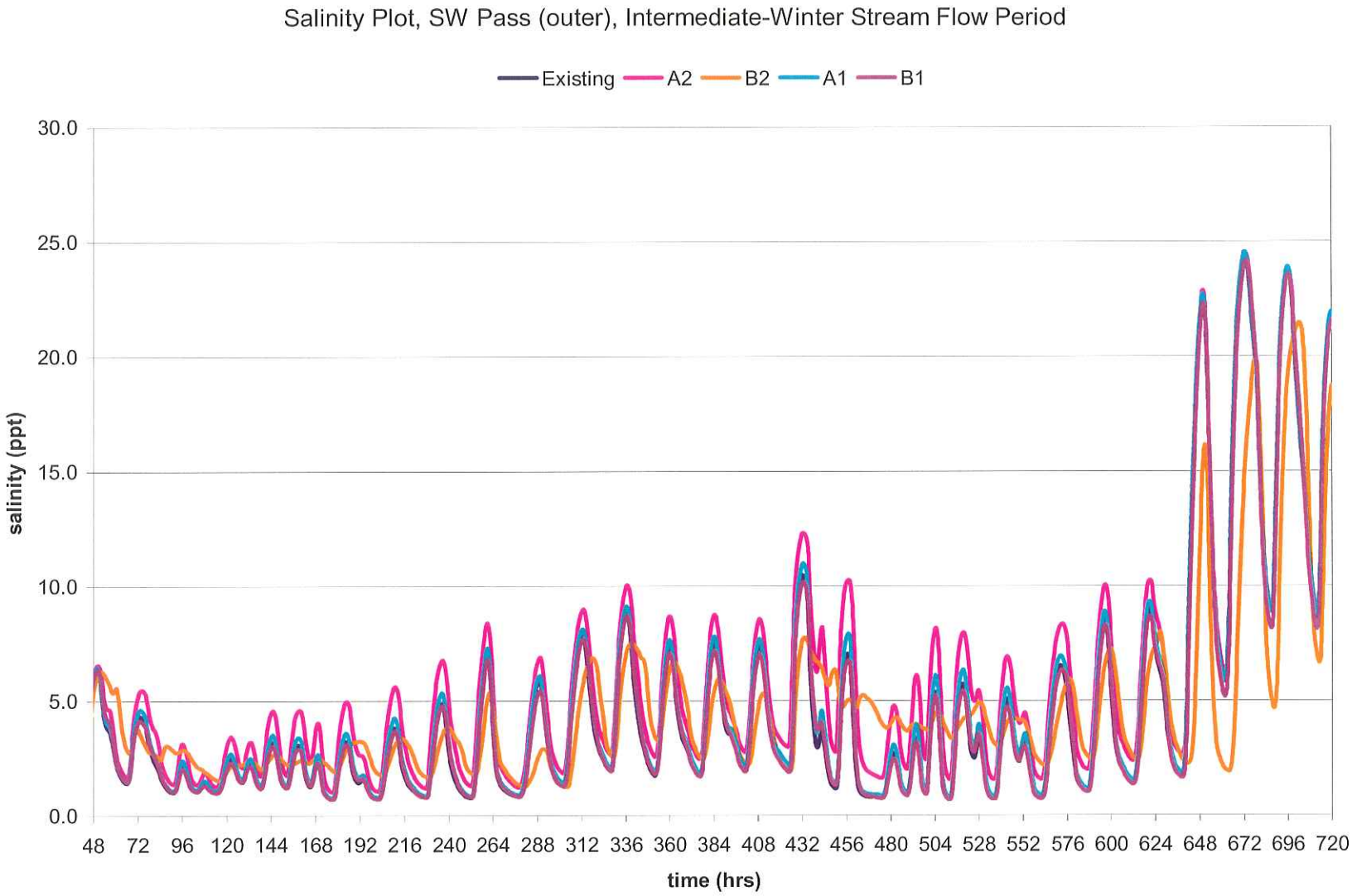
Salinity Plot, SW Pass (outer), Intermediate-Winter Stream Flow Period
Existing
A2
B2
A1
B1
30.0
25.0
20.0
15.0
10.0
5.0
0.0
salinity (ppt)
48 72 96 120 144 168 192 216 240 264 288 312 336 360 384 408 432 456 480 504 528 552 576 600 624 648 672 696 720
time (hrs)

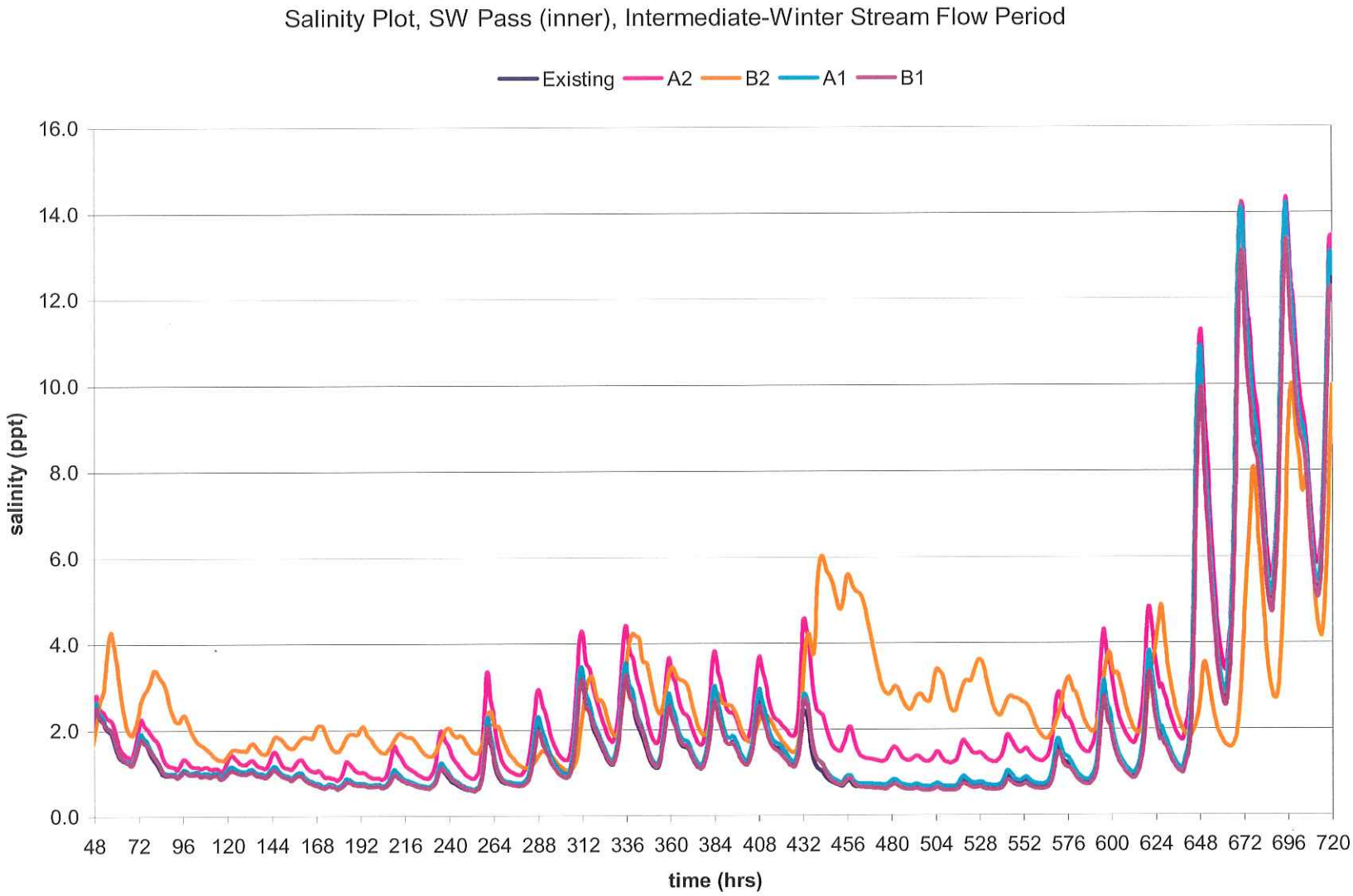
Salinity Plot, SW Pass (inner), Intermediate-Winter Stream Flow Period
Existing
A2
B2
A1
B1
16.0
14.0
12.0
10.0
8.0
6.0
4.0
2.0
0.0
salinity (ppt)
48 72 96 120 144 168 192 216 240 264 288 312 336 360 384 408 432 456 480 504 528 552 576 600 624 648 672 696 720
time (hrs)

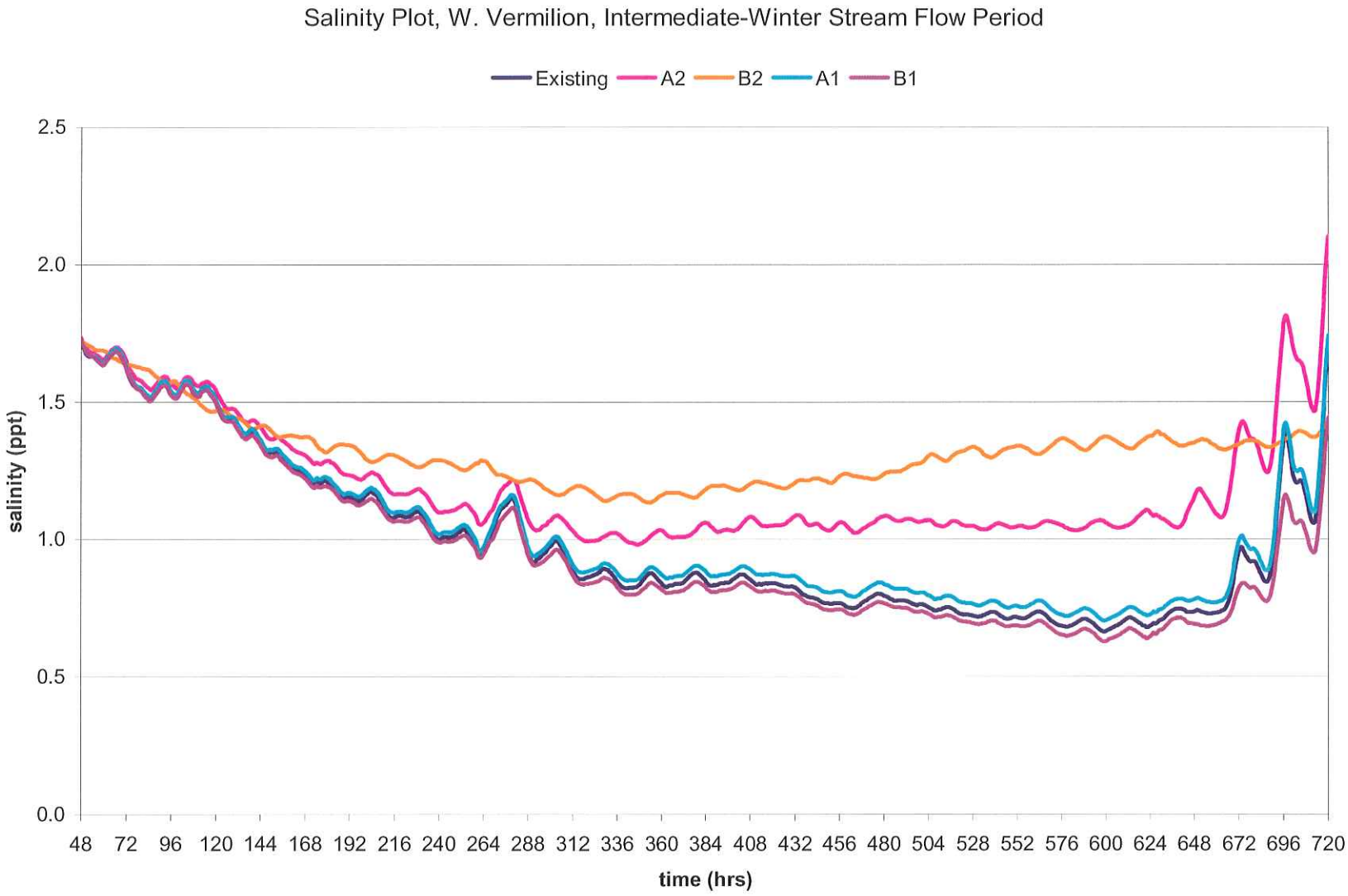
Salinity Plot, W. Vermilion, Intermediate-Winter Stream Flow Period
Existing
A2
B2
A1
B1
2.5
2.0
1.5
1.0
0.5
0.0
salinity (ppt)
48 72 96 120 144 168 192 216 240 264 288 312 336 360 384 408 432 456 480 504 528 552 576 600 624 648 672 696 720
time (hrs)

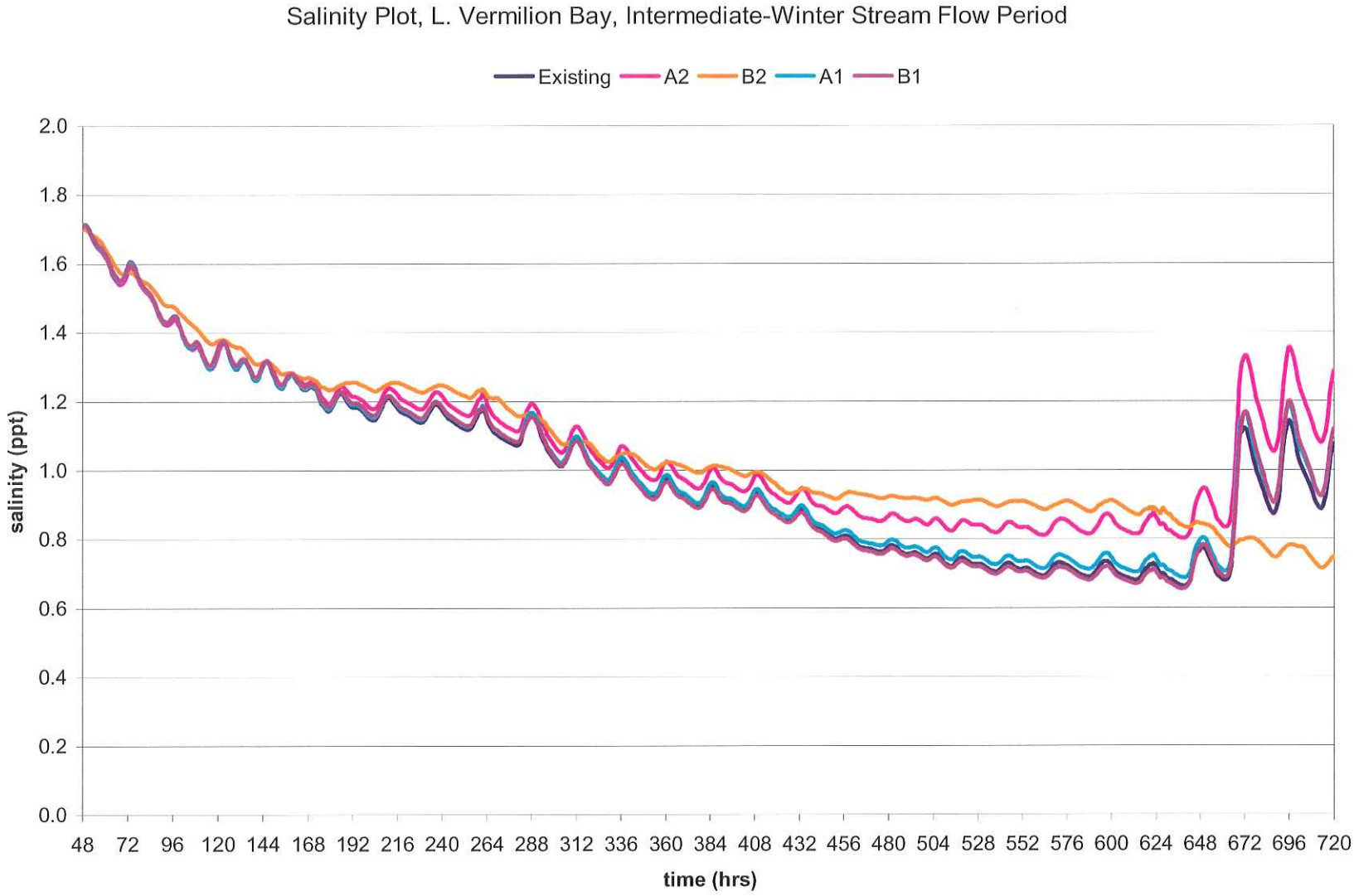
Salinity Plot, L. Vermilion Bay, Intermediate-Winter Stream Flow Period
Existing
A2
B2
A1
B1
salinity (ppt)
2.0
1.8
1.6
1.4
1.2
1.0
0.8
0.6
0.4
0.2
0.0
48 72 96 120 144 168 192 216 240 264 288 312 336 360 384 408 432 456 480 504 528 552 576 600 624 648 672 696 720
time (hrs)

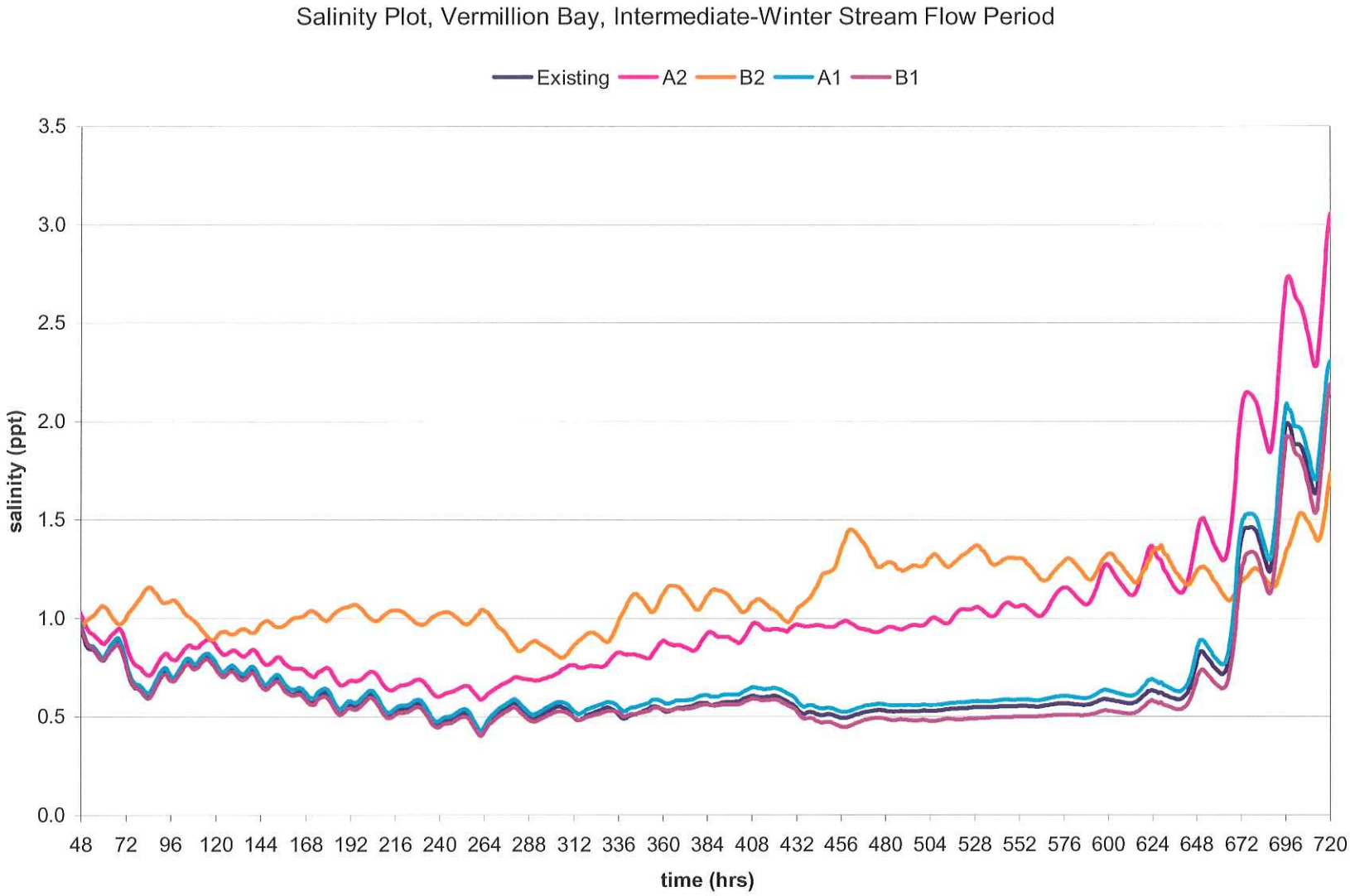
Salinity Plot, Vermillion Bay, Intermediate-Winter Stream Flow Period
Existing
A2
B2
A1
B1
salinity (ppt)
3.5
3.0
2.5
2.0
1.5
1.0
0.5
0.0
48 72 96 120 144 168 192 216 240 264 288 312 336 360 384 408 432 456 480 504 528 552 576 600 624 648 672 696 720
time (hrs)

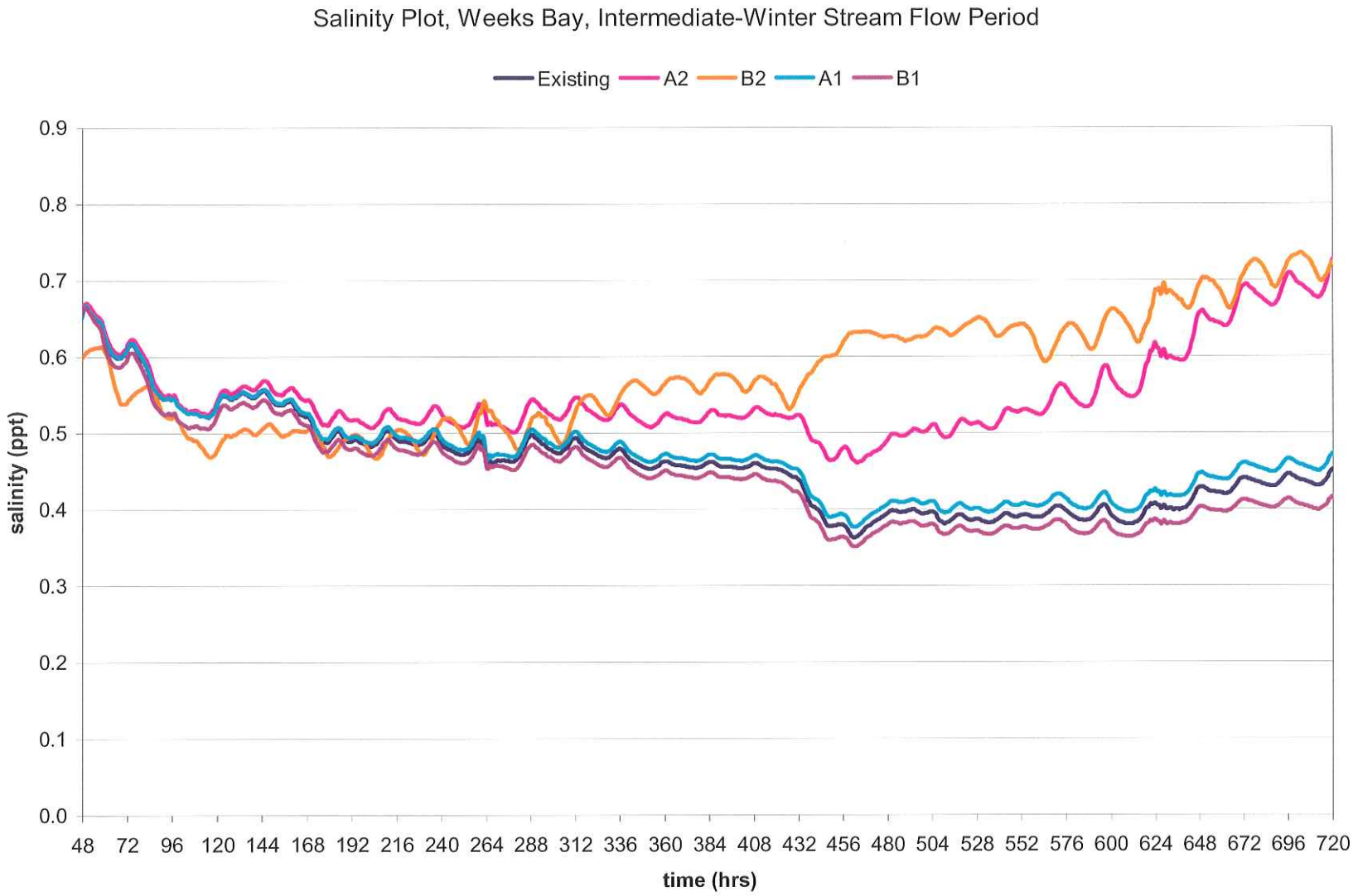
Salinity Plot, Weeks Bay, Intermediate-Winter Stream Flow Period
Existing
A2
B2
A1
B1
salinity (ppt)
0.0
0.1
0.2
0.3
0.4
0.5
0.6
0.7
0.8
0.9
48 72 96 120 144 168 192 216 240 264 288 312 336 360 384 408 432 456 480 504 528 552 576 600 624 648 672 696 720
time (hrs)

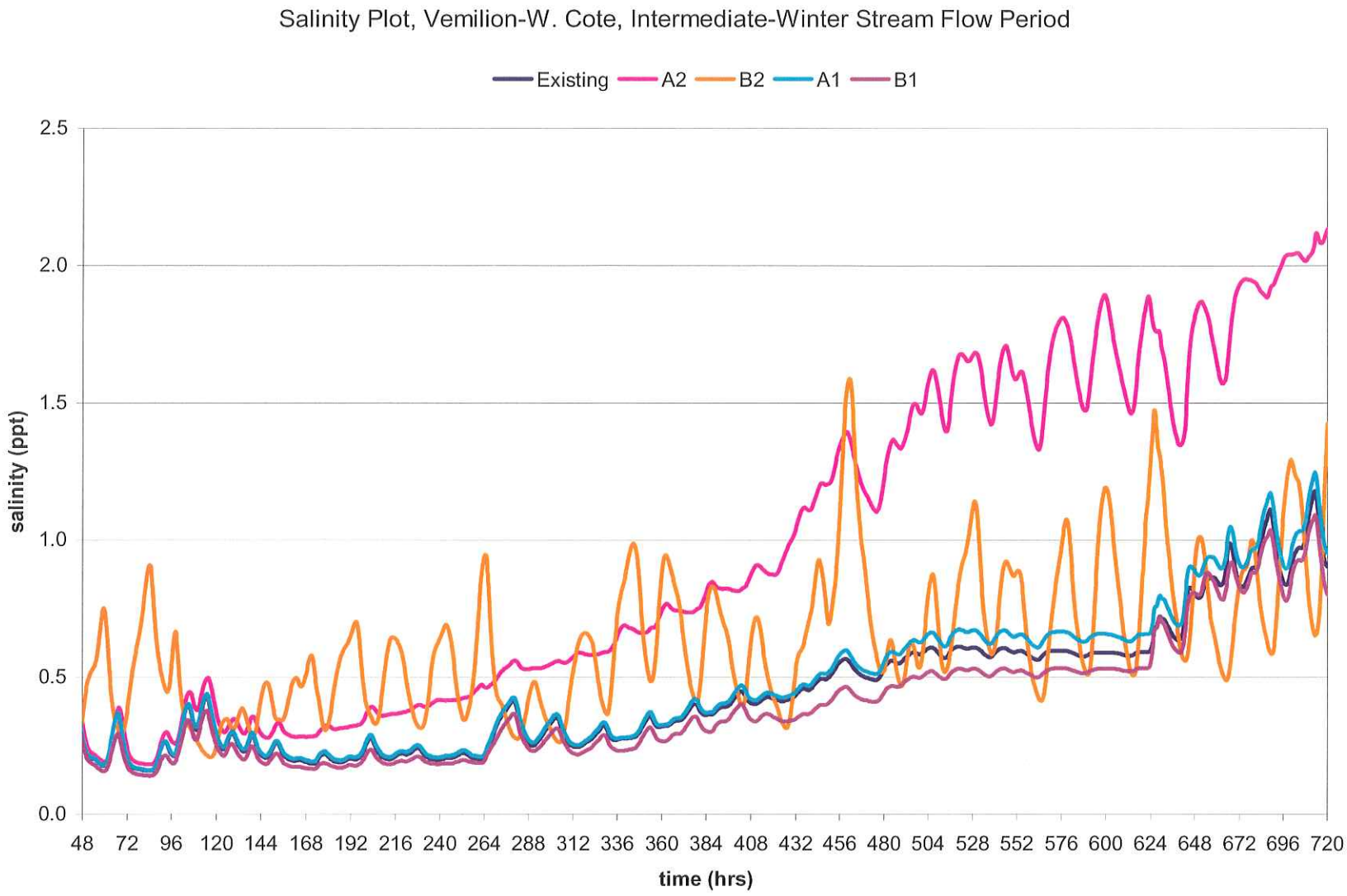
Salinity Plot, Vemilion-W. Cote, Intermediate-Winter Stream Flow Period
Existing
A2
B2
A1
B1
2.5
2.0
1.5
1.0
0.5
0.0
salinity (ppt)
48 72 96 120 144 168 192 216 240 264 288 312 336 360 384 408 432 456 480 504 528 552 576 600 624 648 672 696 720
time (hrs)

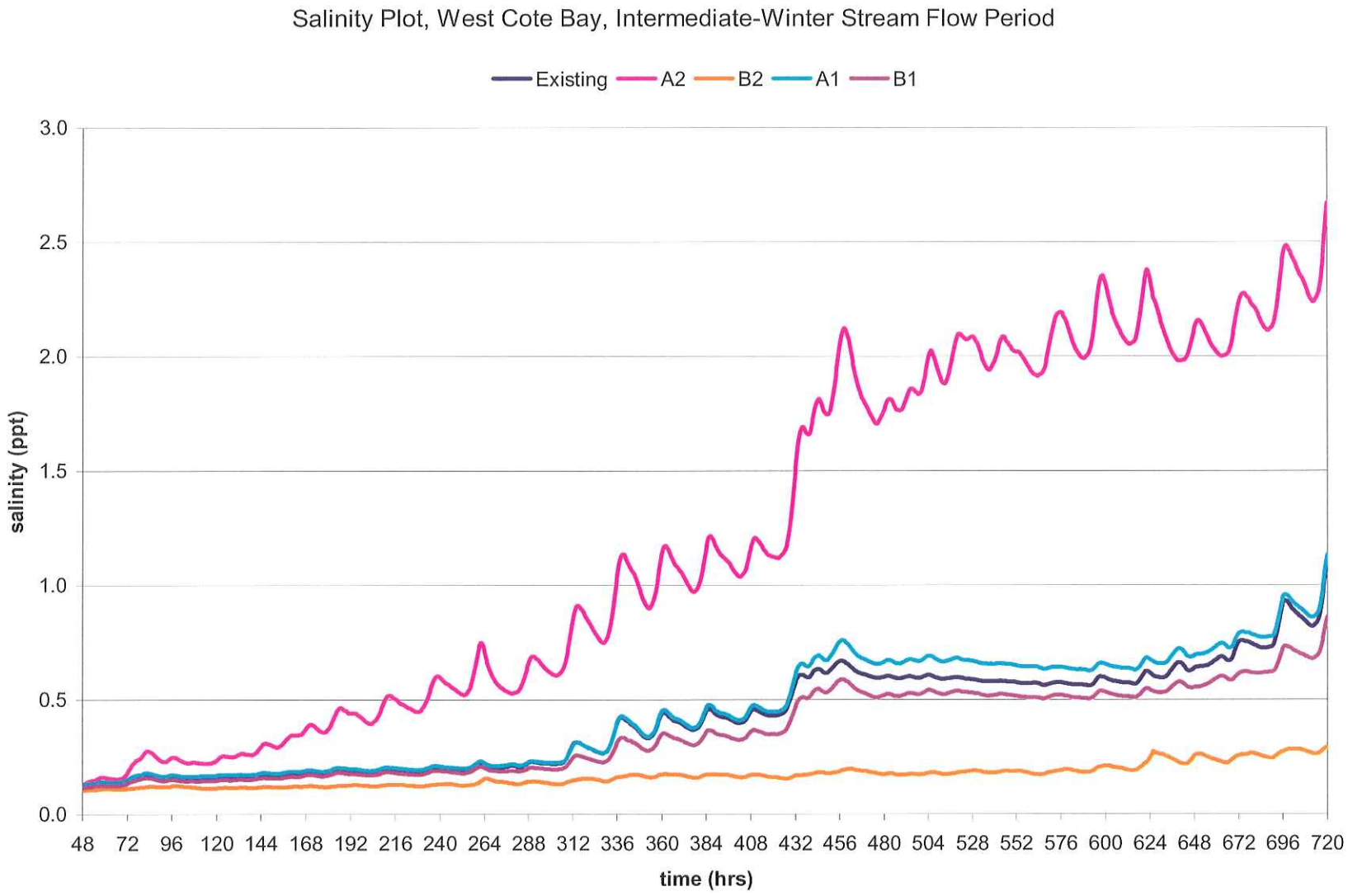
Salinity Plot, West Cote Bay, Intermediate-Winter Stream Flow Period
Existing
A2
B2
A1
B1
3.0
2.5
2.0
1.5
1.0
0.5
0.0
salinity (ppt)
48 72 96 120 144 168 192 216 240 264 288 312 336 360 384 408 432 456 480 504 528 552 576 600 624 648 672 696 720
time (hrs)

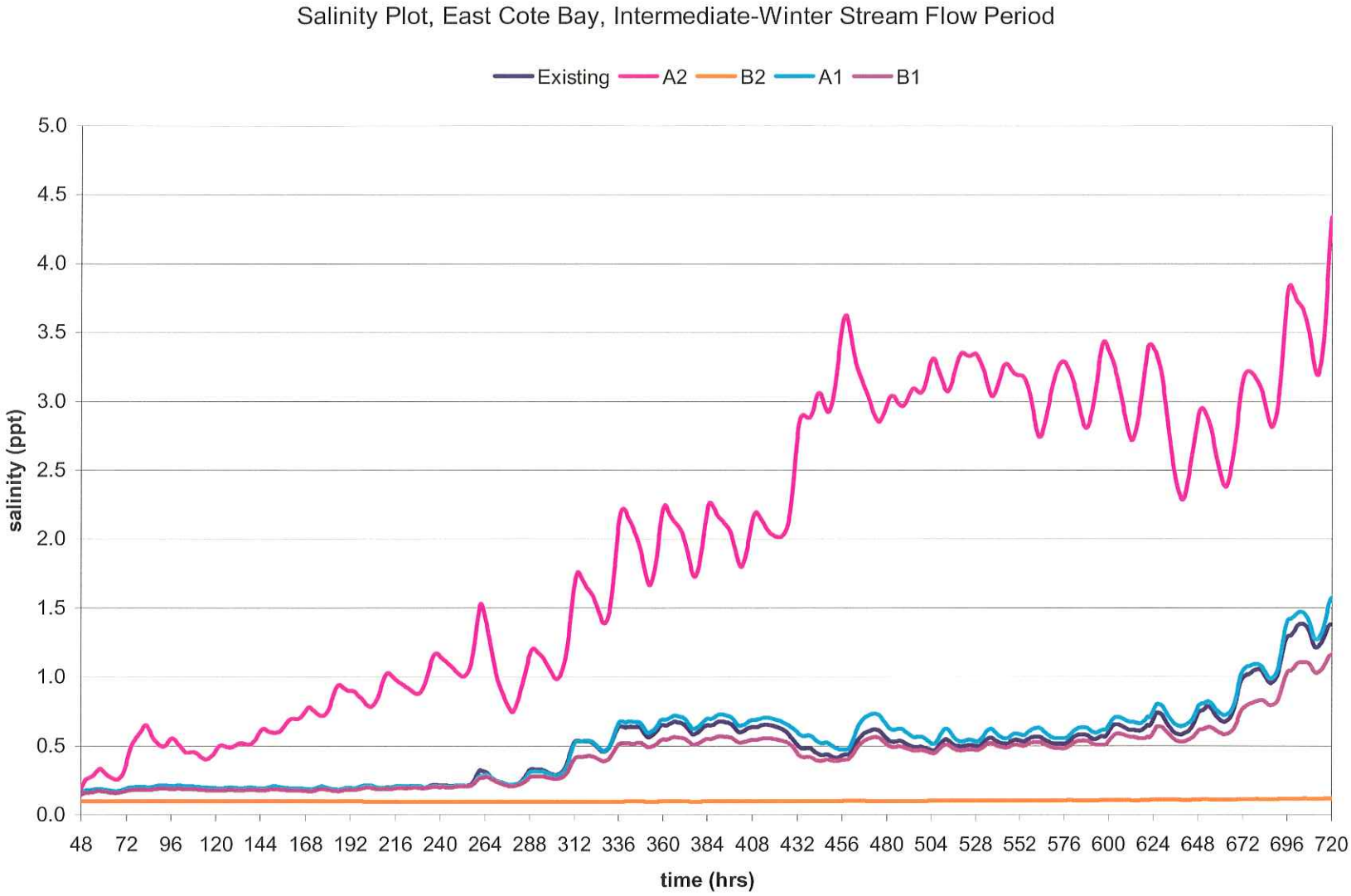
Salinity Plot, East Cote Bay, Intermediate-Winter Stream Flow Period
Existing
A2
B2
A1
B1
salinity (ppt)
5.0
4.5
4.0
3.5
3.0
2.5
2.0
1.5
1.0
0.5
0.0
48 72 96 120 144 168 192 216 240 264 288 312 336 360 384 408 432 456 480 504 528 552 576 600 624 648 672 696 720
time (hrs)

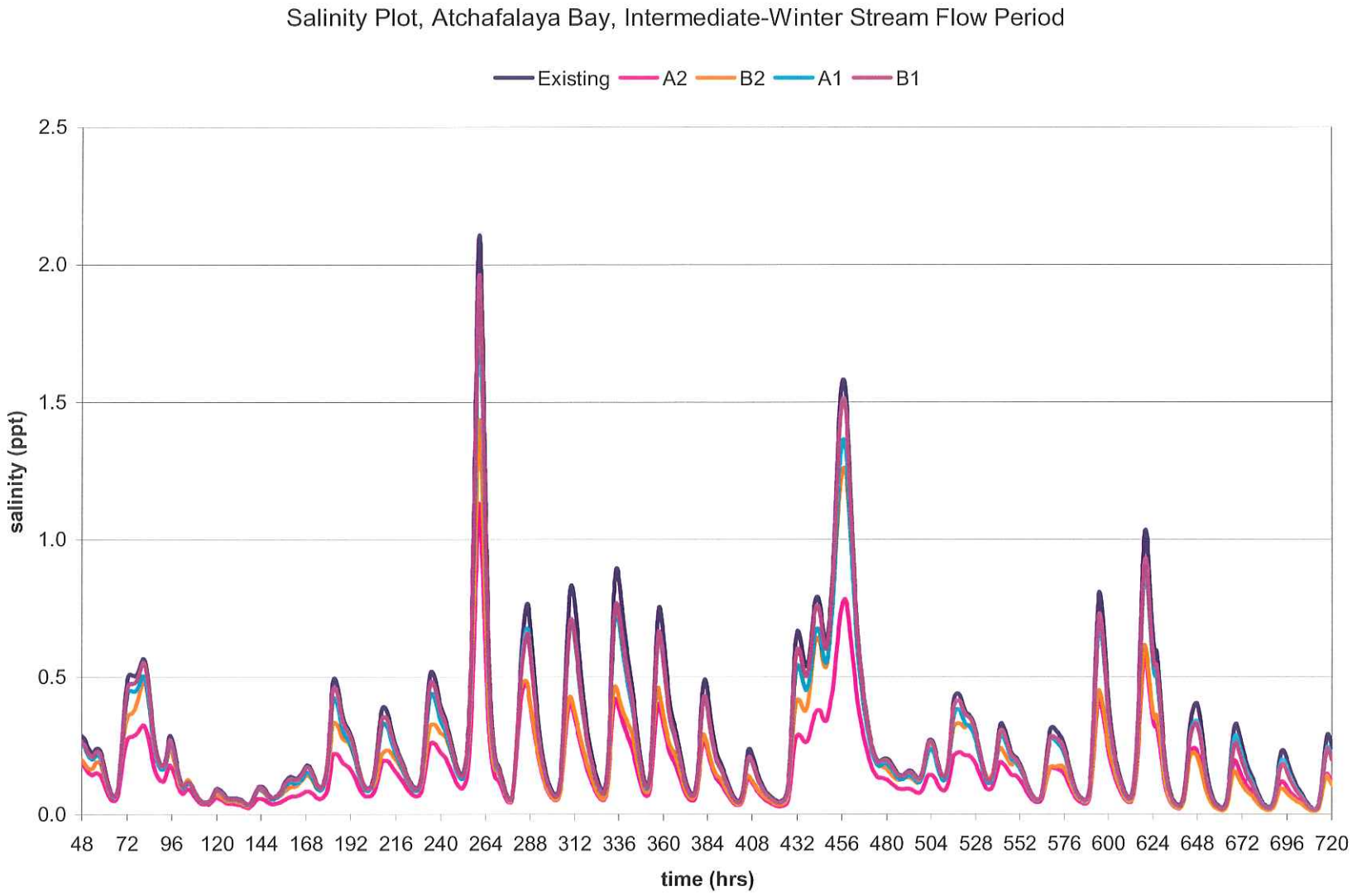
Salinity Plot, Atchafalaya Bay, Intermediate-Winter Stream Flow Period
Existing
A2
B2
A1
B1
2.5
2.0
1.5
1.0
0.5
0.0
salinity (ppt)
48 72 96 120 144 168 192 216 240 264 288 312 336 360 384 408 432 456 480 504 528 552 576 600 624 648 672 696 720
time (hrs)

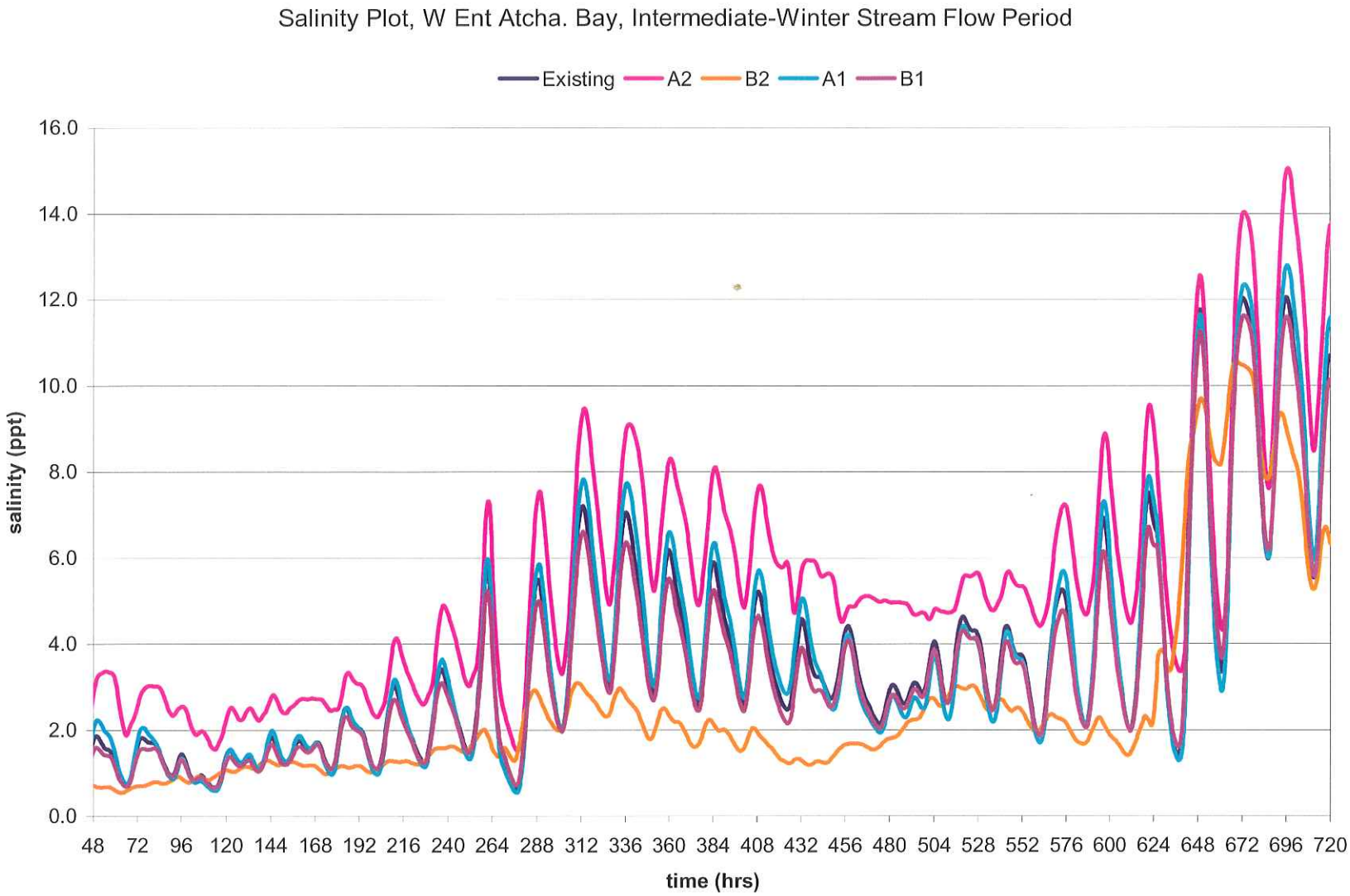
Salinity Plot, W Ent Atcha. Bay, Intermediate-Winter Stream Flow Period
Existing
A2
B2
A1
B1
16.0
14.0
12.0
10.0
8.0
6.0
4.0
2.0
0.0
salinity (ppt)
48 72 96 120 144 168 192 216 240 264 288 312 336 360 384 408 432 456 480 504 528 552 576 600 624 648 672 696 720
time (hrs)

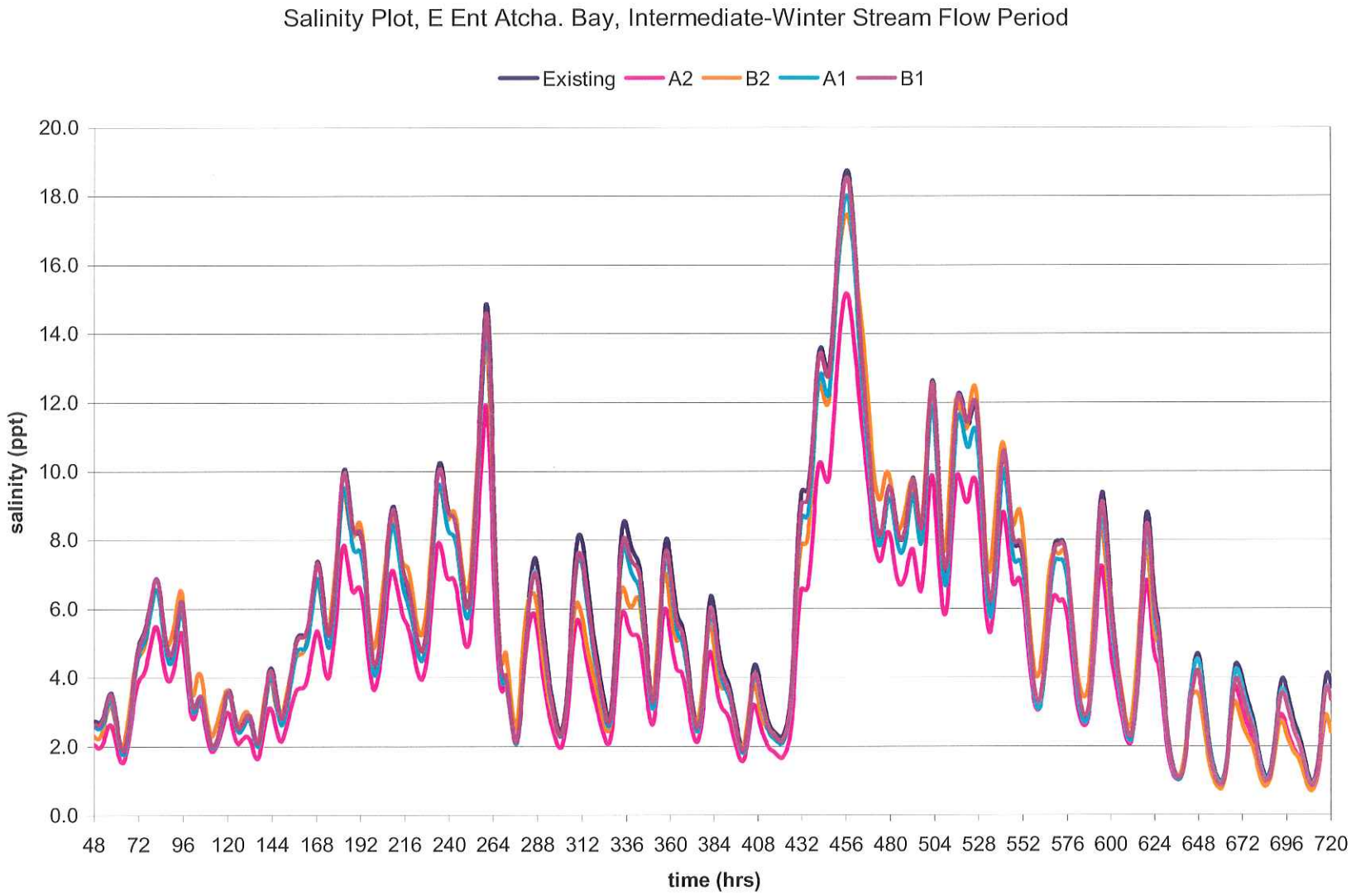
Salinity Plot, E Ent Atcha. Bay, Intermediate-Winter Stream Flow Period
Existing
A2
B2
A1
B1
20.0
18.0
16.0
14.0
12.0
10.0
8.0
6.0
4.0
2.0
0.0
salinity (ppt)
48 72 96 120 144 168 192 216 240 264 288 312 336 360 384 408 432 456 480 504 528 552 576 600 624 648 672 696 720
time (hrs)

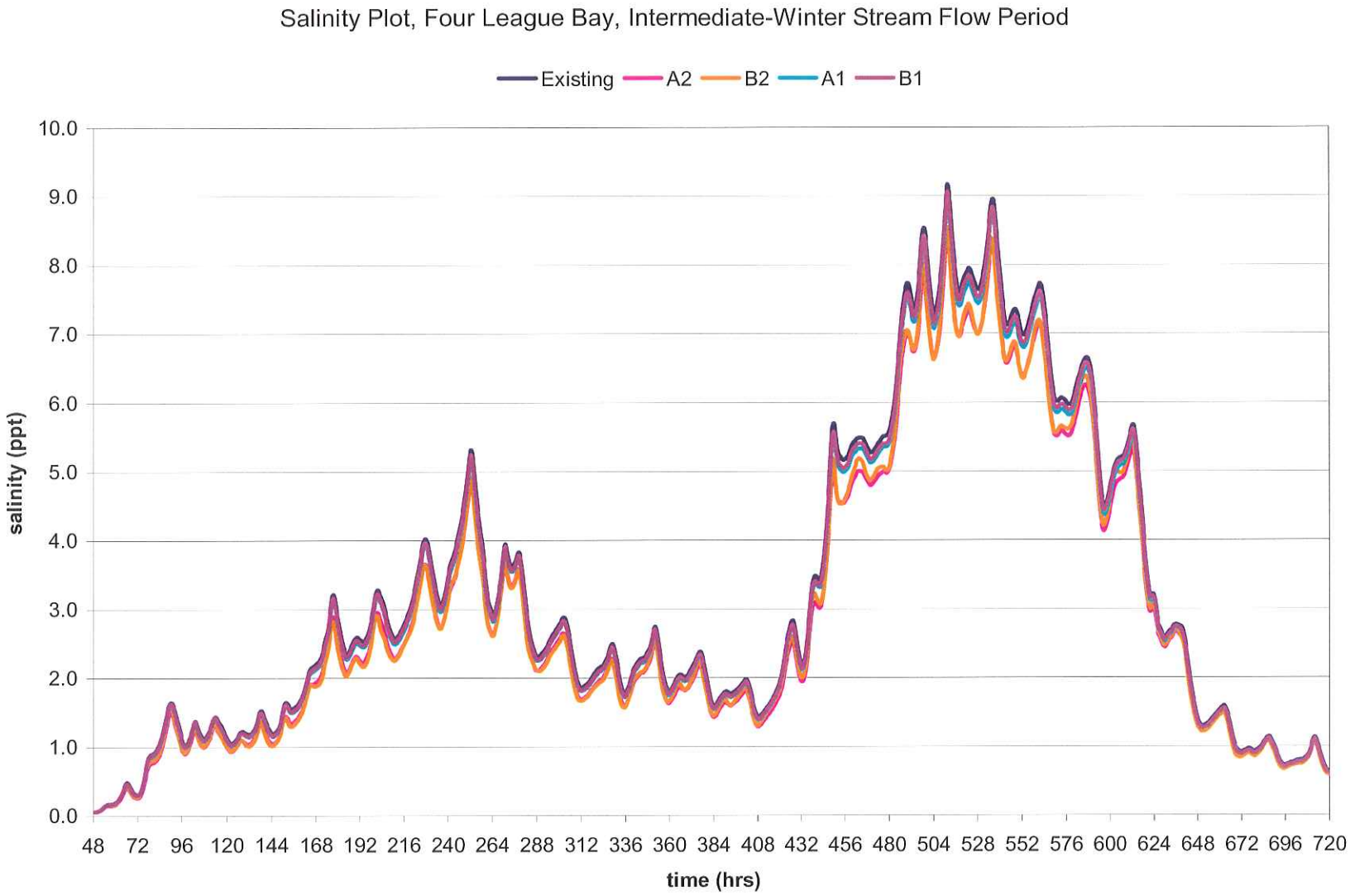
Salinity Plot, Four League Bay, Intermediate-Winter Stream Flow Period
Existing
A2
B2
A1
B1
salinity (ppt)
10.0
9.0
8.0
7.0
6.0
5.0
4.0
3.0
2.0
1.0
0.0
48 72 96 120 144 168 192 216 240 264 288 312 336 360 384 408 432 456 480 504 528 552 576 600 624 648 672 696 720
time (hrs)

Appendix C

Turbidity Time Series Plots

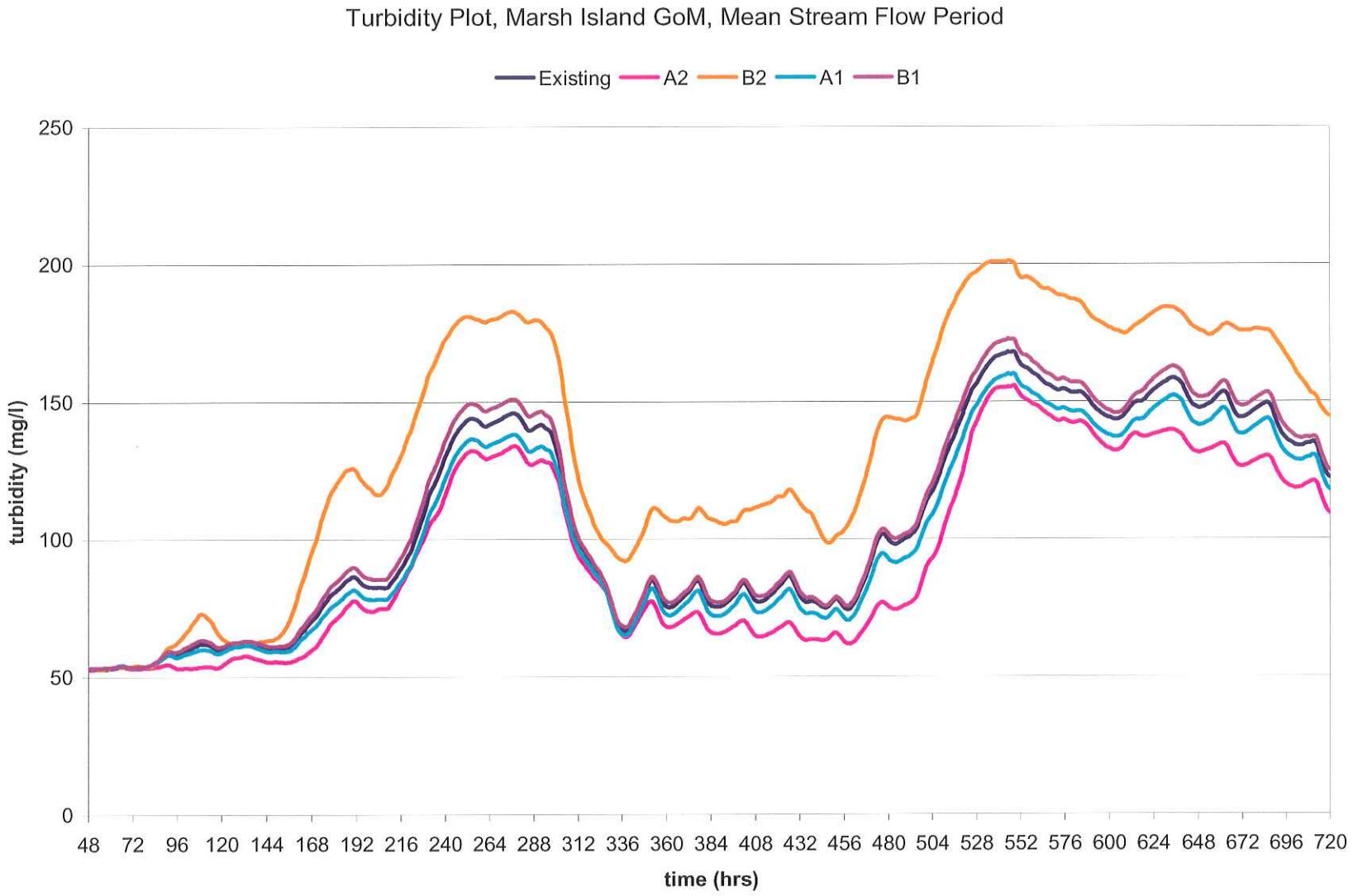
Turbidity Plot, Marsh Island GoM, Mean Stream Flow Period
Existing
A2
B2
A1
B1
250
200
150
100
50
0
turbidity (mg/l)
48 72 96 120 144 168 192 216 240 264 288 312 336 360 384 408 432 456 480 504 528 552 576 600 624 648 672 696 720
time (hrs)

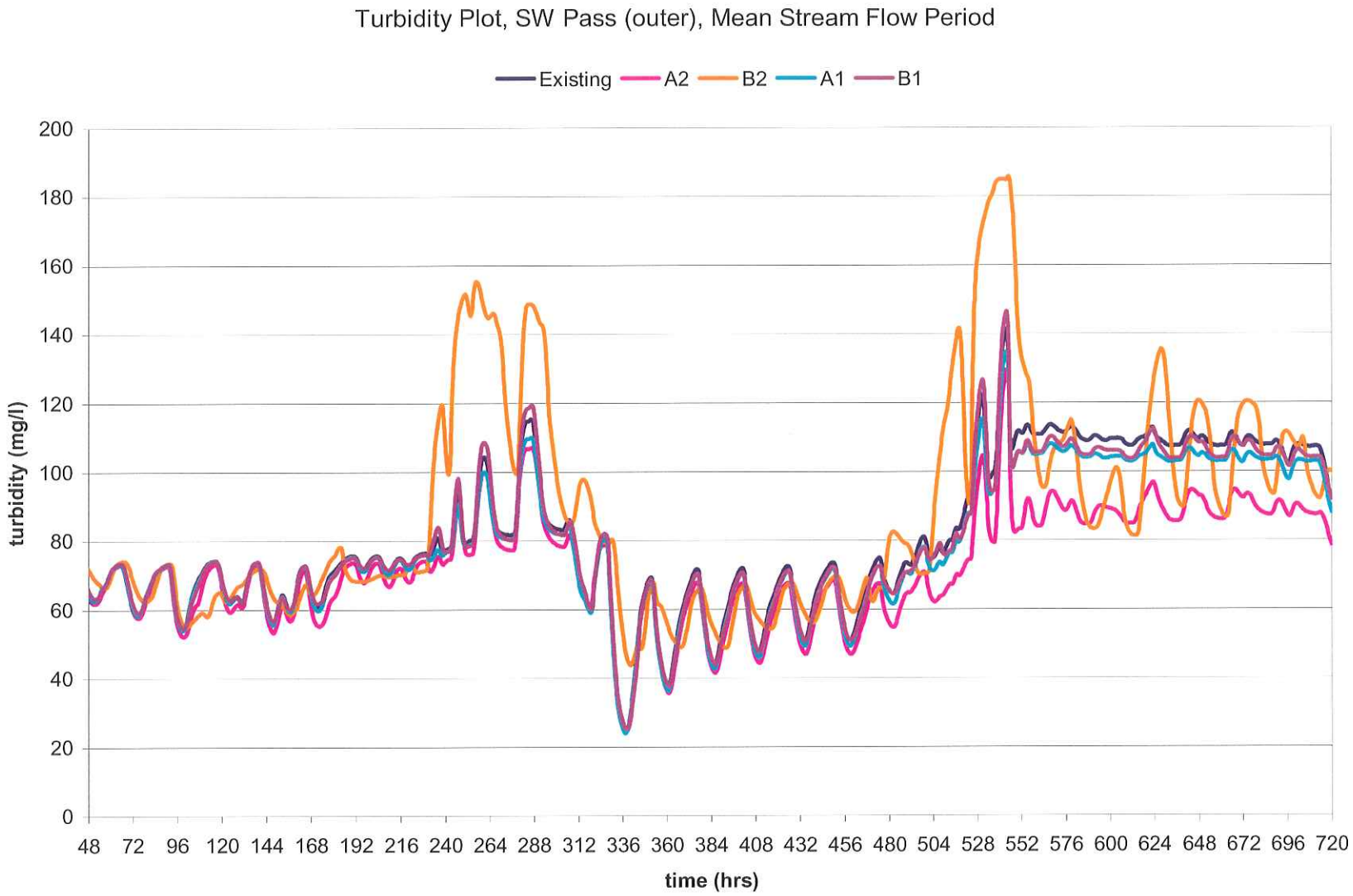
Turbidity Plot, SW Pass (outer), Mean Stream Flow Period
Existing
A2
B2
A1
B1
turbidity (mg/l)
0
20
40
60
80
100
120
140
160
180
200
48
72
96
120
144
168
192
216
240
264
288
312
336
360
384
408
432
456
480
504
528
552
576
600
624
648
672
696
720
time (hrs)

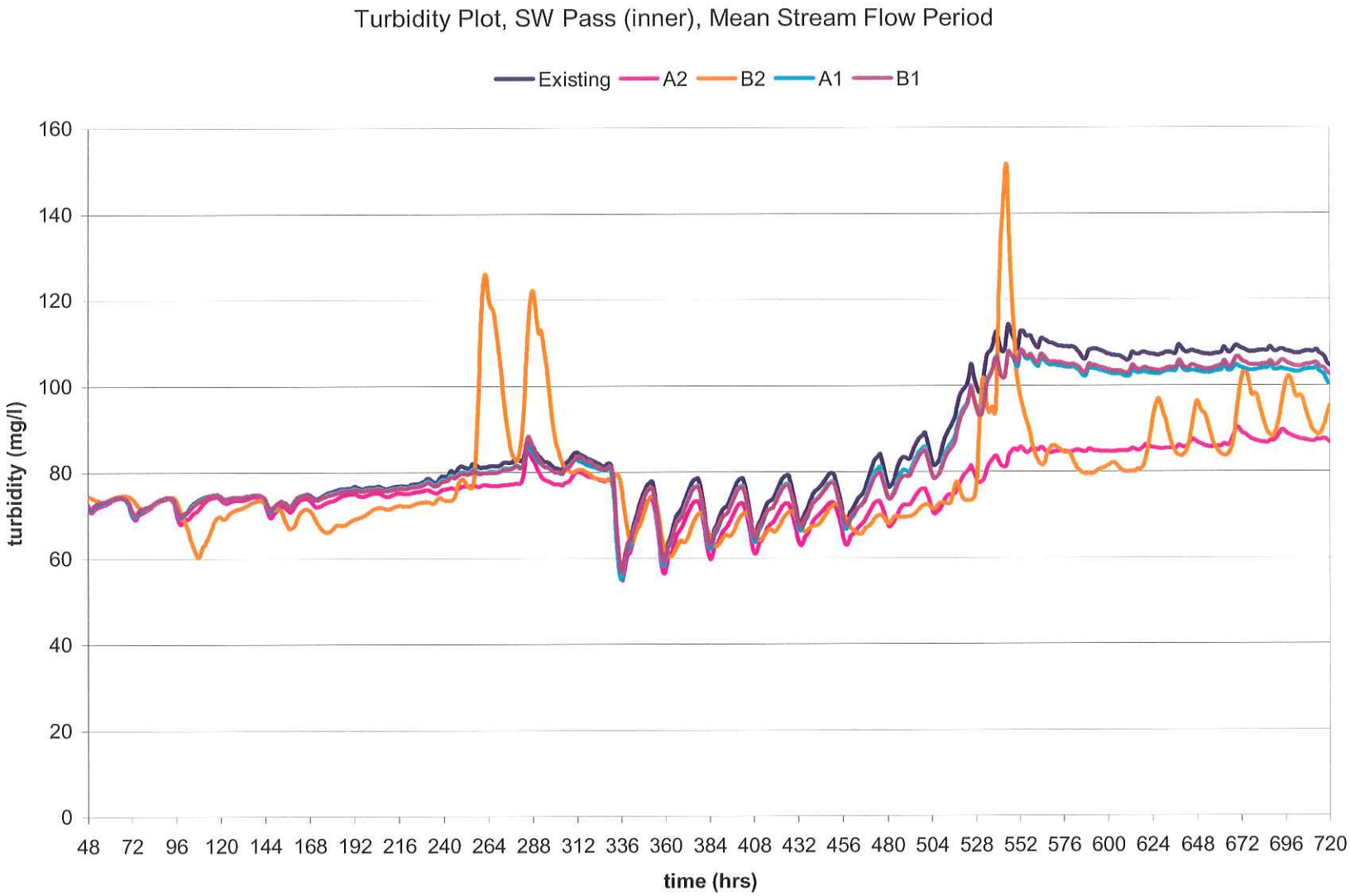
Turbidity Plot, SW Pass (inner), Mean Stream Flow Period
Existing
A2
B2
A1
B1
turbidity (mg/l)
0
20
40
60
80
100
120
140
160
48 72 96 120 144 168 192 216 240 264 288 312 336 360 384 408 432 456 480 504 528 552 576 600 624 648 672 696 720
time (hrs)

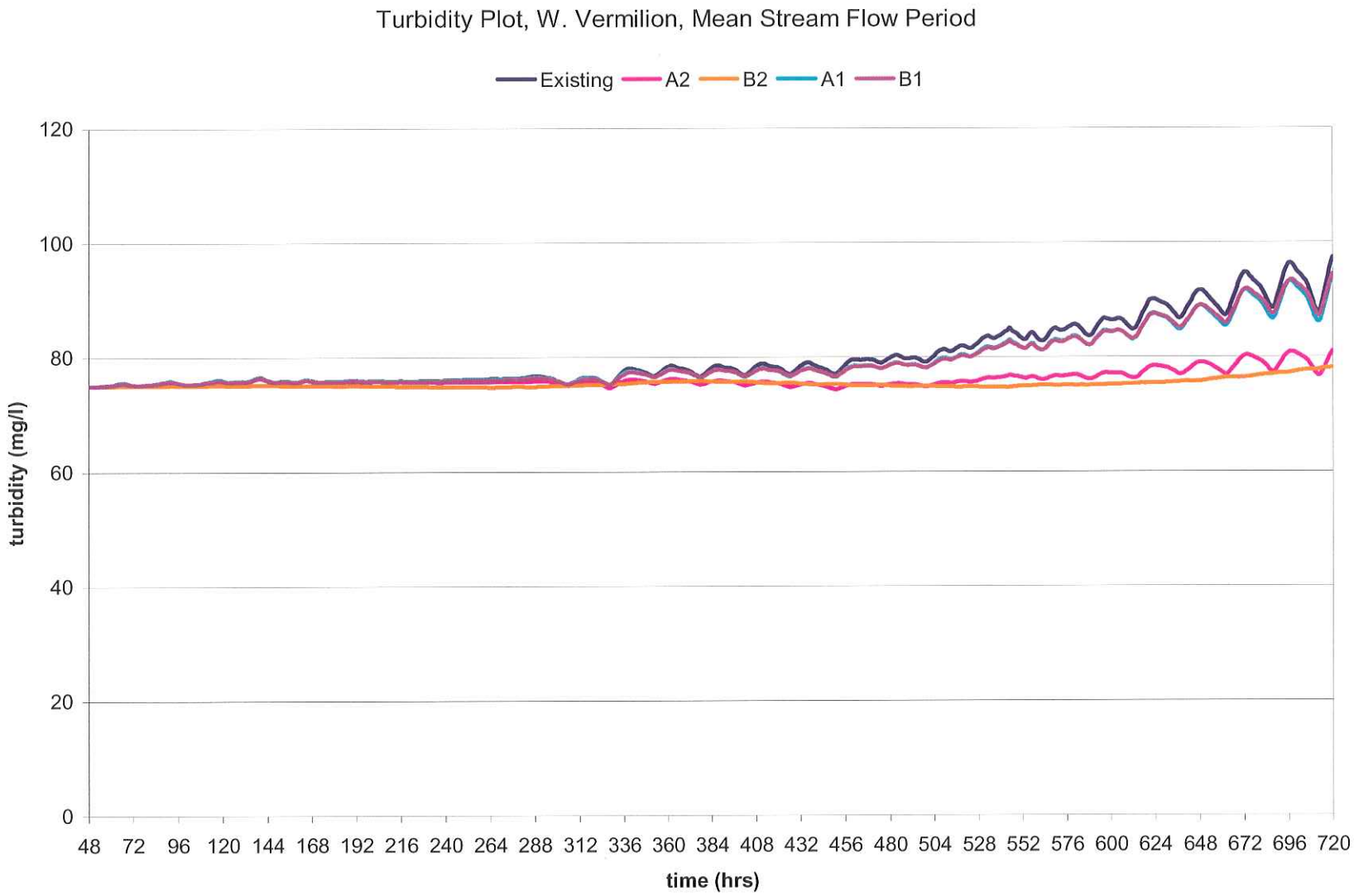
Turbidity Plot, W. Vermilion, Mean Stream Flow Period
Existing
A2
B2
A1
B1
120
100
80
60
40
20
0
turbidity (mg/l)
48 72 96 120 144 168 192 216 240 264 288 312 336 360 384 408 432 456 480 504 528 552 576 600 624 648 672 696 720
time (hrs)

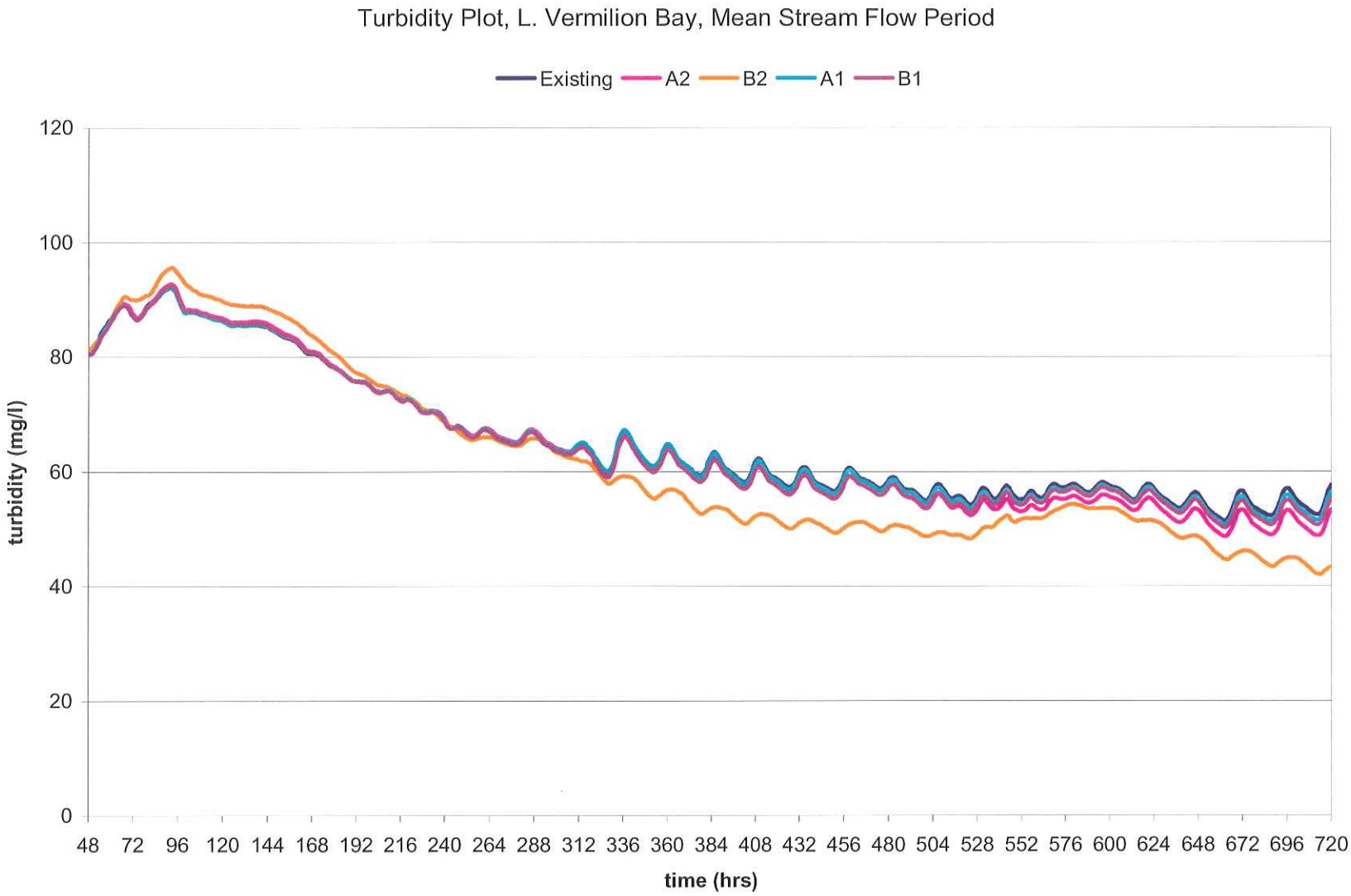
Turbidity Plot, L. Vermilion Bay, Mean Stream Flow Period
Existing
A2
B2
A1
B1
120
100
80
60
40
20
0
turbidity (mg/l)
48 72 96 120 144 168 192 216 240 264 288 312 336 360 384 408 432 456 480 504 528 552 576 600 624 648 672 696 720
time (hrs)

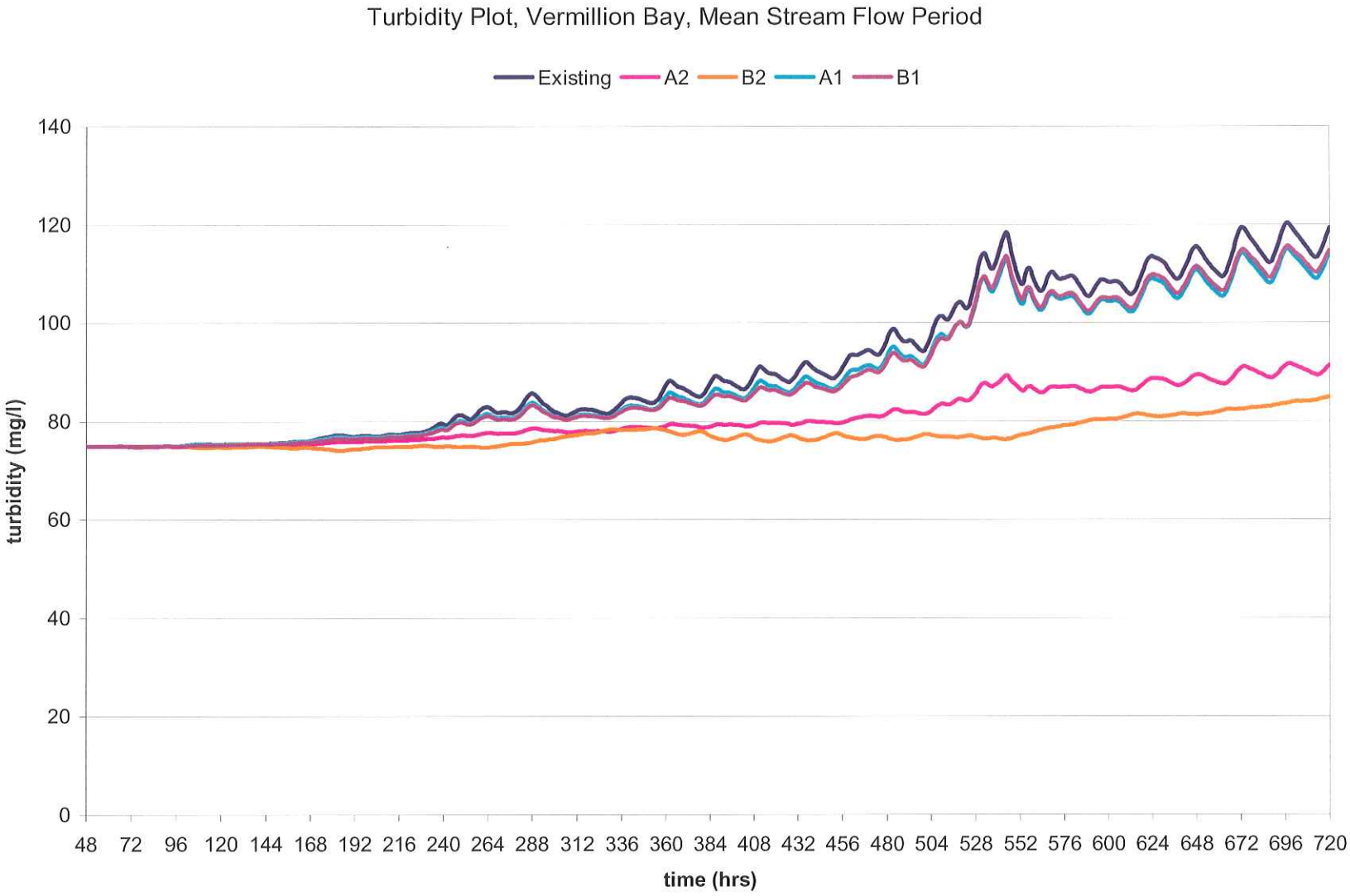
Turbidity Plot, Vermillion Bay, Mean Stream Flow Period
Existing
A2
B2
A1
B1
140
120
100
80
60
40
20
0
turbidity (mg/l)
48 72 96 120 144 168 192 216 240 264 288 312 336 360 384 408 432 456 480 504 528 552 576 600 624 648 672 696 720
time (hrs)

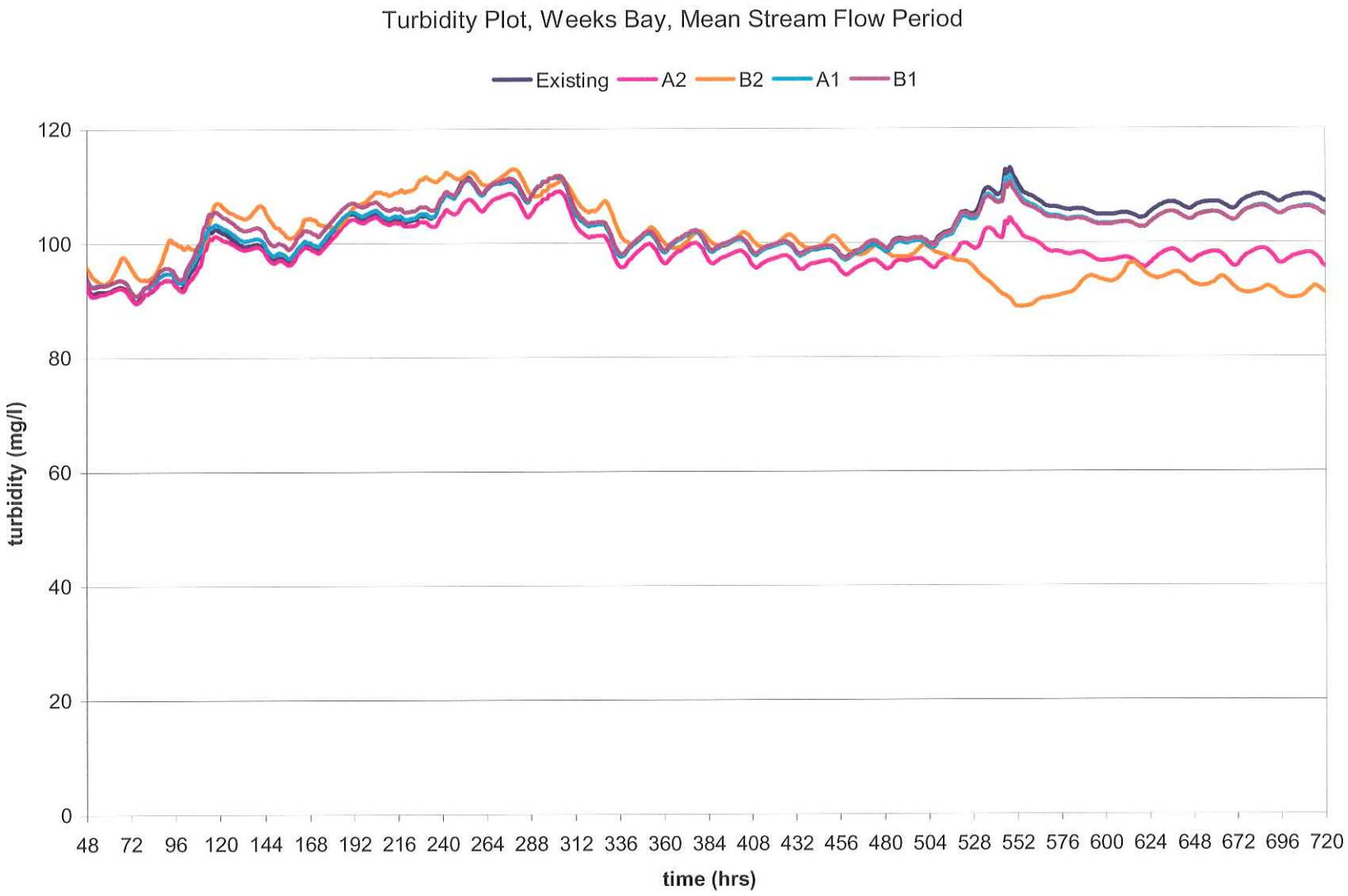
Turbidity Plot, Weeks Bay, Mean Stream Flow Period
Existing
A2
B2
A1
B1
120
100
80
60
40
20
0
turbidity (mg/l)
48 72 96 120 144 168 192 216 240 264 288 312 336 360 384 408 432 456 480 504 528 552 576 600 624 648 672 696 720
time (hrs)

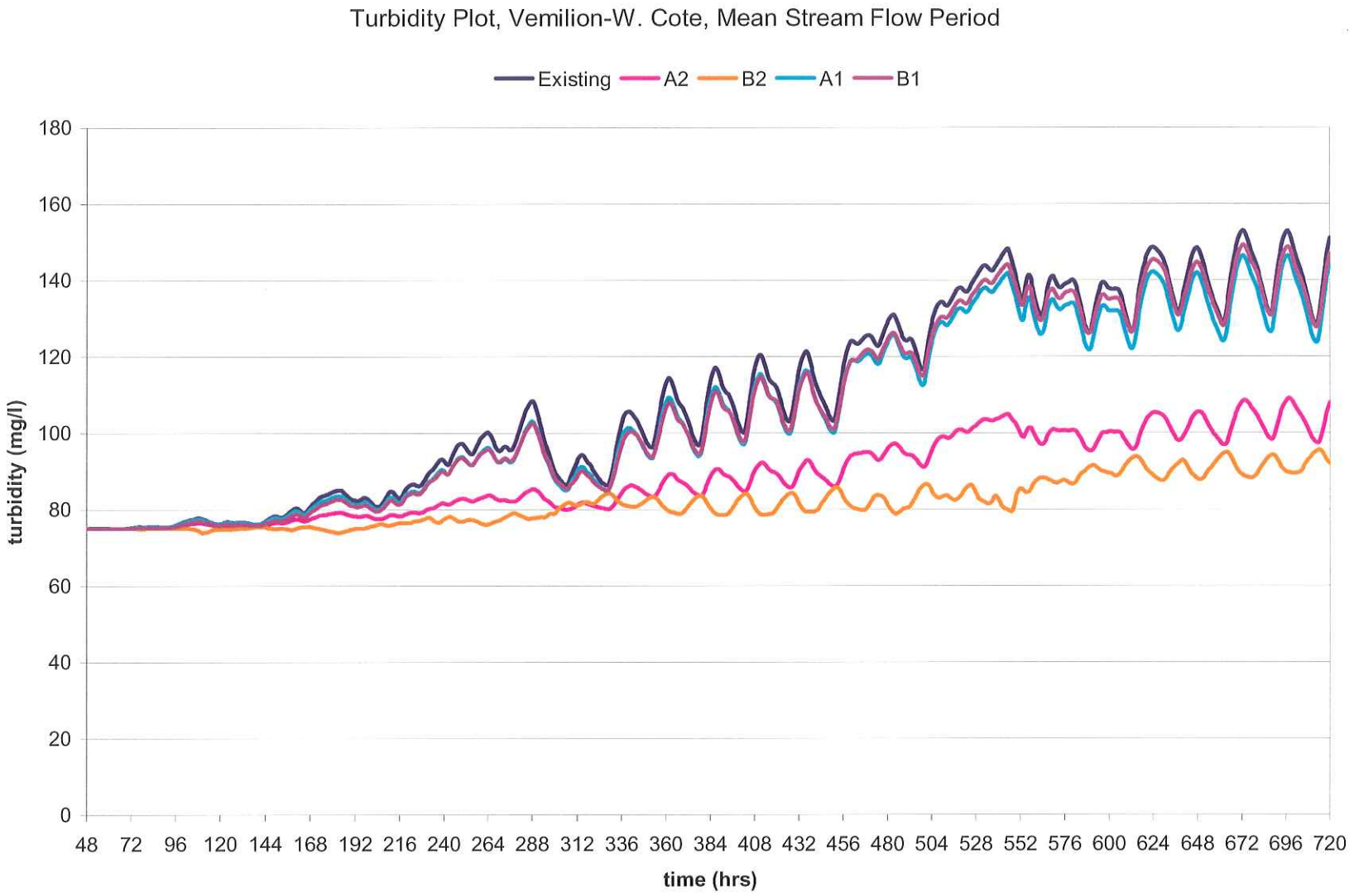
Turbidity Plot, Vemilion-W. Cote, Mean Stream Flow Period
Existing
A2
B2
A1
B1
turbidity (mg/l)
0
20
40
60
80
100
120
140
160
180
48 72 96 120 144 168 192 216 240 264 288 312 336 360 384 408 432 456 480 504 528 552 576 600 624 648 672 696 720
time (hrs)

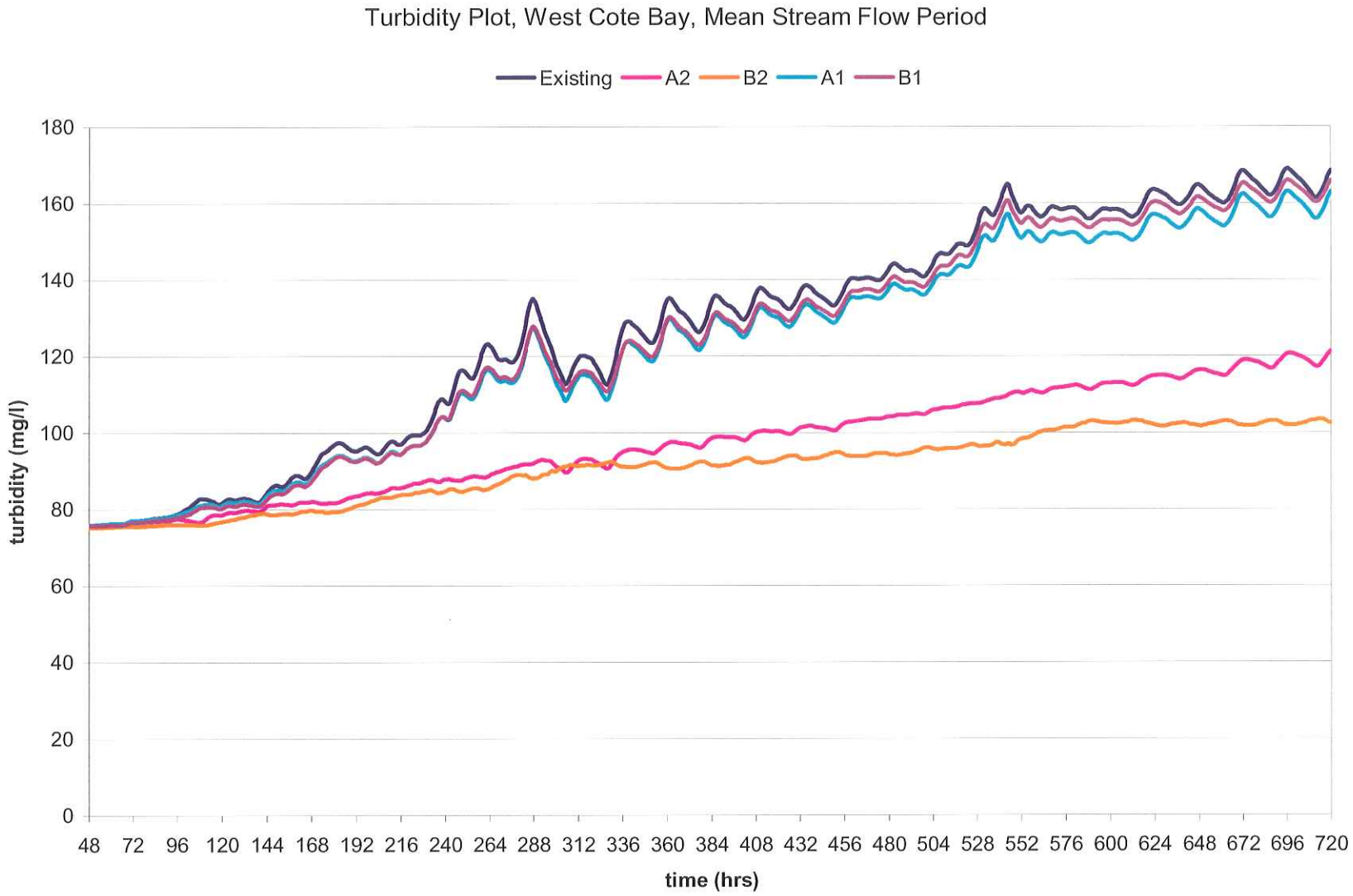
Turbidity Plot, West Cote Bay, Mean Stream Flow Period
Existing
A2
B2
A1
B1
turbidity (mg/l)
0
20
40
60
80
100
120
140
160
180
48 72 96 120 144 168 192 216 240 264 288 312 336 360 384 408 432 456 480 504 528 552 576 600 624 648 672 696 720
time (hrs)

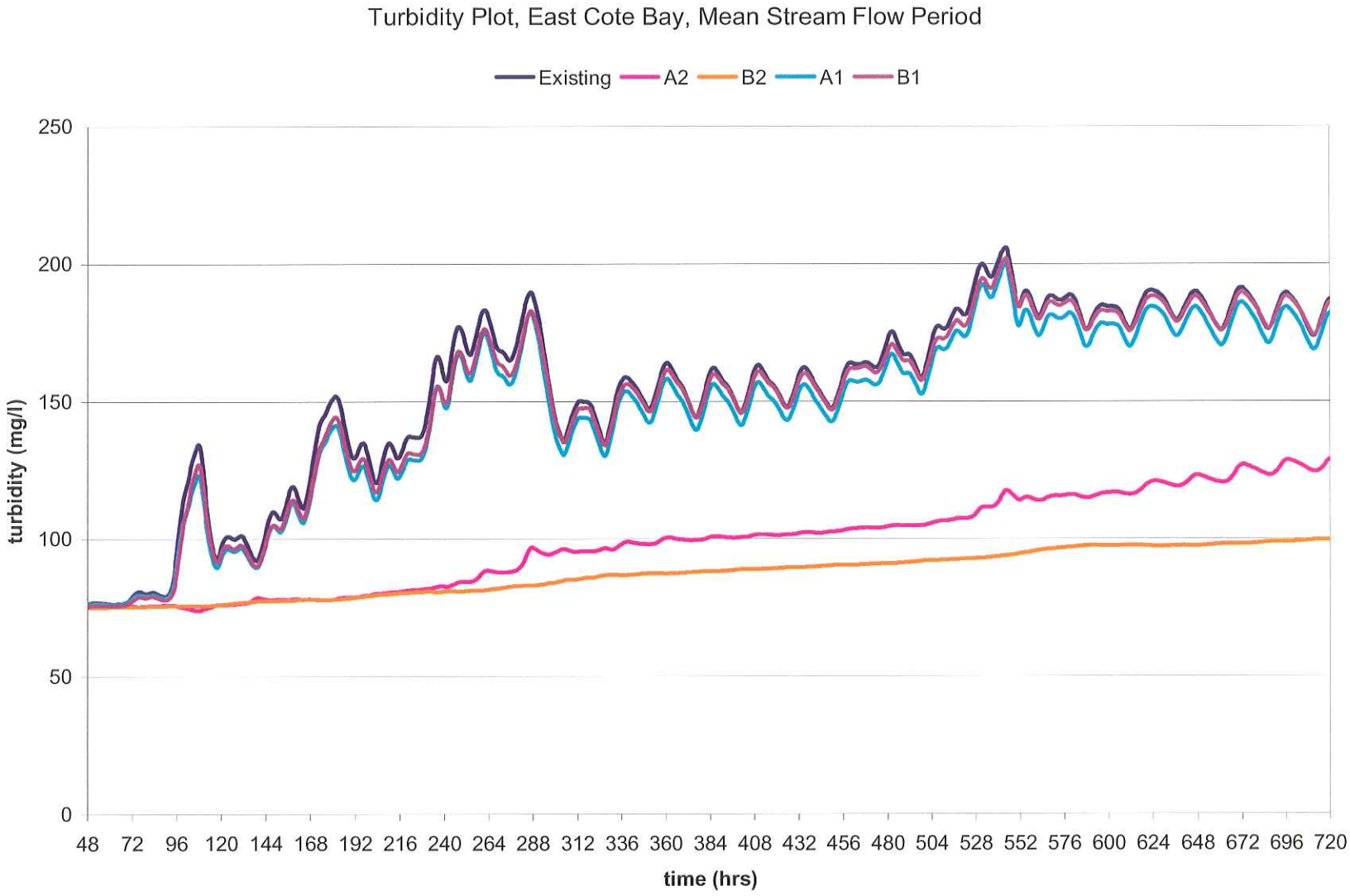
Turbidity Plot, East Cote Bay, Mean Stream Flow Period
Existing
A2
B2
A1
B1
250
200
150
100
50
0
turbidity (mg/l)
48 72 96 120 144 168 192 216 240 264 288 312 336 360 384 408 432 456 480 504 528 552 576 600 624 648 672 696 720
time (hrs)

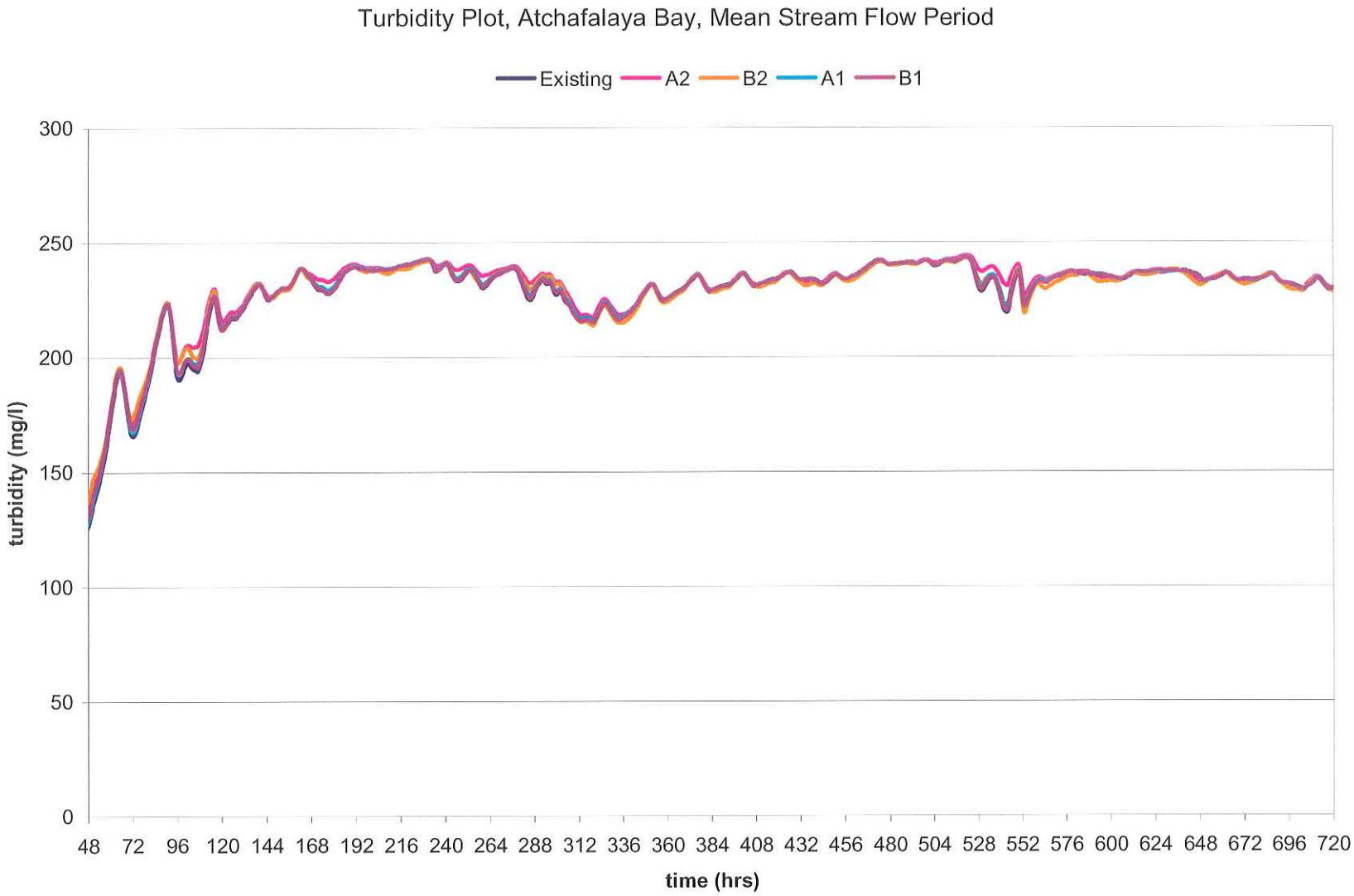
Turbidity Plot, Atchafalaya Bay, Mean Stream Flow Period
Existing
A2
B2
A1
B1
300
250
200
150
100
50
0
turbidity (mg/l)
48 72 96 120 144 168 192 216 240 264 288 312 336 360 384 408 432 456 480 504 528 552 576 600 624 648 672 696 720
time (hrs)

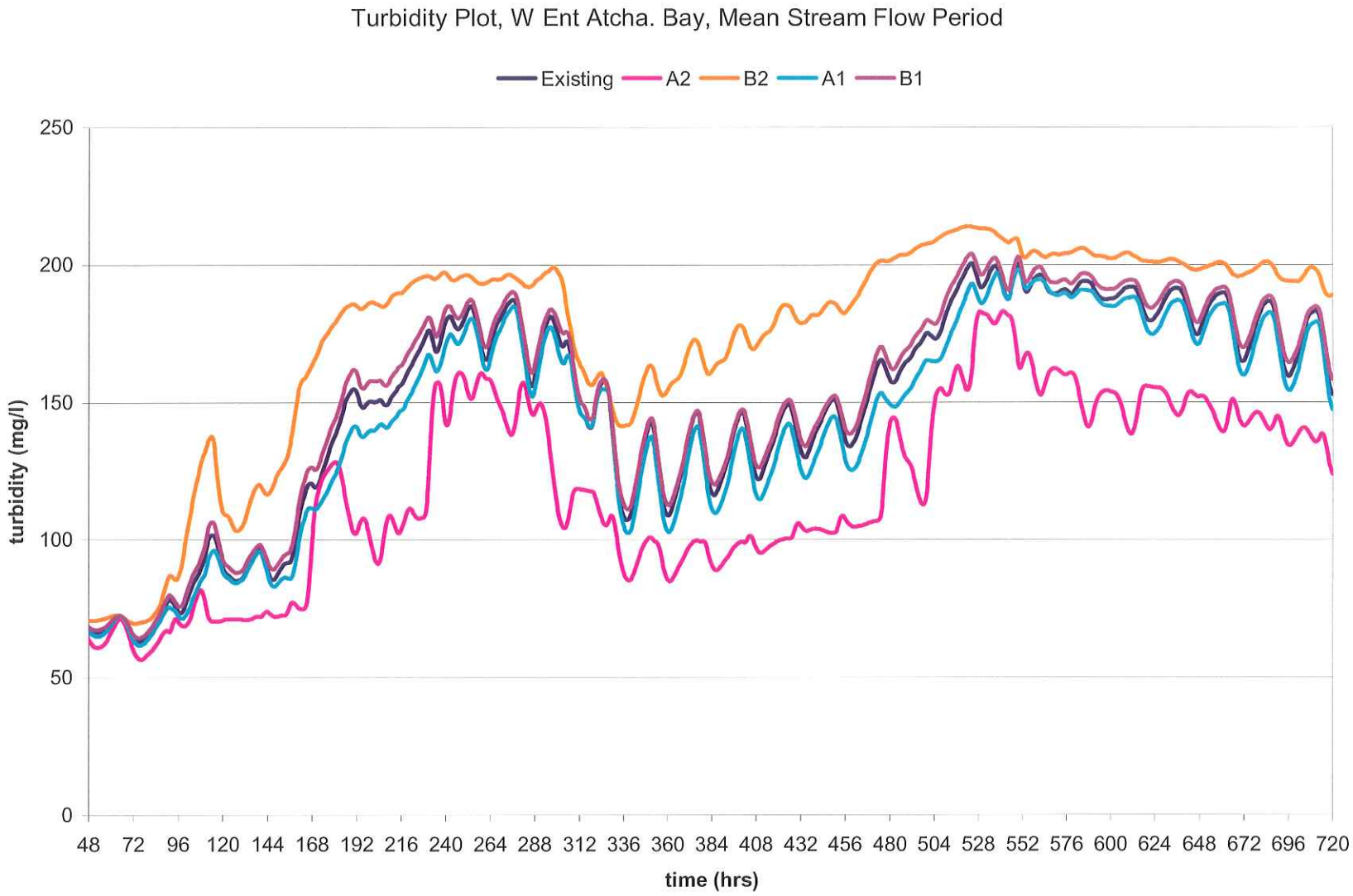
Turbidity Plot, W Ent Atcha. Bay, Mean Stream Flow Period
Existing
A2
B2
A1
B1
250
200
150
100
50
0
turbidity (mg/l)
48 72 96 120 144 168 192 216 240 264 288 312 336 360 384 408 432 456 480 504 528 552 576 600 624 648 672 696 720
time (hrs)

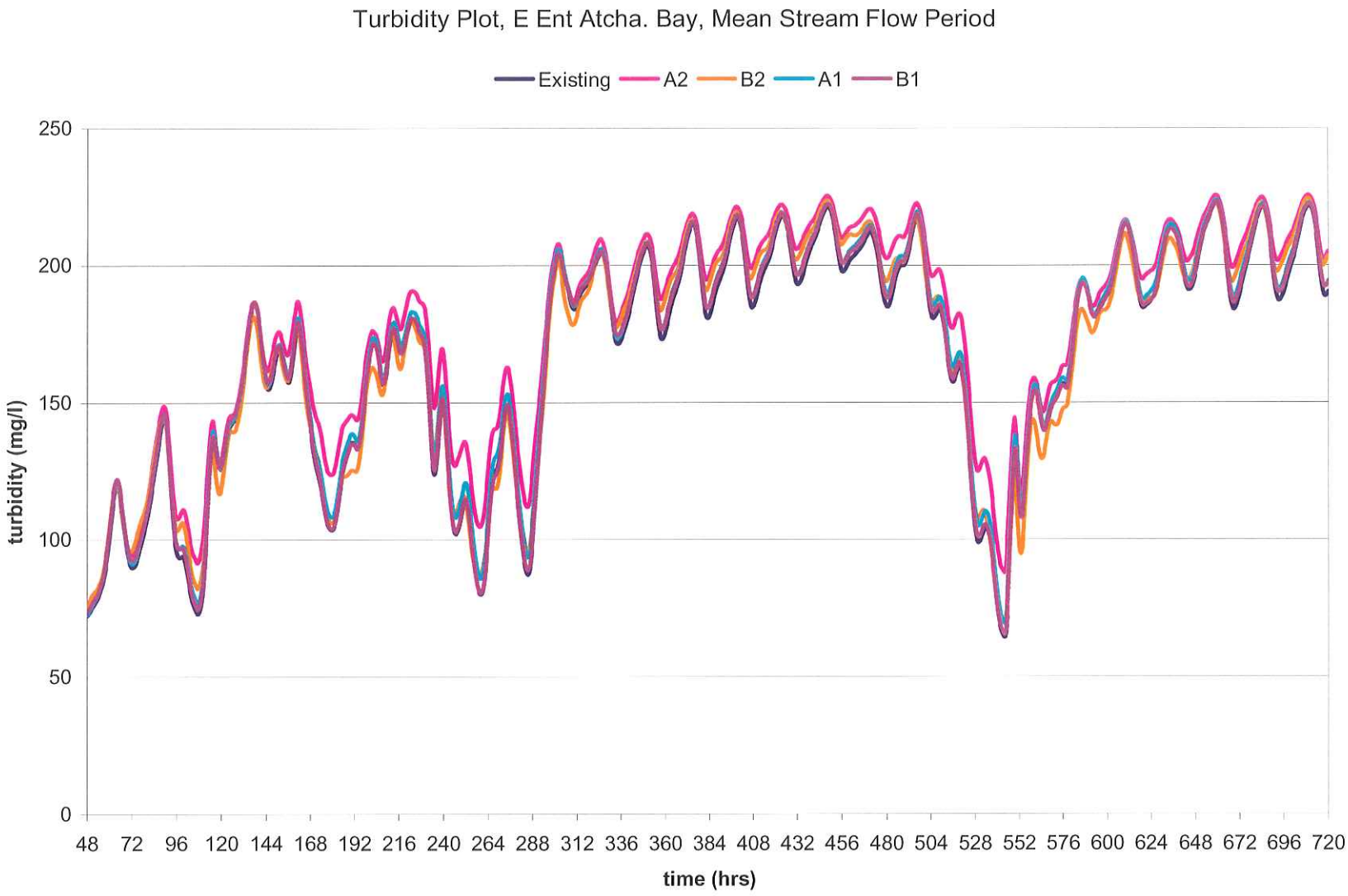
Turbidity Plot, E Ent Atcha. Bay, Mean Stream Flow Period
Existing
A2
B2
A1
B1
250
200
150
100
50
0
turbidity (mg/l)
48 72 96 120 144 168 192 216 240 264 288 312 336 360 384 408 432 456 480 504 528 552 576 600 624 648 672 696 720
time (hrs)

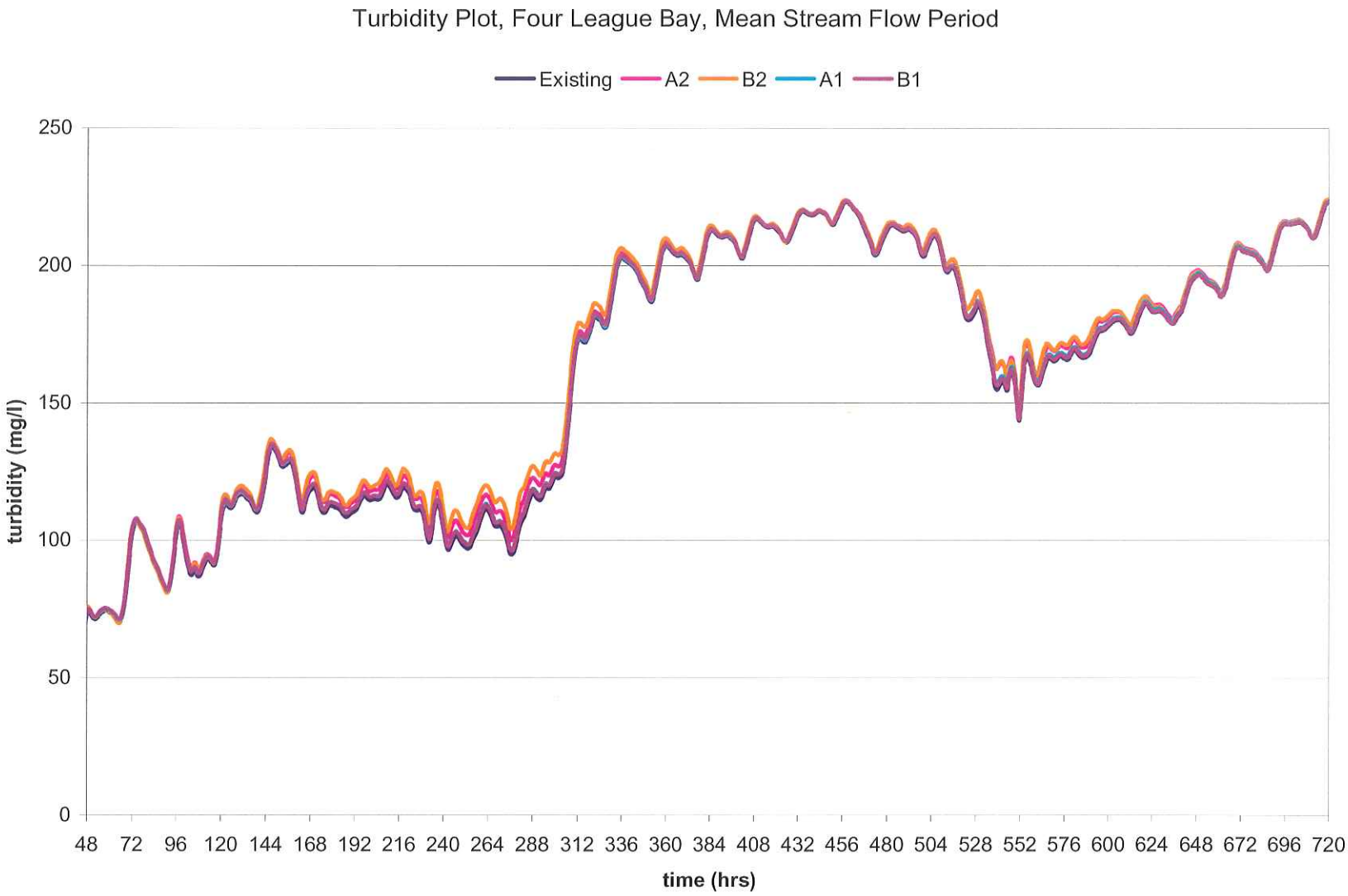
Turbidity Plot, Four League Bay, Mean Stream Flow Period
Existing
A2
B2
A1
B1
250
200
150
100
50
0
turbidity (mg/l)
48 72 96 120 144 168 192 216 240 264 288 312 336 360 384 408 432 456 480 504 528 552 576 600 624 648 672 696 720
time (hrs)

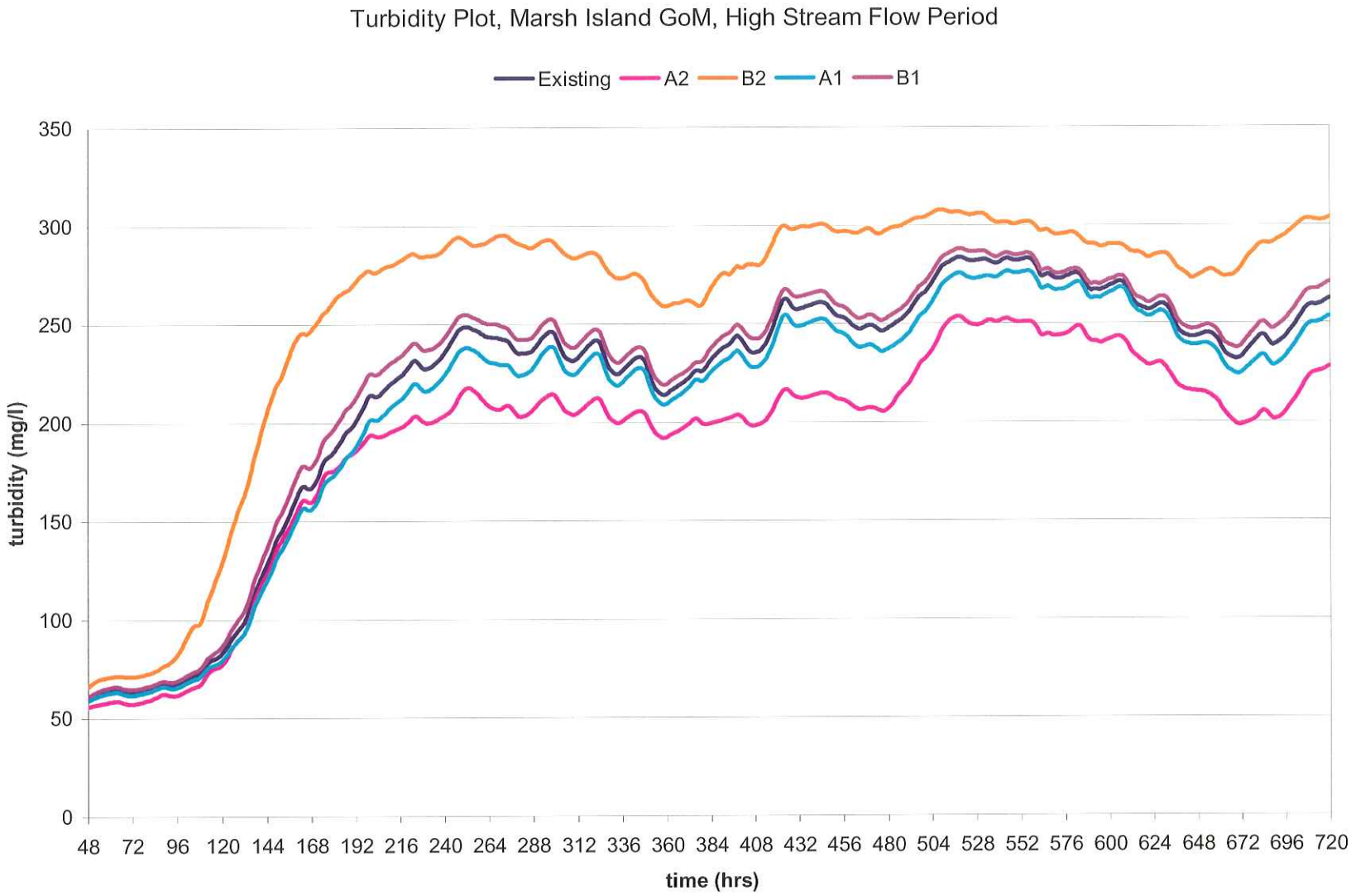
Turbidity Plot, Marsh Island GoM, High Stream Flow Period
Existing
A2
B2
A1
B1
350
300
250
200
150
100
50
0
turbidity (mg/l)
48 72 96 120 144 168 192 216 240 264 288 312 336 360 384 408 432 456 480 504 528 552 576 600 624 648 672 696 720
time (hrs)

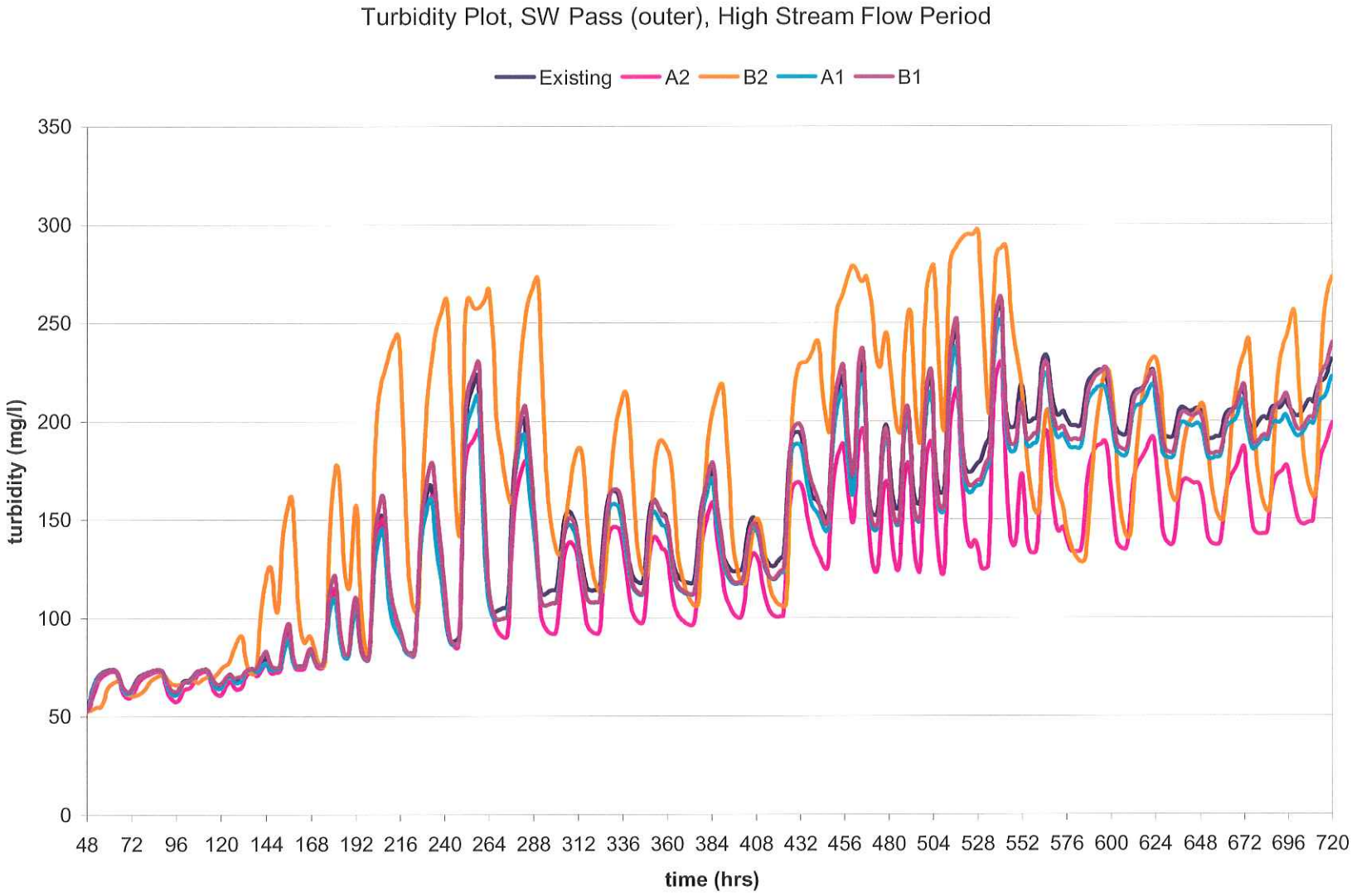
Turbidity Plot, SW Pass (outer), High Stream Flow Period
Existing
A2
B2
A1
B1
350
300
250
200
150
100
50
0
turbidity (mg/l)
48 72 96 120 144 168 192 216 240 264 288 312 336 360 384 408 432 456 480 504 528 552 576 600 624 648 672 696 720
time (hrs)

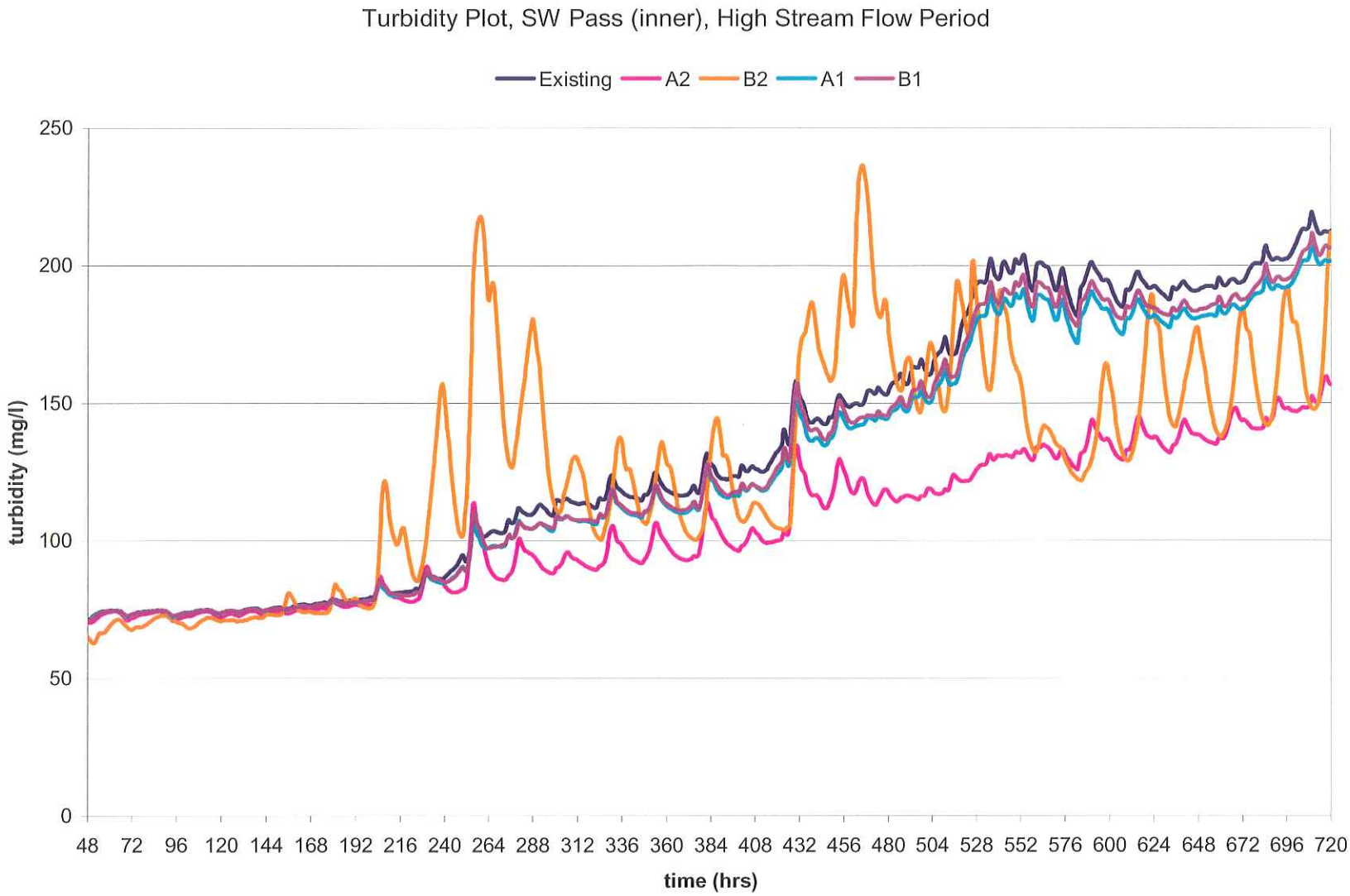
Turbidity Plot, SW Pass (inner), High Stream Flow Period
Existing
A2
B2
A1
B1
250
200
150
100
50
0
turbidity (mg/l)
48 72 96 120 144 168 192 216 240 264 288 312 336 360 384 408 432 456 480 504 528 552 576 600 624 648 672 696 720
time (hrs)

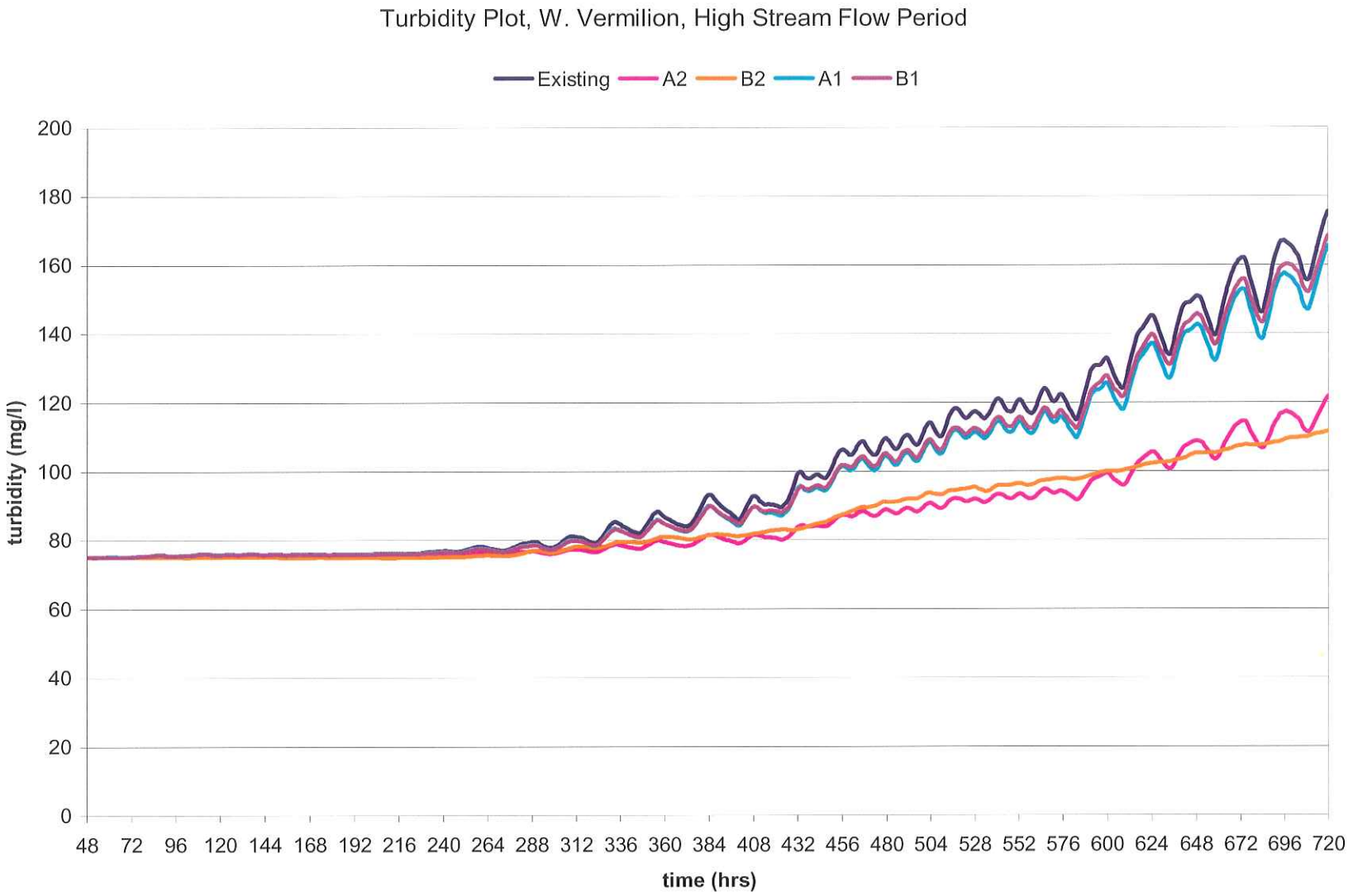
Turbidity Plot, W. Vermilion, High Stream Flow Period
Existing
A2
B2
A1
B1
turbidity (mg/l)
0
20
40
60
80
100
120
140
160
180
200
48 72 96 120 144 168 192 216 240 264 288 312 336 360 384 408 432 456 480 504 528 552 576 600 624 648 672 696 720
time (hrs)

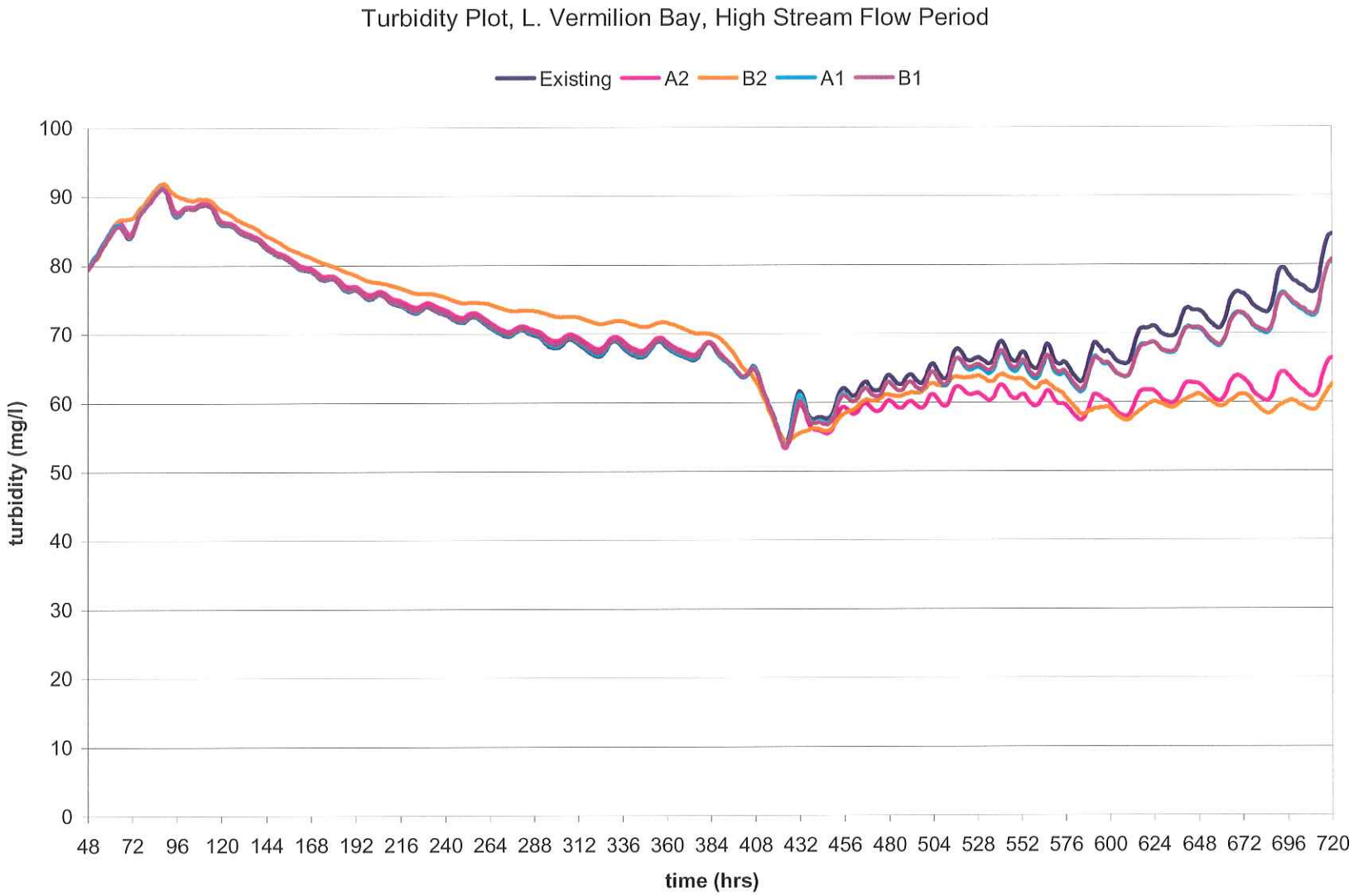
Turbidity Plot, L. Vermilion Bay, High Stream Flow Period
Existing
A2
B2
A1
B1
100
90
80
70
60
50
40
30
20
10
0
turbidity (mg/l)
48 72 96 120 144 168 192 216 240 264 288 312 336 360 384 408 432 456 480 504 528 552 576 600 624 648 672 696 720
time (hrs)

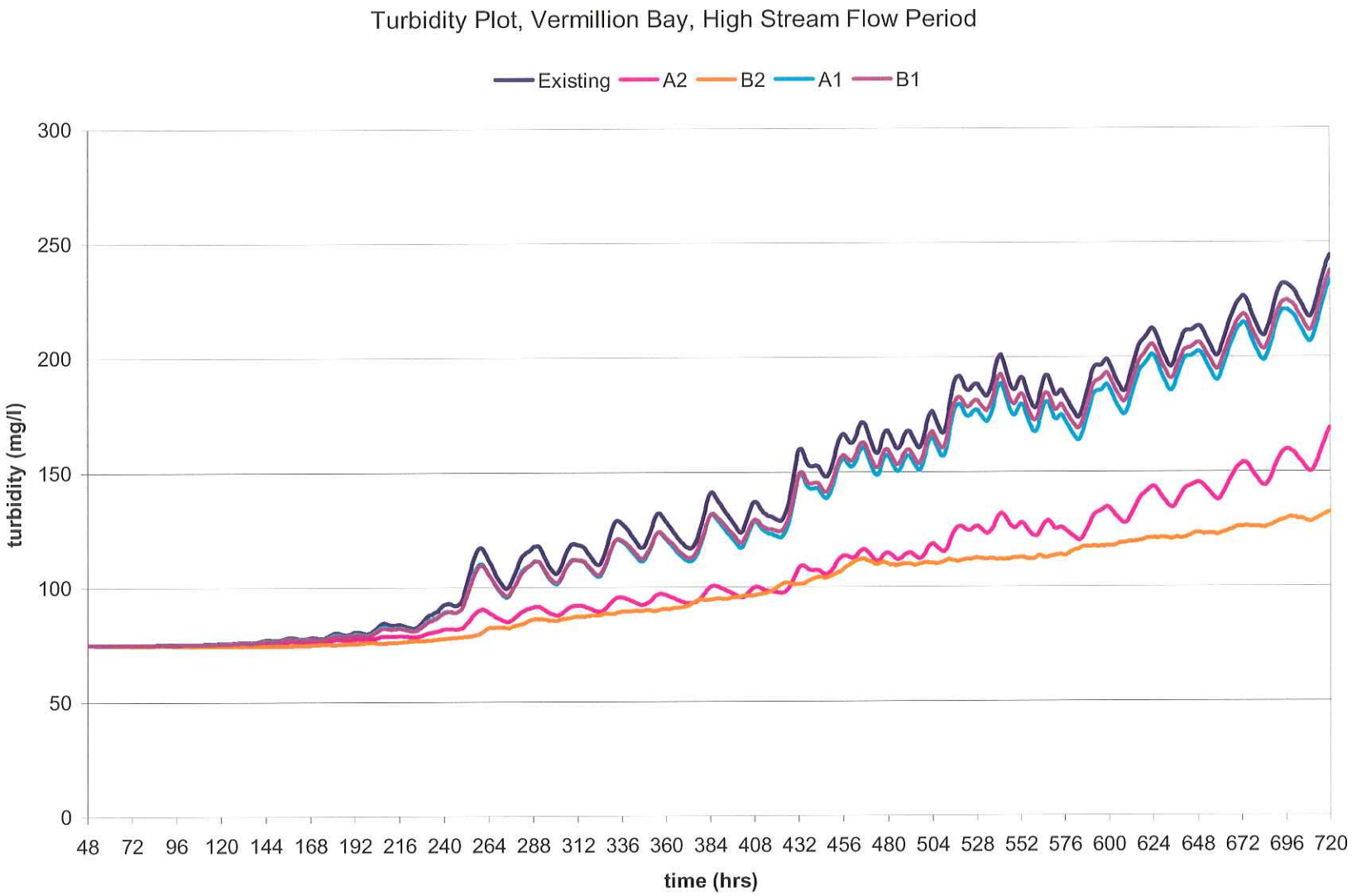
Turbidity Plot, Vermillion Bay, High Stream Flow Period
Existing
A2
B2
A1
B1
300
250
200
150
100
50
0
turbidity (mg/l)
48 72 96 120 144 168 192 216 240 264 288 312 336 360 384 408 432 456 480 504 528 552 576 600 624 648 672 696 720
time (hrs)

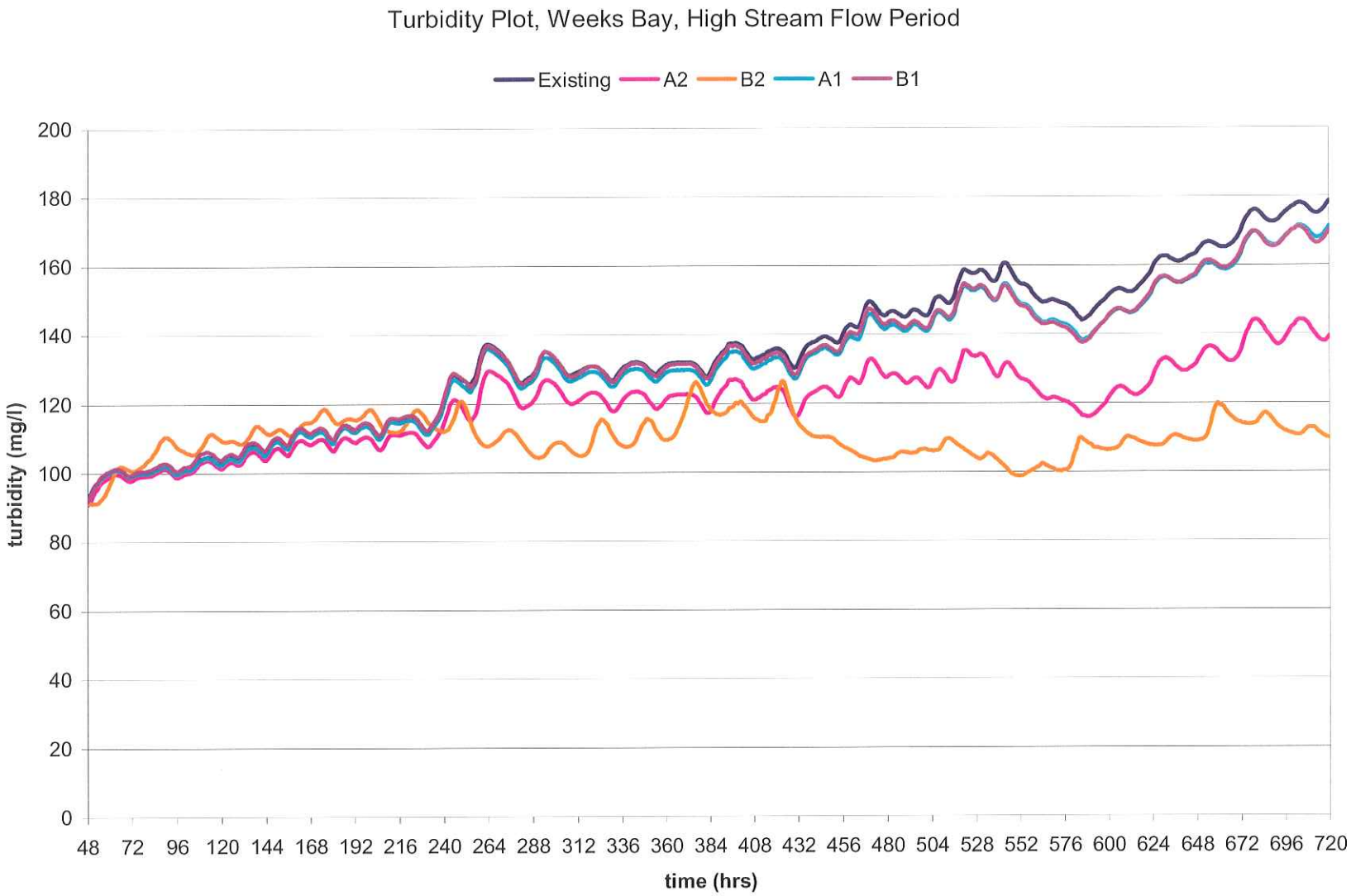
Turbidity Plot, Weeks Bay, High Stream Flow Period
Existing
A2
B2
A1
B1
turbidity (mg/l)
200
180
160
140
120
100
80
60
40
20
0
48 72 96 120 144 168 192 216 240 264 288 312 336 360 384 408 432 456 480 504 528 552 576 600 624 648 672 696 720
time (hrs)

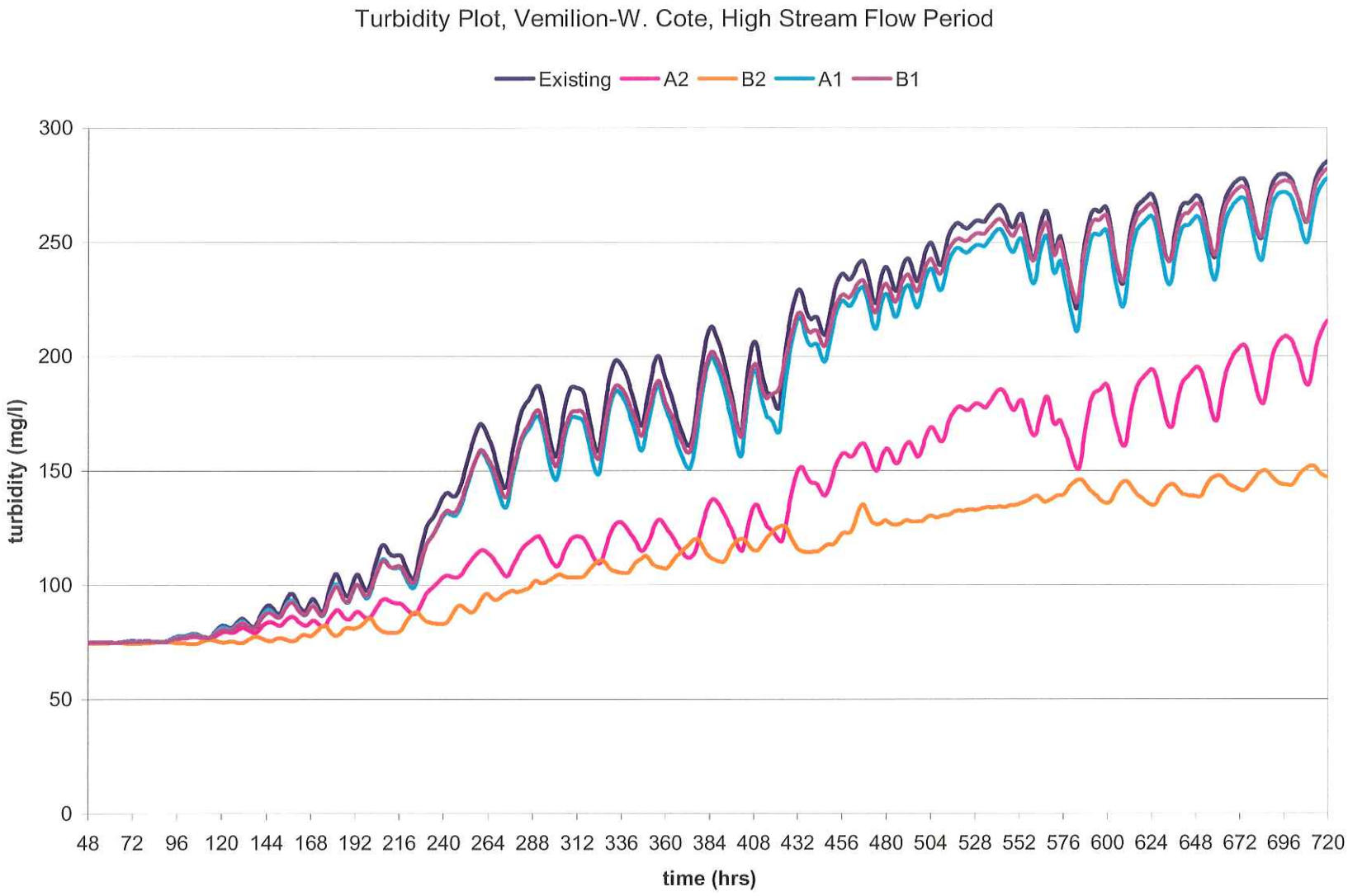
Turbidity Plot, Vemilion-W. Cote, High Stream Flow Period
Existing
A2
B2
A1
B1
300
250
200
150
100
50
0
turbidity (mg/l)
48 72 96 120 144 168 192 216 240 264 288 312 336 360 384 408 432 456 480 504 528 552 576 600 624 648 672 696 720
time (hrs)

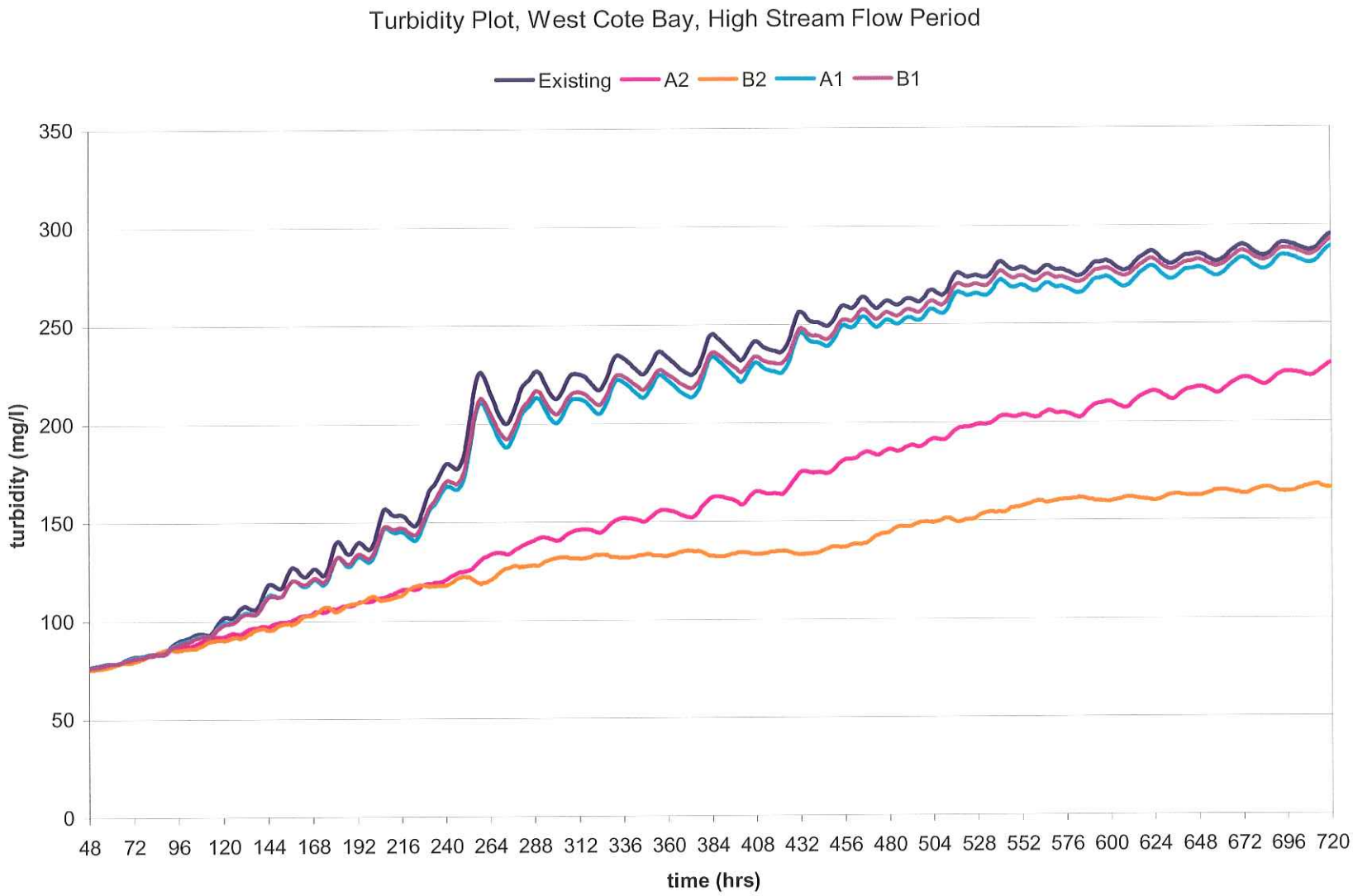
Turbidity Plot, West Cote Bay, High Stream Flow Period
Existing
A2
B2
A1
B1
350
300
250
200
150
100
50
0
turbidity (mg/l)
48 72 96 120 144 168 192 216 240 264 288 312 336 360 384 408 432 456 480 504 528 552 576 600 624 648 672 696 720
time (hrs)

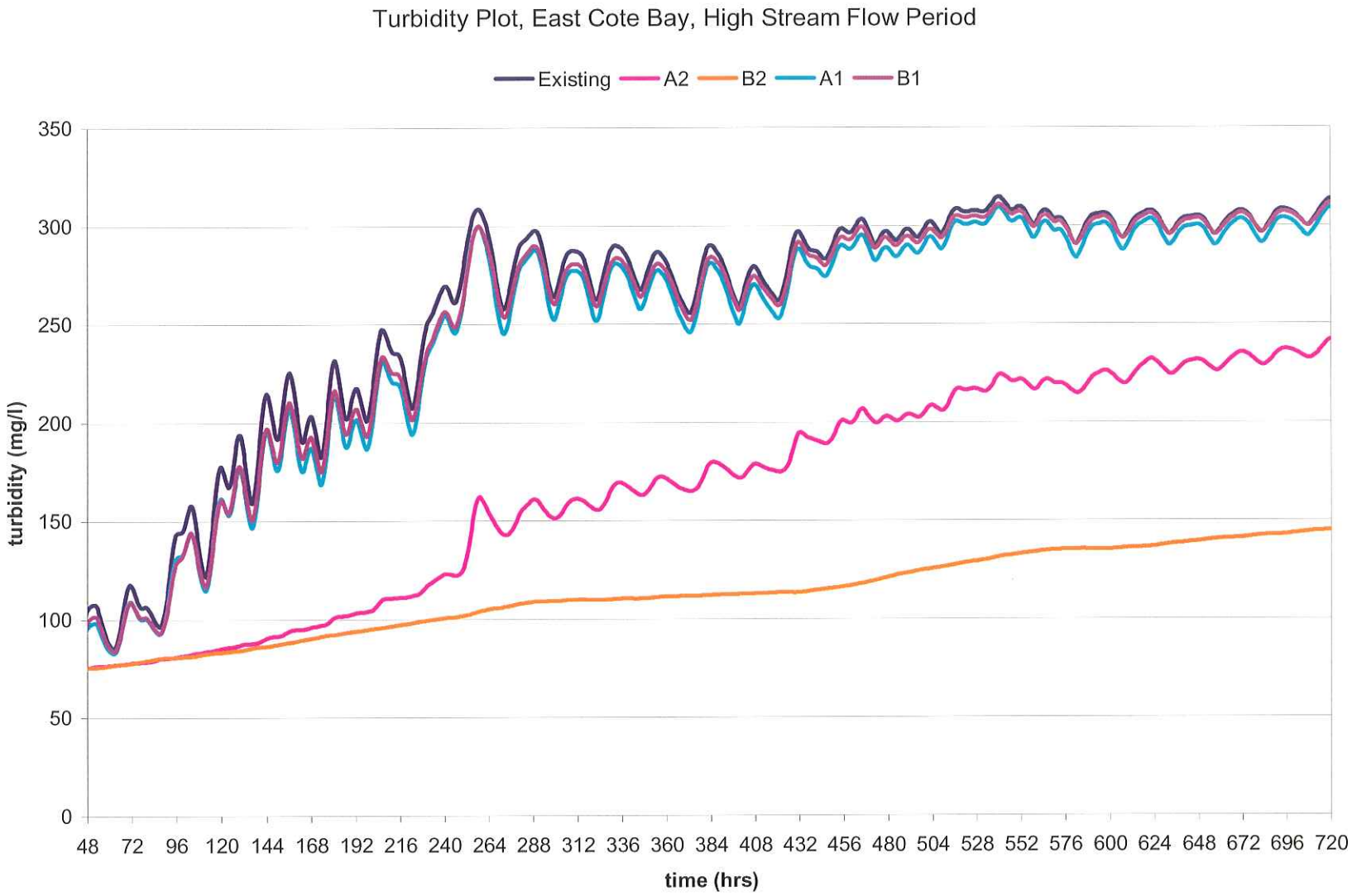
Turbidity Plot, East Cote Bay, High Stream Flow Period
Existing
A2
B2
A1
B1
350
300
250
200
150
100
50
0
turbidity (mg/l)
48 72 96 120 144 168 192 216 240 264 288 312 336 360 384 408 432 456 480 504 528 552 576 600 624 648 672 696 720
time (hrs)

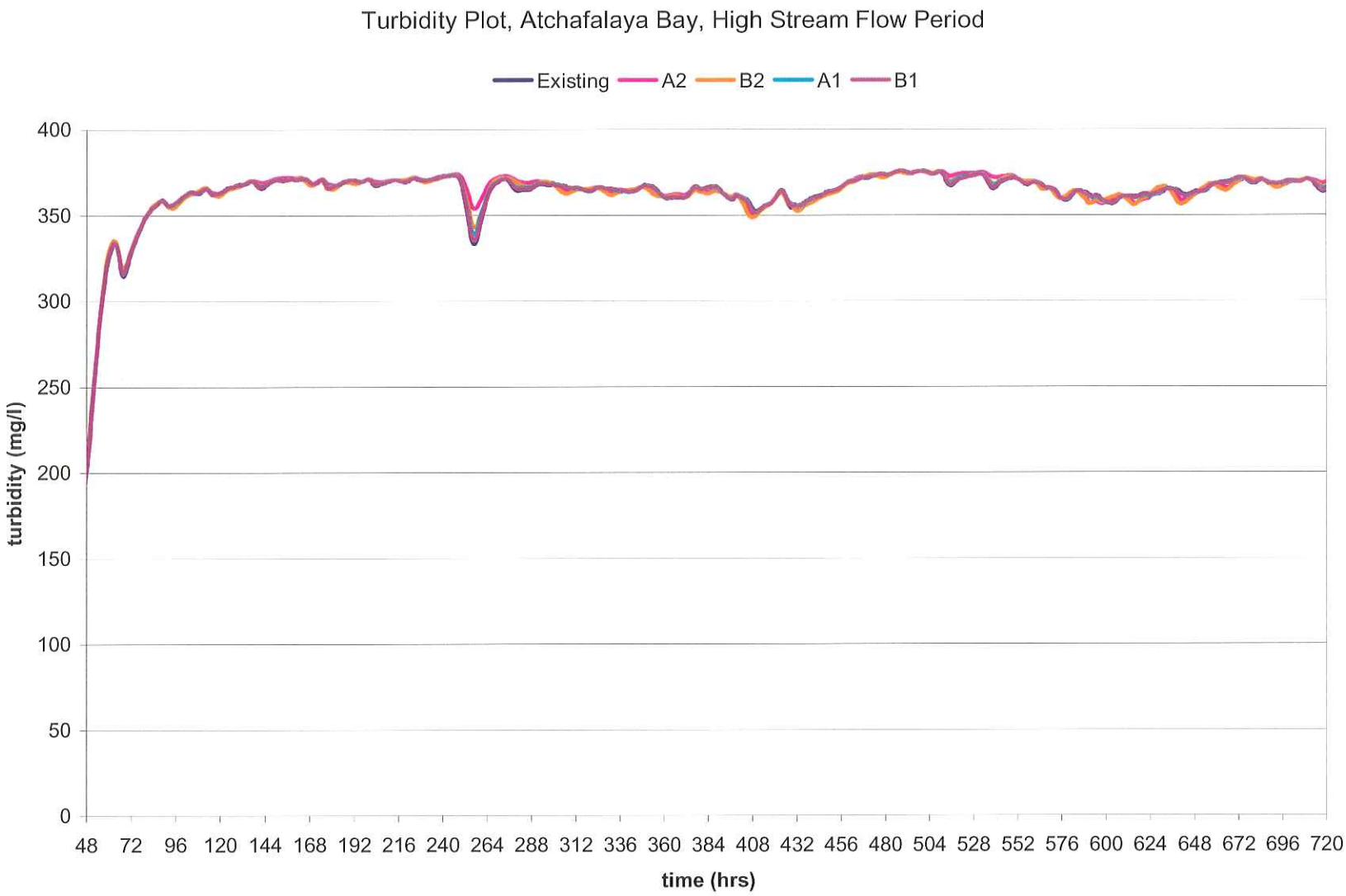
Turbidity Plot, Atchafalaya Bay, High Stream Flow Period
Existing
A2
B2
A1
B1
turbidity (mg/l)
400
350
300
250
200
150
100
50
0
48 72 96 120 144 168 192 216 240 264 288 312 336 360 384 408 432 456 480 504 528 552 576 600 624 648 672 696 720
time (hrs)

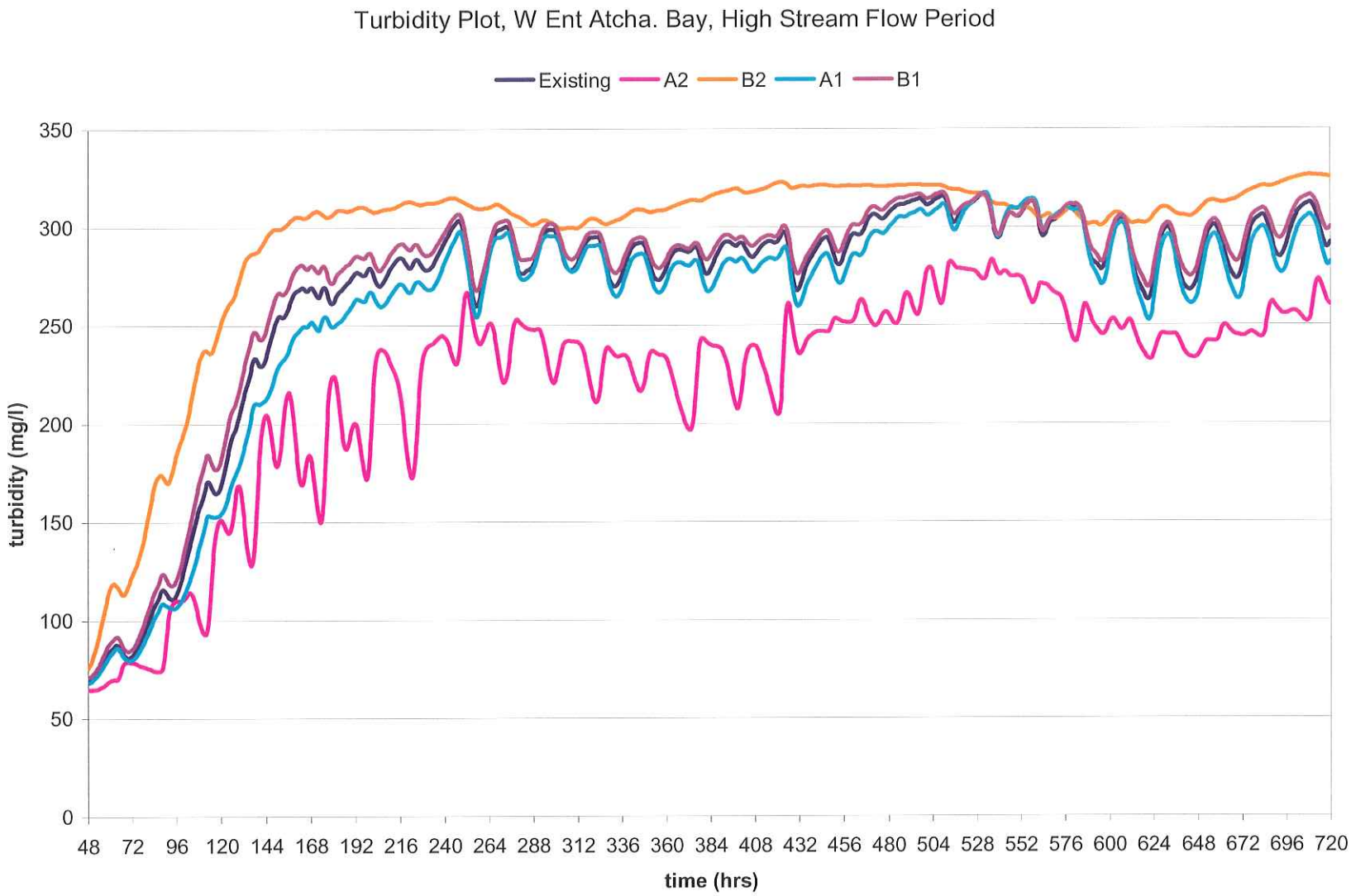
Turbidity Plot, W Ent Atcha. Bay, High Stream Flow Period
Existing
A2
B2
A1
B1
turbidity (mg/l)
0
50
100
150
200
250
300
350
48 72 96 120 144 168 192 216 240 264 288 312 336 360 384 408 432 456 480 504 528 552 576 600 624 648 672 696 720
time (hrs)

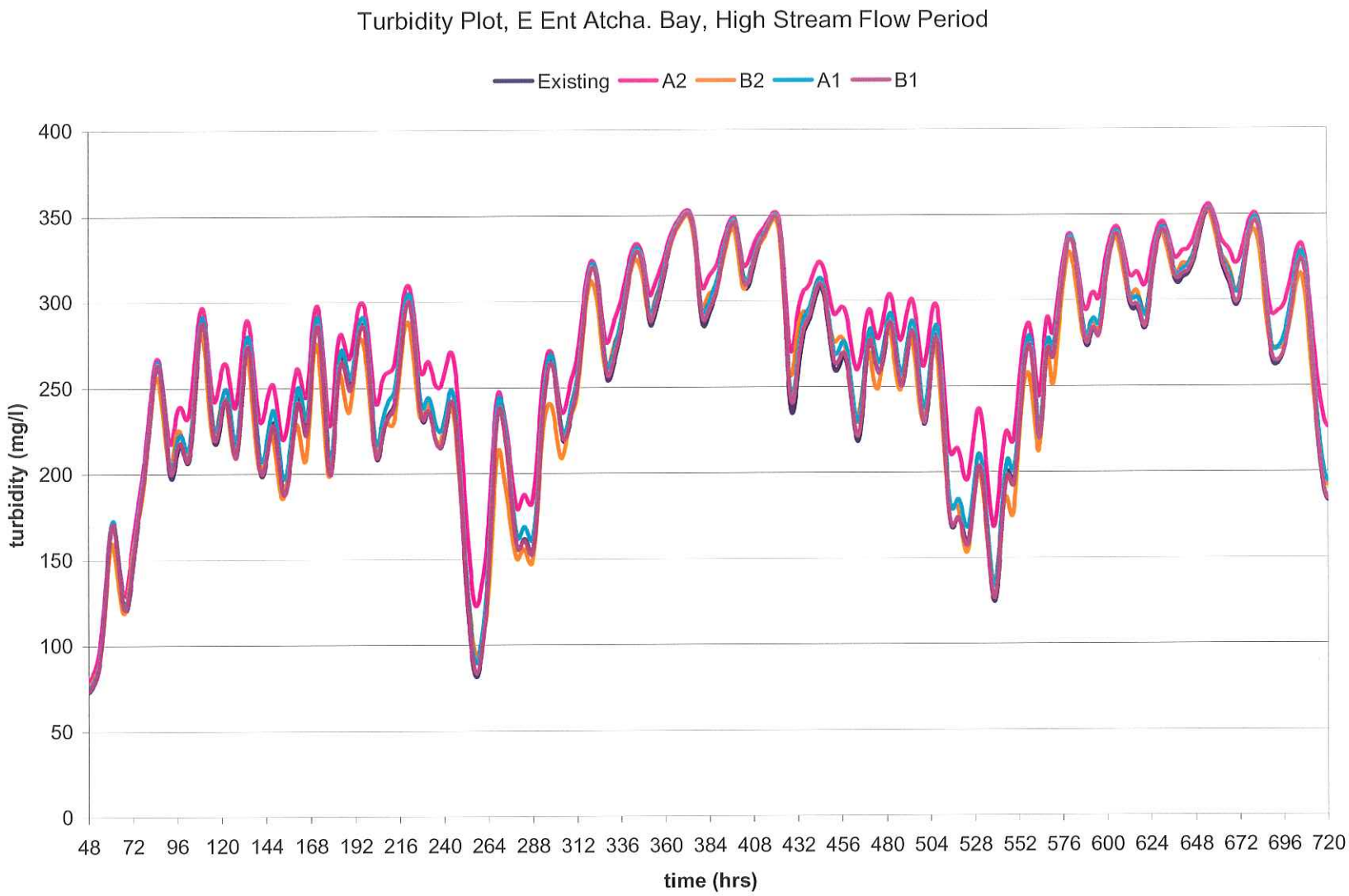
Turbidity Plot, E Ent Atcha. Bay, High Stream Flow Period
Existing
A2
B2
A1
B1
turbidity (mg/l)
0
50
100
150
200
250
300
350
400
48 72 96 120 144 168 192 216 240 264 288 312 336 360 384 408 432 456 480 504 528 552 576 600 624 648 672 696 720
time (hrs)

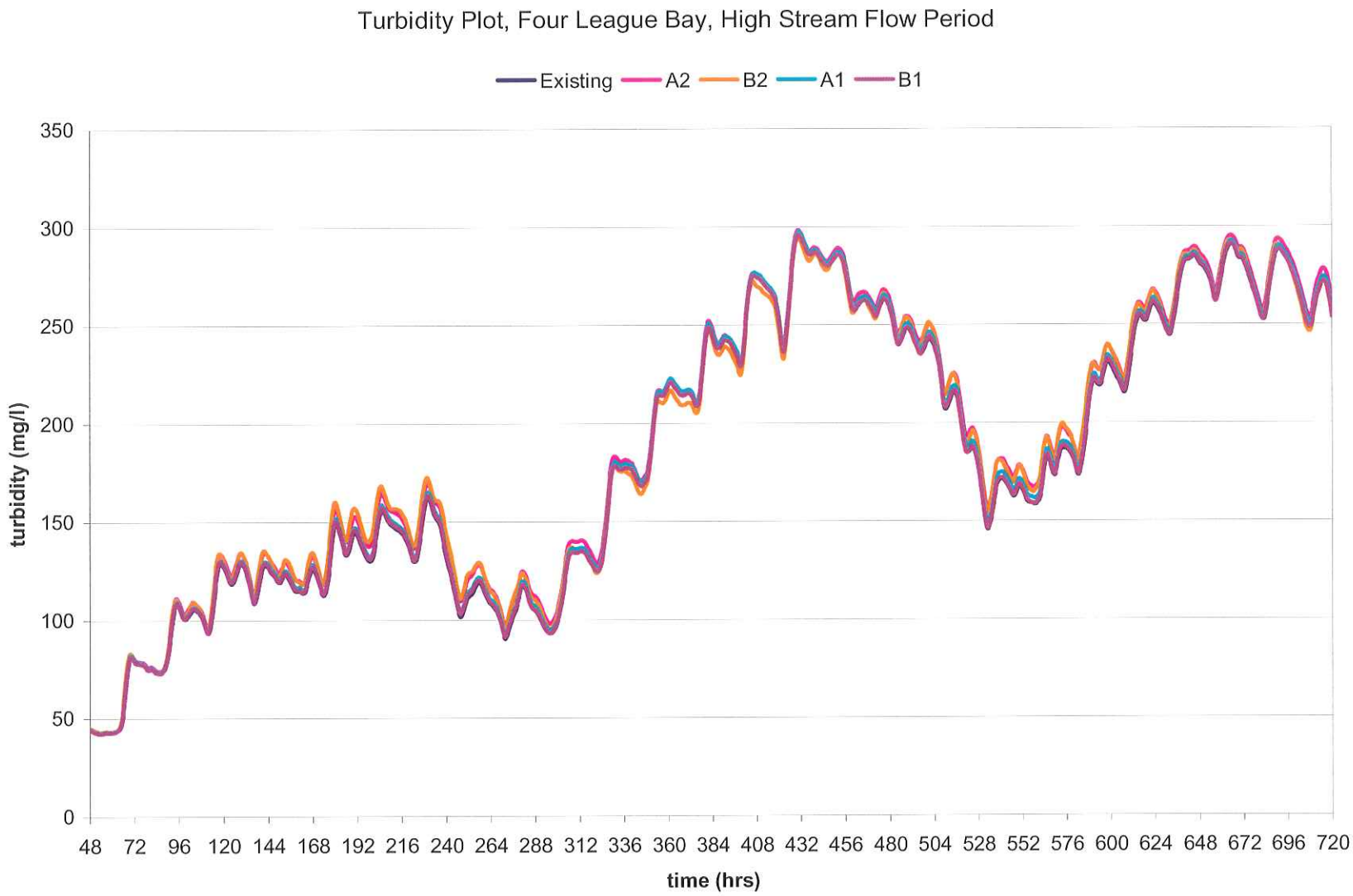
Turbidity Plot, Four League Bay, High Stream Flow Period
Existing
A2
B2
A1
B1
turbidity (mg/l)
0
50
100
150
200
250
300
350
48 72 96 120 144 168 192 216 240 264 288 312 336 360 384 408 432 456 480 504 528 552 576 600 624 648 672 696 720
time (hrs)

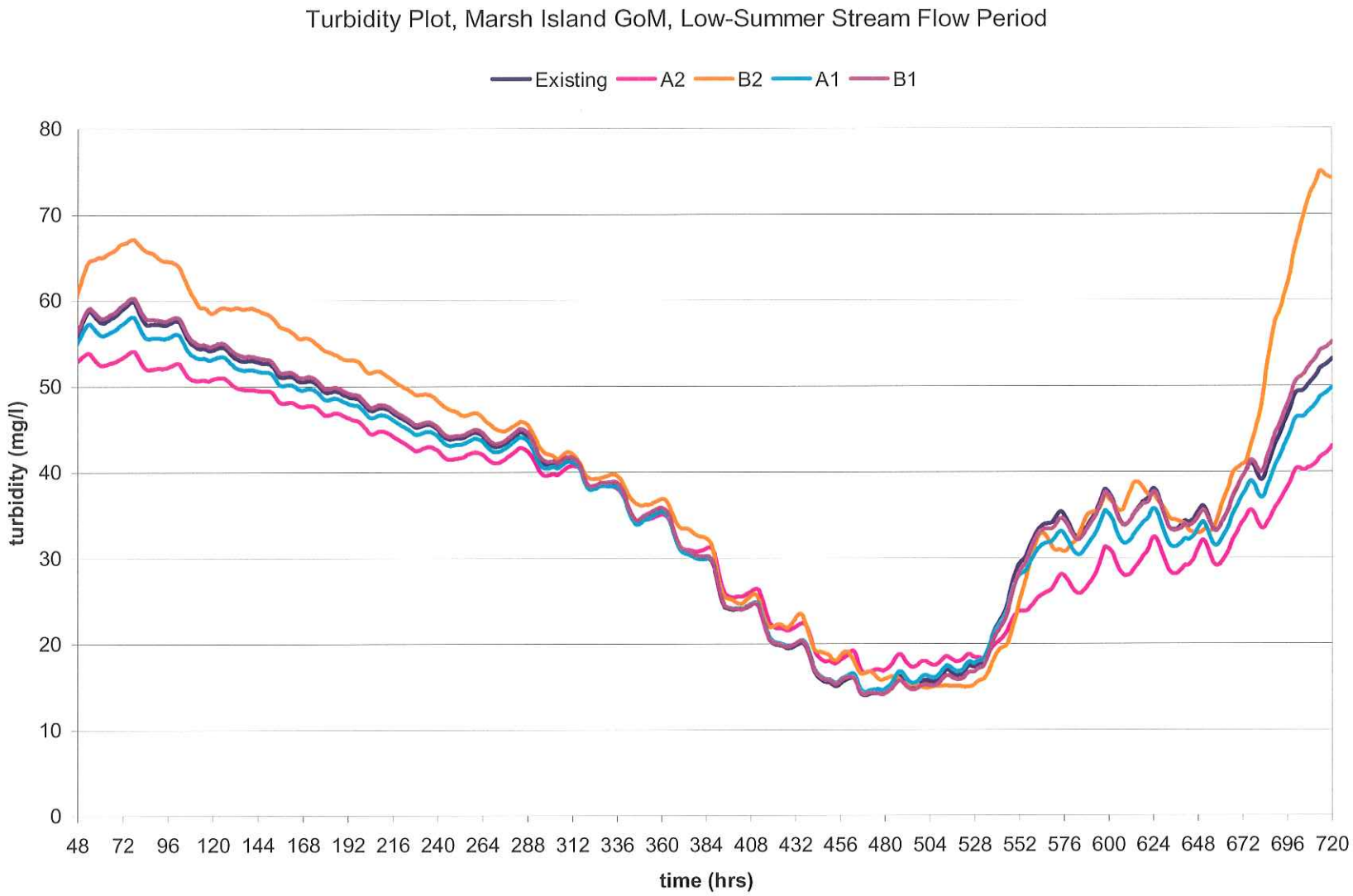
Turbidity Plot, Marsh Island GoM, Low-Summer Stream Flow Period
Existing
A2
B2
A1
B1
turbidity (mg/l)
0
10
20
30
40
50
60
70
80
48 72 96 120 144 168 192 216 240 264 288 312 336 360 384 408 432 456 480 504 528 552 576 600 624 648 672 696 720
time (hrs)

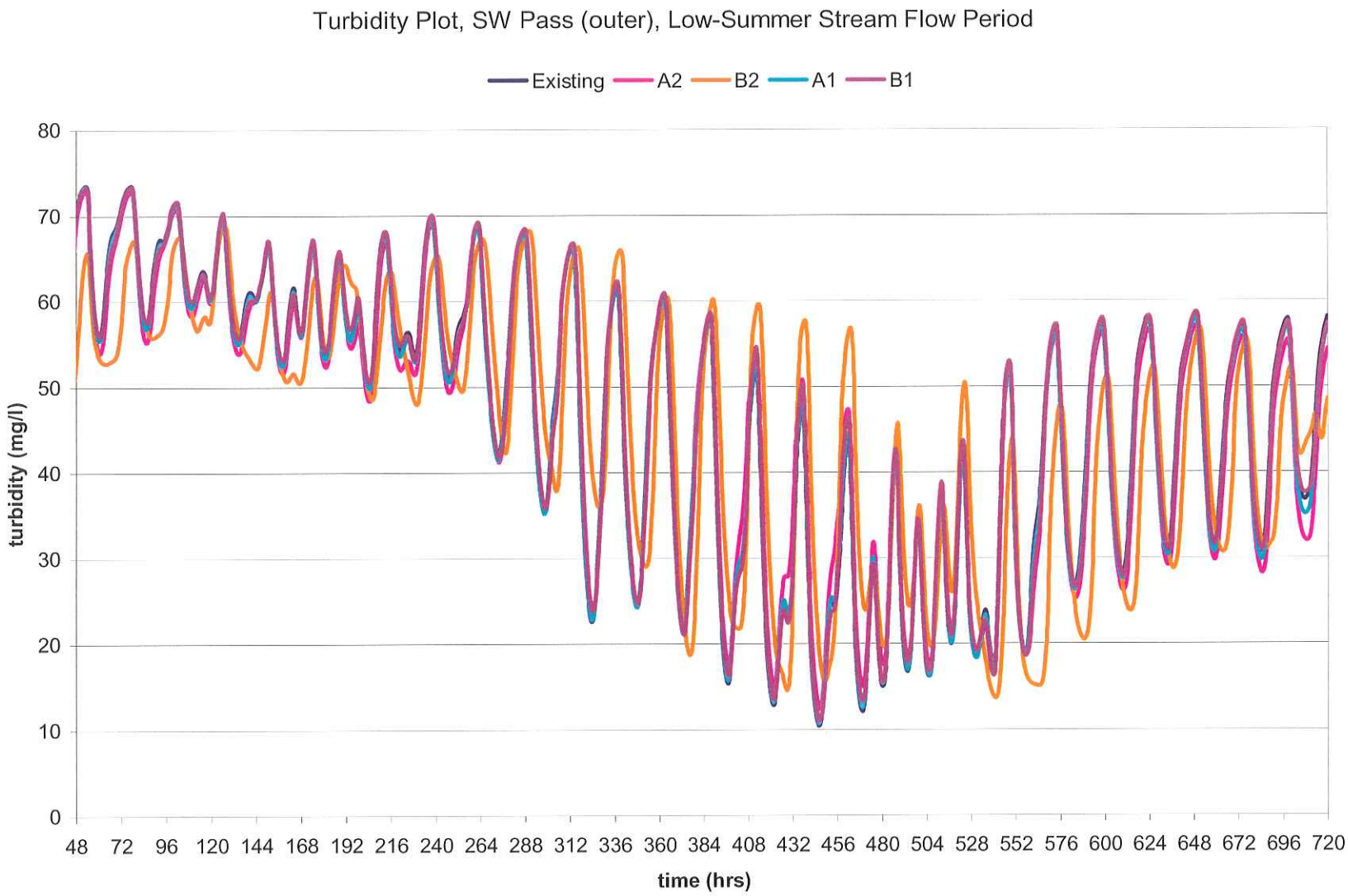
Turbidity Plot, SW Pass (outer), Low-Summer Stream Flow Period
Existing
A2
B2
A1
B1
turbidity (mg/l)
0
10
20
30
40
50
60
70
80
48 72 96 120 144 168 192 216 240 264 288 312 336 360 384 408 432 456 480 504 528 552 576 600 624 648 672 696 720
time (hrs)

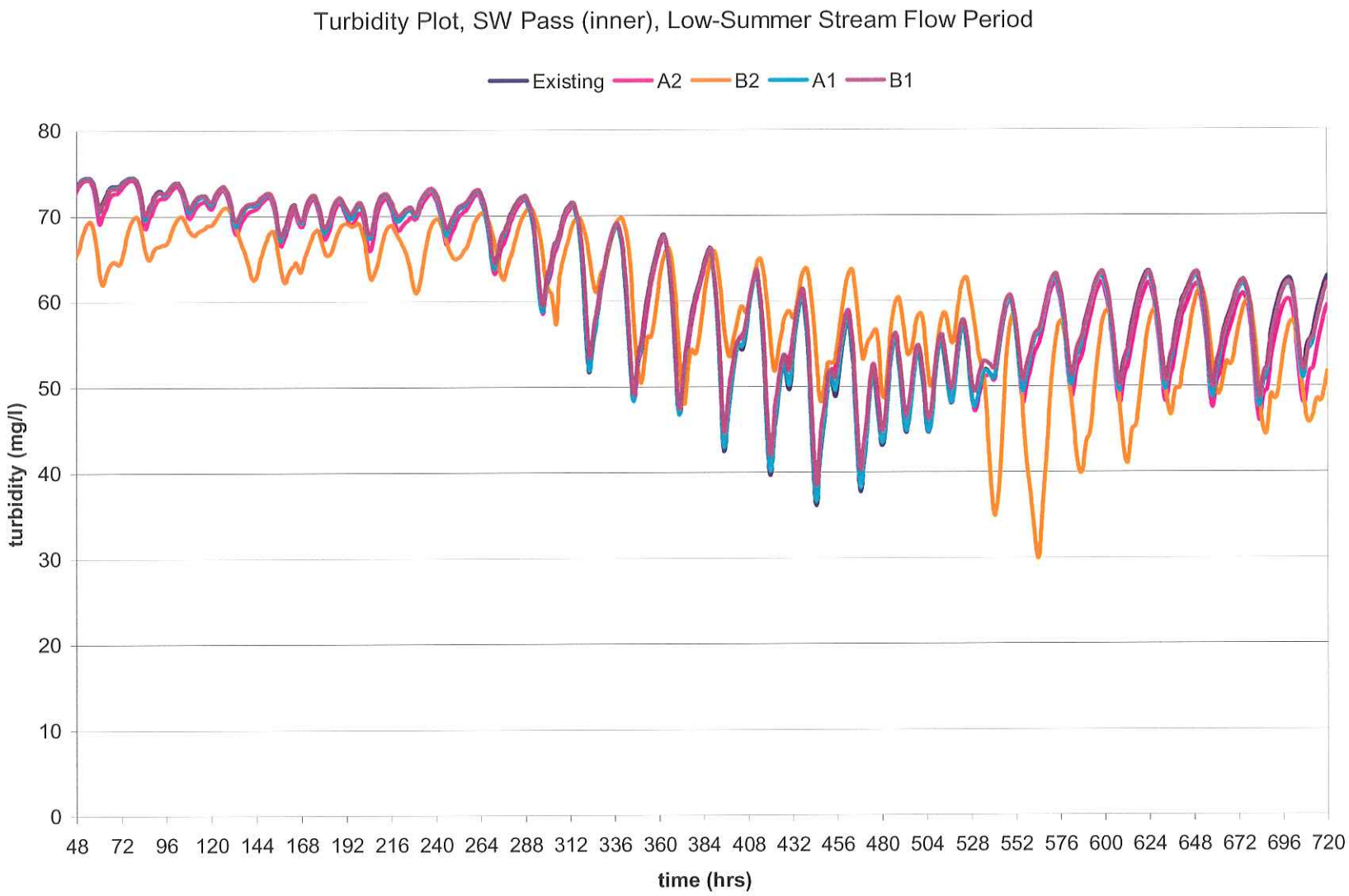
Turbidity Plot, SW Pass (inner), Low-Summer Stream Flow Period
Existing
A2
B2
A1
B1
turbidity (mg/l)
80
70
60
50
40
30
20
10
0
48 72 96 120 144 168 192 216 240 264 288 312 336 360 384 408 432 456 480 504 528 552 576 600 624 648 672 696 720
time (hrs)

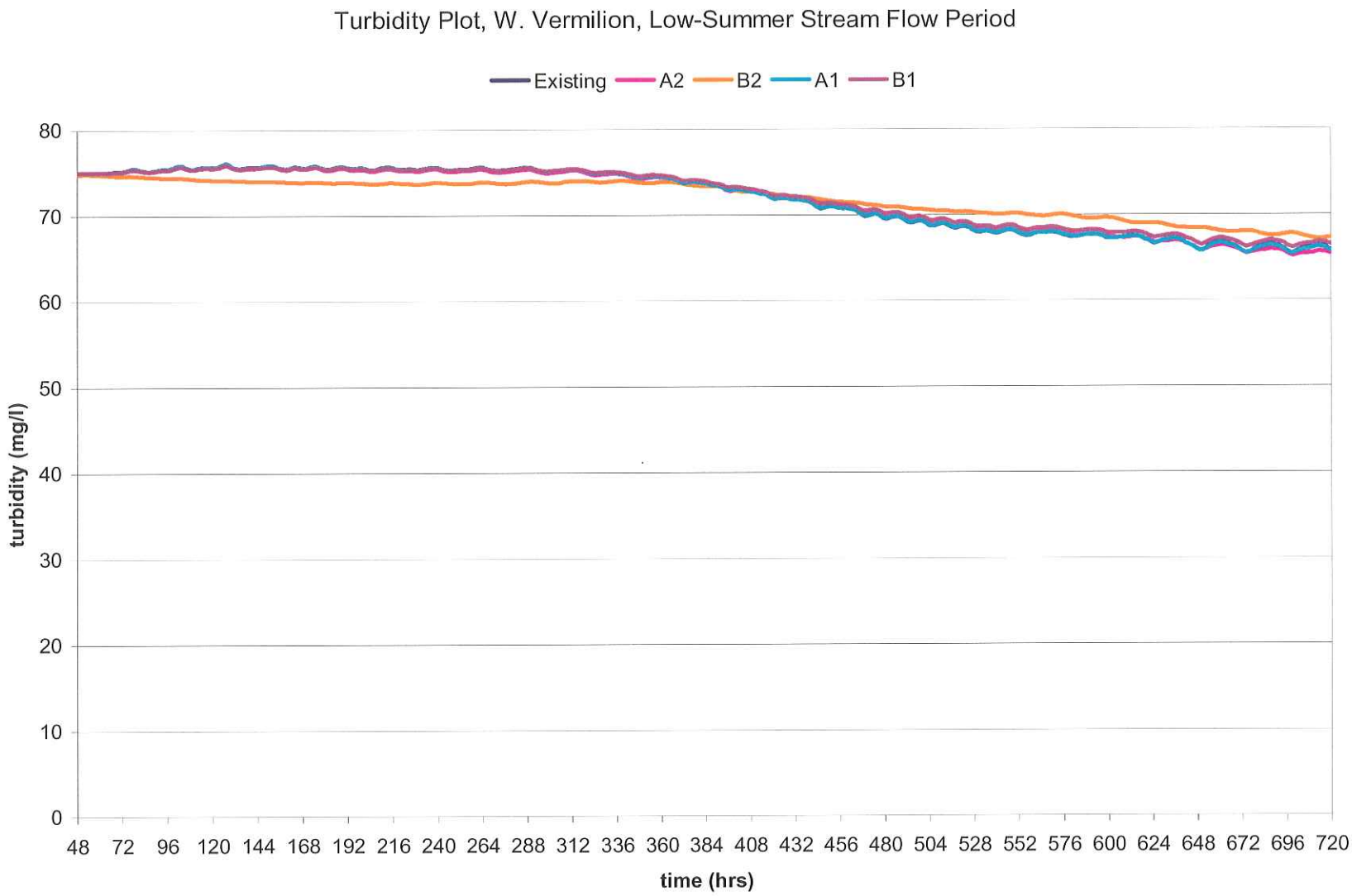
Turbidity Plot, W. Vermilion, Low-Summer Stream Flow Period
Existing
A2
B2
A1
B1
80
70
60
50
40
30
20
10
0
turbidity (mg/l)
48 72 96 120 144 168 192 216 240 264 288 312 336 360 384 408 432 456 480 504 528 552 576 600 624 648 672 696 720
time (hrs)

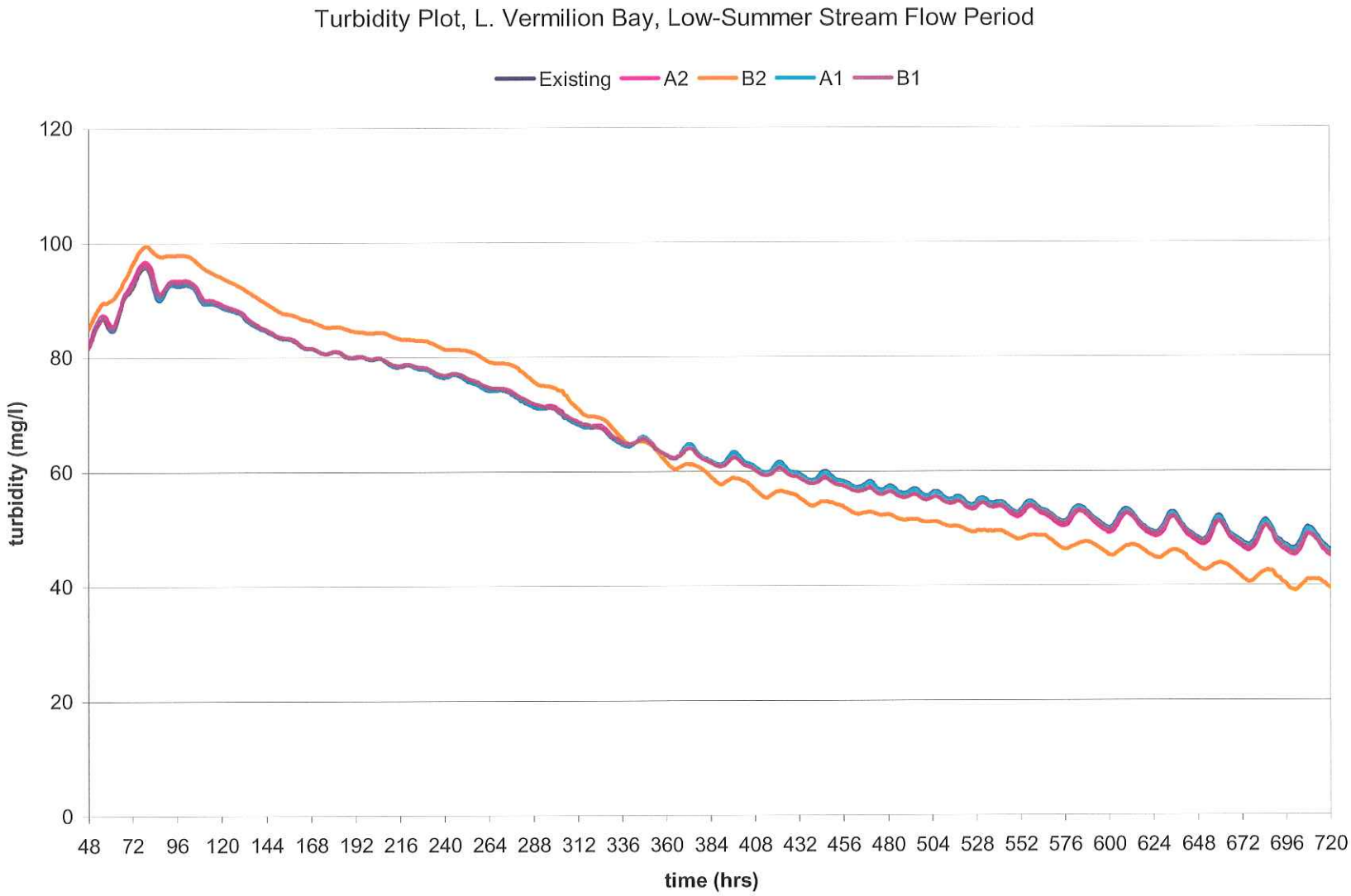
Turbidity Plot, L. Vermilion Bay, Low-Summer Stream Flow Period
Existing
A2
B2
A1
B1
120
100
80
60
40
20
0
turbidity (mg/l)
48 72 96 120 144 168 192 216 240 264 288 312 336 360 384 408 432 456 480 504 528 552 576 600 624 648 672 696 720
time (hrs)

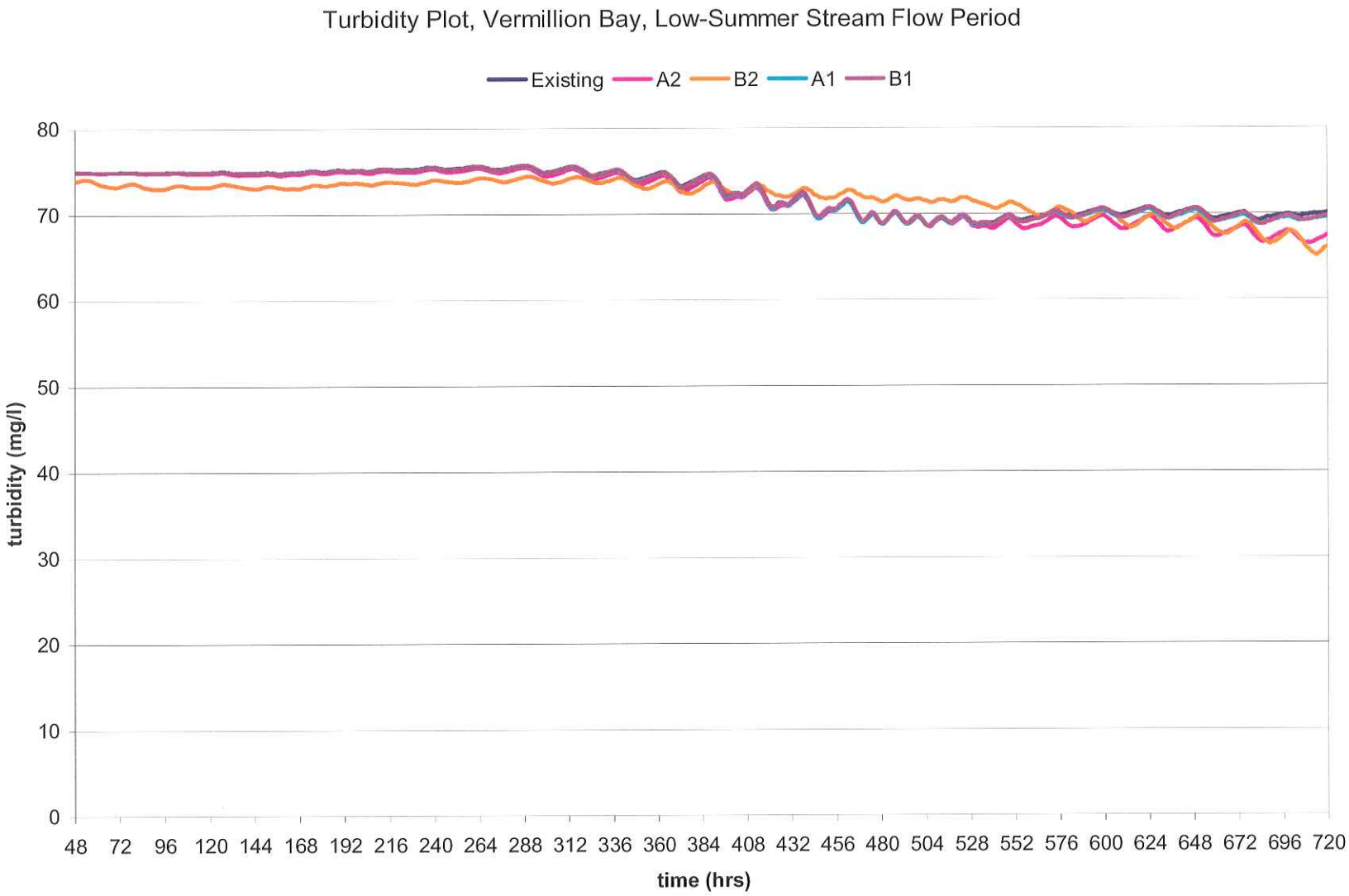
Turbidity Plot, Vermillion Bay, Low-Summer Stream Flow Period
Existing
A2
B2
A1
B1
turbidity (mg/l)
0
10
20
30
40
50
60
70
80
48 72 96 120 144 168 192 216 240 264 288 312 336 360 384 408 432 456 480 504 528 552 576 600 624 648 672 696 720
time (hrs)

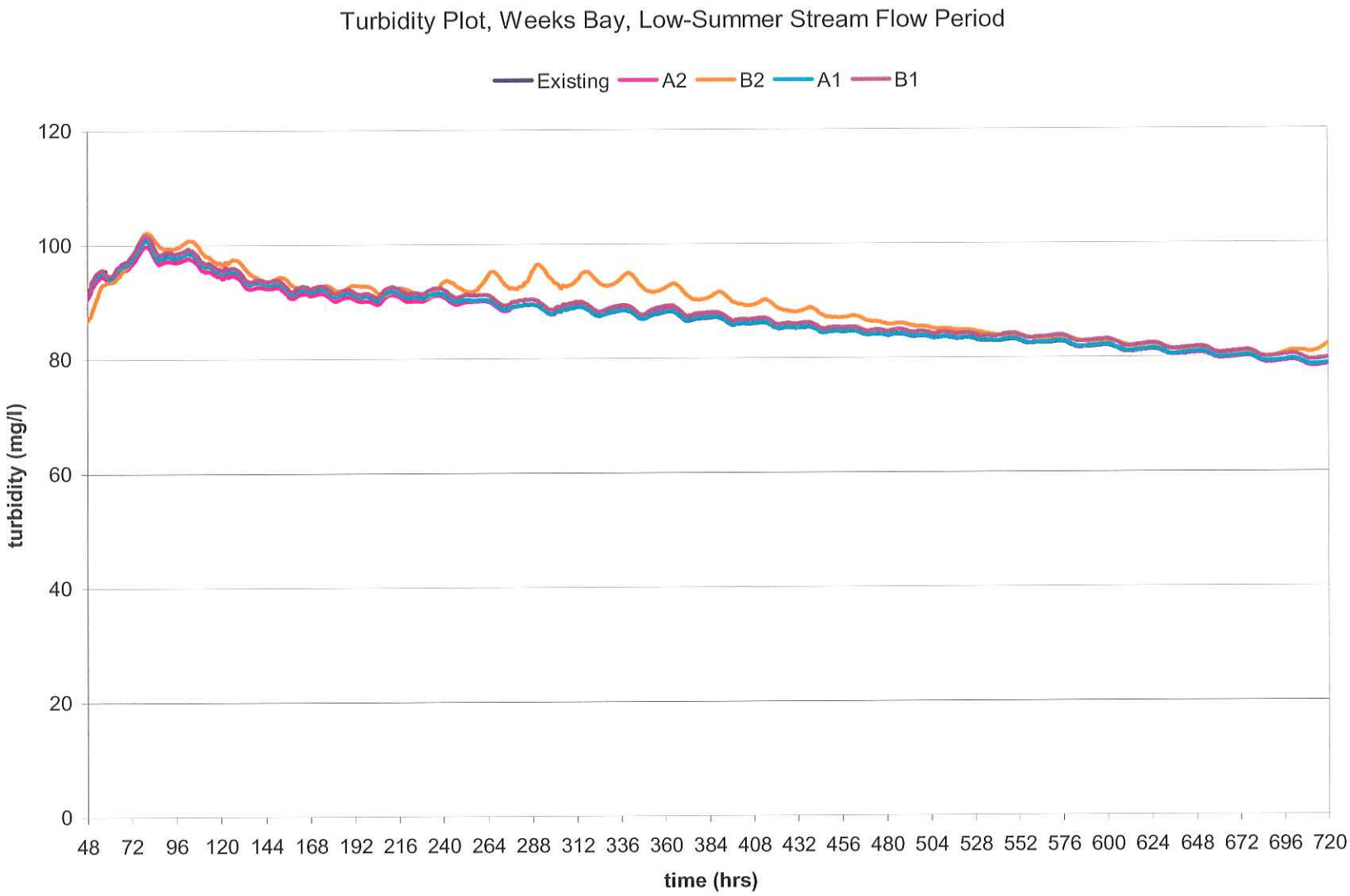
Turbidity Plot, Weeks Bay, Low-Summer Stream Flow Period
Existing
A2
B2
A1
B1
120
100
80
60
40
20
0
turbidity (mg/l)
48 72 96 120 144 168 192 216 240 264 288 312 336 360 384 408 432 456 480 504 528 552 576 600 624 648 672 696 720
time (hrs)

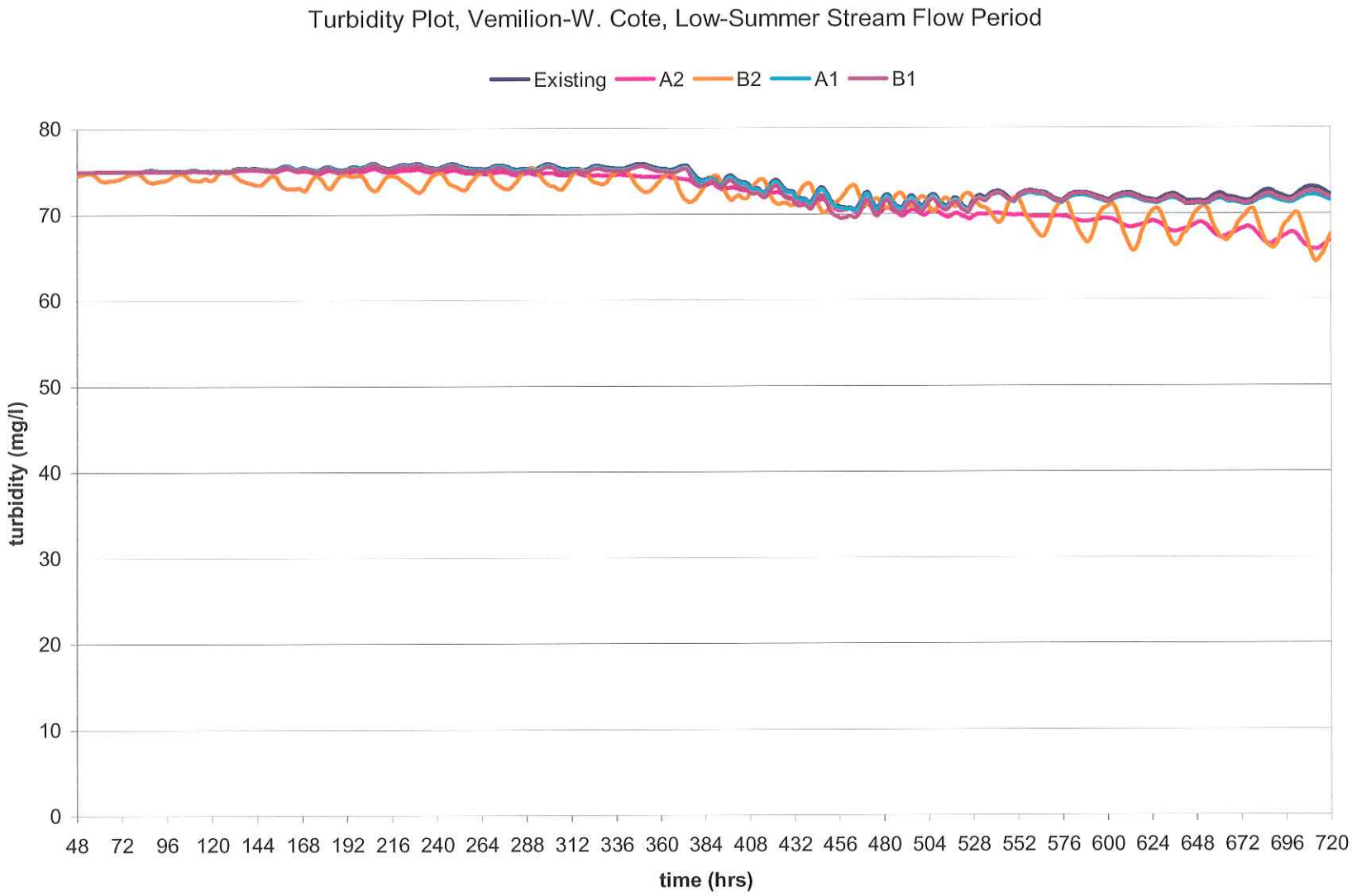
Turbidity Plot, Vemilion-W. Cote, Low-Summer Stream Flow Period
Existing
A2
B2
A1
B1
turbidity (mg/l)
0
10
20
30
40
50
60
70
80
48 72 96 120 144 168 192 216 240 264 288 312 336 360 384 408 432 456 480 504 528 552 576 600 624 648 672 696 720
time (hrs)

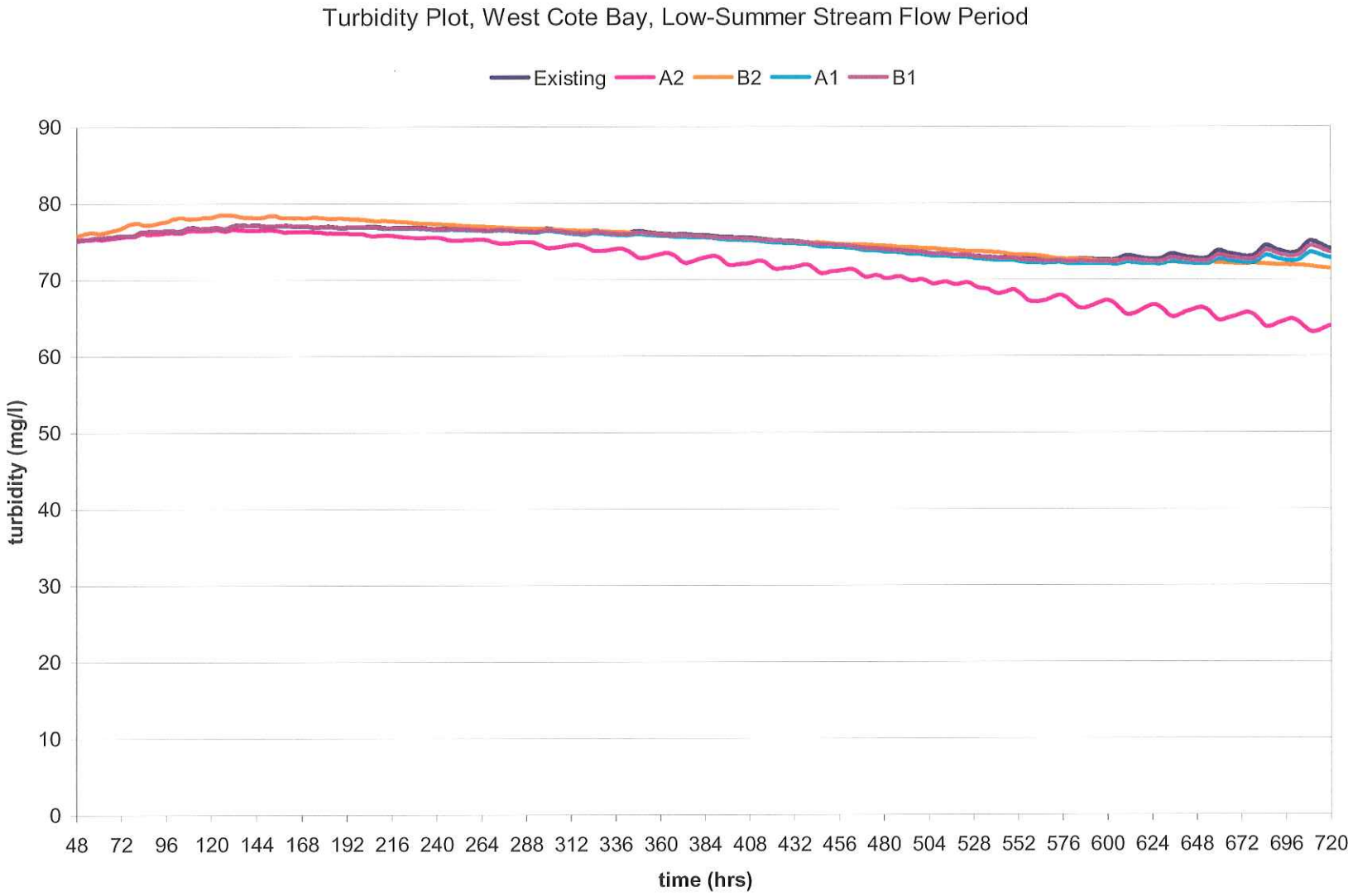
Turbidity Plot, West Cote Bay, Low-Summer Stream Flow Period
Existing
A2
B2
A1
B1
90
80
70
60
50
40
30
20
10
0
turbidity (mg/l)
48 72 96 120 144 168 192 216 240 264 288 312 336 360 384 408 432 456 480 504 528 552 576 600 624 648 672 696 720
time (hrs)

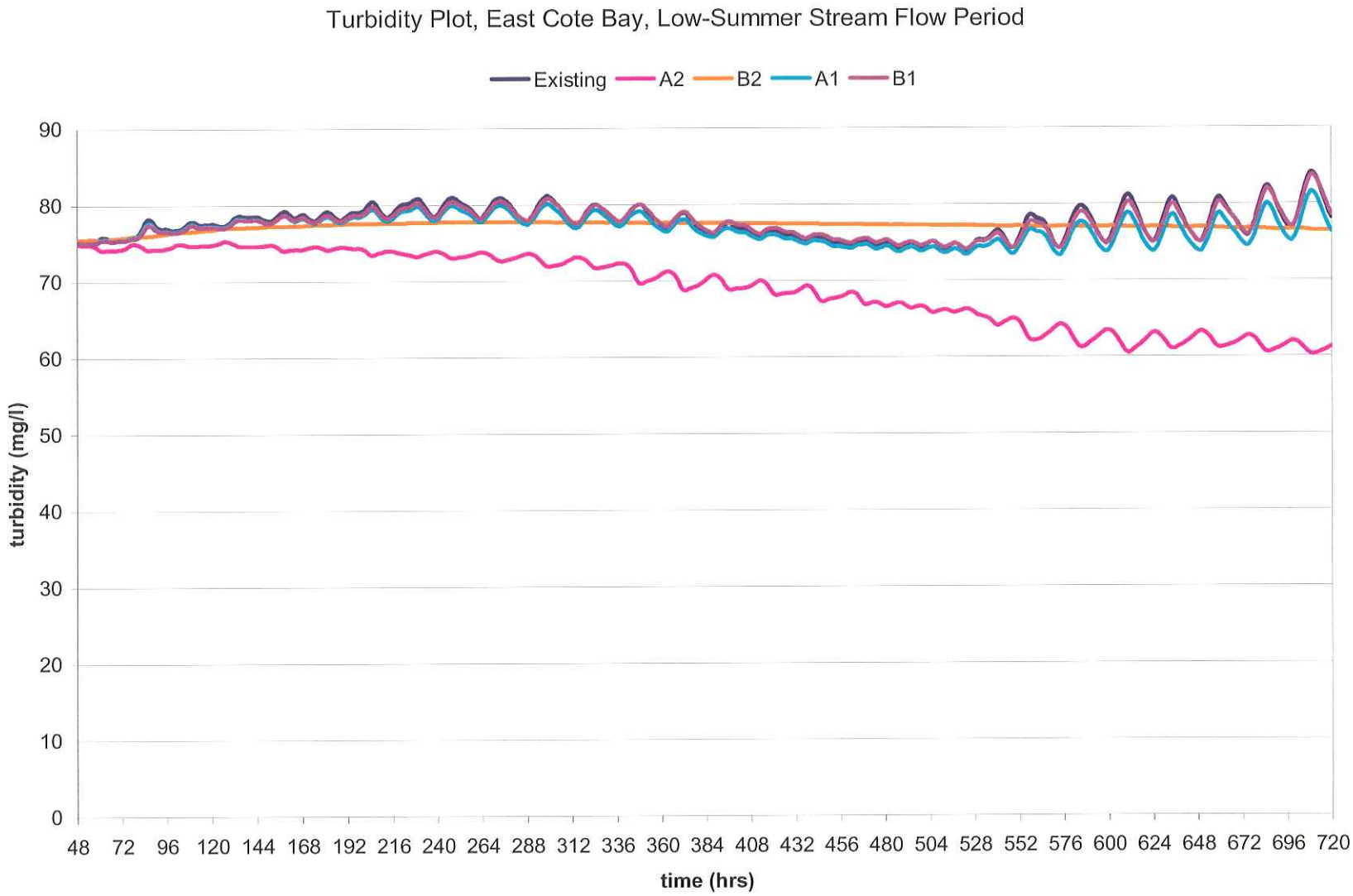
Turbidity Plot, East Cote Bay, Low-Summer Stream Flow Period
Existing
A2
B2
A1
B1
turbidity (mg/l)
0
10
20
30
40
50
60
70
80
90
48 72 96 120 144 168 192 216 240 264 288 312 336 360 384 408 432 456 480 504 528 552 576 600 624 648 672 696 720
time (hrs)

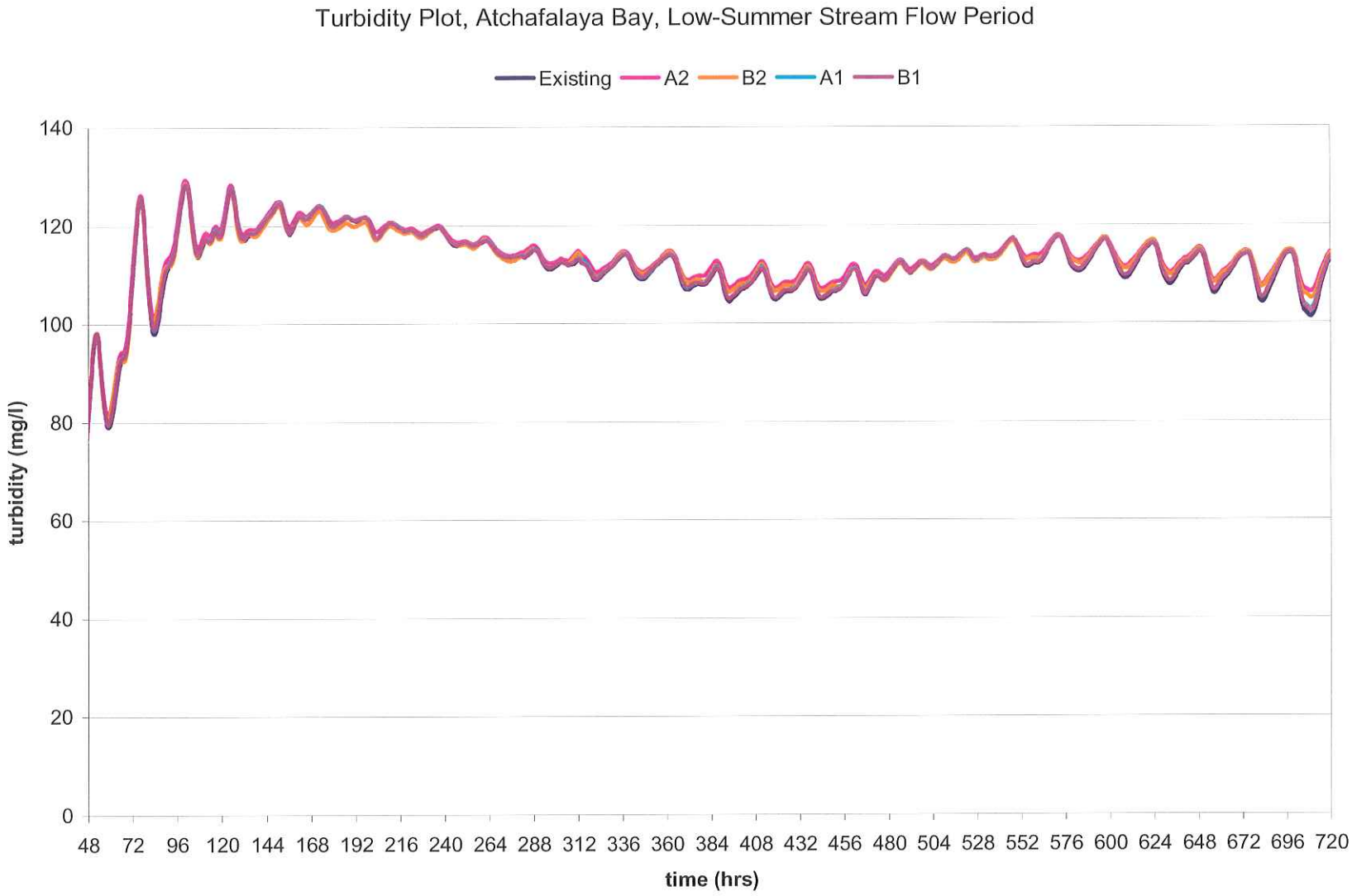
Turbidity Plot, Atchafalaya Bay, Low-Summer Stream Flow Period
Existing
A2
B2
A1
B1
140
120
100
80
60
40
20
0
turbidity (mg/l)
48 72 96 120 144 168 192 216 240 264 288 312 336 360 384 408 432 456 480 504 528 552 576 600 624 648 672 696 720
time (hrs)

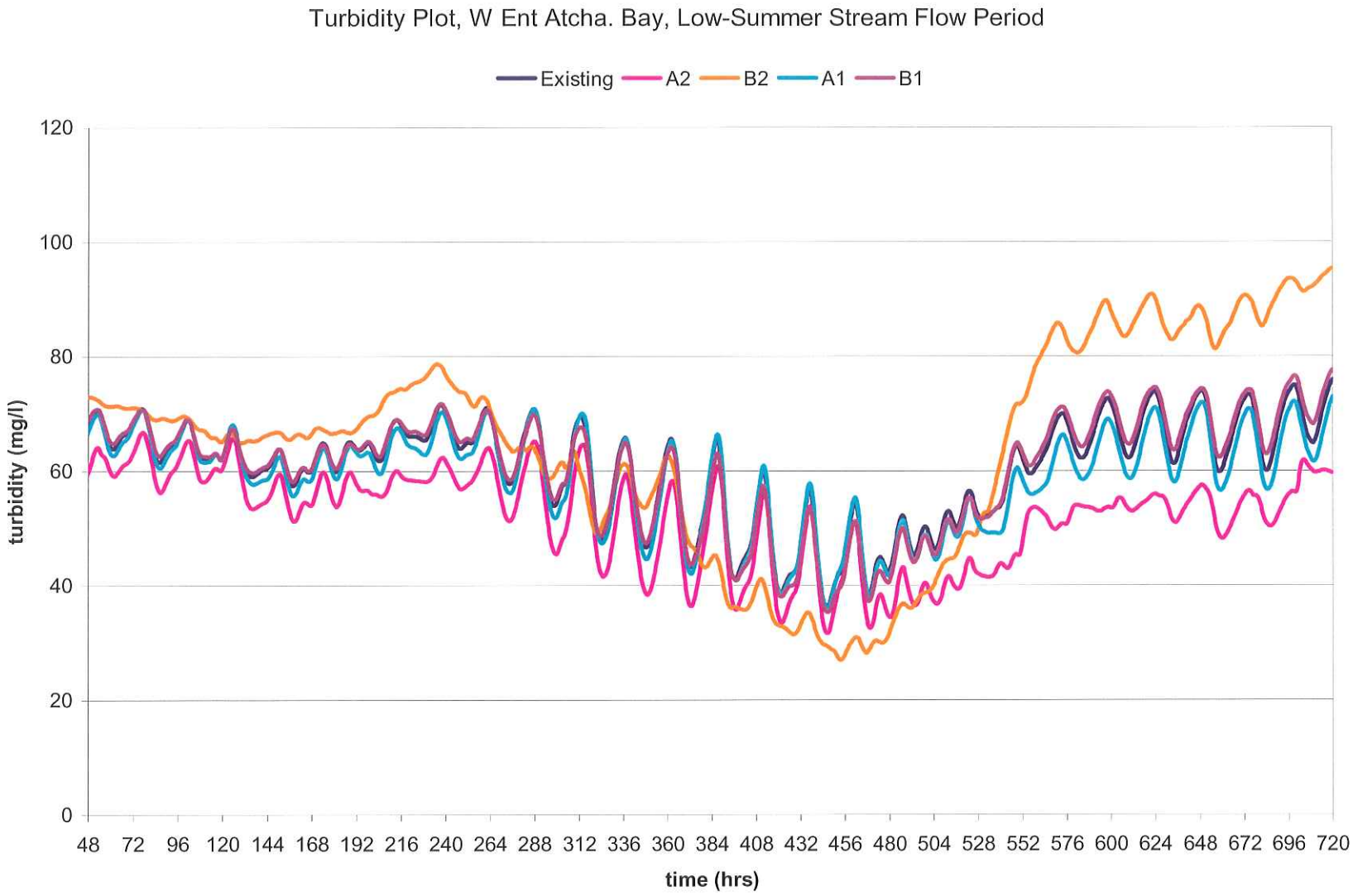
Turbidity Plot, W Ent Atcha. Bay, Low-Summer Stream Flow Period
Existing
A2
B2
A1
B1
120
100
80
60
40
20
0
turbidity (mg/l)
48 72 96 120 144 168 192 216 240 264 288 312 336 360 384 408 432 456 480 504 528 552 576 600 624 648 672 696 720
time (hrs)

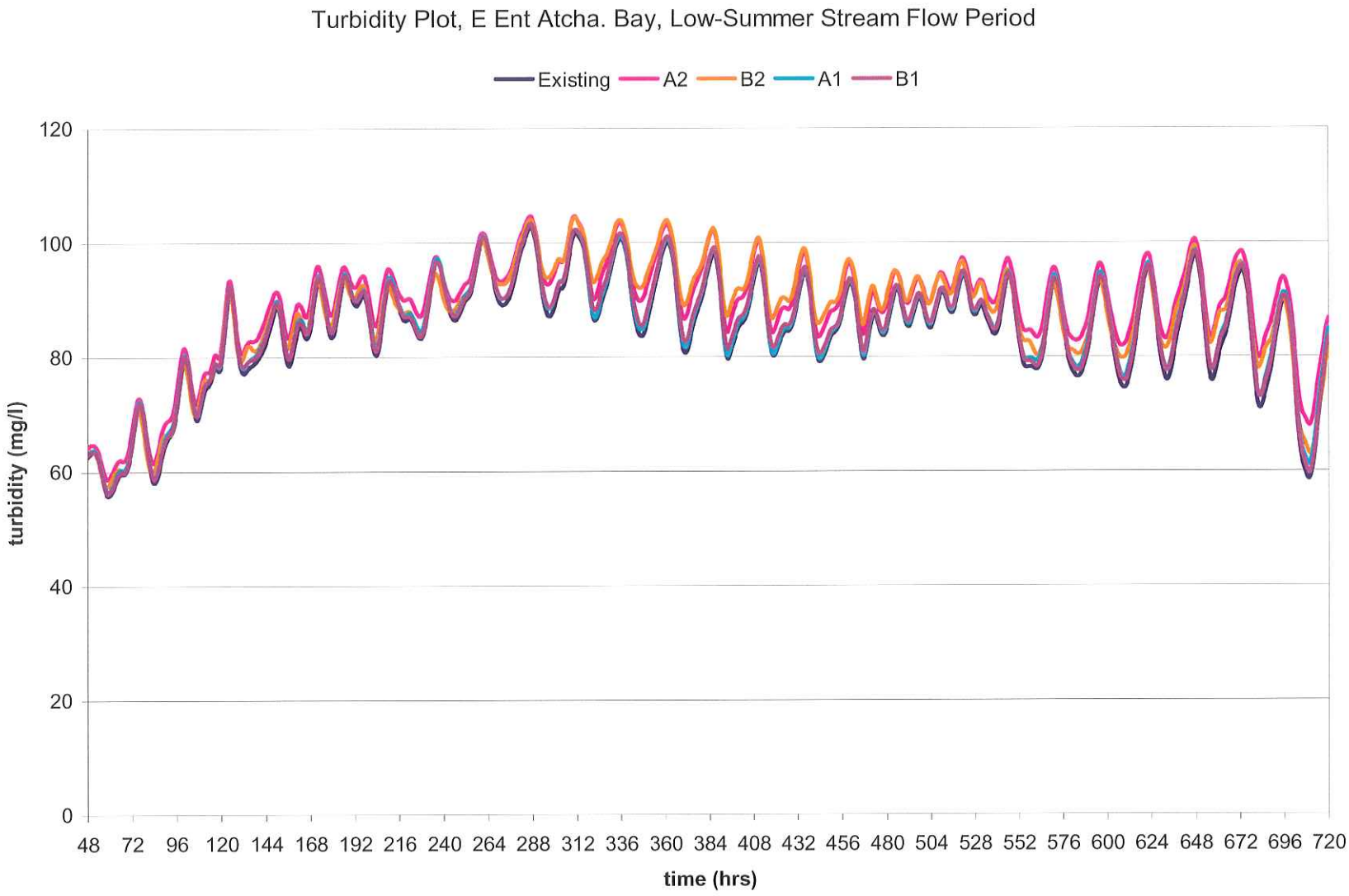
Turbidity Plot, E Ent Atcha. Bay, Low-Summer Stream Flow Period
Existing
A2
B2
A1
B1
120
100
80
60
40
20
0
turbidity (mg/l)
48 72 96 120 144 168 192 216 240 264 288 312 336 360 384 408 432 456 480 504 528 552 576 600 624 648 672 696 720
time (hrs)

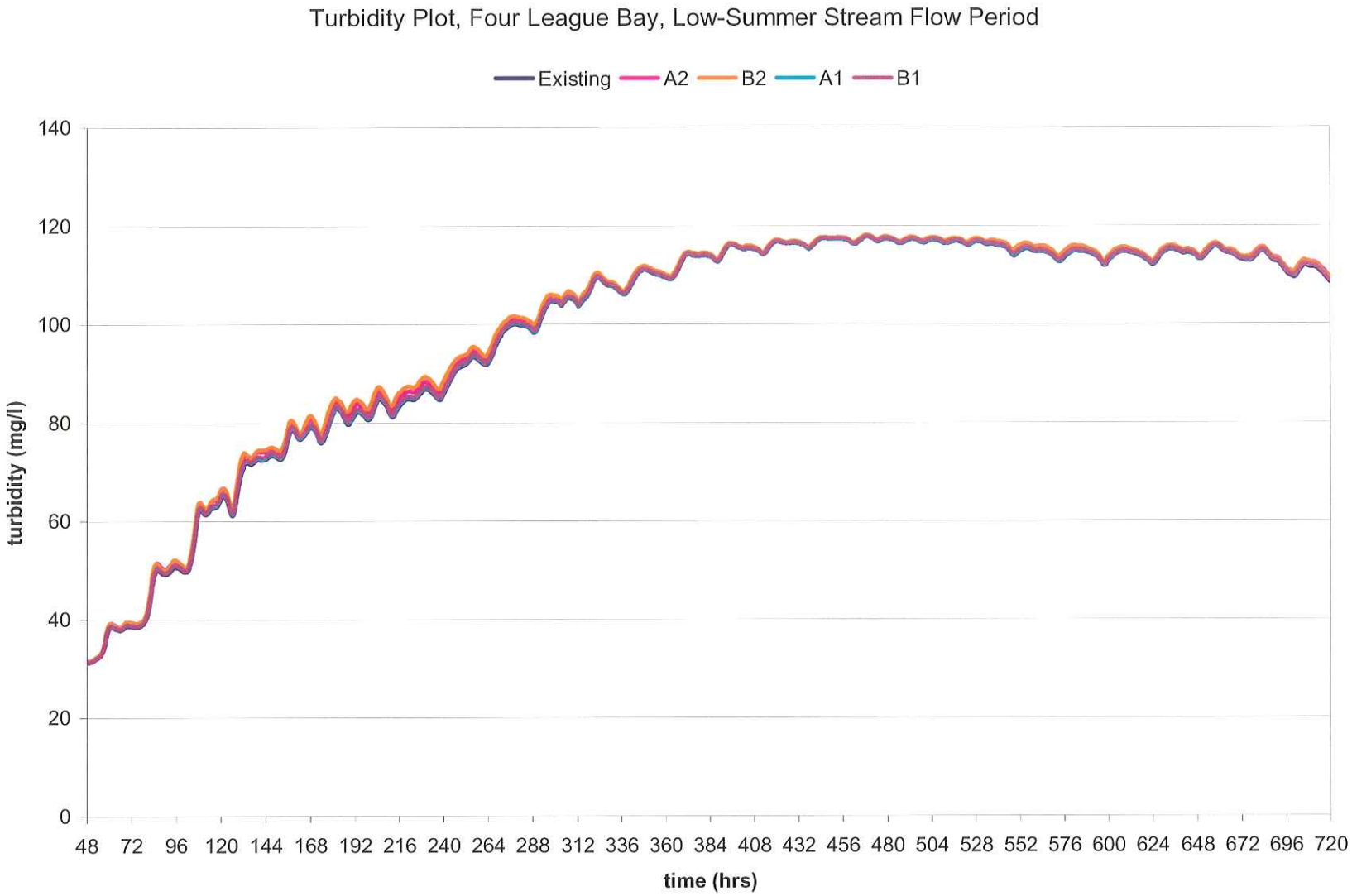
Turbidity Plot, Four League Bay, Low-Summer Stream Flow Period
Existing
A2
B2
A1
B1
140
120
100
80
60
40
20
0
turbidity (mg/l)
48 72 96 120 144 168 192 216 240 264 288 312 336 360 384 408 432 456 480 504 528 552 576 600 624 648 672 696 720
time (hrs)

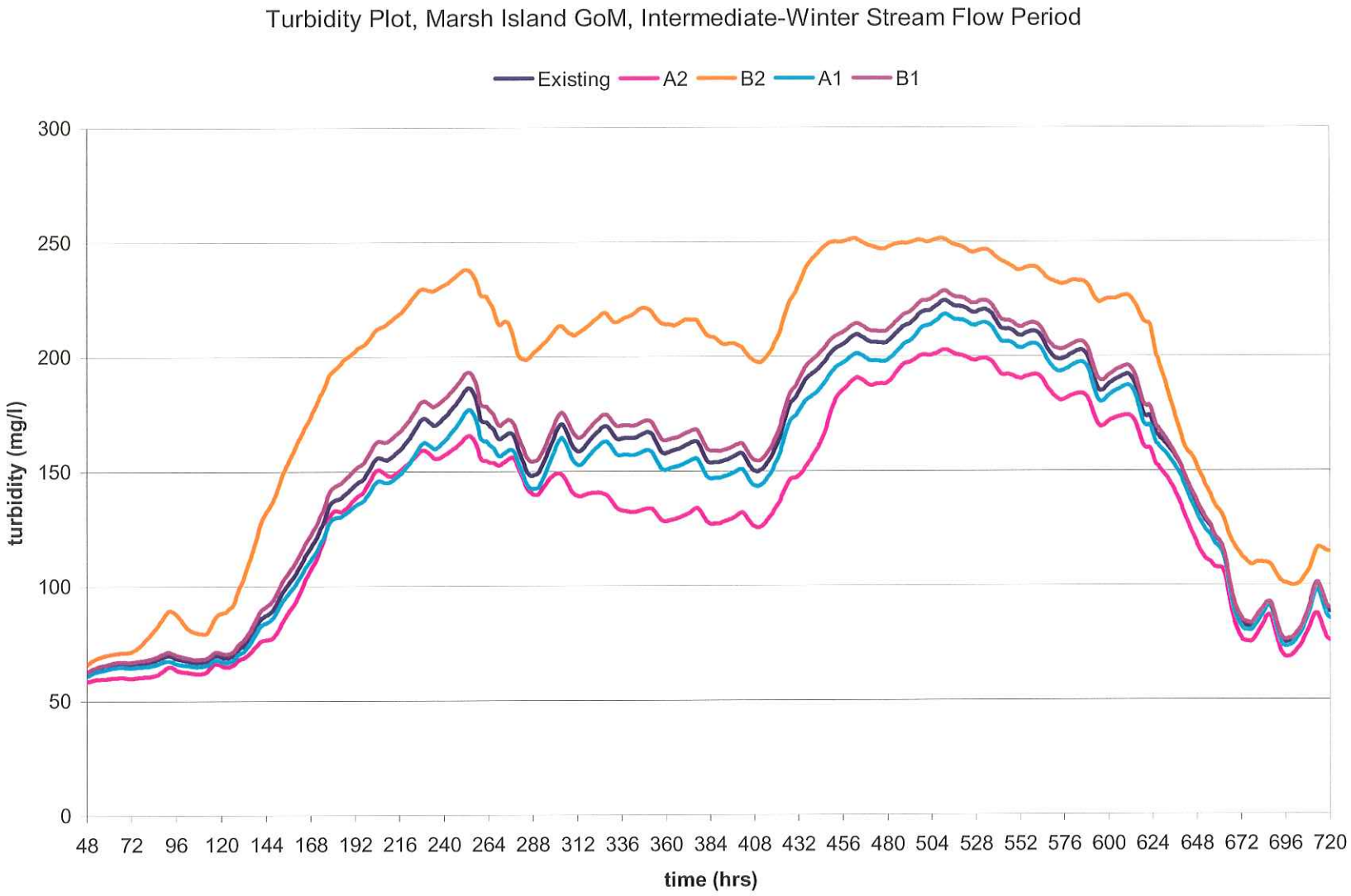
Turbidity Plot, Marsh Island GoM, Intermediate-Winter Stream Flow Period
Existing
A2
B2
A1
B1
turbidity (mg/l)
300
250
200
150
100
50
0
48 72 96 120 144 168 192 216 240 264 288 312 336 360 384 408 432 456 480 504 528 552 576 600 624 648 672 696 720
time (hrs)

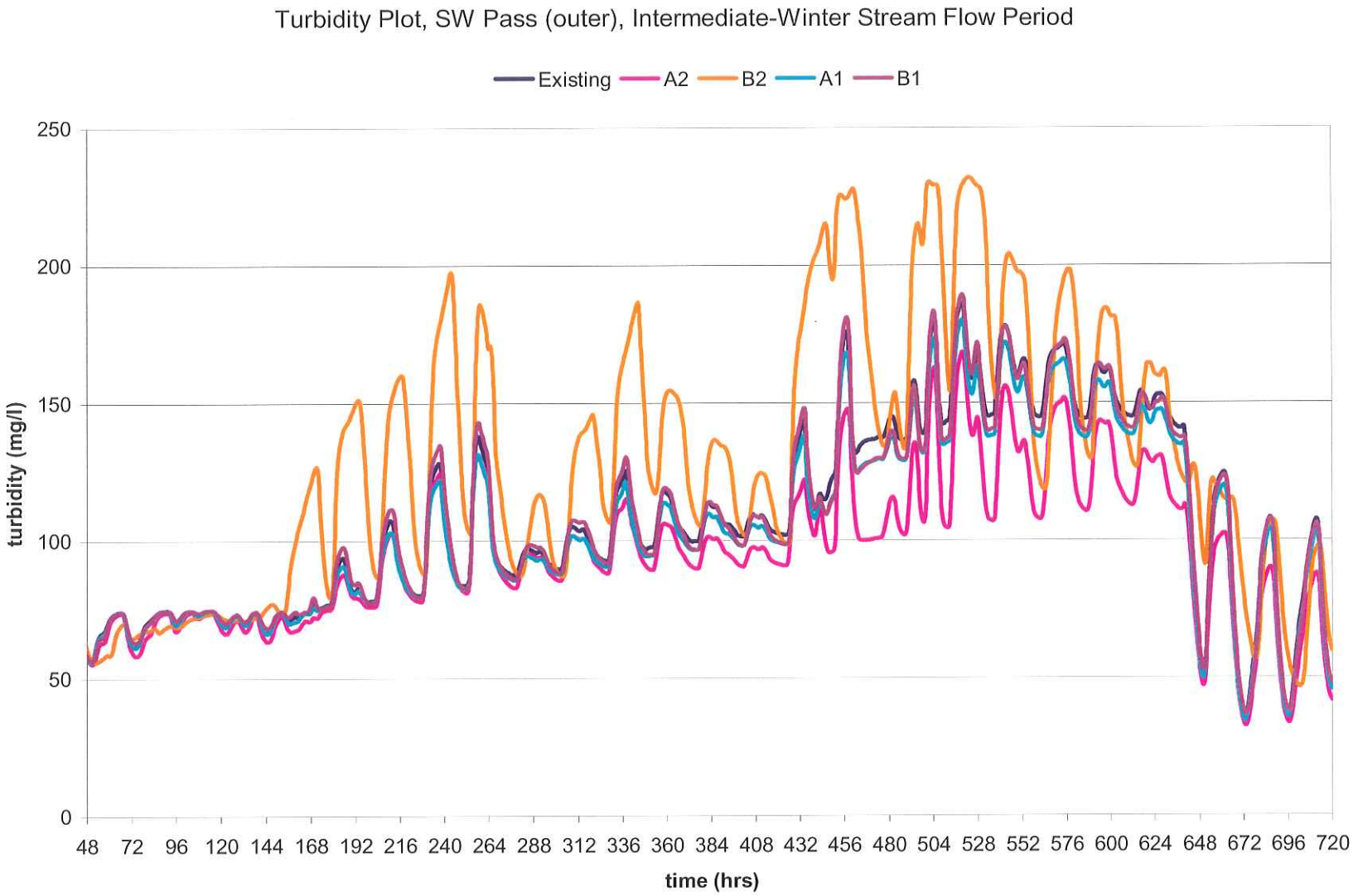
Turbidity Plot, SW Pass (outer), Intermediate-Winter Stream Flow Period
Existing
A2
B2
A1
B1
250
200
150
100
50
0
turbidity (mg/l)
48 72 96 120 144 168 192 216 240 264 288 312 336 360 384 408 432 456 480 504 528 552 576 600 624 648 672 696 720
time (hrs)

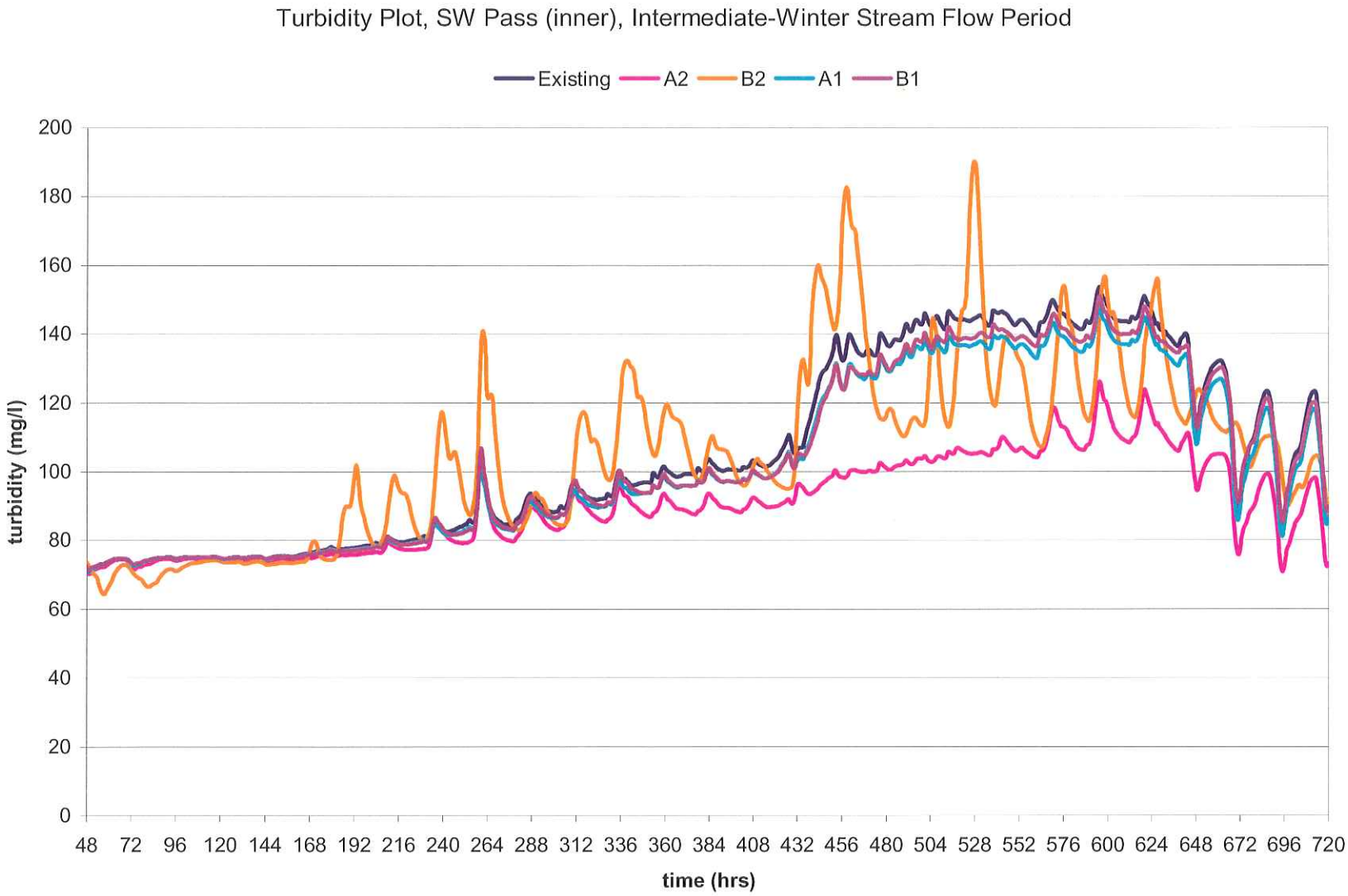
Turbidity Plot, SW Pass (inner), Intermediate-Winter Stream Flow Period
Existing
A2
B2
A1
B1
turbidity (mg/l)
0
20
40
60
80
100
120
140
160
180
200
48
72
96
120
144
168
192
216
240
264
288
312
336
360
384
408
432
456
480
504
528
552
576
600
624
648
672
696
720
time (hrs)

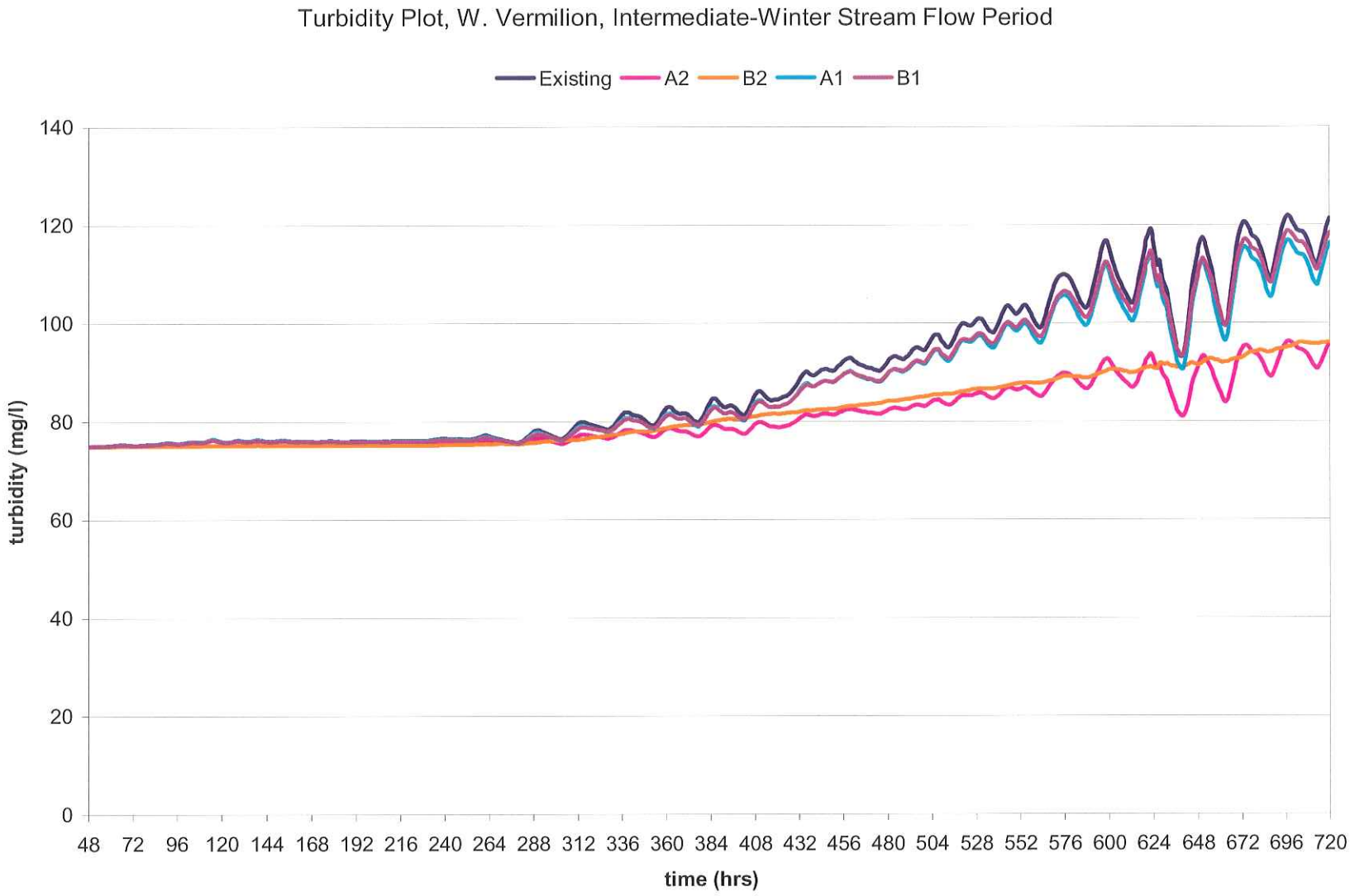
Turbidity Plot, W. Vermilion, Intermediate-Winter Stream Flow Period
Existing
A2
B2
A1
B1
140
120
100
80
60
40
20
0
turbidity (mg/l)
48 72 96 120 144 168 192 216 240 264 288 312 336 360 384 408 432 456 480 504 528 552 576 600 624 648 672 696 720
time (hrs)

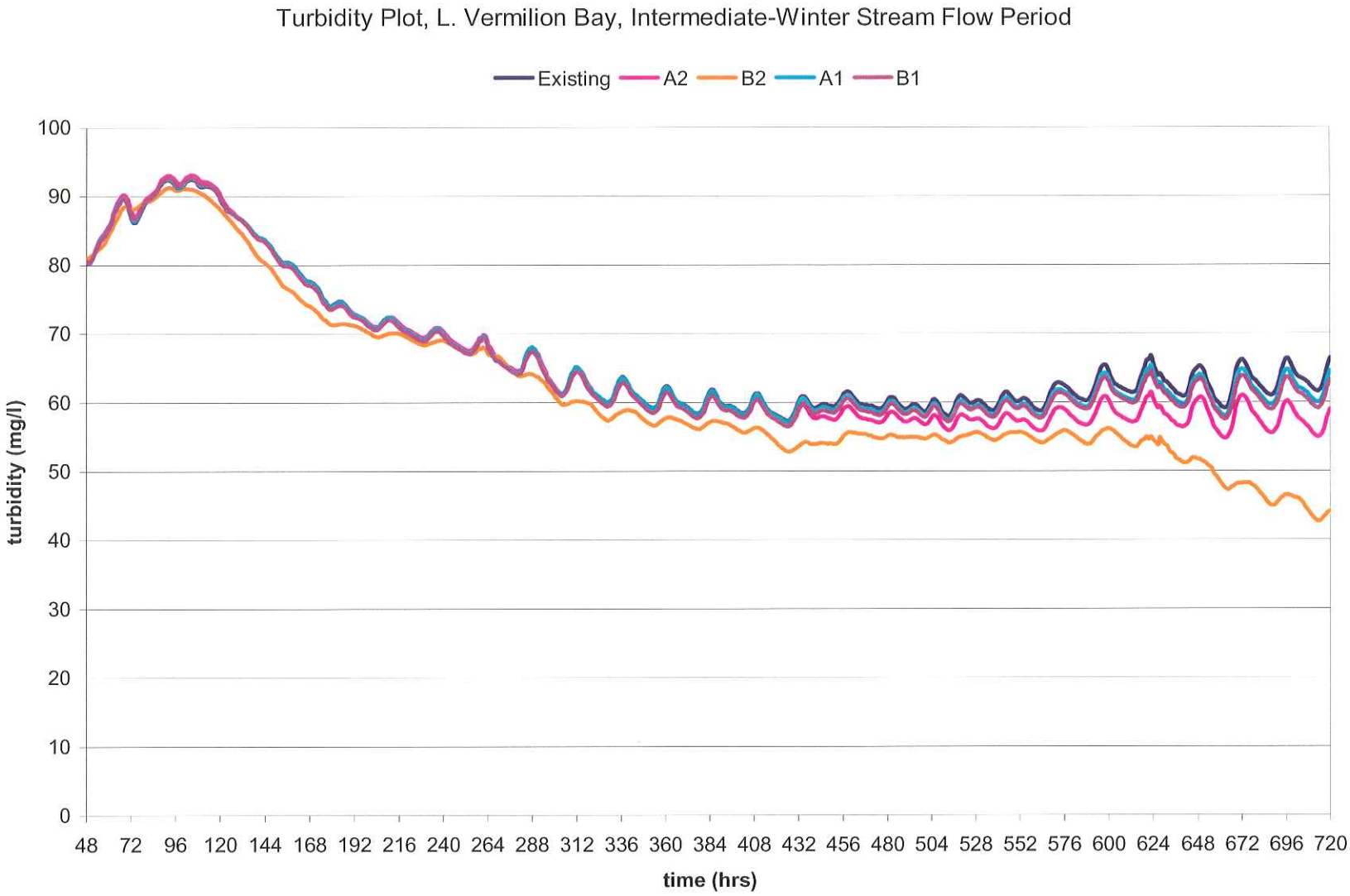
Turbidity Plot, L. Vermilion Bay, Intermediate-Winter Stream Flow Period
Existing
A2
B2
A1
B1
turbidity (mg/l)
100
90
80
70
60
50
40
30
20
10
0
48 72 96 120 144 168 192 216 240 264 288 312 336 360 384 408 432 456 480 504 528 552 576 600 624 648 672 696 720
time (hrs)

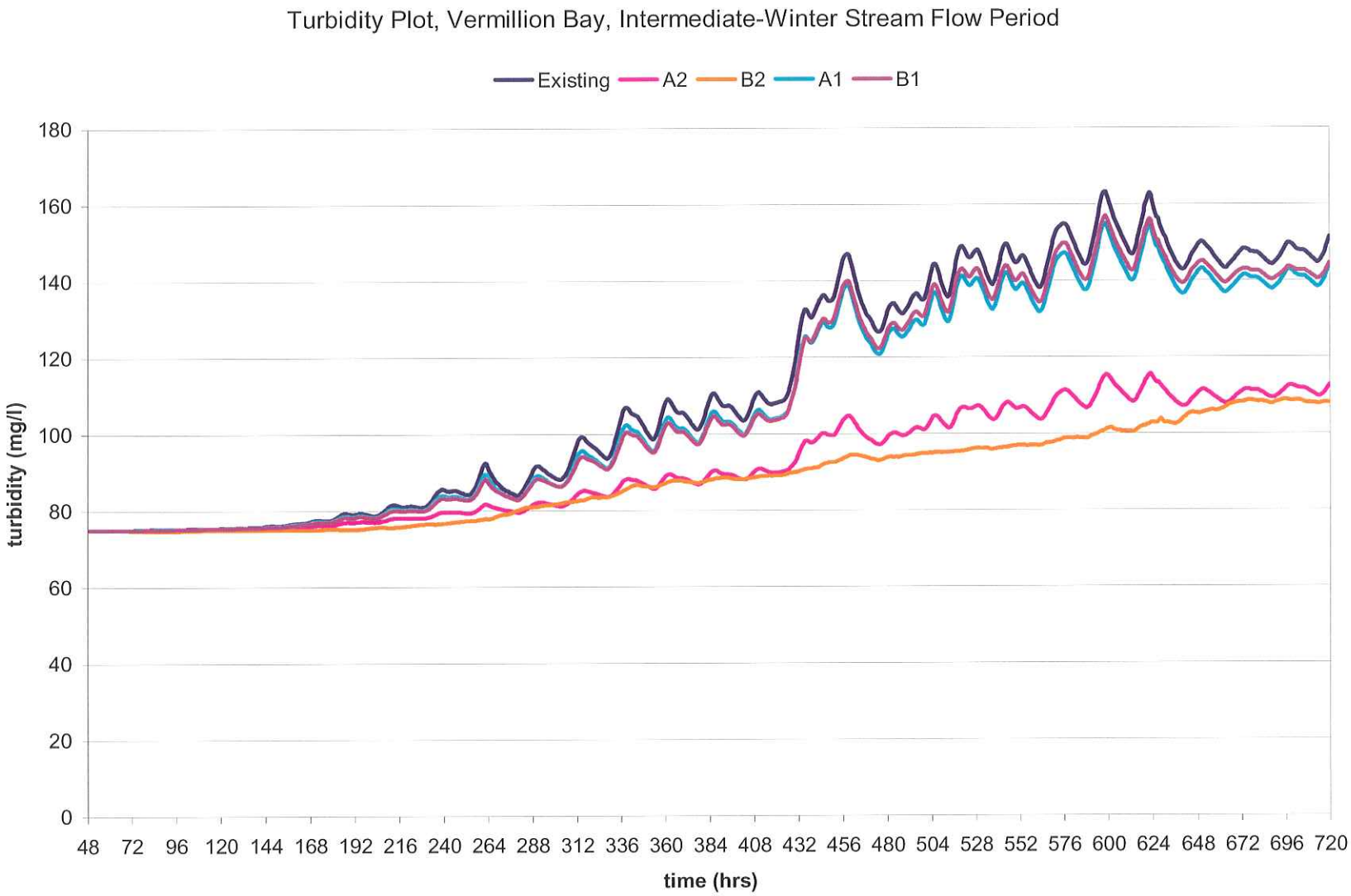
Turbidity Plot, Vermillion Bay, Intermediate-Winter Stream Flow Period
Existing
A2
B2
A1
B1
turbidity (mg/l)
0
20
40
60
80
100
120
140
160
180
48 72 96 120 144 168 192 216 240 264 288 312 336 360 384 408 432 456 480 504 528 552 576 600 624 648 672 696 720
time (hrs)

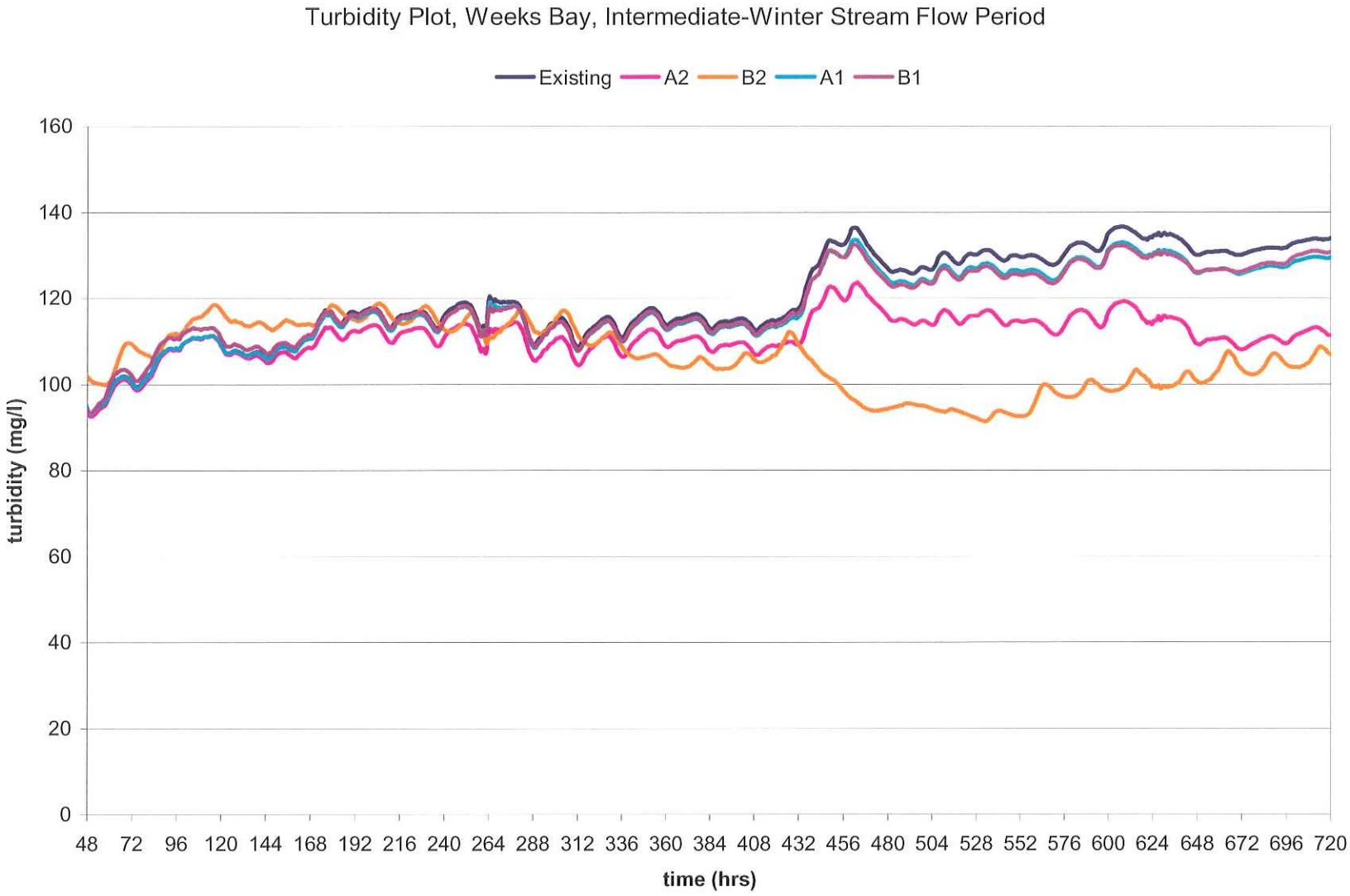
Turbidity Plot, Weeks Bay, Intermediate-Winter Stream Flow Period
Existing
A2
B2
A1
B1
160
140
120
100
80
60
40
20
0
turbidity (mg/l)
48 72 96 120 144 168 192 216 240 264 288 312 336 360 384 408 432 456 480 504 528 552 576 600 624 648 672 696 720
time (hrs)

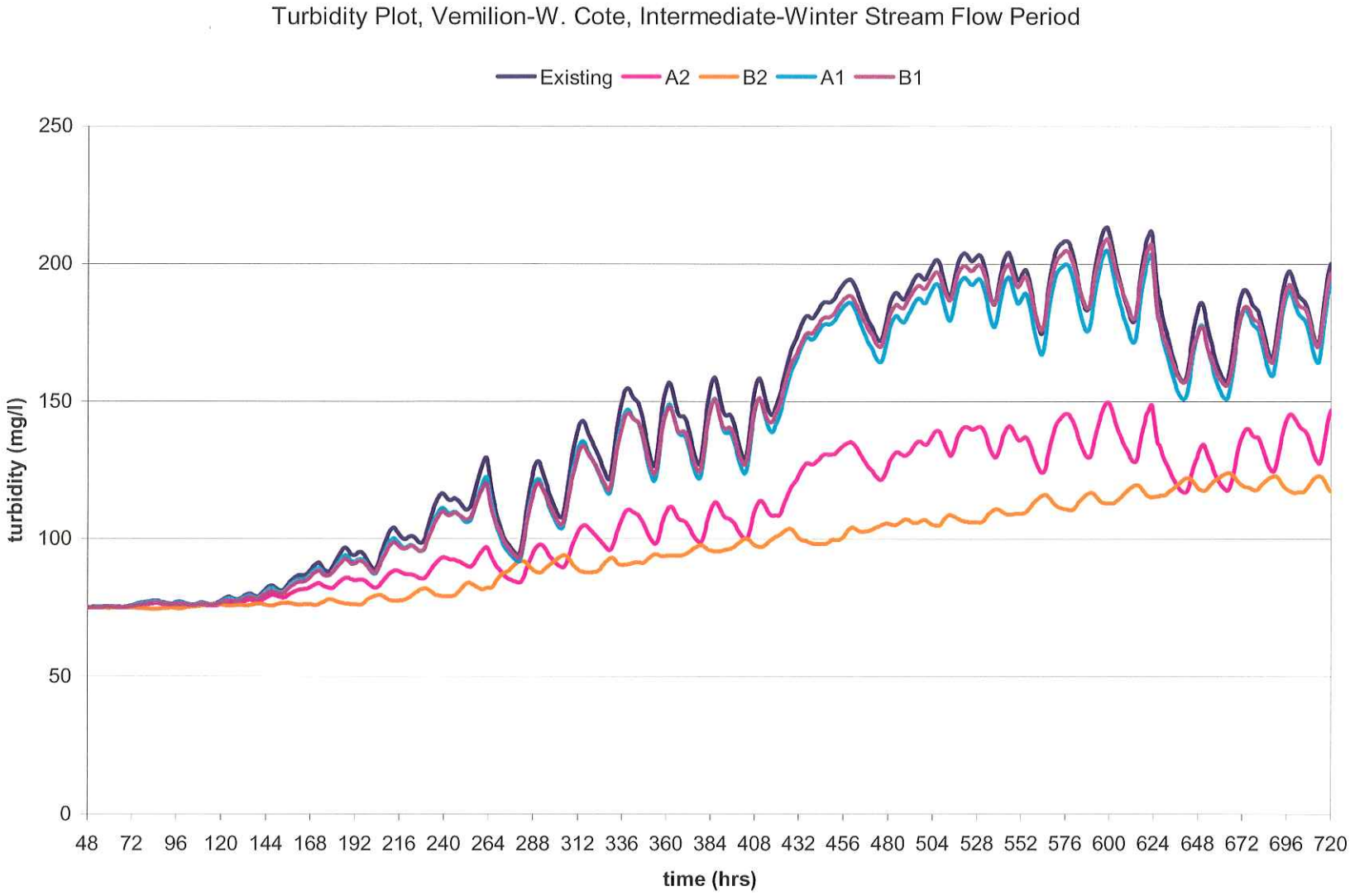
Turbidity Plot, Vemilion-W. Cote, Intermediate-Winter Stream Flow Period
Existing
A2
B2
A1
B1
250
200
150
100
50
0
turbidity (mg/l)
48 72 96 120 144 168 192 216 240 264 288 312 336 360 384 408 432 456 480 504 528 552 576 600 624 648 672 696 720
time (hrs)

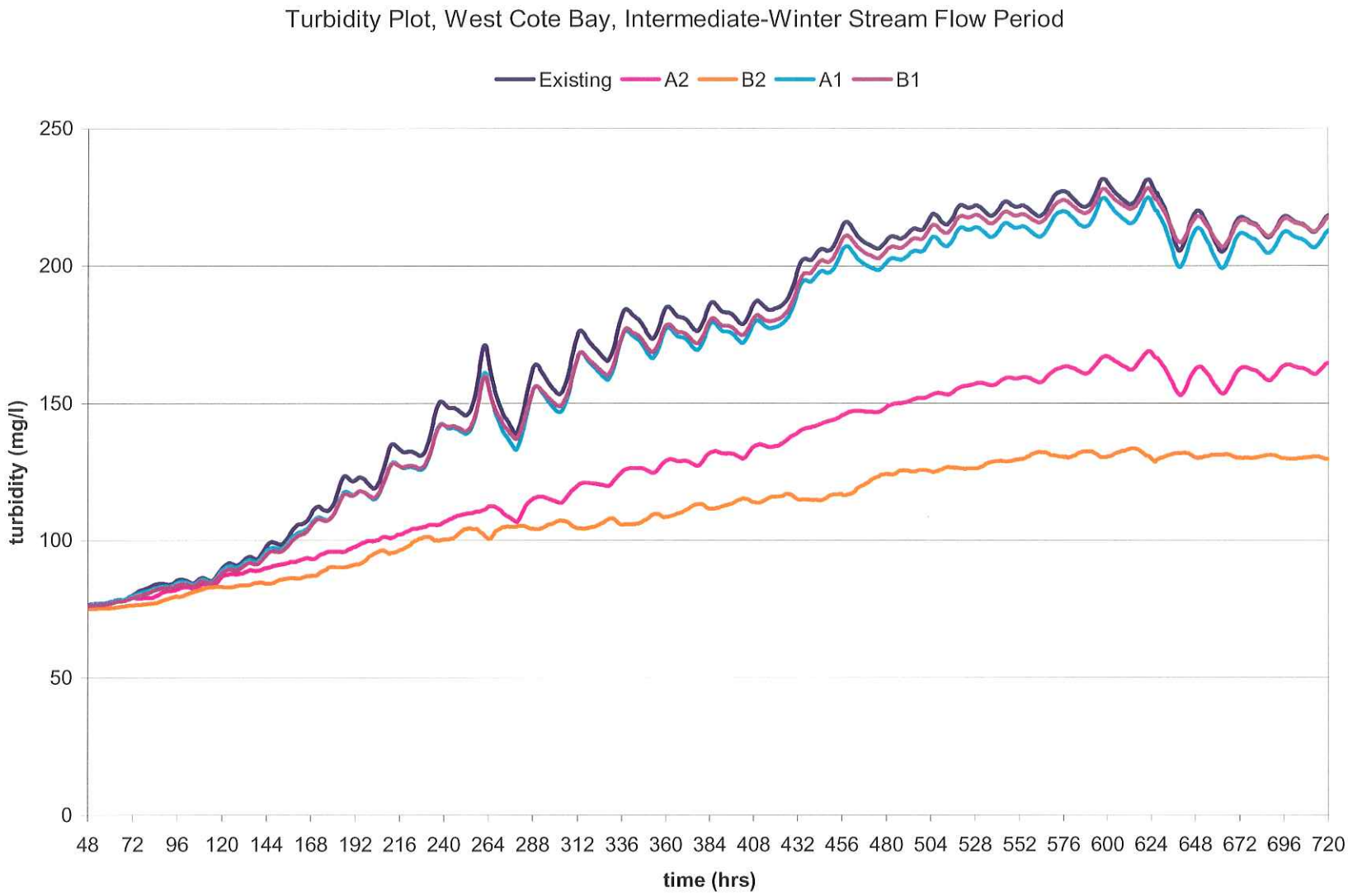
Turbidity Plot, West Cote Bay, Intermediate-Winter Stream Flow Period
Existing
A2
B2
A1
B1
250
200
150
100
50
0
turbidity (mg/l)
48 72 96 120 144 168 192 216 240 264 288 312 336 360 384 408 432 456 480 504 528 552 576 600 624 648 672 696 720
time (hrs)

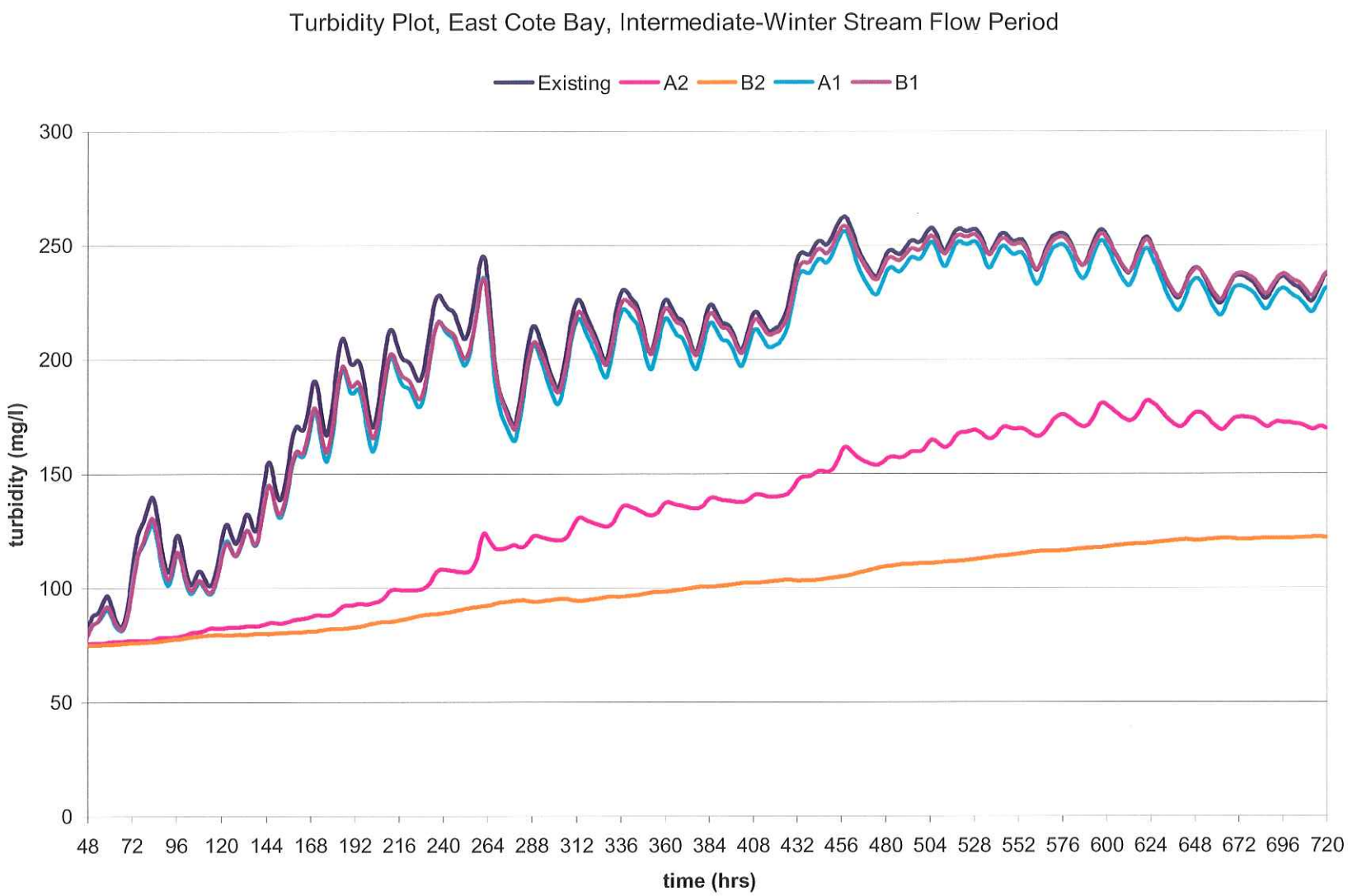
Turbidity Plot, East Cote Bay, Intermediate-Winter Stream Flow Period
Existing
A2
B2
A1
B1
300
250
200
150
100
50
0
turbidity (mg/l)
48 72 96 120 144 168 192 216 240 264 288 312 336 360 384 408 432 456 480 504 528 552 576 600 624 648 672 696 720
time (hrs)

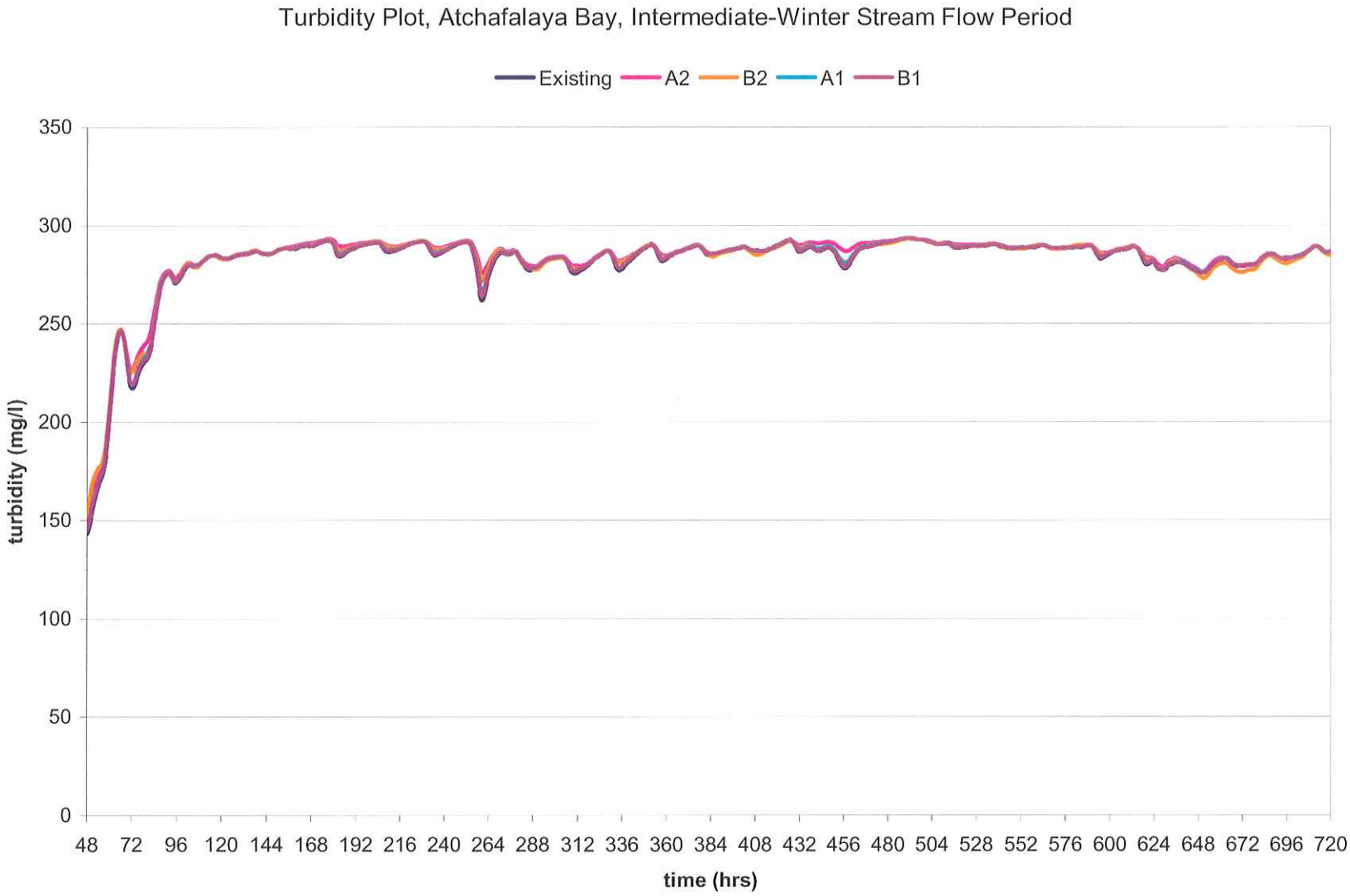
Turbidity Plot, Atchafalaya Bay, Intermediate-Winter Stream Flow Period
Existing
A2
B2
A1
B1
350
300
250
200
150
100
50
0
turbidity (mg/l)
48 72 96 120 144 168 192 216 240 264 288 312 336 360 384 408 432 456 480 504 528 552 576 600 624 648 672 696 720
time (hrs)

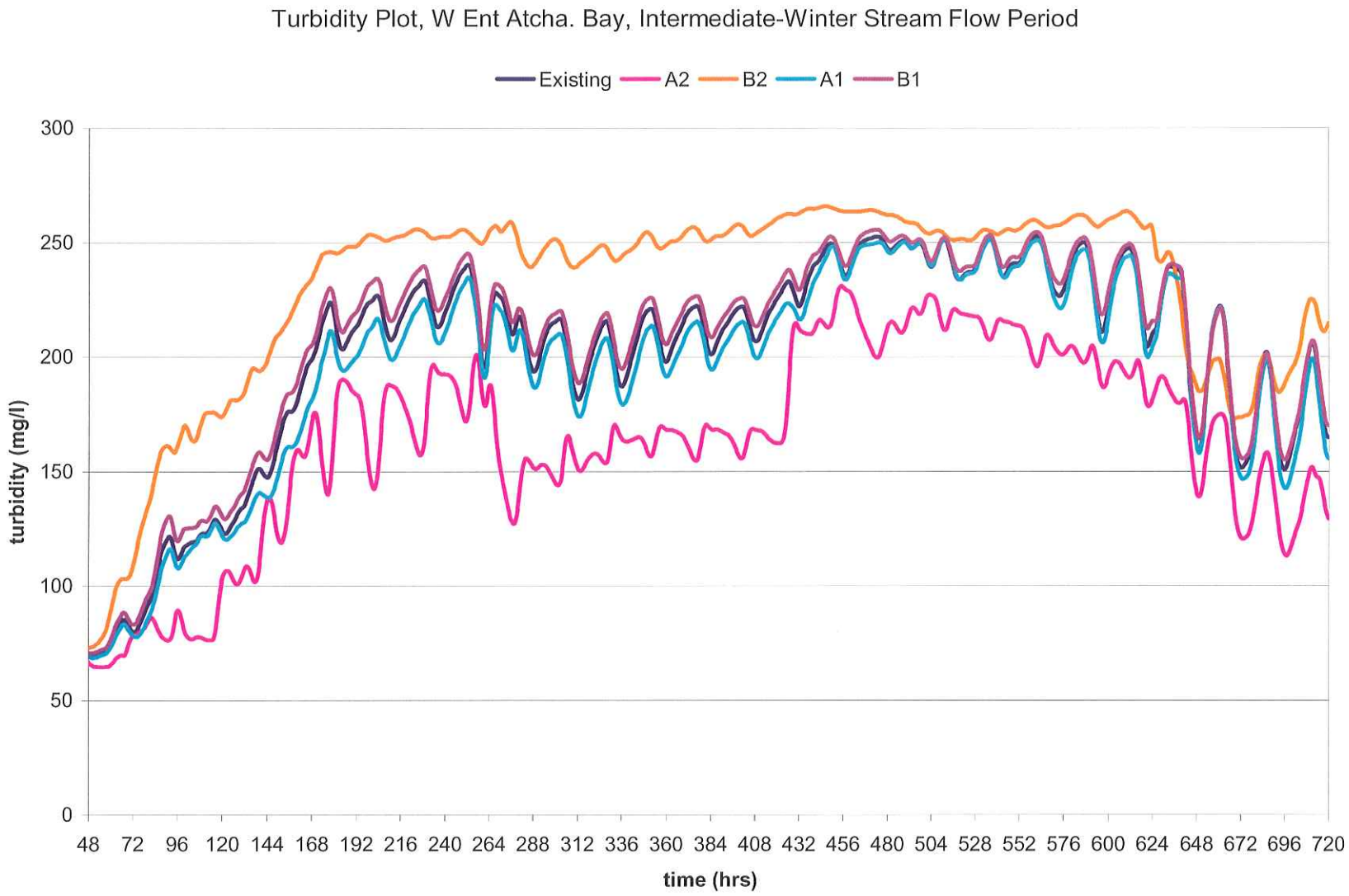
Turbidity Plot, W Ent Atcha. Bay, Intermediate-Winter Stream Flow Period
Existing
A2
B2
A1
B1
300
250
200
150
100
50
0
turbidity (mg/l)
48 72 96 120 144 168 192 216 240 264 288 312 336 360 384 408 432 456 480 504 528 552 576 600 624 648 672 696 720
time (hrs)

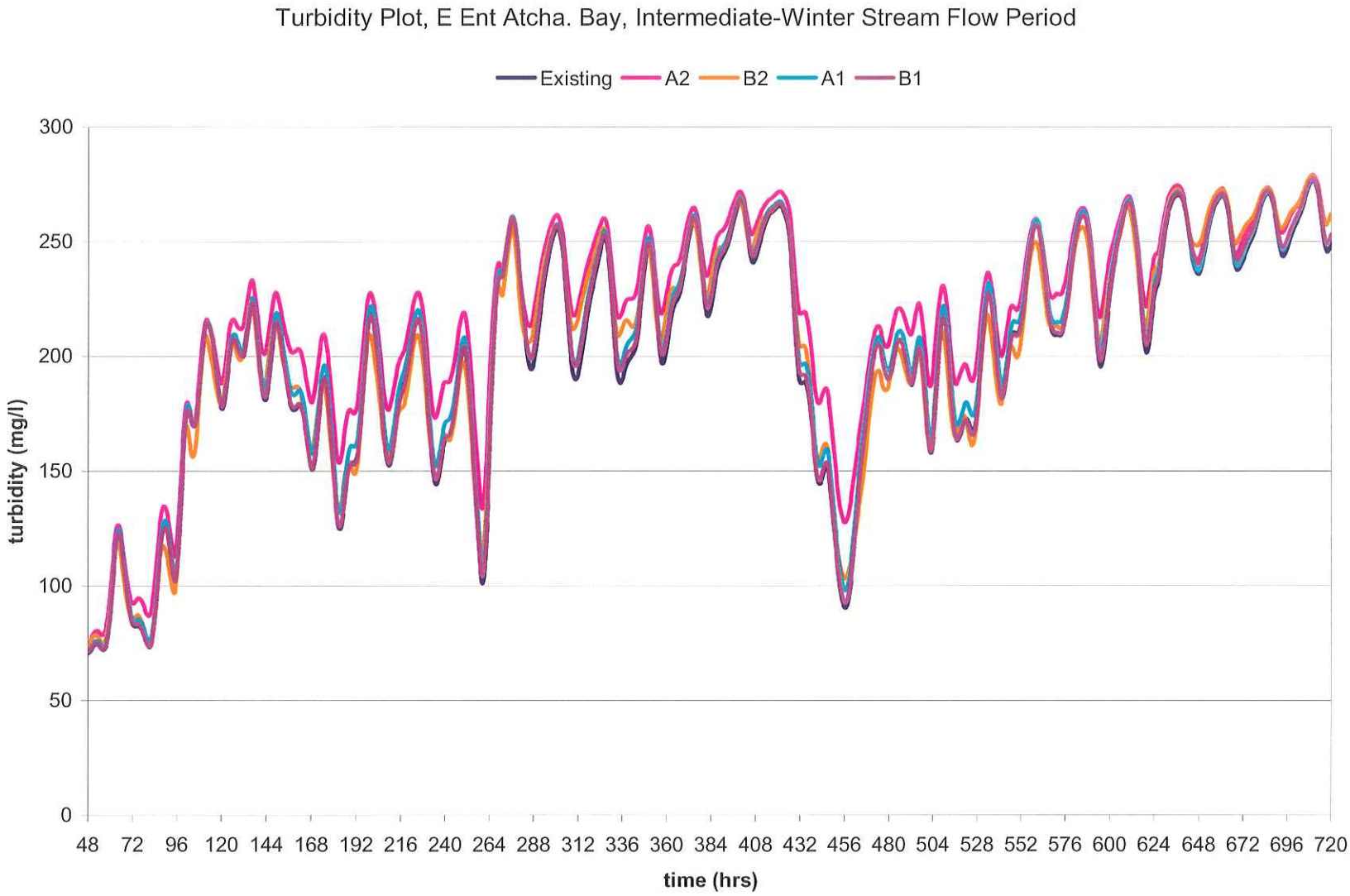
Turbidity Plot, E Ent Atcha. Bay, Intermediate-Winter Stream Flow Period
Existing
A2
B2
A1
B1
turbidity (mg/l)
300
250
200
150
100
50
0
48 72 96 120 144 168 192 216 240 264 288 312 336 360 384 408 432 456 480 504 528 552 576 600 624 648 672 696 720
time (hrs)

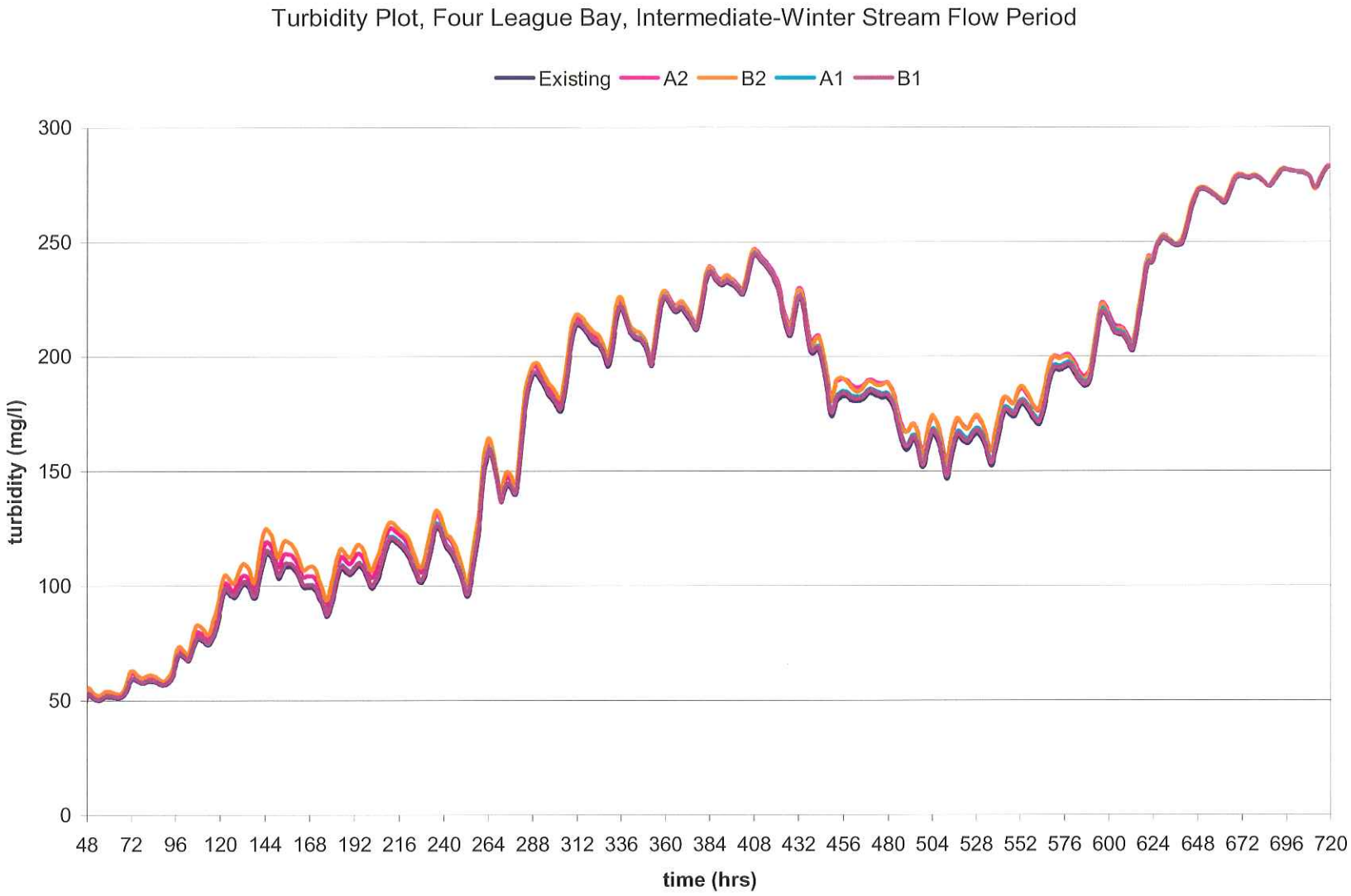
Turbidity Plot, Four League Bay, Intermediate-Winter Stream Flow Period
Existing
A2
B2
A1
B1
turbidity (mg/l)
0
50
100
150
200
250
300
48 72 96 120 144 168 192 216 240 264 288 312 336 360 384 408 432 456 480 504 528 552 576 600 624 648 672 696 720
time (hrs)